SPONSORED BY THE

Federal Ministry
of Education
and Research

Funded by

DFG Deutsche
Forschungsgemeinschaft

German Research Foundation

STATUS CONFERENCE RESEARCH VESSELS 2022

Conference transcript

SCHRIFTENREIHE PROJEKTTRÄGER JÜLICH

„Bibliographic information published by the Deutsche Nationalbibliothek.
Die Deutsche Nationalbibliothek lists this publication in the Deutsche Nationalbibliografie; detailed bibliographic data are available in the Internet at http://dnb.d-nb.de."

Published by
Forschungszentrum Jülich GmbH
Zentralbibliothek, Verlag
52425 Jülich, Germany
Phone: 02461 61-5368
Fax: 02461 61-6103
E-mail: zb-publikation@fz-juelich.de
Internet: www.fz-juelich.de/zb

Edited by and layout
Projectmanagement Jülich, Forschungszentrum Jülich GmbH

Photo credits
Titel (left to right): GEOMAR/Karen Hissmann; Manfred Schulz TV&FilmProduktion/ Max-Planck Institut Bremen; Universität Hamburg/LDF/Denecke

Schriftenreihe Projektträger Jülich Volume 15
ISBN 978-3-95806-608-3

The contributions are abstracts of the results of past research cruises. These results were presented at the virtual Status Conference Research Vessels 2022.

The complete volume is freely available on the Internet on the Jülicher Open Access Server (JuSER) at www.fz-juelich.de/zb/openaccess.

STATUS CONFERENCE RESEARCH VESSELS 2022

Conference transcript

SCHRIFTENREIHE PROJEKTTRÄGER JÜLICH

FOREWORD

Dear participants,

It is my pleasure to welcome you to the 2nd Status Conference Research Vessels 2022 at the Institute for Chemistry and Biology of the Marine Environment (ICBM) of the University of Oldenburg.

Sharing and discussing new scientific results from the many research cruises you conducted and/or participated in in the past years is an exciting, inspiring and important part of marine science and also allows for vital feedback to the Review Panel German Research Vessels (GPF) that works tirelessly to evaluate and advise on scientific cruise proposals. The Status Conference is a venue where you and all participants can relish the results that are the outcome of your hard work that went into devising the science, preparing for and conducting the research cruises, and into analysing and interpreting the data. Importantly, the Status Conference provides a venue to acknowledge this hard work and the work done by all the institutions that make seagoing marine research possible. I therefore want to take the opportunity here to thank you, the GPF, the funding agencies DFG, BMBF and HGF, and the German Research Fleet Coordination Centre for facilitating marine science and hence contributing to the continuous strive to explore, understand and protect our oceans.

I am very excited that this important meeting takes place again at the ICBM and am looking forward to two days of stimulating science, collegial exchange and new inspirations and wish all of you a pleasant stay at the ICBM and in Oldenburg.

KATHARINA PAHNKE
Professor for Marine Isotope Geochemistry, Institute for Chemistry and Biology of the Marine Environment (ICBM), University of Oldenburg

TABLE OF CONTENTS

OVERVIEW

ABSTRACTS

POSTER

OVERVIEW

EMB206, EMB209, EMB213, EMB218, EMB224

The hydrographic-hydrochemical and biological state of the Baltic Sea in 2019 and the variability and ecosystem changes on long time scales

AUTHORS

Department of Physical Oceanography and Instrumentation, Leibniz-Institute for Baltic Sea Research Warnemünde | Rostock, Germany
M. Naumann, V. Mohrholz, M. Schmidt

Department of Biological Oceanography Leibniz-Institute for Baltic Sea Research Warnemünde | Rostock, Germany
J. Dutz

Department of Marine Chemistry Leibniz-Institute for Baltic Sea Research Warnemünde | Rostock, Germany
J. Kuss

THE BALTIC SEA ECOSYSTEM

As an intra-continental sea with a densely populated catchment area, the Baltic Sea is of high economic and social importance for the ambient societies. It is the mission of the Leibniz-Institute for Baltic Sea Research Warnemünde (IOW) to provide knowledge for keeping the Baltic in a good ecological state. Warming, eutrophication and oxygen depletion are the most severe environmental threats the Baltic Sea faces today. The stratification of the water column, resulting from a restricted water exchange, neglectable tides and a positive water balance with a freshwater surplus, is one of the main reasons for a slow overturning circulation and the development of so called extended "dead zones" in the central Baltic Sea. To decipher the development of these hydrographic conditions and the overturning circulation in its full range present and future variability is one of the main aspects of the IOW long term observation programme.

THE ECOSYSTEM STATE OF THE YEAR 2019: METOROLOGICAL/ HYDROGRAPHIC ASSESSMENT

For the southern Baltic Sea area, the Warnemünde weather station recorded in the winter 2018/2019 a "cold sum" of the air temperature of 18.3 Kd leading to a classification as a mild winter season and a ranking as the seventh warmest winter since the beginning of recording in 1948. The summer "heat sum" of 283.1 Kd ranks at 24th position over

the past 71 years and is far below last year's record of 394.5 Kd. The long-term average heat sum is 158.6 +/- 68.9 Kd.

The hydrographic conditions in the deep basins of the Baltic Sea are mainly characterized by stagnation (slow water exchange) and widespread hypoxic to euxinic areas. The water inflowing during the exceptionally warm summer 2018 reached the deep-water of the central Baltic Sea. The Gotland Deep showed record high 8.6 °C at the bottom. Additional pulses of warm water arrived in the Gotland Deep in March and April 2019, but salinity values and concentrations of dissolved oxygen remained mainly unchanged. Three smaller barotropic inflows occurred from autumn 2018 to December /January 2019 and imported 3 Gt of salt into the western Baltic Sea. In the course of the year 2019 another four barotropic inflows but of weak intensity occurred (April, June, September, December). The last one imported 1 Gt of salt. The inflowing water propagated from the Arkona Basin into the southern parts of the eastern Gotland Basin. The bottom salinity values stayed on the high level in the central Baltic Sea caused by the several Major Baltic Inflows in the time span 2014–2016, so that the 2019 events of weak intensity could not ventilate the bottom near water body in the central basins.

HYDROCHEMICAL PARAMETERS

Anoxic and euxinic conditions in the deep waters intensified in 2019. Accordingly, in the eastern Gotland Sea, phosphate and ammonium concentrations were increasing since 2017. In 2019, oxygen was zero in all deep-water reference depths of the key stations Gotland Deep, Farö Deep, Landsort Deep and Karlsö Deep in the central Baltic Seaa. An exception is the deep water in the Bornholm Basin that was intermittently reoxygenated with about 3 ml/l oxygen in March. The annual average of about 1.0 ml/l oxygen, permits a nitrate concentration to 6.8 µmol/l in 2019, the ammonium concentration of 1.5 µmol/l is relatively low. The annual average phosphate concentration wasabout 3.8 µmol/l.

This talk also summarizes data obtained for chlorinated and polycyclic aromatic hydrocarbons (CHC, PAH) in Baltic Sea surface water from the January/February 2019. Observations were performed in areas of the Kiel Bight/Fehmarn Belt up to the Gotland Sea. In general, concentrations for CHC and U.S. EPA PAH decrease from the western Baltic Sea to the Gotland Sea with the exception of the Pomeranian Bight, highest concentrations for PAH and CHC were observed there (ΣPAH_{sum}: 15,000 pg/l, ΣCHC_{sum}: 31.5 pg/l). Among the CHCs highest concentrations were observed for HCB (HCB_{sum}: 6 to 8 pg/L) followed by DDT/metabolites (ΣDDT_{sum}: 3 to 7 (15)pg/L) and PCB_{ICES} (ΣPCB_{sum}: 2 to 9 pg/L). In the Pomeranian Bight concentrations for DDT/metabolites were highest among CHCs. The data depict high contaminant entrainment into the Pomeranian Bight and the Kiel Bight/Fehmarn Belt. Assessment of the results on the basis of the EQS of the Water Framework Directive shows that concentrations of a some high molecular weight PAH might be of concern for marine organisms, particularly in the Pomeranian Bight.

THE BIOLOGICAL STATE

Regarding the pelagic biota, the year 2019 was characterized by an early start of the productive phase. A total of 150 phytoplankton species were recorded on the 5 annual monitoring cruises reported here, marking a high species diversity that is comparable to observations of previous years. The seasonal cycle of phytoplankton growth was characterized by an earlier onset of the spring bloom and higher phytoplankton biomass than measured in 2018, particularly in the southern Baltic Sea areas. Here the spring bloom was dominated by diatoms. The fraction of dinoflagellates and *Mesodinium rubrum* increased towards the Gotland Basin. In May the 2019 spring bloom had already declined. The summer phytoplankton community consisted mainly of dinoflagellates and diazotrophic cyanobacteria in all sampled areas. A bloom of toxic *Alexandrium pseudogonyaulax* dominated the phytoplankton community of the central Arkona basin in July/August with highest abundances so far reported from northern European waters. High cyanobacteria biomass shares were mainly detected in the Bornholm and Gotland basins. The phytoplankton growth period extended well into the autumn: in October a third biomass peak made by diatoms of the genera *Rhizosolenia, Proboscia* and *Cerataulina* was nearly equaling spring bloom biomass levels in the southern Baltic.

The seasonal development of the zooplankton stocks was also characterized by an early start. A total of 50 zooplankton species identified during 2019 marks a medium diversity compared to the previous years. The zooplankton was dominated by the Copepoda and the Copelata. Rotifera and Cladocera were only of minor importance in 2019. They can be very abundant during spring and summer, respectively, but only moderate concentrations of the cladoceran *Bosmina spp.* were found restricted to the eastern Arkona Basin. In spring, high concentrations of the copepod Acartia occured in all areas. In the Kiel Bight and Bay of Mecklenburg *Acartia bifilosa* was dominating, while in the *Arkona Basin*, *A. longiremis* was the major species. The spring and summer abundance of the zooplankton remained below the long term average, particularly Rotifera and Cladocera had a maximum stock size of only 2 % and 40 % of the long-term mean, respectively. In general, the stock size of zooplankton has remained on a very low level since 2010 compared to the preceding decade.

THE LONG-TERM DATA PROGRAMME

The long-term data programme serves to collect long-term data on the variability of the hydrographic, chemical and biological situation in seasonal change from the Bornholm Sea to the central Baltic Sea. Additional measurements in western Baltic Sea, conducted for the national monitoring financed by the Federal Maritime Agency (BSH), complements this dataset. The density of the station network is determined by the requirements of the physical investigations of the dynamics of the water exchange and the Baltic Sea circulation. Chemical-biological investigations are limited to a few selected stations. In addition, permanent measuring stations are operated at key positions, which complement the spatial image in high temporal resolution. The work comprises 45 sea days per year, divided into five trips of about 9 days duration. The measurement programme has

continued to build up time series at key stations continuously since 1969. The results form the necessary basis for research into the natural variability of the Baltic Sea ecosystem, anthropogenic influences and the effects of climate change, and are therefore indispensable for the fulfilment of the IOW's mission. As an example, this long-term data series show an acceleration of oxygen depletion rates analyzing the last three Major Baltic Inflows of strong intensity in detail which occurred in 1993, 2003 and 2014. The observations of this programme support essentially model studies like MEYER et al. (2018) analyzing this oxygen depletion issue on longer time scales of the last 150 years. All data obtained are freely available to researchers and the general public in databases of the Institute (IOWDB), the Federal Environment Agency (MUDAB) and, in an international context, at ICES/HELCOM. They support cooperation in the Baltic Sea region and environmental policy assessments of the ecosystem status of the Baltic Sea.

REFERENCES

Naumann M, Gräwe U, Mohrholz V, Kuss J, et al. Hydrographic-hydrochemical assessment of the Baltic Sea 2019, Marine Science Reports 2020, 114, doi: 10.12754/msr-2020-0114

Zettler M L, Kremp A, Dutz J, Biological assessment of the Baltic Sea 2019, Marine Science Reports 2020, 115, doi: 10.12754/msr-2020-0115

Meier H E M, Väli G, Naumann M, Eilola K, Frauen C, Recently accelerated oxygen consumption rates amplify deoxygenation in the Baltic Sea, Journal of Geophysical Research: Oceans 2018, doi: 10.1029/2017JC013686

ABSTRACTS

AL521 AND AL522

Baltic Sea Integrative Long-term Data Series

AUTHORS

GEOMAR Helmholtz Centre for Ocean Research Kiel | Kiel, Germany
J. Dierking, T. Reusch

STUDY SYSTEM AND QUESTIONS

The Baltic Sea is a macro-regional sea under particularly pronounced anthropogenic pressures, including eutrophication, contaminant accumulation, fishing and non-indigenous species, as well as rapid vectors of change, most notably warming and the spread of oxygen minimum zones. It has therefore been identified as a "time machine" reflecting possible multiple-pressure futures of other coastal areas worldwide, and can serve as a test bed for resource management approaches and solutions under these conditions (Reusch et al 2018). The Baltic is also characterized by a horizontal salinity gradient from the connection to the North Sea in the west to the freshwater-dominated systems in the north-east. In this setting, prominent marine species such as cod are occurring at the very border of their distribution ranges and environmental tolerance limits, and the composition of species pools and food webs changes along the salinity gradient as marine species "drop out" and freshwater species appear in the communities. Both from a fundamental scientific as well as applied resource management perspective, this set-up raises a number questions, including which forcings affect fluctuations and long-term trends in the hydrographic situation and in abiotic parameters, how the interaction of hydrographic change and anthropogenic pressures in turn affects the condition, reproduction, population size and population structure of individual species, as well as the structure and functioning of biological communities and food webs over time. More specific questions include whether change in the Baltic has revealed tipping points or regime shifts, whether and how biological interactions can buffer or promote pressures, and from an evolutionary perspective, how local adaptations and adaptation potential determine the fate of species in this system.

CONCEPT OF THE BALTIC SEA INTEGRATIVE LONG-TERM DATA SERIES

Long-term data series have been highlighted as one of the best available tools to separate short-term fluctuations from long-term directional change (Lotze et al 2012), and thus to understand consequences of global change and anthropogenic pressures for biological systems. To address questions regarding the changing Baltic, the GEOMAR Helmholtz Centre for Ocean Research Kiel and its precursors have assembled one of the best available long-term data and sample series of the pelagic systems of the Baltic Sea, spanning the time period 1986 to the present. The concept has been integrative, i. e., combining hydrographic assessments, surveys and sampling of the planktonic system

(including jellyfish), and measurements and sampling of key fish species including cod, herring and sprat. The spatial focus has been on the deep, productive Bornholm Basin, home of the largest commercial fisheries in the Baltic, where the same station grid has been covered annually (Figure 1), but has also included measurements and sampling along the salinity gradient. The cruises AL521 in April and AL522 in May 2019 contribute to this long-term data series, but have also included additional, project-based work, including intensive food web sampling for dietary tracer analysis and high-quality tissue sampling for genomic work. At the status conference, we will provide an overview of the outcomes and observations of the 2019 cruises, put these new observations in the context of the Baltic Sea Integrative Long-term Data Series, and then present examples of project applications and insights achieved with this data and sample treasure.

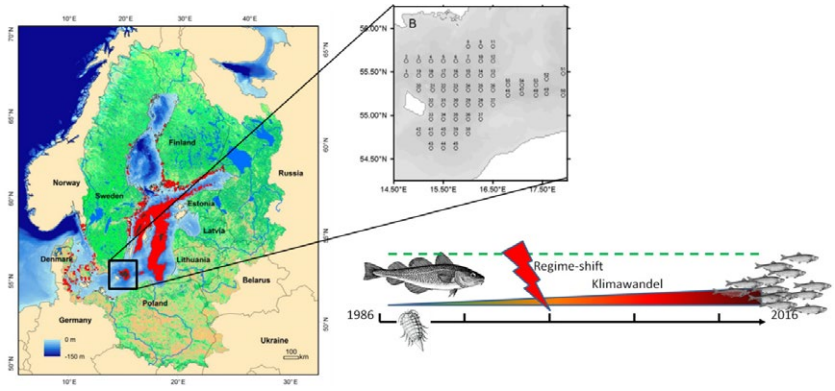

Fig. 1: Study system Baltic Sea (left panel) with a close-up of the station grid in Bornholm Basin (cut-out) covered by the cruises AL521 and AL522 in 2019, and consistently throughout the Baltic Sea Integrative Long-term Data Series since the year 1986. Additional station work took place along the cruise track from Kiel Bight in the western Baltic Sea via Arkona Basin and Bornholm Basin to the Gdansk Deep and Gotland Basin in the east. During the time period 1986 to the present, a regime shift with spreading anoxia in deep water (red areas left panel), a corresponding decline of benthic fauna including the crustacean Saduria entomon and a shift from a cod-dominated to a planktivorous fish dominated system took place in the study area (depicted in the bottom right).

PROJECT APPLICATIONS AND INSIGHTS ACHIEVED

We here focus on two core lines of work and output, spatio-temporal patterns in Baltic cod population structure (Hemmer-Hansen et al 2019, Weist et al 2019) (Figure 2), and the characterization of central Baltic Sea food webs using stable isotope analysis, with a focus on the trophic niches and interactions of fish and jellyfish (Figure 3). We also provide additional examples of time series output, including the retroactive assembly of time series in microplastic concentrations (Beer et al 2018), of the importance of benthic- versus pelagic diet of cod over a period with spreading anoxia, and of cod fecundity over a period of declining fish condition (Köster et al 2020). We close with a short perspective on the tremendous value of integrative long-term data series in a changing world, and provide an outlook both to future cruise plans extending the Baltic Sea Integrative Long-term Data Series, and to project work, including cod genome studies of

signatures of fisheries- and environmentally-induced evolution, and the coupling of dietary tracer and food web model studies.

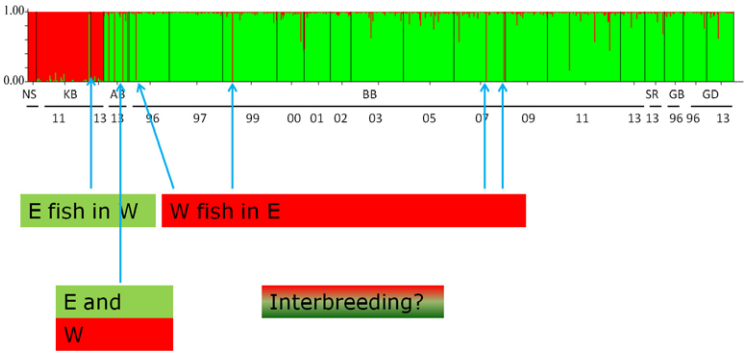

Fig. 2: Spatio-temporally resolved view of genotypic composition of Baltic cod, based on single-nucleotide polymorphism genotyping and Bayesian clustering of 1100 cod individuals from different locations and time points along the Baltic Sea salinity gradient. Results were obtained with the program STRUCTURE 2.3. Each vertical bar represents one individual, and the two colors denote the inferred proportional genotypic contributions of each cluster. Sampling locations sorted from left to right by geographic area from west to east, and chronologically by sampling year within location. The time series shows the presence of two genotypes corresponding to eastern and western Baltic cod, and consistent spatial segregation (with rare occurrence of eastern cod genotypes in the west and western genotypes in the east) of the two stocks. Moreover, the data highlight the co-occurrence but lack of hybridization of western and eastern Baltic cod in the intermediate area Arkona Basin. The rare occurrence of putative eastern Baltic cod in the west, western Baltic cod in the east, and the mixing situation in Arkona Basin are pointed out by arrows. Abbreviations: NS = North Sea, KB = Kiel Bight, AB = Arkona Basin, BB = Bornhom Basin, SR = Stolpe Trench, GB = Gotland Basin, GD = Gdansk Deep.

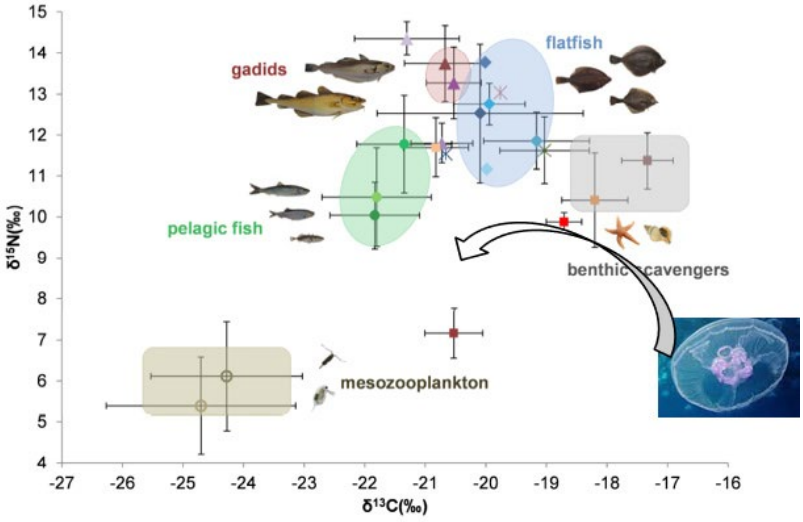

Fig. 3: Characterization of central Baltic Sea food webs with stable isotope dietary tracer analysis. $\delta^{15}N$ is a measure of the trophic position (higher values = higher trophic position), and $\delta^{13}C$ of organic matter sources at the base of the food web and of benthic versus pelagic feeding. At the status conference, we will provide an update on the trophic niches of jellyfish in these food webs (not yet shown here), for which data were collected during cruise AL521 and AL522.

REFERENCES

Beer S, Garm A, Huwer B, Dierking J, Nielsen TG (2018) No increase in marine microplastic concentration over the last three decades – A case study from the Baltic Sea. Science of The Total Environment 621:1272–1279

Hemmer-Hansen J, Hüssy K, Baktoft H, Huwer B, Bekkevold D, Haslob H, Herrmann J-P, Hinrichsen H-H, Krumme U, Mosegaard H, Nielsen EE, Reusch TBH, Storr-Paulsen M, Velasco A, von Dewitz B, Dierking J, Eero M (2019) Genetic analyses reveal complex dynamics within a marine fish management area. Evolutionary Applications 12:830–844

Köster FW, Huwer B, Kraus G, Diekmann R, Eero M, Makarchouk A, Örey S, Dierking J, Margonski P, Herrmann JP, Tomkiewicz J, Oesterwind D, Kotterba P, Haslob H, Voss R, Reusch TBH (2020) Egg production methods applied to Eastern Baltic cod provide indices of spawning stock dynamics. Fisheries Research 227:105553

Lotze, H.K., Sea of Plenty? Historical trends, current issues, and future perspectives on our use of seafood, in Food For Thought: A Multidisciplinary Discussion, R.S. Stewart and K. S.A., Editors. 2012, Cape Breton University Press.

Reusch TBH, Dierking J, Andersson HC, Bonsdorff E, Carstensen J, Casini M, Czajkowski M, Hasler B, Hinsby K, Hyytiäinen K, Johannesson K, Jomaa S, Jormalainen V, Kuosa H, Kurland S, Laikre L, MacKenzie BR, Margonski P, Melzner F, Oesterwind D, Ojaveer H, Refsgaard JC, Sandström A, Schwarz G, Tonderski K, Winder M, Zandersen M (2018) The Baltic Sea as a time machine for the future coastal ocean. Science Advances 4

Weist P, Schade FM, Damerau M, Barth JMI, Dierking J, André C, Petereit C, Reusch T, Jentoft S, Hanel R, Krumme U (2019) Assessing SNP-markers to study population mixing and ecological adaptation in Baltic cod. PLOS ONE 14:e0218127

AL532

Monitoring and Mapping Deformation Offshore Mount Etna

AUTHORS

GEOMAR Helmholtz Centre for Ocean Research Kiel | Kiel, Germany
M. Urlaub, T. Kurbjuhn, A. Steinführer, E. Wenzlaff

Istituto Nazionale di Geofisica e Vulcanologia, Osservatorio Etneo | Catania, Italy
A. Bonforte

INTRODUCTION

Mount Etna at the east coast of Sicily is Europe's largest active volcano. Satellite- based ground deformation observations (GNSS, Interferometric SAR) show that the volcano's south-eastern flank slides seawards at a rate of 2–3 cm per year (Bonforte et al., 2011). Recent seafloor geodetic measurements suggest that also the submerged part of the flank is sliding at a similar rate (Urlaub et al., 2018). However, this observation is spatially limited to one point along the submerged fault that represents the boundary between the stable and unstable sectors of the volcano. The aim of the research cruise AL532 in January 2020 was to map this fault system at the best possible resolution. Therefore, the Autonomous Underwater Vehicle (AUV) ABYSS carried a multibeam echosounder about 80 m above the seafloor, collecting ultra high-resolution data to provide microbathymetric maps with grid spacing as low as 1 m.

RESULTS AND INTERPRETATION

Due to the late arrival of RV ALKOR to Catania, the port of embarkation, the cruise was four days long instead of eleven days as requested. Nevertheless, it was possible to conduct two scientific dives with the AUV providing valuable microbathymetric maps of two areas along the boundary fault. One map covers the area of the seafloor geodetic experiment, which recorded fault activity during a slow slip event in May 2017 with a minimum of 4 cm strike slip and 1 cm dip slip movement. The other map, further downslope, covers the edge of the continental bulge and its transition to the less steep Ionian Basin. Although only 3 km apart, the two maps show very different expressions of what is expected to be one fault. The terrain in the upslope site is steep and rugged and soft sediments are mostly absent. Here, the fault stands out as a very prominent lineament (Fig. 1b). The overall morphology resembles that of terrestrial active strike-slip faults, for example the Elkhorn segment of the San Andreas Fault. Interestingly, the ship-based multibeam data does not resolve the lineament (Fig. 1a) so that we had to revise our previous interpretation of the fault location (compare Fig. 1a and 1b). In contrast, in the lower slope area the terrain is smoother and the fault does not have a surface expression. The presumed fault trace crosses the mouth of Catania Canyon. Hence, there are two

explanations for the absence of a surface fault trace: First, the canyon is highly active and sediments transported in the canyon mask the imprint of the recent fault activity. Second, the downslope part of the fault has not been active recently. Very little is known about the activity of Catania Canyon so that further investigations are necessary to discern between the two hypotheses.

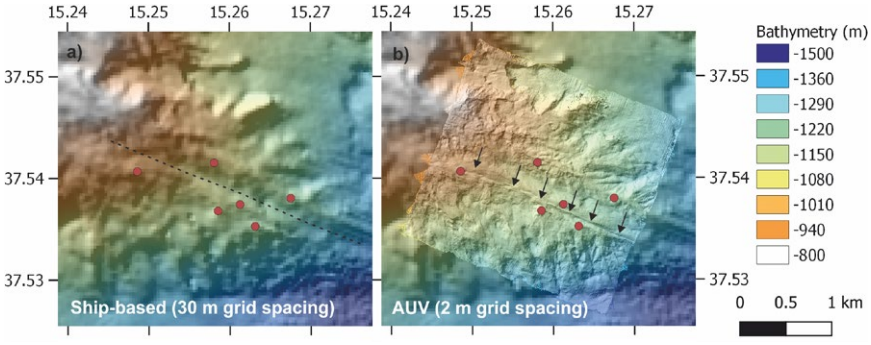

Fig. 1: Comparison of a) ship-based bathymetry and b) AUV microbathymetry of a part of the submerged southern boundary fault of Etna's unstable flank in the area of the seafloor geodetic experiments. The dashed line shows fault location inferred from ship-based bathymetry. Arrows show actual fault location revealed by microbathymetry. Red dots show locations of six seafloor geodetic transponders for the second experiment deployed in August 2020 during expedition SO277. Ship-based multibeam data was acquired during expedition M86/2 with the hull-mounted EM122 multibeam system of RV METEOR (Krastel et al., 2014). Microbathymetry was acquired during AL532 with a Reson SeaBat T50 mutlibeam system carried by AUV ABYSS (Urlaub et al., 2020).

CONCLUSION

With the new microbathymetry we were able to revise our previous interpretation of the fault location inferred from ship-based bathymetry. This result demonstrates the importance of microbathymetry for structural interpretation of seafloor features. Microbathymetry is also crucial for methods that (i) target small-scale seafloor features like seafloor geodesy or (ii) have a limited spatial coverage, such as deep-towed optical approaches or ROV dives. The new microbathymetry data was a key factor for a successful deployment of a new seafloor geodetic array seven months later during RV SONNE voyage SO277. Two very different seafloor expressions of what is assumed to be one fault system raise questions about fault – canyon interaction or abrupt fault segmentation.

REFERENCES

Bonforte A, Guglielmino F, Coltelli M, Ferretti A, & Puglisi G. Structural assessment of Mount Etna volcano from Permanent Scatterers analysis. Geochemistry, Geophysics, Geosystems 2011, 12(2), doi: 10.1029/2010GC003213

Krastel S, Adami C, Beier J, Bialas J, et al. Seismogenic faults, landslides, and associated tsunamis off southern Italy - Cruise No. M86/2, December 27, 2011–January 17, 2012,

Cartagena (Spain) – Brindisi (Italy). METEOR-Berichte 2014, M86/2. DFG-Senatskommission für Ozeanographie, Bremen, 49 pp., doi: 10.2312/cr_m86_2.

Urlaub M, Petersen F, Gross F, Bonforte A et al. Gravitational collapse of Mount Etna's southeastern flank, Science Advances 2018, 4 (10), eaat9700, doi: 10.1126/sciadv.aat9700.

Urlaub M, Bonforte A, Kurbjuhn T, Steinführer A, et al. Alkor-Berichte 2020, AL532, GEOMAR Helmholtz-Zentrum für Ozeanforschung Kiel, Kiel, Germany, 27 pp., doi: 10.3289/CR_AL532.

HE538

Dynamics of benthic communities in protected areas of the German North Sea

AUTHORS

Alfred Wegener Institute Helmholtz Centre for Polar and Marine Research | Bremerhaven, Germany

L. Gutow, J. Beermann

The global oceans are subject to substantial change in response to multiple natural and anthropogenic drivers, including climate change, exploitation of natural resources and pollution (e. g. Myers & Worm 2003; Baum & Worm 2009; Beaugrand et al. 2009; Pörtner & Peck 2010; Poloczanska et al. 2013). Anthropogenic drivers and associated environmental changes are particularly pronounced in shallow coastal waters and shelf seas because of the high degree of industrialization and coastal transformations. Accordingly, coastal ecosystems all over the world are highly disturbed and require efficient management to allow for long-term ecological functioning and sustainable use of natural resources.

For centuries, the southern North Sea is being intensively used and exploited by humans. Among other activities, fisheries, shipping, pollution and the implementation of large offshore infrastructures (oil and gas platforms, offshore wind farms) have sculpted the North Sea ecosystem with profound implications for the structure of habitats and the regional biodiversity (Davis et al. 1982; Gill 2005; Vaissière et al. 2014).

Benthic habitats and communities are intensively used as proxies for the assessment of the environmental status according to several European directives and regional marine conventions. The Federal Republic of Germany is obliged to regularly assess and evaluate the status of the benthic communities in its territorial waters. Within a series of past, ongoing and future research projects funded by the German Federal Agency for Nature Conservation (BfN), the Alfred Wegener Institute Helmholtz Centre for Polar and Marine Research conducts long-term monitoring programs as well as specific targeted investigations on benthic habitats, species assemblages and populations to (1) fulfil the requirements of relevant legislative directives and conventions for the German Exclusive Economic Zone (EEZ) and (2) to evaluate the efficiency of specific conservation and management measures. In particular, the European Habitats Directive Directive, the Marine Strategy Framework Directive (MSFD, directive 2008/56/EG), and the Oslo-Paris convention (OSPAR) provide the framework for these investigations as well as the German Federal Law for Nature Conservation.

During cruise HE538 of RV Heincke benthic communities were investigated in the German Exclusive Economic Zone of the North Sea. The samplings of the in- and epifauna were conducted at the Dogger Bank (60 stations) and at the Sylt Outer Reef (50 stations) (Figure 1).

At both sites, samples were taken to investigate the recovery of the benthic system after cessation of chronic bottom trawling. Exclusion of bottom trawling from both areas is expected to come into force in the years to come. Accordingly, the collection of samples is part of the "Before" phase of this large-scale and long-term impact study. At the Dogger Bank, the investigations addressed the actual sand bank biotope whereas the sampling at the structurally highly diverse Sylt Outer Reef was specifically focused on a scattered coarse sediment biotope ("artenreiche Kies-, Grobsand- und Schillgründe), which is protected under §30 of the German Federal Law for Nature Conservation. At the Dogger Bank, additional samples were taken at the northern slope of the sand bank as part of a long-term monitoring program to fulfil the requirements of the European Habitats Directive. The in- and epifauna were sampled using a van Veen grab, an epibenthos dredge and a towed underwater video system.

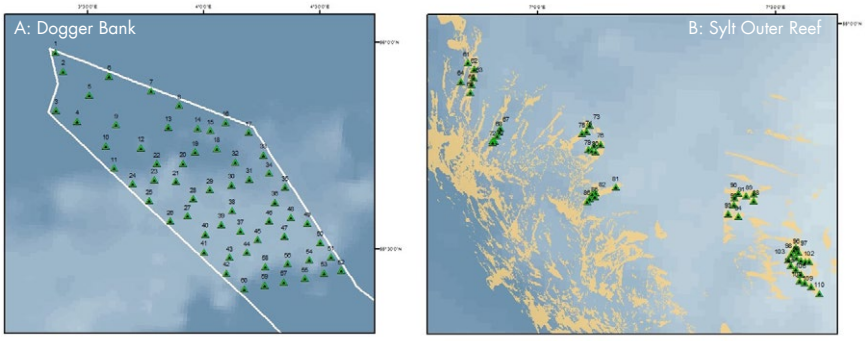

Fig. 1: Sampling stations for benthic in- and epifauna at (A) Dogger Bank and (B) Sylt Outer Reef.

The results allow for the documentation of the spatial and temporal dynamics of the benthic communities in sand bank and coarse sediment biotopes of the North Sea under the influence of chronic bottom trawling. Exemplarily shown are the inter-annual variations in total abundance, species richness, and total biomass of the benthic infauna on coarse sediments at Sylt Outer Reef (Figure 2). It becomes evident that the species richness is experiencing a decline during recent years of the study whereas the abundance and biomass of the infauna remain relatively constant with only minor inter-annual variations.

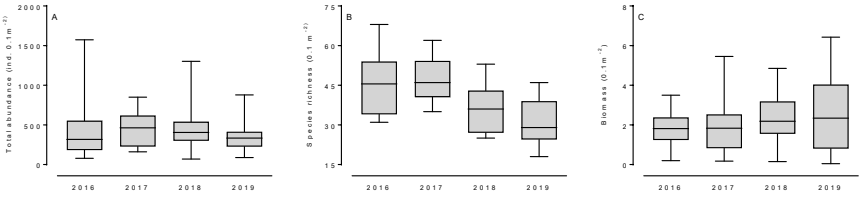

Fig. 2: Inter-annual dynamics of (A) total abundance, (B) species richness, and (C) total biomass of the infauna on coarse sediments at Sylt Outer Reef (samples from the year 2019 were taken during cruise HE538)

The results from these specific investigations will be evaluated in the context of an extensive data set on the benthos of the German North Sea compiled by the Alfred Wegener Institute. The analyses will allow for evaluating the impacts of chronic bottom trawling as well as the potential of different biotope types to recover from one of the major anthropogenic stressors in the German North Sea. In addition to answering these specific environmental research questions, the activities conducted during cruise HE538 contribute to the fulfillment of national sovereign duties of the Federal Republic of Germany according to national and international legislative frameworks for marine nature conservation. Continuous monitoring of the benthic biotopes of the North Sea complement existing data sets and improve our understanding of the structure and functioning of the SE North Sea. The activities during cruise HE538 were conducted in collaboration with external partners in order to optimize the use of the approved ship time.

REFERENCES

Baum JK, Worm B, Cascading top-down effects of changing oceanic predator abundances. Journal of Animal Ecology 2009, 78, 699–714.

Beaugrand G, Luczak C, Edwards M Rapid biogeographical plankton shifts in the North Atlantic Ocean. Global Change Biology, 2009, 15, 1790–1803.

Davis N, van Blaricom GR, Dayton PK, Man-made structures on marine sediments: Effects on adjacent benthic communities. Marine Biology, 1982, 70, 295–303.

Gill AB, Offshore renewable energy: Ecological implications of generating electricity in the coastal zone. Journal of Applied Ecology, 2005, 42, 605–615.

Myers RA, Worm B, Rapid worldwide depletion of predatory fish communities. Nature, 2003, 423, 28–283.

Pörtner HO, Peck MA, Climate change effects on fishes and fisheries: towards a cause-and-effect understanding. Journal of Fish Biology, 2010, 77, 1745–1779.

Poloczanska ES, Brown CJ, Sydeman WJ et al. Global imprint of climate change on marine life. Nature Climate Change, 2013, 3, 919–925.

Vaissière A-C, Levrel H, Pioch S et al. Biodiversity offsets for offshore wind farm projects: The current situation in Europe. Marine Policy, 2014, 48, 172–183.

M111

Dionysus – deep structure of the Ionian Sea and Sicily

AUTHORS

GEOMAR Helmholtz Centre for Ocean Research | Kiel, Germany
H. Kopp, A. Dannowski, D. Klaeschen, I. Klaucke, C. Papenberg, A. Krabbenhoeft

Institut Universitaire Européen de la Mer IUEM | Brest, France
M.-A. Gutscher, D. Dellong, D. Graindorge

Institut Français de Recherche pour l'Exploitation de la Mer IFREMER | Brest, France
F. Klingelhoefer, J. Crozon

Institute of Marine Sciences – National Research Council ISMAR-CNR | Bologna, Italy
M. Rovere

INTRODUCTION AND OBJECTIVES

The 1693 Catania earthquake (60,000 deaths) and the 1908 Messina earthquake (72,000 deaths) are two examples of repeatedly highly destructive earthquakes and tsunamis in southern Italy. The source of the Catania earthquake is uncertain and may have been the shallow NW dipping fault plane of the Calabria subduction zone. Furthermore, controversy still existed regarding the deep structure of the sub-seafloor in the Ionian Sea and the exact nature of the crust. Prior to cruise M111 there were no modern wide-angle seismic data available to image the Africa-Eurasia plate boundary even though it is located in the heart of Europe.

RV METEOR cruise M111 set out to investigate the deep structure of the active margin of southern Italy, the subduction zone and adjacent Ionian Basin to provide important structural information on the south Tethyan. Predominantly seafloor mapping and seismic methods were used (Figure 1) target the three main objectives:

1) Obtain an image of the present day crustal and lithospheric architecture of the plate boundary region between Africa and Eurasia and mapping the exact location or geometry at depth of the Calabrian subduction zone.

2) Unravel the transition from the continental domain to the oceanic portion of the Ionian Sea and the Tethys margin that may be is one of the oldest margins on the planet.

3) Image the present-day wedge geometry and deformation pattern of the margin, including the geometry of the megathrust-fault at depth to improve the regional hazard assessment associated with seismic activity and tsunamogenic threats.

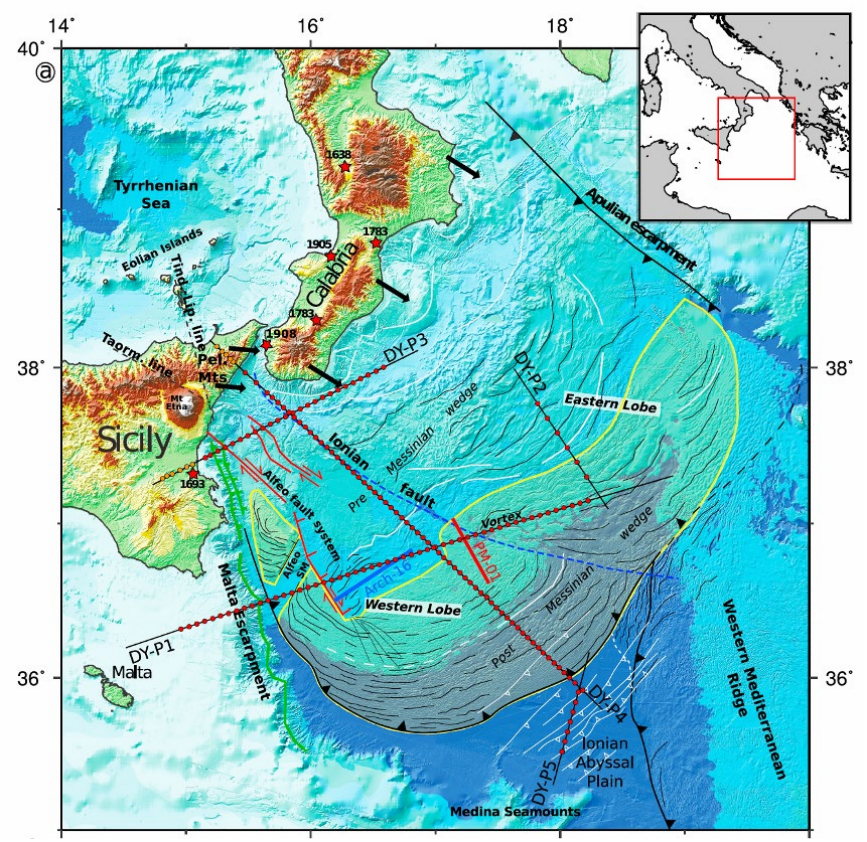

Fig. 1: Interpreted bathymetric map of the Ionian basin (Dellong et al., 2018; Gutscher et al., 2016). Superposed the wide-angle profiles from the M111 cruise (named DY-P1 through DY-P5) with small red dots for the ocean bottom seismometers and orange dots for the land-stations. The red stars show the positions of major earthquakes and their corresponding dates.

DATA AND METHODS

The new data set comprised high-resolution bathymetric data, modern wide-angle seismic refraction data and multichannel reflection mini-streamer data. Five seismic profiles were chosen to run perpendicular to main morpho-tectonic features e. g. Malta Escarpment (DY-P1, DY-P3) or Calabrian accretionary wedge (DY-P3, DY-P4) or across the Ionian Basin seafloor (DY-P5) (Figure 1). Two profiles (DY-P3 and DY-P4) continued onshore with seismometers deployed along two transects on eastern Sicily to provided new coverage of the transition between Sicily and the Calabrian fold-and-thrust belt. The OBS/OBH stations (ocean bottom seismometers/hydrophones) were deployed in highly varying water depth,

ranging from the shallower domains of the Straits of Messina (< 100 m) to the Ionian Abyssal Plain (> 4000 m). Arrivals are locally strongly attenuated due to an irregular salt layer in the Ionian basin. On some OBS, seismic energy is lost at offsets exceeding 40 km, probably due to the presence of strongly reworked sediments. The land stations recorded arrivals up to offsets of 120 km, thus allowing us to additionally constrain the deep geometry of the crust and the Moho discontinuity along the amphibious profiles. The refraction seismic data were modelled using the two-dimensional forward modelling (Zelt & Smith, 1992). We opted for a forward modelling approach instead of a tomographic inversion scheme due to the complex interplay between the thick Messinian evaporate layers and the sedimentary sequences and resulting velocity inversions. The travel time analysis profited from additional input from the multichannel seismic data to image the uppermost portion of the crust. This analysis was conducted in conjunction with gravity modelling from satellite gravity data.

The seafloor mapping reveals important large-scale as well as small-scale features, including active fault zones and segmentation of the subduction zone. The data set was merged with existing data from 6 previous marine geophysical surveys between 2010 and 2015 in order to compile a comprehensive seafloor map of the Ionian Sea and Calabrian subduction system. This surface information combined with the velocity-depth models from the seismic profiles provide a detailed structural overview of the study area.

RESULTS AND DISCUSSION

The seafloor mapping results show that the tectonics and internal mechanics of the Calabrian accretionary wedge vary strongly from one structural domain to the next. The Calabrian wedge can be divided laterally into 2 major lobes and 2 minor lobes: a small trapped lobe (W and NW of Alfeo Seamount), the large SW lobe, the large NE lobe, and a smaller far eastern lobe near the Apulian Escarpment. The boundary between the external (evaporitic wedge) and internal (clastic wedge) is locally expressed by a change in seafloor morphology. Compressional (thrust and folding) tectonics are the primary mode of deformation in the external wedge. Near the E Sicily margin/Straits of Messina area, dextral strike-slip faulting is the dominant mode of deformation. Throughout the internal wedge there is an interplay of compressional and strike-slip deformation.

The deeper anatomy of the Calabrian Arc was mainly resolved using the deep-penetrating wide-angle seismic data in conjunction with and verified by gravity modelling. The sedimentary thickness in the basin is highest at the backstop contact (10–12 km). The Messinian salt layer is imaged along profiles DY-P1, DY-P4 and DY-P5 with a thickness of up to 4 km (Figure 2). A layer of high-velocity sediments is imaged in the southern part of the basin (4.5–4.8 km/s). This high P-wave velocity layer, showing parallel high amplitude reflections has long been described below the Ionian Abyssal Plain (e. g. Gallais et al., 2012 and references therein) and likely represents Jurassic deep-water carbonates. Oceanic crust underlying the basin is ~5 km thick. Crustal thickness increases abruptly at the Malta Escarpment (DY-P1), at the Sicily Margin (DY-P3) and at the Peloritan backstop (DY-P4), indicating the presence of continental crust in these domains.

Particularly interesting features of the Calabrian slab geometry with an extremely shallow average dip of 1.3° of the subducting oceanic crust over the frontal 200 km (deepening from ~11 km to ~16 km). Profile DY-P4 images a slab hinge with an extremely abrupt steepening. The slab dip increases abruptly from 2-5° to 60–70° over a distance of ≤ 50 km.

Along profile DY-P5, roughly 6–7 km thick crust with velocities ranging from 5.1 km/s to 7.2 km/s, top to bottom, can be traced throughout the Ionian Abyssal Plain (Figure 2). In the vicinity of the Medina seamounts at the southern Ionian Abyssal Plain boundary, the crust thickens to about 9 km and seismic velocities decrease to 6.8 km/s at the crust–mantle boundary. In conclusion, the crustal data reveal its oceanic nature and support the interpretation of the Ionian Abyssal Plain as a remnant of the Tethys lithosphere with the Malta Escarpment as a transform margin and a Tethys opening in the NNW–SSE direction. This is in line with the hypothesis that Adria was a rigid promontory of Africa until the beginning of the opening of the Tethys in the early Mesozoic. This places the African Plate margin to the Hellenic subduction zone and the Calabrian subduction zone, and supports an Adria microplate that can move relative to Africa and Europe.

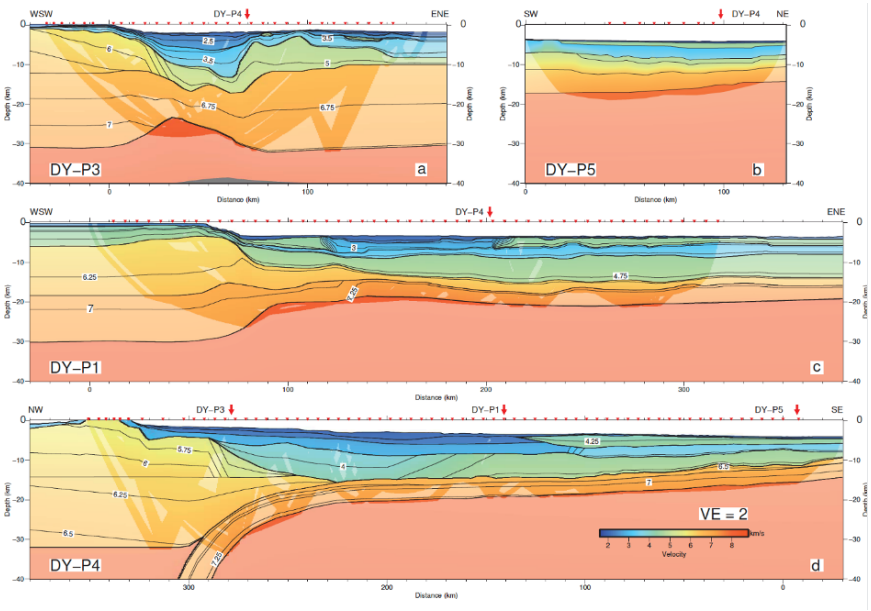

Fig. 2: Final velocity models of the wide-angle seismic profiles DY-P1 through DY-P5. Crossings between the profiles are marked by red arrows and OBS positions by inverted triangles. Vertical exaggeration is 2.

A striking feature is the so-called 'vortex' region (at 17°30'E/37°00'N in Figure 1). The curvature of the vortex indicates counterclockwise rotation, requiring sinistral shear along the boundary between the NE and SW lobes. This observation contradicts the kinematic interpretation of the Ionian Fault as being a major dextral strike-slip fault along the entire boundary between the two lobes and as a major lithospheric tear or STEP fault. The observations drawn from the velocity models (Figure 2) of this study include the following: (1) the deep structure of the Malta Escarpment is different on both profiles (DY-P1 and DY-P3), (2) the deep high-velocity sedimentary layer is absent on the northern profile DY-P3, and (3) the thinned continental crust on DY-P3 shows a greater affinity to the Calabrian backstop than to the Sicilian one. Therefore, we propose that the Ionian Fault system results from the opening of the deep asymmetrical sedimentary basin that found its origin in the collision of the Peloritan with Nubian Sicily and its separation of the Calabrian block. We propose that the thinned continental crust imaged on profile DY-P3 belongs to the Calabrian-Peloritan domains. The most probable location for the STEP fault on both velocity models is the Alfeo Fault system as was previously proposed (Gallais et al., 2013; Gutscher et al., 2016).

REFERENCES

Dellong, D., Klingelhoefer, F., Kopp, H., Graindorge, D., Margheriti, L., Moretti, M., Murphy, S., Gutscher, M.-A., Crustal structure of the Ionian basin and eastern Sicily margin: results from a wide angle seismic survey, J. Geophys. Res. 2018, doi: 10.1002/2017JB015312.

Gallais, F., Gutscher, M.-A., Klaeschen, D., & Graindorge, D., Two-stage growth of the Calabrian accretionary wedge in the Ionian Sea (Central Mediterranean): Constraints from depth migrated multichannel seismic data, Marine Geology 2012, 326-328, 28–45, doi: 10.1016/j.margeo.2012.08.006.

Gallais, F., Graindorge, D., Gutscher, M.-A., and Klaeschen, D., Propagation of a lithospheric tear fault (STEP) through the western boundary of the Calabrian accretionary wedge offshore eastern Sicily (southern Italy), Tectonophysics 2013, 602, 141–152, doi: https://doi.org/10.1016/j.tecto.2012.12.026.

Gutscher, M.-A., Dominguez, S., de Lepinay, B. M., Pinheiro, L., Gallais, F., Babonneau, N., et al., Tectonic expression of an active slab tear from high-resolution seismic and bathymetric data offshore Sicily (Ionian Sea), Tectonics 2016, 35, 39–54, doi: https://doi.org/10.1002/2015TC003898.

Zelt, C. A., and Smith, R. B., Seismic travel-time inversion for 2-D crustal velocity structure, Geophysical Journal International 1992, 108(16–34), doi: 10.1111/j.1365-246X.1992.tb00836.x.

M145

Oxygen and circulation variability in the central and western tropical Atlantic

AUTHORS

GEOMAR Helmholtz Centre for Ocean Research Kiel | Kiel, Germany
P. Brandt, A. Körtzinger

METEOR cruise M145 was the last research cruise of the Kiel Collaborative Research Center 754 "Climate-Biogeochemical Interactions in the Tropical Ocean". Using shipboard and mooring data from the oxygen minimum zone (OMZ) of the eastern tropical North Atlantic (ETNA) the oxygen supply to the ETNA OMZ by the North Equatorial Undercurrent – one of the main supply routes – and its intraseasonal to interannual variability could be quantified. In a first study, in which in-situ data were used to validate a model, it could be shown that the oxygen supply crucially depends on the source water masses of the NEUC. Only if the water of a strengthening NEUC is supplied from within the western boundary current, it can contribute to an enhanced ventilation of the ETNA OMZ. Strengthening of the NEUC fed from the recirculation of the northern branch of the South Equatorial Current (nSEC) might even result in a reduced ventilation (Burmeister et al., 2019). A second study was based on moorings at 5°N, 23°W equipped with current meters and temperature/salinity/oxygen sensors and shipboard measurements along the 23°W repeat section. For the first time, a time series of the NEUC transport could be derived (Fig. 1 g-i). The time series that covers the periods from June 2006 to February 2008 and November 2009 to January 2018 is based on moored velocity observations that were inter- and extrapolated using variability patterns from shipboard ADCP measurements along the 23°W repeat section. In contrast to previous studies (Burmeister et al., 2019; Goes et al., 2013; Hüttl-Kabus and Böning, 2008), neither the moored zonal velocity at 5°N nor the reconstructed eastward NEUC transport exhibits a pronounced seasonal cycle. Both time series are instead dominated by strong intraseasonal eastward flow events which can peak throughout the year (Fig. 1 g-i). Although in the mean meridional ship sections the zonal velocity maximum associated with the NEUC coincides with a local oxygen maximum Fig. 1 a,d, the eastward flow events are only occasionally associated with high oxygen concentrations and thus only occasionally supplied out of the western boundary current (Burmeister et al., 2020).

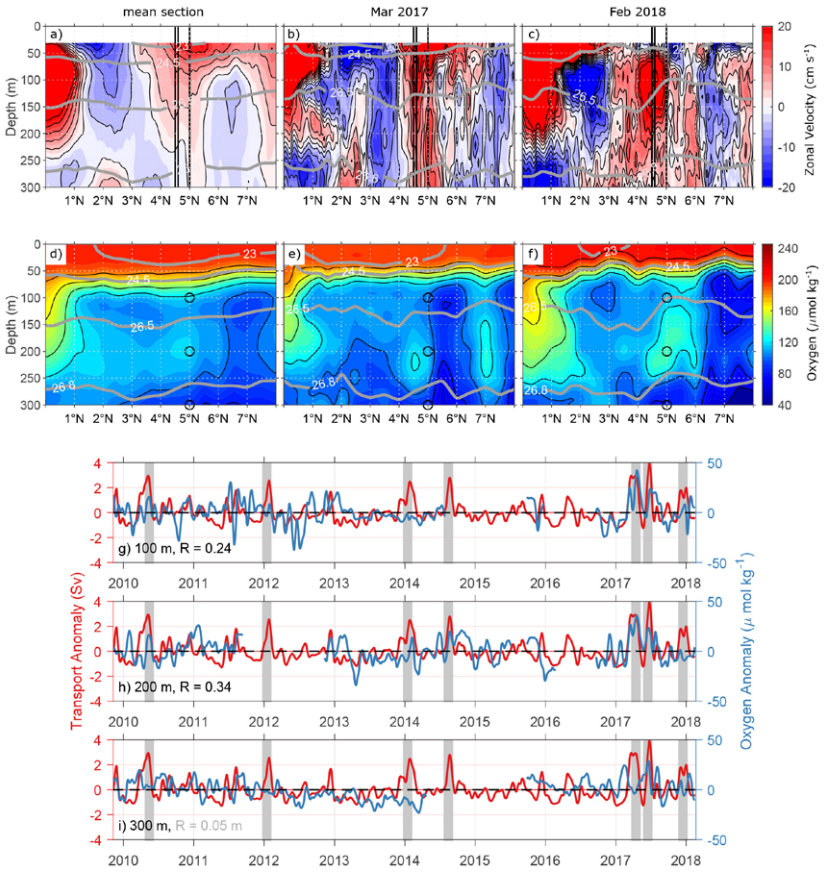

Fig. 1: (a–f) Zonal velocity (a–c) and oxygen (d–f) observations along 23°W with mean sections of all 24 cruises (a,d) and sections taken during Ronald H. Brown cruise PNE 2017 (b,e) and during Meteor cruise M145 (c,f). Grey lines mark neutral density surfaces (kgm^{-3}), black vertical lines (a–c) mark the position of moorings, black circles (d-f) mark single point oxygen measurements. (g–i) 30-day low-pass filtered NEUC transport (red lines) and oxygen anomalies (blue lines) at 5°N, 23°W at a depth of (g) 100m, (h) 200 m, and (i) 300m. Grey bars mark strong NEUC events. R is the correlation coefficient of zonal velocity and oxygen anomalies at zero lag (black/grey color indicate that R is significant/not significant on a 95 % confidence level).

Using mooring and shipboard velocity data from 11°S off Brazil, the mean and the seasonal to interannual variability of the North Brazil Undercurrent (NBUC) could be analyzed. It represents a major pathway of the equatorward thermocline transport within the Subtropical Cells (STCs). Two STC studies were published. The first study by Tuchen et al. (2019) focusses on the mean STCs based on recent data from Argo floats complemented by ship sections at the western boundary as well as reanalysis products to estimate the meridional water mass transports and to investigate the vertical and horizontal structure of the STCs from an observational perspective. Main results are that the thermocline layer convergence is dominated by the southern hemisphere water mass transport (9.0 ± 1.1 Sv from the southern hemisphere compared to 2.9 ± 1.3 Sv from the northern hemisphere) and that this transport is mostly confined to the western boundary.

Compared to the asymmetric convergence at thermocline level, the wind-driven Ekman divergence in the surface layer is more symmetric, being 20.4 ± 3.1 Sv between 10°N and 10°S. The net poleward transports (Ekman minus geostrophy) in the surface layer are in agreement with values derived from reanalysis data (5.5 ± 0.8 Sv at 10°S and 6.4 ± 1.4 Sv at 10°N). A diapycnal transport of about 3 Sv across the 26.0 kgm^{-3} isopycnal is required in order to maintain the mass balance of the STC circulation. This study provides an update for observational estimates of Atlantic STC transports and aims to represent the 21st century mean STCs from an observational perspective.

In a second study by Tuchen et al. (2020) a first observational estimate of transport variability associated with the horizontal branches of the Atlantic STCs in both hemispheres is provided. Thermocline layer transport convergence and surface layer transport divergence between 10°N and 10°S are dominated by seasonal variability. Meridional thermocline layer transport anomalies at the western boundary and in the interior basin are anti-correlated and partially compensate each other at all resolved time scales. It is suggested that the seesaw-like relation is forced by the large-scale off-equatorial wind stress changes through low-baroclinic-mode Rossby wave adjustment. It is shown that anomalies of the thermocline layer interior transport convergence modulate sea surface temperature (SST) variability in the upwelling regions along the equator and at the eastern boundary at time scales longer than 5 years. Phases of weaker (stronger) interior transport are associated with phases of higher (lower) equatorial SST. At these time scales, STC transport variability is forced by off-equatorial wind stress changes, especially by those in the southern hemisphere. At shorter time scales, equatorial SST anomalies are, instead, mainly forced by local changes of zonal wind stress.

Besides the current meters at the 11°S mooring array off Brazil, bottom pressure sensors were also installed at the 300m and 500m isobaths. Together with similar sensors at the eastern boundary off Angola, these bottom pressure measurements were used to derive the first time series of the AMOC in the tropical South Atlantic (Herrford et al. 2020). Over the period 2013–2018, the AMOC and its components are dominated by seasonal variability, with peak-to-peak amplitudes of 12 Sv for the upper-ocean geostrophic transport, 7 Sv for the Ekman and 14 Sv for the AMOC transport. The observed seasonal variability of zonally integrated geostrophic velocity in the upper 300 m is controlled by pressure variations at the eastern boundary, while at 500 m depth contributions from the western and eastern boundaries are similar. Our analyses indicate, that while some of the uncertainties of the AMOC estimates result from the technical aspects of the observational strategy, uncertainties in the wind forcing are particularly relevant for AMOC estimates at 11°S. This work is part of the PhD thesis of Josefine Herrford to be finalized in early 2021.

REFERENCES

Bourlès B, Araujo M, McPhaden M J, Brandt P, et al., PIRATA: A sustained observing system for tropical Atlantic climate research and forecasting, Earth and Space Science 2019, 6, 577–616, doi:10.1029/2018EA000428.

Brandt P, Hahn J, Schmidtko S, Tuchen F P, Kopte R, et al., Atlantic Equatorial Undercurrent intensification counteracts warming induced deoxygenation, Nat. Geosci., doi:10.1038/s41561-021-00716-1, 2021.

Burmeister K, Lübbecke J F, Brandt P, Duteil O, Variability of the Atlantic North Equatorial Undercurrent and its impact on oxygen, J. Geophys. Res. Oceans 2019, 124, 2348-2373, doi:10.1029/2018JC014760.

Burmeister K, Lübbecke J F, Brandt P, Claus M, and Hahn J, Fluctuations of the Atlantic North Equatorial Undercurrent and associated changes in oxygen transports, Geophys. Res. Lett. 2020, 47, e2020GL088350, doi:10.1029/2020GL088350.

Herrford J, Brandt P, Kanzow T, Hummels R, et al., Seasonal variability of the Atlantic Meridional Overturning Circulation at 11° S inferred from bottom pressure measurements, Ocean Sci. 2021, 17, 265–284, doi:10.5194/os-17-265-2021.

Imbol Koungue R A and Brandt P, Impact of intraseasonal waves on Angolan warm and cold events, J. Geophys. Res. Oceans 2021, 126, e2020JC017088, doi:10.1029/2020JC017088.

Tuchen F P, Lübbecke J F, Schmidtko S, Hummels R, and Böning C W, The Atlantic Subtropical Cells Inferred from observations. J. Geophys. Res. Oceans 2019, 124, 7591–7605, doi:10.1029/2019JC015396.

Tuchen F P, Lübbecke J F, Brandt P, and Fu Y, Observed transport variability of the Atlantic Subtropical Cells and their connection to tropical sea surface temperature variability, J. Geophys. Res. Oceans 2020, 125, e2020JC016592, doi:10.1029/2020JC016592.

Ph.D. thesis:

Burmeister, K., On the connection between zonal current variability and oxygen supply of the Eastern Tropical North Atlantic focussing on the North Equatorial Undercurrent, Ph.D. thesis, Christian-Albrechts-Universität zu Kiel, 114 pp., 2019.

Herrford, J., Observing seasonal to decadal variability related to the Atlantic meridional overturning circulation at 11°S, Ph.D. thesis, Christian-Albrechts-Universität zu Kiel, 141 pp., 2021.

Tuchen, F. P., The Atlantic Subtropical Cells - mean state and variability from an observational perspective, Ph.D. thesis, Christian-Albrechts-Universität zu Kiel, 101 pp., 2020.

M146

Henry Seamount Seepage Exploration

AUTHORS

University of Bremen | Bremen, Germany
A. Klügel, H. Villinger, M. Römer

Kiel University | Kiel, Germany
S. Krastel, K.F. Lenz

INTRODUCTION

RV METEOR Cruise M146 (March/April 2018) had the main objective of discovering and documenting fluid venting sites at Henry Seamount, a presumably extinct 126 Ma old volcano located 40 km to the southeast of El Hierro, Canary Islands (Fig. 1). Evidence of recent fluid discharge at this seamount was provided by rock and shell samples from a reconnaissance dredging campaign during cruise M66/1 (Klügel et al. 2011). These authors suggested that seawater infiltrated through basement outcrops of El Hierro's submarine flank, became heated within the oceanic crust, migrated, and finally discharged at Henry Seamount (relief-driven hydrothermal circulation). To test this hypothesis, M146 explored the seamount and the surrounding area in detail by high-resolution reflection seismics, heat flow measurements, high-resolution hydroacoustic mapping by autonomous underwater vehicle (AUV), TV-sled surveys with attached miniature autonomous plume recorder (MAPR), and sediment sampling by gravity corer and Van Veen grab. The work was complemented in 2019 by a follow-up cruise with the Spanish RV Ángeles Alvariño, during which CTD tow-yos were carried out at venting sites and water samples were taken.

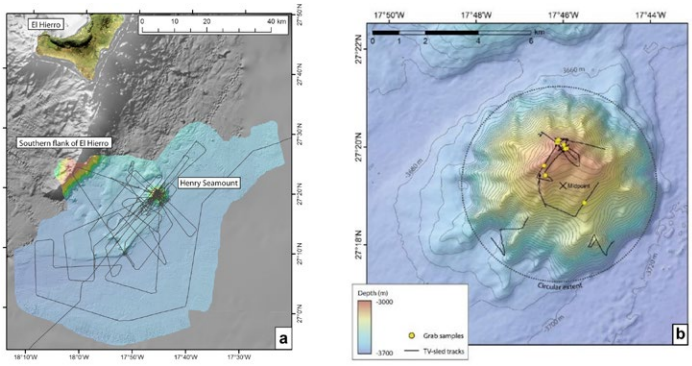

Fig. 1 | a: Shaded-relief map of Henry Seamount and its vicinity showing the area covered by detailed bathymetric surveys during M146 (color-shaded); blue lines indicate the ship track. b: Bathymetric map with locations of TV-sled tracks and sediment grab samples from the seafloor.

INDICATORS FOR HYDROTHERMAL ACTIVITY AT HENRY SEAMOUNT

The dominant manifestation of hydrothermal activity is the occurrence of shells, locally as massive "shell graveyards", in many areas of the seamount. Most shells observed or sampled belong to vesicomyid clams of genus Abyssogena southwardae, which live on H_2S-rich seafloor in symbiosis with sulfide-oxidizing bacteria at hydrothermal vents and cold seeps (Krylova et al. 2010). No living specimen of these clams were found. Radiocarbon ages for 15 shells fall into two groups of 1250–3350 and 13440–19220 years before present; a reservoir age correction would decrease these ages by ~500 years. The observations indicate that hydrothermal activity at Henry Seamount was widespread in the past and is now waning or has ceased. The two groups of shell ages could reflect two distinct pulses or episodes of increased activity.

Evidence for present-day hydrothermal activity at Henry Seamount includes (i) negative oxygen reduction potential (ORP) anomalies a few meters above the seafloor at a number of distinct sites; (ii) confirmation of some of these anomalies by CTD with online ORP sensor when sites were re-visited one year later by the Spanish RV; (iii) slightly enhanced methane concentrations (up to about six times background values) in some bottom water samples taken concurrently to observed ORP anomalies. The data suggest that hydrothermal activity at Henry Seamount is weak and/or diffuse but still ongoing. We identified major venting sites by the co-occurrence of indicators such as dense shell coverage, precipitates, and ORP anomalies. The combined observations reveal widespread past and present hydrothermal activity in the summit area and at the flanks of the seamount (Fig. 2a, 2b).

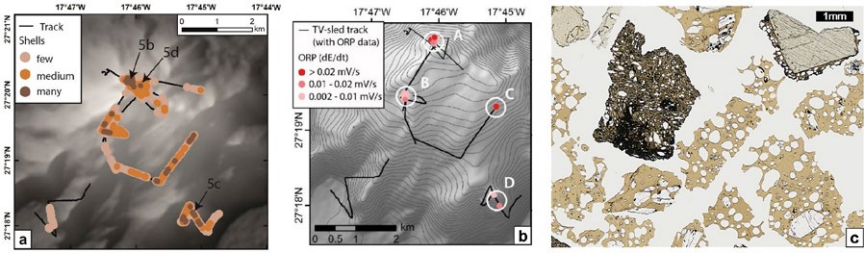

Fig. 2 | a, b: Distribution of clam shells and ORP anomalies at Henry Seamount. Black lines indicate TV-sled tracks, letters A to D indicate main venting sites. c: Microphotograph of fresh glassy basaltic ash, >0.5 mm sieve fraction.

Heat flow values around Henry Seamount are 49 mW/m^2 on average, close to the value expected for 155 Ma ocean crust. The highest value of 83 mW/m^2 was obtained at the seamount summit region. A traverse across the seamount shows some variations in heat flow, but no robust gradient indicative of fluid recharge or discharge comparable to those observed at some other hydrothermally active seamounts (Fisher and Harris 2010). There is, however, a weak gradual increase in heat flow toward the southwestern base of Henry Seamount, which likely reflects hydrothermal circulation that is of relatively recent origin

and/or transient nature (Klügel et al. 2020). This interpretation is consistent with the observation that the chemosynthetic communities are mostly extinct, and that shell ages form two groups of around 1–3 and 13–19 kyrs, respectively.

VOLCANIC ROCK SAMPLES

One unexpected finding of M146 was the recovery of basaltic tephra (heterolithologic coarse ash to small lapilli) and dispersed basaltic rock fragments up to 4 cm in size from the summit area of Henry Seamount at between 3020 and 3240 m water depth. Many ash particles and some rock fragments are glassy and almost unaltered (Fig. 2c). Judging from the freshness of the glass and the thickness of overlying sediment (<20 cm), the volcanic deposits must be relatively young, certainly contemporaneous to subaerial volcanic activity at nearby El Hierro island (<1 Ma). Preliminary U-series data for two samples suggest $^{226}Ra/^{230}Th$ disequilibrium, implying an age of <8 kyrs, although the results may be affected by minor sediment contamination. In contrast, one basaltic fragment that could be Ar/Ar dated yielded ca. 200 ka.

The samples are dominantly alkalic to transitional basalts with chemical and radiogenic isotope compositions similar to subaerial and submarine samples from El Hierro. Analyses of sulfur contents of glasses revealed that the dominant ash type is little degassed and certainly is derived from Henry Seamount, implying rejuvenated activity of this Cretaceous volcano. Most other samples, however, have lower sulfur contents that indicate subaerial or shallow submarine eruption. This leaves El Hierro as the only plausible source for these samples, which raises the question of the mode of transport to Henry Seamount. Subaerial transport of cm-sized basalt fragments over 40 km distance is not possible. The most likely explanation is deposition by the giant Las Playas flank collapse of El Hierro at 145–176 ka (Gee et al. 2001), which passed close to Henry Seamount and may have swept these fragments some 700 m upward along the slope. This scenario is also consistent with the intermixture of various lithologies in our sample suite.

INSIGHTS INTO MAGMATIC SYSTEMS FROM SEISMIC DATA

High-resolution seismic data acquired during M146 was used to investigate the distribution and influence of different phases of magmatic activity in the southeast of El Hierro island. Several acoustic blanking zones were identified as the most prominent features. They show hardly any reflectors, but only some chaotic amplitude patches. Based on their appearance we classified the blanking zones into three different types. Type 1 blanking zones cut all other surrounding seismic units and are related to morphological edifices cropping out at the seafloor, such as Henry Seamount. The respective outcrops have steep flanks, which are traceable in the subsurface. The surrounding reflectors show a slight upward bending and an onlap on these flanks. Type 2 blanking zones show an upward bending of the surrounding reflectors at the sides and on top of the blanking zone. A continuous traceable reflector, characterized by a convex shape, defines the top of this blanking zone type. Type 3 blanking zones show no upward bending of the surrounding reflectors but cuts clearly through bordering reflectors.

We interpret the different blanking zones as follows: Type 1 is related to volcanic edifices, which crop out at the seafloor and cut through all imaged sedimentary units. Type 2 is characterized by upward bending of adjacent reflectors and is most likely caused by hydrothermal doming resulting from saucer-shaped sill intrusions. Type 3 is probably related to fluids or gases that were mobilized by the sill intrusions. Type 1 and 2 blanking zones cluster in the central part of our working area, whereas the blanking zones of type 3 are located on the outskirts. This specific distribution and the occurrence of the varying blanking zone types are combined to make a conceptual model of this area. Our model takes sill intrusions, hydrothermal doming, as well as volcanic outcrops and mobilized fluids into account.

REFERENCES

Fisher AT, Harris RN, Using seafloor heat flow as a tracer to map subseafloor fluid flow in the ocean crust, Geofluids 2010, 10, 142–160.

Gee MJR, Watts AB, Masson DG, Mitchell NC, Landslides and the evolution of El Hierro in the Canary Islands, Marine Geology 2001, 177, 271–293.

Klügel A, Villinger H, Römer M, Kaul N, Krastel S, Lenz K-F, Wintersteller P, Hydrothermal Activity at a Cretaceous Seamount, Canary Archipelago, Caused by Rejuvenated Volcanism, Frontiers in Marine Science 2020, 7, 1001, doi: 10.3389/fmars.2020.584571.

Klügel A, Hansteen TH, Bogaard Pvd, Strauss H, Hauff F, Holocene fluid venting at an extinct Cretaceous seamount, Canary archipelago, Geology 2011, 39, 855–858.

Krylova EM, Sahling H, Janssen R, Abyssogena: A new genus of the family Vesicomyidae (bivalvia) from deep-water vents and seeps, Journal of Molluscan Studies 201, 76, 107–132, doi:10.1093/mollus/eyp052.

M147

Amazon-GEOTRACES – Interactions of trace metals, DOM, and particles in the Amazon estuary and associated plume

AUTHORS

Jacobs University Bremen | Bremen, Germany
A. Koschinsky, A. Hollister

GEOMAR Helmholtz Centre for Ocean Research Kiel | Kiel, Germany
M. Frank, M. Gledhill

Institute for Chemistry and Biology of the Marine Environment ICBM, University of Oldenburg | Oldenburg, Germany
T. Dittmar, M. Seidel

Institute of Geosciences, University Kiel | Kiel, Germany
J. Scholten

M147 Shipboard Scientific Party

The Amazon is Earth's largest river by volume output, making it an important source of trace metals and organic matter to the Atlantic Ocean.To understand trace metal mixing and transport processes of these compounds, the GEOTRACES process study GApr11 (cruise M147) was conducted in 2018 in the Amazon and Pará River estuaries and mixing plume in the tropical North Atlantic Ocean during high river discharge. Size-fractionated water samples were taken with a surface Fish and a CTD-rosette water sampler and surface sediment cores were retrieved with a multicorer from five distinct areas: Amazon River outflow transect, Pará River outflow transect, mangrove belt to the southeast, North Brazil Current, and merged plume north (see Fig. 1, poster abstract, Hollister et al.).

When rivers mix into the ocean, radium (Ra) isotopes are released into the dissolved phase allowing us to apply these isotopes as powerful tracers of river plumes spreading into the ocean. We determined the ^{224}Raex/^{223}Ra activity ratios along the Amazon plume to derive apparent ages and to estimate the residence time of the Amazon waters on the Brazilian continental shelf. Our data suggest that it takes 9–14 days for the Amazon waters to reach the northern continental shelf off French Guyana and 12–21 days to reach the eastern part of the Brazilian continental shelf. Using the apparent ages along the plume, we estimate an average velocity of 37 cm s^{-1} for the northward transport of

the Amazon waters on the continental shelf. These times scales are important information to estimate elemental fluxes to the Atlantic Ocean (Léon et al. in review).

In addition to Ra data dissolved organic and inorganic, carbon (C), and total alkalinity obtained indicate that outwelling of C across the mangrove-ocean continuum represents a major coastal carbon pathway driving bicarbonate storage in the ocean (Cabral et al., 2021).

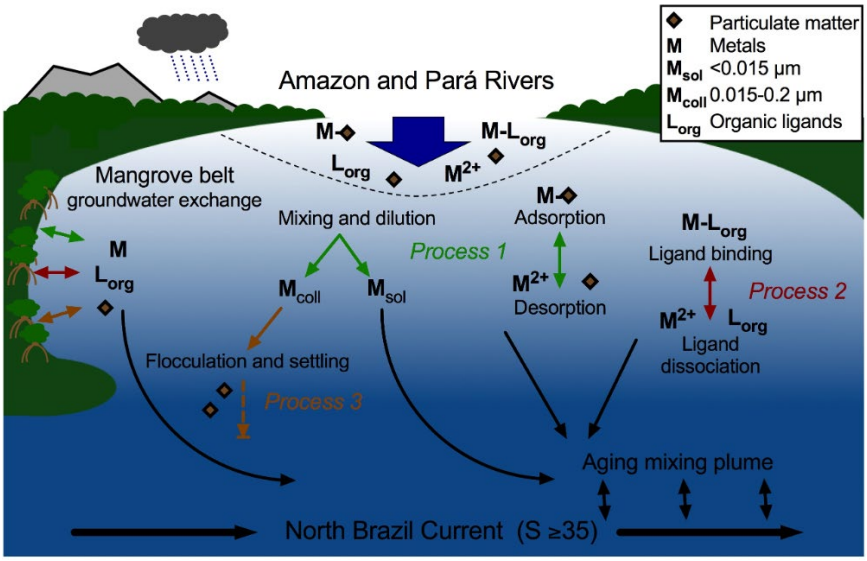

Fig. 1: Sketch demonstrating the different sources of trace metals, particles and organic matter, and their complex interactions in the Amazon and Pará river estuaries and adjacent mangrove belt and plume moving north; Process 1: Metal interactions with particles; Process 2: Solubilisation by metal-binding organic ligands; Process 3: Colloid flocculation and metal removal to sediment

Trace metal processes in the estuarine mixing zone of the Amazon outflow and adjacent continental shelf are strongly influenced by interactions with organic matter, colloidal and particulate matter and pH (Figure 1). Trace metals have been analysed in dissolved and soluble fractions (>0.2 µm, <0.2 µm, <0.015 m, and 10 kDa and 1 kDa by ultrafiltration) as well as in particulate fractions. Furthermore, the hydrophobic organic fraction of trace metals was quantified and characterized. Calculations of metal fluxes from the rivers into the Atlantic are presently done (see poster abstract, Hollister et al).

The distribution of the essential micronutrient copper (Cu) showed negative correlation with salinity and largely followed conservative mixing lines (Hollister et al., 2021). Cu was nearly entirely in the soluble fraction, with the exception of a minor colloidal Cu fraction at lower salinity. Organic Cu-binding ligands were present in excess of Cu throughout the entire salinity range and likely played a role in solubilizing Cu and

preventing adsorption on colloids. Cu-associated organic matter correlated negatively with salinity and appeared to be primarily governed by river input and mixing with seawater. In all dissolved water samples, organic complexation kept free Cu^{2+} below toxic levels (<1 pmol L-1). We found that Cu concentrations remained similar to the 1970s (Boyle et al., 1982) suggesting that the large overall river flow may so far minimize the impact of potential anthropogenic Cu input.

For two other important trace nutrients, nickel (Ni) and cobalt (Co), dissolved Ni was found to be present mostly as weak organic complexes while Co was present as strong organic complexes in the dissolved phase (de Carvalho et al., 2021). Elevated levels of Ni and Co in the mangrove belt were attributed to a possible influx of groundwater and/or desorption process from particulate material. Dissolved species were transported in the estuarine mixing zone as soluble species (<0.015 µm). However, elevated colloidal forms at low salinity may provide a potential removal of dissolved Ni and Co via colloidal flocculation upon seawater mixing.

As a typical representative of particle-reactive elements, dissolved titanium (Ti) showed a non-conservative behavior along the mixing gradients with strong removal at low salinities (correlating with Fe) and some enrichments at particular salinity ranges (Schneider et al., in revision). The results suggest that there was both ad-and desorption of Ti from suspended particles from both riverine and marine sources or flocculation and aggregation of colloids and particulate matter from endmember river as well as resuspension at particular salinity ranges. The 0.015 µm filtered and 10 kDa and 1 kDa ultrafiltered aliquots showed variable distributions of Ti in the different size fractions, depending on the sampling zone.

The less reactive elements molybdenum (Mo), uranium (U) and vanadium (V) partly deviated from their typical conservative behavior observed in seawater. Mo mostly exhibited conservative behavior along the salinity gradient with concentrations above the theoretical mixing line (TML) mostly in the NW section of the Amazon transect. In contrast, most U concentrations in the low salinity region were markedly removed in the water column. Scavenging of U at low salinity waters could be due to adsorption of U to metal oxides (Fe and Mn) or salt-induced aggregation of riverine colloidal material. The observed removal and addition of dissolved V in different sections of the Amazon estuary may be influenced by adsorption to particulates or metal oxides at low salinity region and desorption from re-suspended particles or sediments in the mid salinity region. Nearly all Mo and V were found to be soluble while U was a mix of soluble and colloidal forms.

Estuarine behavior of coupled dissolved and particulate hafnium (Hf) and Rare Earth Element (REE) concentrations and the corresponding radiogenic Hf and neodymium (Nd) isotope compositions was studied with the purpose of using them as tracers of water masses (see also poster abstract, Xu et al.). Previous studies on REEs and radiogenic Nd

isotopes in the Amazon estuary have shown that most of the Nd is already scavenged at low salinities of the surface waters and that most of the Nd reaching the open ocean is released from particles via desorption or partial dissolution at high salinities. First results obtained so far have demonstrated that the Hf concentrations are also very efficiently removed (75 % to 85 % of the dissolved riverine load) at low salinities between 0 and 5 and that the fractional release of Hf from particles in the mid- to high-salinity zone is smaller than that of Nd. Nevertheless, the Hf flux to the open ocean of ~8 x 10^3 mol/yr estimated based on the M147 data clearly demonstrates that the Amazon River is a significant contributor to the Hf budget of the Atlantic Ocean. Combined Nd/Hf isotope compositions and stable Ba isotope compositions of the same samples to be obtained will provide a complete picture of the impact of the Amazon inputs. Dissolved Si isotope compositions from the salinity transect of the surface waters of M147 clearly demonstrate the occurrence of fractionated and elevated Si isotope compositions in the Amazon plume due to diatom utilization of the dissolved $Si(OH)_4$. These data together with data on other major rivers in Zhang et al. (2020) document that the global average stable Si isotope composition entering the ocean is 0.2–0.3‰ higher than that of the rivers themselves due to Si retention in the estuaries.

Surface sediment samples were evaluated for the role of early diagenetic processes within Amazon shelf sediments in the global biogeochemical cycles of phosphorus (P), major cations and iron (Fe) (Spiegel et al., 2021). It was found that Amazon shelf sediments take up potassium (K) from seawater during early diagenesis and release P during frequent resuspension events. Quantification and upscaling of the associated fluxes revealed that these processes taking place on the Amazon shelf are relevant for the global K and P budgets of the ocean. Other than claimed in previous studies, no net uptake of reactive Fe by sediments was detected on the Amazon shelf. Instead, reactive Fe contents in solid particles remain constant and indistinguishable from those of river suspended particles all the way from the shallow shelf to abyssal depths in the western North Atlantic.

Dissolved organic carbon (DOC) concentrations were found to be elevated in the Amazon River plume and in the coastal shelf area close to the mangroves. Terrestrial fluorescent DOM (FDOM) distribution pattern followed closely the DOC concentrations. Aromatic DOM compounds are mainly derived from degraded organic matter from terrestrial land plant production (such as lignin degradation products). DOM aromatic compounds were therefore highly enriched in the river plume confirming previous studies (Seidel et al., 2015). Additional sources were located along the coastal shelf with outwelling porewater from mangrove forests south of the Amazon River mouth. The data suggest that both, the Amazon River, and mangroves are important sources of terrestrial DOM to the ocean.

The preliminary data of the analyses of metal-containing DOM molecular formulae via FT-ICR-MS revealed that Fe- and Cu-containing complexes had primarily aliphatic

character with hydrogen-to-carbon (H/C) ratios >1. The preliminary data indicate an increase of molecular complexity of organic-Cu ligands with a congruent decrease of dissolved Cu concentrations. Consequently, this could imply that even at the lower concentrations in the oligotrophic Atlantic Ocean, Cu is present in biological organic complexes, for example, due to its inherent toxicity. In contrast, we found comparable numbers of Fe-organic complexes in the open-ocean samples compared to the river sample which could imply that Fe is effectively trapped in marine organic complexes even at the very low dissolved iron concentrations in the oligotrophic Atlantic Ocean (see also poster abstract, Seidel et al.).

An approved second cruise to the Amazon region in the dry season (Amazon-GEOTRACES-2, GPF 20-1_057) will help us to develop a holistic understanding of the role of the Amazon for trace metal and DOM fluxes into the Atlantic.

REFERENCES

Boyle EA, Huested SS, Grant B The chemical mass balance of the Amazon Plume—II. Copper, nickel, and cadmium. Deep Sea Res. Part I Oceanogr. Res. Papers 1982, 29, 1355-1364, doi:10.1016/0198-0149(82)90013-9

Cabral, A., Dittmar, T., Call, M., Scholten, J., et al., Carbon and alkalinity outwelling across the groundwater-creek-shelf continuum off Amazonian mangroves. Limnology and Oceanography Letters 2021, doi:10.1002/lol2.10210

de Carvalho LM, Hollister AP, Trindade C, Gledhill M, Koschinsky A, Distribution and size fractionation of nickel and cobalt species along the Amazon estuary and mixing plume, Marine Chemistry, 2021, 236, doi:10.1016/j.marchem.2021.104019

Hollister AP, Whitby H, Seidel M, Lodeiro P, Gledhill M, Koschinsky A Dissolved concentrations and organic speciation of copper in the Amazon River estuary and mixing plume, Marine Chemistry 2021, 234, doi:10.1016/j.marchem.2021.104005

Léon M, van Beek P, Scholten J, Moore W, et al. Use of 223Ra and 224Ra as chronometers to estimate the residence time of Amazon waters on the Brazilian continental shelf, Limnology and Oceanography Letters, in review

Schneider AB, Koschinsky A, Krause CH, Gledhill M, de Carvalho L.M. Dynamic behavior of dissolved and soluble titanium along the salinity gradients in the Pará and Amazon estuarine system and associated plume. Marine Chemistry, 2021, in revision.

Seidel M, Yager PL, Ward ND, Carpenter EJ, Gomes HR, Krusche AV, Richey JE, Dittmar T, Medeiros PM Molecular-level changes of dissolved organic matter along the Amazon river-to-ocean continuum. Marine Chemistry, 2015, doi:10.1016/j.marchem.2015.06.019

Spiegel T, Vosteen P, Wallmann K, Paul, SAL, Gledhill M, and Scholz F Updated estimates of sedimentary potassium sequestration and phosphorus release on the Amazon shelf. Chemical Geology, 2021, 560, doi:10.1016/j.chemgeo.2020.120017

Zhang Z, Cao Z, Grasse P, Dai M, Gao L, Kuhnert H, Gledhill M, Chiessi CM, Doering K, Frank M Dissolved silicon isotope dynamics in large river estuaries. Geochimica et Cosmochimica Acta, 2020, 273, doi:10.1016/j.gca.2020.01.028

M148

Eastern boundary circulation and upwelling off Angola, tropical Atlantic overturning circulation

AUTHORS

GEOMAR Helmholtz Centre for Ocean Research Kiel | Kiel, Germany
M. Dengler, P. Brandt

During RV Meteor cruise M148 a physical oceanography and biogeochemical study was carried out in the tropical South Atlantic along a transatlantic section on the 11°S and in the eastern boundary upwelling region of Angola and Namibia. The cruise combined the foci of the BMBF collaborative projects "Southwest African Coastal Upwelling System and Benguela Niños II (SPACES-SACUS II)" and "Regional Atlantic Circulation and Global Change (RACE II)". The work programme and post-processing of the different data sets collected during the cruise were successfully completed. The data set has contributed to advance understanding of (1) the impact of intraseasonal eastern boundary circulation variability off Angola and Namibia on the interannual climate variability; (2) the physical processes driving upwelling in the tropical eastern boundary upwelling region off Angola, and (3) the variability of the tropical Atlantic Meridional Overturning Circulation (AMOC) and long-term variability of deep water masses in the tropical South Atlantic. In addition to the scientific program, a capacity strengthening program for students and scientists from African and South American countries was carried out. Altogether, nine students from Angola, Benin, Brazil, Argentina and Chile received training during the cruise. The training program was supported by the Nippon Foundation and POGO Ship-board Training Fellowship programme and the BMBF-SACUS project.

IMPACT OF INTRASEASONAL EASTERN BOUNDARY CIRCULATION VARIABILITY ON THE INTERANNUAL CLIMATE VARIABILITY

The eastern boundary circulation off Angola is dominated by the poleward Angola Current (e. g. Kopte et al., 2017). Particularly during austral summer (Nov.–Mar.), the Angola Current transports warm tropical waters into the Benguela upwelling systems (Tchipalanga et al., 2018). Previous studies have suggested that intraseasonal variability of the Angola Current is linked to interannually occurring coastal extreme warm events, the so-called Benguela Niños, causing climate extremes and affecting the marine ecosystem (Shannon et al., 1986). The velocity times series from a mooring at 11°S serviced during M148 and during previous cruises (M120, M131) as well as sea surface temperature and height data sets from satellites were used to analyze the impact of intraseasonal alongshore flow variability on the occurrence of Benguela Niños (Imbol Koungue and Brandt, 2021). At intraseasonal time scale, the variability of the Angola Current is dominated by periods of 90 and 120 days emanating from equatorial forcing

with contribution from local alongshore wind fluctuations (Figure 1). The impact of these intraseasonal waves on the development of the extreme coastal warm or cold events exhibits a tight relationship between sea level and sea surface temperature anomalies in Southern Angola and Northern Namibia with the sea level leading sea surface temperature by about 14 days. These intraseasonal waves contribute to the development of coastal warm and cold events that occur every few years by either enhancing them as for the Benguela Niño in 1995 or damping them as for the coastal warm event in 2001.

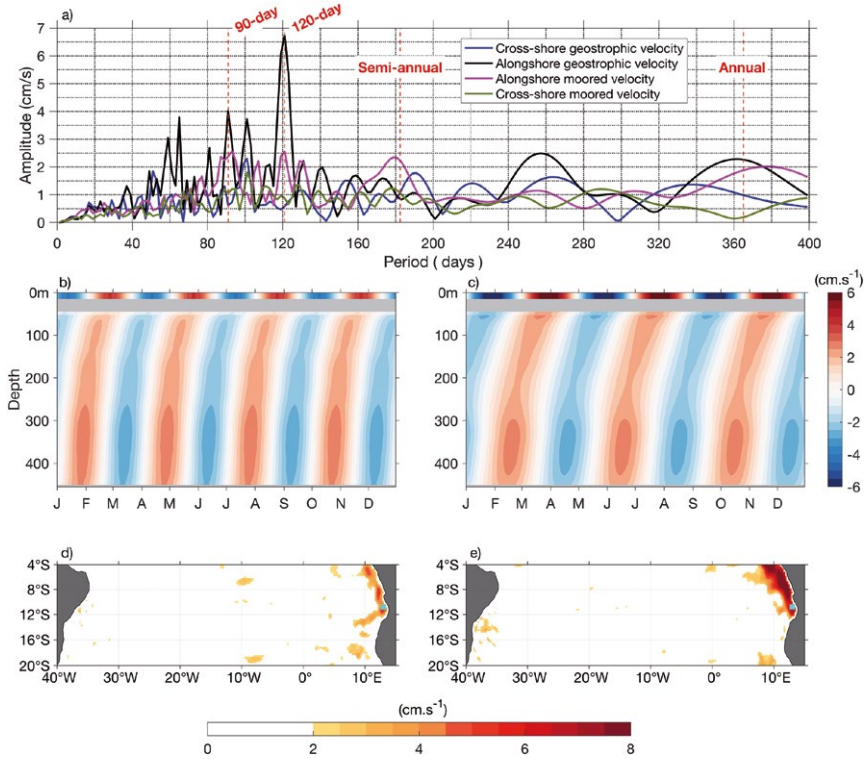

Fig. 1: a) Vertically-averaged periodograms of moored velocities (cross-shore component and alongshore component between 45–450 m) and near-surface absolute geostrophic current velocities from satellite altimetry (cross-shore component and alongshore component at the mooring position). b) 90-day harmonic fit of the alongshore mooring velocities repeated to cover a full year; c) same as b) but for the 120-day harmonic. d) Amplitude of the 90-day harmonic of meridional geostrophic velocity in the tropical South Atlantic; e) same as d), but for the 120-day harmonic. The cyan dots in d) and e) represent the mooring position (from Imbol Koungue and Brandt, 2021).

CAUSES AND EVOLUTION OF THE BENGUELA WARM EVENT IN 2016

Additionally, the data from this cruise contributed to the understanding of the cause of a strong warm event that occurred in the southeastern tropical Atlantic Ocean off Angola and Namibia in January and February 2016 with sea surface temperature anomalies reaching 3°C (Lübbecke et al., 2019). In contrast to classical Benguela Niño events, the

analysis of various direct observations indicates that this warming was not predominantly forced by an equatorial Kelvin wave exciting a coastally trapped wave but instead resulted from a combination of local processes that are related to (1) a weakening of the alongshore, i. e. mainly southerly, winds and (2) enhanced freshwater input through local precipitation and river discharge.

Consistent with the weakened winds, we found a reduction in latent heat loss and a poleward surface current anomaly. The surface freshening, which was detected in satellite observations of sea surface salinity, caused a very shallow mixed layer and enhanced upper ocean stratification. As supported by our moored observations, the shallow layer of warm and fresh surface water was advected poleward by an anomalous surface current that was likely forced by the reduction of the trade winds.

MECHANISMS CONTROLLING UPWELLING OF ANGOLA

The Angolan upwelling has a strong seasonality and biological productivity reaches its maximum in austral winter (June-September). During this period, however, alongshore winds reach their seasonal minimum suggesting that processes other than local wind-driven upwelling contribute to near-coastal cooling and upward nutrient supply. One such mechanism may be turbulent mixing induced by internal tides. To investigate this, we used a three-dimensional ocean model initialized with observed hydrography and observed tidal amplitudes from the moorings to simulate the generation, propagation and dissipation of internal tides at the Angolan continental slope and shelf (Zeng et al., 2020). The simulated internal tides are mainly generated in regions with critical/supercritical topographic slopes typically found between the 200- and 500-m isobaths. Diapycnal mixing due to the internal tides was found to be strongest close to the coast and gradually decreased offshore, thereby contributing to the establishment of cross-shore temperature gradients. The available seasonal coverage of hydrographic data was used to design simulations to investigate the influence of seasonally varying stratification characterized by low stratification in austral winter and high stratification in austral summer. The results show that internal tide characteristics, such as their wavelengths, sea surface convergence patterns and baroclinic structure, have substantial seasonal variations and additionally strong spatial inhomogeneities. However, seasonal variations in the spatially-averaged generation, onshore flux and dissipation of internal tide energy are weak. By evaluating the change of potential energy, it is shown that mixing due to internal tides is more effective during austral winter. We argue that the weaker background stratification during June-August compared to the rest of the season acts as a preconditioning for IT mixing. Additional analysis of the heat budget in the upwelling area including mixing and advective processes controlling upwelling is presented in a separate contribution by Körner et al. (this issue).

AMOC AND WATER MASS CHANGES ALONG 11°S

During M148, bottom pressure sensors moored at the 300 m and 500 m isobaths at the continental slope of Brazil and Angola were serviced, continuing an ongoing effort of

measuring bottom pressure at these locations since 2013. These records were used to derive the first time series of AMOC anomalies in the tropical South Atlantic (Herrford et al. 2021). Over the period 2013–2018, the AMOC and its components are dominated by seasonal variability, with peak-to-peak amplitudes of 12 Sv for the upper-ocean geostrophic transport, 7 Sv for the Ekman and 14 Sv for the AMOC transport (Figure 2).

The observed seasonal variability of zonally integrated geostrophic velocity in the upper 300 m is controlled by pressure variations at the eastern boundary, while at 500 m depth contributions from the western and eastern boundaries are similar. Our analyses indicate, that while some of the uncertainties of the AMOC estimates result from the technical aspects of the observational strategy, uncertainties in the wind forcing are particularly relevant for AMOC estimates at 11°S.

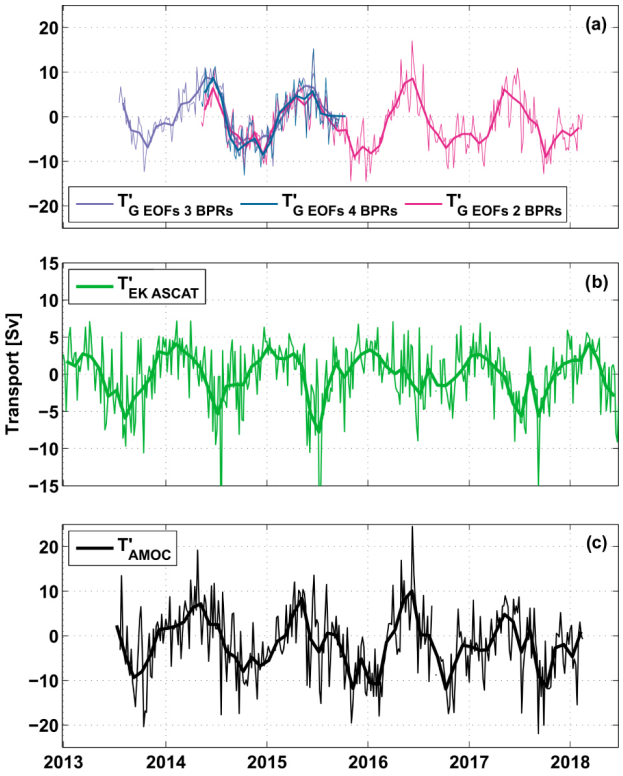

Fig. 2: Anomaly time series at 11° S of (a) the upper-ocean geostrophic transport derived from bottom pressure recorder (BPR) and altimetric sea level measurements, (b) the Ekman transport derived from ASCAT wind stress, and (c) the resulting AMOC anomaly transport. Thin lines represent daily values in a) and 5-daily values in (b, c), bold curves represent monthly averages. Different colors in (a) indicate transport calculations for different sets of bottom pressure records (BPR) – 4 BPRs (petrol), 3 BPRs (purple) and 2 BPRs (magenta) (from Herrford et al., 2021).

DIFFERENCES AND TRENDS OF WATER MASSES IN THE TROPICAL SOUTH ATLANTIC

Differences of water mass characteristics along 11°S were analyzed by comparing hydrographic sections taken in May 1994 (RV Meteor cruise M28/1) and during M148. To account for property changes on isobaric surfaces due to the combined effects of changes along isopycnal surfaces, intrinsic water mass changes, and vertical displacement of the isopycnals, temperature differences calculated on pressure levels as well as temperature and pressure differences calculated on neutral density surfaces. While temperature changes on isobars are very patchy, the signals become clearer when distinguishing between changes in spicyness and heave. The main results were: (1) a strong warming (+ 0.24°C per decade) and oxygen increase above 300 m in the western basin interior and reaching down to 500 m in the western boundary region. (2) in the depth range of the AAIW and uCDW (600–1100 m), the whole western and eastern basin interiors are dominated by a warming and a decrease in dissolved oxygen of 20 µmol kg^{-1} per decade. The warming signal in the western basin patch is twice as large on isobars than on isopycnals, suggesting that it is the result of intrinsic water mass changes as well the vertical displacement of isopycnal surfaces in equal contributions. (3) The entire western basin exhibits an increase in temperature and oxygen within the AABW layers below 4000 m. This work as well as the AMOC anomaly calculation was part of the PhD thesis of Josefine Herrford (Herrford, 2021).

REFERENCES

Herrford J, Brandt P, Kanzow T, Hummels, R., et al. Seasonal variability of the Atlantic Meridional Overturning Circulation at 11° S inferred from bottom pressure measurements, Ocean Science, 2021, 17, 265–284. doi: 10.5194/os-2020-55.

Herrford, J. Observing seasonal to decadal variability related to the Atlantic meridional overturning circulation at 11°S. PhD Thesis, 2021, Mathematisch-Naturwissenschaftliche Fakultät der Christian-Albrechts-Universität zu Kiel, 142 pp. Online copy: https://macau.uni-kiel.de/receive/macau_mods_00001342.

Imbol Koungue R A, Brandt P. Impact of intraseasonal waves on Angolan warm and cold events, Journal of Geophysical Research: Oceans, 2021, 126, e2020JC017088. doi: 10.1029/2020JC017088.

Kopte R, Brandt P, Dengler M, Tchipalanga P C M, Macueria M, Ostrowski M. The Angola current: flow and hydrographic characteristics as observed at 11°S. Journal of Geophysical Research Oceans, 2017, 122, 1177–1189. doi: 10.1002/2016JC012374.

Lübbecke J F, Brandt P, Dengler M, Kopte R, Lüdke J, Richter I, Martins M S, Tchipalanga P C M. Causes and evolution of the southeastern tropical Atlantic warm event in early 2016, Climate Dynamics, 2019, 53, 261–274. doi: 10.1007/s00382-018-4582-8.

Shannon L V, Boyd A J, Bundrit G B, Taunton-Clark J. On the existence of an El Niño-type phenomenon in the Benguela system. Journal of Marine Research, 1986, 44, 495–520. doi: 10.1357/002224086788403105.

Tchipalanga P C M, Dengler M, Brandt P, Kopte R, Macuéria M, Coelho P, Ostrowski M, Keenlyside N S. Eastern boundary circulation and hydrography off Angola-building Angolan oceanographic capacities. Bulletin of American Meteorological Society, 2017, 99, 1589–1605. doi: 10.1175/BAMS-D-17-0197.1.

Zeng Z, Brandt P, Claus M, Greatbatch R., Lamb K, Dengler M, Chen X. Three Dimensional Numerical Simulations of Internal Tides in the Angolan Upwelling Region, Journal of Geophysical Research – Oceans, 2020, resubmitted, doi: 10.1002/essoar.10503264.2.

M148/2

EreBUS – Processes Controlling Greenhouse Gas Emissions from the Benguela Upwelling System

AUTHORS

Max Planck Institute for Marine Microbiology | Bremen, Germany
T. Ferdelman, J. Graf, G. Ho, K. Kitzinger, G. Lavik, S. Littmann, H. Marchant, J. Milucka, W. Mohr, S. Schorn, J. van Arx, M. Kuypers

Institute for the Chemistry and Biology of the Sea (ICBM), Carl von Ossietzky University of Oldenburg | Oldenburg, Germany
P. Böning, F. Gäng, K. Pahnke, S. Garaba, C. Tholen, O. Zielinski, G. Gomez-Saez, Y. Oertel, J. Niggemann

Leibniz Institute for Baltic Sea Research (IOW) | Warnemuende, Germany
V. Mohrholz

Ludwig Maximilian University of Munich | Munich, Germany
W. Orsi, O. Coskun, M. Eitel, R. Frank, R. Morard, P. Rodriguez, A. Vuillemin, G. Wörheide

Center for Marine Environmental Sciences (MARUM), University of Bremen | Bremen, Germany
M. Siccha, M. Kucera

RESEARCH OBJECTIVES

During the Meteor Expedition *EreBUS* (M148/2) we investigated physical processes and biogeochemistry associated with the microbial communities that are relevant for the turnover of key climate-relevant trace greenhouse gases (TGG), such as methane and nitrous oxide, in the Benguela Upwelling System (BUS) and the oligotrophic Angola Gyre (AG) (see Figure 1).

The M148/2 expedition was organized around two major research goals: (1) We examined the factors that control and affect the broad-scale microbial processes leading to production or consumption of TGG in the BUS. This included continuation of the long-term hydrographic observations with moored instruments on the Namibian shelf (mooring maintenance), as well as assessment of the optical properties of color producing agents of seawater (e. g. phytoplankton, dissolved organic matter) in relation to hydrographical conditions. We sought to link bioavailable Fe, whose provenance (dust vs. anoxic

sediment) may be revealed by Fe isotopes to primary productivity and N_2 fixation in the near-shore regions and the AG that feeds into the BUS. Moreover, we investigated the source and fate of dissolved organic matter (including dissolved organic sulfur) compounds in order to understand their impact on microbial respiration and eventually global dissolved organic matter (DOM) stability in the Ocean.

(2) A second major goal was to quantify the processes and identify microbial communities contributing to TGG turnover at key water and surface sediment depths. We took samples to explore the metabolic capacities of these microorganisms, including the contribution of symbiotic microorganisms living with small eukaryotes and fungi for performing cultivation, metagenomics, metatranscriptomic, gene expression stable isotope probing approaches. We assessed the utilization of ammonia and dissolved organic nitrogen compounds (e. g., urea, cyanate) as energy and N-sources for nitrifying microorganisms. We also obtained samples for the ongoing study of planktonic foraminiferal morphology and single-cell DNA analysis, complemented with bulk plankton samples for next generation sequencing (NGS), in order to evaluate the population structure and morphological taxonomy that underpins the majority of paleo-oceanographic methods for determining past ocean properties.

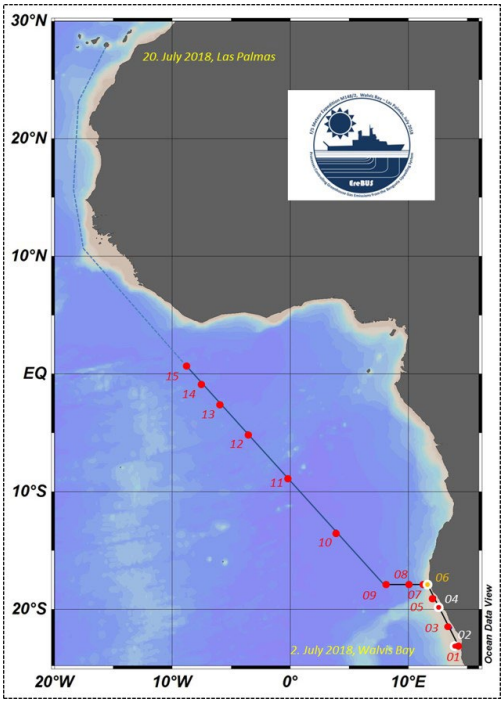

Fig. 1: Cruise track showing the 15 stations occupied during Meteor Expedition M148/2 "EreBUS" showing the sites along the Namibian shelf (Stations 01–06), across the continental slope at 18°S (Stations 06–09) and through the Angola Gyre to the Equatorial Upwelling (Stations 09–15) from 02 to 20 July 2018 (dotted line shows transit only).

RESULTS

The increased availability of nutrients on the Namibian shelf waters was mirrored in high chlorophyll a concentrations (as a proxy for phytoplankton biomass) and high primary production rates at the shelf stations and close to shore (determined ex situ on-deck using ^{13}C incubations). In contrast, N_2 fixation rates (experimentally determined using ex situ ^{15}N on-deck incubations) were measurable but low in these coastal stations (206–208) while rates were higher in the offshore stations in the oligotrophic Angola gyre region and further oligotrophic waters. Interestingly, a subsurface maximum of N_2 fixation rates was observed that is not typical for oligotrophic regions, but this maximum coincided with nutrient-depleted waters potentially derived from different water masses. The patterns of N_2 fixation observed here match those observed for other Oxygen Minimum Zone (OMZ) regions and suggest an advection of essential nutrients further offshore.

We have completed analyses to assess trace element and dissolved organic matter constituents that influence the overall productivity of the BUS. Seawater dissolved rare earth elements (REE) exhibited overall low values at stations M148-202, -203 and -212 but very low values notably in anoxic bottom waters of M148-203, which contrasts with other OMZs (e. g. Mauritania). Fe isotopes in the sediments were isotopically heavier (∂56Fe = 0.3‰) than the lithogenic background, and these sediment endmember values will be used in conjunction continuing investigation of Fe isotopes in the cross-shelf Fe isotope water column (Stations M148-206-210). The presence of glauconite (authigenic Fe silicate) in the sediments of M148-206 as well as quartz and low amounts of organic matter and carbonates (< 2 wt %) indicates changing water column redox conditions combined with reduced sedimentation. This is matched by Mn depletion (Mn < 100 ppm) and lack of Mo enrichments (Mo < 2 ppm) displaying net reducing but not anoxic conditions in the water column.

Higher dissolved organic carbon (DOC) concentrations were observed in the BUS as compared to the open ocean (AG), with DOC concentrations ranging between 55 and 75 µmol L^{-1}. Results from FT-ICR-MS analyses suggested that the concentration of dissolved oxygen was not the main driver for differences observed in the DOM molecular composition. Major differences were found between samples from the shelf and the open ocean with intensity weighted atomic ratios involving nitrogen (N/C, N/O), sulfur (S/C, S/O) and phosphorus (P/C, P/O, N/P) being significantly higher on the shelf compared to the open ocean. Higher S/C and S/O ratios in the sulfidic porewater DOM are indicative of sulfurization of (dissolved organic mater) DOM in the sediments. This first molecular characterization of DOM and dissolved organic sulfur (DOS) in the BUS is an important contribution towards understanding DOM cycling in eastern boundary upwelling systems.

Surface waters on the shelf were oversaturated with respect to the atmosphere for both methane and nitrous oxide, with concentrations of methane reaching up to 11 nM and nitrous oxide up to 30 nM. Across the oligotrophic AG, concentrations of methane and

nitrous oxide were close to atmospheric equilibrium. At three shelf and five offshore stations, stable isotope incubations were carried out to determine rates of methane oxidation, nitrous oxide production and nitrous oxide consumption. Rates of microbial processes involved in both the production and consumption of methane and nitrous oxide were successfully quantified.

Aerobic rates of methane oxidation up to 10 nM d^{-1} were detected at two shelf stations. Processes that contribute to the production of N_2O – ammonia oxidation and denitrification – could also be measured. Overall, denitrification appeared to yield greater rates of N_2O production at two shelf stations. N_2O production rates from labeled ammonia reached up to 125 pM d^{-1} at stations 202 and 204, whereas no significant rates were observed at station 206. Production of N2O from labeled nitrite could be detected at all three coastal stations and reached rates of up to 600 pM d^{-1}. Production and consumption of N_2O at offshore stations was patchy and usually below detection limit.

We could identify putative aerobic methane oxidizing bacteria (Methyloprofundus spp. and Marine Methylotrophic Group 2) in the water column of the shelf stations. With respect to ammonia oxidizing microorganisms, both thaumarchaeal and bacterial nitrifiers were found. Additionally, a wide diversity of putatively denitrifying organisms, ranging from chemolithotrophic sulfur oxidizers to Flavobacteria were also found. The in situ activity of these target taxonomic groups will be further investigated using fluorescence in situ hybridization and nano-scale secondary ion mass spectrometry.

We combined biogeochemical rate measurements, metagenomics and metatranscriptomics to compare the use of urea and ammonia by ammonium oxidizing archaea (AOA) in the oligotrophic Angola Gyre. Within the AG, ammonium and nitrite concentrations were extremely low (<1 µmol L^{-1}), as were concentrations of the dissolved organic nitrogen compounds (urea and cyanate). Intriguingly however, at many stations and depths, urea concentrations were equivalent or greater than ammonium concentrations, suggesting that dissolved organic nitrogen might be an overlooked source of N for ammonia oxidizers. ^{15}N tracer experiments with both ammonia and urea showed that there was no preference for one compound over the other. The AG was dominated by AOA belonging to the genus Ca. Nitrosopelagicus, some of which can grow using urea instead of ammonia. Approximately 30–40 % of the Angola Gyre AOA encoded for and transcribed urease and urea transporters, indicating that they can use urea as an additional substrate to ammonia. This indicates the presence of an AOA community specialized on the use of organic nitrogen.

^{13}C DNA stable isotope probing and gene expression have been conducted on sediment samples and water column samples. These experiments resulted in two serendipitous findings, whereby the activity of both Foraminifera (and a novel group of Archaea called "Lokiarchaeota" were found to be exceptionally high in the gene expression datasets leading to further investigations and subsequent publication (Orsi et al., 2019 and Orsi

et al., 2020). Follow up experiments involve quantifying the 13C uptake by Marine Fungi and comparing this to the carbon utilization by bacteria and archaea. With these transformative results, we have linked the activity of poorly understood groups of marine microbes (foraminifera, Lokiarchaeota, and Fungi) to marine carbon cycling in seawater, OMZs, and sediments.

REFERENCES

Orsi WD, Vuillemin A, Rodriguez P, Coskun ÖK, et al. Metabolic activity analyses demonstrate that Lokiarchaeon exhibits homoacetogenesis in sulfidic marine sediments. Nat Microbiol, 2019, doi:10.1038/s41564-019-0630-3

Orsi WD, Morard R, Vuillemin A, Eitel M et al. Anaerobic metabolism of Foraminifera thriving below the seafloor. The ISME Journal. 2020:2580–94.

M149

Recurrence of tsunamigenic hazards from MeBo drilling records and fluid/solid transfer in the Gulf of Cadiz accretionary prism

AUTHORS

Institute of Geology – University of Innsbruck | Innsbruck, Austria
W. Menapace

MARUM – Center for Marine Environmental Sciences | Bremen, Germany
S. Xu, A. Kopf, A. Hüpers

Historical earthquakes such as the 1755 Lisbon earthquake and tsunami demonstrated that the plate boundary between Eurasia and Africa constitutes a significant earthquake and tsunami threat to neighboring coastal communities. The expedition M149 with R/V Meteor aimed at collecting short and long sediment cores and installing borehole observatories with the seafloor drill rig MARUM-MeBo70 (Meeresboden-Bohrgerät) to obtain records of the past and current tectonic activity of the plate boundary between Eurasia and Africa in the Gulf of Cadiz and Alboran Sea (W Mediterranean Sea).

From July 24 to August 24, 2018, the M149 cruise collected in total 383.2 m of core, conducted 38 in situ heat flow measurements, mapped approximately 12500 km^2 of seafloor and installed 3 borehole observatories in a mud volcano and 2 fault zones (Hüpers et al., 2020). The scientific activities focused on i) two NNW-SSE trending strike-slip faults (Lineament Center and South) cutting through the Gulf of Cadiz accretionary prism; ii) two approximately SW-NE trending strike-slip faults in the Alboran Sea; and iii) adjacent mud volcanoes that are supposed to be hydraulically connected to deeper levels of the fault zones. From July 24 to August 24 in 2018 cruise M149 collected in total 383.3 m of core, conducted 38 in situ heat flow measurements, mapped approximately 12500 km^2 of seafloor and installed 3 borehole observatories. Three new mud volcanoes were discovered during the cruise of which one is located on the SW edge of the accretionary prism - outside of the predominant mud volcano distribution.

Post-cruise analyses of collected pore fluids for minor and major element composition show element patterns related to the mud volcano locations. The pore waters from the mud volcanoes close to the Lineament Center show signals from dissolution of evaporite deposits. Instead, pore waters from mud volcanoes close to the Lineament South show signals from the underlying crust. The observed geochemical patterns imply different fluid source depths. Fluids sampled from the recovered infill of transtensional zones along Lineament Center and South are characterized by elevated Cl concentrations up to 5x times of their seawater value. The ascend of brines along the faults is corroborated by

elevated heat flow values measured during the cruise. For the first time geochemical data gives evidence for the importance of fault zones as main fluid pathways through the Gulf of Cadiz accretionary prism.

Since most MVs in the Gulf of Cadiz are situated close to major strike-slip faults, we selected Meknes and Funky Monkey MVs, which are located in the upper and lower part of the accretionary wedge along different strike-slip fault segments, in order to define fluid mobilization depth and ascent through the accretionary prism (Xu et al., 2021; Figure 1). Consistently with previous studies, we traced back the origin of venting fluids to clay mineral dehydration through major and minor element geochemistry, high content of illite in the mud breccia matrix and calculated reaction temperatures of 60–100 °C using the Mg-Li geothermometer. With the reduced potential of clay mineral dehydration towards the deeper MVs, the enrichment of B and Li with low B/Li values and the inferred crustal-sourced Sr, a stronger crustal input has been hypothesized for Funky Monkey MV. Additionally, we selected fluid samples from the pull-apart basins formed on the two major strike-slip faults to compare with the MVs fluids composition. Based on chemical and isotopic analyses, the fault fluids show no obvious interactions with underlying clay-rich sediments and suggest other sources such as underlying crust for the enrichment of Li and Sr. In agreement with the strong structural control of the diapirs on the area, the fault fluids also show significant geochemical effect from evaporite dissolution which is not obvious in most MVs fluids. Hence, in the Gulf of Cadiz, the MVs located along the major strike-slip faults may have a well-connected deep and shallow fluid system, while the nearby strike-slip faults are deeply rooted and closely linked to salt diapirism, carrying more pristine fluids from the underlying crust. Ongoing work with Sr isotopes will constrain the crustal influence on both MV and fault fluids.

Post-cruise research on recovered sediment cores further showed that the sedimentary infill of such transtensional zones – in particular small pull-apart basins – hosts multiple fining upward sequences degrading from foraminifera-rich ooze at the bottom to hemipelagic nannofossil ooze at the top and which accumulated probably through seafloor gravitational movements in response to the tectonic activity of the faults. Hence, these deposits provide sedimentary records that are ideally suited for paleoseismological studies.

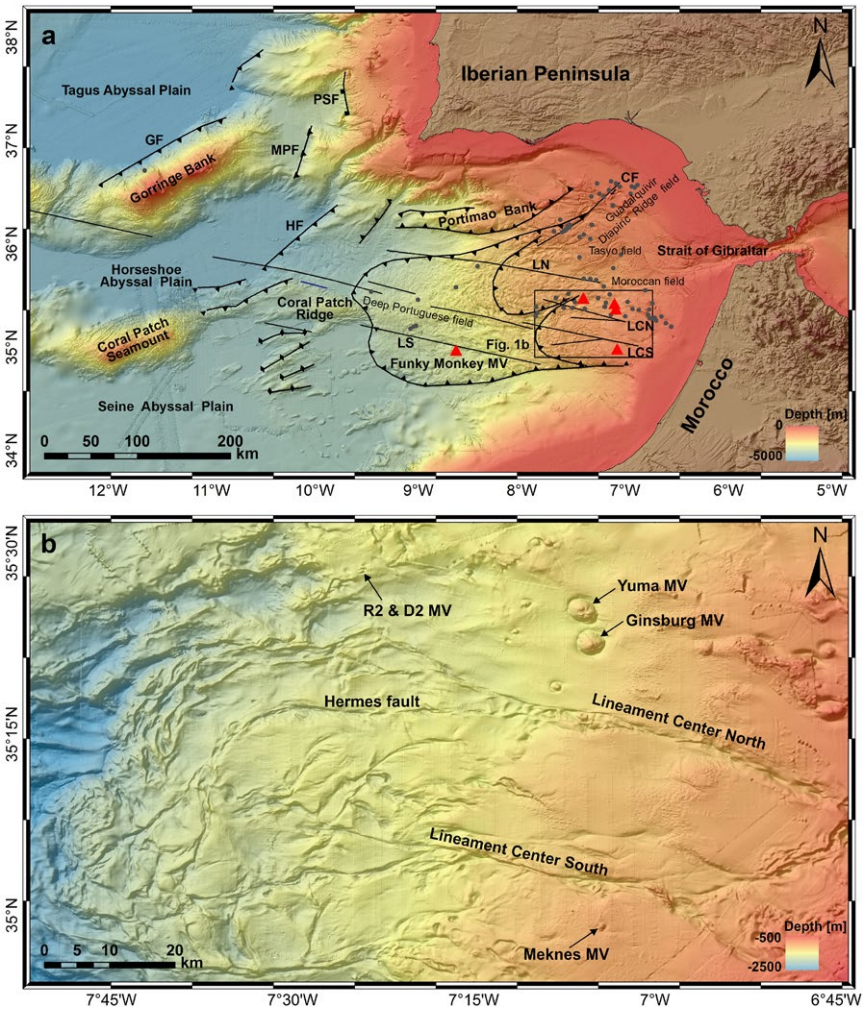

Fig. 1: a) Bathymetry map of the Gulf of Cadiz with main tectonic and morphological features depicted [modified from Cunha et al. (2012); bathymetry from the SWIM compilation of Zitellini et al. (2009)]. The locations of the six MVs investigated in Xu et al. (2021) (red triangles), other MVs known to date (dark gray dots), as well as MV fields and major fault zones are shown. CF Cadiz Fault, GF Gorringe Fault, HF Horseshoe Fault, LN Lineament North, LCN Lineament Center North, LCS Lineament Center South, LS Lineament South, MPF Marques de Pombal Fault, PSF Pereira de Sousa Fault. b) Multibeam bathymetry map of the main study area produced during the M149 cruise.

REFERENCES

Cunha, T.A., Matias, L.M., Terrinha, P., Negredo, A.M., Rosas, F., Fernandes, R.M.S., Pinheiro, L.M., (2012). Neotectonics of the SW Iberia margin, Gulf of Cadiz and Alboran Sea: a reassessment including recent structural, seismic and geodetic data. Geophys. J. Int. 188, 850–872.

Hüpers, A., Menapace, W., Magalhaes, V., Freudenthal, T., Cruise Participants, 2020. Report and Preliminary Results of R/V METEOR Cruise M149: Shipboard and Postcruise

Analysis, Recurrence of Tsunamigenic Hazards from MeBo Drilling Records and Hazard Mitigation Using MeBo Observatories, Las Palmas (Canary Islands) – Cadiz (Spain), 24.07.2018–24.08.2018. Berichte aus dem MARUM und dem Fachbereich Geowissenschaften der Universitat ¨ Bremen, Bremen. doi.org/10.26092/elib/100

Xu, S., Menapace, W., Hüpers, A., & Kopf, A. (2021). Mud volcanoes in the Gulf of Cadiz as a manifestation of tectonic processes and deep-seated fluid mobilization. Marine and Petroleum Geology, 105188. doi.org/10.1016/j.marpetgeo.2021.105188

Zitellini, N., Gracia, E., Matias, L., Terrinha, P., Abreu, M.A., DeAlteriis, G., Henriet, J.P., Danobeitia, J.J., Masson, D.G., Mulder, T., Ramella, R., Somoza, L., Diez, S., (2009). The quest for the Africa-Eurasia plate boundary west of the Strait of Gibraltar. Earth Planet Sci. Lett. 280, 13–50.

M150

Controls in benthic and pelagic BIODIversity of the Azores – BIODIAZ

AUTHORS

Senckenberg am Meer | Wilhelmshaven, Germany
K.H. George, M. Bruhn, F. Iwan, T. Janßen, K. Jeskulke, M. Kagerer, A. Kieneke, A. Ostmann, K. Richter, B. Springer, A. Wehrmann, M. Wilsenack

University of Cologne, Biozentrum, Institute of Zoology | Cologne, Germany
H. Arndt, K. Hermanns, M. Hohlfeld, C. Meyer

Universidade da Madeira, Facultade de Ciências da Vida, Estaçãode Biologia Marinha | Funchal, Madeira, Portugal
M. Kaufmann

Departamento de Oceanografia e Pescas, IMAR – Universidade dos Açores | Horta, Faial, Portugal and Departmento de Biologia, Faculdade de Ciências e Tecnologia | Ponta Delgada, São Miguel, Portugal
S.P. Ávila, C. Loureiro, P. Madeira, C. Pieper

Centro de Investigação em Biodiversidade e Recursos Genéticos, InBIO Laboratório Associado, Polo dos Açores, Universidade dos Açores | Ponta Delgada, São Miguel, Portugal
L. Baptista

Oberösterreichisches Landesmuseum | Linz, Austria
B. Berning

University of Bergen, Department of Biology | Bergen, Norway
F. Carvalho

Departamento de Oceanografia e Pescas, IMAR – Universidade dos Açores | Horta, Faial, Portugal
M. Creemers, A. Defise

Regional Agency for the Development of Research, Technology and Innovation – Oceanic Observatory of Madeira | Funchal, Madeira, Portugal
T. Silva

Interdisciplinary Centre of Marine and Environmental Research | Porto, Portugal
A. Narciso, J. Xavier

Collaboration with:
R. Quartau, Instituto Hidrográfico I Lisboa, Portugal
R.S. Ramalho, Cardiff University I Cardiff, UK

AIMS OF THE CRUISE

METEOR Cruise M150 BIODIAZ provided material from sublittoral down to deep-sea stations to incorporate innovative aspects into the study of seamount and island productivity and their potential role for the establishment of benthic assemblages comprising all size classes (George et al. 2021). The aim was to get a baseline on the diversity, faunal composition and distribution of shelf and deep-sea taxa and related sediments from three different Azorean islands (Flores, Terceira, and Santa Maria) and two adjacent seamounts (Princess Alice Bank, Formigas Bank). Such baseline shall serve to prove fundamental hypotheses regarding the role of seamounts/islands for marine organisms and the principle (bio)-sedimentary processes in the evolution of seamounts. The significance of potential endemism in zoobenthic communities based on the extensively sampled material is studied in the context of the geologic age, topographic isolation, phytoplankton productivity and diversity of the systems.

The scientific staff enclosed the following research groups: 1. CTD, phytoplankton, microplastics; 2. Macro- and megabenthos; 3. Meiobenthos; 4. Nanofauna; 5. Sedimentology. In addition, samples were taken for marine geologists that were not directly involved in the project but had asked for sampling material that would enhance their own studies.

SAMPLING

Altogether, 676 stations were sampled (George et al. 2021) using different gears: Agassiz trawl (AT), Chain sack dredge (KSD), Box corer (KG), Multiple corer (MUC), Brenke-Epibenthos sledge (EBS), Shipek grab (SG), Henning grab (HG), Plankton nets (PN), CTD with bottle rosette (CTD), Underwater videocamera (UWC). In addition, along two orthogonal transects repeated ADCP measurements were made over the summit area of the Formigas Bank in order to confirm zooplankton vertical migration patterns in the acoustic backscatter.

IMPEDIMENTS

Altogether, cruise M150 BIODIAZ was very successful. Almost all targeted stations could be sampled, providing the material needed for carrying out the respective studies. Also, the weather conditions were generally favourable. Nevertheless, some impediments arose:

› The sampling had to be interrupted three times: a fish trawler that had suffered an engine failure was towed to Terceira, and two unforeseen disembarkations at

Sta. Maria and Sao Miguel islands were necessary. Moreover, the tropical storm "Helene" forced us to stop our work at Terceira island and to switch to Sta. Maria; there, we continued by sampling the scheduled transects, and after "Helene" had passed, we steamed back to Terceira and continued the interrupted work.

- Problems for sampling arose because of the topography of the rugged volcanic sea floor around the islands that often presented rocky vertical walls and a coverage with massive boulders, making the sampling not only extremely difficult but leading to several damages on different gears; for instance, both the KSD and the EBS were so badly damaged that they could not be further deployed; the KG suffered strong damages that could fortunately be repaired by the ship's leading engineer, his staff and the deck's fitter; the nets of the AT were burst several times and could be further used only because the bosun and even the captain himself made great efforts to repair them. Major damages were prevented at the depths of 50 and 150 m because the UWC was deployed previously to any gear deployment at these depths, giving insights into the seafloor's topography and condition.

- Nevertheless, the most significant impediment affecting all research groups was related to the onset of the COVID-19 pandemic, leading to a complete breakdown of almost all laboratory work since March 2020. Laboratories had to be closed completely, or only single persons could work. Thus, principally the further treatment of the sampling material, i. e. the centrifugation and sorting of the material, the taxa determination but also all other kind of laboratory work suffered from the lock-down, leading to a dramatic delay in the data acquisition. That resulted in an unexpected reduced success with respect to the striven results. Data acquisition is still in process, so the results presented at the status conference must mostly be considered as preliminary.

RESULTS

As stated above, the COVID-19 pandemic led to a remarkable delay with respect to the data analyses and production of papers. However, a series of manuscripts are in progress (Baptista et al. in prep., George in prep., George et al. in prep., Hohlfeld et al. submitted a, b, Kieneke et al. in prep., Michell et al. in prep., Narciso et al. in prep., Quartau et al. in prep., Schoenle et al. in rev., Zhao et al in prep.), and some data and results were already published (George and Wölfi 2019, Schoenle et al. 2019, Kaufmann et al. 2020, Schoenle et al. 2020, Baptista et al. 2021, Carduck et al. 2021, Kieneke and Todaro 2021, Schoenle et al. 2021, Živaljić et al. 2020a, b).

Particular results are provided here by poster presentations. They consider (i) phytoplankton (Kaufmann et al.), (ii) nanofauna (Hohlfeld et al., Meyer et al.), (iii) meiobenthic major taxa (George et al.), (iv) meiobenthic Copepoda (George), (v) meiobenthic Gastrotricha (Kieneke), (vi) macrobenthic Bryozoa (Baptista et al.), (vii) sedimentology (Wehrmann et al.).

Further first insights are given into:

Microplastics (C. Pieper)

Seawater samples for microplastic analyses were collected and filtered aboard of the RV METEOR during the mission BIODIAZ in 2018.

The analysis of the obtained results will provide knowledge about microplastics vertical distribution in the water column from the sea surface until the deep-sea around the Azorean islands. Moreover, potential transportation and dispersal mechanisms of microplastics will be addressed with the results of the CTD profiles performed during vertical samplings. The analyses are still in process.

Macrobenthic Echinodermata (P. Madeira, S.P. Ávila)

Echinoderms as important component of the Azorean marine benthos is in a desperate need of a renewed look. Therefore, the main task for the BIODIAZ cruise was to collect echinoderm material from depths below 50 m in the archipelago. Echinoderms were retrieved from depths between 50 and 2,547 m. All four echinoderm classes were represented in the collected material; Ophiuroidea was the most abundant in terms of overall individual numbers; Crinoidea were mostly retrieved from material collected at one BIODIAZ station, attached to rock fragments; Holothuroidea were only collected by the AT at depths between 1,535 and 2,547 m. At depths shallower than 500 m, most of the retrieved material was characterized by fragmentary abraded naked echinoid tests of *Genocidaris maculata* A. Agassiz, 1869 and *Echinocyamus* species, most likely indicating that the material was deposited in the seafloor for quite some time and it may not be autochthonous; the few living material collected at depths shallower than 500 m was characterized by ophiuroid species, juveniles of spatangoid echinoids and juveniles of an asterinid sea star.

Most of the echinoid and asteroid specimens collected at depths shallower than 500 m belong to species already known to the area. Nonetheless, the new retrieved material helped to understand the species' geographical and bathymetrical distribution within the Azores waters.

An unexpected result was the observation of echinoid material infested by *Pelseneeria* gastropods. In the North-Atlantic deep waters, the documentation of gastropod parasitism in echinoids is extremely rare. Though this gastropod genus was firstly described for the Azores, it has not been documented in the area since the description of *Pelseneeria striata* Bouchet & Warén, 1986.

Macrobenthic Porifera (F. Carvalho, M. Creemers, A. Defise, J. Xavier)

Pheronema sponges were collected to characterize their ecological roles as habitat and food sources in relation to their associated fauna. To do so, eight sponges were analysed. Entire sponges were measured to obtain their external biometrics and inner morphometrics.

Sponge samples were dissected under stereomicroscope to collect their associated epifauna and infauna. The associated fauna was sorted, individuals were counted and identified to the lowest taxonomic level possible, using the literature and the expertise of specialized taxonomists. More than 250 individuals were collected from the trawl catches belonging to more than 50 different taxa, amongst them the sea urchin *Cidaris cidaris*, polychaetes (Polynoidae, Glyceridae, Nephtyidae), foraminifers, crustaceans such as galathoids (*Uroptychus concolor, Munidopsis serricornis*) and carid shrimps (Pandalidae), and small fish (Macrouridae, *Macroramphosus* sp.).

Sub-samples of *Pheronema* sponges were taken to quantify nutrients and organic content in sponge tissues, to extract the filtered particulate matter for POM quantification, and to obtain their carbon and nitrogen isotopic ratios. Measurements showed that more than 90 % of the sponge total volume is made of empty space, mostly due to their large atrial cavity, and a high porosity (>95 %), hence providing additional space for their associated fauna to shelter in. These results will be linked to the abundance and richness of associated fauna to better understand the role of sponges as a shelter and a habitat.

The results from the isotopic analysis and the mixing models support the trophic role of *Pheronem*a sponges and their filtered particles as food sources for the associated organisms.

Geology (R. Quartau, R. Ramalho, S.P. Ávila)

Under the scope of the PLATMAR project, 118 sediment samples were recovered from the insular shelf of Santa Maria during the cruise PLATMAR 2/2018 (23.08.–12.09.2018) of RV ARQUIPÉLAGO, allowing a sedimentological characterization. Additionally, 7 samples collected during the cruise M150 BIODIAZ (27.08.–02.10.2018) of RV METEOR were also used.

The samples were subjected to grain size, total inorganic carbon (TIC) and total organic carbon (TOC) measurements. The aim was to map the spatial distribution of the sediment characteristics to better understand the depositional setting of the shelf.

The results from the laboratory analysis allowed us to plot the spatial distribution of grain size and $CaCO_3$ and remark several trends:

- The mean grain size is higher on the samples collected at the more exposed shelf sectors to the waves (the northern and western shelves are windward and the southern and eastern shelves are leeward).

- The $CaCO_3$ content in the sediments tends to increase with depth.

- The carbonated skeletal particles have normally a higher grain size than the terrigenous particles, and that explains the grain size increase with depth of the sediments.

- There also appears to be a relationship between shelf width and the $CaCO_3$ content of the sediments, i. e., wider shelves have sediments with higher $CaCO_3$ content.

- The $CaCO_3$ content on sediments consists of carbonated skeletal particles of organisms, such as bryozoans, bivalves, gastropods and foraminifera.

REFERENCES

Baptista L, Berning B, Meimberg H, Melo C, Ávila SP, Curto M. A molecular analysis of the genus Reteporella (Bryozoa: Cheilostomata) in the remote Azores Archipelago. In preparation.

Baptista L, Santos A, Melo C, Rebelo AC, Madeira P, Cordeiro R, Botelho A, Hipólito A, Tavares J, Voelker A, Ávila S. Untangling the origin of the newcomer Phorcus sauciatus (Mollusca: Gastropoda) in a remote Atlantic archipelago. Marine Biology 2021, 168, 9. https://doi.org/10.1007/s00227-020-03808-5

Carduck S, Nitsche F, Rybarski A, Hohlfeld M, Arndt H, Diversity and phylogeny of percolomonads based on newly discovered species from hypersaline and marine waters, European Journal of Protistology 2021, 80, 125808. https://doi.10.1016/j.ejop.2021.125808

George KH. First data on benthic Copepoda of the Meteor cruise M150 Controls in benthic and pelagic BIODIversity of the Azores-Cruise M150 BIODIAZ. In preparation.

George, KH, Wölfl A-C Raw multibeam EM122 data: transits of METEOR cruise M150 (Atlantic). PANGAEA 2019, https://doi.pangaea.de/10.1594/PANGAEA.903545

George KH, Arndt H, Wehrmann A, Baptista L, Berning B, Bruhn M, Carvalho F, Cordeiro R, Creemers M, Defise A, Domingues A, Hermanns K, Hohlfeld M, Iwan F, Janßen T, Jeskulke K, Kagerer M, Kaufmann M, Kieneke A, Loureiro C, Madeira P, Meyer C, Narciso A, Ostmann A, Pieper C, Pointner K, Raeke A, Silva T, Springer B, Wilsenack M. Controls in benthic and pelagic BIODIversity of the AZores BIODIAZ. METEOR-Berichte, Cruise M150, Cádiz–Ponta Delgada, Aug 27–Oct 03, 2021, 74 pp.

George KH, Heitfeld J, Janßen T, Kieneke A, Stein T, Wehrmann A. Sublittoral meiofauna assemblages of three Azorean islands. In preparation.

Hohlfeld M, Meyer C, Schoenle A, Schmidt P, Filz P, Nitsche F, Arndt H. Biogeography, autecology and phylogeny of percolomonads based on newly described species. European Journal of Protistology, Submitted a.

Hohlfeld M, Schoenle A, Arndt H. Horizontal and vertical small-scale patterns of benthic protist communities at the abyssal seafloor. Deep-Sea Research Part I. Submitted b.

Kaufmann M, Springer B, Krahmann G, George KH Physical oceanography (CTD) during Meteor cruise M150. PANGAEA 2020, https://doi.pangaea.de/10.1594/PANGAEA.923929

Kieneke A, Araújo TQ, Hochberg R. Redescription of Crasiella azorensis Hummon, 2008 (Gastrotricha: Macrodasyida) by integrating mitochondrial and nuclear DNA sequence data and microscopy of specimens from São Miguel Island and Formigas Bank (Azores, Portugal). In preparation.

Kieneke A, Todaro MA. Discovery of two 'chimeric' Gastrotricha and their systematic placement based on an integrative approach, Zoological Journal of the Linnean Society 2021, 192, 710–735. Https://doi:10.1093/zoolinnean/zlaa117

Mitchell N, Zhao Z, Quartau R, Moreira S. Sediment transport flux across the shelf of an oceanic island from modelling geochemical data. In preparation.

Narciso A, Springer B, Hoppenrath M, Silva T, Cachão M, Kaufmann M. Pico- and calcareous nanophytoplankton distribution around the Azores Archipelago (Central North Atlantic). In preparation.

Quartau R, Moreira S, Zhao Z, Pombo J, Duarte J, Rodrigues, A. Sedimentary processes on Santa Maria Island shelf (Azores). In preparation.

Schoenle A, Hohlfeld M, Hermanns K, Mahé F, de Vargas C, Nitsche F, Arndt H. Tiny naked eukaryotes dominate diversity of eukaryotes on the deep seafloor. Nature Communications Biology, in revision.

Schoenle A, Hohlfeld M, Rosse M, Filz P, Nitsche F, Arndt H. Global comparison of bicosoecid Cafeteria-like flagellates from the deep ocean and surface waters, with reorganization of the family Cafeteriaceae. European Journal of Protistology 2020, 73, https://doi.org/10.1016/j.ejop.2019.125665

Schoenle A, Hohlfeld M, Hermanns K, Mahé F, de Vargas C, Nitsche F, Arndt H, High and specific diversity of protists in the deep-sea basins dominated by diplonemids, kinetoplastids, ciliates and foraminiferans. Communications Biology 2021, 4(501). https://doi.10.1038/s42003-021-02012-5

Schoenle A, Živaljić S, Prausse D, Voß J, Jakobsen K, Arndt H. New phagotrophic euglenids from deep sea and surface waters of the Atlantic Ocean (Keelungia nitschei, Petalomonas acorensis, Ploeotia costaversata). European Journal of Protistology 2019, 69, 102–116 https://doi.org/10.1016/j.ejop.2019.02.007

Zhao Z, Mitchell R, Quartau R, Moreira S, Rusu L. Threshold of deposition of carbonate-rich sediment on the insular shelf of Santa Maria Island, Azores. In preparation.

Živaljić S, Scherwass A, Schoenle A, Hohlfeld M, Quintela-Alonso P, Nitsche F, Arndt H. A barotolerant ciliate isolated from the abyssal deep-sea of the North Atlantic: Euplotes dominicanus sp. n. (Ciliophora, Euplotia). European Journal of Protistology 2020, 73. https://doi.org/10.1016/j.ejop.2019.125664

Živaljić S, Schoenle A, Scherwass A, Hohlfeld M, Nitsche F, Arndt H. Influence of hydrostatic pressure on the behaviour of three ciliate species isolated from the deep sea. Marine Biology, 2020, 167, 63. https://doi.org/10.1007/s00227-020-3673-3

M152/1

Tracing the unknown: offshore tsunami deposits

AUTHORS

RWTH Aachen University | Aachen, Germany
K. Reicherter, L. Feist, P. Bellanova, J. Schwarzbauer, C. Val-Peón, S. Lechthaler, H. Schüttrumpf

Johannes-Gutenberg University Mainz | Mainz, Germany
A. Vött

University of Cologne | Cologne, Germany
H. Brückner

Center for Marine Environmental Sciences (MARUM), University of Bremen | Bremen, Germany
J. Kuhlmann

University of Coimbra | Coimbra, Portugal
P. Costa

Complutense Universidad | Madrid, Spain
J.I. Santisteban

and the M152 scientific team

INTRODUCTION

In 1755 CE a strong earthquake-generated tsunami caused major inundations, sediment transport and transfer, as well as significant changes of the coastline along the Portuguese coasts. To date, mainly terrestrial coastal archives have been used to characterize various sedimentary parameters of tsunami layers. The continental shelfs, however, may provide extensive sedimentary and geochemical sedimentary archives to achieve a more complete insight into the Holocene tsunami record. While onshore records are more prone to be poorly preserved in time or have been corrupted by human interaction, offshore archives show great preservation potential especially in specific locations in submarine valleys and geomorphological sinks below the storm wave base. So far, only little is known about tsunami backwash processes, as well as about tsunami offshore deposits. In fact, only few offshore sedimentary archives have been studied with regards to tsunami research.

To study these offshore sedimentary records on the Algarve shelf (Portugal), the RV METEOR cruise M152/1 conducted a hydroacoustic profiling and coring campaign along two coastal perpendicular transects. Sub-bottom profiles and sediment cores are examined to study the sedimentological characteristics and the paleoenvironmental effects of event deposits and to assess the tsunami record of the Algarve. Our study aims at a better understanding of the hydrodynamic conditions and transportation processes in the offshore areas, especially regarding tsunami events and their sedimentary footprint. The collected data and samples are analysed in an interdisciplinary multi-proxy approach bringing together geologists, biologists, ecotoxicologists, coastal engineers, geographers and oceanographers.

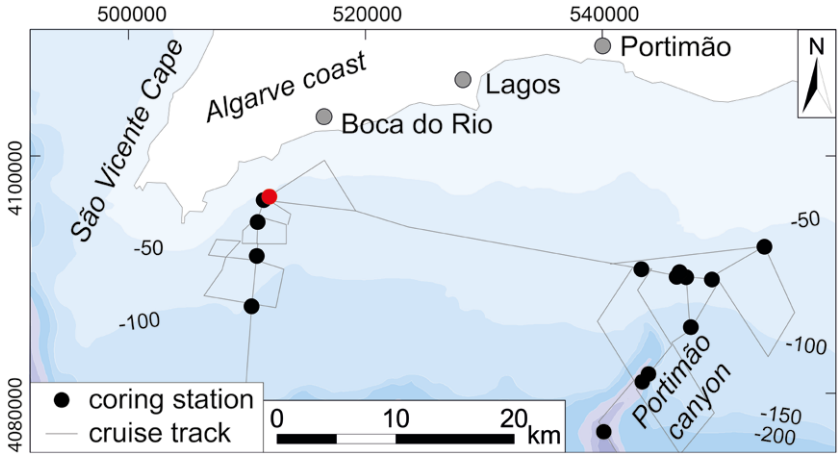

Fig. 1: Cruise track and coring stations of M152/1, the red station marks core GeoB23519-01.

MULTI-PROXY ANALYSES OF THE RETRIEVED CORES

At least two tsunami deposits (1755 CE and ca. 3.4 ka cal. BP) were detected in vibracores obtained from the Algarve shelf seafloor. A multi-proxy approach allowed to differentiate these event deposits from the background sedimentation:

In the upper parts of some cores, a thin layer of coarse silt/ fine sand stands out (e. g. 0.24–0.21 mbsf at GeoB23519-01). The sedimentary and geochemical features slightly contrast with the background. Based on the age-depth model, the layer correlates well to the 1755 CE Lisbon tsunami. The presence of a high pristane/phytane ratio, right below this upper event layer, signals anoxic conditions which often occur in the aftermath of a short-term high energy events, as event deposits seal the underlying strata from oxygen and light. The foraminifera assemblage revealed a lower diversity and density compared to the background sedimentation. In relation to the 1755 CE Lisbon tsunami, pollen samples from the over- and underlying sediments show similar pollen counts and concentration values. A patchy landscape of mixed Mediterranean forests and heathlands

coexist with open areas dominated by Asteraceae, probably due to greatest impact of human activities.

Based on sedimentological features, granulometry and composition, a distinctive ca. 3.4 ka cal. BP layer sharply contrasts with the background sediment. The abrupt distinction of the event layer from the background sedimentation is marked by an erosive base, a complex structure, coarser texture, and distinctive geochemical and geophysical features. A specific deposit configuration with four distinctive sub-units is preserved in cores GeoB23519-01 and 19-02 (1.53–1.18 mbsf). The lowermost part of the deposit shows an erosive base and indications of a traction carpet mode of transport or increasing transport capacity with velocity. A changing foraminifera assemblage indicates mixing features of the event layer and the background material. To form the following massive medium sand sub-unit, a short-term, but high-energy regime and increased transport capacity are needed. Especially in the lower parts of this sub-unit an enrichment in terrestrial organic geochemical markers (n-alkanes, n-aldehydes, phytol) is visible. Interestingly, all these terrestrial markers show variances within the layer, which can be related to different mechanisms during the event or to different phases during a backwash. A general fluvial-driven input of terrestrial material and associated organic compounds onto the Algarve shelf can be seen in the background sedimentation. However, the sudden and significantly enriched concentration shift within the ca. 3.4 ka cal. BP layer indicates the input of large amount of terrestrial material, far more than solely providable by fluvial processes. During a tsunami, large terrestrial areas get inundated, especially areas that are unaffected by riverine activity, thus a significant enrichment of allochthonous terrestrial material and associated organic compounds can be assumed as a potential source for this layer. The foraminiferal assemblage shows a lower diversity and density compared to the background sedimentation, as well as a significant amount of shallow water species that indicate the transport of shallow water taxa towards deeper areas as a consequence of the tsunami backwash. Planktic foraminifera decreased compared to the background and taphonomic features such as abraded tests were identified. Besides the described backwash-driven flow along the seafloor, tsunami backwash can also cause a suspension cloud of fine material, which settles over time and may have formed the normally suspension-graded sub-unit IV. The ca. 3.4 ka cal. BP layer presents a broad longitudinal distribution on the shelf and is traceable from ca. 40 m up to 70 m water depth in the sub-bottom profiles and cores from both, the western and eastern transect. Regarding the ca. 3.4 ka cal. BP event, pollen samples were sterile. Those from the overlying and underlying sediments reached the minimum count of 150 pollen grains and display similar concentration values. From a paleoenvironmental point of view, the landscape was dominated by mixed Mediterranean forests, Mediterranean shrublands, and heaths. Thus, pollen samples indicate similar vegetation before and after the event, so it is not possible to trace any specific continental input in the pollen signal related to the tsunami backwash. A correlation of this event layer with the onshore record of the Algarve is not possible as no paleo-tsunami deposits of this period are known. Nevertheless, the event layer may be associated with paleo-tsunami deposits along the Spanish and Moroccan Gulf of Cádiz with similar ages.

We conclude that offshore tsunami (backwash) research is as yet limited and focuses on specific locations along the shelf. Thus, observed characteristics are strongly site-specific. A thin event layer in the upper parts of some of our cores correlates chronologically with the 1755 CE Lisbon tsunami. Based on the sedimentological and compositional features of the well-preserved ca. 3.4 ka cal. BP event layer, its lateral distribution on the shelf, and increased terrestrial influence, a tsunami backwash scenario can be acknowledged for the formation of this deposit. Thus, our results complement the Algarve's tsunami record with this novel ca. 3.4 ka cal. BP paleo-tsunami. Concisely, offshore sedimentary shelf archives show the potential to extend and improve the understanding of a region's tsunami history, especially when coastal records are incomplete or sparse (De Martini et al., 2021).

OTHER STUDIES RELATED TO M152/1

In order to obtain further information on contaminated areas in connection with the environmental impact of microplastics, water surface samples and (deep sea) sediment were taken and analyzed (Lechthaler et al., 2020). Microfibres, 3 black fibres, were visually detected in 2 of the 20 sediment samples without verifying their polymeric identity. Assuming that they are microplastics, concentration from 0.00–0.29 particles/g dry sediment result. In the eleven water samples, 81.8 % contained microplastics including polymeric identification (0.00–14.09 particles/m^3) with an average contamination of 1.36–4.03 particles/m^3. A significant positive correlation between the microplastic concentration in the water and the average water depth during sampling was identified. This regional study is one of a few that analyzed also deep-sea sediment and provides results about microplastics as anthropogenic contaminants south of the Algarve coast.

The SW coast of the Iberian Peninsula experiences a lack of paleoenvironmental and archaeological data. With the aim to fill this gap, we contribute with a new palynological and geochemical dataset obtained from a sediment core drilled in the continental shelf of the Algarve coast (Val-Peón et al., 2021). Archaeological data have been correlated with our multi-proxy dataset to understand how human groups adapted to environmental changes during the Early-Mid Holocene, with special focus on the Mesolithic to Neolithic transition. Vegetation trends indicate warm conditions at the onset of the Holocene followed by increased moisture and forest development ca. 10–7 ka BP, after which woodlands are progressively replaced by heaths. Peaks of aridity were identified at 8.2 and 7.5 ka BP. Compositional, textural, redox state, and weathering of source area geochemical proxies indicates abrupt palaeoceanographic modifications and gradual terrestrial changes at 8.2 ka BP, while the 7.5 ka BP event mirrors a decrease in land moisture availability. Mesolithic sites are mainly composed of seasonal camps with direct access to the coast for the exploitation of local resources. This pattern extends into the Early Neolithic, when these sites coexist with seasonal and permanent occupations located in inland areas near rivers. Changes in settlement patterns and dietary habits may be influenced by changes in coastal environments caused by the sea-level rise and the impact of the 8.2 and 7.5 ka BP climate events.

REFERENCES

Costa PJM, Feist L, Dawson A, Stewart I, Reicherter K, Andrade C, 2020. Offshore tsunami deposits, Chapter 11. In: Shiki T et al. (eds.) Tsunamiites - Features and Implications, 2nd Edition. https://doi.org/10.1016/B978-0-12-823939-1.00011–2

Costa PJM, Lario J, Reicherter K accepted 2021. Tsunami deposits in Iberia: a succinct review. In: Álvarez-Martí-Aguilar M, Machuca-Prieto F (eds) Historical Earthquakes and Tsunamis in the Iberian Peninsula: An Interdisciplinary Dialogue. Springer, Heidelberg, Germany, Chapter 2 pp.

De Martini PM, Bruins HJ, Feist L, Goodman-Tchernov BN, Hadler H, Lario J, Mastronuzzi G, Obrocki L, Pantosti D, Paris R, Reicherter K, Smedile A, Vött A, 2021. The Mediterranean Sea and the Gulf of Cadiz as a natural laboratory for paleotsunami research: Recent advancements. Earth Sci Rev, 216, 103578. https://doi.org/10.1016/j.earscirev.2021.103578

Lechthaler S, Schwarzbauer J, Reicherter K, Stauch G, Schüttrumpf H, 2020. Regional study of microplastics in surface waters and deep sea sediments south of the Algarve Coast. Regional Studies in Marine Science, 40, 101488. https://doi.org/10.1016/j.rsma.2020.101488

Reicherter K, Vött A, Feist L, Costa PJM, Schwarzbauer J, Schüttrumpf H, Jens H, Raeke A, Huhn Frehers K, 2019. Lisbon 1755, Cruise No. M152/1, 02.11.–14.11.2018, Funchal (Portugal)-Hamburg (Germany): cruise report. METEOR-Berichte M152/1. https://doi.org/10.2312/cr_m152

Val-Peón C, Santisteban JI, López-Sáez JA, Weniger GC, Reicherter K, 2021. Environmental changes and cultural transition in SW Iberia during the Early-Mid Holocene. Appl. Sci. 2021, 11, 3580. https://doi.org/10.3390/app11083580

M152/2

Structural evolution and disintegration of oceanic intraplate volcanoes: The Bathymetrists Seamount Province and its relation to Sierra Leona Rise (eastern equatorial Atlantic)

AUTHORS

University of Hamburg | Hamburg, Germany
C. Hübscher, M. Hartge, T. Häcker, J. Preine, E. Seidel

King Abdullah University of Science and Technology | Thuwal, Saudi Arabia
F. van der Zwan

GEOMAR Helmholtz Centre for Ocean Research Kiel | Kiel, Germany
N. Augustin

OBJECTIVES

The Bathymetrists Seamount Province (BSP; Figure 1) lies north of the Sierra Leone Rise (SLR), a volcanic platform in the eastern Atlantic Ocean between 6° and 9° N. These submarine volcanoes cluster along W–E, N–S, and NE–SW trends, indicating structural control of volcanogenesis. However, melt origins are unknown and may be related to plume volcanism or decompression melting beneath previously unstudied faults and deep transcurrent faults. Building on existing petrologic-geochemical sampling from the Bathymetrists seamounts, the expedition was designed to test the hypothesis that seafloor volcanism of the Bathymetrists seamounts was fed by decompression melting resulting from small-scale convection cells that formed beneath the crust-mantle boundary (Moho) deepening to the Sierra Leone Sill. By means of geophysical profiling and dredge sampling, the particular aims were (1) to understand the interaction between crustal thickness, tectonics and volcanic phases; (2) to investigate the chronological evolution of individual seamounts and seamount chains; (3) to study the structural growth process of elongated seamounts; and (4) to review trigger mechanisms, transport processes and volumes of slope failures.

M152/2 UNDERWAY GEOPHYSICS AND SAMPLING

The objectives were addressed by more than 4000 km high-resolution multi-channel reflection seismic and more than 5000 km of parametric echosounder (Parasound), multi-beam echosounding (EM122), and gravity and magnetic profiles. Rock samples for ground truthing and geochemical research have been collected during 14 dredge stations. As a secondary objective we further determined the concentrations in surface seawater and air and the state of air-sea exchange of a number of nowadays globally banned pesticides and their derivatives.

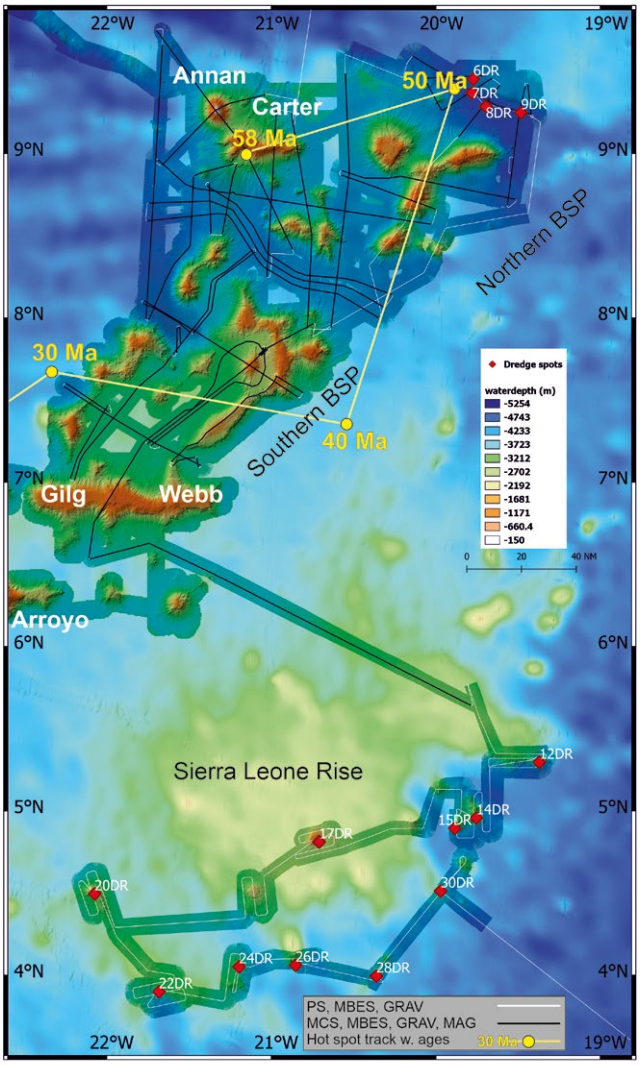

Fig. 1: M152/2 ship track with multi-channel seismic (MCS) profiles and dredging sites. GRAV: gravity; MAG: magnetics; PS: Parasound; MBES: multibeam echosounder. Hot spot track after Long et al. (2020).

RESULTS

BATHYMETRY (VAN DER ZWAN ET AL., IN PREP.)

The joint MBES map resulting from MSM70 (van der Zwan et al., 2018) and M152/2 (Hübscher et al., 2019) covers a total seafloor area of >80,000 km^2 between 10.2°N/23.5°W and 5.3°N/15.5°W (NW and SE corners respectively) with a cell size of 50 m, including a total of 40 seamounts, parts of the Cape Verde Ridge and of the Guinea Fracture Zone (Fig. 1). The mapped seamounts are 5 to 139 km in length and 710 m to 3,930 m in height. The base of the seamounts lays between 4,200 and 3,400 m

depth. While there is no systematic variation in the basal depth, the seafloor enclose between a group of seamounts is always shallower than the seafloor on the outer part of the group. Most of the seamounts have pronounced flat tops and can be described as large guyots. Their summits lay mostly in depths of around 1,000 and 2,000 m but can rise up to a minimum depth of about 210 m and 290 m below sea level in the case of Annan and Arroyo, respectively. Even though talus and gullies deform the original seamount shapes, their main orientation is E–W 85°and SW–NE 50°.

AGE CONSTRAINS

According to petrological analysis of MSM70 samples (Long et al., 2020), the northern BSP evolved first from west to east 58–50 Ma (Fig. 1). The southern BSP emerged east to west 40–30 Ma.

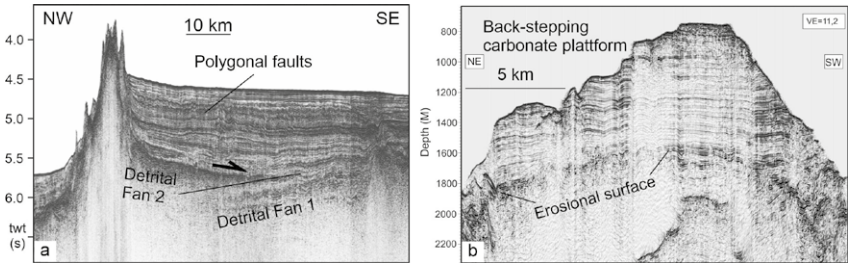

Fig. 2: a) Seismic time section crossing the western rim of the southern BSP and its inner sea sediment infill (Hübscher et al., 2019). b) Seismic depth section showing a carbonate platform the developed on top of a guyot (Häcker, 2020).

A straight forward method for determining the relative age succession between adjacent seamounts by means of seismic interpretation is studying the stacking or onlap pattern of their detrital fans. An instance from the southern BSP is shown in Fig. 2a. The detrital fan from the western seamount chain onlaps the one from the east. Consequently, the western seamount emerged later, which is also consistent with Long et al. (2020).

To develop another method for determining the relative age sequence, Häcker (2020) took the approach of estimating the age of the basal erosion unconformity and the onset of carbonate production through backstripping and subsidence calculations. Fig. 2b shows a depth converted seismic section across one of the carbonate plattforms. This erosional unconformity constrains the carbonate platforms of the guyots downward. The age of the erosional unconformity is also the time after which no significant structural overprinting of the seamount by volcanism has occurred. According to these calculations, the latest time of volcanic activity in the north (Seamount Carter) is 10 Myr before the latest end of volcanism in the south (Seamount Gilg). This relative sequence of development is also consistent with the petrologic results of Long et al. (2020).

POST-VOLCANIC MAGMATISM AND HYDROTHERMAL ACTIVITY

Radaelli (2021) studied magmatic activity and associated fluid flow in the area between the northern and southern BSP. An example is shown in Fig. 3. The data give a clear indication that magma also intruded into or overlapped the sedimentary cover after the volcanic phase. Furthermore, Radaelli (2021) found evidence of Pleistocene to Holocene hydrothermal activity. Recent activity seems likely.

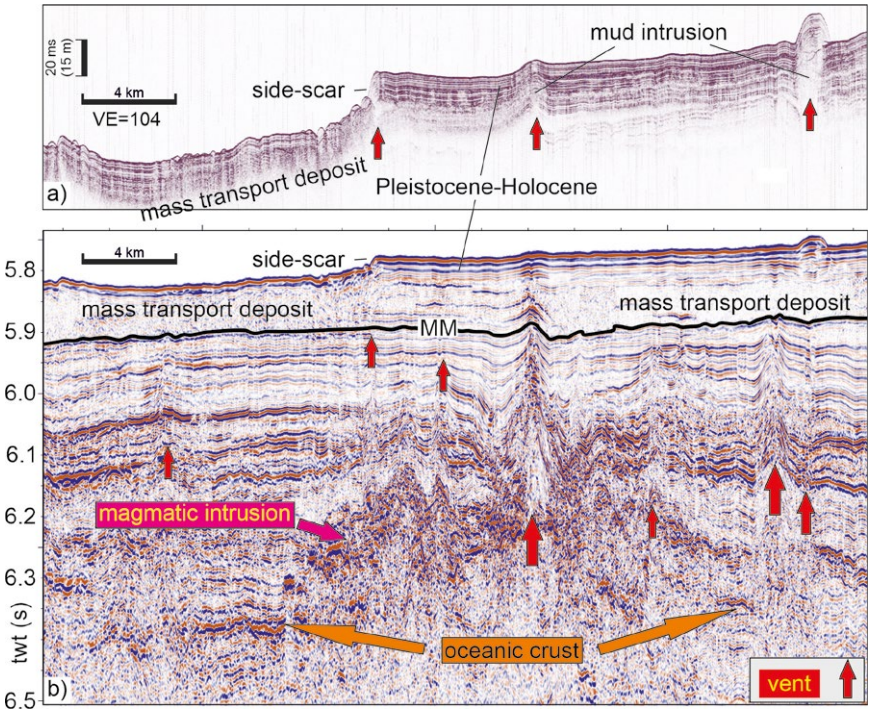

Fig. 3: Parasound (a) and multi-channel seismic (b) line across magmatic intrusion and associated vents. Mud intrusions and mass wasting shape the seafloor.

Hartge (2019) examined bottom simulating reflections (BSR) in seismic data and explained it by diagenesis from Opal-A to Opal-CT. Mapping the depth of this diagenesis front allows estimating of the geothermal gradient from seismic data. This BSR can serve as a proxy for spatial variation in heat flow and thus can be used to identify hot cells in the BSP. Heat flow is elevated both above a studied transform fault and on a volcanic flank. This is interpreted as an indication of magmatic activity. In addition, the correlation of the BSR with fluid upwellings is indicative of hydrothermal activity.

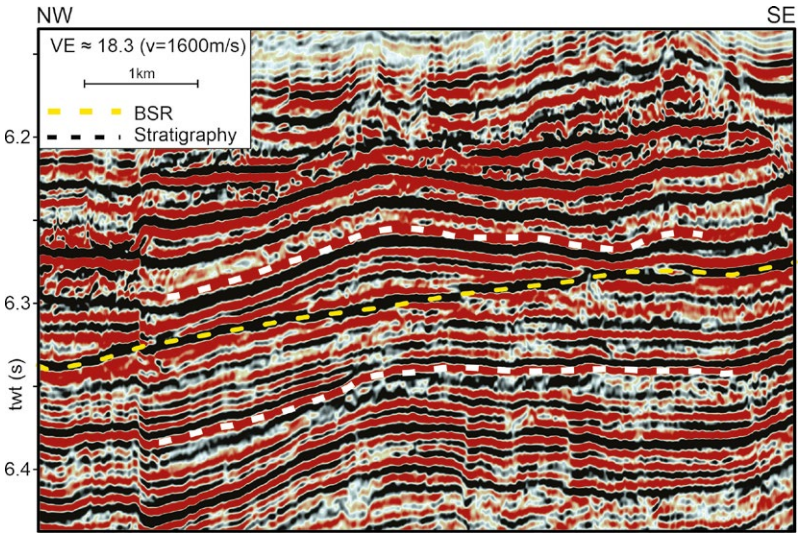

Fig. 4: Seismic time section showing BSR as result of Opal-A to Opal-CT diagenesis (Hartge, 2019). The polarity of the BSR is positive as the sea-floor reflection (not in section).

REFERENCES

Häcker, T., 2019. Altersbestimmung ausgewählter Bathymetrists Seeberge anhandseismischer Profile. BSc-thesis at University of Hamburg (un-published).

Hartge, M., 2019. Opal Conversion related Bottom Simulating Reflector as a Proxy for Heat Flow in the Vicinity of the Bathymetrists Seamounts. BSc-thesis at University of Hamburg (un-published).

Hübscher, C., van der Zwan, F., Grob, H., Häcker, T., Hartge, M., Huster, H., Kretzschmann, L., Lampridou, D., Otte, F., Preine, J., Raeke, A., Schäfer, W., Schade, M., Seidel, E., Warwel, A., Wehmeier, L., Winter, S., 2019. Structural evolution and disintegration of oceanic intraplate volcanoes: The Bathymetrists Seamounts and its relation to Sierra Leona Rise (eastern equatorial Atlantic), Cruise No. M152/2, 03.01.–12.02.2019, Las Palmas (Spain) – Walvis Bay (Namibia), SEDIS. DOI: 10.2312/cr_m152_2.

Long, X., Zwan, F.M. van der, Geldmacher, J., Hoernle, K., Hauff, F., Garbe-Schönberg, C.-D., Augustin, N., 2020. Insights into the petrogenesis of an intraplate volcanic province: Sr-Nd-Pb-Hf isotope geochemistry of the Bathymetrists Seamount Province, eastern equatorial Atlantic. Chem Geol 544, 119599. https://doi.org/10.1016/j.chemgeo.2020.119599

Radaelli, M., 2021. Seismostratigraphic and geomorphological characterization of magmatic intrusions and mud volcanoes in the area of the Bathymetrists Seamounts, Central Eastern Atlantic. MSc-thesis at University of Milano (un-published).

van der Zwan, F. M., 2018. BATHYCHEM The effect of intraplate volcanism on the geochemical evolution of 1074 oceanic lithosphere: Detailed mapping and sampling of the Bathymetrists Seamounts and adjacent 1075 fracture zones, December 26, 2017-February 01, 2018 Mindelo (Cape Verde)-Las Palmas de Gran 1076 Canaria, Canaries (Spain), http://oceanrep.geomar.de/id/eprint/45754.

M153

Trophic Transfer Efficiency in the Benguela Current TRAFFIC

AUTHORS

Leibniz Centre for Tropical Marine Research | Bremen, Germany
W. Ekau, T. Rixen

The cruise METEOR 153 (M153) is a joint effort of several German, Namibian and South African institutes, and contributes to the project TRAFFIC. The overall objective is to expand our knowledge about processes that drive the trophic structures in the northern (nBUS) and southern Benguela Upwelling Systems (sBUS) and govern associated impacts on fisheries and climate. Despite similar primary production rates, there are significant differences in the composition and biomass of fish stocks and top predators. Furthermore, while the nBUS is a substantial source of CO_2 to the atmosphere, the sBUS acts as CO_2 sink. Our aim is to study the food web structure and its functional links in order to analyse the trophic transfer efficiency (TTE) and associated effects on the biologically mediated CO_2 uptake. We hypothesise that, in the nBUS, the pelagic food web structure produces lower fishery yields and higher CO_2 emission whereas, in the sBUS, a more efficient trophic transfer produces higher fishery yields and a net CO_2 uptake.

During M153, different gears have been deployed to measure CO_2 fluxes as well as carbon exports into the deep sea, to assess primary production, and metabolic rates of zooplankton, and fish. Results will be used to develop conceptual models of the two subsystems, explaining how changes in the ecosystem structure affect fisheries and the biologically mediated CO_2 fluxes.

The cruise M153 started on 15 February 2019 in Walvis Bay, Namibia, and ended on 31 March 2019 in Mindelo, Cape Verde Islands. A total of 70 stations, mostly arranged along transects perpendicular to the coast, could be worked up in the Namibian and South African waters. The entire working area reached from about 11°30′ E to the coast and from 20° to 32°S.

Hydrographical investigations were conducted to describe the distribution of water masses in the area and their influence on the shelf and the shallow coastal waters. Vertical profiles of conductivity, temperature, pressure, oxygen, fluorescence, turbidity and photosynthetically active radiance (PAR) were measured during 109 casts at 62 stations.

A high speed remotely operated towed vehicle (ROTV, TRIAXUS, fig. 5.3.1) was deployed on 6 transects to produce transect profiles of temperature, salinity, oxygen, nitrate, and plankton abundance.

To determine C/N/P ratios in the upwelled water, total dissolved inorganic carbon concentration (DIC) and nutrients have been measured in a total of 835 water samples obtained from the CTD rosette at 53 stations. To determine C/N/P ratios in the exported organic matter, four drifter arrays equipped with five sediment traps were deployed at 24-hour and 48-hour stations and four long-term mooring systems have been deployed off Namibia and South Africa. Underway measurements of CO_2 in the water and atmosphere were performed to assess CO_2 uptake and release of the ocean.

Various nets were used to catch different size and taxonomic groups of plankton. An APSTEIN net with 20 µm mesh size was deployed at all phytoplankton stations by hand to collect material between 5 m depth and the surface.

For meso zooplankton a HYDROBIOS MULTINET MIDI (mouth area 0.25 m^2) multiple opening/closing net system was deployed, equipped with five nets (200 µm mesh size) in order to collect vertically stratified mesozooplankton samples. In total, 51 hauls could be realised. For larger mesozooplankton organisms and ichthyoplankton, a towed HYDROBIOS MULTINET MAXI, an RMT and a neuston catamaran were used to estimate the horizontal and vertical distribution of the ichthyoplankton and to assess the zooplankton biomass. The Rectangular Midwater Trawl (RMT) served for large scale overviews on the species communities of epipelagic and mesopelagic fishes.

Underway acoustic measurements by means of an EK80 echosounder were undertaken to estimate biomass and size distribution of pelagic organisms in the areas.

After finishing station work in Namibia, another 13 stations were set on the transit to Mindelo deploying CTD, multinet and neuston catamaran to validate acoustic and chemical underway measurements.

M154

Investigation of sector collapse deposits in the Bouillante-Montserrat Graben – Sector collapse kinematics and tsunami implications

AUTHORS

GEOMAR Helmholtz Centre for Ocean Research Kiel | Kiel, Germany
C. Berndt, D. Kunde, J. Elger, A. Dannowski, S. Kutterolf

Christian-Albrechts-University | Kiel, Germany
M. Kühn, C. Böttner, S. Krastel

University of Bremen | Bremen, Germany
K. Huhn, T. Freudenthal, J. Kuhlmann, R. Gatter

INTRODUCTION

Deep-seated collapses of volcanic islands generate the most voluminous short-term (<1 week) mass movements on Earth. These mass flows are known to trigger large tsunamis. The way in which collapse events emplace mass transport deposits is poorly understood, even though this emplacement process determines the scale of associated tsunamis. Key questions such as whether sector collapse deposits are emplaced in single or multiple events, how they may incorporate seafloor sediment to increase their volume, and how they are related to volcanic eruption cycles and the migration of volcanic centers, remain to be answered. Cruise M154 is part of the comprehensive study of large volcanic island landslide deposits off Montserrat and is directly linked to the IODP drilling campaign in the Lesser Antilles (IODP Expedition 340). Expedition 340 only recovered material from a single site within the volcanic landslide deposits off Montserrat, and even at this site, recovery was not continuous. Through the Meteor cruises M154/1 and M154/2 we were able to document the lateral variation of the well-constrained Deposit 2 (Lebas et al., 2011; Watt et al., 2012), which is critical for understanding how it was emplaced. The main scientific goals of the project are to determine where sector collapses are sourced from; to understand how the mass transport deposits are emplaced; and to understand the relationship between sector collapse, eruption cycles and initiation of new volcanic centers. Combining 3D seismology (M154/1) and MeBo cores (M154/2) provides a unique dataset of the internal structure, composition and source of material throughout a volcanic island landslide.

REFLECTION SEISMIC IMAGING

During M154-1 we acquired a comprehensive geophysical data set including several hundred line kilometers of 2D MCS seismic data and a high-resolution 3D seismic cube

(Figure 1). The 2D seismic data image the extent of the landslide deposits south of Montserrat and recent tectonic activity related to extension across the Bouillante-Montserrat Graben. Interestingly normal faults caused by this extension are the sites of the highest heat flow values measured across the Lesser Antilles (Hornbach et al., 2021). The 3D seismic data image the central and distal parts of Deposit 2 – the best studied mass transport deposit off Montserrat which reaches from the shoreline of Montserrat to the southeast and straddles the adjacent southern Kahouanne Seamounts. The 3D seismic data resolve the important transition from Deposit 2a to 2b. Deposit 2 runs up onto the flank of the Kahouanne Seamounts which is an important boundary condition to determine the initial velocity of the slide material – one of the most important objectives of the cruise.

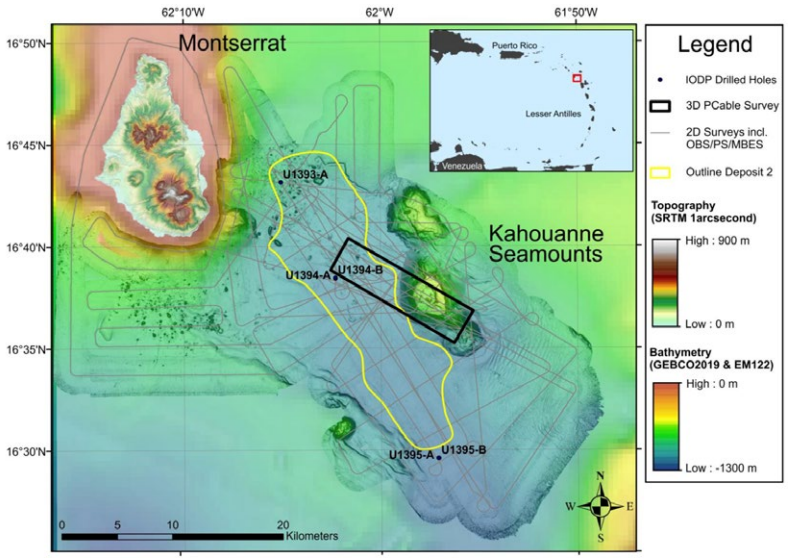

Fig. 1: Seismic surveys carried out during M154/1.

WIDE ANGLE SEISMIC IMAGING

The seismic P-wave velocities of Deposit 2 are necessary to determine the size and depth of the landslide deposit. The P-wave velocities have been derived by forward modeling based on seismic wide-angle reflection and refraction data of six ocean bottom seismometers (OBS) (Kunde, 2020). The forward modeling results were compared to a first-arrival travel time tomography. The 37 km-long profile covers the two largest known mass transport deposits off Montserrat, i. e. Deposit 2 and Deposit 8 (Figure 2). The P-wave velocities within the landslide deposits are in the range of 1700 to 1800 m/s, which is significantly lower than assumed in previous studies that used lower frequency wide angle data. Those studies resulted in velocities about 2000 m/s (Paulatto et al., 2010). Our results are more consistent with IODP borehole data and landslide deposits

elsewhere. They are consistent with a predominantly sedimentary composition of the landslide deposits as opposed to a potential volcanic origin. The shallower Deposit 2 is separated into two parts by a stratified seismic unit. The OBS results show no evidence, that the two parts differ significantly in velocity and composition. However, the stratified layer shows lower P-wave velocity and may consist of hemipelagic rather than volcaniclastic sediments. The results of the travel time tomography are consistent with the forward modeling and earlier work in the area.

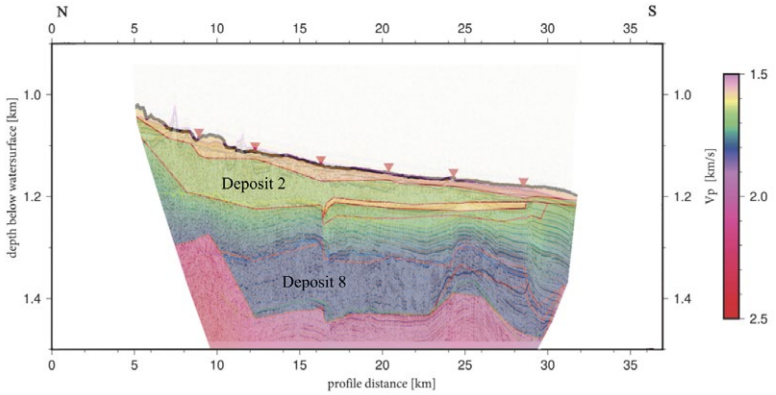

Fig. 2: Best-fitting P-wave velocity model derived from forward modeling of ocean bottom seismometer data (Kunde, 2020).

MEBO70 DRILLING, BOREHOLE LOGGING AND GRAVITY CORING

As major aim of M154-2 was to sample slid masses and undisturbed slope segments off Montserrat, ten MeBo cores at six locations were drilled (Figure 3). In addition, a comprehensive borehole logging program was carried out at five of these sites, in which, a Spectrum Gamma Instrument (SGR), a magnetic susceptibility (MagSus) and Acoustic probe were successfully utilized. These data were supplemented by a newly developed CPT (cone penetration test) probe which was successfully used to measure in situ sediment physical properties. First results point to large variations of physical properties in different sectors of the volcano (BSc Leonie Hönekopp, 2019).

Two MeBo sites were located in the vicinity of IODP Site U1394 in the central part of Deposit 2 (GeoB23714; GeoB23725; Figure 3). In contrast to previous studies, which described a sediment cover of only 5 to 10 m, new PARASOUND data and core materials collected during this expedition revealed that Deposit 2 is overlain by up to 40 m of drape at the graben center where tectonic offsets created accommodation space which hosts several thin younger mass wasting deposits (MSc Olatunde Salami, 2020). Site GeoB23725 was drilled to 55.3 mbsf and penetrated the potential boundary layer between Deposit 2a and 2b. In addition, Deposit 2 was also sampled and logged in the

outer part at Site GeoB23702 down to a depth of 30.3 mbsf and at its edge close to the Kahouanne Seamount down to 25.3 mbsf (GeoB23730). Core recovery was very variable at the different parts of the slide deposit; however, we were able to sample all lithologies at different depth levels including the sediments above and below the potential interface between Deposits 2a and 2b.

Site GeoB23711 served as a reference site slightly north of the slid masses (Figure 3). With a maximum drill depth 70.3 mbsf, both sediment sections associated with Deposit 2 but also sediments older than the concerned volcanic event were drilled. A particularly interesting observation is that two coarse volcaniclastic layers were sampled at a depth of 21.8 mbsf and 28.5 mbsf. Such deposits originate from high energy events associated with volcanic flank collapses. A first interpretation reveals that the shallow layer might correlate with the Deposit 2 horizon. This observation raises the question of how two such high energy volcanic events can travel to such a distal location and fit into the history of the Montserrat volcanic island. Site GeoB23731 serves as a second reference core outside Deposit 2 but south of Montserrat.

This MeBo program was accompanied and supplemented by gravity coring. In total, 21 gravity cores were collected in the vicinity of Deposit 2. In addition, a box corer was deployed eight times, and a grab sampler three times.

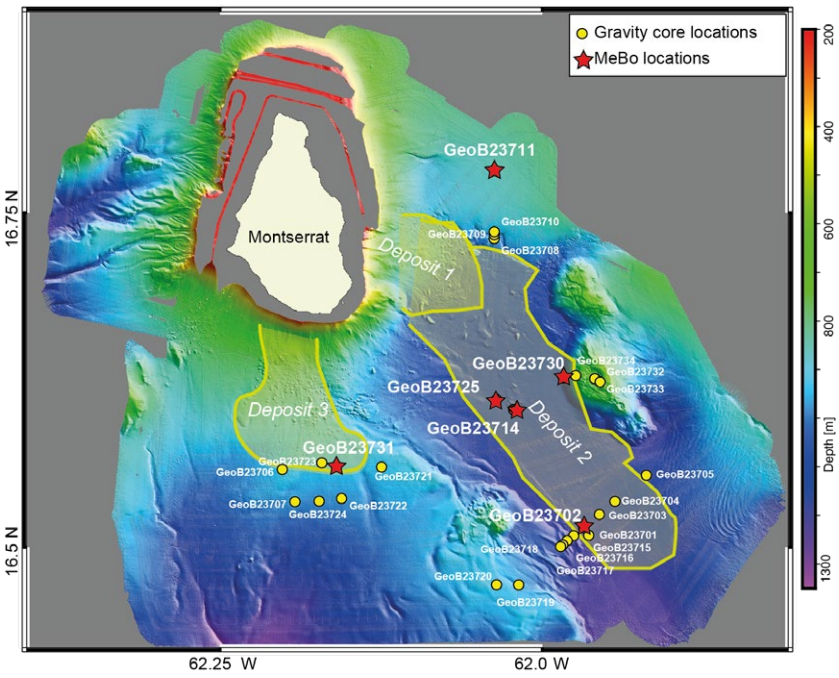

Fig. 3: Working area of M154-2 offshore Montserrat. Bathymetry data were collected during both legs M154-1 and M154-2. Gravity cores are marked by yellow circles and MeBo sites by red stars.

SUMMARY OF PRELIMINARY RESULTS

In spite of adverse weather conditions during the first half of M154/1, we collected a substantial geophysical data set that will allow to address the scientific objectives. As the DFG project to evaluate the data has only started eight months ago, the data evaluation is far from complete and most of the results are so far based on onboard processing of the 2D seismic and hydroacoustic data and the completion of a MSc thesis (Kunde, 2020) that documents the OBS data evaluation. Preliminary results suggest that the main scientific target Deposit 2 definitely consists to a large extent of mobilized seafloor material and is not primarily composed of volcanic flank material. There are indications that it may be sourced from two separate debris flows. As expected before the experiment, the debris flow ran up onto the Kahouanne Seamounts, but the height difference is small suggesting low flow velocities during emplacement. This reconstruction and its implication for tsunamis is the focus of the ongoing work.

The sediment samples collected during M154-2 provide a unique dataset of the internal structure, composition and source of material throughout a volcanic island landslide. Sediments drilled at the location of Deposit 2 consist of massive turbidite sand layers containing both volcanic and bioclastic material rather than volcanic blocks. Intervals of hemipelagic mud and thin turbidites within Deposit 2 most likely represent intervals of remobilised sea floor sediment. In addition, first stratigraphic analyses of sediment samples particularly at the distal site GeoB23702 support the assumption that Deposit 2 consists of two individual events which would explain the internal-reflector-package between Deposits 2a and 2b (i. e. it represents intervening sedimentation (likely volcaniclastic and bioclastic sands, ponded on the Deposit 2a surface). However, this can only be clarified by further sedimentological analyses (including an age dating, detailed compositional analyses of the clast inventories) which will be carried out in the frame of a recently started PhD project funded by the DFG.

REFERENCES

Hornbach, M. J. et al. A Hybrid Lister-Outrigger Probe for Rapid Marine Geothermal Gradient Measurement. Earth and Space Science 8, 1–12 (2020).

Kunde, D. Seismic velocity of sector collapse deposits off Montserrat. MSc Thesis, Christian-Albrechts-University of Kiel, 2020.

Lebas, E. et al. Multiple widespread landslides during the long-term evolution of a volcanic island: Insights from high-resolution seismic data, Montserrat, Lesser Antilles. Geochem. Geophys. Geosyst. 12, (2011).

Paulatto, M et al. [2010]. “Upper crustal structure of an active volcano from refrac-tion/reflection tomography, Montserrat, Lesser Antilles”. Geophysical Journal International 180 (2), pp. 685–696.

Watt, SFL et al. [2012]. “Combinations of volcanic-flank and seafloor-sediment fail-ure offshore Montserrat, and their implications for tsunami generation”. Earthand Planetary Science Letters 319, pp. 228–240.

Hönekopp, L. Korrelation von in situ- und Kernmessungen der Expedition M154-2 zur Identifizierung von vulkanischen Aktivitätszyklen auf Montserrat (Kleine Antillen). (BSc Thesis, Universität Bremen, 2019.

Salami, O. Analysis of shallow mass-transport deposits offshore Montserrat island using Parasound and sedimentary core data for sedimentological characterization (MSc Thesis, Universität Bremen, 2020).

M155

The tsunamigenic gravitational flank collapse of Fogo volcano, Cape Verde Islands and MSM87 – Seismic pre-site survey for an IODP site on the Cape Verde Plateau

AUTHORS

Kiel University | Kiel, Germany
S. Krastel

GEOMAR Helmholtz Centre for Ocean Research Kiel | Kiel, Germany
S. Kutterolf

University of Bremen | Bremen, Germany
A. Klügel

Cardiff University | Cardiff, UK
R. Ramalho

INTRODUCTION

The objectives of the RV METEOR Cruise M155 (May/June 2019) addressed two independent objectives. The first, main objective was the investigation of the deposits of a flank-collapse of Fogo Volcano, which triggered a mega-tsunami approximately 73,000 years ago. The tsunami deposits mapped in the nearby island of Santiago documented run-up heights of more than 270 m (Ramalho et al. 2015). The main goal of Cruise M155 was to determine the geometry, extension, volume, sedimentological characteristics and stratigraphy of the flank-collapse deposits in order to reconstruct the generation and impact of a megatsunami, directly linked to a study of its trigger mechanism. The second objective of Cruise M155 was to collect new high-resolution seismic data as a pre-site survey for an IODP full-proposal, to develop a seismic stratigraphic framework for the Cape Verde Plateau. This data could not be collected due to a compressor failure during Cruise M155 but it was possible to schedule a short cruise in Nov 2019 (MSM87) in order to collect the seismic site survey data.

THE TSUNAMIGENIC GRAVITATIONAL FLANK COLLAPSE OF FOGO VOLCANO, CAPE VERDE ISLANDS

The hydroacoustic data show that the Monte Amarelo flank collapse was much more laterally extensive than previously estimated (Barret et al 2020). The Monte Amarelo deposits proximal to Fogo (MTD-A; distribution shown in Fig. 1a) are characterized by overlapping diffraction hyperbolae (Fig. 1b). We note a progressive transition in the acoustic signature of the deposits from a hyperbolic facies with meter-scale acoustic penetration to a mounded facies draped by ~1.5 m of sediment (Fig. 1c). Southwards,

with increasing distance from Fogo, the acoustic character of the Monte Amarelo deposits changes from being hyperbolae-dominated to being characterized by an acoustically transparent facies (MTD-B; Fig. 1d). A strong internal reflector is imaged in places within the deposits (Fig. 1d). These observations suggest that the deposition of hummocky volcanic debris originating from the failed eastern flank most likely triggered the contemporaneous, multi-phase failure of pre-existing seafloor sediments.

The high-resolution reflection seismic data provide evidence that the Monte Amarelo collapse was a multiphase collapse. The data clearly show the debris avalanche deposits, which are characterized by a hummocky surface with several large blocks and a chaotic seismic facies (Fig. 2). The base of the uppermost debris avalanche deposits can be easily traced. A second debris avalanche deposit is imaged directly beneath, which can be traced even in close proximity of Fogo (Fig. 2). The stacked debris avalanche deposit indicate that the Monte Amarelo collapse was a multiple-phase event (at least two phases). The newly collected high-resolution multichannel-seismic data also allow to image the deeper structures of the volcaniclastic apron surrounding Fogo and the southern Cape Verde Archipelago. The data show a widespread high amplitude reflection package separating a lower sedimentary unit characterized by deformed reflectors and indications for volcanic intrusions and an upper unit which is characterized by abundant mass transport deposits of several sizes in some areas but a relatively undisturbed sedimentary succession in other areas.

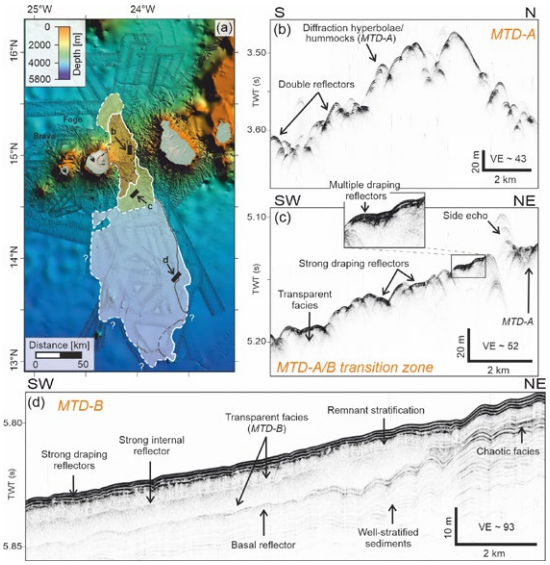

Fig. 1: (a) Map showing the distribution of the debris avalanche deposits (MTD-A), the acoustically transparent/ seismically chaotic MTD-B associated with the Monte Amarelo flank collapse, and a transitional zone where the size of the hummocks decrease with distance from the source. Dashed black line: previous mapped extent of the Monte Amarelo deposits; grey line: eastern margin of the upper part of MTD-B; solid black lines: location of the Parasound lines shown in (b) to (d). (b–d) Parasound profiles highlighting the acoustic character of (b) MTD-A, (c) the transitional zone, and (d) MTD-B. See the text for discussion on the nature of these deposits. VE, vertical exaggeration. Modified after Barret et al (2020).

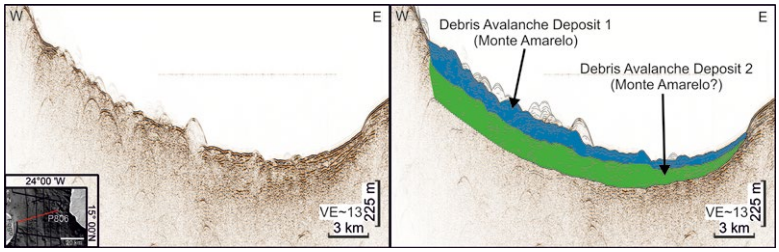

Fig. 2: Multichannel seismic line in close proximity to Fogo. The line shows two stacked debris avalanche deposits.

Acoustic and seismic imaging was complemented by sediment coring. Three east-west coring transects have been performed within the more distal (up to 220 km away) landslide deposits south from Fogo and Santiago (Figure 3). Throughout the study region, cm to decimeter thick turbidite deposits range from coarse to fine sand. These turbidite sands are predominantly of a volcaniclastic and/or mixed volcaniclastic-bioclastic composition, rather than bioclastic composition alone, suggesting that mass-transport processes are directly related to volcanic eruptions or volcanic mass-wasting events. From coring alone, at least 7 volcaniclastic landslide events have been identified (Fig. 3), which are extended by at least 5 more mass transport deposits evident in the seismic and hydroacoustic data. The upper three volcaniclastic layers of proximal core 38 and distal core 14 were compositionally characterized and compared to each other to determine how they differ within the event sequences and with distance (Fig. 3). The work included characterization of smear slide components and subsequent point counting as well as geochemical classification using an electron microprobe. First findings indicate that the upper two volcaniclastic layers of the two cores correlate well stratigraphically, and are petrographically and petrologically very similar. Differences in the abundances, especially of the glass compositional groups, indicate two different collapse events, maybe closely related in age, that tapped more or less the same source area from Fogo volcano. The third layer, however, differs significantly in both petrography and petrology, although the chemical signature indicates that the volcaniclastic material was sourced from Fogo but may represent separate/multiple events. A comparison with the compositional and chronostratigraphic database of Eisele et al (2015) facilitated a first preliminary age estimate of 21 ka to 53 ka for the three volcaniclastic layers. Gravity separation between proximal and distal cores are obvious and underline the importance and benefit of the combined analytic approach to also identify physical separation and mass transport processes that may mask primary provenance signals.

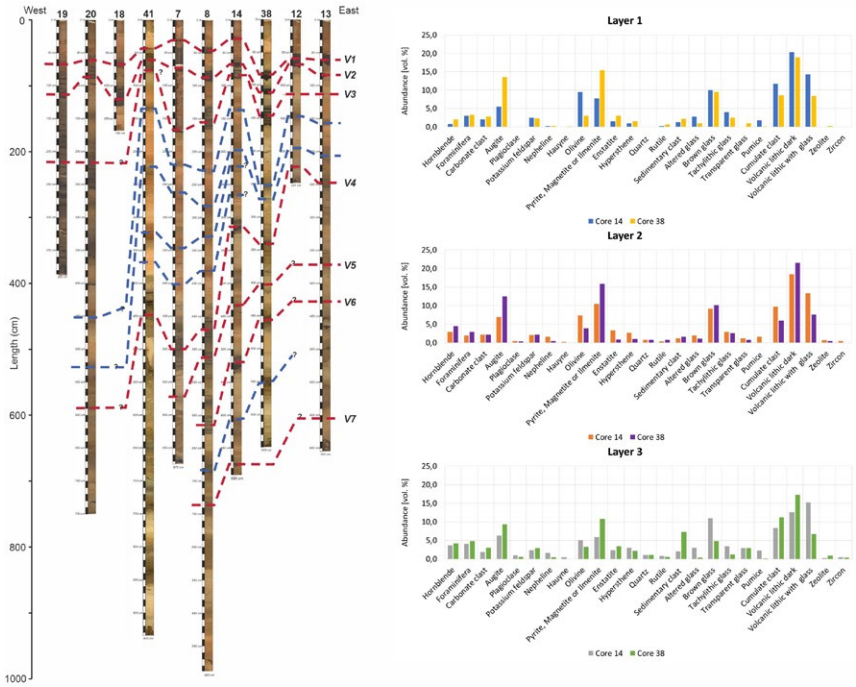

Fig. 3: (Left) Compilation of gravity cores retrieved south of Fogo and Santiago during M155 showing stratigraphic correlations based on visual analysis. Dashed red lines show correlations between different volcaniclastic sand layers (V1-V7). Dashed blue lines show correlation of background sediment layers (reddish-brown horizons). (Right) Point counting analysis showing the average abundance of categorized components in volume percentage [vol. %] of three investigated volcaniclastic layers in distal core 14 (blue) and proximal core 38 (orange).

SEISMIC PRE-SITE SURVEY FOR AN IODP SITE ON THE CAPE VERDE PLATEAU

The IODP full-proposal 973 'Neogene climate of NW Africa' has the following main objectives: i) NW African climate in a warmer world, ii) High productivity, ecosystem and sediment transport response to climate perturbations. Sediment cores should be retrieved between Cape Bojador southeast of the Canary Islands and the deltas of Senegalese and Gambian rivers, including the Cape Verde Plateau. Miocene sediments on the Cape Verde Plateau were already drilled in relatively shallow subsurface depths (ODP Site 659). The aim of this project was to identify new sites where the Plio-Pleistocene is thinner and the Miocene is thicker. The new seismic data is mainly characterized by well-bedded, sub-parallel reflectors. The Pleistocene- Pliocene boundary as well as the Pliocene-Miocene boundary can be clearly identified and traced on the data. The Plio-Pleistocene sediments have a relatively constant thickness of approx. ~140 m. South-East of ODP Site 659, the Pleistocene- Pliocene sediments thin to ~60 m. This site (Fig. 4) represents an optimal drilling location and was selected as primary site. The shallow water depth (2850 m) and the shallow burial of the Miocene deposits will permit full recovery (piston coring) of Miocene strata with well-preserved calcareous microfossils. In

the meantime, IODP proposal 973 was rated excellent and forwarded to the Joides Resolution Facility Board.

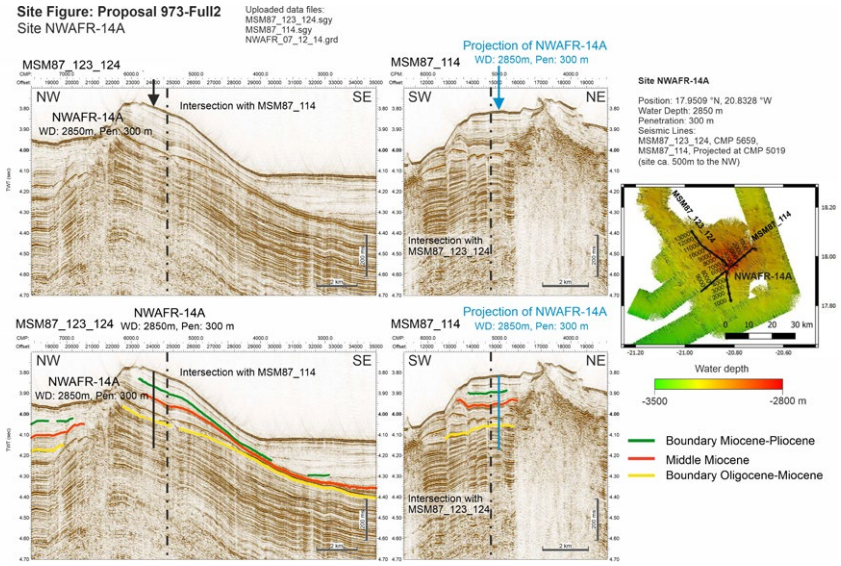

Fig. 4: Site figure for newly suggested primary site NWAFR-14A as submitted to the IODP site survey bank.

REFERENCE)

Barrett R, Lebas E, Ramalho R, Klaucke I, et al. Revisiting the tsunamigenic volcanic flank-collapse of Fogo Island in the Cape Verdes, offshore West Africa. In: Georgiopoulou A. et al. (eds) 2020. Subaqueous Mass Movements and their Consequences: Geol Soc Spec Pub 500, 13-26. doi.org/10.1144/SP500-2019-187

Eisele S, Reißig S, Freundt A, Kutterolf et al. Pleistocene to Holocene offshore tephrostratigraphy of highly explosive eruptions from the southwestern Cape Verde Archipelago. Mar Geol 2015, 369, 233–250

Ramalho RS, Winckler G, Madeira J, Helffrich,G, Hipólito A, Quartau R, Adena K, Schaefer J Hazard potential of volcanic flank collapses raised by new megatsunami evidence. Science Advances 2015, 1:e1500456.

M156

Role of Eddies in the Carbon Pump of Eastern Boundary Upwelling Systems (MOSES Eddy Study I)

AUTHORS

GEOMAR Helmholtz-Centre for Ocean Research Kiel | Kiel, Germany
S. Sommer, N. Adam, K. Becker, A.W. Dale, M. Dengler, A.F. Dilmahamod, Q. Devresse, A. Engel, J.Greinert, J. Hahn, M. Kampmeier, M. Paulsen, M. Perner, M. Schumacher, K. Wallmann, A. Körtzinger

University of Kaiserslautern, Department of Ecology | Kaiserslautern, Germany
H.W. Breiner, S. Katzenmeier, T. Stoeck

The Mauritanian upwelling system (NW Africa) is one of four major eastern boundary upwelling systems. Upwelling of cold, nutrient-, carbon dioxide-rich and oxygen-deficient intermediate waters is driven by trade winds blowing equatorward parallel to the coast and an anticyclonic wind stress curl. The ensuing elevated biological productivity supports major industrial fisheries and a considerable fraction of the global fish catch (Lachkar & Gruber 2012). These systems are vulnerable to various anthropogenic stressors such as ocean warming, acidification, and deoxygenation (Gruber 2011). Furthermore, they are expected to experience changes in trade winds and hence upwelling intensity (Bakun et al. 2010). The major goal of the RV METEOR cruise M156 to Cape Verdian waters and the Mauritanian upwelling area off West Africa (03.07.–01.08.2019) was to contribute to a better quantitative understanding of the effects of mesoscale eddies on (i) CO_2 source/sink mechanisms, (ii) the biological carbon pump in eastern boundary upwelling areas, and (iii) their impact on the oligotrophic periphery including the deep-sea floor.

Eddies are key features of the ocean and responsible for many of its large-scale physical and biogeochemical properties. It has been suggested that eddy-driven subduction of non-sinking particulate organic carbon (POC) may account for up to half of the total springtime export of POC from highly productive subpolar oceans (Omand et al. 2015). Furthermore, eddies may be hotspots of prokaryotic activity and differential community structures (Baltar et al. 2010, Hauss et al. 2016) and have even been shown to be important in the vertical export of organic matter (Fischer et al. 2016) and its transport to deep-sea sediments, thereby directly connecting surface ocean dynamics with the deep ocean (Zhang et al. 2014). The generation of eddies is favored by the interaction of large-scale currents with the bottom topography, islands or headlands, by barotropic or baroclinic instability of currents and fronts, or by atmospheric forcing (e. g. Thomsen et al 2016). By trapping coastal waters of upwelling origin and transporting them westwards into the open ocean, eddies play an important role in the lateral mixing and

transport of physical-biogeochemical properties and thereby modulate biological productivity and material fluxes to the seabed.

Cruise M156 was conducted within the framework of the BMBF-funded project REEBUS (Role of Eddies in the Carbon Pump of Eastern Boundary Upwelling Systems) and the HGF infrastructure project MOSES (Modular Observation Solutions for Earth Systems) by a consortium of physical, biological (benthic microbiology, bacterial plankton, protozoans) and biogeochemical benthic and pelagic oceanographers. The cruise is embedded into a series of the three REEBUS/MOSES cruises M156 (2019), M160 (2019), and M182 (2022).

Specific aims were i. the quantification of solute and particle fluxes within and at the periphery of eddies; ii. to determine the turnover of carbon species, air-sea gas exchange of CO_2, iii. the determination of the protistan and bacterial plankton community structures in the surface layers of an eddy, and iv. to quantify the magnitude and variability of material fluxes of biogenic detritus to the seabed and the remineralization rate of organic matter in the sediment below the eddy corridor. The cruise had two major observational foci, i. an intense benthic/pelagic program along the zonal eddy passage at 18°N. Along this corridor, ranging from 24°20′ to 16°30′W, five benthic/pelagic stations (E1 to E5) in different water depths and distances from the Mauritanian coast were visited (Figure 1). The motivation for this survey has been to resolve zonal gradients in pelagic element cycling as well as of organic matter degradation and burial in the seabed, which in turn could potentially be linked with changes in eddy induced biological productivity. ii. The second focus was a detailed investigation of an individual eddy to investigate physical, biogeochemical and biological processes on meso- to submeso-scales (Figure 1). Satellite data analysis was performed before and during the cruise to identify a suitable eddy from a combination of sea-level anomaly, ocean color (as a chlorophyll a proxy), and sea-surface temperature, supplemented with shipboard current velocity measurements.

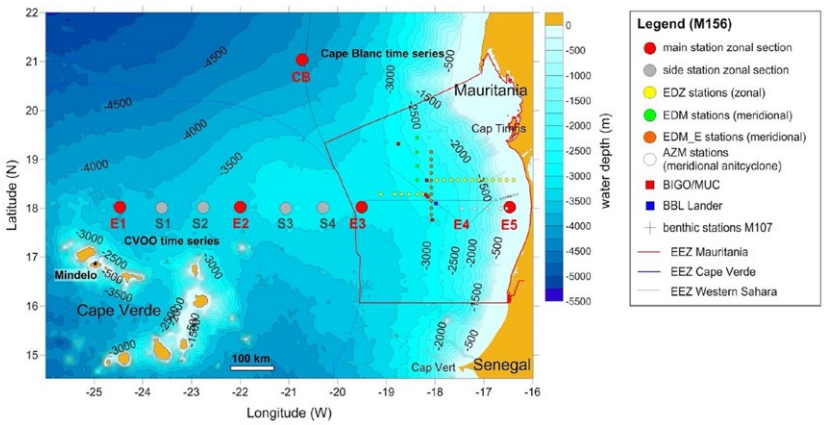

Fig. 1: Station map of RV Meteor cruise M156. The cyclonic eddy position is denoted by EDZ and EDM stations

Vessel mounted ADCP measurements allowed observations of upper-ocean velocities throughout the whole cruise with a main focus on the survey of the 18°W, 18.5°N cyclonic eddy, whose position and extent was determined based on ADCP transects in combination with near real-time satellite altimetry data. Satellite altimetry data suggested a slightly elliptic eddy shape. Considering the meridional distance from maximum eastward to maximum westward swirl velocity, the extension of the eddy of 60 nm was estimated between 18°15'N and 19°15'N. The eddy extended downwards to a depth of several hundred meters.

A total of 37 CTD profiles were performed to survey the cyclonic eddy, which was found to have a low oxygen core with minimum oxygen concentrations well below 20 µmol kg^{-1} between 20 and 50 m depth. Low salinity was observed in the core (corresponding to more South Atlantic Central Water originating from off the Mauritanian coast), whereas the northern and southern eddy boundaries were well oxygenated (80–100 µmol kg^{-1}) and more saline (corresponding to more North Atlantic Central Water from the open ocean). Chlorophyll levels were enhanced at the meridional eddy boundaries in the upper 40 m suggesting more intensified primary production, with highest chlorophyll concentrations at the northern boundary. Correspondingly, turbidity was highest at the northern eddy boundary, but a secondary maximum was observed above the eddy core, at a meridional position where lowest oxygen concentrations were observed.

Further analysis included flow cytometry-based community composition, microbial process rates, such as primary production, secondary production and respiration, in combination with dissolved and particulate organic matter composition in and around the cyclonic eddy. The results from these studies indicate that physical processes shape the small-scale variations in the planktonic community and the composition of particulate and dissolved organic matter. This has consequences for lateral and vertical transport processes of organic carbon and the cycling of carbon in open ocean basins. Importantly, these results contribute to a better understanding of the processes that sustain net heterotrophy in many open ocean basins, Figure 2.

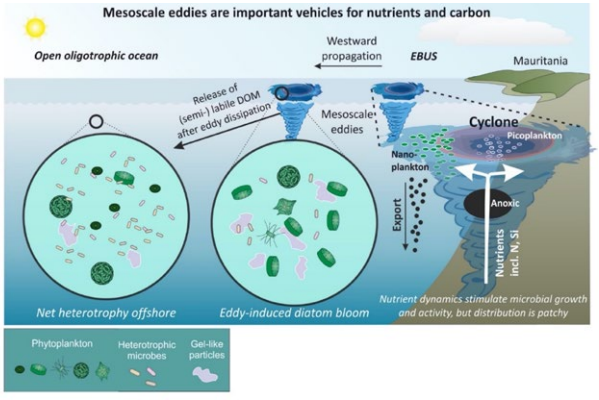

Fig. 2: Eddies as important shuttles for nutrients and carbon to the oligotrophic open ocean (image courtesy K. Becker)

Surprisingly, a red tide of the ciliate Mesodinium rubrum formed in the area of the cyclonic eddy during the cruise. Whether the occurrence of the red tide can be related to the eddy or whether it represents a completely independent phenomenon remains speculative.

A major goal of the benthic biogeochemical program was to quantify the magnitude and variability of material turnover in the sediments underneath the eddy passage and the possibly linkage with eddy-induced enhanced export production. In the oligotrophic deep-sea, organic carbon in sediment is typically degraded by microorganisms using oxygen. Hence, major emphasis was placed on the measurement of total oxygen consumption in situ using landers. In addition to sampling the zonal gradient from the Cape Verde Terrace eastwards to the oxygen depleted waters offshore Mauritania, the seabed underneath the cyclonic eddy was also investigated at the center of the eddy and at its southern and northern periphery at water depths of ~2800 m. When compared to the empirical equation relating total oxygen uptake to water depth provided by Wenzhöfer & Glud (2002), a trend of increased oxygen consumption was discerned, indicating a generally increased organic carbon availability in the eddy area. However, due to the limited database of oxygen uptake rates (n = 9), we were unable to conclusively demonstrate that enhanced oxygen uptake underneath the eddy center was directly related to increased carbon input from the eddy, or whether it merely reflected variability of organic carbon deposition in relation to seafloor topography. Further benthic research included the detailed seafloor imaging and bathymetrical investigation of the seafloor at the different stations to resolve variability of seabed topography and properties likely affecting the accumulation of organic particles at the seafloor.

Outlook: In combination with the upcoming cruise M182 (2023) we will revisit the investigated sites and expand the existing database. One major focus will include the long-term deployment of the Rover Panta Rhei at the seafloor to record a time-series of benthic oxygen consumption, which will reflect enhanced carbon availability during the passage of productive eddies.

REFERENCES

Bakun A, Field DB, Redondo-Rodriguez A, Weeks SJ, Greenhouse gas, upwelling-favorable winds, and the future of coastal ocean upwelling ecosystems. Global Change Biol 2010, 16, doi: 10.1111/j.1365-2486.2009.02094.x

Baltar F, Arístegui J, Gasol JM, Lekunberri I, et al., Mesoscale eddies: hotspots of prokaryotic activity and differential community structure in the ocean. ISME J. 2010, 4, doi: 10.1038/ismej.2010.33

Fischer G, Romero O, Merkel U, Donner B, et al. Deep ocean mass fluxes in the coastal upwelling off Mauritania from 1988 to 2012: variability on seasonal to decadal timescales. Biogeosciences 2016, 13, doi: 10.5194/bg-13-3071-2016

Gruber N, Warming up, turning sour, losing breath: ocean biogeochemistry und global change. Phil. Trans. R. Soc. A 2011, 369, doi: 10.1098/rsta.2011.0003

Hauss H, Christiansen S, Schütte F, Kiko R, et al. Dead zone or oasis in the open ocean? Zooplankton distribution and migration in low- oxygen modewater eddies. Biogeosciences 2016, 13, doi: 10.5194/bg-13-1977-2016

Lachkar Z, Gruber N, A comparative study of biological production in eastern boundary upwelling systems using an artificial neural network. Biogeosciences 2012, 9, doi: 10.5194/bg-9-293-2012

Omand MM, D'Asaro EA, Lee CM, Perry MJ et al. Eddy-driven subduction exports particulate organic carbon from the spring bloom. Science 2015, 348, doi: 10.1126/science.1260062

Thomsen, S, Kanzow, T, Krahmann, G, Greatbatch R et al. The formation of a subsurface anticyclonic eddy in the Peru-Chile Undercurrent and its impact on the near-coastal salinity, oxygen, and nutrient distributions, J. Geophys. Res. Oceans 2016, doi: 10.1002/2015JC010878

Wenzhöfer F, Glud RN, Benthic carbon mineralization in the Atlantic: a synthesis based on in situ data from the last decade. Deep-Sea Res. I 2002, doi: 10.1016/S0967-0637(02)00025-0

Zhang Z, Wang W, Qui B, Oceanic mass transport by mesoscale eddies. Science 2014, 345, doi: 10.1126/science.1252418

M157

First, preliminary results from the coastal Benguela System

AUTHORS

MARUM – Center for Marine Environmental sciences | Bremen, Germany
M. Zabel

IOW – Leibniz Institute for Baltic Sea Research | Warnemünde, Germany
V. Mohrholz, B. Sabbaghzadeh, H. Schulz-Vogt, M. Zettler

GEOMAR – Helmholtz Center for Ocean Research | Kiel, Germany
S. Sommer

The major goal of expedition M157 in fall 2019 was to obtain high-resolution data and samples from shelf and upper slope to document and to understand the variability of the geochemical environment and the present day physical forcing of the Benguela Upwelling System (BUS). For this purpose, comprehensive, multidisciplinary investigations were conducted along three transects perpendicular to the coast of Namibia at about 17,3°S, 23°S and 25°S. The work concentrated in particular on four selected locations, two on each of the southern transects, at which almost all devices could be deployed and all planned measuring methods and sub-sampling could be carried out. This program was complemented by comparative studies at numerous other stations along the three transects, as well as profiling measurements in the water column between all stations and on the transit from Cape Verde Islands to the working area. The geochemical measurements showed that, as expected at this time of year, the oxygen content in the bottom water was not completely depleted. A total of 330 deployments of different devices at 49 individual stations with water depth between 32 m and 2078 m were used to collect and gained extremely valuable samples and sensor data.

The processing of the samples obtained has been delayed by at least one year due to the multiple restrictions in the wake of the Covid 19 pandemic. For this reason, the reported results here can unfortunately only be considered preliminary at this early stage.

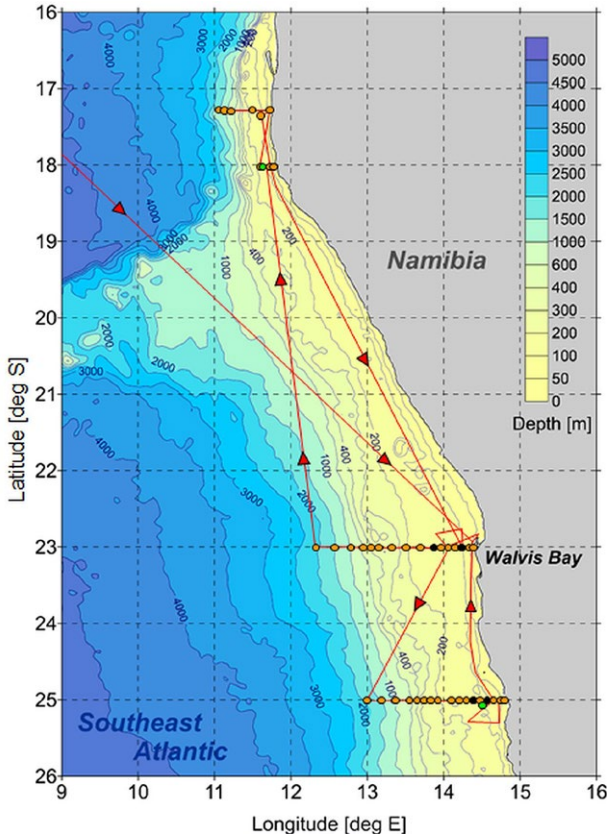

Fig. 1: Track chart of R/V METEOR Cruise M157 with locations of sampling along the three transects.

HYDROGRAPHY

The focus of hydrographic investigations during the cruise was on the impact of short term upwelling variability on oxygen and nutrient supply to the shelf, and on the response of primary production to short term upwelling peaks. As expected for the season the hydrographic data gathered on the Namibian shelf depict a typical upwelling situation. Over the mud belt the bottom water was strongly oxygen depleted but not anoxic, due to significant ventilation by ESACW that was transported northward along the shelf. The oxygen distribution was strongly controlled by the water mass distribution of central water. Enhanced mixing processes in the bottom boundary layer and at the shelf edge enforced the vertical exchange of nutrients and oxygen. The combination of high resolution Nutrient profiles with the Microstructure measurements delivered estimates of vertical nutrient fluxes, and hints to layers with biological driven sources and sinks of nutrients.

MARINE CHEMISTRY

The surface profiles of trace gases i. e. nitrous oxide (N_2O) and methane (CH_4) revealed the co-occurrence of the maximal concentrations in the vicinity of the main upwelling cells

confirmed by a strong negative correlation between trace gas concentrations and sea surface temperature (SST), indicator of upwelling event. The most significant pattern in the distribution of trace gas was a steep cross-shelf gradient, in consequence with coastal upwelling and with concentrations increasing up to 400 nmol L^{-1} with respect to methane around Walvis Bay. We also speculate the indication of upwelling filaments of northern and central Namibian cells, in few kilometers off shore along the transections, in line with the high surface trace gas. N_2O was mainly concentrated in the mid-layers of the water columns with the core of N_2O-rich waters located around 400m depth associated with the South Atlantic Central Water (SACW). Also, shelf topography like a marked steepness in the slope in regions along 17°S may facilitate low oxygen waters to be upwelled in the presence of stronger winds result in sub-surface concentrations higher than off Walvis Bay irrespective of higher regional concentrations. So, it is suggested that the balance between subsurface inventories and transport processes result in regional gradients of N_2O in the Benguela upwelling system. Maximal CH_4 concentrations were recorded within the entire water column in the vicinity of Walvis Bay, associated with the shallow water depths and an extremely organic-rich underlying mud-belt, serving as a substrate for methane production and maintaining the water column concentrations. However, no clear pattern of CH_4 distributions within the water column was found and few local higher concentrations of CH_4 in the upper water might be associated with in situ CH_4 production. It is suggested that two sources of CH_4 within the water column in the region is present; a sedimentary source with restricted diffusive efflux to the atmosphere due to CH_4 consumption via methanotrophic activity, and an upper source of in situ biogenic production of CH_4 by bacteria within the oxygenated layer with greater impact on atmospheric CH_4 flux.

MACROBENTHIC ECOLOGY

In a study of transcriptomic response to oxygen fluctuations, we had results that highlighted the probable importance of anaerobic succinate production (via PEPCK) and mitochondrial and proteome quality control mechanisms in responses to oxygen fluctuations of the OMZ bivalve *L. bicuspidatus*. The reaction of *Lembulus bicuspidatus* to oxygen fluctuations implies parallels to that of other hypoxia-tolerant bivalves, such as intertidal species.

In a study of trophic ecology and nitrogen metabolism of the molluscs *Lucinoma capensis, L. biscuspitadus, Nassarius vinctus* we found that chemoautotrophic productivity (symbionts and free-living bacteria) and sedimented diatoms are the base of the food web of important benthic species at the seafloor of the Namibian shelf. We also, for the first time, showed that the deeper water lucinid symbionts rely on ammonium assimilation to obtain nitrogen rather than nitrogen fixation, as is typical of all shallow water lucinid symbionts. Here, surprisingly, the Candidatus Thiodiazotropha sp. symbionts are shown to be incapable to assimilate N_2, very likely due to the high availability of other inorganic nitrogen sources present in the reducing environment.

In order to investigate the biodiversity of the Namibian upwelling area, we analyzed the material from several expeditions over the past 15 years. Essential input came from the

material obtained on the M157 expedition. Several new species for science have been discovered. Interestingly, the core area of the upwelling zone in particular is home to several new species that appear to be well adapted to this harsh environment.

Biological invasions continue to increase around the world, with impacts on many coastal marine systems. A large number of vectors for the spreading of marine organisms are conceivable, e. g. aquaculture, ship traffic, pet trade and tourism. The present study demonstrates the permanent risk of non-native species being moved from anywhere (here over a distance of probably up to 10,000 km) to Namibia. A randomly initiated sampling of the colonization of a moon pool of a research vessel in the port of Walvis Bay yielded mostly previously unknown non-native species for Namibian waters.

IN SITU FLUX MEASUREMENTS AND EXPERIMENTS

In situ flux measurements of major elements were performed at the center and fringe of the Namibian mudbelt system at 23°S and 25°S in water depths of about 120 m using two BIGO type lander (BIGO, Biogeochemical Observatory). Overall, the rate measurements nicely reflect the bottom water redox conditions, which at the northern and the southern mud-belt system is strongly modulated by the mixing of two different water masses rendering the northern mud-belt system strongly susceptible to oxygen depletion, whereas the southern mud-belt system is characterized by mild oxygen deficiency. The northern mud-belt center stations were characterized by high uptake rates of sulfate of up to 238 mmol m^{-2} d^{-1} indicating microbial sulfate reduction as the main pathway of organic matter degradation. At these sites, oxygen, nitrate and nitrite became rapidly depleted within a few hours giving rise to strongly enhanced phosphate, ammonium and sulfide release of up to 9, 116, 128 mmol m^{-2} d^{-1} respectively. These fluxes are extremely high in comparison to previous flux measurements in this region and other oxygen minimum zones worldwide, highlighting the potential of the northern mud-belt sediments to strongly contribute or even initiate sulfidic events. In contrast, the fluxes determined at the center of the southern mud-belt system, did not show a strong temporal variability as determined for the northern sites, and their magnitudes were generally much lower reflecting the better availability of electron acceptors for organic matter, sulfide oxidation and other secondary processes. Increased access to bottom water nitrate for sulfide oxidizing Thiomargarita might further contribute to efficient sulfide removal and ecosystem health at 23°S.

SEDIMENT GEOCHEMISTRY

Based on the elemental composition of the sediments, the potential origin of the terrigenous fraction and possible temporal changes should be investigated in a first step. For this purpose, We reconstruct the provenance of aluminosilicate sediment deposited over the last 4 kyr from the Namibian Mudbelt from Site GeoB 23812-25 (23°S). Using multivariate statistical techniques (Q-mode factor analysis, constrained least squares multiple linear regressions) on major, trace and rare earth element composition of bulk sediment, we fingerprint and quantify three aluminosilicate components (Namaqualand,

Damaraland, Witwatersrand/Kapvaal), and calculate their mass accumulation rates through time. Based on the elemental composition of the sediments, the first step was to investigate the potential origin of the terrigenous fraction and possible changes over time. There is a clear trend in the proportion of mineral constituents carried by the Orange River. Two primary processes are discussed as possible causes, a quantitative change due to changing erosion efficiency combined with changes of the precipitation intensity in the source region and/or a change in the strength of the Benguela Coastal Current. Both scenarios would have considerable significance for assessing the evolution of Benguela coastal upwelling or the geochemical environments there. A corresponding manuscript is in preparation.

In a further approach, the contents of redox-sensitive elements (especially Mo and U) will be investigated to reconstruct the potentially changing oxygen availability in the mud belt region. Results to date also indicate a change within the last 4kyr. The complex sedimentological depositional conditions require a high degree of system and process understanding to reliably interpret the obtained data. The upcoming 2nd EVAR expedition in early 2022 should provide further insights. This includes the recovery of suspended material and high-resolution sediment acoustic recordings.

Initial results from the *Geomicrobiology* and *Microbial Ecology* working groups will also be presented at the status conference.

PUBLICATIONS (SO FAR)

Amorim K, Piontkivska H, Zettler ML, Sokolov E, Hinzke T, Nai AM, Sokolova IM, Transcriptional response of key metabolic and stress response genes of a nuculanid bivalve, Lembulus bicuspidatus from an oxygen minimum zone exposed to hypoxia-reoxygenation. Comparative Biochemistry and Physiology Part B, Biochemistry and Molecular Biology 2021, 256: 110670

Zettler ML, Alf A, A new Polititapes (Bivalvia, Veneridae) from Namibia. Archiv für Molluskenkunde 2021, 150: 1–4 https://doi.org/10.1127/arch.moll/150/001-004

Zettler ML, Hoffman L, A wide distribution of Waisiuconcha haeckeli (Bivalvia: Vesicomyidae) in the eastern Atlantic Ocean. Miscellanea Malacologica 2021, 9: 1–3

Zettler ML, Hoffman L, New species in Galeommatoidea (Bivalvia) from Namibia. Iberus 2021, 39: 195-208 https://doi.org/10.5281/zenodo.5039263

Zettler ML, Hoffman L, Nuculana cornidei (Bivalvia: Nuculanidae) from Namibia. Miscellanea Malacologica 2021, 9: 5–9

Zettler ML, An example for transatlantic hitchhiking by macrozoobenthic organisms with a research vessel. Helgoland Marine Research 2021, 75:4

M158

Trans-Atlantic Equatorial cruise I

AUTHORS

GEOMAR Helmholtz Centre for Ocean Research Kiel | Kiel, Germany
P. Brandt, R. Kiko

METEOR cruise M158 in the following called Transatlantic Equatorial Cruise I (TRATLEQ I) was an interdisciplinary cruise focusing on upwelling in the tropical Atlantic, its physical forcing, its importance for biological production and plankton communities, associated chemical cycles, as well as on the current system setting the background conditions for the downward carbon export. This cruise represents the first physical, chemical, biogeochemical and biological measurement program covering a whole equatorial section from the eastern to the western boundary and from the surface to the bottom.

During TRATLEQ I for the first time the Equatorial Undercurrent (EUC) was measured with direct velocity measurements across the whole basin. Together with the velocity measurements, hydrographic data of temperature, salinity, oxygen among others were obtained (Fig. 1). The EUC was captured, flowing eastward along the equator with a core depth of about 80 m shallowing toward east (Fig. 1c).

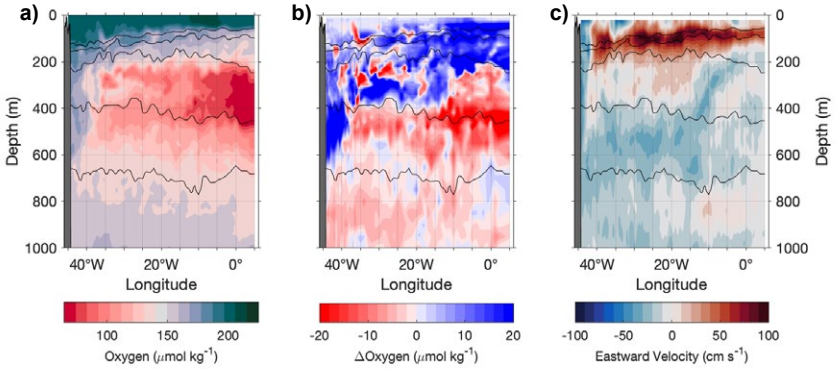

Fig. 1: Shipboard measurements along the Atlantic equator in Sep./Oct. 2019. a, Dissolved oxygen concentration. b, Dissolved oxygen anomaly relative to the climatological year-2000 state. c, Eastward velocity. Grey areas mark bottom topography at the western boundary. Black lines mark the 25 kg m^{-3}, 26 kg m^{-3}, 26.5 kg m^{-3}, 27 kg m^{-3} and 27.25 kg m^{-3} isopycnals.

During TRATLEQ I, also the long-term mooring at the equator, 23°W was serviced. This mooring now provides an almost 20-year time series that shows besides low-vertical

mode seasonal variability, high-vertical mode interannual variability also decadal variability of the EUC. Using this data, we could show that the EUC strengthened by more than 20 % over the decade 2008–2018 (Fig. 2). This EUC strengthening was associated with increasing subsurface oxygen concentrations and a thickening of the upper-ocean oxygenated layer in the equatorial Atlantic, thereby counteracting climate warming-induced deoxygenation in this region. The EUC strengthening was found to be mainly forced by trade wind changes in the western tropical North Atlantic. A comprehensive 60-year dataset additionally revealed that the recent oxygen increase in the upper equatorial Atlantic was associated with multidecadal variability characterized by low oxygen concentrations in the 1990s and early 2000s and high oxygen concentrations in the 1960s and 1970s. The observed oxygen variability seems to be linked to a compression and expansion of the habitat of tropical pelagic fish and must be accounted for when evaluating possible consequences of deoxygenation for marine ecosystems and fisheries (Brandt et al. 2021).

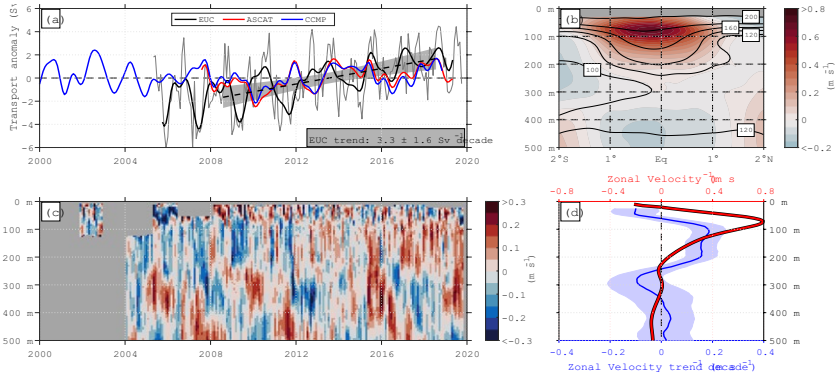

Fig. 2: The Atlantic Equatorial Undercurrent (EUC) at 23°W. a, EUC transport anomaly (monthly data, grey thin line; mean and annual and semi-annual harmonics subtracted and 270-day low-pass filtered, black thick line; ten-year (August 2008 to July 2018) trend, black dashed line; with 95 % confidence interval, grey shading) and STC transport anomaly calculated from Ekman divergence between 10°N and 10°S using different wind forcing products (ASCAT, red; CCMP, blue; mean and annual and semi-annual harmonics subtracted and 270-day low-pass filtered). b, Mean eastward velocity (color) and dissolved oxygen (µmol kg-1, contours) from shipboard measurements after. c, Time series of eastward velocity anomaly at the equator with mean and seasonal cycle subtracted. d, Ten-year (August 2008 to July 2018) trend in eastward velocity (blue, with 95 % confidence interval, light blue shading) and mean eastward velocity (red) at the equator.

Data from the long-term mooring at the equator at 23°W was also used to analyze the intraseasonal variability of the zonal velocity in the equatorial Atlantic and of the alongshore velocity at the eastern boundary of the tropical Atlantic Ocean. Pronounced oscillations of alongshore velocity and sea level off Angola at periods of about 90 and 120 days were observed. Similar spectral peaks are detected along the equator suggesting an equatorial forcing via equatorial and coastally trapped waves. Equatorial variability at 90 days is enhanced only in the eastern Atlantic likely forced by local zonal wind fluctuations. Variability at 120 days is generally stronger and linked to a second

equatorial basin mode covering the whole equatorial basin. Besides forcing of the 120-day variability by equatorial zonal winds, additional forcing of the resonant basin mode likely originates in the central and western tropical North Atlantic. The coastally trapped waves generated at the eastern boundary by the impinging equatorial Kelvin waves that are detected through their variations in sea level anomaly are associated with corresponding sea surface temperature anomalies delayed by about 14 days. Off Angola, those intraseasonal waves interfere with major coastal warm and cold events that occur every few years by either enhancing them as for the Benguela Niño in 1995 or damping them as for the warm event in 2001 (Imbol Koungue and Brandt, 2021).

The equatorial mooring data (Fig. 2) were further used to validate a new method to derive characteristics of high vertical mode fluctuation of the zonal velocity, the equatorial deep jets (EDJ) from Argo float measurements. In the last few years, Argo floats have added a significant amount of measurements at intermediate depth. In this study we therefore revise estimates of the EDJ scales based on Argo float data. Mostly, we use velocity data at 1000m depth. Very weak or no EDJ signals can be detected in the Indian and Pacific Oceans. In the Atlantic, however, the EDJ signal is strong at 1000m depth, allowing us to obtain robust estimates of their frequency, amplitude, phase, zonal wavelength, and meridional structure. Additionally, we present a new estimation of their vertical structure throughout the Atlantic basin, based on an equatorial geostrophic velocity reconstruction from hydrographic Argo float measurements from depths between 400 and 2000 m. Earlier studies have mostly estimated the Atlantic EDJ scales from shipboard data. Our new estimates from Argo float data thus provide an independent EDJ scale assessment, as well as having smaller uncertainties than those from earlier studies (Bastin et al., 2021, submitted).

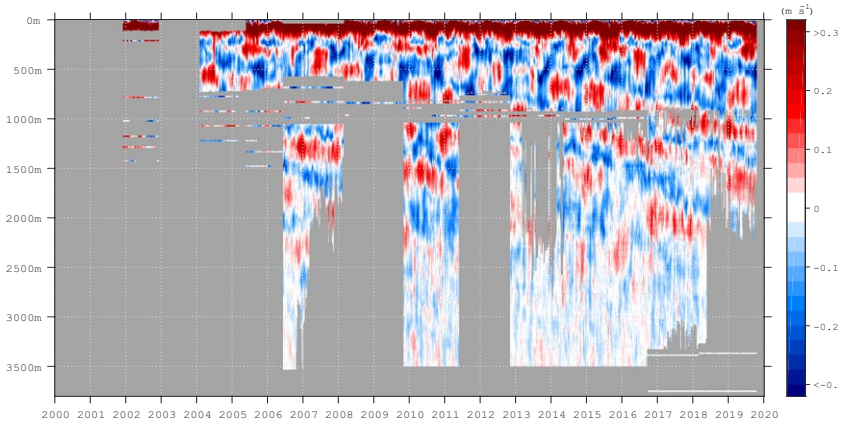

Fig. 3: Equatorial zonal velocity at 23 W measured by moored current meters. Positive values indicate eastward velocity, negative westward velocity.

REFERENCES

Brandt P, Hahn J, Schmidtko S, Tuchen F P, Kopte R, et al., Atlantic Equatorial Undercurrent intensification counteracts warming induced deoxygenation, Nat. Geosci., doi:10.1038/s41561-021-00716-1, 2021.

Imbol Koungue R A and Brandt P, Impact of intraseasonal waves on Angolan warm and cold events, J. Geophys. Res. Oceans 2021, 126, e2020JC017088, doi:10.1029/2020JC017088.

Bastin S, Claus M, Brandt P, and Greatbatch R. J., Atlantic equatorial deep jets in Argo float data, J. Phys. Oceanogr., submitted July, 2021.

M159

Circulation off Brazil

AUTHORS

GEOMAR Helmholtz Centre of Ocean Research Kiel | Kiel, Germany
M. Visbeck, P. Handmann, R. Hummels

The expedition "Circulation off Brazil" with its interdisciplinary work program was concerned with documenting the variability of the western boundary current systems off Brazil. The deep measurements along 11°S focused on the Atlantic Meridional Overturning Circulation (AMOC). Off the coast of Brazil, the research looked at the transport variability of the North Brazil Undercurrent (NBUC) – as a part of the AMOC and subtropical cells (STC) – on intra seasonal to decadal time scales. The section along 35°W provided additional information on water mass property changes and the connection to equatorial signals.

The research program of M159 (Fig. 1) covered three main research areas that are 1) the coastal area off Brazil, 2) the equatorial Atlantic via the 35°W section and 3) the area north of the Cap Verde Islands concerning the CVOO mooring.

Focus areas were the 11°S and 5°S zonal sections off Brazil and the meridional section along 35°W between ~5°S and 6°N. The work off Brazil covered the western boundary current system, which plays an essential role in the meridional overturning circulation. The meridional section along 35°W covers the zonal branches of the equatorial current system.

M159 focused on the maintenance and data recovery of the mooring array at 11°S. The mooring observatory at 11°S is providing vital data for the analysis of the variability of the NBUC and the deep western boundary current (DWBC). The NBUC reacts very sensitive to fluctuations of the AMOC and the subtropical cell (STC) and therefor forms a key region for the Atlantic circulation. The data collected during the cruise is part of a long-term mooring observatory of velocity, temperature and salinity time series off the Brazilian coast 11°S and hydrographic time series along 11°S and 5°S. The collected data, in combination with data collected at 11°S at the Angolan Coast, will be used to determine the transport of the NBUC, DWBC and the AMOC. The first tropical AMOC time series at 11°S focusing on seasonal variability was recently published (Herrford et al. 2021). In combination with previously collected data and data which will be collected in the future intra-seasonal to decadal variability of these time series will be analyzed. The updated NBUC and DWBC time series until 2019 including the data recovered on M159 (Fig. 2) were recently used to validate the tropical boundary current transports in the high-resolution ocean model VIKING20X (Biastoch et al. 2021).

In addition, the section between 5°S and 6°N was sampled for the first time in the last 16 years and will be used to analyze changes in water mass properties and water mass pathways across the equator to get insights into the signal propagation across the hemispheres as well as along the equator in combination with the 23°W section which was covered during another cruise. An interesting aspect was the analysis of the warming observed between the new data and a survey from 2003 (Fig. 3). The temperature difference is certainly patchy due to the energetic equatorial current system. However, when averaged over the section one can clearly see the strong upper ocean warming between 0.5 and 1.5°C. A less dramatic but still noticeable warming can be detected down to 1800m depths.

The study area north of the Cape Verde Islands at the CVOO mooring is aiming for a better understanding of the role of mesoscale eddies for the lateral transport of biogeochemical properties and their coupling to the carbon pump. By recovering and redeploying the CVOO mooring hydrographic, biogeochemical and velocity data were recovered in order to analyze long term variability at this location.

In addition to the scientific work, the expedition provided training of young researchers from developing countries. The Partnership for Observation of the Global Ocean (POGO) sponsored, in collaboration with GEOMAR, two training fellows from Nigeria and Argentina under its Nippon Foundation-Partnership for Observation of the Global Ocean (NF-POGO) Shipboard Training Fellowship program. The training provided hands-on, sea-going experience to young scientists from developing countries, and the opportunity to be involved in an internationally renowned scientific program.

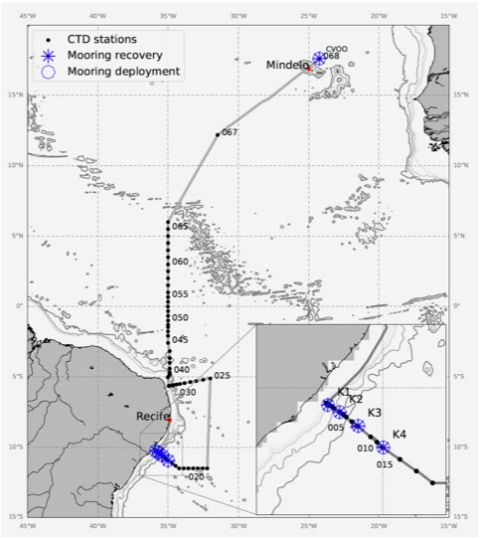

Fig. 1: Bathymetric map with cruise track of R/V METEOR cruise M159 (grey solid line) including locations of CTD/UVP/LADCP/AZFP stations, mooring recoveries and redeployments.

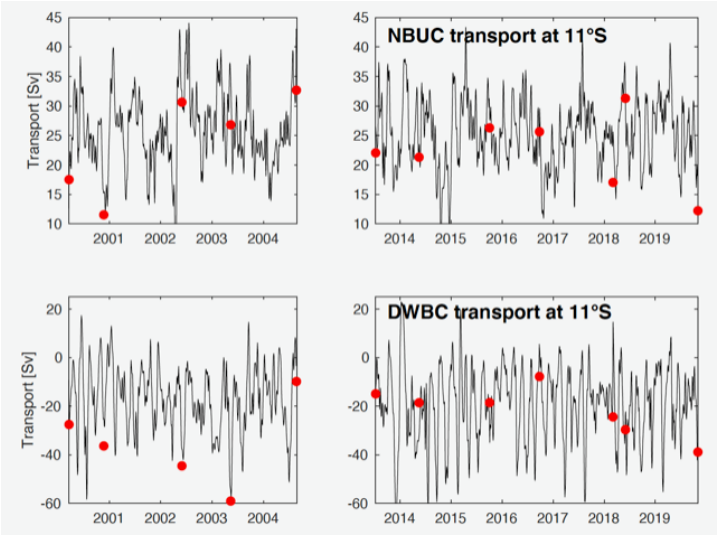

Fig. 2: Transport time series of the NBUC (upper panels) and DWBC (lower panels) based on all available moored velocity records from the array at 11°S. The red dots indicate the transports obtained from the shipboard measurements while doing the maintenance of the array.

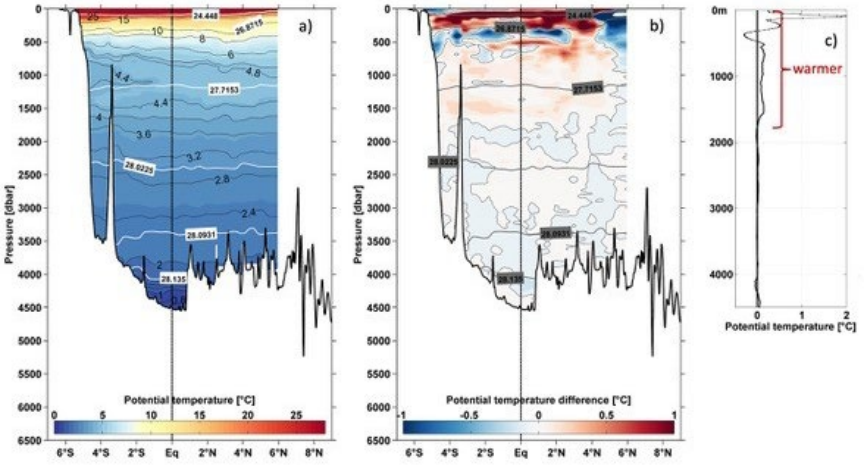

Fig. 3: Temperature sections along 35°W and their changes over the last 16 years. a) shows the temperatures from M159, b) shows the difference between 2019 and 2003, and c) section average warming as a function of depths. One can clearly see the warming over the upper 1600m water depths.

REFERENCES

Hummels, R., Brandt, P., Dengler, M., Fischer, J., Araujo, M., Veleda, D., et al. (2015). Interannual to decadal changes in the Western boundary circulation in the Atlantic at 11°S. Geophysical Research Letters, 42, 7615–7622. https://doi.org/10.1002/2015GL065254

Biastoch, A., Schwarzkopf, F. U., Getzlaff, K., Rühs, S., Martin, T., Scheinert, M., ... & Böning, C. W. (2021). Regional imprints of changes in the Atlantic meridional overturning circulation in the eddy-rich ocean model VIKING20X. Ocean Science Discussions, 1–52.

Herrford, J., Brandt, P., Kanzow, T., Hummels, R., Araujo, M., and Durgadoo, J. V.(2021): Seasonal variability of the Atlantic Meridional Overturning Circulation at 11°S inferred from bottom pressure measurements, Ocean Sci., 17, 265–284, https://doi.org/10.5194/os-17-265-2021

Herrford, J. (2021). Observing seasonal to decadal variability related to the Atlantic meridional overturning circulation at 11° S (Doctoral dissertation).

M160

Role of Eddies in the Carbon Pump of Eastern Boundary Upwelling Systems (MOSES/REEBUS Eddy Study II)

AUTHORS

GEOMAR Helmholtz Centre for Ocean Research Kiel | Kiel, Germany
A. Körtzinger, B. Fiedler, M. Dengler, J. Karstensen, T. Fischer, A. Engel, K. Becker

Helmholtz Centre Hereon | Geesthacht, Germany
B. Baschek, P. Calil, J. Horstmann, L. Merckelbach, R. Röttgers, M. Hieronymi

University of Bremen | Bremen, Germany
M. Iversen, G. Fischer, N. Moradi

Alfred Wegener Institute for Polar and Marine Research | Bremerhaven, Germany
M. Iversen, C. Flintrop

University of Kaiserslautern | Kaiserslautern, Germany
T. Stoeck

and further members of the M160 team

Cruise M160 was part of the concerted MOSES/REEBUS Eddy Study featuring three separate but connected research expeditions of RV METEOR (M156, M160, M182). It aimed at developing both qualitative and quantitative understanding of the role of physical-chemical-biological coupling in ocean eddies for the biological pump. The study followed three major hypotheses to be addressed by the three MOSES/REEBUS field campaigns:

(1) Mesoscale and sub-mesoscale eddies play an important role in transferring energy along the energy cascade from the large-scale circulation to dissipation at the molecular level.

(2) Mesoscale and sub-mesoscale eddies are important drivers in determining onset, magnitude and characteristics of biological productivity in the ocean and contribute significantly to global primary production and particle export and transfer to the deep ocean.

(3) Mesoscale and sub-mesoscale eddies are important for shaping extreme biogeochemical environments (e. g., pH, oxygen) in the oceans, thus promoting specific source/sink functions for greenhouse gases.

Cruise M160 employed the 'Modular Observation Solutions for Earth Systems' (MOSES) infrastructure of the Helmholtz Association (HGF). MOSES is an observing system developed by the centers in the HGF Research Field Earth and Environment (moses.eskp.de/home) that comprises highly flexible and mobile observation modules, which are designed to investigate the interactions of short-term events and long-term trends across Earth compartments.

Scientifically the MOSES/REEBUS Eddy Study was embedded into the MARE:N collaborative project REEBUS (Role of Eddies in the Carbon Pump of Eastern Boundary Upwelling Systems – Demonstration Case Canary Current System, www.ebus-climate-change.de/de/reebus). The ultimate goal REEBUS in general and cruise M160 in particular was to contribute significantly to our understanding of how ocean eddies generated in one of the major eastern boundary upwelling systems, i. e. the Canary Current system, shape and mediate ocean productivity and vertical carbon export via the biological carbon pump. For this purpose, we planned to carry out a detailed high-resolution, multi-parameter, interdisciplinary study of two individual eddies in Cabo Verdean waters (Fig. 1). The study was based on an interdisciplinary approach demonstrated successfully during the 2014 "Eddy Hunt Project" (GEOMAR & Kiel University; Fiedler et al. 2016, Fischer et al. 2016, Grundle et al. 2017, Hauss et al. 2016, Karstensen et al 2017, Löscher et al. 2015, Schütte et al. 2016).

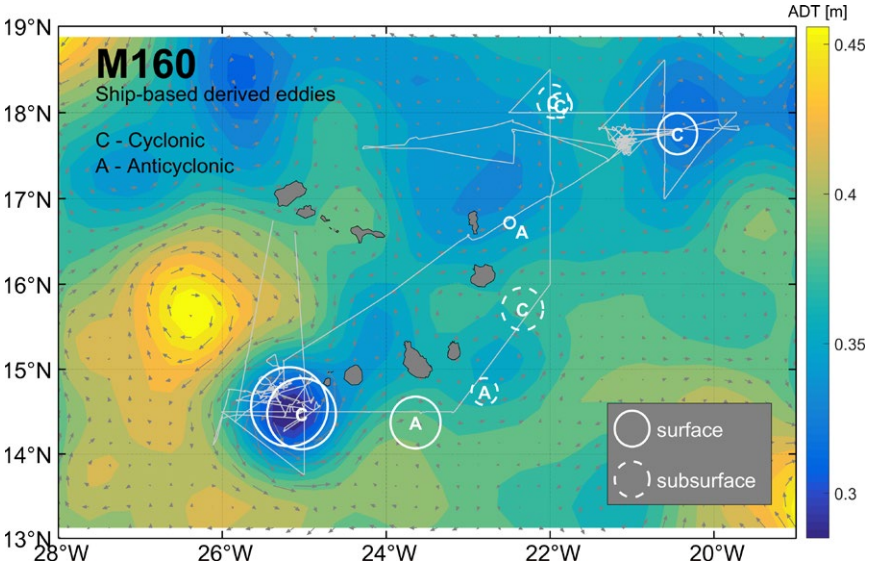

Fig. 1: Track chart of R/V METEOR Cruise M160 with location of cyclonic and anticyclonic eddies.

The general concept of the eddy study started with a detailed survey of mesoscale properties of an eddy. This included the current field in the upper 1200 m as well as physical and a whole suite of biogeochemical and biological properties at the surface and in the upper 1200 m of the water column. On the basis of this survey and with the aid of remote sensing information of temperature, currents and ocean color information – both from satellites and the research glider plane STEMME (Fig. 2, D-KNFH of University of Applied Sciences in Aachen) – the exact locations of the sub-mesoscale studies were determined. Both mesoscale and sub-mesoscale studies featured a large range of observational techniques that were deployed in a concerted way. Special attention was given to the frontal region at the boundary of the eddies where strong vertical and horizontal sub-mesoscale motion is concentrated in sharp fronts at the surface connecting matter exchange with the surface layer and across the eddy boundary. Elucidating these contrasting roles by connecting the large range of relevant scales was a major and novel aim of the study.

Fig. 2: Chief pilot Philipp Hilker and Prof. Burkard Baschek before departure of motorglider STEMME (left) and overflight of RV METEOR as seen from the plane (middle) and from the vessel (right).

In contrast to the other two legs (M156, M182), MOSES/REEBUS Eddy Study II during M160 did not include any benthic work but focused entirely on the pelagic dynamics within eddies. It accomplished a multi-disciplinary, multi-parameter and multi-platform study of two discrete cyclonic eddies in an unprecedented complexity. The pre-cruise search for discrete eddies suitable for detailed study during M160 had already started several months prior to the cruise. Remote sensing data products (sea surface height, sea surface temperature, ocean color/chlorophyll a) were used in combination with eddy detection algorithms and numerical modelling to identify and track promising eddy candidates across the entire eddy field off West Africa. In addition, 2 gliders and 1 waveglider had been sent out from Mindelo/Cabo Verde for autonomous pre-cruise mapping of the potential working area north of the Cabo Verdean archipelago.

At the start of M160, a few suitable eddies – mostly of cyclonic type – had been identified, some of which were outside the safe operation range of the motorglider plane for airborne observations. As technical problems delayed the flight operations, the first cyclonic eddy (center at 14.5°N/25°W) for detailed study was chosen to the southwest of the island of Fogo. It was decided to carry out an initial hydrographic survey of the eddy followed by the deployment of a suite of autonomous instruments (gliders,

waveglider, floats, drifters, short-term mooring). Such instrumented, we left this first eddy and transited – via a strong anticyclonic feature southwest of the island of Santiago – to the region northeast of the island of Sal, i. e. in the working range of the glider plane. During the transit, a full suite of underway measurements as well as a CTD/RO section along 22°W (16°–18.5°N) were carried in search for sub-surface expressions of anticyclonic eddy features.

In the northeast, we had identified the second strong cyclonic eddy (center at 18°N/22.5°W) which was chosen for detailed study starting with a complete hydrographic survey (ADCP, CTD/RO, other routine station work). After completion of the mesoscale work program, we identified a strong and dynamic frontal region at the southwestern rim of the cyclonic eddy, which was chosen for the first sub-mesoscale study with the parallel aerial observation component. There, also the first dye release experiment was carried out which consisted release of the rhodamine WT fluorescent dye itself followed by an intense multi-platform survey of the vertical and horizontal spreading of the initial dye streak. This work was supported and partly guided by aerial observation of the research motorglider Stemme, which was still somewhat compromised by technical issues and meteorological conditions (high cloud cover, Saharan dust event). Nevertheless, this first dye release experiment was successful and showed rapid movement of the dynamic meandering front.

After completion of work on this second eddy and execution of a focused sampling program at the Cape Verde Ocean Observation, RV METEOR returned to the first eddy for continuation of the work started there in the beginning of the cruise. This was accompanied by a relocation of the airbase of Stemme from the international airport of Sal to the domestic airport of Fogo. The further execution of the eddy study at this first eddy, which again included a complete hydrographic survey followed by a mesoscale eddy study with dye release, was therefore possible with aerial observations providing important guidance for work on RV METEOR.

Overall, M160 accomplished an extremely intense and complex work program with 212 instrument deployments during station work, 137 h of observation with several towed instruments and a wide range of continuous underway measurements throughout the cruise. Up to about 30 individually tracked platforms (Saildrones, gliders, wavegliders, drifters, floats) were in the water at the same time providing unprecedented orchestrated observation capabilities in an eddy. All planned work components were achieved and all working groups acquired the expected numbers of instrument deployments and sampling opportunities (Fig. 3).

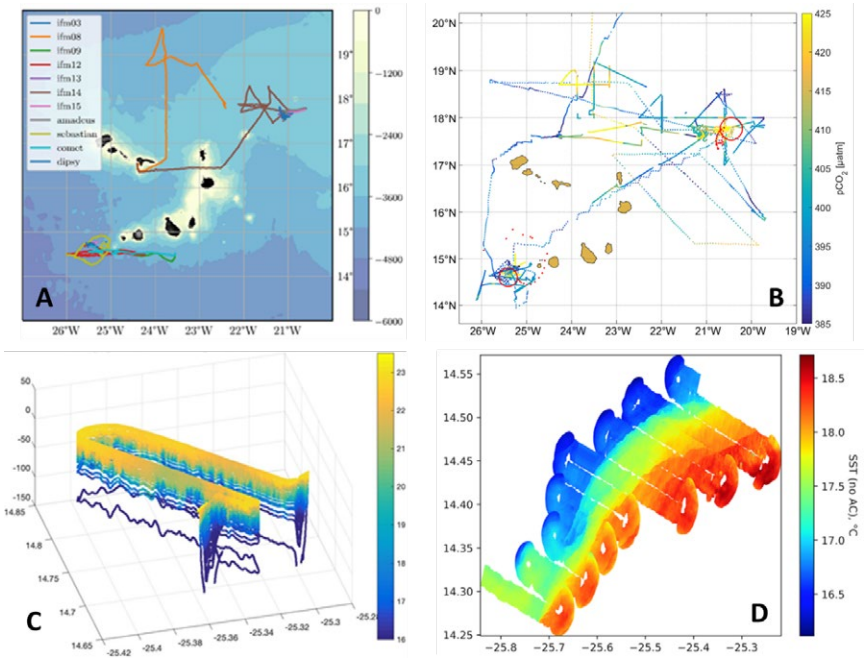

Fig. 3: Examples of deployments of autonomous or airborne instruments for high-resolution observations: (A) Tracks of all deployments of the 11 gliders used during M160, (B) Map of surface pCO2 as measured by RV METEOR, 2 Saildrones, and 2 Wave Gliders during M160, (C) 3D visualization of temperature measurements performed by the Towed Instrument Array system (TIA) during M160 on 13/12/2019, and (D) composite map of sea surface temperature from a flight of the Stemme on 12/12/2019 at the southeastern edge of the mesoscale eddy that was located to the southwest of the island of Fogo.

REFERENCES

Fiedler, B., D. Grundle, F. Schütte, J. Karstensen, C.R. Löscher, H. Hauss, H. Wagner, A. Loginova, R. Kiko, P. Silva, and A. Körtzinger, 2016. Oxygen utilization and downward carbon flux in an oxygen-depleted eddy in the Eastern Tropical North Atlantic. Biogeosciences 13: 5633-5647, doi: 10.5194/bg-13-5633-2016.

Fischer, G., J. Karstensen, O. Romero, K.-H. Baumann, B. Donner, J. Hefter, G. Mollenhauer, M. Iversen, B. Fiedler, I. Monteiro, and A. Körtzinger, 2016. Bathypelagic particle flux signatures from a suboxic eddy in the oligotrophic tropical North Atlantic: production, sedimentation and preservation. Biogeosciences 13: 3203–3223, doi: 10.5194/bg-13-3203-2016.

Grundle, D.S., C.R. Löscher , G. Krahmann, M.A. Altabet, H.W. Bange, J. Karstensen, A. Körtzinger, and B. Fiedler, 2017. Low oxygen eddies in the eastern tropical North Atlantic: Implications for N_2O cycling. Sci. Rep. 7, 4806, doi: 10.1038/s41598-017-04745-y.

Hauss, H., S. Christiansen, F. Schütte, R. Kiko, M. Edvam Lima, E. Rodrigues, J. Karstensen, C.R. Löscher, A. Körtzinger, and B. Fiedler (2016). Dead zone or oasis in the open ocean? Zooplankton distribution and migration in low-oxygen modewater eddies. Biogeosciences 13: 1977–1989, doi: 10.5194/bg-13-1977-2016.

Karstensen, J., F. Schütte, A. Pietri, G. Krahmann, B. Fiedler, B., Grundle, H. Hauss, A. Körtzinger, C.R. Löscher, P. Testor, N. Viera, and Martin Visbeck (2017). Upwelling and isolation in oxygen-depleted anticyclonic modewater eddies and implications for nitrate cycling. Biogeosciences 14: 2167–2181, doi: 10.5194/bg-2016-34.

Löscher, C.R., M.A. Fischer, S.C. Neulinger, B. Fiedler, M. Philippi, F. Schütte, A. Singh, H. Hauss, J. Karstensen, A. Körtzinger, S. Künzel, and R.A. Schmitz (2015). Hidden biosphere in an oxygen-deficient Atlantic open-ocean eddy: future implications of ocean deoxygenation on primary production in the eastern tropical North Atlantic. Biogeosciences 12: 7467–7482, doi: 10.5194/bg-12-7467-2015.

Schütte, F., J. Karstensen, G. Krahmann, H. Hauss, B. Fiedler, P. Brandt, M. Visbeck, and A. Körtzinger, (2016). Characterization of "dead-zone" eddies in the tropical Northeast Atlantic Ocean. Biogeosciences 13: 5865-5881, doi: 10.5194/bg-13-5865-2016.

M161

Contributions to EUREC4A

AUTHORS

Max Planck Institute for Marine Microbiology | Bremen, Germany
W. Mohr

Max Planck Institute for Meteorology | Hamburg, Germany
S. Kinne

Institute of Geophysics – Polish Academy of Sciences | Warsaw, Poland
D. Baranowski

EUREC⁴A – ATOMIC

Climate-cooling trade-wind cumulus clouds are poorly represented in climate models (too few, optically too dense). In addition, small changes to these clouds (e. g. cover, water content) have a strong impact on our climate. Thus, measurements across a range of cloud field realizations are required not just to capture these cloud properties but also interactions of these clouds with their environment (including the ocean). Goals are an improved understanding of the (cloud-life) relevant processes for the development of subsequent parameterizations to better represent unresolved processes and scales in modeling. Europe via EUREC⁴A (Stevens et al. 2021) and the United States via ATOMIC combined their research infrastructures for a month-long (mid-Jan to mid-Feb 2020) campaign over the western subtropical Atlantic. During this field experiment east of Barbados – with its downwind cloud monitoring Barbados Cloud Observatory (BCO) site – four aircraft with cloud in-situ and remote sensing instrumentation probed the atmosphere. Aircraft sampling was complemented by the ground-monitoring of four research vessels (including the R/V METEOR [M161] and R/V MARIA S. MERIAN [MSM89]). These research vessels captured properties of the ocean, the state and transport at the ocean surface and atmospheric properties via in-situ and remote sensing capabilities. The position of the R/V METEOR during the field experiment was chosen to sample statistics on clouds and environmental properties near 57 °W in longitude between 12 and 15 °N in latitude, well upwind of the BCO site and within the domain of aircrafts' operations, as illustrated in Figure 1.

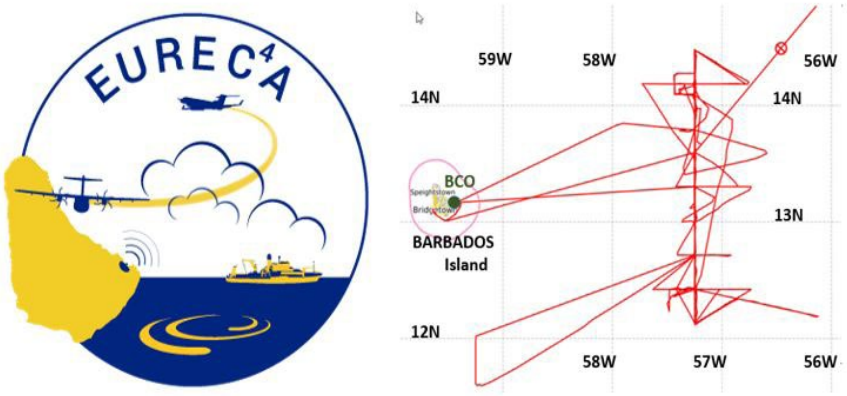

Fig. 1: Field campaign logo (with METEOR image) and the METEOR-covered track.

The complementary atmospheric and oceanic equipment, in addition to the on-board instruments (CTD for regular profiling, thermosalinograph for continuous hull-depth temperature and salinity samples, ADCP for subsurface currents data and meteorological data for atmospheric state data and solar and thermal broadband radiation data), are listed in Tables 1 and 2 including the primary derived properties.

Table 1: Complementary atmospheric equipment for M161

Instrument	Institute	Properties
94GHz cloud bal.radar	LIM	cloud structures/profiles, vertical velocity
microwave radiometer	LIM	profiles (temperature, humidity)
spectrometer	LIM	cloud optical depth, cloud droplet radius
ceilometer	MPI-M	cloud base, profile (lower aerosol)
cloud-cameras	MPI-M	cloud images (visible and thermal)
sun-photometer	MPI-M/NASA	aerosol (AOD, size), water vapor
RAMAN-lidar	MPI-M	profiles (aer, depol, T, w-vap), cloud base
wind-lidar	DUT/FrauHB	vertical winds in lower troposphere
eddy fluxes (front, top)	UNI-HH	momentum, sensible & latent heat fluxes
piccaro	UNM	water vapor vert transport (via isotopes)
Palmex Rain sampler	ETHZ	precipitation

Instrument	Institute	Properties
MAX-DOAS	MPI-C	trace-gases
WRAS	MPI-C	in-situ: aerosol size-distribution
PAX	IOPAN	in-situ: absorption and scattering coeff.
LOCOMOTIVE	U.Warsaw	In-situ: (aerosol) particle mass
radiosondes	MPI-M	profiles (T,RH,p,wind) up to 30 km
UAV	IG-PAS	lower trop in-situ profiles (T,RH,p)
cloud (balloon)-kite	MPI-DS	lower trop in-situ: turbulence, microphys.

Table 2: Complementary oceanic equipment for M161

Instrument	Institute	Properties
Seagliders / Autonaut	UEA	near surface water: T, salinity, velocity
ARGO floats	BSH	upper ocean state monitoring
CTD and incubations	MPI-MM	Biogeochemical processes

The data analysis so far has primarily focused on assuring the quality of the measured properties and slowly studies are underway involving temporal property associations (if not for process understanding so at least for modeling constraints). On a coarser temporal scales studies are on the way, exploring latitude dependencies (northern track vs southern track data), data at low (first two weeks) and high (last two weeks) aerosol loads, data at low and high wind speeds and data at low and high relative humidity statistics. Also, time-series (to BCO or R/V MARIA S. MERIAN side-by-side events) and statistics associations with HALO aircraft overpasses are planned.

CTD profiling during M161 has been the primary tool for monitoring of subsurface ocean physical properties across the core EUREC^{4}A/ATOMIC domain. Salinity structure showed a consistent maximum at about 100 m with near surface, mixed layer water being significantly (1–2 PSU) fresher. A temperature inversion (sometimes exceeding 1 °C) was often encountered at the bottom of the mixed layer (~80 m depth). The magnitude of the salinity variability in the top 200 m as well as the existence and strength of a temperature inversion showed both meridional and temporal variability during the observation period.

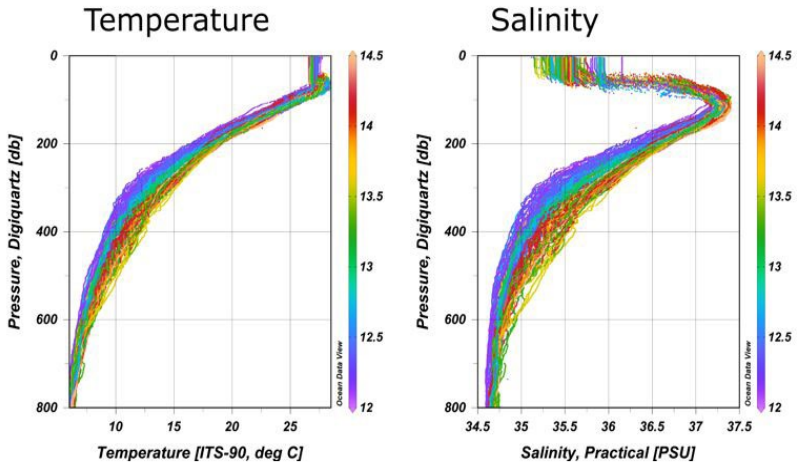

Fig. 2: All temperature (left) and salinity (right) profiles collected during EUREC4A part of the M161 cruise. Data colored by latitude. Many profiles exhibit temperature inversion at the bottom of the mixed layer (~80 m) coinciding with the salinity maximum.

The Western tropical North Atlantic is a nutrient-limited yet productive region where some of the highest rates of dinitrogen gas (N_2) fixation in the ocean have been found so far. Our aims of the M161 cruise were: i) to identify unknown N_2-fixing microorganisms, that likely play a role in this region, including those that have previously been indicated in other studies, ii) to study the dynamics of cyanobacterial N_2-fixing microorganisms due to the high influx of Saharan dust in this region, iii) to investigate the importance of N_2-fixing and non-N_2-fixing microorganisms in the production of the trace greenhouse gas methane (CH_4) and iv) to determine the factors driving the spatial and temporal variability of N_2 fixation rates in the Western tropical North Atlantic. The results will help us understand what is driving N_2 fixation, the largest source of N to the ocean, and associated processes at the meso- and submesoscale level in order to improve global biogeochemical models. So far, we have determined preliminary data for the base biogeochemical parameters such as nutrient and chlorophyll a concentrations as well as for rates of primary production, N_2 fixation and CH_4 production from methylphosphonate at the twelve biogeochemical stations sampled during the cruise (Fig. 3). These data confirm the distribution of chlorophyll a in surface waters (Fig. 3) with concomitant higher rates of primary production and N_2 fixation in the southern half of the M161 study area. Ongoing analyses include the comparison of these data to other data obtained during the cruise such as oceanographic and aerosol properties, the analyses of metagenomic and metatranscriptomic sequencing data to obtain insights into active microorganisms and levels of nutrient limitation, and single-cell activity analyses of cyanobacterial N2-fixing microorganisms.

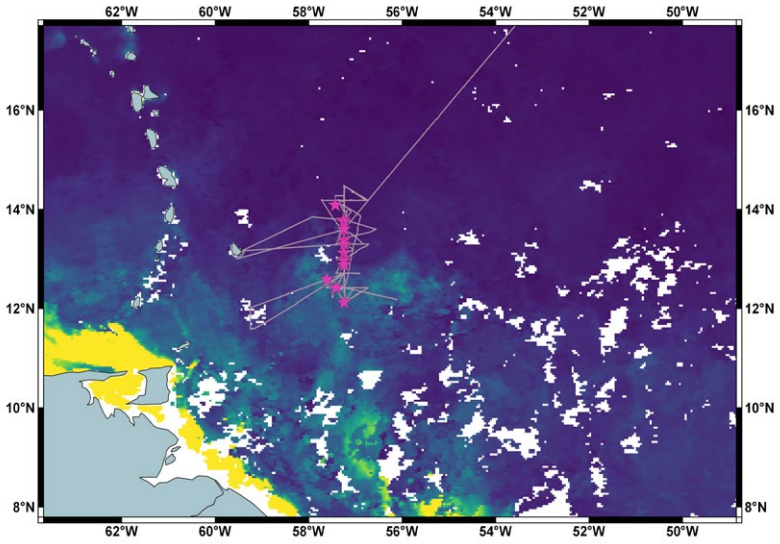

Fig. 3: Map depicting the M161 cruise track off the coast of Barbados. The background color indicates surface chlorophyll concentrations (monthly composite for February 2020) obtained from satellite imagery (NASA Goddard Space Flight Center, Ocean Ecology Laboratory, Ocean Biology Processing Group; (2018): Sea-viewing Wide Field-of-view Sensor (SeaWiFS) Ocean Color Data, NASA OB.DAAC. doi: 10.5067/ORBVIEW-2/SEAWIFS/L2/OC/2018. Accessed on 2020/03/30) with warmer colors representing higher chlorophyll concentrations. Pink asterisks show the twelve biogeochemical stations.

REFERENCE

Stevens B, Bony S, Farrell D, et al. EUREC4A, Earth System Science Data 2021, 13 (8): 4067–4119. doi: 10.5194/essd-13-4067-2021

MSM44 AND MSM66

Reconstruction of past ice sheet dynamics, palaeoceanography and plankton ecology in the Baffin Bay

AUTHORS

Alfred-Wegener-Institute Helmholtz Centre for Polar and Marine Research | Bremerhaven, Germany
B. Dorschel, P. Slabon

MARUM – Center for Marine Environmental sciences, University of Bremen | Bremen, Germany
D. Hebbeln, M. Kucera

MSM44 and MSM66 with RV Maria S. Merian were multidisciplinary research expeditions to the Baffin Bay, a key area for palaeo-climatic, palaeoceanographic and palaeontological research. Major past and recent northern hemisphere ice sheets, including the Laurentide ice sheet (LIS) and Greenland ice sheet (GIS), drain(ed) into this enclosed embayment (e. g. Pieńkowski et al., 2014; Simon et al., 2014). In addition, the Baffin Bay is a major interglacial gateway (blocked during glacial periods) for fresh water and ice transport from the Arctic to the North Atlantic with main connections through the Nares Strait and the Lancaster Sound (Campbell and de Vernal, 2009; Jennings et al., 2011; Tang et al., 2004). During the above-mentioned expeditions, data and samples were collected to reconstruct the retreat histories of the LIS and GIS and palaeoceanographic conditions and sedimentation in the Baffin Bay since the Last Glacial Maximum (LGM).

Glacigenic landforms, such as e. g. moraines, drumlinoid landforms, megascale glacial lineations (MSGL), and grounding zone wedges (GZW), preserved along the shelf edge and on the shelves of Baffin Bay, provide information on the maximum extent of the ice sheets and the dynamics of ice sheet retreats in the area. Dated shelf sediments helped furthermore to constrain the timing of ice sheet retreat and advance events, thus providing a stratigraphic framework for the ice-dynamic processes.

The distribution of glacigenic landforms on the eastern shelf of Baffin Bay indicate that grounded ice streams of the GIS reached across the shelves to the shelf edge at their maximum extents during the LGM (Fig. 1). Retreat of the ice margin from the LGM to the recent position was not continuous and not synchronous. In the northeast Baffin Bay, the retreat of the GIS on the outer shelf was slow continuous and stepwise. Further to the south, it was more episodic with phases of stabilization. Large GZW complexes evidence repeated times of ice margin stabilization (Fig. 1). In addition, indications for temporary

ice margin advances were identified (Slabon et al., 2016). A series of GZWs and moraines in Clyde Fjord on the western side of Baffin Bay indicates that also the retreat of the LIS was episodic since the LGM.

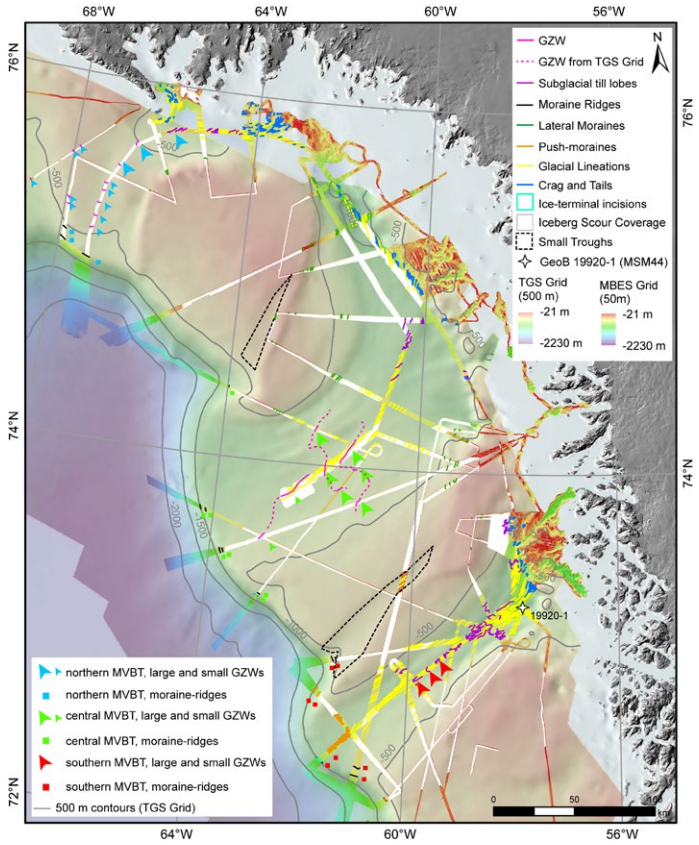

Fig. 1: Glacial landforms identified from bathymetric data collected during expedition MSM44 (Slabon et al., 2016).

The dynamics of the ice sheets around Baffin Bay are closely coupled to the palaeoceanography of the North Atlantic, particularly the inflow of warm water from the Labrador Sea into Baffin Bay (Simon et al., 2014). However, a remarkable temporal mismatch between the largely microfossil-based reconstructions of Holocene Atlantic-water inflow/influence in the Labrador Sea and Baffin Bay and grain size-based current strength reconstructions from the adjacent North Atlantic with a time lag by > 2ka hampered a distinct paleoceanographiy reconstruction for Baffin Bay. A new sediment core-based current strength record from the West Greenland shelf off Nuuk (GeoB 19905-1) now allowed a detailed reconstruction of Atlantic Water (AW)-inflow to the Labrador Sea via the West Greenland Current (WGC). It reveals a very good alignment of the Holocene AW-inflow into Labrador Sea with the Holocene Speed Maximum

documented in the North Atlantic (Fig. 2; Weiser et al. (2021)). The observed lag between the microfossil-based records and the Holocene Speed Maximum can be explained when considering the presence of an extended meltwater lens that prevented the shoaling of the inflowing Atlantic waters. Once the meltwater discharge waned after the cessation of large-scale melting of the surrounding ice sheets, the AW could influence the surface waters, independently of the strength of its inflow. Only then was an effective ocean-atmosphere heat transfer enabled, triggering the comparably late onset of the regional Holocene Thermal Maximum (Fig. 2). Furthermore, sediment geochemical analyses show that short term cooling events, such as the 8.2 ka event related to the final drainage of glacial Lake Agassiz, lead to glacier advances of the Greenland Ice Sheet. Since the grain size data show that these events had no influence on the AW-inflow to the north eastern Labrador Sea, these advances must have been caused by atmospheric cooling. Thus, this new record shows that (i) in this region, surface water-based proxies register AW influence rather than inflow, (ii) the AW-inflow into the Labrador Sea is controlled by the circulation in the North Atlantic, but (iii) its impact on an effective ocean-atmosphere heat transfer was hindered by a prevailing meltwater lens in the early Holocene, i. e. until the cessation of large-scale melting of the surrounding ice sheets (Weiser et al., 2021).

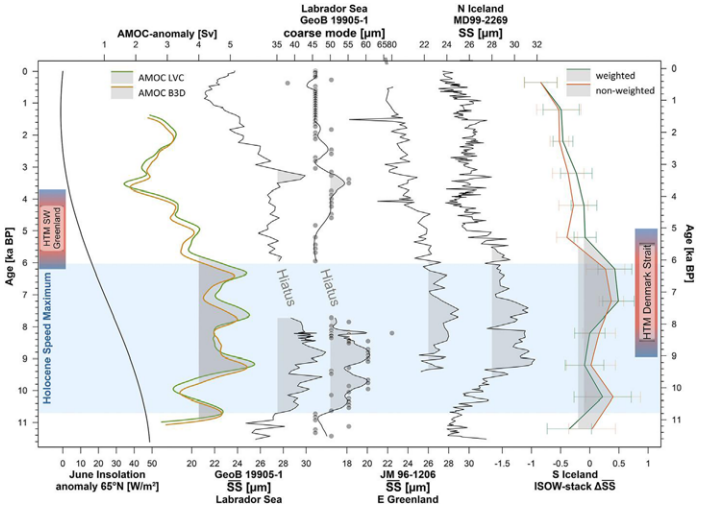

Fig. 2: Compilation of current strength reconstructions from the North Atlantic and the Labrador Sea in relation to insolation and regionally varying Holocene Thermal Maxima (HTM; after Kaufman et al. (2004)), grey shaded areas mark the respective Holocene Speed Maxima (HSM), blue shading indicates general HSM-timeframe. Atlantic Meridional Overturning Circulation (AMOC) anomaly from Ritz et al. (2013), JM96-1206 and MD99-2269 sortable silt mean grain size (SS) from McCave and Andrews (2019), Iceland-Scotland Ridge Overflow Water (ISOW)-stack from Thornalley et al. (2013), and GeoB 19905-1 record from Weiser et al. (2021).

The circulation in Baffin Bay obviously is closely connected to the sea ice cover, which is a critical component of the climate system, known to influence ocean circulation, earth's

albedo, and ocean–atmosphere heat and gas exchange. In the NE Baffin Bay, off NW Greenland, Melville Bugt in the northeast Baffin Bay is a climate-sensitive region characterized by strong seasonal sea ice variability and strong melt-water discharge from the GIS. For this region, a new sea ice record, based on sea-ice proxy IP25 and open-water phytoplankton biomarkers (brassicasterol, dinosterol and HBI III) based on core GeoB19927-3, provdied the first centennial-scale resolution Holocene record of sea ice variability (Saini et al., 2020). A cold interval between prior to ~9.4 ka BP, characterized by extensive sea ice cover and very low local productivity, is succeeded between ~9.4-8.5 ka BP by reduced sea ice cover, enhanced GIS spring melting, and strong influence of the WGC. From ~8.5 until ~7.8 ka BP, a cooling event is recorded by ice algae and phytoplankton biomarkers. These indicate an extended sea ice cover, possibly related to the opening of Nares Strait connecting the Baffin Bay to the Arctic Ocean in the north, which may have led to an increased influx of Polar Water into NE-Baffin Bay. The interval between ~7.8 and ~3.0 ka BP is characterized by generally reduced sea ice cover with millennial-scale variability of the (late winter/early spring) ice-edge limit, increased open-water conditions (polynya type), and a dominant WGC carrying warm waters at least as far as the Melville Bugt area. During the last ~3.0 ka BP, the biomarker records do not reflect the late Holocene 'Neoglacial cooling' observed elsewhere in the Northern Hemisphere, possibly due to the persistent influence of the WGC and interactions with the adjacent fjords. When integrated with marine and terrestrial records from other circum-Baffin Bay areas (Disko Bay, the Canadian Arctic, the Labrador Sea), the Melville Bugt biomarker records point to close ties with high Arctic and Northern Hemispheric climate conditions, driven by solar and oceanic circulation forcing (Saini et al., 2020).

REFERENCES

Campbell DC, de Vernal A, Marine geology and paleoceanography of Baffin Bay and adjacent areas. Nain, NL to halifax, NS, August 28-September 23, 2008. Cruise report of CCGS Hudson Expedition 2008029, Natural Resources Canada 2009,(Open File 5989), 201

Jennings AE, Sheldon C, Cronin TM, Francus P, Stoner J, Andrews JT, The Holocene History of Nares Strait: Transition from Glacial Bay to Arctic-Atlantic Throughflow, Oceanography 2011, 24(3), 26–41, doi:http://dx.doi.org/10.5670/oceanog.2011.52.

Kaufman DS, Ager TA, Anderson NJ, Anderson PM, Andrews JT, Bartlein PJ, Brubaker LB, Coats LL, Cwynari LC, Duvall ML, Dyke AS, Edwards ME, Eisner WR, Gajewski K, Geirsdóttir A, Hu FS, Jennings AE, Kaplan MR, Kerwin MW, Lozhkin AV, MacDonald GM, Miller GH, Mock CJ, Oswald WW, Otto-Bliesner BL, Porinchu DF, Rühland K, Smol JP, Steig EJ, Wolfe BB, Holocene thermal maximum in the western Arctic (0–180°W), Quaternary Science Reviews 2004, 23(5–6), 529–560, doi:https://doi.org/10.1016/j.quascirev.2003.09.007.

McCave IN, Andrews JT, Distinguishing current effects in sediments delivered to the ocean by ice. II. Glacial to Holocene changes in high latitude North Atlantic upper ocean flows, Quaternary Science Reviews 2019, 223105902, doi:https://doi.org/10.1016/j.quascirev.2019.105902.

Pieńkowski AJ, England JH, Furze MFA, MacLean B, Blasco S, The late Quaternary environmental evolution of marine Arctic Canada: Barrow Strait to Lancaster Sound, Quaternary Science Reviews 2014, 91184–203, doi:http://dx.doi.org/10.1016/j.quascirev.2013.09.025.

Ritz SP, Stocker TF, Grimalt JO, Menviel L, Timmermann A, Estimated strength of the Atlantic overturning circulation during the last deglaciation, Nature Geoscience 2013, 6(3), 208–212, doi:https://doi.org/10.1038/ngeo1723.

Saini J, Stein R, Fahl K, Weiser J, Hebbeln D, Hillaire-Marcel C, de Vernal A, Holocene variability in sea ice and primary productivity in the northeastern Baffin Bay, arktos 2020, 6(1), 55-73, doi:https://doi.org/10.1007/s41063-020-00075-y.

Simon Q, Hillaire-Marcel C, St-Onge G, Andrews JT, North-eastern Laurentide, western Greenland and southern Innuitian ice stream dynamics during the last glacial cycle, Journal of Quaternary Science 2014, 29(1), 14–26, doi:https://doi.org/10.1002/jqs.2648.

Slabon P, Dorschel B, Jokat W, Myklebust R, Hebbeln D, Gebhardt AC, Greenland ice sheet retreat history in the northeast Baffin Bay based on high-resolution bathymetry, Quaternary Science Reviews 2016, 154182–198, doi:https://doi.org/10.1016/j.quascirev.2016.10.022.

Tang CCL, Ross CK, Yao T, Petrie B, DeTracey BM, Dunlap E, The circulation, water masses and sea-ice of Baffin Bay, Progress in Oceanography 2004, 63(4), 183–228, doi:http://dx.doi.org/10.1016/j.pocean.2004.09.005.

Thornalley DJR, Blaschek M, Davies FJ, Praetorius S, Oppo DW, McManus JF, Hall IR, Kleiven H, Renssen H, McCave IN, Long-term variations in Iceland–Scotland overflow strength during the Holocene, Clim. Past 2013, 9(5), 2073–2084, doi:https://doi.org/10.5194/cp-9-2073-2013.

Weiser J, Titschack J, Kienast M, McCave IN, Lochte AA, Saini J, Stein R, Hebbeln D, Atlantic water inflow to Labrador Sea and its interaction with ice sheet dynamics during the Holocene, Quaternary Science Reviews 2021, 256106833, doi:https://doi.org/10.1016/j.quascirev.2021.106833.

MSM51 AND MSM62

Baltic Sea Littorina Stage and Deep Ventilation – LISA I & II

AUTHORS

Institute of Geosciences, Kiel University | Kiel, Germany
R. Schneider

Leibniz Institute for Baltic Sea Research | Warnemünde, Germany
M. Moros, T. Neumann

Cruises MSM51 and MSM62 were dedicated to perform seismo- and hydroacoustic surveys, sampling of Holocene sediments, and to investigate the water column wintertime mixing close to sea-ice limits. The primary goals were to improve our understanding of variations in the ventilation of the deeper Baltic, considering the effects of postglacial sea-level rise and isostatic uplift, next to climatic forcing during Holocene. In particular, we wanted to investigate in detail the impact of the Littorina transgression on the inflow of saline waters into the western Baltic and assess the potential for future diminution of ventilation in the central and northern deeper basins due to isostatic uplift. As the influence of saline water inflow into these basins is likely to decrease, the role of wintertime deep mixing in deep water oxygenation of the northern basins was one main target. Moreover, new hydroacoustic surveying in the western Baltic basins during maximum sea ice extent and deployment of a new vibro-corer system in silty-sandy sediment drifts and transgressive deposits in the inflow region of the Great Belt and the Kattegat were an important progress for a quantitative assessment of Holocene water and sediment budgets as well as to account for the impact of budget changes on the Baltic Sea ecosystem during the Littorina Stage.

With respect to the latter, first investigations of the new vibro-corer retrieved sediment cores from the western Baltic contributed to a new synthesis for the timing of the Littorina transgression flooding the western Baltic straits (Bennike et al., 2021). Most of the ages based on shells of marine molluscs imply that the northern part of the Great Belt region was inundated about 8.9 cal. ka BP, slightly before the central part of the Great Belt at about 8.2 cal. ka BP, while in the southwestern Baltic it took place about 7.0 to 8.1 cal. ka BP. The brackish-water phase before may have lasted for about 500 to 1000 years. In contrast, youngest lake deposits without signs of marine influence are dated 8.8 cal. ka BP (Great Belt), 8.7 cal. ka BP (Little Belt) and 8.5 cal. ka BP (Arkona Basin).

For the northern and central Baltic Basins, the first results of the geological work in progress, addressing the sediment dynamics and spread of anoxia during the Littorina Stage, support the scenario of past changes in the occurrence of deep-water formation

and its effects on sediment redistribution as published in Moros et al. (2020). Former and new hydroacoustic surveys of the Baltic Sea seabed reveal the. so far not much explored, occurrence of sediment contourite drifts and re-suspension at greater water depths. In addition, radiocarbon dating of bulk sediments indicates numerous age reversals. Results of previous and new hydrographic measurements combined with those from geological studies now indicate that a deep-water formation process significantly affected the seabed dynamics during regional climatically cold phases during the last 7,000 years (Fig. 1). It is very likely, that during colder periods newly formed bottom waters caused widespread re-suspension of organic carbon-rich laminated sediments. originally deposited during the preceding warm periods in shallower areas. Probably, this material was transported to and re-deposited in the deeper parts of the Baltic Sea sub-basins north of the Baltic Sea Klint, a topographic high, that acted as a hydrographic barrier for deep-water formed in the northern Baltic. Moreover, deep-water formation produced bottom currents that led to the formation of sediment contourite drifts at water depths of > 200 m in the Bothnian Sea, the Åland Deep and northern central Baltic Sea sub-basins.

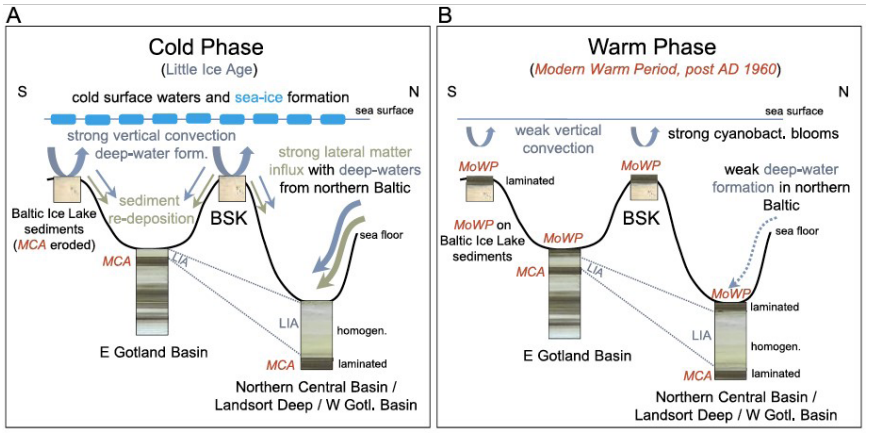

Fig. 1: Schematic sketches of deep-water formation processes on sediment accumulation during a cold (A) and a warm (B) phase with strong and weak formation, respectively, in sub-basins south and north of the Baltic Sea Klint. South of the Klint, during the cold Little Ice Age (LIA: blue) phase (A) strong local winter convection erodes laminated sediments accumulated in shallower areas and not affected during the warm Medieval Climate Anomaly due to weaker convection (MCA: red italic). North of the Klint, strong sediment influx via deep water inflow from the northern Baltic caused a much higher thickness of homogenous sediments accumulated during the LIA (A). During the recent Modern Warm Period (MoWP post AD 1960: red italic), however, deep water formation weakened and laminated sediments accumulate also at shallower water depths (B). (from Moros et al. 2020).

Such features are not observed for the warm climate intervals implying a much weaker deep convection and ventilation in the northern basins then. Furthermore, since bottom water ventilation in the Baltic Sea is generally assumed to be determined solely by the inflow of oxygen-rich, saline water from the North Sea, our geological findings postulate that for the northern basin deep-water formation is a key process for ventilation and

spread of anoxia of bottom waters in addition. However, if this process was much weaker during warm climate periods as the data suggests, this raises the immediate question about the conditions of deep basin ventilation under even warmer conditions in the future.

REFERENCES

Bennike O, Jensen J B, Nørgaard-Pedersen N, Andresen K J, Seidenkrantz M-S, Moros M, Wagner B, When were the straits between the Baltic Sea and the Kattegat inundated by the sea during the Holocene? Boreas 2021, 50, 1079–1094, doi.org/10.1111/bor.12525. ISSN 0300-9483.

Moros M, Kotilainen TP, Snowball I, Neumann T, Perner K, Scherff I, Meier MHE, Leipe T, Zillén L, Sinninghe Damsté J, Schneider RR, Is 'deep-water formation' in the Baltic Sea a key to understanding seabed dynamics and ventilation changes over the past 7,000 years? Quaternary International 2020, 550, 55–65, doi.org/10.1016/j.quaint.2020.03.031.

MSM70

Detailed Mapping and Sampling of the Bathymetrists Seamounts and Adjacent Fracture Zones

AUTHORS

King Abdullah University of Science and Technology | Thuwal, Saudi Arabia
F.M. van der Zwan

GEOMAR Helmholtz Centre for Ocean Research | Kiel, Germany
N. Augustin

Kiel University | Kiel, Germany
C.D. Garbe-Schönberg

STRESS CONTROLLED PLACEMENT AND GEOCHEMISTRY OF THE BSM

Intraplate volcanism is one of the major surface manifestations of magma production with a unique and distinct chemical composition. Nevertheless, the origin of some of these intraplate volcanic provinces is not entirely clear, as they can be related to either mantle plumes or the presence of large fault systems. One example is the poorly investigated Bathymetrists Seamount Chain in the central-eastern Atlantic. This intraplate volcanic province has been associated with the Sierra Leone Rise mantle plume but is also located in an area with dense and extended transform fault systems related to the final breakup of Africa and South America.

The BATHYCHEM (MSM70, Dec 2017–Febr 2018) cruise aimed to characterize the structure, age, and composition of the Bathymetrists Seamounts and adjacent fracture zones to understand their origin and formation mechanism, which will allow a better assessment of how intraplate volcanism forms and modifies the structure and composition of oceanic lithosphere through time. The MSM70 expedition undertook high-resolution hydroacoustic mapping and dense rock sampling of the study area to achieve these aims. The new bathymetric maps (50 m resolution) revealed a complicated pattern for the emplacement of the seamounts and indicated that most of the seamounts resemble guyots capped by carbonated platforms, phosphorites, and abundant manganese-iron crusts. In addition, the morphological analyses of the seamounts together with geodynamic modeling indicated tectonically determined volcano emplacement following complex crustal fault patterns related to the local stress regime during left-lateral shear of multiple transform faults (van der Zwan et al., in prep). Igneous samples from 27 volcanic seamounts revealed dense basaltic samples and vesicular volcanoclastic material of mafic origin containing pyroxenes, amphiboles, and biotite. Geochemically, the

recovered lavas have alkali ocean island basalt compositions (e. g., Nb/Yb>25 at TiO2/Yb=1.2) and indicate that melts were generated by low degrees of deep melting of the mantle. The distinct HIMU isotopic signatures indicate a plume-like origin for the magmas of the Bathymetrists Seamounts (Long et al., 2020). The combination of the rock chemistry and the morphological characteristics of the volcanoes indicate that a deep mantle plume formed the Bathymetrists Seamounts. At the same time, the complex shear-fault structures in the crust and lithosphere provided the melt pathways.

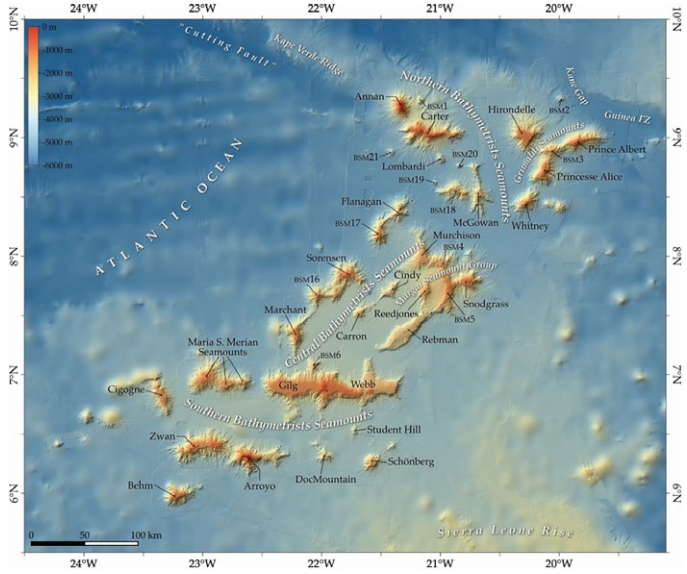

Fig. 1: Combination of low- (GEBCO) and high-resolution ship bathymetry (from expeditions MSM70 and M152/2) of the Bathymetrists Seamounts in the central-eastern Atlantic (from van der Zwan et al., in prep.).

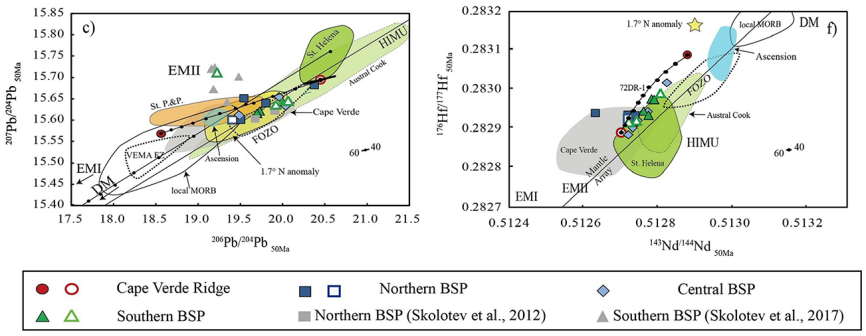

Fig. 2: Initial (age-corrected) Nd-Pb-Hf isotope ratios of investigated lavas from the Bathymetrists Seamounts and Cape Verde Ridge shown in comparison to literature samples of surrounding volcanic provinces (see Long et al., 2019 for details). The samples fall on mixing lines (shown with 10 % increments) between the depleted Cape Verde Ridge lava 5DR-5 (believed to reflect local upper mantle) and enriched Cape Verde Ridge sample 5DR-8 (assumed to closest resemble the proposed BSP plume composition). From Long et al., 2020

REFERENCES

Long X, van der Zwan FM, Geldmacher J, Hoernle K, Hauff F, Garbe-Schönberg CD, Augustin N, Insights into the petrogenesis of an intraplate volcanic province: Sr-Nd-Pb-Hf isotope geochemistry of the Bathymetrists Seamount Province, eastern equatorial Atlantic. Chemical Geology 2021, 544, 119599.

van der Zwan FM, Augustin N, Le Saout M, Wölfl A-C, Schade M, Seidel E, Lampridou D, Follmann J, Antonio RJ, Heinath V, Köse MC, Krach L, Long X, Miluch J, Schönberg J, Hübscher C, Geldmacher J, Hoernle K, Garbe-Schönberg C-D, The Bathymetrists Seamount Chain: a structurally controlled intraplate volcanic province. In preparation for Geomorphology

MSM71

LOBSTER – Ligurian Ocean Bottom Seismology and Tectonics Research

AUTHORS

GEOMAR Helmholtz Centre for Ocean Research | Kiel, Germany
H. Kopp, D. Lange, I. Grevemeyer, A. Dannowski, F. Wolf, L. Murray-Bergquist

Christian-Albrechts-University Kiel | Kiel, Germany
M. Thorwart

Institut de Physique du Globe de Paris IPGP | Paris, France
W. C. Crawford

Université Grenoble Alpes, Université Savoie Mont Blanc, CNRS, IRD, UGE, ISTerre | Grenoble, France
A. Paul

Istituto per la dinamica dei processi ambientali IDPA-CNR | Milano, Italy
G. Caielli, R. de Franco

INTRODUCTION AND OBJECTIVES

The Ligurian Sea has a complex geodynamic setting manifested in pronounced variations in crustal thickness. Topographic gradients in the area are the largest for the entire Alpine-Mediterranean domain, rising from -2500 m in the Ligurian basin to >3000 m in the Alpine-Apennine orogen over a distance of less than 100 km. The northern margin of the Ligurian Basin shows notable seismicity at the Alpine front, including frequent magnitude 4 events. Seismicity decreases offshore towards the Basin centre and Corsica, revealing a diffuse distribution of low magnitude earthquakes.

The Ligurian Basin is a back-arc basin that opened by the south-eastward trench retreat of the Apennines-Calabria-Maghrebides subduction zone. Late-Oligocene-to-Miocene rifting caused continental extension and subsidence. Yet it remains unclear if rifting caused continental break-up and seafloor spreading. The kinematic boundaries around the Ligurian Basin are poorly resolved, in particular the transition from the continental domain to the oceanic domain at its northern termination (Figure 1). The recent deformation in the Ligurian Sea results from compression along its northern margin, but rates of deformation are very low.

Both, the LOBSER active seismic experiment conducted during MSM71 as well as the long-term AlpArray ocean bottom seismometer (OBS) network recovered during MSM71, provide new active and passive seismic data of excellent quality to characterise the lithospheric structure and to shed light on today's active deformation in the Ligurian Sea. The AlpArray OBS network consists of stations from IPGP, DEPAS pool and GEOMAR that were deployed with RV Pourquoi Pas?. Further, the AlpArray OBS network contributes to the European AlpArray initiative and complements the AlpArray seismic network that consisted of several hundred closely spaced broadband land seismometers that cover the entire Alpine orogen.

The scientific aim of the LOBSTER project is manifold: (1) characterisation of the crust and upper mantle of the Ligurian Basin and the transition from the oceanic to the continental domain; (2) understanding the structures and kinematics of rifting during the opening of the Ligurian Sea; (3) imaging the prolongation of the Alpine front; and (4) studying the recent deformation in the Ligurian Basin and the surrounding coastal areas as imaged through local seismicity.

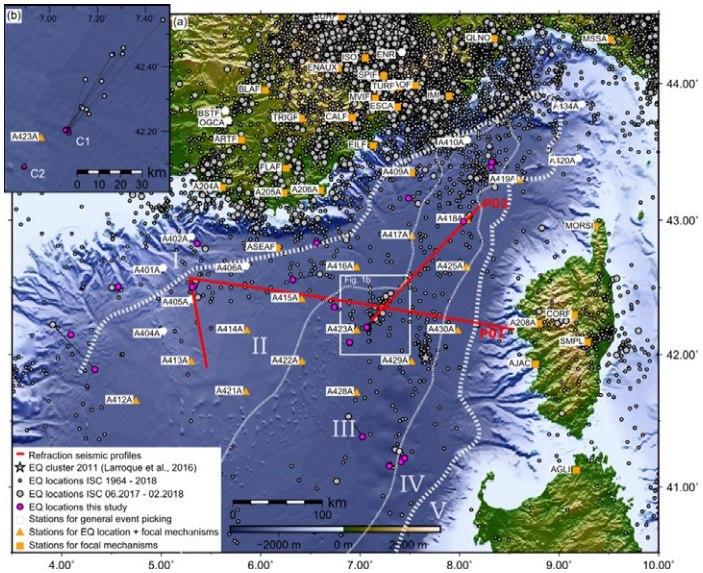

Fig. 1: Bathymetric map of the Ligurian Sea and surrounding. Superposed the wide-angle profiles from the MSM71 cruise (red lines P01 and P02), orange triangles and squares for the long-term broad-band ocean bottom seismometers and land-stations. The magenta circles show the locations of earthquakes during June 2017 and February 2018. White dashed lines mark the different proposed crustal domains: continental domain (I and V), transitional domain (II and IV), and oceanic domain (III).

DATA AND METHODS

To tackle the described aims, two wide-angle seismic refraction lines were shot (Figure 1). The active seismic shots where used to determine the directions of the horizontal seismometer

components and control the timing and location of the long-term AlpArray OBS network stations. Simultaneously to the OBS shot recordings, multi-channel seismic (MCS) data were acquired on a mini-streamer. Profile P01 was extended by three land stations.

Refraction seismic data were picked manually and served as input for travel time tomography (Tomo2D, Korenaga et al., 2000). MCS data were used to identify the geometry of the uppermost sedimentary layers. Additionally, gravity modelling is applied to prove the seismic modelling and extend the profile north-eastwards towards the Italian coast.

Local seismic events were picked on the data from the AlpArray OBS network and other permanent and AlpArray land stations. After this initial picking, the work focused on two earthquake clusters of 16 events (M2.5 or smaller) that occurred from June to November 2017. The fault plain solutions from P-wave and amplitude ratios of P- and S-waves of the vertical component were calculated.

Ambient noise cross-correlation technique was applied on the AlpArray OBS network data combined with AlpArray land stations in the coastal area. In addition, the cross-correlation technique was also applied to time windows of teleseismic events recorded on the same stations. Data processing of the OBS data included correction for tilt and compliance. Group velocity dispersion curves were calculated. A crucial step was to separate fundamental modes and higher modes of the Rayleigh waves by picking the dispersion curves by hand. In the marine ray paths, SE in the basin, higher modes were primarily observed. The Fast Marching Surface Tomography (FMST, Rawlinson and Sambridge, 2004; 2005) was used to perform a surface wave tomography for group velocities of ambient noise data and teleseismic data. 3D group velocity maps were generated.

Recently, the second phase of the SPP 4DMB started. In the scope of the new project a 3D body wave tomography will be performed using airgun shots and earthquakes recorded on OBS and land stations. The results will be combined with geologic observations in a tectonic reconstruction.

RESULTS AND DISCUSSION

The P-wave velocity models along the active seismic profiles p01 and p02 in the Ligurian Basin show a high velocity gradient of ~1 s-1 for the uppermost ~1.5 km, interpreted as Plio-Quaternary sediments with velocities increasing from ~2.2 km/s at the seafloor to ~3.5 km/s at ~1.5 km depth. They overlay a thick Messinian salt unit that is characterised by velocities of ~4.4 km/s and shows salt tectonism. Underneath the salt unit, Pre-Messinian and Tortonian sediments have been accumulated with seismic velocities of up to ~5.7 km/s. Towards Corsica, the sedimentary units thin out, while they reach a thickness of up to 7 km in the basin centre. Seismic velocities of up to 6.8 km/s are observed along both profiles for the crust. Profile p02 images the gradual NE–SW decrease in crustal thickness as a result of increased continental stretching towards SW caused by the counter-clockwise rotation of the Corsica-Sardinia block. Profile p01

images the crustal stretching along the opening direction. At the Corsican margin, the Moho is deepening extremely from ~11 km to ~24 km depth within a short distance of 30 km. Based on seismic velocities, we interpret that the crust imaged along both profiles is of continental nature and that rifting failed before oceanic spreading was initiated.

The data from the AlpArray OBS network confirm that the entire Ligurian Basin is characterised by sparse but wide-spread micro-earthquakes of low magnitudes. The OBS recorded between June 2017 and February 2018 two earthquake clusters that show thrust faulting mechanisms, supporting a model of inversion of the Ligurian Basin, in which the basin's centre is under compression and stresses are taken up by reactivated faults in the crust and uppermost mantle. Compressional forces are probably related to Africa-Europe plate convergence and the major part of these forces in the Ligurian Basin are taken up at its northern margin. The location of the cluster events and their focal mechanisms indicate that they occurred in reactivated pre-existing rift-related structures. Slightly different striking directions of faults in the basin centre compared to faults further east and hence away from the rift basin may reflect the counter-clockwise rotation of the Corsica-Sardinia block. A high mantle S-wave velocity of Vs=4.7 km/s and a low Vp/Vs ratio of 1.72 reveal a strengthening of the crust and uppermost mantle during the Oligocene-Miocene rifting.

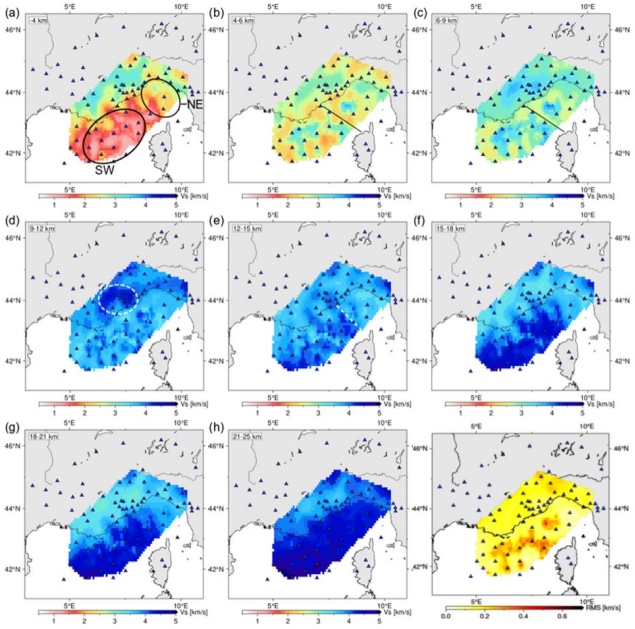

Fig. 2: 2D shear velocity maps (for different depths intervals) derived from 1D inversion of group velocity maps. Annotations in (a) mark the southwestern and central (SW) and the northeastern (NE) Ligurian Basin. The dashed circle in (d) marks a high-velocity area north of Nice and the dashed white line in (e) represents the proposed prolongation of the Alpine front. Panel (i) shows the root mean square (RMS) value for the 1D shear-wave-inversion in map view (i. e. one RMS value per grid point). Blue triangles mark the stations used in this study.

The ambient noise analysis and the correlation of teleseismic events resulted in the first 3D high-resolution seismic group and shear velocity models for the Ligurian Basin. Onshore, our results compare well with existing larger-scale ambient noise studies. We reveal a high-velocity area at the Argentera Massif, approximately 10 km below sea level. Offshore, the lithospheric structure in the Ligurian Basin mostly mimics the geometry of the basin. Shear-wave velocity maps (Figure 2) indicate a gradual deepening of the Moho from 12–15 km in the SW basin centre towards 20–25 km in the NE basin and a rapid deepening from the basin axis to the northern margin. Based on the low Vp/Vs ratios of 1.74, comparable to the local seismicity study, we exclude mantle serpentinisation in the basin centre. In the SW part, the opening of the basin is more developed, but we do not observe oceanic crust in our study area, which is in good agreement with the findings from the two active seismic profiles.

REFERENCES

Korenaga, J., Holbrook,W. S., Kent, G. M., Kelemen, P. B., Detrick, R. S., Larsen, H.-C., Hopper, J. R., and Dahl-Jensen, T., Crustal structure of the southeast Greenland margin from joint refraction and reflection seismic tomography, J. Geophys. Res.-Sol. Ea. 2000, 105, 21591–21614, doi: https://doi.org/10.1029/2000JB900188.

Rawlinson, N. and Sambridge, M., Wave front evolution in strongly heterogeneous layered media using the fast marching method, Geophys. J. Int. 2004, 156, 631–647, doi: https://doi.org/10.1111/j.1365-246X.2004.02153.x.

Rawlinson, N. and Sambridge, M., The fast marching method: an effective tool for tomographic imaging and tracking multiple phases in complex layered media, Explor. Geophys. 2005, 36, 341–350, doi: https://doi.org/10.1071/EG05341.

MSM72

Variability and Trends in Physical and Biogeochemical Parameters of the Mediterranean Sea

AUTHORS

GEOMAR Helmholtz Centre of Ocean Research Kiel | Kiel, Germany
T. Tanhua

Institute of Oceanography, University of Hamburg | Hamburg, Germany
D. Hainbucher

The last decades have seen dramatic changes in the hydrography and biogeochemistry of the Mediterranean Sea. The complex bathymetry, highly variable spatial and temporal scales of atmospheric forcing, convective and ventilation processes contribute to generate complex and unsteady circulation patterns and significant variability in biogeochemical systems. Part of the variability of this system can be influenced by anthropogenic contributions. Consequently, it is necessary to document details and to understand trends in place to better relate the observed processes and to possibly predict the consequences of these changes.

The main objective of cruise MSM72 was to contribute to the understanding of long-term changes and trends in physical and biogeochemical parameters, such as the anthropogenic carbon uptake and to further assess the hydrographical situation after the major climatological shifts in the eastern and western part of the basin, known as the Eastern and Western Mediterranean Transients.

The survey was carried out from 2nd of March to 3rd of April 2018. The cruise started on Iraklion, Greece and ended in Cadiz, Spain (Figure 1)c. The main focus of the cruise was on an east-west transect across the Western and Eastern Mediterranean Sea starting east of Crete and ending near the Strait of Gibraltar (figure 1), which is a repeat of the hydrographic line in GO-SHIP called MED1. Sections were additionally conducted across some important passages: The Strait of Otranto, Kasos Strait, Antikythera Strait, Strait of Sicily and Strait of Gibraltar, in order to characterize the incoming and outgoing flows. CTD stations in the Eastern Ionian Sea were carried out to quantify the flow of the Levantine Surface Water (LSW) into the Adriatic Sea and to track the outflow of the Adriatic Deep Water (AdDW) into the Ionian Sea.

During the thirty-three days of the cruise we carried out measurements of hydrographic and biogeochemical variables along-track with the classical approach i. e. CTD, lADCP, uCTD instrumentation and bottle samples on highly resolved sections across the

Mediterranean Sea. The high resolution of CTD stations, enhanced for the physical parameters by additional uCTD measurements, allowed us to resolve the eddy field on the sections, the analysis was also supported and complemented by satellite data. Most sections and CTD-positions followed previous sampling strategies to allow long-term trend analyses. Along the different sections, CTD stations including sampling of chemical parameters were conducted approximately every 30 nm, CTD without sampling about every 15–20 nm and with even smaller spacing in the Straits. In addition, underway CTD measurements and ADCP measurements were performed between CTD stations.

The water sampling program included measurements of all level 1 variables as defined by GO-SHIP (i. e. oxygen, macronutrients, transient tracers and the carbonate system,) and measurements of the biogeochemical variable such as 13C, nitrous oxide (N_2O) and dissolved organic carbon (DOC) isotopes of nitrate isotopes of organic particulate matter, particulate matter optical properties, particulate organic carbon and particulate nitrogen and their stable isotopes (Chaikalis et al., 2021). These data were used to quantify trends and variability of ventilation and biogeochemical cycles, in particular uptake of anthropogenic carbon.

The transient tracer observations during MSM72 added to a time-series of such observations that quantify the variability of deep ventilation of the Mediterranean Sea (Figure 2). The new observations were able to more specifically determine the strength of deep convection over time (Figure 3, Li and Tanhua, 2020).

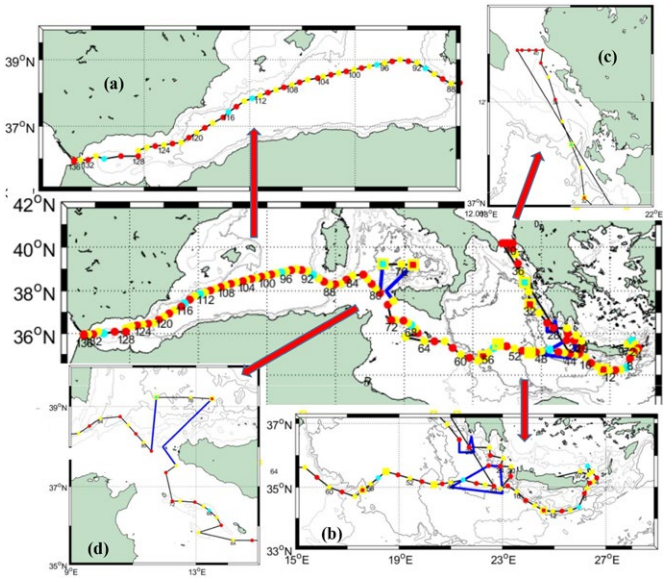

Fig. 1: Station Map. Yellow dots: CTD without any chemical sampling, red dots: CTD with chemical sampling, cyan dots: CTD with chemical and additional sampling of isotopes, yellow squares: deployment of drifter and floats, blue lines: fine resolved uCTD and ADCP tracks. Black lines: Track with uCTD casts between CTD stations.

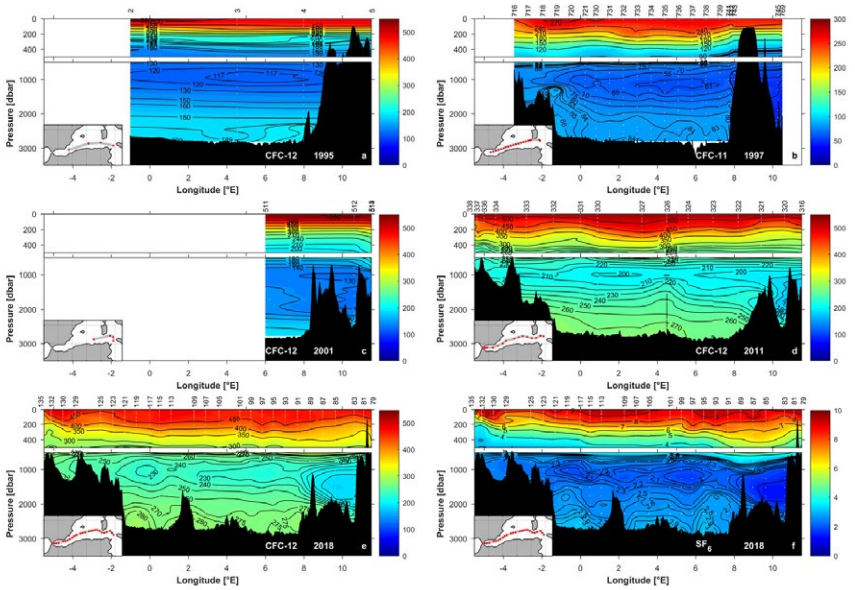

Fig. 2: Time series of transient tracer sections in the Western Mediterranean Sea, the result from MSM72 in the bottom row (Li and Tanhua, 2020).

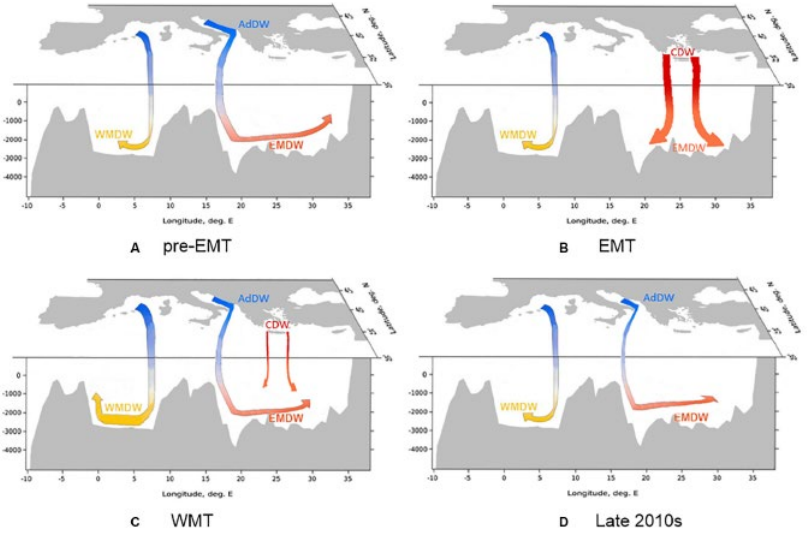

Fig. 3: Schematic figures of the Mediterranean deep overturning circulation (A) before the EMT, (B) during the EMT, (C) during the WMT, and (D) in the late 2010s, Colors highlight the approximate change in salinity (blue = low salinity and red = high salinity). Thickness of arrows represents the approximate change in source intensity (thick = high intensity and thin = low intensity). Water masses are defined as follows: AdDW, Adriatic Deep Water; CDW Cretan Deep Water; EMDW, Eastern Mediterranean Deep Water; WMDW, Western Mediterranean Deep Water (Li and Tanhua, 2020).

REFERENCES

Chaikalis, S., Parinos, C., Möbius, J., Gogou, A., Velaoras, D., Hainbucher, D., Sofianos, S., Tanhua, T., Cardin, V., Proestakis, E., Amiridis, V., Androni, A., and Karageorgis, A.: Optical Properties and Biochemical Indices of Marine Particles in the Open Mediterranean Sea: The R/V Maria S. Merian Cruise, March 2018, Journ10.3389/feart.2021.614703al, 9, 2021.

Li, P. and Tanhua, T.: Recent Changes in Deep Ventilation of the Mediterranean Sea; Evidence From Long-Term Transient Tracer Observations, Journ10.3389/fmars.2020.00594al, 7, 2020.

MSM73 AND MSM83

Sustained observations of the Atlantic Meridional Overturning Circulation at 47°N

AUTHORS

IUP – Institute of Environmental Physics, University of Bremen | Bremen, Germany
C. Mertens, M. Rhein, D. Kieke, R. Steinfeldt

MARUM – Center for Marine Environmental Sciences, University of Bremen | Bremen, Germany
M. Rhein, D. Kieke, S. Wett, H. Nowitzki

BSH – Federal Maritime and Hydrographic Agency| Hamburg, Germany
M. Moritz, K. Jochumsen, B. Klein

The Atlantic Meridional Overturning Circulation (AMOC) is an essential component of the Earth's climate system. The AMOC is responsible for the transport of heat, freshwater, and dissolved gases in the ocean. Climate models project an AMOC decline between 10 % and 50 % by 2100, with serious implications for climate and sea level. Whether the AMOC has already weakened in response to anthropogenic climate change is an open question motivating multiple sustained AMOC observing systems (Frajka-Williams et al., 2019; McCarthy et al., 2020; Rhein 2019). Despite the importance of the large-scale circulation in the North Atlantic to the climate system, the internal flow field is known only qualitatively, neither the mean nor the variability and trends have been quantified. In a long-term study we investigated the North Atlantic current field at 47°N using a combination of inverted echo sounders deployed at the seafloor and moored current meters in the boundary current regions to quantify the components of the AMOC at this latitude (Fig. 1). Subsequently continuous records are established from a combination of the moored time-series, shipboard hydrographic measurements, and satellite altimetry.

The North Atlantic Current (NAC) is only about 100–150 km wide but imports 106 Sv into the Newfoundland Basin, making the NAC one of the strongest currents in the world ocean. Constrained by the bathymetry, more than half of the northward flow recirculates to the south in close proximity to the NAC (-44 Sv). The NAC and its return flow are significantly anti-correlated: A stronger NAC inflow corresponds to a stronger recirculation (Rhein et al., 2019). The mean flow in the interior Newfoundland Basin between 37°W and 31°W, is -28 Sv to the south, more sluggish and without permanent features. This part of the circulation seems to be independent from the NAC system and the boundary current, since no significant correlation with these individual time series was found.

Combining the northward NAC transport and the recirculation in the Newfoundland Basin results in a net northward transport in the interior of 34 Sv which is comparable to the eastward transport across the MAR (Nowitzki et al., 2021).

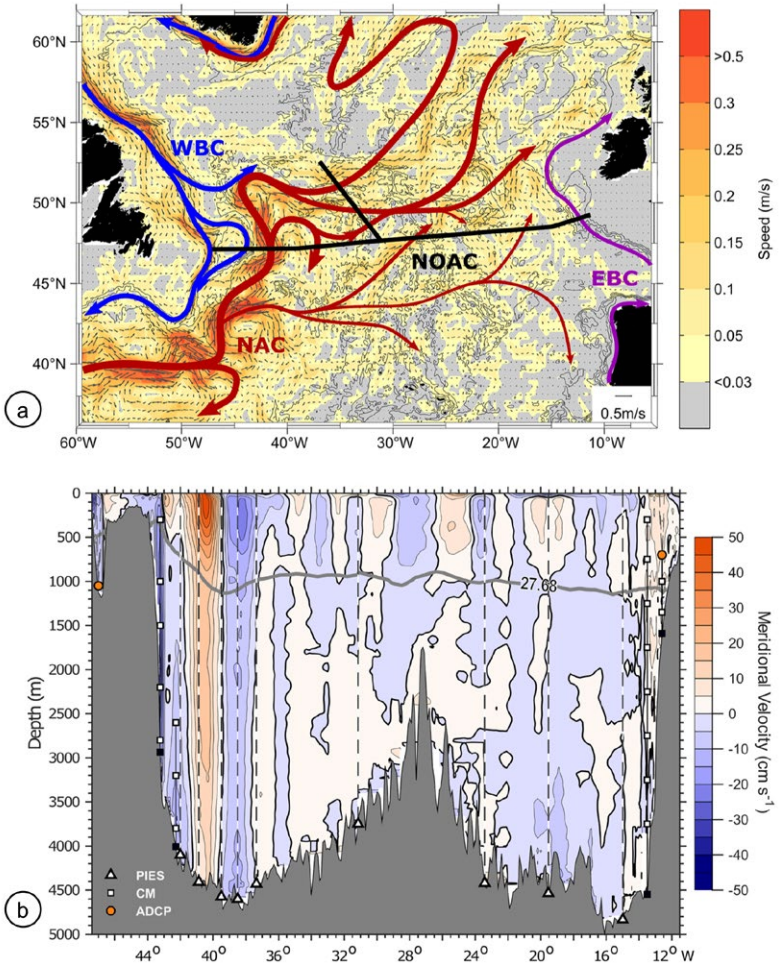

Fig. 1: (a) Schematic circulation with a focus on the NAC and the location of the North Atlantic Changes (NOAC) array. Contours and vectors are mean geostrophic surface velocity in 2016/2017 from satellite altimetry. The western boundary current (WBC) here combines the flow paths of the West Greenland Current, the Labrador Current and the Deep Western Boundary Current. The eastern boundary current system (EBC) here combines the flow paths of the Mediterranean Outflow Water and the slope current. (b) Meridional velocities at the NOAC array from repeat lowered acoustic Doppler current profiler (LADCP) measurements. The locations of PIES are shown as vertical dashed lines, current measurements (ADCPs and current meters) at the western and eastern boundaries are shown as symbols (from Nowitzki et al., 2021).

In the eastern part of the array the data reveal an additional pathway from the south across 47°N with a mean northward transport of 9 Sv contributing about 20 % to the

total inflow into the eastern subpolar basin. The transport time series of this pathway is anticorrelated to the zonal transport across the MAR, damping the interannual variability of the total transport into the subpolar eastern North Atlantic.

The temporal variability of the water transports across 47°N that was derived from the shipboard and the moored observations turned out to be highly correlated with sea surface height measurements from satellite altimetry, a result that was then used to calculate a longer time series of transport fluctuations directly from the altimeter measurements. The analysis reveals significant decadal trends (despite the large variability on all time scales) in the interior transport contribution. For the meridional transport in the interior eastern basin, a positive trend of 2.0 Sv per decade was found, that partly balances the negative decadal trend of −6.0 Sv observed in the interior western basin. The transport trends are linked to irregular decadal trends in sea surface height and thus most likely caused by regionally different warming of the water column. The decadal trends of sea surface height in the subpolar North Atlantic are generally positive and, at 47°N, strongest at the western and eastern boundaries. In the interior, the trends are not significant at many locations, and patches of negative and positive trends are in close proximity along the perceived pathways of the NAC. Combined with the positive trend at the boundaries, this leads to a weakening horizontal pressure gradient and thus to decreasing interior northward transports in the west and a strengthening of the pressure gradient in the east corresponding to an increasing northward transport.

At the eastern boundary a long term mean transport of about 3 Sv was found. The time series shows strong variability that is linked to a dynamic eddy field, especially a stationary cyclonic circulation pattern near the mooring array, and meandering of current branches originating from the North Atlantic Current (Moritz et al. 2021). Analyzing the time series of the AMOC at 47°N and comparing it with other observational AMOC time series will extend the understanding of meridional coherence and the processes important for variability and trends.

REFERENCES

Frajka-Williams, E, IJ Ansorge, J Baehr, HL Bryden, M Paz Chidichimo, SA Cunningham, G Danabasoglu, S Dong, KA Donohue, S Elipot, NP Holliday, R Hummels, LC Jackson, J Karstensen, M Lankhorst, I Le Bras, S Lozier, EL McDonaugh, CS Meinen, H Mercier, BI Moat, RC Perez, CG Piecuch, M Rhein, M Skrokoz, KE Trenberth, S Bacon, G Forget, G Goni, P Heimbach, D Kieke, J Koelling, T Lamont, G McCarthy, C Mertens, U Send, DA Smeed, M van den Berg, D Volkov, and C Wilson (2019), Atlantic Meridional Overturning Circulation: Observed transports and variability. Frontiers in Marine Science, 6:260, doi:10.3389/fmars.2019.00260.

McCarthy, GD, PJ Brown, CN Flagg, G Goni, L Houpert, CW Hughes, R Hummels, M Inall, K Jochumsen, KMH Larsen, P Lherminier, CS Meinen, BI Moat, D Rayner, M Rhein,

A Roessler, C Schmid, and DA Smeed, Sustainable observations of the AMOC: Methodology and Technology, Reviews of Geophysics (2020), 58, e2019RG000654, doi:10.1029/2019RG000654.

Moritz, M, K Jochumsen, D Kieke, B Klein, H Klein, M Köllner, M Rhein (2021), Volume transport time series and variability of the North Atlantic eastern boundary current at Goban Spur, Journal of Geophysical Research: Oceans, 126, e2021JC017393, doi:10.1029/2021JC017393.

Nowitzki, H, M Rhein, A Roessler, D Kieke, C Mertens (2021), Trends and transport variability of the circulation in the subpolar eastern North Atlantic, Journal of Geophysical Research: Oceans, 126, e2020JC016693, doi:10.1029/2020JC016693.

Rhein, M, Taking a close look at ocean circulation (2019), Science, 363, 456–457, doi:10.1126/science.aaw3111.

Rhein, M, C Mertens, A Roessler (2019), Observed transport decline at 47°N, western Atlantic, Journal of Geophysical Research: Oceans, 124, doi:10.1029/2019JC014993

MSM74

Western Subpolar North Atlantic Variability

AUTHORS

GEOMAR Helmholtz Centre for Ocean Research Kiel | Kiel, Germany
J. Karstensen, M. Visbeck, P. Handmann

OCEAN VARIABILITY AT 53°N AND INTEGRATION IN THE OSNAP ARRAY

Since 1997 the transport of the Deep Western Boundary Current (DWBC) water masses that compose the North Atlantic Deep Water (NADW) is observed with the aid of a mooring array (53°N Array) at the exit of the Labrador Sea (Figure 1). The array provides high temporal resolution records and the data analysis can consider time scales from hours to decades. The transport time series (Figure 2, left) shows a clear multiannual variability (6 to 9 year cycle) with an amplitude of more than 10 Sv (1Sv=10^6m3sec^{-1}) which seems to be increasing in recent years. Considering the time series as a whole, a general trend towards less transport can be identified. While the decadal variability has been shown in phase with low frequency wind forcing, the general trend needs further analysis.

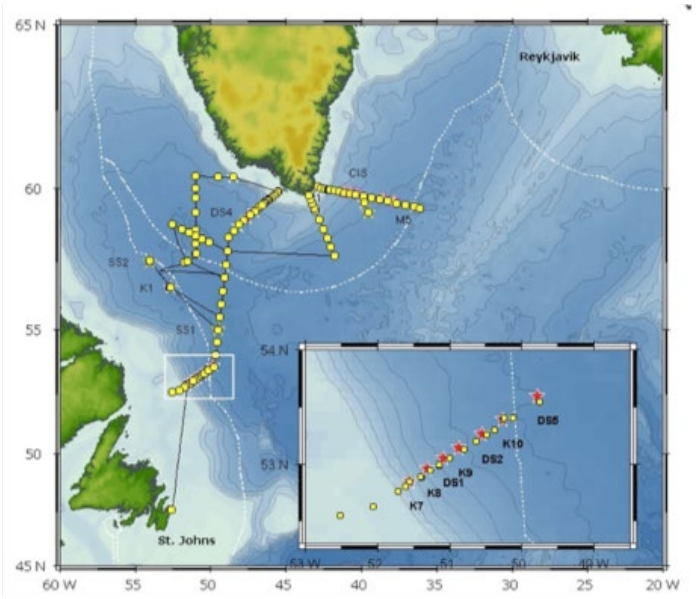

Fig. 1: Station map of MSM74: yellow dots: CTD stations, red crosses: mooring locations, the black line markes the ship track. EEZ regions of the neighbouring countries are shown for reference. The inset lower left provides a detailed view on the operations in the 53°N Array area.

In 2014 the international OSNAP overturning array was set up, combining observational efforts from various countries and coordination a joint analysis of data in order to estimate the basin wide overturning transport in the subpolar North Atlantic (Fig. 2, right). In reference to the 53°N Array, the OSNAP period is marked by an increase in transport from a low of about 20Sv in 2014 to a maximum of 32Sv at the end of the 2017. However, the overturning transport in the OSNAP West section (Labrador Sea) varies only marginally by a couple of Sv's with no trend. It is not much of a surprise maybe that no directly linkage between overturning and transport in the DWBC at the 53°N array can be seen. The 53°N Array considers only the "southward" (along the topography) transport and thus the transport is much larger as it is rather the strength of the horizontal circulation and not the overturning that is observed. Therefore, the first comprehensive study on the mean structure of the DWBC at the Greenland side (Pacinini et al. 2020) is very important as a benchmark for further analysis of variability. The trend that is observed in the 53°N Array transports may indicate large-scale changes in the density structure of the subpolar gyre system and which requires further investigation, in particular because Li et al. (2021) did not report boundary density structure to be responding in concert with the variability.

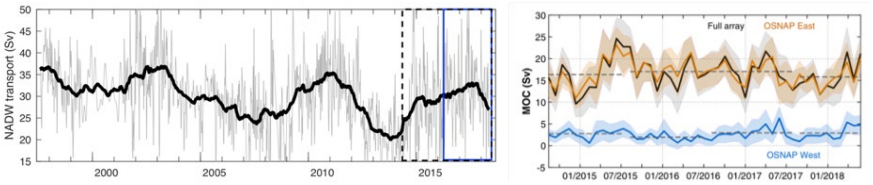

Fig. 2: (left) Total (below 400m) southward transport across the 53NArray. Blue square: MSM74 data recovery; black broken square: OSNAP period. (right) 30-day meridional overturning transport estimated from the full OSNAP array (black), and separating into eastern (red) and western (blue) SPNA (Liu et al. 2021).

One key finding from the subpolar overturning estimate (Lozier et al. 2019, Liu et al. 2021) was the overturning to be concentrated in the eastern subpolar gyre and not on the western side where the deep convection areas are located. Although models indicated this pathway earlier, this was the first observational estimate of were the overturning occurs and that no direct link to the deep convection was identified on multiannual timescales. However, the overturned water masses transit the deep convection areas being part of the DWBC and while they do that they exchange mostly in a lateral way water with the deep convection areas. This lateral exchange is potentially an important source of tracer renewal in the DWBC and hence in Northatlantic Deep Water. In a recent study (Koelling et al. in review) determined the importance of lateral fluxes on DWBC oxygen content using MSM74 in combination with earlier cruises and moored sensors data, as well as data from Argo floats. The study estimated the export of oxygen from the subpolar gyre associated with Labrador Sea Water (LSW) supplies about 71 % of the oxygen consumed annually in the upper North Atlantic Deep Water layer in the

Atlantic Ocean between the equator and 50°N. Consequently, if deep convection in the Labrador Sea is important for replenishing oxygen to the deep oceans, meaning that possible changes in LSW formation rate, and Labrador Sea ventilation in general, could have wide-reaching impacts on marine life. The study also high-lights the important information that can be obtained by expanding the moored arrays with biogeochemical sensors in order to estimate implication of transport variability on non-physical properties and processes. The timescale dependence of co-variability between oxygen, hydrography and velocity is currently investigated in a MSc thesis (Leimann 2021).

REPRESENTATION OF MESOSCALE EDDIES IN SATELLITE DATA

A dedicated mesoscale ocean eddy survey was done during a high wind period of the MSM74 cruise and later analyzed by Bendinger (2020). Making use of the characteristic velocity of a Rankine Vortex, the ship underway ADCP section data was used to reconstruct eddy parameters of current festures encountered during the cruise (e. g. location of centre, diameter, velocity structure). During the cruise real-time maps of Sea Level Anomalies (SLA) from Copernicus Marine Environmental Monitoring Service (CMEMS) were used to design an adaptive survey plan for eddies in real-time. The anticipated SLA of the ship-based eddy reconstructions differed surprisingly strong from the gridded satellite-based maps from CMEMS (Figure 3). The satellite-based maps overestimate not only the extend of the SSH anomaly but also its location and often maybe even missing completely eddies. It was interesting to see that in many cases the original satellite along-track data (also shown in Figure 3) agreed well with the anticipated SLA of the eddies estimates from the ship data. The observations motivated further investigations, also using very high-resolution ocean model data to test the impact of ship sampling (e. g. impact of accuracy of eddy reconstruction on ship track locations in a mesoscale eddy). This analysis is currently prepared for publication (Bendinger at al., in preparation).

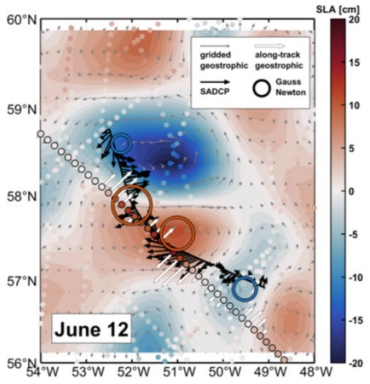

Fig. 3: SSH anomaly gridded map (contour) against observational ship current data (black arrows) for the 12. June 2018 in the Labrador Sea. The colored dots show the altimeter data that was used to create the gridded map via the AVISO+ satellite data service. The red and blue circles mark mesoscale eddies that have been identified from the near surface velocity ship data (red: anticyclonic, blue: cyclonic rotation).

REFERENCES

Bendinger, A., Characteristics of Mesoscale and Submesoscale Eddies in the Labrador Sea: Observations vs. Model, Master thesis CAU Kiel, 2020, 75pp.

Koelling, J., Atamanchuk, D., Karstensen, J., Handmann, P., and Wallace, D. W. R.: Oxygen export to the deep ocean following Labrador Sea Water formation, Biogeosciences Discuss. [preprint], https://doi.org/10.5194/bg-2021-185, in review, 2021.

Li, F., Lozier, M.S., Bacon, S. et al. Subpolar North Atlantic western boundary density anomalies and the Meridional Overturning Circulation. Nat Commun 12, 3002, 2021, doi: 10.1038/s41467-021-23350-2 8.

Lozier, M.S. et al. (2019) A Sea Change in Our View of Overturning – First Results from the Overturning in the Subpolar North Atlantic Program, Science, 363, 516–521, February 1, doi: 10.1126/science.aau6592.

Pacini, A., R.S. Pickart, F. Bahr, D.J. Torres, A. Ramsey, J. Holte, J. Karstensen, M. Oltmanns, F. Straneo, I.A. Le Bras, G.W.K. Moore, and M.F. de Jong, Mean conditions and seasonality of the West Greenland boundary current system Journal of Physical Oceanography, 50, 2849-2871, 2020, doi: 10.1175/JPO-D-20-0086.1.

Leimar, I., Temporal and spatial varibiliyt of properties in the Deep Western Boundary Current at 53°N in the Labrador Sea, Master thesis CAU Kiel, 2021

MSM76

Nordic Seas Exchanges

AUTHORS

Alfred-Wegener-Institute Helmholtz Centre for Polar and Marine Research | Bremerhaven, Germany
T. Kanzow, R. McPherson, D. Aydin

Department 1 of Physics and Electrical Engineering, University of Bremen | Bremen, Germany
S. Kritsotalakis

1. SUMMARY

During the expedition MSM76 we (1) continued the monitoring of the Denmark Strait overflow (DSO) transport using moorings, (2) carried out a process study in the region of intense mixing downstream of Denmark Strait, (3) studied the subsurface circulation of warm Atlantic Water on the shelf of Northeast Greenland and its impact on marine terminating glaciers in East Greenland, and (4) continued to monitor the circulation of Atlantic Water in the West Spitsbergen Current in Fram Strait. While the work conducted towards the monitoring aspects was successful, most scientific progress has been made regarding the goals (2) and (3). Regarding mixing within the DSO plume, we have been able to classify the mesoscale activity from a mooring cluster in terms of amplitudes, eddy types and propagation. We have subsequently successfully undertaken analyses to link the mesoscale variability to vertical mixing within the DSO plume. Regarding the East Greenland work, we have been able for the first time to come up with a description of the circulation within the Scoresby Sund-Nordvest Fjord system.

2. SCIENTIFIC RESULTS

2.1 Mixing and eddy dynamics in the DSO plume downstream of the sill

Aim and work conducted: Roughly 200 km downstream of the Denmark Strait sill (DSS) a large part of the mixing and entrainment-induced warming of the DSO plume has already been accomplished. This is why the observation-based estimates of horizontal heat flux (Voet and Quadfasel, 2010) and vertical heat flux (Paka et al., 2013) taken at this site reveal too low values to explain the bulk warming of the DSO plume upstream. The aim of the MSM76 expedition was to carry out a study of the interaction between eddy dynamics and mixing in the area of strongest flow of the DSO plume significantly further upstream. It consisted of a rhombus-shaped cluster of 4 moorings approximately 120 km downstream of the DSS (Fig. 1). This was accompanied by densely space CTD-LADCP sections across the DSO plume and yoyo-CTD stations near the mooring cluster.

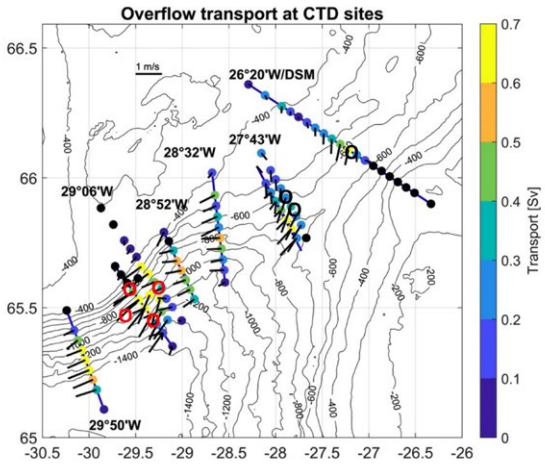

Fig. 1: The transport (color coded) of overflow waters (pot. temperature < 2 °C and pot. density σ0> 28 kg m^{-3}) is displayed at each CTD station. The black lines indicate the velocity amplitude and direction of the DSO plume layer. The red circles denote the positions of the mooring cluster.

Time mean flow field and eddies: The area of the mixing study turned out to be well-chosen with flow speeds of the DSO plume exceeding those both at the sill and 45 km downstream by roughly 70 %. Eddy-resolving numerical ocean simulations confirmed this area of the DSO gravity current to exhibit a maximum in the eddy kinetic energy. We developed and applied an algorithm to automatically detect eddies and their characteristics – built on Darelius et al. (2011) and Moritz et al. (2019). A total of 6 cyclones and 3 anti-cyclones are detected passing through the mooring array.

Eddy-related instabilities in the DSO: Paka et al (2013) and Schaffer et al. (2016) had studied this interaction, however in a region further downstream where most of the mixing (warming) of the DSO has already been accomplished. Our analyses reveal that shear instabilities in the interfacial layer (IL) of the plume and the AW (ambient water above the plume) are linked to the departure or transition of the plume. During these phases the along-stream velocity core is fully developed and creates strong vertical shear in the IL and AW.

Small-scale mixing: The role of shear instabilities in driving dissipation and entrainment in the interfacial layer of the DSO plume has been highlighted by North et al. (2018), showing that high transport-flows exhibit elevated amplitudes of dissipation compared to low transport-flow. Schaffer et al. (2016) connected the passage of the dense DSO plume with bottom-intensified cyclonic eddy motion and suggested that the latter contributed to lateral and vertical mixing between plume and ambient water.

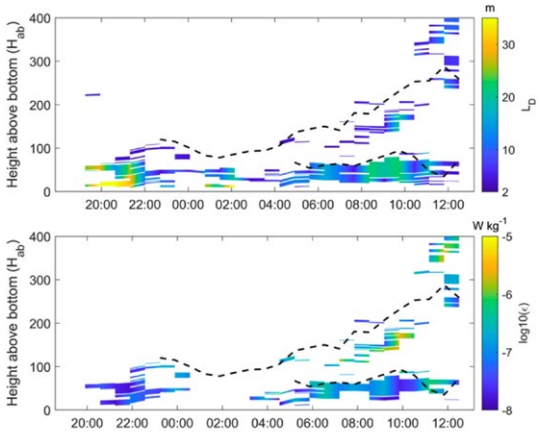

Fig. 2: Thorpe scales (top panel) and the logarithm of dissipation (bottom panel) from the yo-yo cast 120 km downstream of the DSS sill, between 18 and 19 August, 2018 (time in UTC). Black dashed lines indicate the upper limits of the bottom (BL) and interfacial (IL) layers of the DSO plume.

The focal of this study was to connect the mesoscale eddy field detected from the mooring time series with vertical turbulent mixing in the interfacial layer of the DSO. The Yo-Yo cast (Fig. 2) captures an arrival event of the DSO plume after which the interfacial layer (IL) of the plume rapidly grows in thickness from 75 to 200m altitude. Vertical mixing was quantified via Thorpe scales, LT. The rate of dissipation of turbulent kinetic energy, ε, and the entrainment rate, wE, were then derived under the assumption that the LT is equivalent to the Ozmidov scale (Dillon, 1982). Turbulent overturns were present throughout the whole Yo-Yo cast in the DSO plume (Fig. 2). ε ranged between 10^{-8} W kg^{-1} and 10^{-5} W kg^{-1}. The largest ε values are observed in the mid-levels of the IL (Fig. 2). Following the thickening of the IL, patches of dissipation migrate upward. Our moored time series demonstrate that anti-cyclonic mesoscale activity is present throughout the duration of the Yo-Yo cast, temporally coinciding with the two major turbulent events in Fig. 2. Thus, the events in the IL appear to be driven by mesoscale activity above the plume.

2.2 Circulation of Atlantic Water on the east Greenland Shelf/Scoresby Sund

Aims and work: Prior to MSM76 there was no information in the scientific literature regarding the circulation within Scoresby Sund and its exchange with the Greenland shelf. CTD-LADCP sections were accomplished across the mouth of Scoresby Sund, across the entries to Nordvest Fjord (within Scoresby Sund).

Results: Based on the data sets obtained during MSM76, and by combining them with measurements from the MSM65 expedition we have come up with a first description of the circulation (Seifert et al., 2019). The subsurface circulation at the fjord mouth is characterized by an inflow of Atlantic Water into Scoresby Sund in the northern part of the mouth and an outflow of Atlantic Water in the southern part (Fig. 3, upper left panel), suggesting boundary currents to be present at either margin. In order to quantify the strength of the fjord-shelf

exchange, cumulative cross-section transports have been computed for the two sections at the fjord mouth, yielding maximum inflows lies of 60 and $100 \cdot 10^3$ m s^{-1} (Fig. 3, lower left panel), respectively. With the Rossby Radius of deformation amounting to 6 km, and the outer Scoresby Sund exhibiting typical widths of 35 km, boundary currents along its margins represent plausible features of the circulation.

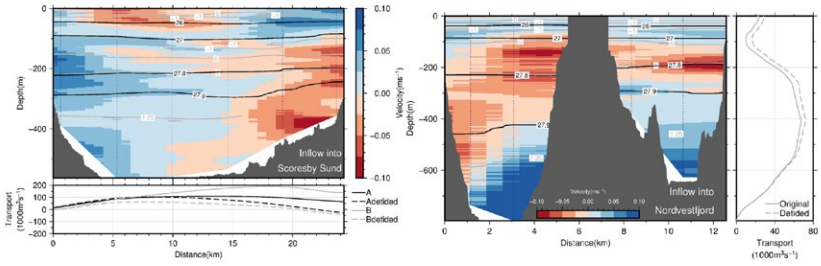

Fig. 3: The upper left panel displays the across-section velocity along the mouth of Scoresby Sund. Blue shading denotes inflow into Scoresby Sund. In the lower panel the cumulative volume transport into Scoresby Sund from two sections is displayed (solid black and gray lines, respectively). The middle panel displays the across-section velocity at transition between Scoresby Sund and Nordvestfjord. Blue shading denotes inflow of waters into Nordvestfjord. The right panel displays the cumulative volume transport into Nordvestfjord.

At the transition between the outer Scoresby Sund and Nordvestfjord (Fig. 3, middle panel) a bottom intensified inflow of Atlantic Water at densities exceeding 27.9 kg m^{-3} is found to replenish the warm bottom waters found in Nordvestfjord, amounting to $65 \cdot 10^3$ m s^{-1}. The outflow from Nordvestfjord is found to occur mainly at mid-depths confined to a layer bounded below by the 27.9 kg m^{-3} and the 0°C isotherm at the top. Thus, at the transition of the outer Scoresby Sund to Nordvestfjord, where the fjord becomes narrow, no evidence for horizonal recirculations are found. Here the flow seems reminiscent of classical estuarine circulations (Straneo and Cenedese, 2014).

REFERENCES

Darelius E, Fer I, & Quadfasel D Faroe Bank Channel Overflow: Mesoscale Variability. Journal of Physical Oceanography 2011, 41(11), 2137–2154, doi:10.1175/JPO-D-11-035.1

Dillon T M, Vertical overturns: A comparison of Thorpe and Ozmidov length scales. Journal of Geophysical Research 1982, 87(C12), 9601–9613, doi:10.1029/JC087iC12p09601

Moritz M, Jochumsen K, North R P, Quadfasel D & Valdimarsson H, Mesoscale Eddies observed at the Denmark Strait sill, J. Geophys. Res. Oceans 2019, 124, 7947–7961.

North R P, Jochumsen K, & Moritz M, Entrainment and energy transfer variability along the descending path of the Denmark Strait overflow plume, Journal of Geophysical Research Oceans 2018, 123, 2795–2807, doi:10.1002/2018JC013821

Paka V T, Zhurbas V M, Rudels B, Quadfasel D, Korzh A, & Delisi D Microstructure measurements and estimates of entrainment in the Denmark Strait overflow plume, Ocean Science 2013, 9(6), 1003–1014, doi:10.5194/os-9-1003-2013

Schaffer J, Kanzow T, Jochumsen K, Lackschewitz K, Tippenhauer S, Zhurbas V M, et al. Enhanced turbu lence driven by mesoscale motions and flow-topography interaction in the Denmark Strait Overflow plume, Journal of Geophysical Research: Oceans 2016, 121, 7650–7672, doi:10.1002/2016JC011653

Seifert M, M Hoppema C Burau, C Elmer A Friedrichs, JK Geuer, U John, T Kanzow, BP Koch, C Konrad, H van der Jagt, O Zielinski and MH Iversen Influence of glacial meltwater on summer biogeochemical cycles in Scoresby Sund, East Greenland, Frontiers in Marine Science 2019, 6 (412), doi: 10.3389/fmars.2019.00412.

Straneo F, & Cenedese C, The dynamics of greenland's glacial fjords and their role in climate, Annual review of marine science 2014, 7, 89–112

Voet G, & Quadfasel D, Entrainment in the Denmark Strait overflow plume by meso-scale eddies, Ocean Science 2010, 6(1), 301–310, doi:10.5194/os-6-301-2010

MSM78

Strategies for Environmental Monitoring of Marine Carbon Capture and Storage – PERMO2

AUTHORS

GEOMAR Helmholtz Centre for Ocean Research Kiel | Kiel, Germany
C. Berndt, J. Karstens, E. Kossel, M. Haeckel, C. Deusner

Christian-Albrechts-Unversity | Kiel, Germany
C. Böttner

University of Southampton | Southampton, UK
B. Callow, R. Gehrmann, J. Bull, R. James, I. Falcon-Suarez

INTRODUCTION

Expedition MSM78 took place from the 16th until the 25th of October 2018. The research cruise MSM78 was part of STEMM-CCS project and its main aim was to collect sediment cores for geochemical and geotechnical analyses using BGS' RockDrill2.

The main scientific goals of STEMM-CCS were to develop new monitoring strategies for offshore storage of CCS (Flohr et al., 2021). PERMO2 contributed to WP3 of the STEMM-CCS project (Robinson et al., 2021) and the first objective was to constrain the bulk permeability of an existing chimney structure, i. e. to assess the amount of aqueous and gassy fluids that may move through these structures over time. Secondly, we tried to constrain the temporal evolution of fluid migration through pipe structures over time, i. e. do they transport fluids continuously or episodically and if episodically is it likely that CO_2 storage may initiate a new episode of migration. Finally, we set out to test the hypothesis that chimney structures in seismic data represent indeed fault networks created by hydro-fracturing and not bulk mobilization of sediments as a diapir or subsidence of sediments in the style of a breccia pipe.

OPERATIONS

Drilling was originally planned for the second leg of research cruise MSM63 in May 2017, but this had to be cancelled because a bolt had fallen into one of the pod drives during maintenance operations and the second leg of MSM63 was cut too short for drilling. Although the replacement cruise took place in the northern North Sea in fall, relatively calm weather conditions allowed to drill with RockDrill2 for four consecutive days during which a total of 22.6 m of sediment cores could be recovered (Fig. 1 and 2). Due to the limited duration of the cruise, only pore water samples were taken from the cores. The rest of the cruise, i. e. when the weather was

not suitable for drilling, was used to acquire further hydroacoustic data and several gravity cores.

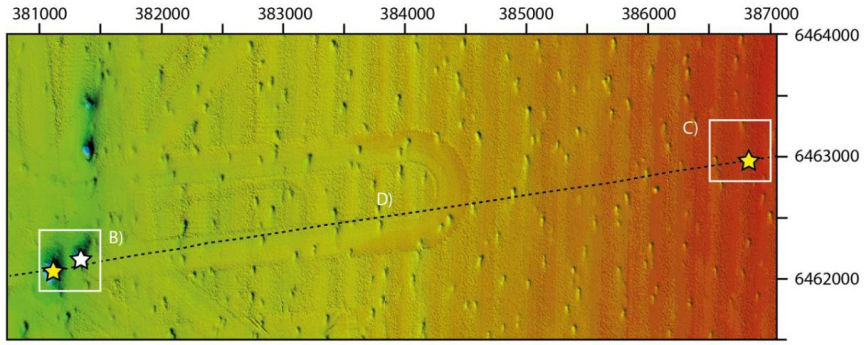

Fig. 1: Location of the RockDrill2 boreholes in Scanner Pockmark (B) and reference site (C). Coordinates in UTM zone 31, WGS 84. Water depth range from 170 m in Scanner Pockmark to 149 m at the reference site. Note, the two pockmark classes: deep-seated ones like Scanner, Scotia and Alkor to the north of Scanner and numerous meter-deep pockmarks farther east. Dashed line shows Fig. 2 (from Karstens et al., 2019).

Physical properties

The sediment cores were logged at intervals of 1 cm using a GEOTEK multi-sensor core logger at the BOSCORF laboratory of the National Oceanography Centre Southampton. Bulk density was measured using gamma ray attenuation. Porosities were estimated from the measured bulk density using fixed grain and porewater densities. Resistivity was measured by inducing a high-frequency time-varying electric field. A receiving coil offset by 2 cm detected the magnetic field induced in the sample which is directly proportional to the material conductivity. The MSCL data show an increase in electrical resistivity with depth and a decrease in porosity (Fig. 3a). These physical properties were then used to calculate electrical resistivity from the controlled-source electric data acquired during MSM67 (Gehrmann et al., 2021).

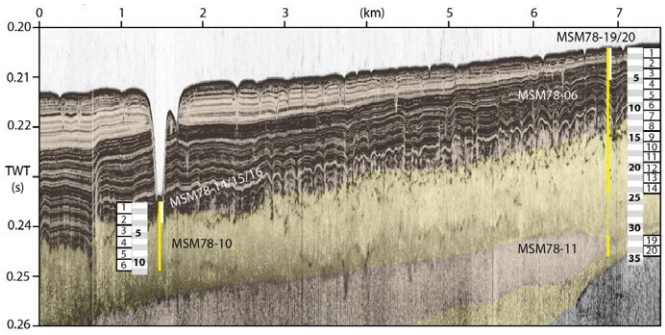

Fig. 2: Parasound profile through the two RockDrill2 sites: Scanner Pockmark in the west (left) and the reference site in the east (right) (from Karstens et al., 2019). For location see Fig. 1.

GEOTECHNICAL WORK

Both the gravity cores and the RockDrill2 cores have been scanned using an X-ray micro-CT scanner. These results were analyzed for sediment structure and texture (Callow et al. in press). Furthermore, it is planned to measure the geotechnical properties of the RockDrill2 cores with a triaxial shear cell under various gas flows and simultaneous imaging using a CT scanner to understand how gas is migrating through the sediments.

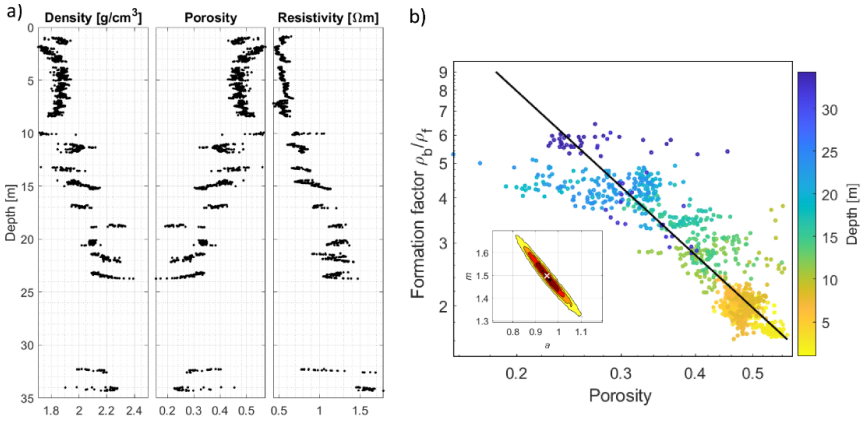

Fig. 3: (a) Density, density-derived porosity and electrical resistivity from MSCL measurements on sediment cores acquired by drill rig RD2 at a reference site 6 km North East of the pockmark (Karstens et al., 2019); (b) Formation factor (bulk vs. fluid resistivity ratio) versus porosity from MSCL measurements colour-coded by depth, and Archie's empirical relationship (black line) with best-fit Archie parameters a = 0.95 and m = 1.5 (white cross in probability density of a and m, inlay) (after Gehrmann et al., 2021).

REFERENCES

Callow, B. et al. Seismic chimney characterisation in the North Sea – Implications for pockmark formation and shallow gas migration. Mar Petrol Geol 133, 105301 (2021).

Flohr, A. et al. Towards improved monitoring of offshore carbon storage: A real-world field experiment detecting a controlled sub-seafloor CO_2 release. International Journal of Greenhouse Gas Control 106, 103237 (2021).

Gehrmann, R. A. S. et al. Porosity and free gas estimates from controlled source electromagnetic data at the Scanner Pockmark in the North Sea. International Journal of Greenhouse Gas Control 109, 103343 (2021).

Karstens, J., Böttner, C., Edwards, M., Falcon-Suarez, I., Flohr, A., James, R., Lichtschlag, A., Maicher, D., Pheasant, I., Roche, B., Schramm, B., Wilson, M., 2019. RV MARIA S. MERIAN Fahrtbericht/Cruise Report MSM78 – PERMO 2,

Edinburgh – Edinburgh (U.K.) 16.10.–25.10.2018. GEOMAR Report N.Ser. 048. 10.3289/GEOMAR_REP_NS_ 48_2019.

Robinson, A. H. et al. Multiscale characterisation of chimneys/pipes: Fluid escape structures within sedimentary basins. International Journal of Greenhouse Gas Control 106, 103245 (2021).

MSM79

Preliminary results: Marine carbon production, export, relocation and degradation off NW Africa and Carbon release from thawing permafrost of the European tundra

AUTHORS

Center for Marine Environmental Sciences – MARUM, University of Bremen | Bremen, Germany
K. Zonneveld, G. Mollenhauer, E. Roza, G. Versteegh

The scientific activities of cruise MSM79 in November 2018 focused on organic carbon and processes that steer its turnover. The cruise contained two legs. During the first leg, high-resolution sediment archives that record the melting of European permafrost at the end of the last ice age approximately 20,000 years have been collected in front of the English Channel. During the second leg, key aspects of the ocean carbon pump during active upwelling off Cape Blanc (NW Africa) have been studied. First results have been published in two peer-reviewed publications (Versteegh et al., 2020; Zonneveld et al., 2021) and two master studies.

Here we present an overview on the preliminary results from both legs with focus on investigations on a seven-day drifting trap survey, modern and post-depositional alteration molecular characteristics of particulate organic matter particles of known origin and an 18-years sediment trap study.

The drifting trap survey was carried out in an active upwelling cell covering the transition from active upwelling to upwelling relaxation/stratification. For 7-days the export production of organic- and calcareous dinoflagellate cysts and planktonic foraminifera were followed (Fig. 1). Highest export flux of both phyto- and zooplankton occurred in the active upwelling phase with exception of the calcareous dinoflagellates that had highest fluxes during upwelling relaxation. In all organism groups a clear species succession was observed.

Identification of the molecular characteristics of organic planktic foraminifera linings and organic dinoflagellate cysts reveal that these are specific for the organism and on species level respectively. Effects of post depositional aerobic degradation on molecular characteristics of organic microfossils reveal that although aerobic sediment contained excellent preserved specimens, their molecules were highly affected by volcanisation as one of the diagenetic processes. It also shows that the best preservation of molecular structure is not necessarily, where most organic matter is preserved. These results are important for understanding the nature and fate of sedimentary organic matter.

From the worldwide longest sediment trap series, results of a survey of 18-year duration are presented. This survey that has been carried out at the rim of the active upwelling area off Cape Blanc, reveals that the system is highly dynamic with strong sub-annual and interannual variability. Long-term changes in phyto- and zooplankton export flux and association composition are being observed as well as interannual cyclicity. Although individual upwelling events show some coherence, the phyto- and zooplankton export flux association composition appeared to be event specific.

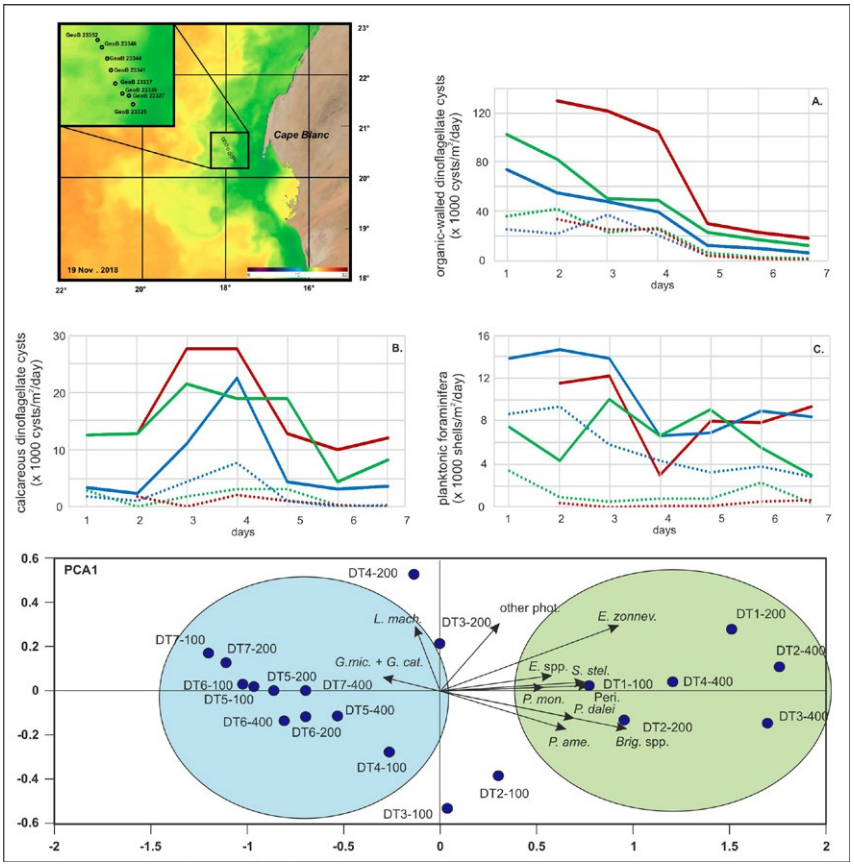

Fig. 1: Export flux of A: organic dinocysts, B: calcareous dinocysts, C: planktonic foraminifera (7-days drifting trap survey). Blue, green, red lines: collection at 100 m, 200 m, 400 m. Solid: total cysts/tests, dotted: cysts/tests with cell content. PCA analysis. Green field: organic dinocysts + samples characteristic for upwelling (DT-1 to DT-3) and bleu: upwelling relaxation/stratification (DT-5 to DT-7).

REFERENCES

Versteegh G.J.M, Houben A.J.P., Zonneveld K.A.F. Better molecular preservation of organic matter in an oxic than in a sulfidic depositional environment: evidence from Thalassiphora pelagica (Dinoflagellata, Eocene) cysts. Biogeosciences 2020, 17, 3545–3561, 2020.

Zonneveld K.A.F., Donner B., Meiland J., Versteegh G.J.M. Export flux succession of dinoflagellate cysts and planktonic foraminifera in an active upwelling cell off Cape Blanc (NW Africa). European Journal of Phycology, 2021, doi: 10.1080/09670262.2021.1885066

MSM79/2, SO267/2, MSM82/2, SO268/3

References

AUTHORS

Max-Planck-Institute for Meteorology | Hamburg, Germany
S. Kinne

COLLECTION OF OCEANIC REFERENCE DATA

Atmospheric data for aerosol, trace-gases and clouds were collected to address the need for atmospheric reference data over oceans. Sub-groups of always (7 to 14) scientists from different research institutes and universities under the lead of Stefan Kinne participated on many transit cruises over the last five year, including the transits of MSM79/2, SO267/2, MSM82/2 and SO268/3. Using the sun and the sky as background, atmospheric properties can be determined at higher accuracy than via satellite remote sensing. Thus, for the collection of reference data on atmospheric aerosol and atmospheric trace-gases the participating scientists operated several sun-photometers (among them a calibrated NASA instrument of the Maritime Aerosol Network) and several MAX-DOAS instruments. The measurements were further complemented by a vertically profiling ceilometer and by sky imaging cameras to add statistics on cloud properties. In addition, the participating science staff always included a couple geodesy scientists, who analyzed bathymetric oceans floor data and prepared those data for the database of the Seabed 2030 initiative. Finally, the transit cruises also offered opportunities to release new ARGO floats (sampling robots) to maintain oceanic monitoring capabilities.

MSM79/2

The MSM79/2 transit cruise departed Mindelo (Capo Verde) on Dec 6, 2018 and reached Bahia de las Minas (Panama) on Dec 18, 2018. Under the logo MOOR-1 the extra instruments (that were operated and whose data were analyzed) were several sun-photometers, two differential absorption spectrometers, a ceilometer and a cloud camera-system. In addition, recorded oceanic state and ocean-floor data were analyzed and five ARGO floats from Germany were deployed in international waters.

SO267/2

The SO267/2 transit cruise departed Suva (Fiji) on Jan 28, 2019 and reached Manzanillo (Mexiko) on Feb 14, 2019. Under the logo MORE-1, the extra instruments (that were operated and whose data were analyzed) were several sun-photometers, three differential absorption spectrometers, a ceilometer and a cloud camera system. In addition, recorded ocean-floor data in international waters were processed.

MSM82/2

The MSM 82/2 transit cruise departed Montevideo (Uruguay) on Apr 26, 2019 and Las Palmas (Canary, Is., Spain) on May 14, 2019. Under the logo MOOR-2 the extra instruments (that were operated and whose data were analyzed) were a sun-photometer, a differential absorption spectrometer, a ceilometer and a cloud camera system. In addition, recorded ocean-floor data in international waters were processed.

SO26/3

The SO268/3 transit cruise departed Vancouver (Canada) on May 6, 2019 and reached Singapore on Jul 7, 2019. Under the logo MORE-2, the extra instruments (that were operated and whose data were analyzed) were four sun-photometers, three differential absorption spectrometers, a ceilometer and a cloud camera. In addition, recorded ocean-floor data were processed in international waters and 23 ARGO floats from the US were deployed.

sunphotometers: Samples of the direct sun-light, at times when the sun was not obscured by clouds, offer detail on atmospheric properties by direct attenuation (aerosol) and differential absorption (trace-gases). Sampled aerosol data with calibrated MICROTOPS instruments of the Maritime Aerosol Network (Smirnov et al, 2009, 2011) were immediately sent to NASA for inclusion into the MAN data-base http://aeronet.gsfc.nasa.gov/new_web/maritime_aerosol_network.html. Atmospheric aerosol loads, via daily averages for the aerosol optical depth (AOD) of all four transit-cruises are summarized in Figure 1.

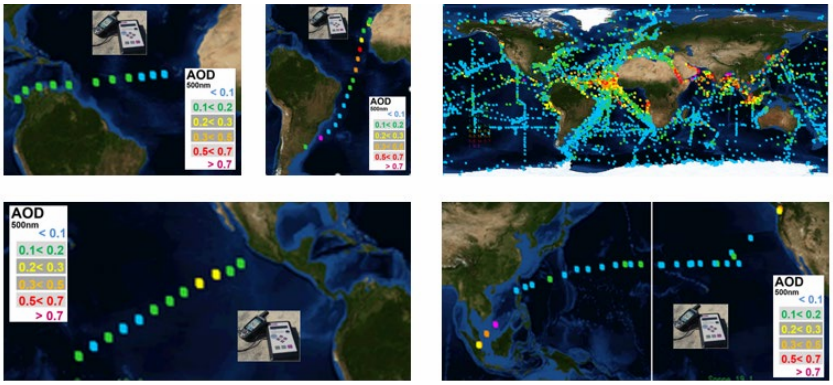

Fig. 1: daily AOD averages (also illustraing the vessel tracks) during MSM79-2 (top left), MSM82-2 (top center), SO267-2 (bottom left) and SO268-3 (bottom right) transit are shown in the context off all shipborne samples contributed to the MAN data-base over the last 18 years (top right).

MAN data information has been is statistically (monthly and 1x1 deg. lat/lon binned) applied, to improve global distributions of aerosol properties (Kinne 2019a). And in an application (with temporal, spatial and vertical scaling from global modeling) of this

climatology in an off-line radiative transfer code the aerosol radiative effects and likely aerosol climate impacts were determined (Kinne 2019b). The handheld operated MICROTOPS instrument also sampled the atmospheric water vapor content – via differential solar absorption. The same technique, though at much higher spectral resolution was used by the solar tracking BRUCKER instrument of the U.Heidelberg to determine Greenhouse gas concentrations. The extracted atmospheric loads were compared after the cruise to simulations and to satellite data (Knapp et al., 2021).

sky-spectrometers: A different technique to extract atmospheric absorption is the combined use of multi-spectral data at different elevations above the horizon. Two MAX-DOAS (Multi-AXis Differential Optical Absorptions Spectrometer) instruments of MPI-C and KMNI and a Pandora instrument of the FU-Berlin examined the near surface concentrations of pollutants as illustrated from the MSM79/2 cruise in Figure 2.

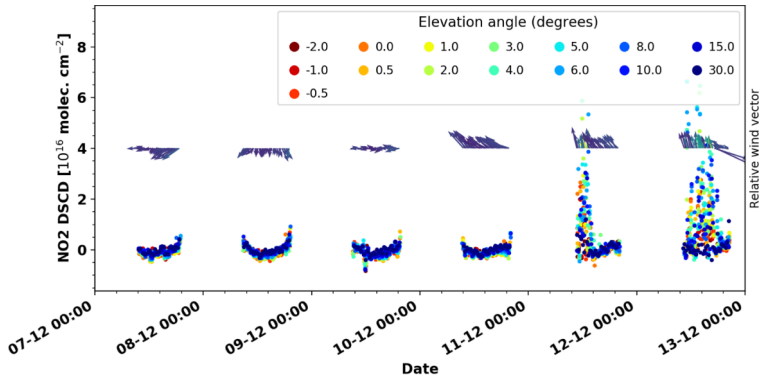

Fig. 2: NO_2 (direction) differential slant column densities for oceanic background conditions during MSM79-2. The various colors represent different data based on different elevation views. Dec12 and 13 data are contaminated by ship exhaust as relative wind vectors (center arrows) indicate an exhaust transport into scanned air.

The after cruise data analysis involved comparisons to satellite retrievals (Wang et al., 2020) and a closer look at a case of very low oxygen dimer (O4) concentrations during very low atmospheric aerosol loads (Wagner et al., 2021).

cloud-camera and **ceilometer:** a cloud camera system of the MPI-Met provided continuously visible and thermal images of the sky. Thermal data inform, in addition to cover and structure, also on cloud altitude (which for accuracy was calibrated by a ceilometer). A pair of simultaneous visible and thermal images of an upward sky-scene is presented in Figure 3 and cloud base statistics is summarized in Figure 4.

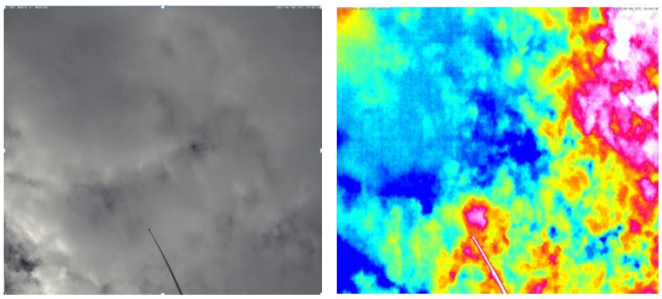

Fig. 3: an image pair of an upward looking cloud camera (ca 35 deg FOV) in the visible region (left) and thermal window region (right), The color in thermal image indicates sky temperature (red=warmer → low clouds, dark blue=colder → cloud-free).

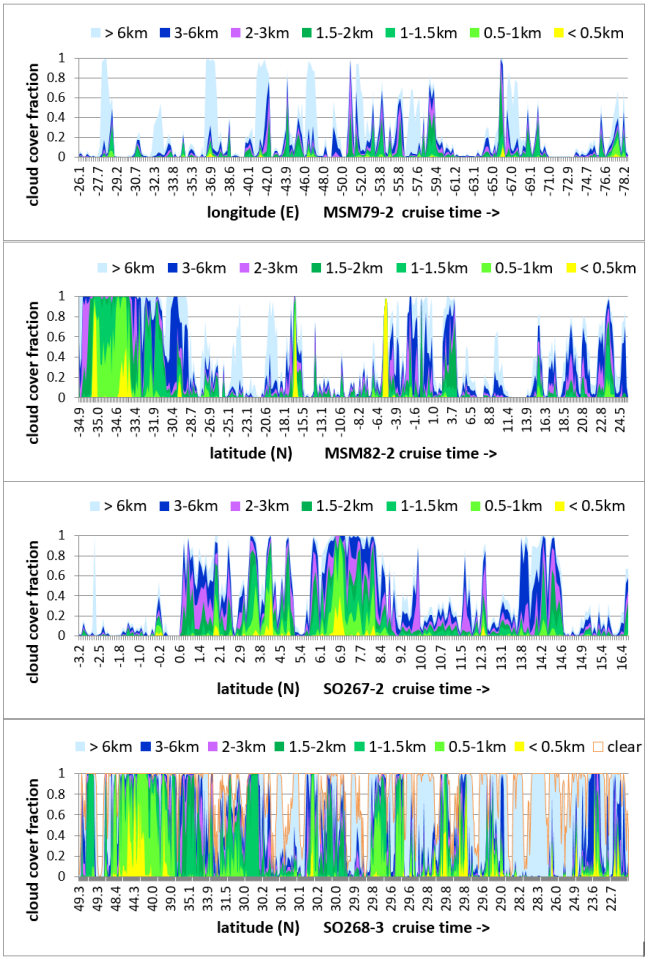

Fig. 4: Hourly averages of cloud cover fraction as function of the cruise track by the thermal camera images. Cloud fractions are presented as function of cloud-base altitude-regimes, according to the color scale. Cloud-free fractions are in white.

Cloud-base statistics (of thermal camera and ceilometer) complement retrieved cloud top altitudes of satellite data and are important for more accurate estimates of LW downward radiative fluxes and surface processes.

Atmospheric relationships: Many atmospheric properties varied during the cruise, including relative humidity, temperature and wind-speed at the surface. This offered opportunities to establish general relationships based on hourly averages. The relationship between aerosol load (AOD) and wind-speed is presented in Figure 5.

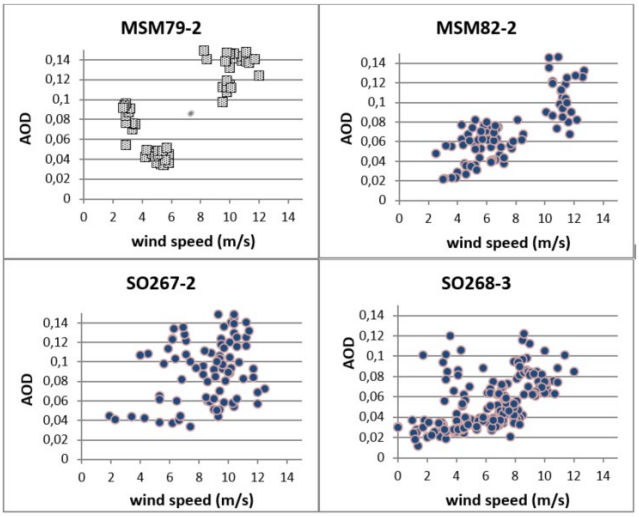

Fig. 5: Relationships of hourly wind-speeds and hourly lowest aerosol amounts (AOD) during MSM79/2, MSM82/2, SO267/2 and SO268/3.

The relationships illustrate the minimum AOD to be expected as function for surface winds, which is highly relevant for remote region AOD constrains to aerosol satellite retrievals (Kinne, 2009) and to global modeling (Kinne et al. 2006). The lowest AODs over oceans are near 0.02 at calm conditions. Minimum AOD values start to increase when wind-speeds exceed an 8m/s threshold, with is consistent with the appearance of whitecaps and then the release of extra seasalt aerosol into the atmosphere.

Bathymetric analysis: Hydroacoustic recorded data were prepared for the database of the "Seabed 2030" ocean floor mapping initiative. (https://seabed2030.gebco.net/). Selected high resolution paths of the seafloor depth of from transit cruises are presented in Figure 6.

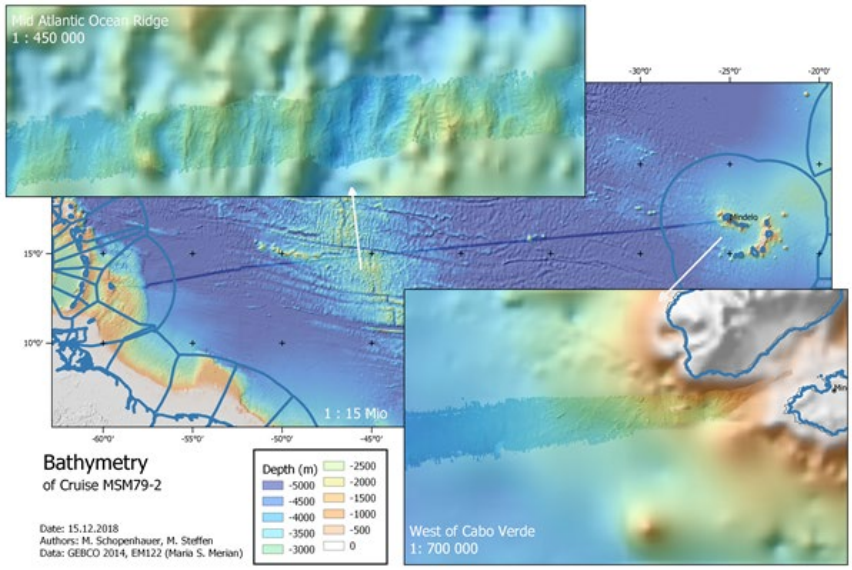

Fig. 6: Overview map of the bathymetric survey (from the Cape Verde Island to Barbados) during MSM 79/2 and two high resolution samples over the Atlantic ridge (top) and west of Mindelo (bottom)

ARGO floats: As part of an international collaboration (http://www.argo.uscd.edu) ca 3000 floats (unmanned robots) monitor the state (e. g. temperature, salinity, currents) of oceans down to depths of 2000 m. Due to a float's limited lifetime of about 5 years, always new floats (as on MSM 79/2 and SO 268/3) need to be added (preferably in float sparse oceanic regions) to maintain upper ocean observing capabilities. Pictures of float releases are presented in Figure 7.

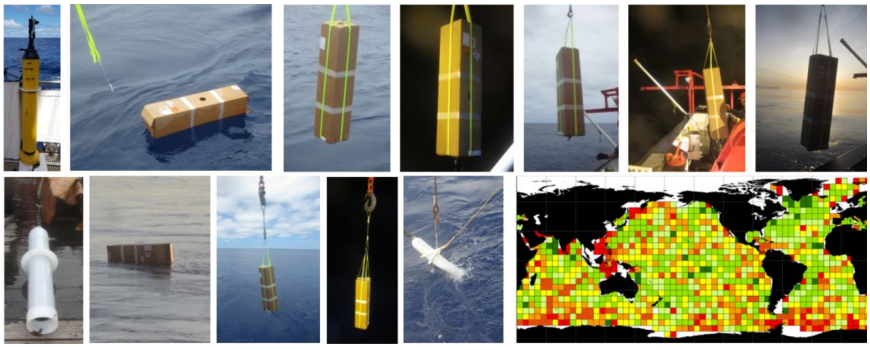

Fig. 7: ARGO floats (left top: teledyne left, left bottom: new US version usually deployed in a carton), deployment pictures during SO268/3 and a regional density (red: too sparse, green: OK) map of floats over oceans (right) as of Dec 2019.

REFERENCES

Kinne, S., The MACv2 Aerosol Climatology, Tellus B: Chemical and Physical Meteorology, 2019a, 71, 1, 1–21.

Kinne, S., Aerosol radiative effects with MACv2, ACP 19, 2019b, 10919–10959.

Kinne, S., Remote sensing data combinations-superior global maps for aerosol optical depth. Satellite Aerosol Remote Sensing Over Land, A.Kokhanovsky and G. de Leeuw, Springer ISBN: 978-3-540-69396-3, 2009.

Kinne, S., et al., An AeroCom initial assessment – optical properties in aerosol component modules of global models, 2006, ACP, 6, 1–22.

Knapp, M., et al., Shipborne measurements of XCO2, XCH4, and XCO above the Pacific Ocean and comparison to CAMS atmospheric analyses and S5P/TROPOMI, Earth Syst. Sci. Data Discuss., 2021, 13,199–211.

Smirnov, A., et al., Maritime aerosol network as a component of AERONET – first results and comparison with global aerosol models and satellite retrievals, Atmos. Meas. Tech., 2011, 4, 583-597.

Smirnov, A., et al., Maritime Aerosol Network as a component of Aerosol Robotic Network, J. Geophys. Res., 2009, 114, D06204, doi:10.1029/2008JD011257.

Wagner, T., et al., Quantitative comparison of measured and simulated O4 absorptions for one day with extremely low aerosol load over the tropical Atlantic, AMT, 2021, 14, 3871–3893.

Wang, P., et al., Shipborne MAX-DOAS measurements for validation of TROPOMI, Atmos. Meas. Tech., 2020, 1413–1426.

MSM80

Coastal Upwelling System in a Changing Ocean (CUSCO)

AUTHORS

University of Bremen – BreMarE – Bremen Marine Ecology | Bremen, Germany
H. Auel, A. Schukat on behalf of the cruise participants and the BMBF-CUSCO project partners

Leibniz-Institute for Baltic Sea Research (IOW) | Warnemünde, Germany
V. Mohrholz

The MSM80 research cruise with R/V Maria S. Merian to the Humboldt Current upwelling system off Peru in December 2018 / January 2019 was the field campaign of the BMBF-funded joint research project CUSCO – "Coastal Upwelling System in a Changing Ocean – Trophic Transfer Efficiency of the Humboldt Current Upwelling System off Peru" in cooperation with the Peruvian marine and fisheries research institute IMARPE.

Eastern Boundary Upwelling Systems (EBUS) are among the most productive marine ecosystems, providing 7 % of total marine primary production and 20 % of global marine fish landings, but accounting for only <2 % of the ocean area. Although the four major EBUS have similar upwelling intensities and similar primary productivity per unit area, the Humboldt Current Upwelling System (HUS) provides five to eight times higher fisheries yields per unit area than the other systems.

Such an enormous fish production despite similar primary production levels as in other EBUS can only be explained by a much higher trophic transfer efficiency (TTE) in the HUS compared to other EBUS. Therefore, the overall objective of CUSCO and of the MSM80 research cruise was to elucidate the reasons for the extremely high productivity at upper trophic levels and how the mechanisms will respond to global climate change. In interdisciplinary cooperation, biological and physical oceano-graphers collaborated with marine ecologists, biogeochemists, and fisheries scientists in order to trace carbon and energy fluxes through the marine foodweb and to study how different upwelling intensities affect overall TTE.

Specifically, research during MSM80 focused on the following topics:

(i) Phytoplankton composition and primary production under different upwelling regimes.

(ii) Length of the food chain between primary producers and harvested species via trophic biomarkers (stable isotopes, fatty acids).

(iii) Role of filter feeders (e. g. krill). Since filter feeders efficiently consume a wide range of prey sizes, they form less complex food webs with a higher overall TTE.

(iv) Gelatinous zooplankton, since they are often "dead ends" of the food chain and predators and competitors for small pelagic fish.

(v) Abundance, distribution and prey spectra of pelagic and mesopelagic fishes.

(vi) Effects of physical-biological boundaries (meso-scale eddies, upwelling filaments, margins of the oxygen minimum zone) on zooplankton dynamics.

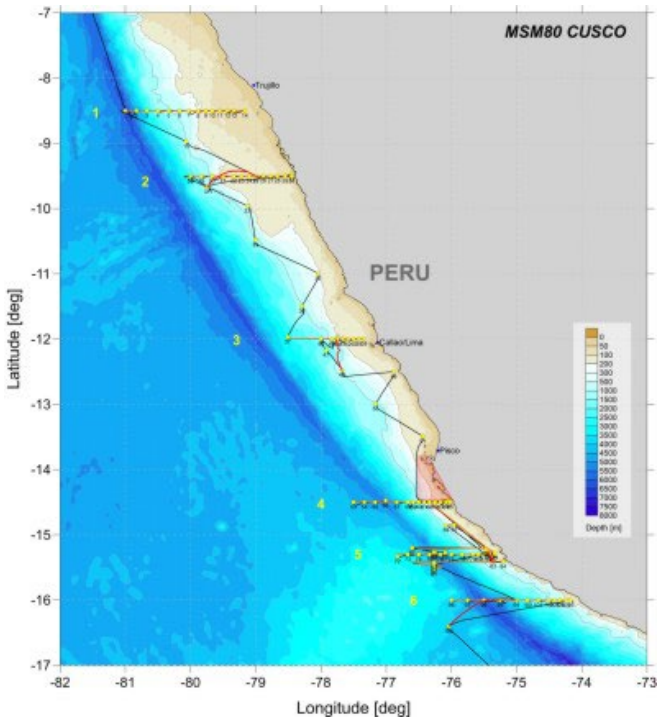

Fig. 1: Station map and cruise track of MSM80. Yellow dots indicate the positions of CTD/MSS stations. The orange lines depict the ScanFish transects. The red lines indicate the deployments and pathways of the drifting surface mooring. The thin black line is the ship track (provided by IOW team).

The research cruise MSM80 started on 20th December 2018 in Bahia Las Minas, Panama, and ended on 31st January 2019 in Valparaiso, Chile. In total, 106 stations were sampled, covering the continental shelf (200 m) and continental rise (1000 m) along the Peruvian coastline from 8°30'S to 16°30'S and concentrating along six sections perpendicular to the coast (Fig. 1). CTD/rosette water sampler casts, plankton nets of different sizes, and optical profilers were deployed to establish hydrographic

parameters, abundance, biomass, and biodiversity of the pelagic community. Dietary spectra and trophic levels of key species were studied with trophic biomarkers (fatty acids, stable isotopes $\delta^{15}N$, $\delta^{13}C$). Respiration (optode respirometry) and egg production measurements were conducted on board to establish energy budgets and TTEs of dominant zooplankton species. Additionally, information on diapycnal mixing was gathered by microstructure measurements with an MSS profiler. A towed CTD (ScanFish) was used to supply high resolution hydrographic data at water mass boundaries and fronts. The temporal evolution of upper layer dynamics was studies with several short-term deployments of a drifting surface mooring.

The first and second transects covered the wide and shallow shelf area off northern Peru. The central shelf was sampled with the third transect off Callao. The transects four, five and six were carried out on the narrow southern shelf between 14.5°S and 16°S, the main working area during the cruise. Between those transects, a number of stations were sampled near the shelf edge (1000 m bottom depth) and on the shelf (200 m) to gather additional information on the spatial distribution of water masses and pelagic communities.

During the time of the MSM80 cruise, upwelling was generally weak to moderate along most of the Peruvian coastline. However, at several stations, the succession state of the pelagic community indicated recent upwelling days to weeks before. The covid-19 pandemic since March 2020 has caused delays in the processing and analysis of samples and data from the MSM80 cruise, and BMBF has recently prolonged the CUSCO project period for another year till the end of 2022 in order to compensate for the pandemic-related delays. In addition, Peru is still in the process of establishing national regulations related to the Nagoya protocol, which has affected the publication of molecular genetic research results. Nevertheless, we were already successful in publishing part of the MSM80 results, in particular those revealing the central role of key zooplankton species and their life-cycle adaptations for the high TTE of the HUS.

Pelagic communities in the HUS differ from those in other EBUS by the dominance of four biomass-rich crustacean species in addition to the Peruvian anchovy *Engraulis ringens*, the key small pelagic fish in the system. The key crustaceans include the copepods *Calanus chilensis* at the surface and *Eucalanus inermis* in the pronounced oxygen minimum zone, the krill *Euphausia mucronata*, and the endemic, semi-pelagic squat lobster *Pleuroncodes monodon*, resulting in an overall rather simple food web with a restricted number of major trophic pathways and high TTE (Massing et al., in review). In addition, squat lobsters play an important role in the benthic-pelagic coupling. By partly feeding on benthic resources and by diel vertical migration, they seem to provide a unique pathway for returning carbon and energy from the sea floor to the epipelagic layer, increasing the food supply for pelagic fish. These mechanisms result in a very efficient food web, channeling energy towards higher trophic levels and partially explaining the "Peruvian puzzle" of enormous fish production in the HCS (Massing et al., in review).

Moreover, key zooplankton species have developed specific life-history adaptations to cope with the peculiar environmental conditions of the HUS, including high primary productivity and a very pronounced, shallow oxygen minimum zone. The copepod *Calanus chilensis*, for instance, did not conduct ontogenetic vertical migrations with a dormant stage at depth, as typical for closely related counterparts in other EBUS. By contrast, in the HUS C. *chilensis* was almost exclusively restricted to the surface layer (50–0 m) above the oxygen minimum zone (Schukat et al. 2021). Surprisingly, the regional distribution of *C. chilensis* secondary production extended much further offshore (>200 km from the coast) than is typical of other EBUS. Compacted biomass concentrations of *C. chilensis* in the surface layer from the shelf (≤3 g DM dry mass m^{-2}) to offshore waters (≤1.5 g DM m^{-2}) facilitate easy and efficient foraging by predators such as juvenile Peruvian anchovies (Schukat et al. 2021). Thus, the compacted biomass and high productivity of *C. chilensis* at the surface derived from its adaptive life-history traits and biological-physical response to the pronounced shallow oxygen minimum zone in the HUS apparently also contribute to the superior TTE and, hence, enormous fisheries yield of the HUS.

REFERENCE

Schukat A, Hagen W, Dorschner S, Correa Acosta J, Pinedo Arteaga EL, Ayón P, Auel H, Zooplankton ecological traits maximize the trophic transfer efficiency of the Humboldt Current upwelling system, Progress in Oceanography 2021, 193, 102551

Massing JC, Schukat A, Auel H, Auch D, Kittu L, Pinedo Arteaga EL, Correa Acosta J, Hagen W, Towards a solution of the "Peruvian Puzzle": Pelagic food-web structure and trophic interactions in the northern Humboldt Current upwelling system off Peru, Frontiers in Marine Science, in review

MSM82

Rio Grande Rise

AUTHORS

GeoZentrum Nordbayern, Friedrich-Alexander-University Erlangen-Nuremberg | Erlangen, Germany
K. Haase, J. O'Connor, P. Hoyer, M. Regelous

Alfred Wegener Institute Helmholtz Centre for Polar and Marine Research | Bremerhaven, Germany
W. Geissler, T. Altenbernd, W. Jokat

GEOMAR Helmholtz Centre for Ocean Research Kiel | Kiel, Germany
S. Homrighausen, F. Hauff, J. Geldmacher, K. Hoernle

AIMS OF THE CRUISE AND SAMPLING PROGRAM

The Walvis Ridge in the eastern South Atlantic Ocean is one of the first proposed plume tracks and is the only volcanic trail on the African plate that connects continental flood basalts to active hotspot volcanoes. Thus, it has been studied relatively well and its magmatic evolution has been defined. In contrast, much less is known about the western South Atlantic with the Rio Grande Rise (RGR) and its relation to the plume model in continental rifting and opening of the South Atlantic. The RGR is considered to have formed on the South American plate together with WR while the Tristan-Gough hotspot was located close to the Mid-Atlantic spreading ridge (MAR). However, long-lived volcanism and mantle tomography suggest that another hotspot has produced a different kind of volcanic track connecting the RGR to Jurassic flood basalts in Brazil. Recent geophysical and petrological studies suggested that the RGR could be a fragment of a detached continental margin that has been preserved as a 'microcontinent' embedded in plume-influenced oceanic crust. Cruise MSM82 carried out geophysical surveys and dredge sampling in order to better define the structure, age and composition of the RGR.

GEOPHYSICAL RESULTS

Seismic refraction and gravity data were acquired along two NNE-SSW trending seismic lines. They cross the western and eastern RGR, respectively. The Cruzeiro do Sul Lineament (CdSL), a series of NW-SE trending troughs which cut the Eastern Rio Grande Rise (ERGR) and Western Rio Grande Rise (WRGR), was imaged along both profiles. The main objectives of our geoscientific investigations were to study the nature of the crust, the evolution of the Rio Grande Rise and the formation of the CdSL.

Based on P-wave velocity models derived by forward modelling and supplemented by a gravity models, the crustal structure and partly also the upper mantle structure along both profiles could be constrained. Unfortunately, no seismic reflection data were acquired during the cruise due to a malfunction of the streamer. Since the seismic refraction data are of good quality, the structure of the CdSL could be examined despite the lack of MCS data. The CdSL is well-imaged along both profiles and up to 8 km deep faults cut the upper crust. The faults at the northern flank of the graben are much steeper than at the southern flank along both profiles.

Our two P-wave velocity models show that up to 2 km thick sediments cover the RGR in its eastern and western part. Below, the upper 5 km of the crust along both profiles consist of 2–3 layers with velocities increasing from 4.4–6.4 km/s with depths. The crust of the WRGR is up to 30 km thick, while the crust of the ERGR is thinner and only half as thick (15 km). The differences in crustal thickness are due to the varying thickness of the lowermost crust, which has a maximum thickness of 25 km at the WRGR and only 10 km at the ERGR. A common feature of the lowermost crust in the east and west is a high velocity lower crust with velocities of up to 7.4 km/s at the base. While a high-velocity upper mantle (up to 8.6 km/s) is partly present below the western RGR, such high upper mantle velocities are not observed along the eastern profile, which could also be a result of a partially poor data coverage in the upper mantle along our eastern profile.

With the exception of the crustal thickness, the crustal structure along both profiles is very similar. Velocity-depth profiles indicate that the crustal structure of the RGR is typical for oceanic plateaus/submarine ridges. Additionally, thickness and crustal velocities of the WRGR are similar to the crustal structure of Walvis Ridge. No indications for the existence of a detached microcontinent or a continental sliver situated in the RGR have been identified along our two seismic lines.

PETROLOGIC AND GEOCHEMICAL RESULTS

Major and trace element concentrations were determined on 47 whole rock samples dredged during MSM82 from the flanks of a long rift valley that cuts through the eastern (E) and western (W) parts of the RGR. Further, new geochemical data are provided from DSDP Site 516 and the Jean Charcot Seamount Chain (JCSC). Trace element modelling suggests that the WRGR was affected by at least two stages of volcanism. The magmatic system changed from a configuration with high degrees of shallow mantle melting to one with deep melting of an enriched source. The second stage of volcanism was affected by the JCSC. In comparison, the lavas from the ERGR show high degrees of shallow mantle melting but exhibit an alkaline character and higher ratios of Nb/Zr, Nb/Yb and Th/Yb than depleted MORB. Thus, the ERGR lavas were formed at or close to a plume-influenced spreading centre. All samples from the RGR have high Nb/Th, Ce/Pb and Nb/La similar to oceanic basalts, indicating that they have not undergone significant contamination by a continental component showing low values of these ratios. Therefore, there is no

compelling geochemical evidence for continental crust below the RGR and rather, the plateau probably formed by volcanic processes of a large igneous province.

All recovered rocks from MSM82 are characterized by a pronounced DUPAL-signature, characterized by high Δ 7/4, Δ 8/4, $^{87}Sr/^{86}Sr$ and low $^{143}Nd/^{144}Nd$ ratios relative to normal mid-ocean ridge basalts. The Sr-Nd-Pb isotope ratios from the Rio Grande Rise (RGR; 38 samples recovered during MSM82 and 4 samples from DSDP Site 516) lie largely within the compositional array of the Tristan-Gough hotspot track on the African plate. Samples recovered from the western RGR (WRGR) have a more enriched continental-like signature (higher $^{87}Sr/^{86}Sr$ ratios and lower $^{143}Nd/^{144}Nd$ ratios) compared to the eastern RGR (ERGR). If the continental signature derives from intra-crustal contamination of an embedded microcontinent in the oceanic fabric of the RGR, we would also expect a more pronounced continental signature in Pb isotope ratios, which is not observed. Additionally, on diagrams of differentiation versus continental signature proxies (i. e., MgO vs. $^{143}Nd/^{144}Nd$) the most primitive samples from the ERGR have variable isotope ratios most likely reflecting melting source heterogeneities rather than continental intra-crustal contamination. Based on the similar geochemical signature, temporal and geodynamic constraints (i. e., plate motion models), the RGR and Walvis Ridge share most likely a co-genetic origin formed by the Tristan-Gough mantle plume.

The Tristan-Gough hotspot track comprises two distinct enriched compositional types, which are spatially separated: 1) the long-lived Gough-type composition forming the Walvis Ridge and easternmost sub-track leading to Gough island, and 2) the Tristan-type composition emerging at the southwestern tip of the Walvis Ridge and forming the westernmost sub-track leading to Tristan da Cunha. The RGR, on the other hand, cannot be unambiguously assigned to one of the enriched compositional types. The Sr-Nd isotope ratios of the RGR lie largely within the Gough-type compositional array. The Pb isotope ratios, which most clearly separate the both compositional types, have a higher Tristan-type affinity, possibly indicating that the geochemical zonation of the Tristan-Gough hotspot emerged earlier than previously assumed, which provides important insights into the temporal geochemical evolution of the Tristan-Gough hotspot track.

The JCSC lavas lie largely within the compositional array of the RGR in Sr-Nd-Pb isotope ratio diagrams and form overall linear trends from an enriched continental-like signature to a more depleted component similar to the South Atlantic MORB, but with higher Pb isotope ratios. In contrast to the RGR we have no evidence for the emplacement age so far, which is essential to calculate the initial isotope ratios for a more detailed evaluation.

MSM82/2

Morphology of the headwall area of the Sahara slide (NW-Africa); Measuring Over Ocean References; Mapping sequences to protists morphospecies from the Atlantic

AUTHORS

Kiel University | Kiel, Germany
S. Krastel

Max Planck Institute for Meteorology | Hamburg, Germany
S. Kinne

Max Planck Institute for Dynamics and Self-Organization | Göttingen, Germany
E. Bodenschatz

University of Cologne | Cologne, Germany
F. Nitsche

INTRODUCTION

RV MARIA S. MERIAN Cruise MSM82/2 was a transit cruise from Montevideo to Las Palmas. Three proposal were realized during the cruise. Hydroacoustic data and gravity cores were collected in the headwall area of the Sahara slide (Proposal 'Morphology of the headwall area of the Sahara Slide, NW-Africa'. Atmospheric data were collected in the frame of the proposal 'Measuring Over Ocean References'. These measurements included shipboard-based estimates of atmospheric aerosol and trace-gases as well as cloud properties. A major success was the test of a CloudKite. The proposal 'Mapping sequences to protists morphospecies from the Atlantic' aimed in studying the biodiversity of pelagic protists in an area, which has not been investigated extensively yet. Surface water samples were taken every 5° latitude.

MORPHOLOGY OF THE HEADWALL AREA OF THE SAHARA SLIDE, NW-AFRICA

Submarine mega-slides with an involved material of several hundreds of cubic kilometers pose a major threat due to their potential to destroy offshore infrastructure and trigger devastating tsunamis. The Sahara Slide Complex affected an area of about 48,000 km^2 at the northwestern African continental margin. Previous studies focused on its distal depositional zone and the uppermost headwall area, but the reconstruction of individual slide events forming the entire headwall area was impossible. New hydroacoustic and sedimentological data collected during Cruise MSM82/2 reveal great morphological

heterogeneity of the Sahara Slide Complex with three distinct headwall areas (the upper, southern and lower headwall area). Individual headwall areas were formed by multiple failures along different levels of glide planes. The slide deposits cover well stratified sediments in the upper and southern headwall area. Sliding occurred along distinct and widespread glide planes pointing to failures along pronounced weak layers. Glide planes are found at different stratigraphic levels for individual headwall areas suggesting a repetitive process for the formation of weak layers. We assume that this process is driven by climate. The lower headwall presents a distinct single and continuous headwall compared to the multiple minor headwalls of the upper and southern headwall. The lower headwall area is characterized by stacked slide deposits. Sediment cores allow to date individual slide events. The lower headwall was formed at ~ 60 ka, followed by the northeastern part of the upper headwall area at 14 ka. The main slide of the upper headwall area occurred at 6 ka, followed by sliding in the southern headwall area. The youngest slide event (~2 ka) is found at the upper headwall. This pattern proofs the long history of landsliding in this area continuing into the recent past (Fig. 1).

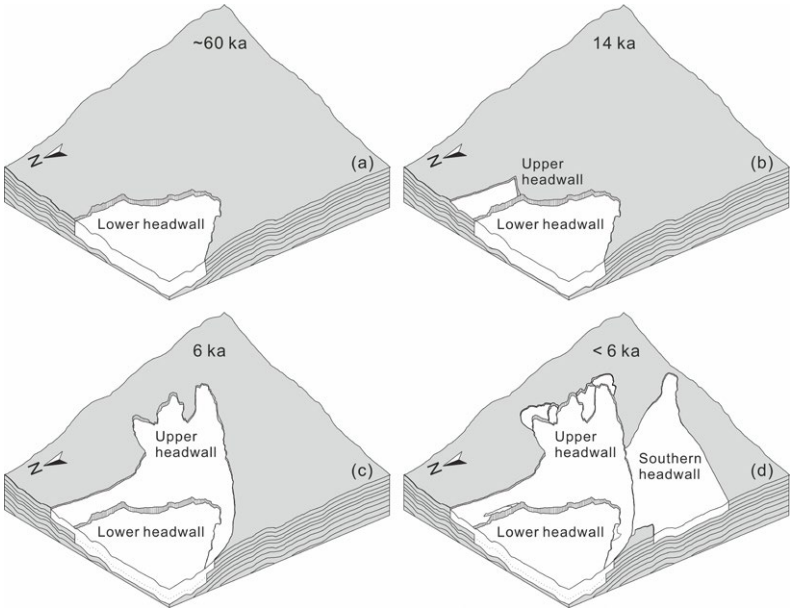

Fig. 1: Conceptional model for the successive slide events in the headwall area of Sahara Slide Complex from 60 to 2 ka (taken from Tang et al., 2021)

MEASURING OVER OCEAN REFERENCES

Atmospheric data for aerosol, trace-gases and clouds were collected to address the need for atmospheric reference data over oceans. Using the sun and the sky as background, atmospheric properties can be determined at higher accuracy than via satellite remote sensing. Thus, for reference data on atmospheric aerosol and trace-gases a

sun-photometer (Smirnov et al, 2009) and a MAX-DOAS were operated. Accessible at http://aeronet.gsfc.nasa.gov/new_web/maritime_aerosol_network.html the aerosol data have been used in climatology updates (Kinne, 2019) and in a study linking properties of aerosol and trace-gases (Wagner et al., 2021). Atmospheric reference samples were complemented by a vertically profiling ceilometer and by sky imaging cameras to add statistics on cloud properties. The sub-group's science staff also included a geodesy scientist, which prepared ocean floor data for the Seabed 2030 initiative database and many MPI-DS scientists, which operated a new lower atmospheric in-situ sampling test platform: Max-Planck Cloud Kite (MPCK). Images of its operation are presented in Figure 2. At times two balloon-kites were needed to lift the (ca 60kg) heavy instrument packages, designed to capture turbulence (via high frequency pressure, temperature and humidity sensors) and cloud microphysics (size, shape) from 30cm down to sub-millimeters scales.

Fig. 2: Images of the cloud kite operation during MSM82/2

MAPPING SEQUENCES TO PROTISTS MORPHOSPECIES FROM THE ATLANTIC

Heterotrophic protists are unicellular eukaryotes present in all ecosystems and play a key role in microbial food webs. Our study during Cruise MSM82/2 focused on heterotrophic protists from surface water of a transect across the South and North Atlantic Ocean (35 °S to 23 °N). With a high isolation and cultivation effort, we tried to get insights into protist species richness and community patterns of a total of 15 sampling stations. We were able to isolate, cultivate and sequence (SSU rDNA) over 50 protistan strains, i. e. choanoflagellates, kinetoplastids, cercozoans, ancyromonadids and apusomonadids (Fig. 3). With this, we broadly extended the molecular data on marine species present in the Atlantic Ocean. Our isolation and cultivation effort on craspedid choanoflagellates extended the recently introduced genus Hartaetosiga (Carr et al., 2017) by 14 strains and transcriptomic data of nine of these strains. Morphometric data showed no distinct

morphological traits allowing for a species delineation, indicating a cryptic species complex within the genus. Based on cultivation, morphological data and molecular analyses, we could describe a new species, H. australis. This new species was recorded only from sampling stations in the Southern Hemisphere, indicating a potential biogeographic distribution likely caused by the Equatorial Counter Current (ECC), dividing the northern and southern surface waters.

This study extends our knowledge on the taxonomy and phylogeny of different groups of heterotrophic protists and demonstrates that biogeographically patterns might be present within several groups like choanoflagellates. It also highlights the necessity of further taxonomic and phylogenetic studies on ubiquitous species like kinetoplastids, to understand their dispersal and role in the microbial food web.

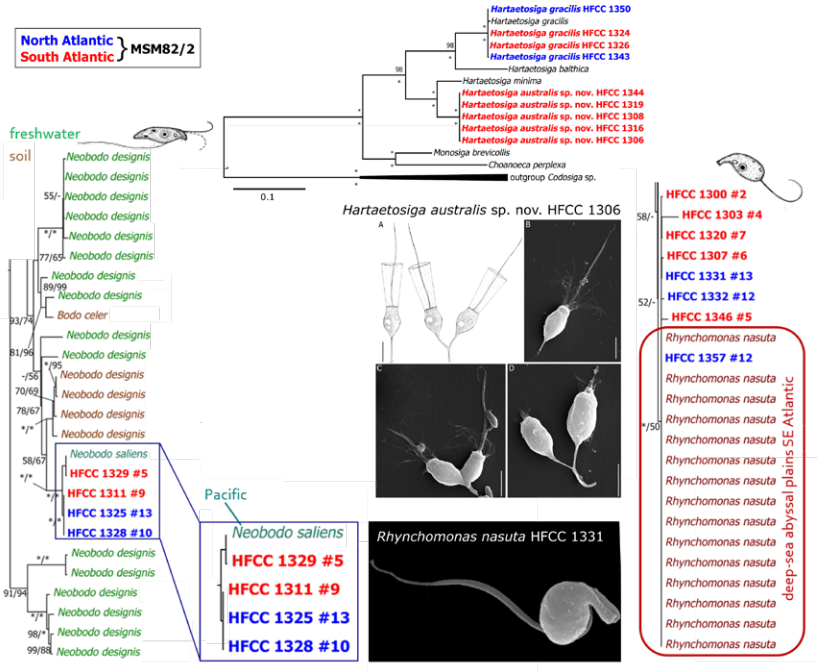

Fig. 3: Selection of protistan diversity and potential biogeographical separation from the Atlantic Ocean (cruise MSM82/2) exemplified by craspedid choanoflagellates (see phylogenetic analyses in the upper part and morphology (scheme and SEM) of the newly described Hartaetosiga australis sp. nov.) and the phylogeny of kinetoplastids (left: clade of Neobodo designis, right: Rhynchomonas nasuta with SEM image) extended by new strains investigated from the North (blue) and South (red) Atlantic.

REFERENCES

Carr M, Richter D, Fozouni P, Smith TJ, Jeuck A, Leadbeater B, Nitsche F, A six-gene phylogeny provides new insights into choanoflagellate evolution, Molecular Phylogenetics and Evolution, 2017, 107, 166–178

Kinne S, The MACv2 Aerosol Climatology, Tellus B: Chemical and Physical Meteorology, 2019, 71, 1, 1–21

Smirnov A, et al., Maritime Aerosol Network as a component of Aerosol Robotic Network, Journal of Geophysical Research, 2009, 114, D06204, doi:10.1029/2008JD011257.

Tang Q, Düring A, Unverricht D, Lenz K-F, Krastel S, New acoustic and gravity core data for multiple failures in the headwall area of Shara Slide Complex off northwestern African continental margin, Annual meeting of the DGG 2021, Kiel

Wagner T, et al., Quantitative comparison of measured and simulated O4 absorptions for one day with extremely low aerosol load over the tropical Atlantic, AMT, 2021, 14, 3871–3893.

MSM84

Holocene and deglacial history of the Labrador Shelf and Lake Melville

AUTHORS

Alfred Wegener Institute for Polar and Marine Research | Bremerhaven, Germany
C. Gebhardt, J. Matthiessen

University of Bremen, Institute of Geography | Bremen, Germany
C. Ohlendorf

University of Kiel, Institute of Geoscience | Kiel, Germany
F. Gross, R. Schneider

and the MSM84 Expedition Team

INTRODUCTION

The Labrador shelf is a key area for palaeoclimatic and palaeoceanographic investigations. During deglaciations of the Laurentide Ice Sheet (LIS), large quantities of freshwater were released through the Labrador fjord-trough systems into the Labrador Sea and the North Atlantic. These freshwater pulses had a profound influence on the strength of the Atlantic meridional overturning circulation, which in turn significantly influenced the climate of the Northern Hemisphere. The major drainage system, Hudson Bay in the northernmost part of the Labrador shelf, is well-investigated as are the areas around Newfoundland and Nova Scotia. Large parts of the Labrador shelf, however, remained rather unexplored. So far, the dynamics of the LIS were mostly reconstructed based on marine sediment cores derived mainly from the North Atlantic, relatively far away from the actual LIS margin. Direct evidence from glacial features on the shelf, i. e. direct evidence on the temporal and spatial retreat of the LIS, was not available.

The overarching goal of the expedition was to reconstruct the spatial and temporal history of LIS retreat in its eastern sector with special emphasis on the Wisconsinan glaciation. The working program of MSM84 consisted of a series of complementary methods: (1) sediment coring, (2) hydroacoustics including PARASOUND and multibeam echosounder, and (3) seismic profiling.

During expedition MSM84, we therefore performed a sampling program for deglacial to Holocene sediment sequences from areas that were once overlain by the LIS. The cores were taken from three large trough systems on the Labrador Shelf, namely the Cartwright, Hopedale, and Okak troughs (Fig. 1). In addition, to span a wide range from the shelf

break to as far inland as possible, and hence cover a wide range of LIS retreat at the end of the last glacial, we also entered the 250 m deep Lake Melville inlet system at ca. 54°N. This lake system is connected to the Labrador Shelf through a small link of ca. 30 m water depth, the "Rigolet Narrows".

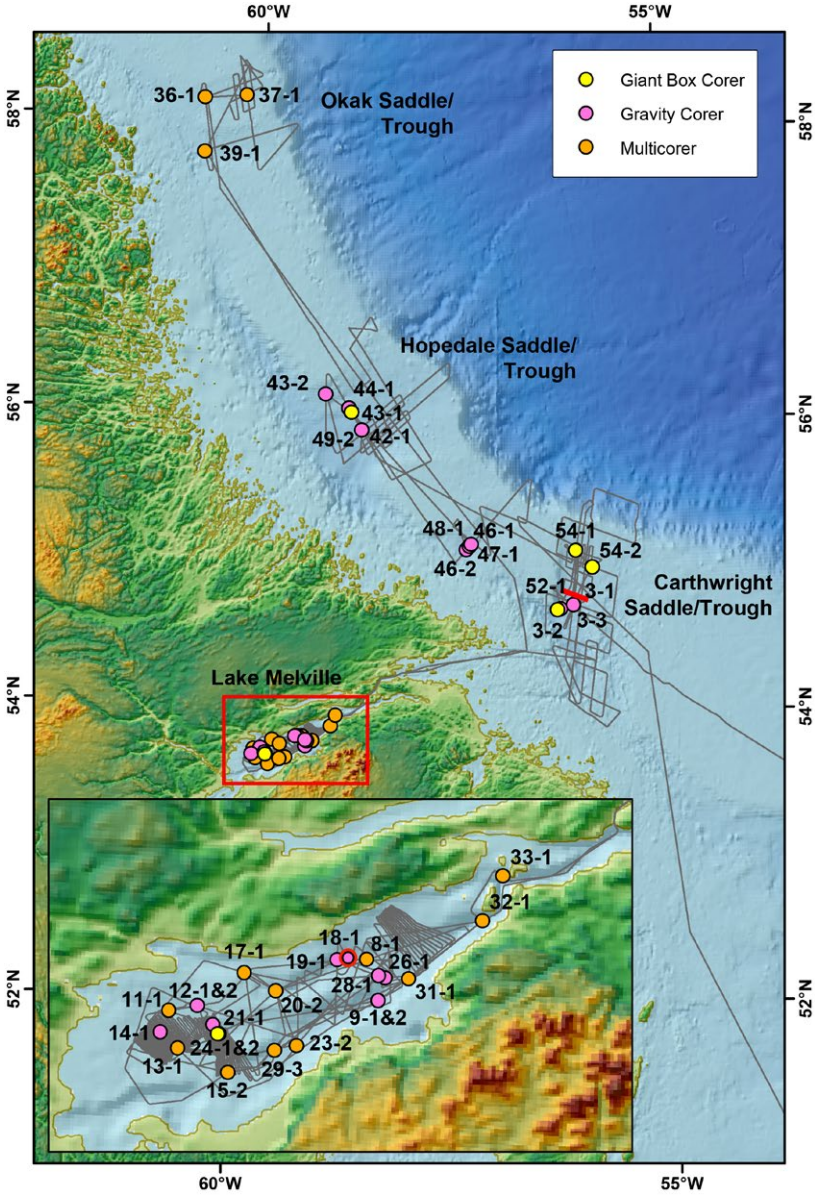

Fig. 1: Research area with location of sediment cores and tracklines of Parasound and bathymetry. Seismic profiles were gathered in the trough systems of the Labrador Shelf. Core MSM84_18-1 shown in Fig. 2 and profile 707 displayed in Fig. 3 are marked in red.

In addition, ca. 3000 km of high-resolution seismic profiles were collected from the three glacial troughs. Along the entire trackline of MSM84, Parasound and multibeam bathymetry data were collected, and systematic mapping of glacial features on the seafloor (lakefloor) was performed in Lake Melville.

LAKE MELVILLE

Previous seismic studies in Lake Melville have shown that a thick sequence of sediments (up to 400 m) is deposited in a rather narrow valley (Syvitsky and Lee, 1997). The 250 m water depth may have allowed this lake to persist below the LIS, and hence make it a candidate for retrieval of sediments that date back in time further than the last deglaciation. First results from a 14 m long gravity core show clayey silt to slightly sandy silt, a prominent turbidite that is likely found basin-wide, and varying physical properties (Fig. 2). Preliminary ^{14}C dates indicate that the cores retrieved in Lake Melville span at least the entire Holocene.

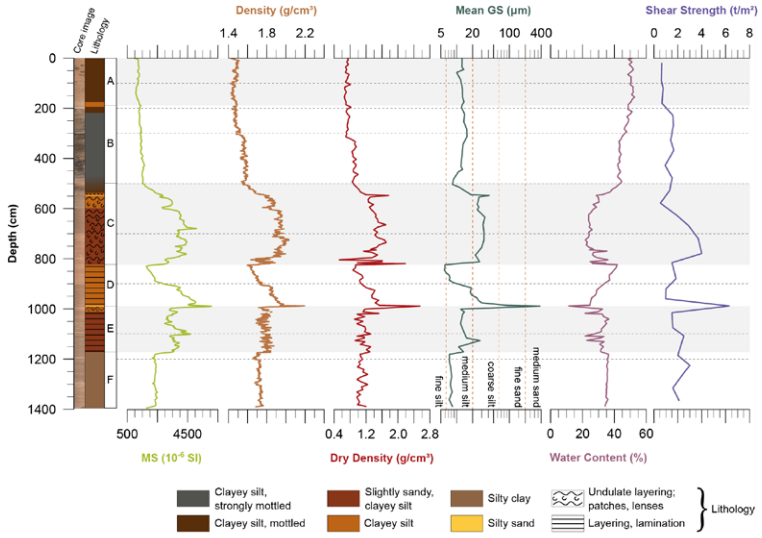

Fig. 2: Lithology and physical properties of core MSM84_18-1, located in Lake Melville. Lithological units A and B are relatively homogeneous, but B exhibits a large number of black mottles. Unit C is marked by an increase in magnetic susceptibility, density, larger grain size, and slightly enhanced shear strength. Unit D is a pronounced turbidite that is encountered in large parts of the western Lake Melville. Unit E is relatively similar to C. Unit F is strikingly homogenous, fine-grained, with low magnetic susceptibility and density (Kowalski, 2020).

LABRADOR SHELF

The shelf is characterized by a series of cross-shelf troughs that were initially excavated by ice streams at the outer border of the LIS. High-resolution seismic profiles were taken along and across the trough axes and onto the neighboring inter-trough banks. Data from the Cartwright Trough show different seismic facies types, major horizons and seismic units, erosional unconformities, deeply cut depressions, U- and V-shaped channels and

mound structures that can be associated to glacial phases, i. e. both advances and retreats of the LIS. The glacial deposits are overlain by glaciomarine and Holocene postglacial sediments that often are well-stratified.

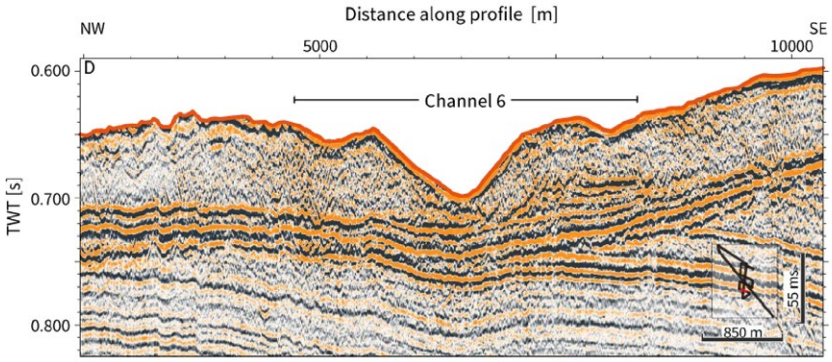

Fig. 2: V-shaped depression (channel 6) flanked by two U-shaped depressions, on NW-SE trending profile p707 (Martínez Bautista, 2021).

REFERENCES

Martínez Bautista, O, Quaternary geological evolution and paleo-landscape reconstruction of the Cartwright Saddle (Labrador Shelf, Canada): Analysis of high-resolution reflection seismic data, MSc thesis 2021, Christian-Albrechts-Universität zu Kiel, Germany, Faculty of Mathematics and Natural Sciences, 75pp.

Kowalski S, Multi-proxy analysis of a Late Glacial-to-Holocene sediment sequence from Lake Melville, Canada, MSc thesis 2020, University of Bremen, Germany, Physical Geography, 48pp.

Syvitski JPM and Lee, HJ, Postglacial sequence stratigraphy of Lake Melville, Labrador, Marine Geology 1997, 143: 55–79.

MSM85

Submarine meltwater around Greenland

AUTHORS

IUP – Institute of Environmental Physics, University of Bremen | Bremen, Germany
C. Mertens, O. Huhn, D. Kieke, M. Rhein

MARUM – Center for Marine Environmental Sciences, University of Bremen| Bremen, Germany
D. Kieke, M. Rhein

The accelerated melting of the Greenland Ice Sheet (GrIS) under a warming climate is one of the major causes of global sea level rise. Surface melting due to atmospheric warming, iceberg calving, and inflow of warm and saline Atlantic Water into the cavities beneath the floating ice tongues of the large marine-terminating outlet glaciers contribute to the increased melting observed over the past decades. This submarine melting induced by the Atlantic Water yields colder and fresher outflow that is eventually exported toward the shelf break and presumably into the boundary current. The meltwater from the GrIS could also affect the regional density structure and circulation. Knowledge about the actual submarine melting rates is, however, limited and often based on indirect remote sensing methods. The increasing release of meltwater into the ocean is expected to have an impact on the deep water formation in the North Atlantic causing it to decrease. Since the deep water formation and spreading contribute to the lower limb of the Atlantic Meridional Overturning Circulation, identifying, tracking, and quantifying the oceanic submarine meltwater content and its variability is of high interest.

The noble gases helium (He) and neon (Ne) provide a valuable tool to identify and quantify the components of glacially modified water. Atmospheric air is trapped in the ice matrix during formation of the meteoric ice. When the glacial ice above the sea water melts from below, these gases are completely dissolved in the water due to the enhanced hydrostatic pressure at the base of the ice shelf or glacier. The so called, submarine melt water (SMW) is thus highly enriched in He and Ne (e.g. Huhn et al., 2018, Huhn et al., 2021). At Antarctica surface melt does not play a role, because of the freezing-point air temperatures throughout the year, while around Greenland, where summer temperatures are higher, surface and submarine melting are of similar importance. For the ice-tongue glaciers, most of the SMW is released via melting beneath the ice tongue. For tidewater glaciers, a minor part is discharged by melting of the vertical tidewater face, but the major part is discharged through melting of icebergs, so that here the SMW injection points are mostly inside the fjords along the trajectories of the icebergs.

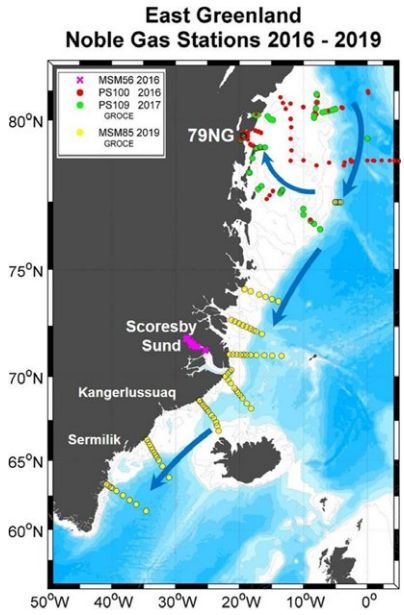

Fig.1: Stations with noble gas samples along the eastern coast of Greenland. The blue arrows indicate the East Greenland Current and the circulation on the northeast Greenland shelf.

For the three remaining largest ice tongues, all located in northern Greenland, thecontribution of submarine melting to the glacial runoff is about 80 %. In 1960–1990, that is a time period with a stable GrIS, the ice discharge (iceberg calving and submarine melting) from glaciers with ice tongue and tidewater glaciers covered about 54 % of the total freshwater flux. Downstream, at the southern tip of Greenland, the analysis of noble gas data revealed that the presence of SMW is mostly confined in the upper 400 meters in the boundary current, while it could not be detected in the interior of the basins (Rhein et al., 2018).

The major goal of the observations on Maria S. Merian cruise MSM85 was to determine the distribution of glacial melt water along the east Greenland shelf and in the East Greenland Current using the noble gases helium and neon as tracers. The work program consisted of 160 CTD stations along eight hydrographic sections that were crossing the Greenland Shelf and the East Greenland Current at different latitudes in the Irminger and Greenland Seas (Fig. 1). A total of 720 water samples for noble gas analysis were collected. The cruise MSM85 was part of the BMBF program GROCE (Greenland Ice Sheet – Ocean Interaction). The goal was to close the gap between observation in the north obtained on the Polarstern cruises (PS100 and PS109 in 2016 and 2017), and data from Maria S. Merian cruise MSM43 (2015) in the south. We evaluate hydrographic, velocity and noble gas measurements with focus on the Greenland boundary current systems, and the aim at obtaining a large-scale view on the submarine meltwater distribution around Greenland and discuss the different regional regimes around Greenland.

REFERENCE

Huhn O, M Rhein, T Kanzow, J Schaffer, J Sültenfuß (2021), Submarine meltwater from Nioghalvfjerdsbræ (79 North Glacier), Journal of Geophysical Research: Oceans, 128(7), e2021JC017224, doi:10.1029/2021JC017224.

Huhn O, T Hattermann, PED Davis, E Dunker, HH Hellmer, KW Nicholls, S Østerhus, M Rhein, M Schröder, J Sültenfuß (2018), Basal melt and freezing rates from first noble gas samples beneath an ice shelf, Geophysical Research Letters, 45, 8455—8461, doi:10.1029/2018GL079706.

Rhein M, R Steinfeldt, O Huhn, J Sültenfuß, T Breckenfelder, Greenland submarine melt water observed in the Labrador and Irminger Sea (2018), Geophysical Research Letters, 45, doi:10.1029/2018GL079110.

MSM86

Results from MSM86 to the Vesteris Seamount

AUTHORS

Geoscience Faculty and MARUM, University of Bremen | Bremen, Germany
W. Bach

GeoZentrum Nordbayern, University Erlangen-Nuremberg | Erlangen, Germany
K.M. Haase

GEOMAR Helmholtz Centre for Ocean Research Kiel | Kiel, Germany
U. Hentschel Humeida, B. Slaby

Institute of Geology, University of Hamburg | Hamburg, Germany
J. Peckmann

Department of Geosciences and Geography, University of Helsinki | Helsinki, Germany
C. Beier

The research program of RV MARIA S. MERIAN cruise MSM86 Vesteris Seamount was aimed at improving our understanding of the evolution of Vesteris Seamount, a large and lone intraplate volcano in the Greenland Sea. We had also planned to sample other basement highs in the region to determine their age and origin. Our research objectives include (1) resolving mantle melting dynamics and source composition and their bearing for the geodynamic evolution of the northern North Atlantic, (2) reconstructing the volcanic growth of Vesteris Seamount and its partial destruction by slope failures, (3) investigating the diversity of sponges and the microbiomes they host at Vesteris Seamount and other basement highs, and (4) examining the colonization of volcanic rocks by microorganisms, including fungi and bacteria, and determining the relation between rock alteration and endolithic life. Our work focused on four main areas (1) the main edifice of the Vesteris Seamount, (2) the volcanic edifices along the Logi Ridge and Southern Seamount, (3) the northeastern area, and (4) Luise Boyd Seamount on the northern flank of Mohns Ridge (Figure 1).

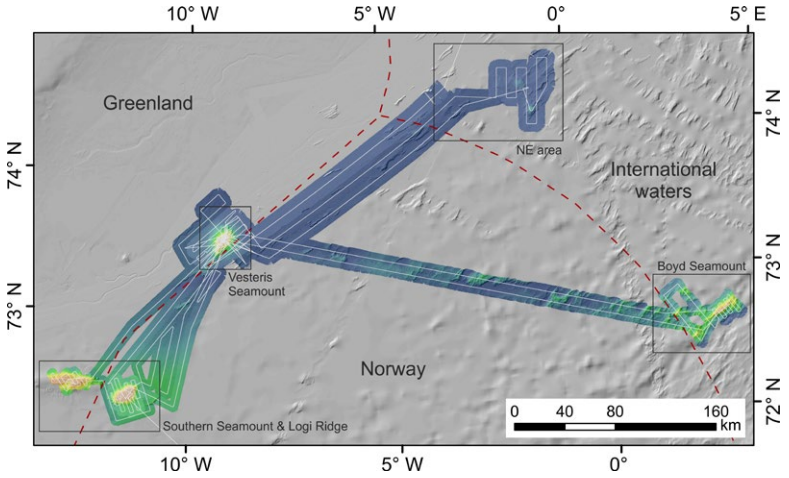

Fig. 1: Cruise track and MBES bathymetry of MSM86. The location of the four work areas are indicated. Background GEBCO bathymetry data is shown as gray hillshade.

Hydroacoustic surveys yielded high-resolution maps of bathymetric and backscatter properties of the seafloor. Geological and biological sampling was conducted using the Remotely Operated Vehicle (ROV) MARUM-SQUID (at Vesteris Seamount) and the TV-guided grab (in all four work areas). Rock sampling at Vesteris Seamount showed a predominance of effusive and pyroclastic rocks, the latter of which are particularly abundant in water depths <300 m. Basement in water depths >1000 m is commonly covered by diamictic muds with dropstones, so outcrops are discontinuous and scattered. The sediments contain occasional layers of ash or volcanic sand. In water depths < 300 m, thick spiculite mats, consisting of sponge needles and bryozoans are virtually continuous (cf. Henrich et al., 1992) and made rock sampling difficult. The rocks we collected comprise vesicular alkali basalts, olivine-clinopyroxene bearing basanites and hyaloclastites, which are particularly abundant in the summit area.

Southern Seamount has steep flanks that lead from >2000 m to a large and flat plateau at 400 m water depth. Sampling the slopes yielded mostly muds and dropstones, but angular pieces of basaltic rock were also recovered. The plateau at the summit is not perfectly flat, as our maps clearly show scouring marks produced by drifting icebergs that grounded and eroded the top of the volcano. Similarly, Logi Ridge has a flat and iceberg-scoured plateau at 500 m water depth; its flanks are less steep. There are small volcanic cones in water depths >600 m. Sampling those cones and the slopes merely gave diamictic muds with dropstones.

In the northeastern area, we mapped two basement highs that are roundish features rising above the abyssal plain by more than 1000 m. The westernmost of the two yielded hydrothermally altered olivine gabbro, while the other one had Mn-oxide coated pieces of mantle peridotite next to small pieces of serpentinite und chrysotile veins embedded in

mud. These results clearly indicate that both basement highs are not volcanic in origin but instead represent ocean core complexes that formed 40 Ma at the Mohns Ridge.

Much closer to the Mohns Ridge is the Luise Boyd Seamount, only 12 km north of the spreading axis. Our mapping and rock sampling indicates that Luise Boyd Seamount represents an off-axis seamount that formed along the flanks of the Mohns Ridge. We did not find evidence that the seamount represents a modern oceanic core complex analogous to those sampled in the northeastern area.

A total of 700 samples include 163 rocks, of which 122 are from Vesteris Seamount, and > 400 biological specimen. In particular, we sampled several distinct morphotypes of sponges (Porifera) at the different seamounts in the working area. That show a much higher diversity than previously recognized (Henrich et al. 1992). Sponges of the genus *Geodia* were the most abundant, accounting for 152 samples followed by the genus *Stelletta* with 31 sampled specimens. In general, the collection is dominated by sponges of the class Demospongiae (278 samples), but the ROV footage indicates that glass sponges (class Hexactinellida) are also very common and diverse in this area and we were able to collect 54 specimens of this group mainly of the order Lyssacinosida. Additionally, we observed and collected other fauna, such as anemones, crinoids, amphipods, ascidian, crustaceans, bryozoans and polychaetes

Initial post-cruise work focused on the (1) the petrological and morphological evolution of Vesteris seamount and (2) geobiological studies of rock-hosted microorganisms. The sponge samples collected are part of a large 16S amplicon sequencing study of the phylogenetic diversity of sponges and the microbiomes they host.

(1) The high-resolution bathymetry survey data collected during MSM86 was used in a detailed raster terrain analysis of Vesteris Seamount, distinguishing cones, irregular volcanic ridges, volcanic debris fans, U-shaped channels and lava flows (Figure 2; Unger-Moreno et al., accepted). The slope angles, ruggedness index and slope direction were combined with backscatter images to aid geologic interpretation. The new data show that the entire structure is a northeast to southwest elongated stellar-shaped seamount with an elongated, narrow summit surrounded by irregular volcanic ridges, separated by volcanic debris fans. Whole-rock geochemical data of 78 lava samples form tight liquid lines of descent with MgO concentrations ranging from 12.6 to 0.1 wt. %, implying that all lavas evolved from a similar parental magma composition. Video footage from six ROV dives shows abundant pyroclastic and hyaloclastite deposits on the summit and on the upper flanks, whereas lavas are restricted to flank cones. The seamount likely formed above a weak zone of the lithosphere possibly related to initial rifting parallel to the Mohns Ridge, but the local stress field increasingly affected the structure of the volcano as it grew larger. Thus, we conclude that the evolution of Vesteris Seamount reflects the transition from deep, regional lithospheric stresses in the older features to shallower, local stresses within the younger volcanic structures similar to other oceanic intraplate volcanoes.

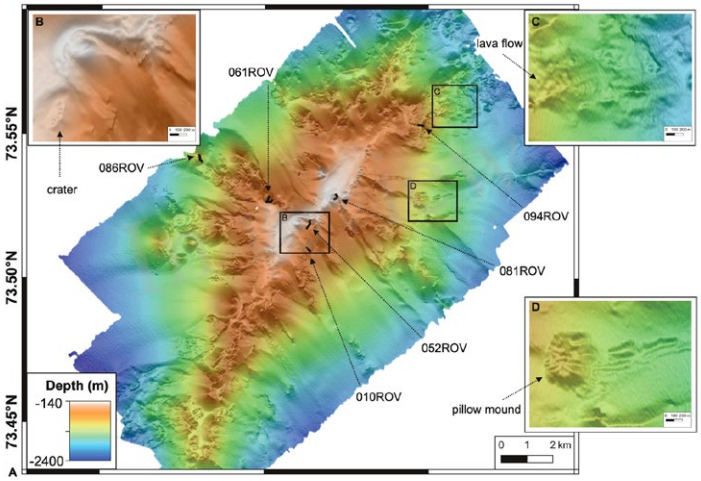

Fig. 2: (A) Close-up of the central part of Vesteris Seamount. The DEM has a resolution of 3 m and shows the tracks of the ROV dives. (B) three craters and a constructional cone in the summit area. (C) Close-up of lava flows on one of the irregular ridges. (D) close-up of a pillow mound on the eastern slope. From Unger-Moreno et al. (accepted)

(2) Rock-dwelling microorganisms like bacteria or fungi are able to mediate ion mobility and therefore contribute to erosion or deposition in such a system. It was known from previous work that the vesicular volcanic rocks of Vesteris seamount provide a habitat for marine fungi (Ivarsson et al., 2015). We investigated samples from MSM86 using x-ray microscopy to image the interconnected porosity that allowed microorganisms to colonize the rock interiors. The microorganism-infested samples show dense networks of intergrown filaments and laminated secondary mineralization filling the pore space and following a system of micro fissures through the rock. We documented the sequence of mineralization and the extraordinary content of body fossils, consisting of a range of mineral phases, including iron oxide, clay and manganese oxide minerals.

REFERENCES

Henrich R, Hartmann M, Reitner J, Schäfer P. Freiwald A, et al. (1992) Facies belts and communities of the Arctic Vesterisbanken Seamount (Central Greenland Sea). Facies 27, 71–104

Ivarsson M, Peckmann J, Tehler A, Broman C, Bach W, et al. (2015): Zygomycetes in vesicular basanites from Vesteris Seamount, Greenland Basin – A new type of cryptoendolithic fungi. PLoS ONE 10(7), e0133368.

Unger Moreno KA, Thal J, Bach W, Beier C, Haase KM (accepted): Volcanic structures and magmatic evolution of the Vesteris Seamount, Greenland Basin, Frontiers of Earth Sciences

MSM88

A seafloor mapping campaign to fill the gaps in the grid

AUTHORS

GEOMAR Helmholtz Centre for Ocean Research Kiel | Kiel, Germany
A.C. Wölfl, C.D. Devey

High resolution bathymetry data is crucial to understand the seafloor and associated processes. Nevertheless, only 20 percent of the seafloor is mapped to modern standards, which means that the majority of our oceans is still unmapped, unobserved, and unexplored, especially in the deep sea. In order to address this problem, the Nippon Foundation-GEBCO Seabed 2030 Project was launched in 2017. This project aims to bring together all available bathymetric data to complete the freely available GEBCO digital map by 2030. Seabed 2030 is a collaborative effort that supports and coordinates mapping activities worldwide and relies on cooperation and data sharing from the scientific community. In 2021, UNESCO's IOC even announced Seabed 2030 as one of the first actions endorsed as part of the United Nations Decade of Ocean Science for Sustainable Development.

The aim of the cruise legs MSM88/1 and MSM88/2 was to make a contribution to this global approach and to map a previously uncharted region in the Atlantic using the ship's multibeam system. The work area was chosen based entirely on the lack of available bathymetric data. The individual research interests of the cruise Chief Scientists explicitly played no part in this choice. The region surveyed is situated in international waters between 14° and 17° North in the Atlantic Ocean and stretches from the exclusive economic zone of Cabo Verde in the east to the Guadeloupean and Martinican EEZ in the west. Before the cruise only sparse bathymetric data were available from the area, especially the eastern part was virtually unsurveyed based on the data holdings of the IHO Data Centre for Digital Bathymetry (DCDB), with only some old single beam and low-resolution multibeam measurements known for some transit lines and parts of the Mid-Atlantic Ridge. The features mapped during MSM88 included the Mid-Atlantic Ridge, which is obviously one of the most prominent features in the working area, but also smaller ridges and fracture zones, seamounts, ocean core complexes, channel and graben structures as well as flat plains.

During this cruise, a total of approximately 250,000 km² were mapped. This is the second-largest contiguous bathymetry data set freely available in the world (after the MH370 search area in the southeastern Indian Ocean with 279,000 km²). The bathymetry datasets obtained on MSM88/1 and MSM88/2 are part of the DAM (German Marine Research Alliance) pilot project underway research data and are freely

available as “underway” data at the PANGAEA Data Publisher and at the IHO DCDB, from where it will be integrated into future editions of the GEBCO digital map series. With this mapping effort, Germany and the German marine science community made a major contribution to advancing our knowledge of the shape of the seafloor, important "base knowledge" for such diverse fields as habitat mapping, ecosystem connectivity research, ocean circulation and mixing among others.

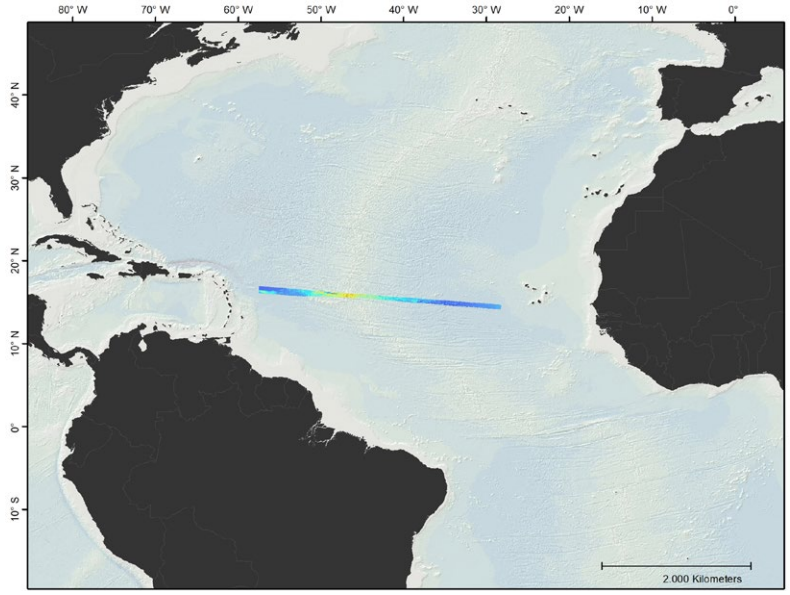

Fig. 1: Overview of the work area showing high resolution bathymetry data obtained during MSM88. GEBCO digital map in the background.

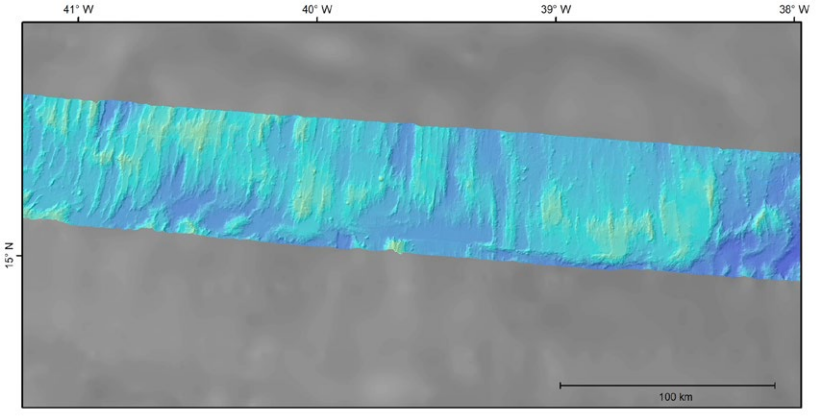

Fig. 2: Close up of the MSM88 bathymetry grid east of the Mid-Atlantic Ridge. GEBCO digital map in the background.

REFERENCES

Devey C, Wölfl A-C, Multibeam bathymetry raw data (Kongsberg EM 122 entire dataset) of RV MARIA S. MERIAN during cruise MSM88/1, GEOMAR – Helmholtz Centre for Ocean Research Kiel, PANGAEA 2020, doi:10.1594/PANGAEA.919112.

Wölfl A-C, Devey C, Multibeam bathymetry raw data (Kongsberg EM 122 entire dataset) of RV MARIA S. MERIAN during cruise MSM88/2, GEOMAR – Helmholtz Centre for Ocean Research Kiel, PANGAEA 2020, doi:10.1594/PANGAEA.919112.

MSM89

The ocean mesoscale component in the EUREC4A++ field study

AUTHORS

GEOMAR Helmholtz Centre for Ocean Research Kiel | Kiel, Germany
J. Karstensen, M. Dengler

Max Planck Institute for Meteorology | Hamburg, Germany
S. Kinne

Max Planck Institute for Marine Microbiology | Bremen, Germany
G. Lavik

University of Hohenheim, Stuttgart | Germany
V. Wulfmeyer, D. Lange

MULTIPLATFORM OBSERVING OF THE AIR/SEA INTERFACE

It probably is fair to say that EUREC4A was one the largest and most comprehensive field studies for understanding the coupled ocean/atmosphere system in the western tropical North Atlantic ever executed (Figure 1). EUREC4A made use of latest observing technology on various observational platforms, most remarkably 4 research ships, 4 research air-planes and a dedicated long-term ground station (*Barbados Cloud Observatory*, BCO), and augmented by autonomous sampling devices (Stevens et al. 2021). The EUREC4A-Ocean/Atmosphere (EUREC4A-OA) cruise on Maria S. Merian was part of this EUREC4A initiative focusing on the specific of air/sea interaction linked to meso- and submesoscale oceanic features (eddies, fronts) and operating in waters under the influence of the northwestward propagating North Brazil Current (NBC) rings (Region C in Figure 1). The list of the various devices used on the ship is presented in Stevens et al. (2021) and recent publications describe the processes in consolidating data from various sources and assessing the data quality (Stephan et al. 2021, Bosser et al. 2021, l'Hegaret et al. in preparation, Lange et al. conference abstract). The challenge in data analysis is to link the various data streams as such that the temporal evolution of the processes in ocean and atmosphere are identified and attribute them to possible effects of coupling between two media.

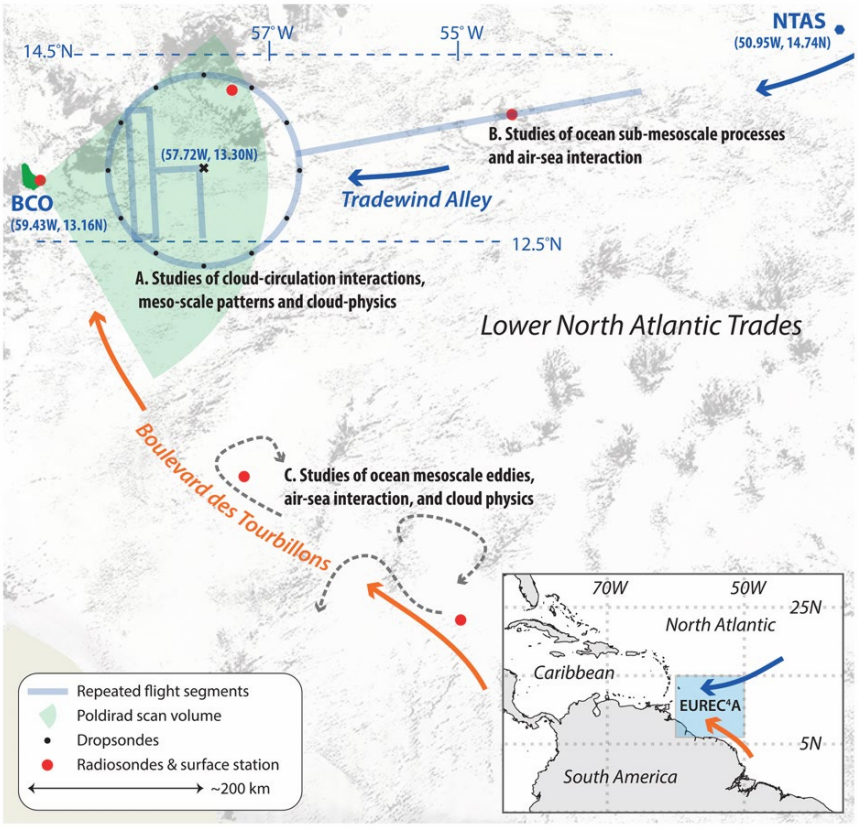

Fig. 1: EUREC4A study area: (A) The "EUREC4A-Circle" defines the airborne sounding array. (B) Tradewind Alley - band following the direction of the trades between the Northwest Tropical Atlantic Station (NTAS) and BCO. (C) Area under the impact of propagating NBC rings (also called Boulevard des Tourbillons). The background shows a negative of the cloud field taken from the 5 February 2020 MODIS-Terra (ca. 14:30 UTC) overpass.

IMPACT OF FRESHWATER FILAMENTS

In the Eddy boulevard region (C in Figure 1) we designed our observations as such that they surveyed through freshwater filaments that frequently occur here. One study (Reverdin et al. 2021) documented how freshwater from the Amazon reaches the open ocean up to 12°N in the northwest tropical Atlantic in January to March. The classical view is that the water is channeled along the shelf to the Caribbean Sea. However, making use of the Maria S. Merian MSM89 and the accompanying cruise by N/O l'Atalante in combination with satellite observations we could document the temporal evolution of a freshwater plume. This plume separated from the shelf near 55°W north off French Guiana on February 2–5, 2021. This fresher water was stirred by a NBC rings up to 12°N before mostly spreading westward. The near-surface water was initially very stratified at least until 10-m from the surface. More than 14 days later and 400 km farther north, salinity as low as 33.3 with mixing depths on the order of only 20-m was still encountered. The total area of the freshwater plume reached 100,000 km^2 with a flow

of freshwater on the order of 0.15 Sv (10^6 m^3s^{-1}) during 10 days. This phenomenon seems to be triggered by changes in the wind direction on the shelf closer to the equator, and has also been observed in satellite products in 7 out of 10 years since 2010.

We further investigated for the region the processes driving the variability of air-sea CO_2 fluxes at different scales (Olivier et al. 2021). In-situ surface fugacity of CO_2 (fCO2), salinity and temperature combined with maps of satellite salinity, chlorophyll-a and temperature highlight contrasting properties in the region. Using the various data available, a local reconstruction of the Air-sea CO_2 flux was estimated also showing the deviation with global reconstructions (Figure 2). In February 2020, the area is a CO_2 sink (-1.7 $TgC.month^{-1}$), previously underestimated by a factor 10 (Figure 2, right). The NBC rings transport saline and high fCO2 water indicative of their equatorial origins and are a small source of CO_2 at regional scale. Their main impact on the variability of biogeochemical parameters is through the filaments they entrain into the open ocean (see Reverdin et al. 2021 above). During the campaign, a nutrient rich freshwater plume from the Amazon River was entrained from the shelf up to 12°N and caused a phytoplankton bloom leading to a significant carbon drawdown (~20 % of the total sink). On the other hand, saltier filaments of shelf water rich in detrital material act as strong local sources of CO_2. Spatial distribution of fCO2 is therefore strongly influenced by ocean dynamics south of 12°N. The less variable North Atlantic subtropical water extends from Barbados northward. They represent ~60 % of the total sink due to their lower temperature associated with winter cooling and the strong winds.

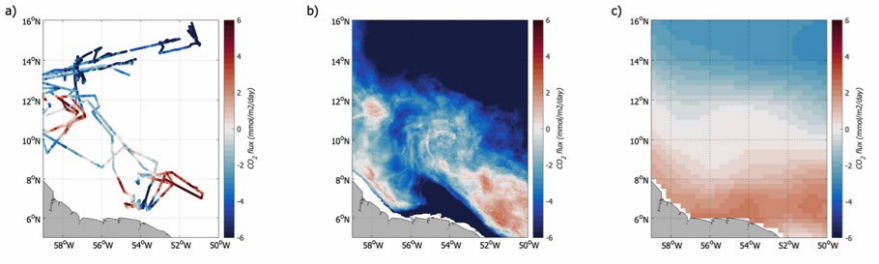

Fig. 2: a) Air-sea CO_2 flux measured in Jan-Feb 2020 during the EUREC4A-OA/ATOMIC cruise. b) Air-sea CO_2 flux reconstructed over February 2020. c) February climatology of the air-sea CO_2 flux over 1998-2015.

DIURNAL CYCLE

The diurnal cycle (DC) is considered a most fundamental mode of variability in the tropics. The DC can be experienced in the ocean as well as in the atmosphere and detecting the DC in the various data sets and understanding linkages in DC between ocean and atmosphere is a major science objective for EUREC4A-OA. One interest is the momentum flux between ocean and atmosphere. In a first study by Lösel (2021) looked at the impact of surface water velocities on air sea exchange in momentum and heat fluxes using the COARE3.6 algorithms. The study showed that on average the current

feedback (CFB) during the cruise generated more frequent higher than lower heat and momentum fluxes. Regions with maximum surface currents where connected to the occurrence of NBC rings and here the CFB increased the heat fluxes by up to 8 % and the momentum flux by 18 %. However, the study also showed the importance of obtaining measurement of the real surface currents (e. g. by X-Band radar) because the often-used Acoustic Doppler Current Profiler typically start resolving currents at depth greater 15m and where already substantial shear may occur relative to the surface.

This shear was further investigated and linked to a DC (Figure 3). For this purpose, the surface and 15m depth currents were rotated by 45° to account for the theoretical momentum flux response of the ocean (Ekman theory). It could be shown that the along-flow shear clearly has a DC (Figure 3, left), while the across-flow shear has not (Figure 3, middle). Likewise, the wind speed has a DC that is in phase with the sea-surface temperature (SST; Figure 3, right). This link between along flow shear and SST is interpreted as a diurnal warming signal and confirmed by observations of the vertical stratification. Furthermore, the diurnal warming may create a very shallow mixed layer which in turn supports a momentum trapping that in turn explains the diurnal cycle in along-flow shear – and this, despite the fact that the momentum input (wind speed) is lower when the trapping is most intense.

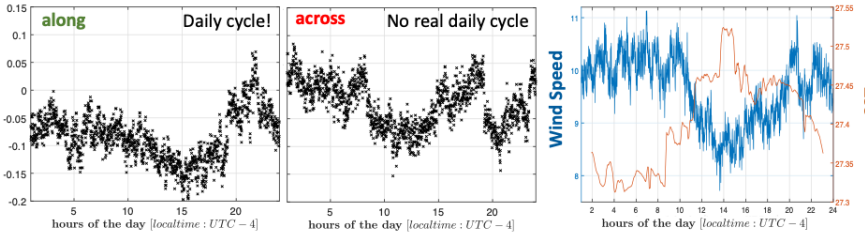

Fig. 3: Shear between surface and 15 m depth current: left) for the along-flow component and the middle) across-flow component. Right) DC for wind speed and SST. Note, only data with surface current from X-Band radar was considered.

REFERENCE

Stevens, B., et al., EUREC4A, Earth Syst. Sci. Data, 2021, 13, 4067–4119, https://doi.org/10.5194/essd-13-4067-2021.

Stephan, C. C., et al. Ship- and island-based atmospheric soundings from the 2020 EUREC4A field campaign, Earth Syst. Sci. Data, 2021, 13, 491–514, https://doi.org/10.5194/essd-13-491-2021.

Bosser, P., Bock, O., Flamant, C., Bony, S., and Speich, S., Integrated water vapour content retrievals from ship-borne GNSS receivers during EUREC4A, Earth Syst. Sci. Data 2021, 13, 1499–1517, https://doi.org/10.5194/essd-13-1499-2021.

L'Hegaret. P., et al. (in preparation) A coherent and quality controlled ocean data set from the EUREC4A field experiment, in preparation for Earth Syst. Sci. Data

Reverdin, G., Olivier, L., Foltz, G. R., Speich, S., Karstensen, J., Horstmann, J., et al. Formation and evolution of a freshwater plume in the northwestern tropical Atlantic in February 2020. Journal of Geophysical Research: Oceans 2021, 126, e2020JC016981. https://doi.org/10.1029/2020JC016981

Olivier, L. et al. Impact of North Brazil Current rings on air-sea CO_2 flux variability in winter 2020, submitted to Biogeosciences 2021.

Rudloff, D., Observations of Vertical Propagation of Near Inertial Waves in a Complex Vorticity Field, MSc thesis, CAU University Kiel, 52pp., 2021

Lösel, C., The Impact of varying Surface Conditions on Air/Sea Heat and Momentum Fluxes during the MSM89 Cruise, Bachelor thesis, CAU University Kiel, 44pp., 2021

POS530

First scientific survey of munition dump sites in the German Baltic Sea (2018) during MineMoni I

AUTHORS

GEOMAR Helmholtz Centre for Ocean Research Kiel | Kiel, Germany
J. Greinert, M. Kampmeier, A. Beck, E. Achterberg

Institute of Toxicology and Pharmacology for Natural Scientists, University Medical School Schleswig-Holstein | Kiel, Germany
E. Maser, J. Strehse

MOTIVATION

During and after WW-II large amounts of munition have been deployed and dumped into the seas around Europe. According to historic research 300.000 tons of conventional munitions and 5.000 tons of chemical weapons have been deposited in the German waters of the Baltic Sea. In contrast, the North Sea contains around 1.300.000 tons of conventional and 9.000 tons of chemical munition (Böttcher, 2011). Besides unexploded ordnance from combat and bombing, all kind of munitions from onshore munition depots have been dumped in nearshore areas along the coastline. In addition to shipping the munition to official dump sites, it was common practice to commence with throwing munition over board along the way to the designated areas (Böttcher 2011). This and the dislocation of ordnance by fishing activities and currents, create substantial uncertainty about the exact location and extent of undersea conventional munitions even where relatively good records of disposal exist. This makes it difficult to predict locations with increased risk of biological exposure to toxic munition-associated chemicals.

Cruise MineMoni I with RV POSEIDON (POS530; 1st to 21st October 2018) took place within the framework of the BMBF – funded UDEMM project (Environmental monitoring for the delaboration of munition in the sea). There were two overarching goals in this cruise: One was to test and verify the best practices developed in the UDEMM project during a large-scale Baltic sampling and mapping cruise (→ blueprint for coming monitoring cruises). The second is to acquire the first scientifically acquired baseline data set of the contamination by munition contaminants (incl. TNT and other TNT metabolites) in the vicinity of some of the munition dump sites in the Baltic Sea. Three main sites were chosen based on historic reconstruction work prior to the survey. The transits to and in between those sites were planned along former constraint routes during WWII. These routes were main target of the British Air Force and mines and bombs can be expected along these ways. During transits water samples were taken with CTD-rosette-mounted Niskin bottles in regular distances in order to get a dense cluster of TNT measurements

across the German Baltic Sea. First action inside the dedicated research areas always was high-resolution hydroacoustic multibeam mapping. Based on the on-board processed bathymetric maps, stations for the following sampling and observation program were planned. This included additional water sampling, the deployment of mussel bags for biomonitoring with divers, AUV surveys for visual inspections using the GIRONA 500 system, Subbottom Profiler and ADCP surveys, underwater video transects and sediment sampling. By using these methods the areas were surveyed and analyzed in terms of their munition content and distribution (as objects on the seafloor, but also as dissolved compounds within the water column), their sedimentary composition (subseafloor and surficial sediments) and their water current regime.

Cruise POS530 proofed to be indeed a very good blueprint for a monitoring layout and thus was adopted for the two-following cruise MineMoni II and III with RV ALKOR (AL548 in 2020 and AL567 in 2021). Results shown here are almost exclusively from POS530 and do NOT represent the current state of knowledge anymore.

RESULTS
ACOUSTIC SEAFLOOR MAPPING

Most of the working areas have not been mapped in high resolution before and only single findings or information in historic documents existed prior the cruise. AS RV POSEIDON did not have a shallow water multibeam available, we installed an a RESON T50 system in the moonpool and accepted the additional work to very accurately calibrate the system with its RTK stabilized position information. The knowledge gain we derived from this procedure is nowadays the base for similar installations on RV ALKOR and LITTORINA. The exemplarily shown maps in Figure 1, give an indication of how munition objects look like on the seafloor and show the continuously growing mapped area in Lübeck Bay.

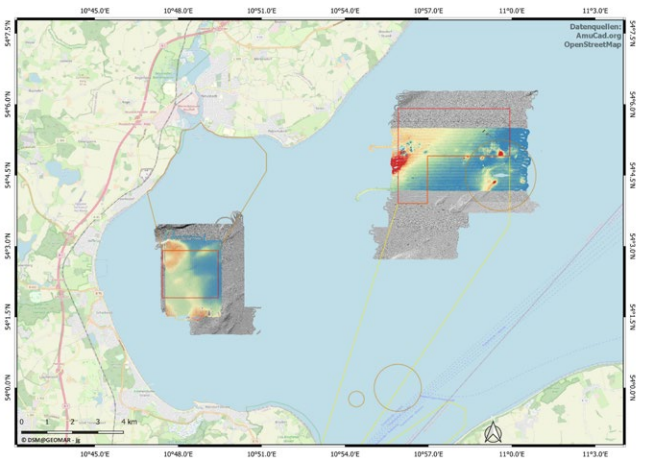

Fig. 1a: Lübeck Bay with bathymetric data acquired during POS530 (color) and data recorded in 2020 and 2021

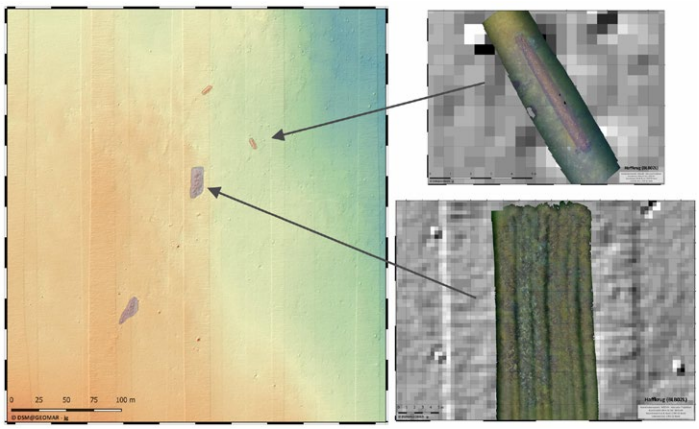

Fig. 1b: Examples of a torpedo and munition box pile in working area Haffkrug in Lübeck Bay. The imagery was taken with the AUV

Manual annotation, using ground truth knowledge from visual investigations shows that in the Pelzerhaken area (east; 10.3 km^2) more than 1,690 single objects and more than 127 areas of piles of munition boxes and bombs could be identified. The total munition covered area is 34,955m2 (~ 5 football fields). Munition has been found outside the dedicated dump areas. In Haffkrug (west; 4.1km^2) less munition was found, here 24 torpedoes, 171 other single objects and 28 munition piles were detected and many of them visually inspected. Haffkrug was the second dedicated dump area in Lübeck Bay and thus the amount of munition is less. However, significant amounts lie outside the dedicated and in nautical charts indicated munition dump area.

MUNITION COMPOUND MAPPING

For the first time a dedicated and wide spread water sampling was undertaken. Onshore lab-based analyses revealed a wide spread occurrence of munition compounds, not one sample was analyzed where the concentrations of all potential compounds where below the quantification limit. This for the first time showed the real scale of the chemical contamination. Spatial coverage of water sampling was particularly high-resolution at known munitions contamination sites (e. g., Fehmarn Sound, Lübeck Bight), which had not been previously investigated during the UDEMM project. During POS530, 114 CTD stations were run and 552 individual water samples were taken. The preliminary spatial distribution of TNT is shown in Figure 2. TNT concentrations were highest near the shore, especially in Kiel Bay and Fehmarn Sound, although some high concentrations were also found near Gelting Bight and Lübeck Bight. Increased values corresponded to generally known ammunition contamination, although some sites, such as the Fehmarn Belt, have a higher water flow and may reflect transport from other sites. The lowest concentrations were found off Rostock and in the Arkona Basin.

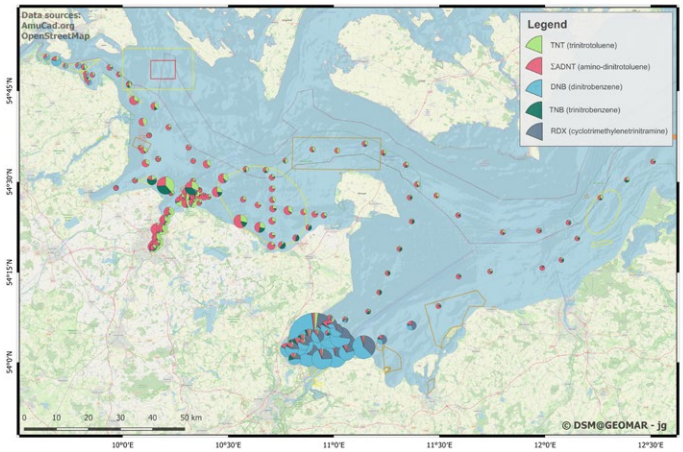

Fig. 2: Map showing different munition compounds in POS530 samples.

Depending on the water depth, vertical profiles included between three and nine depths. The vertical distribution of munition compounds generally showed the highest concentrations near the seabed (Figure 6). Significant spatial differences were observed between the different munition compounds analyzed. The munition compounds shown in Figure 24 were all derived from primary explosives (TNT = trinitrotoluene, RDX = 1,3,5-Trinitro-1,3,5-triazinane, DNB = dinitrobenzene, TNB = trinitrobenzene), but not all of these compounds showed enrichment at the same sites. For example, TNT and TNB concentrations were highest in Kolberger Heide, while RDX and DNB were highest in Lübeck Bight. Relatively high DNB concentrations were also found in Gelting Bight.

POS531

Benthic-pelagic coupling in sandy sediment regions and its interactions with the biological carbon in the open ocean

AUTHORS

MARUM – Center for Marine Environmental Sciences, University of Bremen | Bremen, Germany
M. H. Iversen, S. Swoboda, H. Marchant, S. Ahmerkamp, J.-H. Hehemann, H. Buck-Wiese, F. M. Jaladdin

Alfred Wegener Institute for Polar and Marine Research | Bremerhaven, Germany
M. H. Iversen

Max Planck Institute for Marine Microbiology | Bremen, Germany
H. Marchant, S. Ahmerkamp, J.-H. Hehemann, H. Buck-Wiese, F. M. Jaladdin

Institute for Chemistry and Biology of the Marine Environment | Oldenburg, Germany
K. Schwalfenberg

Leibniz Centre for Tropical Marine Research | Bremen, Germany
A. Chennu

OFF-SHORE ADVECTION OF SHELF-PRODUCED ORGANIC MATTER

The transfer of organic matter from the surface ocean to the ocean floor is a key regulator of atmospheric CO_2, the exclusive food source for life in vast areas in the deep sea, and the main pathway for the long-term storage of carbon in the sediments (Volk and Hoffert, 1985). However, the mechanisms of (trans)formation, translocation, degradation and preservation of organic matter and (bio)minerals within the water column and at the seafloor are hardly understood. Algal blooms form dissolved and particulate organic matter, which together with (bio)minerals aggregate into settling particles that shuttle carbon and other elements into the deeper ocean (Ploug et al., 2008a, 2008b, Iversen and Robert, 2015). Along its vertical path, this flux is rapidly attenuated by microbial activity, making the oceans a "gigantic heterotrophic digester" that is directly tied to atmospheric carbon dioxide levels (Hedges, 1992, van der Jagt et al., 2018). Our understanding of chemical transformation processes and the origin and age of settling particles is insufficient due to the inherent chemical complexity of organic matter in the ocean and the poorly constrained transport mechanisms of organic matter and (bio)

minerals through the water column and at the sea floor (Iversen et al., 2010). The magnitude of export depends on how the particle flux is transformed as it falls. To understand the functioning of the ocean's biology and chemistry, we need to understand what controls both the horizontal and vertical transport of material through the water column.

Often there is little correlation between organic matter production in the surface ocean and export at depth due to large lateral movement of the settling material (Karakas et al., 2006, Iversen et al., 2010). This decoupling depends on the particle characteristics (e. g., size and shape, (bio)mineral content, density and composition of an aggregate) (Iversen and Ploug, 2010). However, while residing for days to months close to the surface layer, particles are prone to transport, resulting in integration of different temporal and spatial scales into one sinking particle. As a result, seasonally variable current regimes may lead to biases in the temporal and spatial integration represented by a particle collected at a specific depth. Before we understand mechanisms leading to delayed export and lateral transport, it is difficult to predict the origin of particles collected at depth. Identifying the trajectories and origins of individual falling particles will elucidate specific transformation and turnover processes of organic matter through the water column.

Lateral transport processes from ocean margins to offshore regions can cause substantial decoupling of surface water productivity and material reaching the open ocean seafloor (Karakas et al., 2009, Iversen et al., 2010). However, conventional deep ocean sediment traps and benthic lander measurements average all settling particles and do not differentiate between particles transported vertically and horizontally. It is therefore difficult to predict the relative contribution of 'fresh' organic material arriving from vertical fluxes of fast-settling particle versus the 'older' organic matter within slowly-sinking particles transported laterally over long distances. Lateral transport from the shelfs to the open ocean are especially pronounced in Eastern Boundary Upwelling Ecosystems (EBUEs) where upwelling is driven by alongshore winds, leading to offshore advection of surface water, which is replaced by colder and nutrient-rich subsurface waters. The EBUEs are characterized by the occurrence of large filaments with high chlorophyll concentrations that can be transported as far as 450 km offshore (Fischer et al., 2009). The filaments off Cape Blanc (NW Africa) are the largest among the EBUEs and are known as ('giant Cape Blanc filament', Van Camp et al., 1991).

Several studies have investigated the processes driving lateral advection of surface production in EBUS and the consequential role for carbon displacement and export via the biological pump (Helmke et al. 2005, Amos et al. 2019, Chabert et al. 2020, Bonino et al. 2021, Lovecchio et al. 2017, Santana-Falcón et al. 2020, Frischknecht et al. 2018). However, despite being a constant feature of EBUS, the role of particle clouds on the carbon export in these areas has rarely been addressed, and a comprehensive assessment of their contribution is lacking to date (Freudenthal et al. 2001, Fischer et al. 2009).

The data collected during RV Poseidon cruise POS531, provided data that has helped us to understand the impact from horizontal advection on deep ocean carbon export. We have combined this data with a 23 years long time-series of deep ocean carbon fluxes off Cape Blanc, Mauritania. This allowed us to assess the inter-annual and inter-seasonal contribution from off-shore advection of shelf-produced organic matter to deep ocean carbon export. Our results suggest that off-shore advection from the shallow shelf can contribute with up to 60 % of the organic carbon exported to the deep ocean in the Cape Blanc upwelling region (Figure 1). These results strongly suggest that we need to reassess the export mechanisms in upwelling regions.

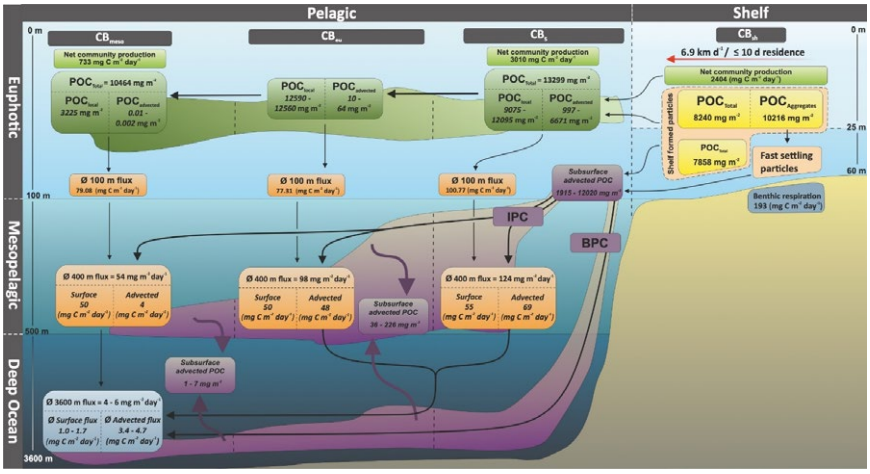

Fig. 1: Schematic of particle sources and sinks at the upwelling region off Cape Blanc. Excess production is laterally transported from the shallow shelf to the open ocean as surface or subsurface advected particulate organic carbon (POC). Surface advected POC forms a surface filament at the shelf break, while subsurface advected POC forms the intermediate and benthic nepheloid layers at ~<500 m and ~3500 m, respectively. Italic font indicates calculated values while regular fonts indicate measured values. POC_{total} represents the POC standing stock in the water column. Deep ocean carbon fluxes are collected by the Cape Blanc long-term sediment trap time-series (see Fischer et al. 2015), while the shallow data (<400 m) were collected as part of the process studies that were carried out during the POS531 expedition.

REFERENCES

Amos CM, Castelao R M, Medeiros PM, Offshore transport of particulate organic carbon in the California Current System by mesoscale eddies, Nature Communications 2019, 10(1), 1–8, doi:10.1038/s41467-019-12783-5.

Bonino G, Lovecchio E, Gruber N, Münnich M, Masina S, Lovino D, Drivers and impact of the seasonal variability of the organic carbon offshore transport in the Canary Upwelling System, Biogeosciences Discussions 2020, 1–30, doi:10.5194/bg-2020-470.

Chabert P, d'Ovidio F, Echevin V, Stukel MR, Ohman MD, Cross-Shore Flow and Implications for Carbon Export in the California Current Ecosystem: A Lagrangian Analysis. Journal of Geophysical Research: Oceans 2021, 126(2), 1–14, doi:10.1029/2020JC016611.

Fischer G, Reuter C, Karakas G, Nowald N, Wefer G, Offshore advection of particles within the Cape Blanc filament, Mauritania: results from observational and modelling studie, Progress in Oceanography 2009, 83, 322–330.

Fischer G, Romero O, Merkel U, Donner B, Iversen MH, Nowald N, Ratmeyer V, Ruhland G, Klann M, Wefer G, Deep ocean mass fluxes in the coastal upwelling off Mauritania from 1988 to 2012: Variability on seasonal to decadal timescales, Biogeosciences Discussions 2015, 12(21), 17643–17692, doi:10.5194/bgd-12-17643-2015

Freudenthal T, Neuer S, Meggers H, Davenport R, Wefer G, Influence of lateral particle advection and organic matter degradation on sediment accumulation and stable nitrogen isotope ratios along a productivity gradient in the Canary Islands region, Marine Geology 2001, 177, 93±109.

Frischknecht M, Münnich M, Gruber N, Origin, Transformation, and Fate: The Three-Dimensional Biological Pump in the California Current System, Journal of Geophysical Research: Oceans 2018, 123(11), 7939–7962, doi:10.1029/2018JC013934.

Hedges JI, Global biogeochemical cycles: Progress and problems. Mar. Chem. 1992, 39, 67–93.

Helmke P, Romero O, Fischer G, Northwest African upwelling and its effect on offshore organic carbon export to the deep sea, Global Biogeochemical Cycles 2005, 19(4), 1–16, doi:10.1029/2004GB002265.

Iversen MH, Nowald N, Ploug H, Jackson GA, Fischer G, High resolution profiles of vertical particulate organic matter export off Cape Blanc, Mauritania: degradation processes and ballasting effects, Deep Sea Research I 2009, doi:10.1016/j.dsr.2010.03.007.

Iversen MH, Ploug H, Ballast minerals and the sinking carbon flux in the ocean: carbon-specific respiration rates and sinking velocities of marine snow aggregates, Biogeosciences 2010, 7, 2613–2624.

Iversen MH, Robert ML, Ballasting effect of smectite on aggregate formation and export from a natural plankton community, Marine Chemistry 2015, 175, 18–27.

Karakas G, Nowald N, Blaas M, Marchesiello P, Frickenhaus S, Schlitzer R, High-resolution modeling of sediment erosion and particle transport across the northwest African shelf, Journal of Geophysical Research 2006, 111, doi:10.1029/2005JC003296.

Karakas G, Nowald N, Schäfer-Neth C, Iversen MH, Barkmann W, Fischer G, Marchesiello P, Schlitzer R, Impact of particle aggregation on vertical fluxes of organic matter, Prog. Oceanogr. 2009, 83, 331–341.

Lovecchio E, Gruber N, Münnich M, Lachkar Z, On the long-range offshore transport of organic carbon from the Canary Upwelling System to the open North Atlantic, Biogeosciences 2017, 14(13), 3337–3369, doi:10.5194/bg-14-3337-2017.

Ploug H, Iversen MH, Fischer G, Ballast, sinking velocity, and apparent diffusivity within marine snow and fecal pellets: Implications for substrate turnover by attached bacteria, Limnology and Oceanography 2008a, 53 (5), 1878–1886.

Ploug H, Iversen MH, Koski M, Buitenhuis ET, Production, oxygen respiration rates, and sinking velocity of copepod fecal pellets: Direct measurements of ballasting by opal and calcite, Limnol. Oceanogr. 2008b, 53, 469–476.

Santana-Falcón Y, Mason E, Arístegui J, Offshore transport of organic carbon by upwelling filaments in the Canary Current System, Progress in Oceanography 2020, 186(March), 102322, doi:10.1016/j.pocean.2020.102322.

van der Jagt H, Friese C, Stuut JB, Fischer G, Iversen MH, The ballasting effect of Saharan dust deposition on aggregate dynamics and carbon export: Aggregation, settling, and scavenging potential of marine snow, Limnol. Oceanogr. 2018, doi: 10.1002/lno.10779.

Van Camp L, Nykjaer L, Mittelstadt E, Schlittenhardt P, Upwelling and boundary circulation off Northwest Africa as depicted by infrared and visible satellite observations, Progress in Oceanography 1991, 26. 357–402.

Volk T, Hoffert MI, Ocean carbon pumps: analysis of relative strengths and efficiencies in ocean-driven atmospheric CO_2 changes, in: Sundquist, E.T., Broecker, W.S. (Eds.), The Carbon Cycle and Atmospheric CO_2: Natural Variations Archean to Present 1985. AGU, Washington D.C., pp. 99–110.

POS532

Coastal deep-sea biodiversity, ecological interactions, carbon flux and oceanography of Cabo Verde

AUTHORS

GEOMAR Helmholtz Centre for Ocean Research Kiel | Kiel, Germany
H.J. Hoving, K. Hissmann , V. Merten, S. Scheer, A.C. Hans, H. Hauss

Atlantic Technical University | Mindelo, Republic of Cabo Verde
R. Freitas

Smithsonian Institute | Washington D.C., USA
K. Osborn

During cruise POS532, which took place in February 2019 off Cabo Verde, we proposed to test the hypothesis that large gelatinous macrozooplankton and cephalopods (e. g. tunicates, hydrozoans) 1. have a relatively high diversity and 2. provide a significant carbon source and carbon vector from midwater to the ocean floor in Cape Verde. To test this hypothesis, we studied 1) the distribution, diversity and abundance of gelatinous organisms and cephalopods in the epi-, meso, and bathypelagic zone, 2) the role of gelatinous taxa in transporting carbon through the pelagic foodweb to the seafloor and 3) their behavior and associations. We worked in the coastal deep sea off Santo Antão and Fogo, as well as in the open ocean at the time series station CVOO and a cyclonic eddy 355km southwest off the island Fogo. The island volcanoes combined with the steep island slopes allowed us to work in deep waters, close to shore, benefitting from the shelter that the high island topography provided. The manned submersible JAGO was used for mesopelagic surveys down to 400 m, to document the behaviour and associations of deep-sea organisms and to collect living specimens.

Fig. 1: RV Poseidon and the deployment of submersible JAGO off Fogo (Photo Jens. Klimmeck)

In total, we performed 17 dives exploring the water column and seafloor for more than 45 hours. With JAGO we were able to capture the first specimens of the polychaete *Poeobius*, allowing a new species description (Osborn et al. in prep.). Submersible dives also documented new records of benthic fish, crustaceans and a cephalopod. Additionally, multinet tows and JAGO enabled the capture and description of a new species of *Paraphronima* amphipod (Stenvers et al. 2021a), while additional hyperiid amphipods collected were used to complete a study of unusual brain evolution (Lin et al. 2021). With JAGO we observed the first reefs of the giant oyster in Cabo Verde waters, and collected a new species of benthic gastropod (*Tritonia hirondelle*) which is now described and published. Overall, 542 individual organisms were preserved for genetic analysis (COI) and are being prepared for cataloguing in museum collections, and 3054 scientific photographs of specimens were collected.

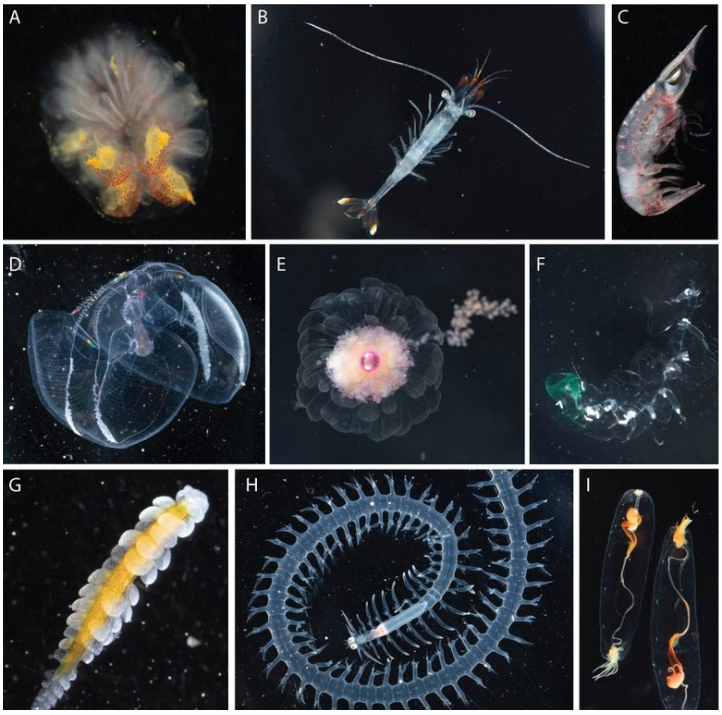

Fig. 2: Exemplar animals collected. A. A pyrosome (Chordata, Tunicata), *Pyrosoma atlanticum*. B. An unknown shrimp (Crustacea, Decapoda) repeatedly found associated with *P. atlanticum*. C. A hyperiid amphipod (Crustacea) *Leptocotis*. D. A lobate ctenophore, *Ocyropsis*. Two siphonophores (Cnidaria, Hydrozoa) *E. Athorybia* and *F. Lilyopsis*. Three polychaete worms (Annelida) G. Typhloscolidae, H. Alciopidae, and I. a male and female specimens of a new species of *Poeobius*. (Hoving et al 2019)

Our insights into the vertical zonation of the benthic habitat and community obtained from submersible dives and bottom video transects with the Ocean Floor Observation System represent among the first information of this kind on the deepwater fauna around

the Cabo Verde islands. We performed pelagic video transects down to 3000 m, in combination with net sampling in the upper 1000m. Environmental DNA (eDNA) metabarcoding on 168 seawater samples (from between 50 and 2500 m), using an 18S rRNA universal cephalopod primer pair, and a species-specific primer pair for Taningia danae resulted in the detection 32 taxa. This sampling contributed to a complete list of Cabo Verde cephalopods, and allowed us to conclude that Cabo Verde is a biodiversity hotspot in the Atlantic Ocean. This data also contributed to test the hypothesis that Cabo Verde is biogeographically isolated from other Macaronesian islands. Finally, it enabled prediction of which taxa may contribute to the biological carbon pump in Cabo Verde waters (Merten et al. submitted).

Fig. 3: The benthic octopus *Pteroctopus tetracirrhus* and the pelagic octopus *Vitreledonella* as observed by submersible JAGO off Cabo Verde

The sample and video analyses are finalized and allowed the documentation and quantification of the ecological and biogeochemical role of *Pyrosoma atlanticum* in the pelagic and benthic deep-sea ecosystem of Cabo Verde. This pelagic tunicate is an upwelling-favored species largely absent from the oligotrophic open ocean, but present in large numbers in the leeward coastal waters of Cape Verde. We surveyed the wake eddy chain off Fogo with a focus on a productive cyclone that was already 355 km away from the islands, and contained an extremely high abundance of P. *atlanticum* (Stenvers et al. 2021b). The cyclone had a radius of 44 km and a mean propagation speed of 5.1 km d^{-1}. ADCP and CTD transects in combination with remote sensing further allowed a detailed reconstruction of the effect of the islands on currents and productivity. The derived quantities resemble those of island wakes lee of Hawaii and Gran Canaria (Hans 2019). Combining data from multinet, PELAGIOS video transects and submersible surveys, we quantified daily vertical migration which occurred between the surface and 400 m. The regional carbon deposited on the seafloor by pyrosome carcass deposition was 15.09 ± 17.89 (s. d.) mg C m^{-2}. Observations in the water column show that a range of taxa, including fish and crustaceans, use pyrosomes as substrate in midwater. On the seafloor pyrosomes are scavenged upon by molluscs and crustaceans (Stenvers et al. 2021b).

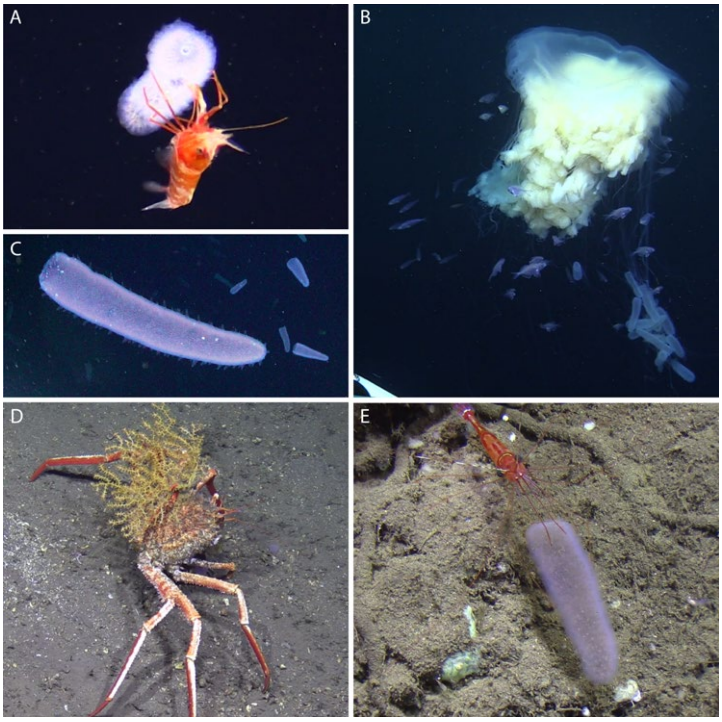

Fig. 4: Pelagic (A,B) and benthic (D,E) animals associated with P. atlanticum (C.) in the eastern tropical North Atlantic, observed in February 2018 and 2019. (A) Unidentified Oplophoridae sp. and (B) *Drymonema gorgo* feeding on pyrosomes. (C) *Pyrosoma atlanticum* (D) An unidentified decorator crab, (E) *Pandalopsis* sp. feeding on pyrosomes. (Stenvers et al 2021)

We also had several activities to communicate the work onboard to the general public, including photography, filming, drone filming and interviews. On board we produced an interview with participating scientists which was broadcasted on Cape Verdean national television while we were sailing. Scientist also gave seminars at the Ocean Science Centre Mindelo after the end of the cruise. The POS532 team wrote in total five contributions to the Oceanblogs, https://www.oceanblogs.org/capeverde/, and the cruise was also described in a publication „Von Wasserwirbeln und Feuerwalzen" for the GEOMAR News magazine issue 01/2019.

REFERENCES

Hans AC Island Wakes off Cape Verde BSc thesis 2019 Christian Albrecht University Kiel 36 pp.

Lin C, Hoving HJT, Cronin TW, Osborn KJ, Strange eyes, stranger brains: exceptional diversity of optic lobe organization in midwater crustacean. Proceedings of the Royal Society B. 2021 288, 2021216. doi.org/10.1098/rspb.2021.0216.

Merten V, Bayer T, Reusch TBH, Puebla O, et al. An integrative assessment combining net sampling, in situ observations and eDNA analysis identifies Cabo Verde as a cephalopod biodiversity hotspot in the Atlantic Ocean. In Revision Frontiers in Marine Science

Ortea J, Moro L, El FS Poseidon rinde homenaje al Hirondelle: descripción de una nueva especie de Tritonia Cuvier, 1798 (Mollusca: Nudibranchia) de las aguas profundas de las islas de Cabo Verde para celebrar las singladuras de un yate carismático. Avicennia 2020, 27: 29–34.

Stenvers VI, Gonzales BC, Goetz FE, Hemmi JM, Jessop A-L, Lin C, Hoving HJT, Osborn KJ, Extraordinary eyes reveal hidden diversity within a holopelagic genus Paraphronima (Amphipoda: Hyperiidae). Deep Sea Research Part I 2021 Volume 177, 103610

Stenvers V, Hauss H, Osborn K, Neitzel P, Merten V, Scheer St, Robison BH, Freitas R, Hoving HJT, Distribution, association and role in the biological carbon pump of Pyrosoma atlanticum (Tunicata, Thaliacea) off Cabo Verde, NE Atlantic:. Nature Scientific Reports 2021 11, 9231. https://doi.org/10.1038/s41598-021-88208-5

POS533

Natural and anthropogenic sources of marine trace gases in the oceanographic and biogeochemical regime of the Subtropical North East Atlantic | POS533-AIMAC – Atmosphere-Ocean-Islands-Biogeochemical interactions in the Macaronesian Archipelagos of Cabo Verde, the Canaries and Madeira

AUTHORS

GEOMAR Helmholtz Centre for Ocean Research Kiel | Kiel, Germany
M. Mehlmann, B. Quack, H. Hepach

Department of Atmospheric Sciences, RSMAS, University of Miami | Miami, USA
E. Atlas

Institute of Space and Atmospheric Studies, University of Saskatchewan | Saskatoon, Canada
S.Tegtmeier

The POSEIDON cruise POS533 – AIMAC (Atmosphere–ocean–island-biogeochemical interactions in the Macaronesian Archipelagos) investigated the influence of the Cape Verdes, the Canary Islands, and Madeira on the physics, chemistry and biology of the surrounding subtropical North- East Atlantic ocean. High oceanic and atmospheric concentrations of iodinated, brominated and chlorinated methanes from marine sources are often found near coastlines and their air – sea exchange impact tropospheric and stratospheric ozone depletion and therewith air quality and human health. The abundance of the organic bromine compounds bromoform ($CHBr_3$) and dibromomethane (CH_2Br_2) is generally related to a common marine source, which is not well characterized.

The tropical processes are of special importance for the changing chemistry and composition of the stratosphere. Stratospheric ozone is mainly created in the tropical lower stratosphere and transported upwards and towards the winter pole by large-scale atmospheric circulation. Most long-lived and short-lived trace gases in tropospheric air enter the stratosphere in the tropics and follow the same transport pathways.

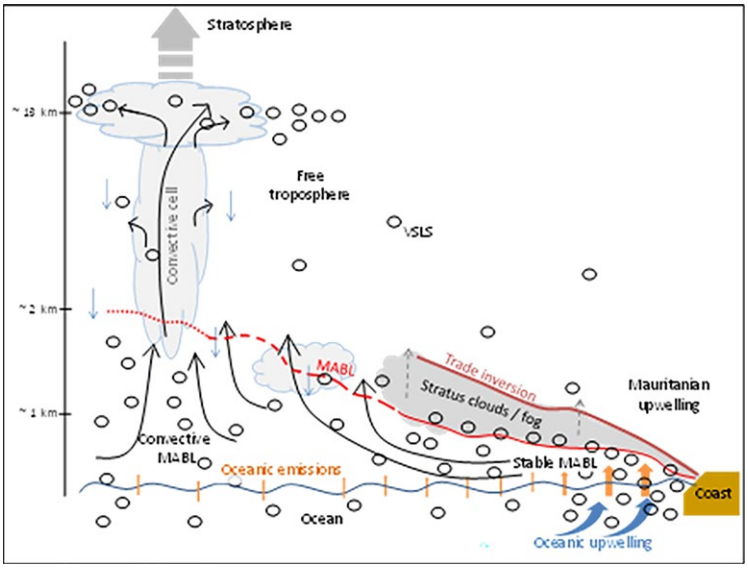

Fig. 1: Transport of air masses in the Marine Boundary layer (MABL) from the subtropics, enriched in very short-lived trace gases (VSLS) from the oceans, coasts and islands, towards lower latitudes under the trade inversion and uplift to the stratosphere in tropical deep convection. The organobromine gases from the locally increased fluxes are transported by the trade winds from their source regions in the extra tropics towards the equator, where deep convection can transport them to the stratosphere.

METHOD

The POS533 cruise started on 28th of February 2019 in Mindelo on Sao Vicente (Cape Verde), and crossed nearby the archipelagos islands Santo Antao, Sao Nicolau, Fogo, Santiago, Boavista and Sal. Five days of transit against the northeastern trade winds towards the Canaries was followed by a transect through the coastal waters of Hierro, La Gomera, Tenerife, and Gran Canary. After a stopover in Las Palmas (Gran Canary) the ship sailed northwards, carried out two transects leeward of Madeira, made a stop in Funchal, where the sampling ended and the cruise ended in Las Palmas on the 22nd of March 2019. *Underway air, water and depth profile sampling was conducted.*

TEMPERATURE, SALINITY, OXYGEN AND FLUORESCENCE IN THE WATER COLUMN

Distinctive differences of the mean seawater properties existed for three island groups. Surface temperatures were highest at Cape Verde (22–23 °C), followed by the Canaries (19.0 °C) and Madeira (18.0 °C) (Figure 2). In the ocean interior, the mean temperature profile for Cape Verde (red) was lowest and the Madeira (blue) mean interior temperature was highest. While Cape Verde mean temperature homogeneously decreased with depth, Canaries (green) and Madeira mean temperatures exhibited a change in temperature decrease at around 1000 m depth, where Mediterranean water (MW) is located.

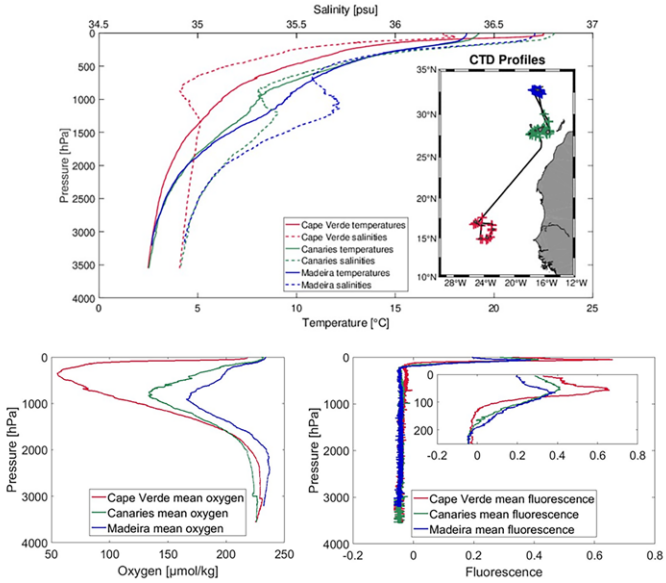

Fig. 2: Mean temperature, salinity, fluorescence, and oxygen profiles. Cape Verde CTD stations: red, Canary Islands CTD stations: green, Madeira CTD stations: blue. The Cape Verde mean salinity was lower (SACW) than salinity around the Canary Islands and Madeira (higher saline ENACW) in the upper 1000 m. The highest salinities were found in the Canary surface waters. The oxygen profiles during POS533 showed a decrease from the surface to around 400 m depth for Cape Verde, and a decrease to 900 m depth for the Canaries and Madeira. Cape Verde oxygen decreased down to under 60 µmol kg^{-1}, while the minima around the Canary Islands and Madeira reached 140 and 160 µmol kg^{-1}. Subsurface fluorescence (indicator of phytoplankton abundance) maxima were found in all three archipelagos. The highest fluorescence was found at Cape Verde at around 50 m depth. Canary Islands fluorescence maximum was at around 40 m depth and Madeira had a fluorescence maximum at around 60 m depth. Below 200–250 m fluorescence was zero for all profiles.

HALOCARBON SURFACE DISTRIBUTIONS

High CHBr3 was measured around the Canaries, where several samples exceeded 100.0 pmol L^{-1}. Similar high concentrations were found in the harbours of Mindelo with 241.5 pmol L^{-1} and Funchal 314.1 pmol L^{-1}, while the highest concentration during the cruise of 1480.0 pmol L^{-1} was measured in Las Palmas harbour. $CHBr_3$ reached 63.4 pmol L^{-1} at the south of Santiago and was elevated around 30 pmol L^{-1} between 22–24 °N during the first transit, between Cape Verde and the Canaries. Low $CHBr_3$ surface concentrations of < 10 pmol L^{-1} were found in all areas, except for the Canaries, while Madeira showed the lowest concentrations < 5 pmol L^{-1}.

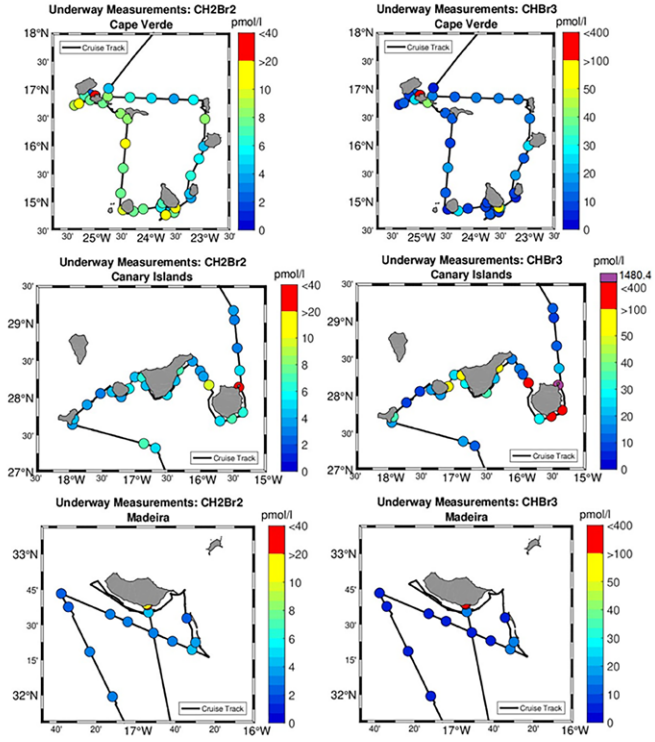

Fig. 3: CH_2Br_2 and $CHBr_3$ underway measurements along POS533 cruise track (black line). Top figures: Cape Verde samples, middle figures: Canary Islands samples, bottom figures: Madeira samples. Highest CH_2Br_2 concentrations at Cape Verde often exceeded 10.0 pmol L^{-1}, specifically around the western and southern islands. It was also high in the harbours with 36.5 pmol L^{-1} in Mindelo, 21.1 pmol L^{-1} in Funchal and 31 pmol L^{-1} in the Las Palmas harbour sample. Similar to $CHBr_3$, CH_2Br_2 was elevated with around 8.0 pmol L^{-1} between 22–24°N during the transit, and low concentrations of < 5 pmol L^{-1} were found in all regions, while the lowest concentrations were again detected in Madeira waters.

CONCLUSIONS

The oceanic halocarbon concentrations measured in coastal regions of Cape Verde, the Canaries and Madeira were much higher than found during previous studies in the region. These high concentrations were linked to both natural and anthropogenic causes. The cruise revealed that anthropogenic sources increased oceanic $CHBr_3$ emissions significantly close to some islands, especially at the Canaries, while heterotrophic processes in the ocean increased the flux of CH_2Br_2 from the sea to the atmosphere in the Cape Verde region.

Cape Verde was found to be an area of rich biological productivity that produces halocarbons in the surface and upper ocean. Upwelling favored biological production conditions, low oxic conditions and microorganisms in deeper waters of the thermocline likely convert $CHBr_3$ to CH_2Br_2. This conversion results in elevated CH_2Br_2 surface water concentrations and small ratios of $CHBr_3$ to CH_2Br_2 around Cape Verde. This region was

therefore a significant source of CH_2Br_2 to the atmosphere, which was reflected in high atmospheric CH_2Br_2 mixing ratios. Around the Canaries an anthropogenic influence on $CHBr_3$ was visible in unique high ratios of $CHBr_3$ to CH_2Br_2, which was likely caused from coastal anthropogenic disinfection processes used in power plants and desalination technologies. $CHBr_3$ concentrations of more than 1,400 pmol L^{-1} (Las Palmas harbor), several samples more than 100 pmol L^{-1} (Gran Canary coasts), and a $CHBr_3$ sea-air flux of on average 6,700 pmol m^{-2} h^{-1} indicated that industrial discharges likely influence the marine production in coastal waters and the atmosphere. Elevated halocarbon surface concentrations at Mindelo and Funchal harbours also displayed a visible anthropogenic signal leading to increased flux of the compound from the ocean to the atmosphere.

Wind speed positively influences the halocarbon sea-air flux to the atmosphere, which led to on average 4.5–6.6 fold higher halocarbon fluxes on the windward sites of the islands, where wind speeds were on average twice to three times higher as they were leeward of the island. In the windward sites of islands around the Canaries, the sea-air flux was largest, because strongly elevated surface concentrations, containing an anthropogenic signal, contribute to the flux in addition to the strong wind on these sites.

The cruise revealed that the major sources of both compounds for the atmosphere were spatially separated between the Macaronesian Archipelagos. $CHBr_3$ sea-air fluxes were dominated by anthropogenic sources, while heterotrophic processes in the ocean increased the CH_2Br_2 sea-air flux.

The data give new insights into important oceanographic and biogeochemical cycles in the Subtropical North Atlantic and how they are impacted by anthropogenic activities. As anthropogenic disinfection processes, which release marine derived $CHBr_3$ in coastal areas increase, and as more CH_2Br_2 may be produced from increased heterotrophy in a warming, deoxygenated ocean, both sources could supply higher fractions of stratospheric bromine in the future, with yet unknown consequences for stratospheric ozone.

REFERENCE

Mehlmann M, Quack B, Atlas E, Hepach H, Tegtmeier S, Natural and anthropogenic sources of bromoform and dibromomethane in the oceanographic and biogeochemical regime of the subtropical North East Atlantic, Environmental Science: Processes & Impacts 2020, 22(3): 679–707. https://doi.org/10.1039/C9EM00599D

POS534

Monitoring gas discharge from the seafloor in the North Sea

AUTHORS

GEOMAR – Helmholtz Centre for Ocean Research Kiel | Kiel, Germany
M. Schmidt, M. Haeckel, A. Dale, J. Gros, C. Böttner, S. Sommer, P. Linke, E. Achterberg, K. Wallmann

National Oceanography Centre | Southampton, United Kingdom
A. Flohr, D. Connelly

To test new offshore CO_2 leak-detection strategies and technology, a 2-vessel campaign was conducted in May 2019 with RV Poseidon (POS534) and RRS James Cook (JC180) in an area near the Goldeneye offshore platform located in the British EEZ, central North Sea (Fig. 1). The Goldeneye site was considered by the British Government and by Shell for storage of captured CO_2 into a depleted gas reservoir at about 2800 mbsf (Lower Cretaceous sandstone reservoir rock).

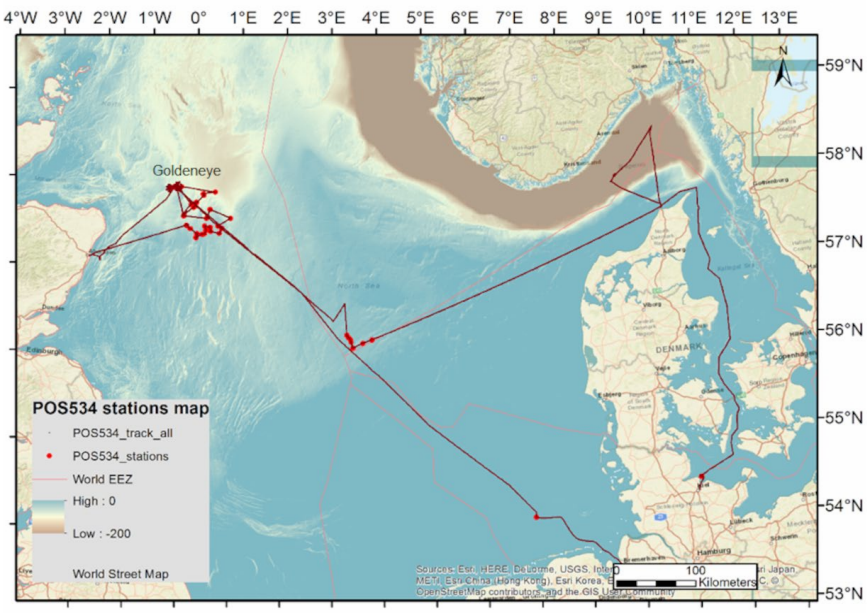

Fig. 1: Map of POS534 (Leg 1 and 2) cruise track and stations (red dots).

First a CO_2/tracer-release experiment was installed at the seafloor (~120 mbsl) from onboard RRS James Cook to mimic an unintended emission of CO_2 from a subsurface CO_2 storage site into the surface sediment (i. e. sandy mud, Witch Ground formation). A total of 675 kg of CO_2 were injected into the shallow sediments (~3 m below seafloor), at continuous flow rates between 6 and 143 kg per day for about 11 days. Then a combination of novel techniques, adapted versions of existing techniques, and well-proven standard techniques were used to detect, characterize and quantify gaseous and dissolved CO_2 in the sediments and the overlying seawater (Fig. 2).

The controlled release of CO_2 (+ tracers) into the surface sediment and consequently into the bottom water was monitored during POS534-Leg 1 by hydroacoustic water column imaging and an ADCP was used to constrain plume transport during the release experiment. The near- and far-field water chemistry was investigated by using towed equipment i. e. a Video-CTD water sampler rosette equipped with additional O_2, pH-, CO_2/CH_4-sensors. Water samples were collected during the release experiment from pumped water and from Niskin bottles of the rosette.

The POS534 Leg 2 cruise concentrated on sediment (0–6 m) sampling in the vicinity of the CO_2-release spot after the seafloor installations had been removed by RRS James Cook. Sediment cores recovered by Gravity corer and Multicorer were partly processed onboard and undisturbed sediment cores were stored for further land-based physical and biogeochemical investigations and experiments.

Moreover, as offshore wells are considered a weakening of the overburden above gas reservoirs the newly developed hydroacoustic and chemical monitoring techniques were also applied above selected abandoned well sites in the British EEZ during transit.

Main results from POS534 cruise were the background definition of porewater (e. g. DIC, TA, etc.) and sediment biogeochemistry (e. g. TOC<0.6 %), benthic nutrient fluxes, oxygen uptake (<6 mmol m^{-2} d^{-1}) and a sulfate-methane transition zone at about 20 mbsf in the prevailing sandy mud of the upper Witch Ground formation (Dale et al., 2021). Compared to background data the CO_2-release experiment increased porewater alkalinity and major and trace element composition (e. g. Si, Ca, Mg, Fe, Mn) due to silicate and carbonate dissolution and a temperature increase of up to 5°C from exothermal bubble dissolution reaction (Lichtschlag et al., 2021; De Beer et al., 2021).

The release of CO_2 bubbles into the bottom water was monitored by active and passive hydroacoustic surveying, ROV sampling and AUV imaging, and various sensors deployed near the bubble strings (Flohr et al., 2021). However, as CO_2 bubbles are completely dissolved at about 4–5 m above seafloor they are hard to detect or quantified during surveying. Thus, a multi-purpose Video-CTD was applied to monitor the much bigger dissolved CO_2 plume moving in the near field above the release site (Gros et al., 2021). The detected dissolved pCO_2 concentration anomalies and the water chemistry

(Martinez-Cabanas et al., 2021) were combined with water current data measured by ADCP and physical parameters of the water column (Esposito et al., 2021), finally to be used in a bent plume model (TAMOC) to quantify the CO_2 release (Fig. 3; Gros et al., 2021). The simulated plume distribution and CO_2 release rate fit the measured data very well and indicated that about 35 % of the injected CO_2 was retained by the sediment during the highest injection rate scenario of 143 kg per day.

Parallel to ROV and AUV operations from RRS James Cook at the release site RV Poseidon operated far away from the site during daytime to further investigate abandoned oil and gas wells for gas leakage. The hydroacoustic surveys of selected abandoned wells were conducted with a newly developed Kongsberg Echosounder/ADCP device (ES70/EC150). The target selection was based on existing industry 3D seismic data, which covered about 1800 abandoned wells in a 22000 km² large region of the British EEZ. Gas leakage was detected at 28 out of 43 surveyed well heads and leakage probabilities within the 3D data set were calculated for abandoned wells considering distance to subsurface shallow gas accumulations which could have been penetrated during drilling (Fig. 4; Böttner et al., 2020). Combining the leakage analysis with published methane release rates of abandoned wells in the Norwegian EEZ (Vielstädte et al., 2015) methane emission rates of 0.7–4.2 kt CH_4 per year were estimated for the ~1800 wells in the study area. Overall, abandoned wells provide a major source for methane in the North Sea, of which about 40 % is estimated reaching the atmosphere (Vielstädte et al., 2017).

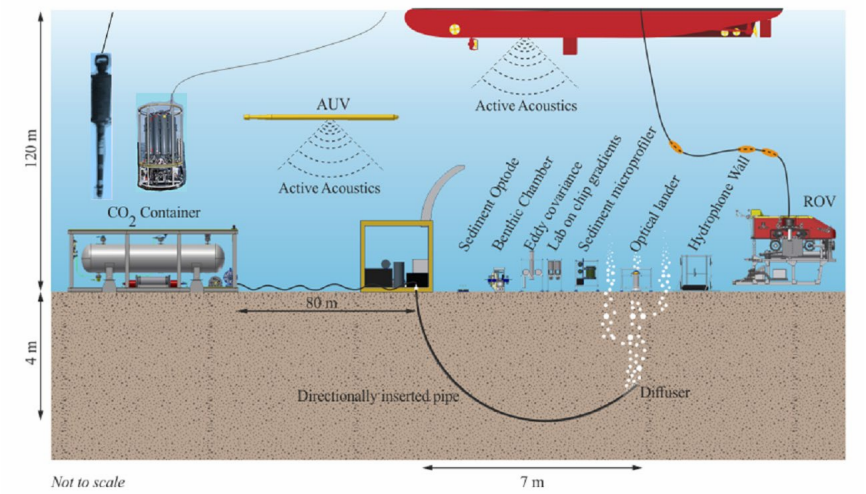

Fig. 2: Schematic overview of the CO_2 release experiment and a selection of deployed detection methods (modified after Flohr et al., 2021).

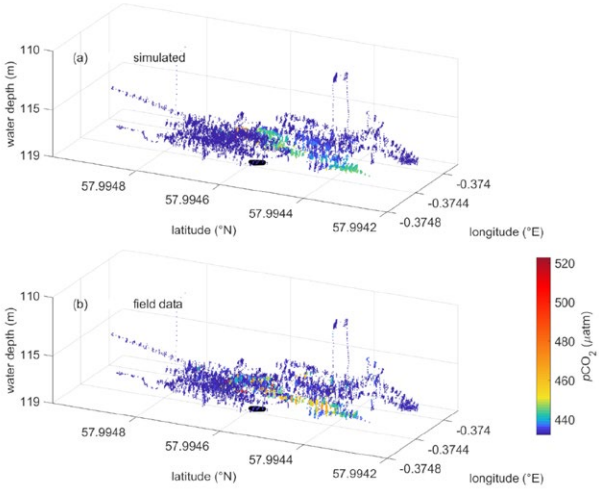

Fig. 3: Comparison of simulated (a) and measured (b) spatial distribution of pCO_2 in the water column during injection of 143 kg CO_2 per day into sediment at Goldeneye. The black shape indicates the bubble release site (Gros et al., 2021).

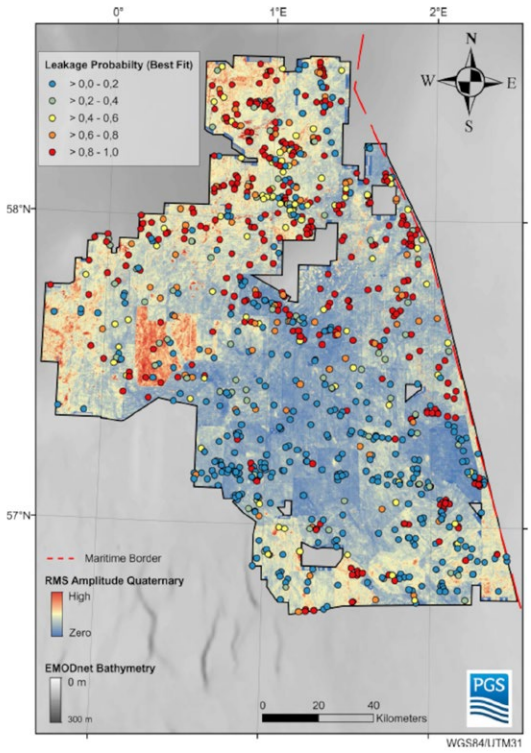

Fig. 4: Root Mean Square (RMS) amplitude map of shallow gas distribution in the subsurface of the study area in the British EEZ. Abandoned wells are marked by different colours (blue, zero – red, high) reflecting their probability for leakage (Böttner et al., 2020).

ACKNOWLEDGEMENT

The PO534 cruise has received funding from the European Union's Horizon 2020 research and innovation programme under grant agreement No. 654462 (Strategies for Environmental Monitoring of Marine Carbon Capture and Storage).

REFERENCES

Böttner C., Haeckel M., Schmidt M., Berndt C., Vielstädte L., Kutsch J.A., Karstens J., Weiß T., Greenhouse gas emissions from marine decommissioned hydrocarbon wells: leakage detection, monitoring and mitigation strategies, International Journal of Greenhouse Gas Control, 2020, 100, 103119. DOI 10.1016/j.ijggc.2020.103119.

de Beer D., Lichtschlag A., Flohr A., van Erk M.R., Ahmerkamp S., Holtappel M., Haeckel M., Strong J., Sediment acidification and temperature increase in an artificial CO_2 vent, International Journal of Greenhouse Gas Control, 2021, 105, 103244.

Esposito M., Martinez-Cabanas M., Connelly D.P., Jasinski, D., Linke P., Schmidt M., Achterberg, E.P., Water column baseline assessment for offshore Carbon Dioxide Capture and Storage (CCS) sites: Analysis of field data from the Goldeneye storage complex area. International Journal of Greenhouse Gas Control, 2021, 109, 103344. DOI 10.1016/j.ijggc.2021.103344.

Dale A.W., Sommer S., Lichtschlag A., Koopmans D., Haeckel M., Kossel E., Deusner C., Linke P., Scholten J., Wallmann K., van Erk M.R., Gros J., Scholz F., Schmidt, M., Defining a biogeochemical baseline for sediments at Carbon Capture and Storage (CCS) sites: An example from the North Sea (Goldeneye), International Journal of Greenhouse Gas Control, 2021, 106, 103265. DOI 10.1016/j.ijggc.2021.103265.

Flohr A., Schaap E., Achterberg E.P., et al., Towards improved monitoring of offshore carbon storage: A real-world field experiment detecting a controlled sub-seafloor CO_2 release, International Journal of Greenhouse Gas Control, 2021, 106, 103237. DOI 10.1016/j.ijggc.2020.103237.

Gros J., Schmidt M., Linke P., Dötsch S., Triest J., Martinez-Cabanas M., Esposito M., Dale A.W., Sommer S., Flohr A., Fone J., Bull J.M., Roche B., Strong J.A., Saw K., Brown R., Koopmans D., Wallmann K., Quantification of dissolved CO_2 plumes at the Goldeneye CO_2-release experiment, International Journal of Greenhouse Gas Control, 2021, 109, 103387. DOI 10.1016/j.ijggc.2021.103387.

Lichtschlag A., Haeckel M., Olierook D., Peel K., Flohr A., Pearce C.R., Marieni C., James R.H., Connelly D.P., Impact of CO_2 leakage from sub-seabed carbon dioxide storage on sediment and porewater geochemistry. Open Access International Journal of Greenhouse Gas Control, 2021, 109, 103352. DOI 10.1016/j.ijggc.2021.103352.

Martinez-Cabanas M., Esposito M., Gros J., Linke P., Schmidt M., Triest J. Achterberg, E.P., Deviations from environmental baseline: Detection of subsea CO_2 release in the water column from real-time measurements at a potential offshore Carbon Dioxide Storage site. International Journal of Greenhouse Gas Control, 2021, 109, 103369. DOI 10.1016/j.ijggc.2021.103369.

Vielstädte L., Haeckel M., Karstens J., Linke P., Schmidt M., Steinle L., Wallmann K., Shallow gas migration along hydrocarbon wells – An unconsidered, anthropogenic source of biogenic methane in the North Sea, Environmental Science & Technology, 2017, 51(17), 10262–10268.

Vielstädte L., Karstens J., Haeckel M., Schmidt M., Liebetrau V., Reimann S., McGinnis D. F., Linke P., Wallmann K., Quantification of methane emissions at abandoned gas wells in the Central North Sea. Marine and Petroleum Geology, 2015, 68, 848–860.

POS535 AND POS524

Geoscientific Investigations of Hydrothermal Sites along the Arctic Mid-Oceanic Ridge during Cruises POS535 (Loki2GrimseyEM) and POS524 (GrimseyEM)

AUTHORS

GEOMAR Helmholtz Centre for Ocean Research Kiel | Kiel, Germany
S. Hölz, A. Haroon, S. Martins, S. Petersen

POSEIDON CRUISES POS535 AND POS524

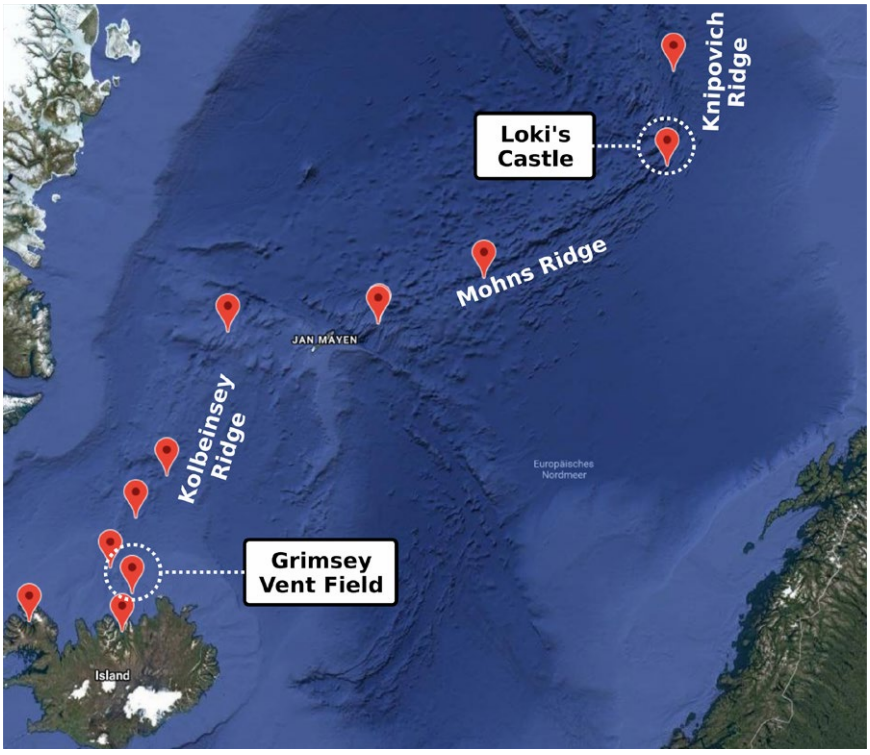

Fig. 1: Arctic Mid-Oceanic Ridge (AMOR) with the two working areas Grimsey Hydrothermal Field (GHF) and Loki's Castle and additional vent fields from Beaulieu (2015).

During the two research cruises POS524 (2018) and POS535 (2019), investigations were carried out onboard RV Poseidon at hydrothermal sites located along the Arctic Mid-Oceanic Ridge (AMOR). Both cruises visited the Grimsey Hydrothermal Field (GHF), which is located offshore northern Iceland. During the latter cruise, we also sailed further

North and carried out experiments at the hydrothermal site "Loki's Castle". During these cruises, we investigated, to what extent active hydrothermal systems and potential mineralizations may be detected and characterized in the marine environment by using electromagnetic (EM) experiments. We used different EM experiments, which allow for different depths of investigations (DOIs):

- The inductively coupled, mobile MARTEMIS system (marine transient electromagnetic induction system) uses transmitter and receiver coils in a coincident loop configuration mounted in a frame with a size of approximately 4×4m^2 to detect conductive features down to a depth of ~30mbsf (Hölz et al., 2015).

- The Coil2Dipole experiment (Safipour et al., 2017), for which we use the mobile MARTEMIS source as transmitter and several stationary OBEM (ocean bottom EM) receiver nodes. This experiment offers a greater DOI of about 120mbsf.

- The CAGEM system, a transmitter with two perpendicular, horizontal dipoles mounted to a frame, which allows for a dual-polarization measurement with a DOI of ~300mbsf.

Electromagnetic investigations were accompanied by CTD measurements, measurements with a temperature probe using a 220 cm long sensor string and by direct sampling with a gravity corer with a 300 cm long core barrel.

INVESTIGATIONS AT THE GRIMSEY HYDROTHERMAL FIELD

A first interpretation of TEM data acquired with the MARTEMIS system is depicted in Fig. 2 in terms of a stitched section of 1D inversions. Slightly increased conductivities (turquoise, orange) can be seen at the actual vent site, which is marked by the floating map above the bathymetry. However, most striking is a good conductor (yellow blob), which stretches from the hydrothermal field to a probable fault scarp in the West. We believe that this area of high conductivities could be due to mineralizations beneath the seafloor. However, high conductivities could also indicate a phase separation of high temperature fluids into a saline (=more conductive) brine remaining within the seafloor and a less saline phase being vented at the hydrothermal field further to the East. The existence of a conductive body to the West of the hydrothermal field was further confirmed by data from the Coil2Dipole experiment, which was evaluated as part of a Bachelor thesis (Barnscheidt, 2019). Additionally, elevated temperatures (15.5°C & 17.0°C @220cm) measured with the temperature probe at locations to the West of the active field also indicate increased activity in this area. Sulfides occur as disseminated particles and isotope analyses show a bimodal distribution with δ34S ranging between -21.7–0.4‰ indicating reduction of seawater sulfate by sulfate reducing bacteria for very negative values and the influence of hydrothermal fluids for values around zero, where sulfur is leached from mid-ocean ridge basalts (MORB). Further geochemical and sedimentological analyses are pending.

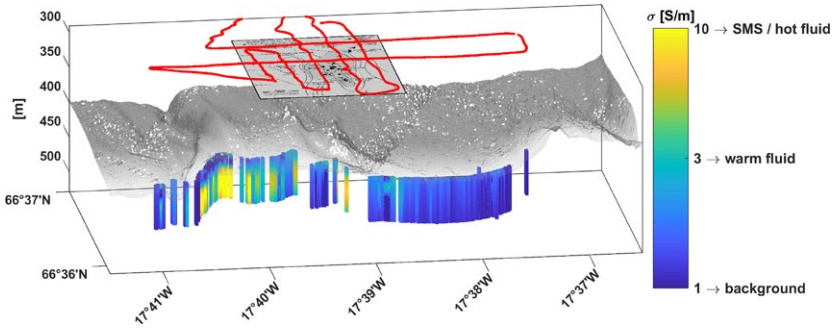

Fig. 2: TEM experiment at the GHF with track of the MARTEMIS system (red), location of the hydrothermal site (floating inlay, map from Hannington et al., 2001), bathymetry and a stitched conductivity section of 1D inversion results.

These results are exciting, because geophysical and more specifically electromagnetic methods can open a window into the subsurface and lead other scientific disciplines (e. g. geochemistry, microbiology) to areas that they may not have considered as targets of interest in the past. In the marine environment, these disciplines have so far concentrated very much on the obviously active areas and targets, e. g. chimneys at vent sites. With an interdisciplinary approach, we can break new grounds here and, thus, gain new insights.

We have successfully proposed to continue investigations at the GHF in a cruise to be carried out in the summer of 2023 (FS Alkor or FS Heincke). We aim to take additional core samples (up to 5 m length), which will then hopefully give a first insight into the microbiology of this CO_2 rich vent field (GEOMAR cooperation between FB2 and FB4). The obtained samples will also be analyzed as part of the granted project "High CO_2 – metabolic responses and bioeconomic opportunities" (Helmholtz Innovation Pool, Thematic Cluster 2), which is a collaboration between Forschungszentrum Jülich, Geoforschungszentrum Potsdam and GEOMAR. As outlook, we also plan to apply for a MeBo drilling project (up to 70 m depth) in the spring of 2023, which will be in coordination with Prof. Bach and Dr. Freudenthal (University of Bremen/Marum).

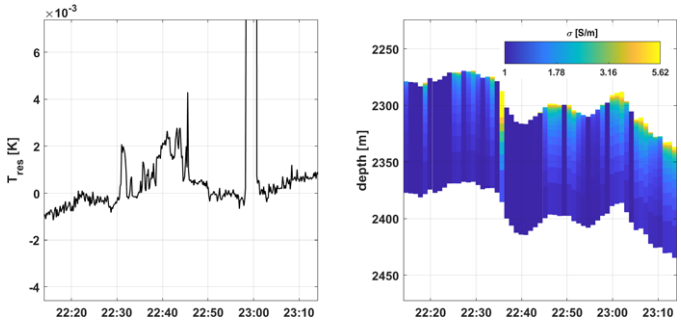

Fig. 2: TEM experiment at the GHF with track of the MARTEMIS system (red), location of the hydrothermal site (floating inlay, map from Hannington et al., 2001), bathymetry and a stitched conductivity section of 1D inversion results.

INVESTIGATIONS AT THE HYDROTHERMAL SITE "LOKI'S CASTLE"

Additional experiments carried out at the vent site "Loki's Castle" (LC, see Fig. 1) showed distinct anomalies in the acquired CTD data, which coincide with elevated anomalies in the conductivity section derived from EM data (Fig. 3). However, when comparing this section to the one obtained at GHF (see Fig. 2) it seems evident that elevated conductivities are confined to the very shallow part of the section. We argue that this comparison demonstrates that the type of host geology (GHF → sedimentary; LC → basalt / mudstones) dictates the potential size/volume of mineralization generated by hydrothermal systems.

First results from the investigations at LC were presented and discussed during an informal workshop held at the end of October 2019 at the University of Bergen (Organizers: Dr. M. Sommer, University Bergen, Dr. S. Hölz, GEOMAR) with 22 participants from scientific/educational (U of Bergen, NTNU, GEOMAR), governmental (NGU – Geological Survey of Norway) and commercial (Equinor) entities.

REFERENCES

Barnscheidt, K.C.: Qualitative und quantitative Auswertung eines neuartigen marinen elektromagnetischen „Coil2Dipole" Experiments. Bachelor thesis, 71pp., Christian-Albrechts-Universität zu Kiel, supervised by Dr. S. Hölz and Prof. C. Berndt.

Beaulieu, S.E., Baker, E.T., German, C.R.: Where are the undiscovered hydrothermal vents on oceanic spreading ridges? Deep Sea Research Part II,121, 202–212.

Hannington, M., Herzig, P., Stoffers, P., Scholten J., Botz, R. Garbe-Schönberg, D., Jonasson, I.R., Roest, W. & Shipboard Scientific Party, 2001: First observations of high-temperature submarine hydrothermal vents and massive anhydrite deposits off the north coast of Iceland. Marine Geology, 177, 199–220.

Hölz, S., Jegen M., Petersen S. & Hannington, M.: How to Find Buried and Inactive Seafloor Massive Sulfides using Transient Electromagnetics – A Case Study from the Palinuro Seamount in the Tyrrhenian Sea. Talk with extended abstract during UMC conference, Tampa Bay, 1.11.–6.11.2015.

Safipour, R., Hölz, S., Jegen, M., Swidinsky, A.: On electric fields produced by inductive sources on the seafloor, Geophysics, 2017, vol. 82, E297–E313.

POS536

Abundance, composition and distribution of microplastics in the North Atlantic Garbage Patch

AUTHORS

GEOMAR Helmholtz Centre for Ocean Research Kiel | Kiel, Germany
M. Lenz, E. Achterberg, A.J. Beck, E. Borchert, A. Engel, M. Haeckel, T. Hamm, U. Hentschel Humeida, E. Kossel, N. Ory

University of Siena | Siena, Italy
L. Galgani

BACKGROUND

The input of plastic waste into the oceans is currently between 10 and 20 million tons per year (Jambeck et al. 2015, Borelle et al. 2020), while the mass of plastic waste that is floating in the central areas of the ocean basins, the so-called garbage patches, only amounts to 0.27–1.00 *10^6 t (Eriksen et al. 2014, Lebreton et al. 2018). This discrepancy has been explained by various processes, for instance by the fact that 40 % of the introduced plastic debris has negative buoyancy and sinks to the seafloor soon after release. A further, much smaller part with positive buoyancy is deposited along the coastlines, while the remaining material is assumed to reach the open ocean. There it fragments into particles too small to be recognized by surveys and/or gets transferred by vertical transport from the sea surface to deeper water layers and finally to the seafloor. This vertical pathway presumably constitutes the largest sink for plastic debris on the planet. However, so far no observational data exist on the export of this material to the deep sea and the mechanisms facilitating this transport, including the presumably very relevant biota-plastics interactions. The latter could comprise the ingestion of small plastic pieces by pelagic marine animals such as zooplankters, which may take the material with them to deeper water layers during their vertical migrations and excrete it there. In this way, microplastics could eventually reach the deep sea and accumulate there. However, little knowledge exists on the trophic transfer through as well as on the accumulation of plastic debris in open ocean food webs and on the environmental impact it may have on deep sea ecosystems. Consequently, no quantitative models exist that could help to assess vertical transport rates in the oceanic environment. The main objective of cruise POS 536 was to obtain data that provide information on the abundance and composition of microplastics at the ocean surface and in different water depths as well as in various pelagic animals.

METHODS AND GEAR

The working area was located at the mid-northern margin of the inner accumulation zone of the North Atlantic garbage patch, where debris loads of up to 2 500 g per km^2 have

been documented at the sea surface (Cózar et al., 2014). It is south-west of the Azores near the Mid-Atlantic Ridge and was visited by RV POSEIDON from mid-August to mid-September 2019. In order to quantify the occurrence of large-sized marine debris in this sea area, the abundance of floating objects was recorded from the forecastle in a visual litter survey. This was done over a total of 50 hours during 10 transits between stations. The majority of litter items encountered (99 %) were identified as plastics, while the vast majority of these objects were smaller 10 cm. Only 1 % was larger than 90 cm, while 3 % were larger than 50 cm. At 36 stations, a neuston catamaran equipped with a 300 µm net was towed with 4 knots for 20 minutes to sample the sea surface. Furthermore, at 10 stations bongo nets with a mesh size of 300 µm were towed horizontally in three water depths (10, 100, 300 m), while WP2 plankton nets with a mesh size of 100 µm were lowered to 500, 1000 and 1500 m. Both nets served to capture plankton organisms and suspended microplastic particles at various depths. To also assess microplastics smaller than 100 µm, which are either suspended/sinking in the water column or which are embedded in organic aggregates ("marine snow"), *in situ* pumps and sediment traps were used. The *in situ* pumps were deployed at six stations to water depths of 50, 75, 150 and 300 m and were equipped with 10 µm stainless steel filters. The sediment traps were organized in eight arrays that were mounted on PVC cross frames to collect sinking material at 50 m, 100 m, 150 m, 200 m, 300 m, 400 m, 500 m and 600 m. Each array contained twelve Particle Interceptor Traps (PITs, with a collection area of 0.0038 m^2). The PVC crosses were fixed to a steel cable which, in turn, was fastened to a buoy and several floats. This structure was deployed from the vessel twice during POS 536 and drifted autonomously in the study area for five days before it was taken back on board. In order to also obtain data on the abundance of microplastics on the seafloor, sediment samples were collected at seven stations from depths between 2200 and 3100 m using a box corer. Finally, hydrographic data and water samples were collected at 19 stations using a CTD with a water samples rosette.

PRELIMINARY RESULTS

After the cruise, all samples were brought to GEOMAR where they are currently processed. In order to characterize the captured microplastics, the particles must be extracted from the environmental matrix in which they are contained. In case of the sediment samples, this is done by means of density separation and filtration. Then, any particles that may be microplastics are collected from the filters and are chemically analyzed using a Raman spectroscope. All bongo net samples were first scanned and the scans were uploaded into the ecotaxa database to analyse species diversity and abundance. By this, four groups of organisms were identified to be of interest for microplastic gut analysis: Euphausicae as filter feeders, chaetognaths as predators, copepods as the most abundant group of organisms and fish. These groups were separated from the rest of the sample material and are currently digested using enzymes as well as KOH. Microplastic particles in the size range 20–100 µm will then be filtered off the residues and will get analyzed with a Raman spectroscope. From the material collected with the neuston catamaran, a total of 5509 particles were picked, of which

5165 were identified as plastics with a hyperspectral imaging system at GEOMAR. The most common polymer type was polyethylene, the second was polypropylene and only two particles were polystyrene. In addition to identifying the polymer type, the microbial film on 73 of these particles was sampled on board of RV POSEIDON and its composition is currently analyzed. So far, 600 bacterial genomes have been reconstructed. These data allow insights into the colonization of plastics by microbes in the open ocean. The sample material from the sediment traps was analyzed by Pyrolysis GC-MS and by FT-IR spectroscopy, and both methods revealed the presence of microplastics (< 1000 µm) at almost all depths that were sampled. The water samples and the filters from the *in situ* pumps were analysed for their content of Uranium and Thorium, since the Uranium-Thorium disequilibrium provides information about the rate of vertical particle transport in the water column. The depletion of Thorium at some of the sampled stations indicates a substantial vertical particle transport. With the help of models of ocean circulation at GEOMAR, which also capture mesoscale ocean currents and eddies, the drift of the particles is currently reconstructed in order to gain information about their origin. Furthermore, we are investigating the role of eddies for the horizontal transport of microplastics in the open ocean. This talk will outline the objectives of POS 536, explain the methods used and give an overview over the results as obtained until the time of the talk.

REFERENCES

Borelle SB, Ringma J, Law KL, Monnahan CC, Lebreton L, McGivern A, Murphy E, Jambeck J, Leonard GH, Hilleary MA, Eriksen M, Possingham HP, De Frond H, Gerber LR, Polidoro B, Tahir A, Bernard M, Mallos N, Barnes M, Rochman CM Predicted growth in plastic waste exceeds efforts to mitigate plastic pollution. Science 2020, 369, 1515–1518.

Cózar A, Echevarría F, González-Gordillo JI, Irigoien X, Úbeda B, Hernández-León S, Palma ÁT, Navarro S, García-de-Lomas J, Ruiz A, Fernández-de-Puelles ML, Duarte CM Plastic debris in the open ocean. Proceedings of the National Academy of the Sciences of the USA 2014, 111, 10239–10244.

Eriksen M, Lebreton LCM, Carson HS, Thiel M, Moore CJ, Borerro JC, Galgani F, Ryan PG, Reisser J Plastic pollution in the world's oceans: more than 5 trillion plastic pieces weighing over 250,000 tons afloat at sea. 2014, PLoS ONE 9, e111913.

Jambeck JR, Geyer R, Wilcox C, Siegler TR, Perryman M, Andrady A, Narayan R, Law KL Plastic waste inputs from land into the ocean. Science 2015, 347, 768–77.

Lebreton LCM, Slat B, Ferrari F, Sainte-Rose B, Aitken J, Marthouse R, Hajbane S, Cunsolo S, Schwarz A, Levivier A, Noble K, Debeljak P, Maral H, Schoeneich-Argent R, Brambini R, Reisser J Evidence that the Great Pacific Garbage Patch is rapidly accumulating plastic. Nature 2018, 8, 4666.

POS537

Biofilm-like habitat at the sea-surface: A mesocosm study during POS537

AUTHORS

University of Oldenburg, Institute of Chemistry and Biology of the Marine Environment | Wilhelmshaven, Germany
O. Wurl, T.B. Robinson, M. Striebel

Spanish Institute of Oceanography (CSIC) | Malaga, Spain
I. Ferrera, A.M. Cabello

Departament de Genètica i de Microbiologia, Universitat Autònoma de Barcelona | Bellaterra, Spain
C.R. Gazulla

Institut de Ciències del Mar (CSIC) | Barcelona, Spain
M.M. Sala

CESIMAR Centro para el Estudio de Sistemas Marinos | Puerto Madryn, Argentina
R. Gonçalves

Universiti Putra Malaysia | Seri Kembangan, Malaysia
N.I.H. Mustaffa

The sea-surface microlayer is the boundary interface between the atmosphere and ocean, covering about 70 % of the Earth's surface. With a typical thickness of 60–100 µm, the sea-surface microlayer has physicochemical and biological properties that are measurably distinct from underlying waters. Because of its unique position at the air-ocean interface, the sea-surface microlayer is central to a range of global biogeochemical and climate-related processes. More recent studies indicate that the sea-surface microlayer is an aggregate-enriched biofilm environment with distinct microbial communities (Stolle et al., 2010, Wurl et al., 2016). The redeveloped paradigm pushes the sea-surface microlayer into a new and wider context that is relevant to many ocean and climate sciences, including marine carbon cycle (Reinthaler et al., 2010), air-sea gas exchange (Mustaffa et al., 2020) and aerosol production (Wilson et al., 2015).

The overall objective of this expedition has been to gain a mechanistic understanding of the formation of a biofilm-like habitat at the sea surface. In a time- series (several days),

we have investigated the dynamics of biofilm formation and light conditions as primary force (i. e. natural dark/light cycle and controlled dark conditions). We have modified old lift rafts as floating mesocosms and covered them with UV transmitting and UV blocking foil. Another set of mesocosm served as dark control. In addition, we have conducted deck incubations to gain additional information on the influence by UV radiation and light on chemical and biological composition of natural sea-surface microlayer and near-surface water.

Six mesocosms modified from decommissioned lift rafts were deployed. The bottom of the lift rafts was cut out to have a floating oval shape with a site of approximately 2.8 meter x 1.5 meter. The roof structures, also inflatable, were used to attach UV transmitting and UV blocking foil (each two mesocosm), two mesocosms remain their original cover as dark control. In total we deployed six mesocosms (Figure 1). The mesocosms were attached to each other, randomly, in a chain. The free floating mesocosm were sampled when the weather permitted, but typically in the morning and the afternoon, from the small boat. The sea-surface microlayer was collected using the glass plate technique (Figure 2), and the volume of collection restricted to the 30 % of the total volume of the sea-surface microlayer within the mesocosm assumed thickness of 100 µm). At the time, bulk water samples were collected from 1 meter depth as reference.

Fig. 1: Deployment of six free floating mesocosms during POS 537.

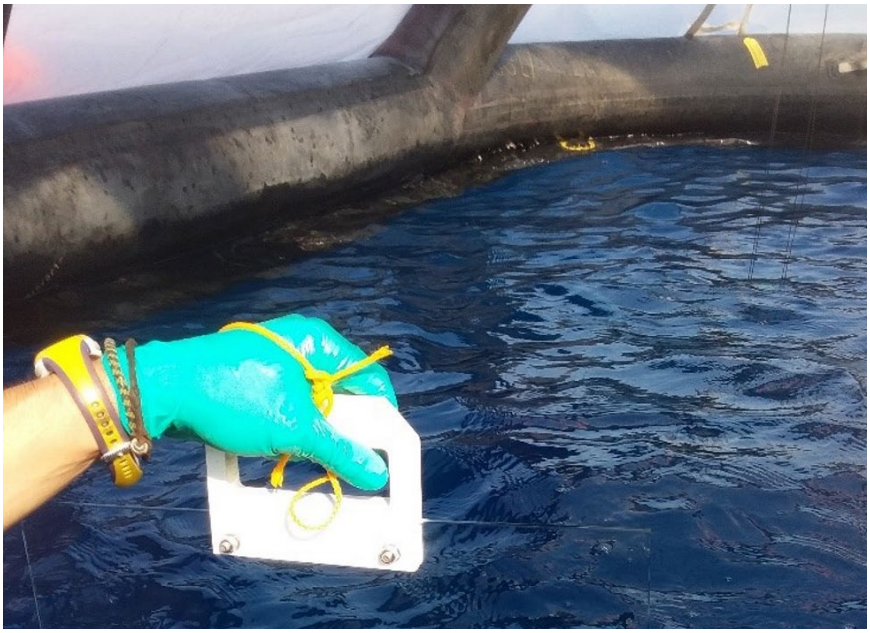

Fig. 2: Sampling mesocosms from the small boat for the SML and underlying bulk water.

In addition, we collected water samples from the upper surface layer with the CTD to conduct incubation experiments. Seawater samples from 10 different depths were collected and filled 200 cell cultures bottles with and were treated with three light treatments, i. e., blue, red and green and a control treatment (grey) for > 2 weeks. This experiment aims to understand how phytoplankton community at different depths respond to different light penetration in the ocean. An additional incubation experiments were set up at a later point of the cruise, to investigate the effect of grazing by zooplankton on transparent exopolymer particles; the latter an essential component of biofilms observed on the sea surface.

TEP results showed that changes of TEP concentrations in the SML were higher than ULW with the highest changes seen in the dark mesocosms, then mesocosms allowing light (UV+) and then mesocosms blocking UV light (UV-). Patterns in changes of TEP concentration over time were similar for both the dark and UV light admitting mesocosms while the UV blocking mesocosm showed little change in TEP over time. Potential diurnal patterns were observed in the dark and UV+ mesocosms but further time series analysis is required to confirm such patterns and to discern their potential causes.

Overall our results showed differences between the sea-surface microlayer and the bulk water as reference. In terms of carbon utilization based on a Biolog ®Ecoplates assay, we found that widest utilization occurred in dark mesocosms, then mesocosms allowing all light (including UV), and then the mesocosms which blocked UV light. It indicates

different microbial communities may have developed with various capacity in the utilization of different carbon sources. The optical density was also highest in the dark mesocosm, although we did not observe clear trends for the cell abundance in terms of enrichment in the sea-surface microlayer. We focused on the enzyme activities of ß-glucosidase, which is involved in the utilization of dimers of cellulose, chitobiase for the degradation of chitin, leucyl aminopeptidase, which degrades the proteinaceous components of DOM, and alkaline phosphatase, involved in the hydrolysis of organic phosphoesters. The activities of alkaline phosphatase and chitobiase did not differ significantly among the different light treatments, but leucyl aminopeptidase and ß-glucosidase showed higher activities in the dark mesocosm.

We conducted on-board an incubation experiment on the growth of phytoplankton collected at various water depth and incubated under different light conditions, that means incubated under four different light spectra foils, i. e., control (425–770 nm), blue (430–530 nm), red (600–750 nm) and green (425–600 nm). Light intensity was reduced to a mean of 43.7 % of ambient light using the foils. Different light treatments affect significantly the growth rate of phytoplankton ($F=28.11$, $p<0.001$). Phytoplankton incubated under blue light treatment showed the highest growth rate, meanwhile phytoplankton growing under green light had the lowest growth rates (Figure 3). The Shannon index of the pigment diversity was significantly affected by the light treatments, water depth and their interaction. In general, diversity was significantly lower in samples grown under green light treatment ($p<0.0001$) (Fig. 3C). Samples under green light treatment showed the most differences between the depths.

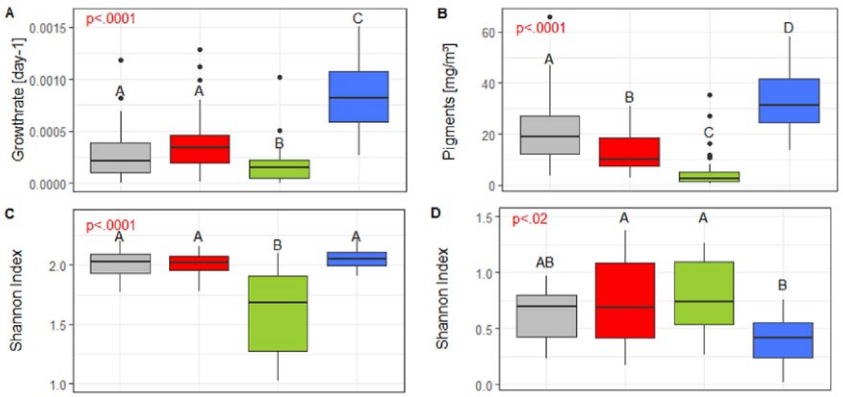

Figure 3: Effect of different light treatment considering from all water depths together on (A) growth rate, (B) total pigment concentration, (C) Shannon Index of phytoplankton pigments, (D) Shannon Index of phytoplankton community composition. Colors represent light treatments, grey indicates control.

In conclusion, our experiment demonstrate that different light sources lead to changes in community growth rate, pigment composition, and content. Although our results showed

an interaction of light and water depth, our expectation, that communities from different water depths show different adaptions to the light treatments in terms of their growth, pigment composition and content could not be confirmed.

For additional onboard experiment on deck, zooplankton (copepods) were collected from the surface water with a neuston net and individually separated into plastic bottles filled with water from sea-surface microlayer or bulk water. The bottles were exposed to two light treatments with and without UV radiation, inside a water bath to ensure constant temperature. After 24 hours of incubation, zooplankton survival and TEP (among other variables) were measured. Results indicate that zooplankton survival was higher than 5 % in all bottles. TEP concentrations increased during the incubation in all treatments and with the presence of zooplankton. This indicates TEP production by the activity of zooplankton, and we assume sloppy feeding to increase TEP concentrations.

REFERENCES

Mustaffa N I H, Ribas-Ribas M, Banko-Kubis H M, Wurl O, Global reduction of in situ CO_2 transfer velocity by natural surfactants in the sea-surface microlayer, Proceedings of the Royal Society A 2020, 476(2234), 20190763.

Reinthaler T, Sintes E, Herndl G J, Dissolved organic matter and bacterial production and respiration in the sea-surface microlayer of the open Atlantic and the western Mediterranean Sea, Limnology and Oceanography 2008, 53(1), 122–136.

Stolle C, Nagel K, Labrenz M, Jürgens K, Succession of the sea-surface microlayer in the coastal Baltic Sea under natural and experimentally induced low-wind conditions, Biogeosciences 2010, 7(9), 2975–2988.

Wilson T W, Ladino L A, Alpert P A, Breckels M N et al., A marine biogenic source of atmospheric ice-nucleating particles, Nature, 2015, 525(7568), 234–238.

Wurl O, Stolle C, Van Thuoc C, Thu P T, Mari X, Biofilm-like properties of the sea surface and predicted effects on air–sea CO_2 exchange, Progress in Oceanography 2016, 144, 15–24.

POS538

High-resolution 2D and 3D reflection seismic analysis of tsunamigenic eruptions in the Christiana-Santorini-Kolumbo Volcanic Field, Southern Aegean Sea (Greece)

AUTHORS

GEOMAR Helmholtz Centre for Ocean Research | Kiel, Germany
J. Karstens, G.J. Crutchley, C. Berndt, F. Schmid

University of Hamburg | Hamburg, Germany
C. Hübscher, J. Preine

MOTIVATION AND AIMS

Volcanic tsunamis caused more than 60,000 casualties since AD 1600. They can be generated by submarine explosions, earthquakes, caldera subsidence, slope instabilities and pyroclastic flows or a combination of these processes (Auker et al., 2013; Day, 2015). The reconstruction of the tsunami source mechanisms of a volcanic eruption is a complex task and the most common approach is to compare numerical simulations with tsunami observations (if available). This approach is limited by the availability and accuracy of input parameters for specific source mechanisms, e. g. volumes and velocity of slide masses, dynamics of deformation processes, depth and strength of explosions. Volcanic eruptions and earthquakes in the Christiana-Santorini-Kolumbo Volcanic Field have repeatedly triggered devastating tsunamis including the 1600 BCE Minoan Eruption of Santorini, the AD 1650 eruption of Kolumbo, and the AD 1956 Amorgos earthquake. The Minoan Eruption tsunami affected large areas of the eastern Mediterranean and contributed to the demise of the Minoan culture on Crete, while the effects of the AD 1650 Kolumbo and the AD 1956 Amorgos tsunamis were limited to the islands around the Christiana-Santorini-Kolumbo Volcanic Field. Although intensively studied in recent decades, the potential tsunami source parameters of these events remain poorly constrained. POS538 aimed to (1) provide constraints about the volcano-tectonic evolution of the CSKVF, (2) to parameterize various potential source parameters associated with these tsunamis, and (3) to collect site survey data for IODP Expedition 398 (proposal 932-Full).

SEISMIC EXPERIMENT

During POS538, we conducted 2D and 3D reflection seismic surveys as well as a ocean-bottom seismometer refraction seismic experiment covering the Christiana-Santorini-Kolumbo Volcanic Field in October 2019 (Fig. 1; Karstens et al., 2020). The acquired P-Cable 3D seismic dataset covers an area of ~40 km^2 including the Kolumbo edifice and the newly discovered Oia Fault to the north. We collected more than 650 km of 2D

reflection seismic profiles. These were used as site survey data for IODP proposal 932-Full, which has been approved and is now scheduled as IODP Expedition 398 for December 2022 to February 2023. Furthermore, we deployed six Ocean-Bottom-Seismometers (OBS) to construct a 2D velocity model for the subsurface of Kolumbo and to record local earthquakes and other active volcanic or hydrothermal events.

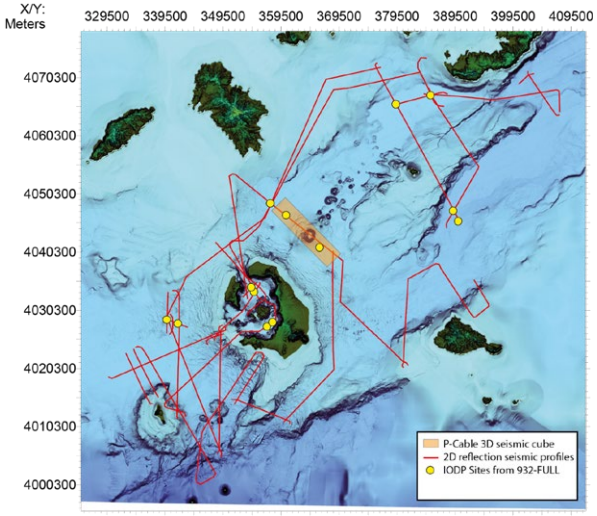

Fig. 1: Overview of the datasets acquired during POS538. Coordinates in UTM zone 35, WGS84.

RESULTS

VOLCANIC EVOLUTION OF THE CHRISTIANA-SANTORINI-KOLUMBO VOLCANIC FIELD

The analysis of the high-resolution 2D seismic dataset allowed us to reconstruct the first consistent chronological framework for the Christiana-Santorini-Kolumbo Volcanic Field by linking seismic interpretation to the onshore volcanic sequences (Fig. 2; Preine et al., 2021). The analysis revealed that volcanic activity developed in four distinct phases, which are controlled by large-scale tectonic activation phases of the rift system, and that the volcanism in the Christiana-Santorini-Kolumbo Volcanic Field evolved from many small volcanic centers to a focused system forming the Santorini Edifice (Preine et al., 2021). A distinct shift in volcanism from a phase of relative volcanic dormancy to widespread volcanism correlates temporally with the emplacement of a previously unknown, large-scale (up to 125 km^3) mass-transport deposit, which highlights the complex interplay of tectonics, volcanism and mass-transport (Preine et al., submitted). Furthermore, the new seismic datasets enable us to link individual seismic units to the products of specific volcanic eruptions (e. g., the 1600 BCE Minoan Eruption, the AD 754 Kameni Eruption and the AD 1650 Kolumbo eruption), highlighting the great potential of high-resolution reflection seismic experiments for marine volcanology.

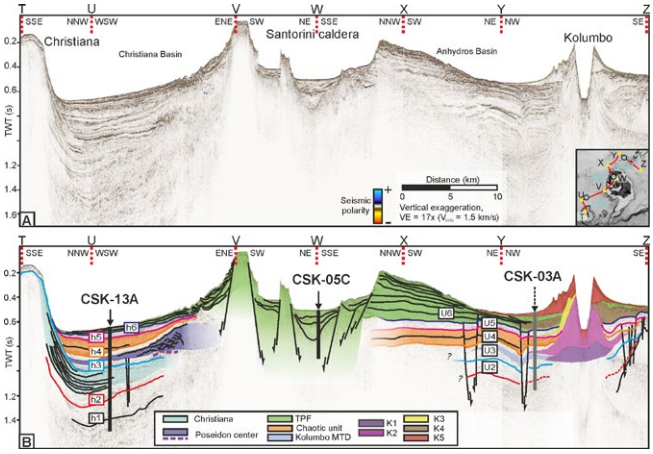

Fig. 2: Seismic profile crossing the major volcanic centers of the CSKVF. B) Interpretation of the main stratigraphic units and drill sites of IODP Expedition 398 after Preine et al., (2021).

3D SEISMIC ANALYSIS OF THE AD 1650 KOLUMBO CONE

First analyses of the high-resolution P-Cable 3D seismic dataset revealed a prominent deformation structure in northwestern flank of Kolumbo. This indicates that the volcanic cone formed during the AD 1650 eruption was affected by deep-seated deformation, which may have played a role in triggering the associated tsunami (Fig. 3). We will investigate whether the deformation represents a structural weakness zone, which may be relevant for Kolumbo's long-term slope stability. The 3D seismic dataset also covers the Oia Fault, which is part of the Santorini-Amorgos Tectonic Zone. There is an ongoing debate to what extent the Santorini-Amorgos Tectonic Zone is transtensional which will be analyzed based on the 3D seismic imaging of the fault geometries.

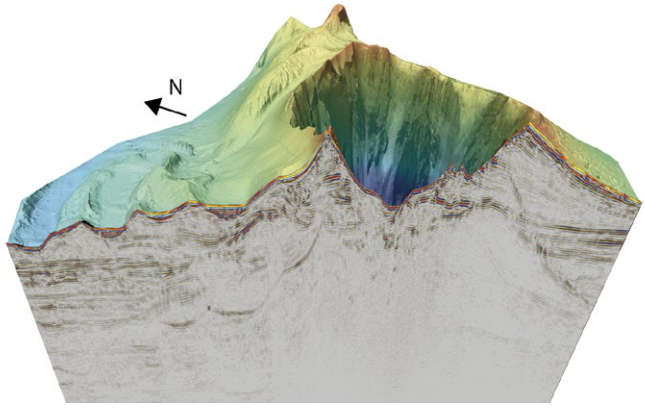

Fig. 3: 3D view into the 3D seismic dataset of the Kolumbo edifice revealing deformation of the northwestern flank of the AD 1650 volcanic cone.

IODP EXPEDITION 398

The 2D seismic profiles acquired during POS538 cover all proposed drill sites of IODP Expedition 398 (a subset is seen in Fig. 2B), while the 3D seismic dataset covers one drill site aiming to constrain Kolumbo's history. The data collected during POS538 played a crucial role for the IODP proposal 932-Full and provide important constraints for the upcoming drilling operations. In order to achieve the main objectives of IODP Expedition 398, it is necessary to extend the stratigraphic models from core and log data regionally throughout the rift basins and the caldera, which will be achieved by core-log seismic integration using the presented datasets.

REFERENCES

Auker MR, Sparks RSJ, Siebert L, Crosweller, HS, Ewert J, 2013. A statistical analysis of the global historical volcanic fatalities record. Journal of Applied Volcanology Society and Volcanoes 2013, 2:2.

Day S, Chapter 58 – Volcanic Tsunamis, In The Encyclopedia of Volcanoes (Second Edition), edited by Haraldur Sigurdsson, Academic Press, Amsterdam, 2015, pp. 993–1009. doi.org/10.1016/B978-0-12-385938-9.00058-4.

Karstens J, Crutchley G J, Elger J, Kühn M, Schmid F, Dalla Valle G, Preine J, Nomikou P, R/V Poseidon Cruise Report 538 – THESEUS Tsunami hazard of explosive submarine eruptions, 7th October – 28th October 2019, Cartagena (Spain) – Heraklion (Greece) . GEOMAR Helmholtz Centre for Ocean Research, Kiel, Germany, 2020, 106 pp. doi: 10.3289/cr_pos538.

Preine J, Karstens J, Hübscher C, Nomikou P, Schmid F, Crutchley G J, Druitt T, Papanikolaou D, Spatio-Temporal evolution of the Christiana-Santorini-Kolumbo volcanic field, South Aegean. Geology 2021. doi: 0.1130/G49167.1

Preine J, Karstens J, Hübscher C, Crutchley G J, Druitt T, Schmid F, Nomikou P, The Hidden Giant: How a rift pulse triggered a disaster cascade of sector collapses and voluminous secondary mass-transport events in the early evolution of Santorini. Submitted to Earth and Planetary Science Letters

POS539

Microbial processes involved in the N- and C-cycles in the western basin of the Black Sea (MicroliNC)

AUTHORS

Max Planck Institute for Marine Microbiology | Bremen, Germany
H. Marchant, J. Milucka

ABSTRACT

The Black Sea is a large inland sea located between Europe and Asia. An insufficient supply of oxygen and a high flux of organic matter (e. g. from Danube discharge) have turned this water body into the world's largest anoxic basin. The Black Sea is meromictic, containing permanently anoxic waters below its pycnocline (currently at 80–150 m). The upper oxic and lower anoxic waters are separated by a stable and well-defined suboxic zone. The sediments below the anoxic water column are a substantial source of methane, which is derived from both biogenic and thermogenic sources. As such, the Black Sea has a water column inventory of 96 Tg of methane (CH_4), making it the largest marine water reservoir of dissolved methane (Reeburgh et al., 1991). Furthermore, the Black Sea is a net source of this potent greenhouse gas to the atmosphere; 0.05–0.2 Tg CH_4 are lost from this basin annually (Kessler et al., 2006).

In the Black Sea, biological methane removal is understood to occur through its oxidation with oxygen and/or sulfate. However, in recent years, nitrogen oxides, such as nitrate and nitrite, have emerged as potentially important electron acceptors for methane oxidation. Nitrate and nitrite are present in the Black Sea, and both tend to disappear in the suboxic zone suggesting a local sink for these nitrogen species. Nitrite has been shown to serve as an electron acceptor for the oxidation of ammonium by anammox bacteria (Kuypers et al., 2003) but it remains to be seen whether it might also serve as electron acceptor for methane oxidation in the suboxic zone of the Black Sea.

The occurrence of nitrogen-coupled methane oxidation would directly link the C and N cycle in the Black Sea. Given the intense methane turnover in this system, methane-linked respiration of nitrogen oxides could also have a significant effect on the nitrogen cycle of the Black Sea. Additionally, respiration of nitrogen oxides during methane oxidation could contribute to the production of a different greenhouse gas, nitrous oxide (N_2O), which is formed as the end product of denitrification by some methanotrophs.

Determining rates of microbial turnover of climate-relevant greenhouse gases (methane and nitrous oxide) and identification of the responsible microorganisms was one of the research aims of the R/V POSEIDON cruise POS539. This cruise took place in the

northwestern basin of the Black Sea (42°30'N to 44°N and 29°E to 31°E) between November 6th and 21st, 2019. The cruise area encompassed the western shelf and slope of the Black Sea basin (Figure 1).

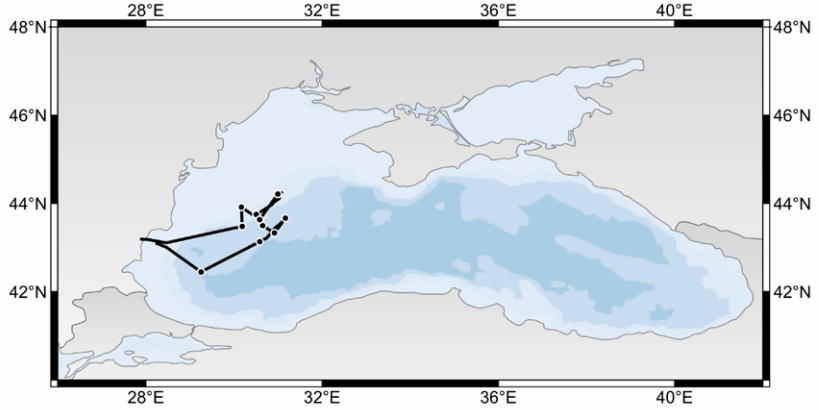

Fig. 1: The cruise track of the research cruise POS539 of R/V Poseidon in the western basin of the Black Sea.

The cruise track stretched between ca. 42°30'N and 44°N and 29°E and 31°E. Ten stations were sampled within this area that were roughly arranged in two perpendicular transects. The first transect included stations in the western basin, with water depths over 2000 m. The second transect stretched from the western basin towards the shelf, and the water depths of stations in this transect ranged between ca. 2000 m to ca. 80 m. Two additional stations were sampled on the slope for paleo-oceanographic studies.

Preliminary data of the recorded oceanographic conditions of the water column agree with the known water properties of this basin. At all stations, water temperature dropped from ca. 17°C at the surface to ca. 8°C at 50 m depth and remained stable throughout the rest of the water column. Chlorophyll was only detected in the mixed surface layer (upper ca. 25 m) and no deep chlorophyll maximum was observed. This was expected due to the lower photosynthetic activity usually associated with late autumn. Water density and salinity increased with increasing depth of the water column, as a consequence of the vertical mixing of saline bottom Mediterranean waters with freshwater originating from the riverine input. Oxygen concentrations dropped rapidly to zero at ca. 100–120 m, in accordance with the expected water properties. Below the oxycline, waters were anoxic and sulfidic (i. e. euxinic).

Sediment and water samples, including suspended particle material, were collected from water depths representing the various redox zones of the Black Sea (i. e. suboxic, oxic-anoxic transition, anoxic). Metabolic rates will be quantified from tracer experiments that were setup onboard after their analyses by isotope-ratio mass spectrometry. Further work

in progress includes the analyses of microbial diversity and in situ activity using metagenomic and metatranscriptomic sequencing.

Overall, the samples retrieved on this cruise will serve to investigate the activity and physiology of microorganisms involved in the conversion of nitrogen compounds and degradation of organic carbon under various oxygen conditions. Apart from microbial greenhouse gas cycling, other research questions will be investigated, such as (i) the metabolic activity and biogeochemical impact of archaeal ammonia oxidizers, (ii) the composition and stability of organic matter, more specifically polysaccharides, under different redox conditions, and (iii) the biomarker record of the freshwater-to-marine transition in this basin.

The Black Sea represents an ideal natural laboratory for studies of microbial processes at various redox conditions. Together, the results of the interdisciplinary POS539 cruise will help to mechanistically understand and quantify carbon and nitrogen cycling in this unique marine habitat.

REFERENCES

Kessler JD, Basin-wide estimates of the input of methane from seeps and clathrates to the Black Sea, Earth and Planetary Science Letters 2006, 243, doi:10.1016/j.epsl.2006.01.006.

Kuypers MMM, Anaerobic ammonium oxidation by anammox bacteria in the Black Sea, Nature 2003, 422, doi.org/10.1038/nature01472.

Reeburgh WS, Black Sea methane geochemistry, Deep Sea Research Part A 1991, 38, doi.org/10.1016/S0198-0149(10)80030-5

SO263

TongaRift Volcanism, hydrothermal activity and vent biology

AUTHORS

GeoZentrum Nordbayern, Friedrich-Alexander-University Erlangen-Nuremberg | Erlangen, Germany
K. Haase, M. Regelous, M. Keith, J. Falkenberg, B. Storch, M. Schönhofen-Romer

Department of Geosciences, University of Bremen | Bremen, Germany
W. Bach, A. Diehl, P. Monien, S. Sopke

Jacobs University | Bremen, Germany
C. Kleint, F. Wilckens, D. Ernst, A. Moje, A. Koschinsky

AIMS OF THE CRUISE AND SAMPLING PROGRAM

The research program of RV Sonne cruise SO236 TongaRift aimed at determining the relation between the igneous, hydrothermal, and tectonic processes occurring during island arc and back-arc formation. During the cruise to the northernmost Tonga island arc and associated NE Lau back-arc basin we focused on (1) the Niua arc volcano, (2) the seamounts south of Niua, (3) an island arc and fore-arc stratigraphic profile, (4) the Niuatahi caldera, and (5) the North East Lau Spreading Centre (NELSC) as the main sampling and research targets. We performed 17 dives using MARUM ROV QUEST 4000, 62 TV grabs, 22 volcanic rock corers, as well as 19 CTDs and performed 11 hydroacoustic surveys. Hydrothermal plumes were determined and investigated using the CTD and Mini Autonomous Plume Recorders (MAPRs) attached to selected TV grab, CTD and rock corer deployments. Hydrothermal activity was found at Niua North and South, along the caldera ring fault of the southern and northern caldera rim of Niuatahi, and at the Maka volcanic edifice on the NELSC. Hydrothermal plumes and fluids were sampled using the CTD and isobaric gas-tight (IGT) fluid samplers attached to the ROV Quest.

VOLCANISM AND HYDROTHERMAL ACTIVITY AT NIUA ARC FRONT VOLCANO

Niua is a large (~140 km^2) rectangular volcanic structure situated in an E-W-striking rift basin in the northernmost Tonga Ridge. The lavas recovered from the Niua volcanic structure mainly consist of dacites and rhyolites with MgO contents of 0.3 to 1.1 wt. %. Although the volcano can be separated morphologically into northern and southern Niua, the lava compositions are homogenous, suggesting similar sources of the magmas. In contrast to the typical lavas of the Tonga island arc, those from Niua are enriched in Nb and Ta as well as in other incompatible elements. Radiogenic isotope compositions of the Niua and several volcanoes further south indicate an inflow of

Samoa plume mantle into the arc front, as well as an input of fluids from subducted pelagic sediments.

The submarine hydrothermal system of Niua South (Tonga arc) consists of numerous black-smoker type chimneys emitting fluids with temperatures (up to 325°C) near the seawater boiling curve at ~1170 m water depth (Falkenberg et al., 2021). Multiple generations of sulfide precipitation in the chimneys reflect the evolution from an early low-temperature stage dominated by seawater mixing to a mature high-temperature boiling stage. Low-temperature (~240°C) framboidal pyrite and sphalerite are enriched in seawater-derived (Mo) and low-temperature elements like Tl, Mn, Pb, Ag, whereas euhedral pyrite and chalcopyrite form at high-temperature (~300°C) concentrating elements like Co, Se, and Sn. Gold occurs in solid-solution and as boiling-induced particles of native Au, electrum and Au-rich Bi-tellurides in the sulfides. Lead isotope data indicate that hydrothermal fluids scavenged metals not only from the deeper Tonga basement in the reaction zone, but also from young volcanic host rocks in the upflow zone. Sulphur isotope data exclude a magmatic volatile influx and indicate shallow subseafloor fluid-seawater mixing.

INFLUENCE OF THE SUBDUCTING LOUISVILLE SEAMOUNTS AND OF THE SAMOA PLUME ON THE NORTHERN TONGA MAGMAS

The compositions of lavas from volcanoes in the northernmost Tonga island arc and the associated back-arc imply not only variable subduction of pelagic sediments and altered oceanic crust, but also effects of subducted material from the Louisville Seamount Chain (LSC) as well as inflow of mantle from the Samoa plume. New geochemical and isotope data of lavas from six young submarine volcanoes of the northernmost Tonga island arc front show that the LSC signal is ~50 km wider than previously shown, implying an earlier effect of the subducting LSC. In contrast, the northernmost Tonga Arc front lavas are relatively enriched in Nb and Ta and their Nd, Hf and Pb isotope compositions resemble rejuvenated Samoa hotspot lavas. These unusual compositions indicate that Samoa plume mantle is flowing southwards beneath the northern Tonga Arc and Lau Basin apparently guided by rifting of the Tonga lithosphere. The mantle wedge beneath North Tonga was depleted by prior melting events, before re-enrichment by a partial melt enriched in highly incompatible elements. A fluid component was later added from a mixture of subducted pelagic sediment and LSC volcanic material.

VOLCANISM AND HYDROTHERMAL ACTIVITY AT THE NIUATAHI REAR-ARC VOLCANO

Niuatahi has a diameter of 15 km and forms an unusually large volcanic structure in the rear-arc of the northern Tonga island arc ~175 km west of the trench (Anderson et al., 2021). The volcano has an ~400 m deep caldera with a diameter of 8 km. Lavas show basaltic to basaltic andesite composition on the caldera rim and a small cone outside the caldera, whereas dacitic to rhyolitic lavas occur inside the caldera. This implies longer stagnation of the magmas beneath the caldera than during the initial formation of the

volcano. The caldera probably formed by eruption of voluminous dacite flows outside the caldera causing variable subsidence of its floor. Different generations of ring faults were active, cross-cutting several volcanic cones in the caldera and at its rim. Some of these ring faults form pathways for ascending hydrothermal fluids. The trace element composition of the lavas shows a strong influence of slab components on a highly depleted mantle source. Interestingly, the Pb isotope composition of Niuatahi lavas implies transport of subducted LSC material into the rear-arc mantle.

Hydrothermal activity at Niuatahi caldera was discovered at three vent sites (South Central, Southwestern Cone and Northern Cone) at 1607 to 1699 m water depth. Additionally, the young Motutahi cone in the caldera center is known to release magmatic SO2. Measured temperatures range up to 334°C and pH values were as low as 2.8. The sampled fluids are depleted in Mg, sulfate, and U, but enriched in metals like Fe, Mn, K, and Li and dissolved gases (e. g., H_2S, CO_2, H_2) relative to seawater. Low chlorinity of the fluids at South Central indicates fluid boiling, which is associated with the lowest pH (2.8–3.1), highest H_2S and lowest H_2, CH_4 and CO_2 concentrations at the three vent sites. Hydrothermal fluids from the Northern and Southwestern Cone show a similar geochemical composition with lower Fe/Mn ratios and H_2S concentrations than those from South Central, suggesting an influence by subsurface cooling and sulfide precipitation. The fluid data do not show a contribution of magmatic SO_2 compared to the $\delta^{34}S$ values of hydrothermal sulfides that are as low as -10.6 ‰ fat Niuatahi South-Central (Peters et al., 2021). The new data from Niuatahi caldera suggest that hydrothermal fluids in subduction-related systems show a high spatial compositional variability, and are affected by a strong temporal variability possibly due to varying input of magmatic volatiles.

The variable temperatures and salinities of the fluids from the different vent sites at Niuatahi caldera cause distinct Te/As and Te/Au ratios in hydrothermal pyrite, sphalerite, and chalcopyrite. Sulfur isotope and trace element compositions of sulfides from the hottest vents at Niuatahi South Central suggest a contribution of magmatic SO_2 to the hydrothermal system leading to an enrichment in volatile elements (e. g., Se, Bi, Te). By contrast, the distal northern caldera wall-hosted hydrothermal system is decoupled from the magmatic SO_2 source. Thus, the observed hydrothermal processes cause distinct metal contents in associated sulfides. Thus, Niuatahi caldera represents a continuum ranging from magmatic volatile- to seawater-dominated fluid venting. The variable processes lead to distinct compositions with selective trace element enrichments, such as Te, Se, and Co in the central caldera compared to Au, Zn, and Pb at the northern caldera wall. These results have important implications for the exploration of polymetallic sulfide mineralisations on the modern seafloor and in the geological record.

VOLCANISM AND HYDROTHERMAL ACTIVITY AT THE NORTH EAST LAU SPREADING CENTER

Abundant volcanic activity occurs in the back-arc region of the northern Tofua island arc where the Northeast Lau Spreading Centre (NELSC) propagates southwards into older

crust causing the formation of numerous seamounts at the propagating rift tip. An off-axis volcanic diagonal ridge (DR) occurs at the eastern flank of the NELSC, linking the large rear-arc volcano Niuatahi with the NELSC. New geochemical data from the NELSC, the southern propagator seamounts, and DR reveal that the NELSC lavas are tholeiitic basalts, whereas the rear-arc volcanoes typically erupt lavas with boninitic affinity. The sharp geochemical boundary may reflect the viscosity contrast between off-axis hydrous harzburgitic mantle and dry fertile mantle beneath the NELSC. The new data do not indicate an inflow of Samoa plume mantle into the NELSC, confirming previously published He isotope data. The NELSC magmas form by mixing of an enriched and a depleted Indian Ocean-type upper mantle end-member implying a highly heterogeneous upper mantle composition in this area. Most NELSC lavas are little affected by a slab component implying that melting is adiabatic beneath the spreading center. The DR lavas show the influence of a component from the subducted Louisville Seamount Chain, which was previously thought to be restricted to the nearby arc volcanoes Niuatoputapu and Tafahi. This signature is rarely detected along the NELSC implying little mixing of melts from the low-viscosity hydrous portion of the mantle wedge beneath the rear-arc volcanoes into the melting region of the dry mantle beneath the NELSC.

Maka volcano on the NELSC shows hosts two active hydrothermal vent sites emitting fluids of distinct composition at 1525 to 1543 m water depth (Klose et al., 2021). The fluids of the Maka hydrothermal field are characterized by temperatures up to 329°C, pH values ranging between 2.79 and 3.03, as well as low concentrations of Mg and sulfate. At Maka South, white fluids are venting with temperatures up to 301°C, pH values between 4.53 and 5.42, and relatively high concentrations of Mg and sulfate. Metals like Li and Mn are typically enriched relative to seawater together with H2S. A three-component mixing process is suggested for Maka South including seawater, a boiling-induced low Cl vapor, and a black smoker-type fluid similar to that of the Maka hydrothermal field. Trace element contents in hydrothermal pyrite agree the with contribution from these fluid end-members. Pyrite precipitating from Cl-poor vapor-rich fluids at Maka South is characterized by high As/Co suggesting a boiling-induced element fractionation between the vapor (As) and liquid phase (Co). By contrast, pyrite from the "normal" black smoker-type chimneys from the Maka hydrothermal field have lower As/Co and higher Co/Ni ratios.

REFERENCES

Anderson, M. O., C. Norris-Julseth, K. H. Rubin, K. M. Haase, M. D. Hannington, A. T. Baxter, and M. S. Stewart (2021), Geologic and structural evolution of the NE Lau Basin, Tonga: Morphotectonic analysis and classification of structures using shallow seismicity, Front. Earth Sci., 9, 665185. doi: 10.3389/feart.2021.665185.

Falkenberg, J. J., M. Keith, K. M. Haase, W. Bach, R. Klemd, H. Strauss, I. A. Yeo, K. H. Rubin, B. Storch, and M. O. Anderson (2021), Effects of fluid boiling on Au and volatile element enrichment in submarine arc-related hydrothermal systems, Geochim. Cosmochim. Acta, 307, 105–132. doi: 10.1016/j.gca.2021.05.047.

Klose, L., M. Keith, D. Hafermaas, C. Kleint, W. Bach, A. Diehl, F. Wilckens, C. Peters, H. Strauss, R. Klemd, K. Haase, and A. Koschinsky (2021), Trace element and isotope systematics in vent fluids and sulphides from Maka volcano, North Eastern Lau Spreading Centre: Insights into three-component fluid mixing, Front. Earth Sci., 9, 776925. doi: 10.3389/feart.2021.776925.

Peters, C., H. Strauss, K. Haase, W. Bach, C. E. J. de Ronde, C. Kleint, and V. K. Stucker (2021), SO2 disproportionation impacting hydrothermal sulfur cycling: Insights from multiple sulfur isotopes for hydrothermal fluids from the Tonga-Kermadec intraoceanic arc and the NE Lau Basin, Chem. Geol., 120586. doi: 10.1016/j.chemgeo.2021.120586.

SO265

Papanin Ridge and Ojin Rise Seamounts (Northwest Pacific): Dual Hotspot Tracks formed by the Shatsky Mantle Plume

AUTHORS

GEOMAR Helmholtz Centre for Ocean Research Kiel | Kiel, Germany
A. Dürkefälden, J. Geldmacher, M. Portnyagin, R. Werner, F. Hauff, K. Hoernle

Institute of Geosciences, Kiel University | Kiel, Germany
D. Garbe-Schönberg

EarthByte Group, School of Geosciences, The University of Sydney | Sydney, Australia
D. Müller

INTRODUCTION AND GEOLOGICAL BACKGROUND

Although previous findings support an origin of the Shatsky Rise igneous plateau (Northwest Pacific) through interaction of a mantle plume with a mid-ocean ridge triple junction, the evidence for the involvement of a mantle plume is equivocal. The identification of an intraplate hotspot track emanating from the plateau could solve this controversy. Two structures are directly adjacent to Shatsky Rise: Papanin Ridge and the Ojin Rise Seamount province. The major aim of this study was to test if any of these structures were formed as intraplate hotspot tracks by an alleged Shatsky mantle plume. Nearly 50 successful dredge hauls were conducted during R/V SONNE expedition SO265 in 2018 on Papanin Ridge and Ojin Rise Seamounts (Geldmacher et al., 2018). Here we present geochemical (major and trace element) data from volcanic whole rock and glass samples and combine them with plate tectonic reconstructions. This extended abstract is a summary of the recently published Dürkefälden et al. (2021) paper, whereas a companion study (including the results of radiogenic isotope measurements and $^{40}Ar/^{39}Ar$ dating) is currently under preparation.

The emplacement of Shatsky Rise took place in the Late Jurassic to Early Cretaceous during a period of frequent magnetic field reversals enabling the reconstruction of its original tectonic setting. Accordingly, the plateau formed along the path of a northeastward moving triple junction between the Pacific, Izanagi and Farallon plates (Nakanishi et al., 1999). The more than 500 km long Papanin Ridge represents the northeastern continuation of the main plateau and was initially still formed at the triple junction (thick dashed gray line in Fig. 1b). After magnetic chron M4, however, the ridge no longer lay on the path of the triple junction. Thus, the northeastern end (bend) of Papanin Ridge could have formed by intraplate volcanism above the tail of a mantle

plume. If so, we would expect that lavas from both parts of Papanin Ridge would differ geochemically. We have therefore subdivided the Papanin Ridge lavas into a southwestern (Papanin Ridge SW) and a northeastern (Papanin Ridge NE) part (Fig. 1).

The Ojin Rise Seamounts are located east of Shatsky Rise's northern Shirshov Massif extending over ~650 km to the ESE. The seamount province comprises approximately 80 individual seamounts and resides on crust that formed between M13 to M1 (~135–122 Ma).

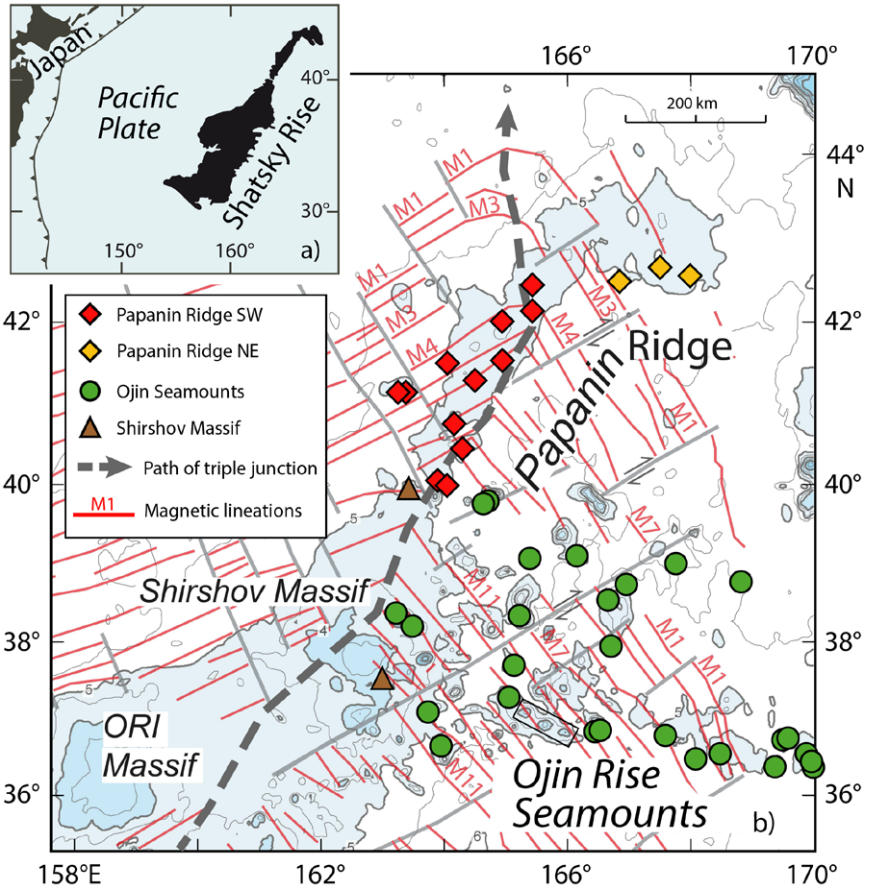

Fig. 1: a) Overview map of Shatsky Rise. b) Close-up map of Papanin Ridge emanating from the northern part of Shatsky Rise and the Ojin Rise Seamounts east of Shirshov Massif showing the sample locations of this study in different colors depending on their structural affiliation. Map modified after Sager et al. (2010) with magnetic anomaly lineations (red) after Nakanishi et al. (1999).

RESULTS AND DISCUSSION

Papanin Ridge lavas range from N-MORB to E-MORB compositions and overlap with the prevailing Shatsky main plateau lava compositions. Since trace element variations reflect

both mantle source and melting conditions, this observation suggests that Papanin Ridge most likely formed from the same source and under similar melting conditions and therefore in a similar tectonic regime as Shatsky Rise. The fact that Papanin Ridge shows much less volume and elevation than the main Shatsky plateau could either indicate that the plume source was already waning or that lesser amounts of plume material were drawn into the melting zone beneath the retreating triple junction.

Since the NE part of Papanin Ridge did no longer form at the triple junction, we expected to find higher ratios of incompatible over less incompatible elements (e. g., increased Th/Yb) and/or possible greater depletion in heavy rare earth elements (HREEs; e. g. higher Tb/Yb) resulting from greater average depth/lesser degree of melting. However, no such geochemical differences are observed between lavas from Papanin SW and Papanin NE. We therefore conclude that the NE part of Papanin Ridge was also formed by plume-ridge interaction (drainage of plume material into a spreading center), albeit not at the retreating triple junction (see below).

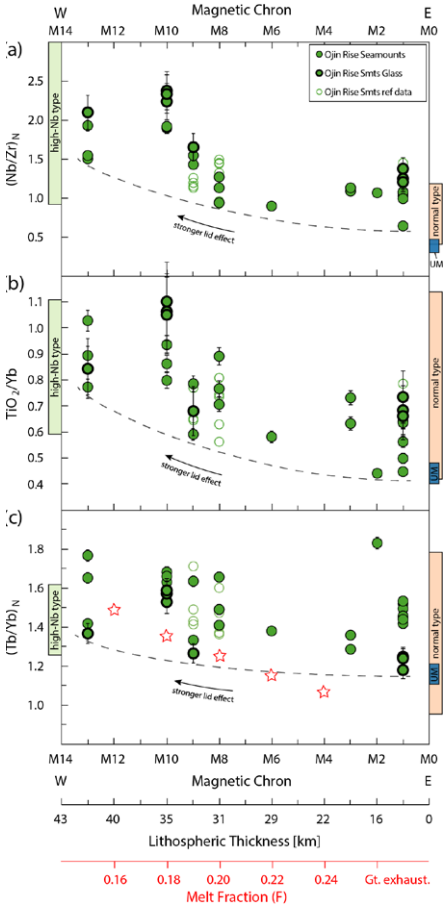

Fig.2: Ojin Rise Seamount lavas (normalized to primitive mantle values after Hofmann, 1988) show a systematic spatial change in composition with lithospheric thickness, which becomes particularly clear if only the (alteration-free) glass data are considered. Also shown are the compositional ranges of Shatsky Rise magma types after Sano et al. (2012) and upper mantle (UM). To correct for lateral offset of crust segments by fracture zones, we plot the degree of enrichment against the magnetic chron of the crust segment on which the respective seamounts were emplaced, serving as proxy for lithospheric age and thus thickness.

In contrast to Papanin Ridge, Ojin Rise Seamount lavas range toward higher enrichment of incompatible over less incompatible elements (reaching an OIB signature) and show a stronger depletion of HREEs. This indicates that these seamounts could indeed be formed in an intraplate setting beneath a lithospheric lid by overall lower degrees and higher pressures of partial melting and therefore are likely to represent the hotspot track of the Shatsky plume. The lavas, however, display a wide compositional range pointing to generation beneath variably old/thin lithosphere. If the seamounts were not formed directly at the spreading ridge but on already existing oceanic crust at some distance from the spreading center, their lava chemistry should therefore reflect a stronger lid effect (thicker lithosphere) in the NW and a weaker lid effect toward the SE due to progressively thinner lithosphere closer to the spreading center (e. g., Niu et al., 2011). In fact, we observe that seamount lava chemistry becomes gradually depleted toward the E (Fig. 2a) and greater depletion in HREE (2 b,c).

Based on our new geochemical results, we attempt to reconstruct the formation of late stage Shatsky Rise and the Ojin Rise Seamounts (Fig. 3) by using plate rotation parameters of Matthews et al. (2016) and Wessel and Kroenke (2008): The SW part of Papanin Ridge was formed along the path of the triple junction by drainage of plume material into the northward-retreating triple junction while the plume center was still be somewhere beneath Shirshov Massif (S) (Fig. 3a). After chron M4 (Fig. 3b), the triple junction lost connection with the plume source and the NE part of Papanin Ridge was formed by drainage of plume material into the Pacific-Farallon spreading center. At around 124 Ma (chron M2), the drift of the Pacific plate changed from a southwestern to western direction. This change was accompanied by a significant slowdown of absolute plate motion consistent with the assumed quasi-stationary position of the Shatsky plume center (stem). At latest when large-scale drainage of plume material along the retreating spreading ridge ceased, the emplacement of the Ojin Rise Seamounts on the Pacific plate began in an intraplate setting (Fig. 3c). The initially very slow absolute westward Pacific plate motion allowed a more widespread distribution of upwelling plume material beneath the lithosphere resulting in a scattered cluster of seamounts instead of a narrow hotspot track. With the shift to a more pronounced NW direction and drastic acceleration of plate speed after 118 Ma (Fig. 3d), the overall width of the province progressively narrowed down toward the SE. Consequently, this fast movement rapidly brought the plume stem beneath progressively younger lithosphere consistent with the observed spatial geochemical gradient in the lavas (Fig. 2). It is conceivable that the eventual cessation of the Ojin Rise hotspot track reflects beginning deflection and anew drainage of upwelling plume material into the nearby located Pacific-Farallon spreading center and thus the inception of Hess plateau formation.

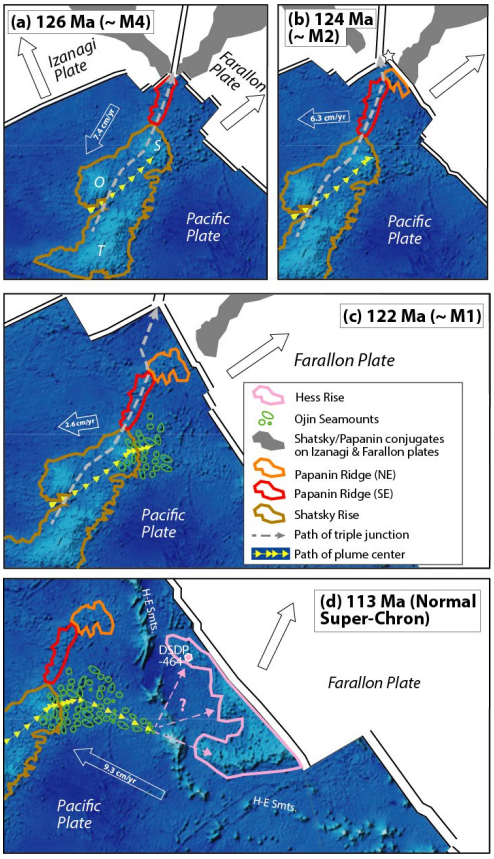

Fig 3: Reconstruction using the GPlates software from Müller et al. (2018) with rotation parameters from Matthews et al. (2016) and Wessel and Kroenke (2008). The motion path of the plume center (pointing in the opposite direction to plate motion) is shown with yellow arrows at 1 m.y. increments starting at 134 Ma near Ori Massif (O).

The recognition of two hotspot tracks and in particular of the Ojin Rise Seamounts as an intraplate hotspot track that is directly linked to Shatsky plateau volcanism both in terms of geochemistry and plate tectonic reconstructions confirms the long-disputed involvement of a mantle plume for the formation of Shatsky Rise.

ACKNOWLEDGMENTS

We thank Captain L. Mallon and his skillful crew on the R/V SONNE for their support. We also appreciate fruitful discussions with T. Sano and M. Tejada. We acknowledge funding of the cruise and this study by the German Ministry of Education and Research (BMBF; 03G0265A to JG, KH and RW).

REFERENCES

Dürkefälden A, Geldmacher J, Portnyagin M, Garbe-Schönberg D, et al. Papanin Ridge and Ojin Rise Seamounts (northwest Pacific): dual hotspot tracks formed by the Shatsky plume, Geochemistry Geophysics Geosystems 2021, 22(9), doi:10.1029/2021GC009847.

Geldmacher J, Hauff F, Werner R, Cruise Report SO265 – Shatsky evolution: evolution of the Shatsky Rise hotspot system, Yokohama (Japan) – Kaohsiung (Taiwan), 26.08.–11.10.2018., GEOMAR Report 2018, N. Ser. 047, 258 pp, doi: 10.3289/geomar_rep_ns_47_2018.

Hofmann A W, Chemical differentiation of the earth: the relationship between mantle, continental crust, and oceanic crust, Earth and Planetary Science Letters 1988, 90(3), 297–314, doi:10.1016/0012-821X(88)90132-X.

Matthews K J, Maloney K T, Zahirovic S, Williams S E, et al. Global plate boundary evolution and kinematics since the late Paleozoic, Global and Planetary Change 2016, 146, 226–250, doi:10.1016/j.gloplacha.2016.10.002.

Müller R D, Cannon J, Qin X, Watson R J, et al. GPlates: building a virtual earth through deep time. Geochemistry Geophysics Geosystems 2018, 19(7), 2243–2261, doi:10.1029/2018gc007584.

Nakanishi M, Sager W W , Klaus A, Magnetic lineations within Shatsky Rise, northwest Pacific Ocean: implications for hotspot-triple junction interaction and oceanic plateau formation. Journal of Geophysical Research 1999, 104(B4), 7539–7556, doi:10.1029/1999jb900002.

Niu Y, Wilson M, Humphreys E R, O'Hara M J, The origin of intra-plate ocean island basalts (OIB): the lid effect and its geodynamic implications. Journal of Petrology 2011, 52(7–8), 1443–1468, doi:10.1093/petrology/egr030.

Sager W W, Sano T, Geldmacher J, Proceedings IODP, 324, Tokyo (Integrated Ocean Drilling Program Management International, Inc.) 2010, doi:10.2204/iodp.proc.324.102.2010.

Sano T, Shimizu K, Ishikawa A, Senda R, et al. Variety and origin of magmas on Shatsky Rise, northwest Pacific Ocean. Geochemistry Geophysics Geosystems 2012, 13(8), doi:10.1029/2012GC004235.

Wessel P, Kroenke L W, Pacific absolute plate motion since 145 Ma: An assessment of the fixed hot spot hypothesis. Journal of Geophysical Research 2008, 113(B6), doi:10.1029/2007jb005499.

SO266/1

Methane hydrate deposits offshore Taiwan – Results from MeBo cores drilled during the R/V SONNE cruise

AUTHORS

MARUM – Center for Marine Environmental Sciences and Department of Geosciences, University of Bremen | Bremen, Germany
G. Bohrmann, T. Freudenthal, S. Mau, T. Pape

GEOMAR Helmholtz Centre of Ocean Research Kiel | Kiel, Germany
C. Berndt, C. Deusner, J. Elger, K. Wallmann

Research Center for Future Earth, National Taiwan University | Taipei, Taiwan
S. Lin

Department of Geosciences, National Taiwan University | Taipei, Taiwan
J.-N. Chen, K.-Y. Chen

Department of Life Sciences, National Chung Hsing University | Taipei, Taiwan
S.-C. Chen, M.-C. Lai

Institute of Oceanography, National Taiwan University | Taipei, Taiwan
T.-T. Chen, L.-F. Fan

Institute of Earth Sciences, Acdemia Sinica | Taipei, Taiwan
W.-C. Chi

Department of Earth Sciences, National Chung Hsing University | Taipei, Taiwan
A. Lin

Department of Oceanography, National Sun Yat-sen University | Kaohsiung, Taiwan
T.-H. Tu

Taiwan Ocean Research Institute, National Applied Research Laboratories | Kaohsiung, Taiwan
P.-S. Yu

The presence of gas hydrates in marine sediments southwest of Taiwan is well known from seismic investigations because widespread distribution of bottom simulating reflectors (BSRs). BSRs were mapped along the passive continental margin south of the Chinese shelf as well as along the active ocean margin of plate convergence. The main goal of the R/V *Sonne* cruise SO266 was to increase our knowledge about gas hydrate occurrence and distribution in sediments southwest of Taiwan. To learn more about hydrate systems and their dynamics at passive and active margins MeBo drillings were performed. We drilled eleven holes at six sites, four holes at the passive margin and seven holes at the accretionary margin. In total 834 m were drilled and 419 m were cored with 83 % recovery. Borehole logging was conducted at five of the eleven MeBo200 deployments. We used a spectrum gamma ray probe that records natural gamma ray intensity and analyses for potassium, uranium and thorium concentrations in the drilled formations. Electrical resistivity was measured using a dual induction probe and the sonic tool was used for measuring p-wave velocity in the formation. Although no direct sampling of gas hydrate specimen were taken hydrate occurrence in the sediments was indicated by several gas hydrate proxies like negative chloride anomalies in the pore water, cold spots detected by infrared thermal scans on cores, changes in resistivity and lithological parameters.

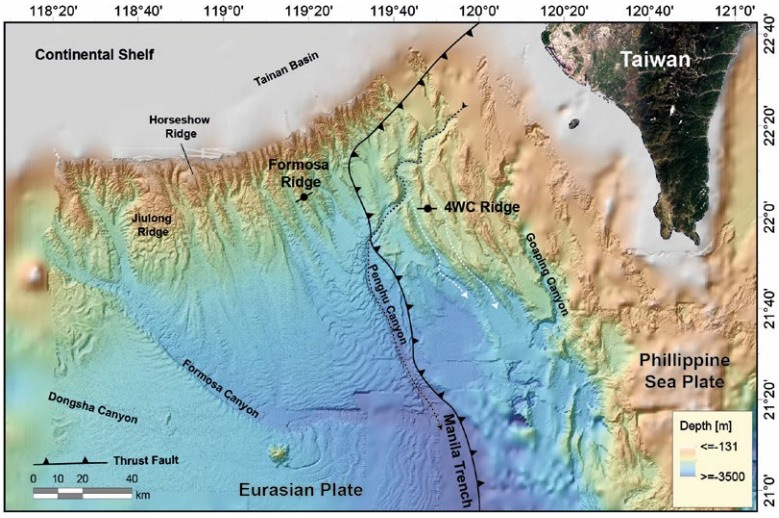

Fig. 1: Bathymetric map of southwest Taiwan. The outer deformation front of the accretionary wedge is also indicated which separates the Eurasian plate in the west from the Phillippine sea plate in the east. Bathymetric information are from multi-beam data of R/V SONNE cruises SO177 and SO266 and GEBCO data.

Four holes were drilled at southern summit of Formosa Ridge (Fig. 1) down to 126 meters below seafloor (mbsf) and recovered homogeneous carbonate-bearing clay as a dominant lithology. Inferred from chloride concentrations of the pore water, low gas hydrate contents were encountered within a shallow depth interval of 15–42 mbsf and

below 100 mbsf. Gas hydrate saturation values between 1–10 % were found at the shallow interval and higher values of up to 38 % at the deep interval are probably related to sealing effect of carbonate nodules which occur between 85–95 mbsf. This interval of carbonate nodules is well expressed in high amplitude reflections of the seismic records and by gamma ray logging data.

Four holes were drilled at Four-Way Closure Ridge (Fig. 1), a typical anticlinal ridge of the accretionary wedge, to reach high amplitude reflectors above the bottom simulating seismic reflector. A maximum drilling depth of 140.40 m was reached, and hydrate presence starts in 65 mbsf continuing down-core with a range of 1–10 % gas hydrate saturation in fine-grained homogenous clay. An abrupt change to higher gas hydrate saturation values of up to 80 % occurs below 109 mbsf where silty and sandy turbidite layers are often intercalated. High gas hydrate contents occur only in the sand layers and not in the fine-grained sediments intercalated to the sand deposits. According to seismic surveys, such sandy turbidites are often found in deeper layers within the gas hydrate stability zone, especially on the eastern flank of the Four-Way Closure Ridge, and form typical high gas hydrate reservoirs which may stay for the entire accretionary wedge southwest of Taiwan.

REFERENCE

Mau, S, Tu, TH, Becker, M, dos Santos Ferreira, C, Chen, JN, Lin, LH, Wang, PL, Lin, S and Bohrmann, G (2020) Methane seeps and independent methane plumes in the South China Sea offshore Taiwan. Frontiers in Marine Science, 7. doi:10.3389/fmars.2020.00543

SO267

ARCHIMEDES – Integrated Geodynamic, Magmatic and Hydrothermal Studies of the Fonualei Rift System, NE Lau Basin

AUTHORS

GEOMAR Helmholtz Centre for Ocean Research | Kiel, Germany
H. Kopp, C. Devey, R. Werner, S. Petersen, P. Brandl, A. Dannowski, F. Schmid, A. Jegen, M. Riedel, I. Klaucke, N. Augustin, M. Rothenbeck, S. Martins, N. Diller, T. Kurbjuhn, S. Lange, F. Petersen, F. Hampel

Federal Institute for Geosciences and Natural Resources | Hanover, Germany
M. Schnabel, U. Barckhausen, M. Engels, I. Heyde, B. Schramm

University of Ottawa | Ottawa, Canada
M. Hannington

Vrije Universiteit Amsterdam | Amsterdam, The Netherlands
A. Beniest

GFZ German Research Centre for Geoscience Helmholtz Centre Potsdam | Potsdam, Germany
M. Weber

University of Ottawa | Ottawa, Canada
M. Engelbert-Stewart

Geological Survey of Canada | Québec, Canada
P. Mercier-Langevin

MOTIVATION AND OBJECTIVES

The research project ARCHIMEDES deals with the geological evolution of an emerging microplate mosaic in the NE-Lau Basin, a region with the fastest growing crust on Earth. The goal was to determine the sequence of events that caused the breakup of an island arc and the associated magmatic-hydrothermal activity. The study area is situated in a unique location where all relevant tectonic processes of crustal growth along convergent plate margins can be observed in their entirety. The research objective was to answer a number of important questions about the crustal growth in complex arc-backarc systems: At what stage of structural and thermal development of the crust is the break-up of the island arc and the formation of spreading centers on the seafloor initiated? What are the

types of faults and what is the role of pre-existing crustal structures? Where are the boundaries of the developing microplates? One objective was to identify and determine the nature of the island arc crust just prior to break-up and to determine how it influences the formation and rifting. In doing so, our investigations confirm the early hypothesis for the development of the Lau Basin as a dense mosaic of microplates.

INTEGRATED GEOPHYSICAL, GEOLOGICAL AND GEOCHEMICAL STUDIES

During cruise SO267 a total of 110 stations were performed, including 146 ocean bottom seismometer (OBS) and ocean bottom magnetotelluric (OBMT) stations. The seismic program included 9 profiles (1,065 km of multi-channel seismic and 673 km of refraction seismic data) with more than 25,000 shot points by a 84 l source array. The multichannel seismic reflection (MCS) data were acquired using a 3,900 m active cable and a fixed shot point distance of 50 m. The geophysical program was complemented by 8 AUV dives (910 line-km), 41 dredges, and 21 heat flow and 6 gravity core stations on the same sections. During the geologic mapping, more than 46,600 km^2 were surveyed using high-resolution multibeam and backscatter data. Approximately 500 samples of igneous and sedimentary rocks, including samples of island arc crust, of volcanic cones near the island arc front, from volcanic ridges and volcanic edifices on young ocean crust, as well as from older backarc crust, were collected. The faults and the crustal structure were investigated at the southern end of the Fonualei Rift Spreading Center (FRSC), at the overlap between the FRSC and the Mangatolu Triple Junction (MTJ), as well as in the intraplate region between the FRSC and the Central Lau Spreading Center (CLSC). These areas were each investigated by a combination of seafloor mapping and sampling along with multiparameter geophysical surveys and seismic reflection and refraction imaging to decipher the architecture of the rifting process and the nature of the underlying mantle. Our investigations suggest a rather diffuse plate boundary between the southern tip of the FRSC and the CLSC, and a northward progression of the FRSC, overtaking the eastmost arm of the MTJ here. Our geologic mapping in this region shows that the Northeast Lau Spreading Center (NELSC) is forming a new triple junction. The scenarios have consequences for mantle flow, the composition of island-arc volcanoes and the magmatic and hydrothermal budget of the growing Niuafo'ou microplate, which has been verified by extensive rock sampling and geochemistry studies. These results have important implications for the understanding of crustal growth processes in ancient greenstone belts, including the distribution of deposits.

DEEP CRUSTAL STRUCTURE

The internal structure of the deforming backarc crust of the northern Lau-Basin was investigated using combined 2D reflection and refraction seismic data with acquired potential field data, geologic mapping, and petrologic results. All MCS lines have been processed up to post-stack time migration. Due to the cable length the resulting seismic velocities allowed for reliable depth conversion of the seismic sections. The imaging of the median valley of the southern FRSC demonstrates that it is characterized by a mixture

of extrusive mounds and tilted sedimentary strata. It does not resemble a classical spreading center. These findings show that the formation of the FRSC was a result of tectonic extension in combination with unfocussed extrusive magmatic activity. The northern part around MTJ shows a broader central valley, characterized by small sedimentary basins in combination with horst and graben structures. The southern part of the northern Lau Basin shows no recent plate boundary within the seismic images. These observations let us conclude that the northern Lau Basin is underlain by one single Niuafou'ou-Tonga microplate, which is in the stage of crustal rifting within its northern part.

Large parts of the region are characterized by buried faults within the lower sedimentary layers, while recently active faults are mainly found along the branches of the MTJ and along the FRSC. This points to a two-stage evolution of the northern Lau Basin: an earlier phase of extension was distributed over a broad region, while recent extension is focussed along the central rift structures MTJ and FRSC. A joint assessment of sediment thicknesses and crustal ages deduced from magnetic Chrons shows that the transition between the broad and narrow rifting should have taken place at around 1.85 Ma.

Results of a P-wave tomography model and a density model suggest that crustal accretion within the southern FRSC occurs through a combination of extension of the island arc crust and magmatic activity (Schmid et al., 2020). The absence of magnetic reversals within the FRSC supports this, and suggests that the formation of new ocean crust by seafloor spreading has not yet contributed to crustal accretion. The backarc crust that forms the southern Niuafo'ou microplate has a heterogeneous structure that includes several crustal blocks. However, some regions have a crustal structure that resembles typical oceanic crust, suggesting that they were formed by seafloor spreading. Other crustal blocks have a structure that resembles the crust of a volcanic arc or a "hydrated" oceanic crust formed in a spreading center under the influence of water from the subducted plate. Throughout the backarc region, a lower crust with high velocity (Vp 7.2–7.5 km^{-1}) was found, indicating magmatic accretion of crustal material on the underside of the plate, probably supported by elevated upper mantle temperatures in this region. The origin of the seismicity within the rift and the interaction of magmatism and tectonics during its early evolution into the backarc spreading zone were investigated by Schmid et al. (2021) using a 32-day OBS deployment that recorded microearthquakes in the Southern Fonualei Rift spreading center (S-FRSC). The majority of the epicenters were concentrated along the central part of the axial valley that marks the active ridge axis. Few events were associated with the prominent faults that border the axial valley. About 450 events are concentrated around 17°42′S and show a strong similarity in their waveforms. Most of these events were associated with a 138 hour-long earthquake swarm. The recorded earthquake swarm was located at the transition between two segments, indicating that this activity is mainly tectonic in nature. Global teleseismic data were combined with a kinematic analysis of mapped seafloor structures to identify directions in motion along the main structures in different parts of the Lau Basin (Baxter et

al., 2020). Despite the regional extent, it was found that the majority of the seismic events occur along large transcurrent faults rather than on normal faults. The relevant moment tensors (CMTs), which were determined for large (Mw> 5), shallow (<30 km) seismic events were compared with the orientations

of lineaments on the seafloor mapped using ship-based echosounder data and satellite altimetry data. By matching the possible focal planes of the CMTs with the orientations of the lineaments, the most likely solutions of the fault planes were determined and thus the highly variable stress regime in the basin was constrained.

VOLCANIC ACTIVITY

Brandl et al. (2020) investigated the recent volcanic activity near the FRSC, which occurred immediately after cruise SO267. In August 2019 a large pumice raft appeared as the surface expression of a submarine volcanic eruption in the study area. Reconstructing the drift path of the pumice raft with the help of satellite imagery pointed to volcano "F" in the Tofua arc NW of the island of Vava'u as the most likely source. Volcano F is a large volcanic complex at the southern tip of FRSC. ESA's Sentinel-2 satellite has detected the onset of the submarine eruption on August 6, 2019, and the subsiding of the eruption on August 8, followed by observations of the drifting pumice raft through August 14. The start time is consistent with T-phase records at seismic stations on the island of Niue and Rarotonga, as well as the signal delay time of 733 s between the two stations with an origin at or near volcano "F". Before the eruption, a series of earthquakes was recorded in the vicinity of volcano "F". The series began on August 5 with an M_b 4.7 event, followed by at least six shallow earthquakes (M_b >3.9) on August 6. On August 8, a >136.7 km^2 raft of pumice appeared at the sea surface. The modeled minimum volume of 8.2-41.0*10^6 m^3 corresponds to 2.5-12.3*10^6 m^3 of dense rock. The results confirmed that the eruption of volcano "F", despite its location on the island arc front, occurred in an area of local extent. The volcano also shows geochemical differences with the neighboring Fonualei and Late island arc volcanoes. The basal diameter of the volcanic field is >50 km with a large central caldera measuring 8.7 x 6 km with a floor at ~700 m water depth. The top of the post-caldera cone complex had a summit depth of 35 m below sea level in 2004. The volcanic morphology of the volcano and two documented eruptions (2001 and 2019) indicate a highly active volcanic system that warrants future investigation and monitoring.

REFERENCES

Baxter A, Hannington M, Stewart M, et al. Shallow seismicity and the classification of structures in the Lau back-arc basin. Geochemistry Geophysics Geosystems 2020, 21(7), e2020GC008924, 1–25, doi:10.1029/2020GC008924.

Brandl P, Schmid F, Augustin, N, et al. The 6–8 Aug 2019 eruption of 'Volcano F' in the Tofua Arc, Tonga, Journal of Volcanology and Geothermal Research 2020, 390:106695, 1–9, doi:10.1016/j.jvolgeores.2019.106695.

Schmid F, Kopp H, Schnabel M, et al. Crustalstructure of the Niuafo'ou microplate and Fonualei Rift and Spreading Center in theNortheastern Lau Basin, southwestern Pacific, Journal of Geophysical Research 2020, 125, e2019JB019184, 1–21. doi:10.1029/2019JB019184.

Schmid F, Cremanns M, Augustin N, et al. Microseismicity and lava flows hint at magmato-tectonic processes near the southern tip of the Fonualei Rift and Spreading Center in the Lau Basin, Journal of Geophysical Research 2021, 126, e2020JB021340, 1–36. doi: 10.1029/2020JB021340.

SO267/2

On the road across the Pacific with underway measurements

AUTHORS

Institute for Chemistry and Biology of the Marine Environment, Carl von Ossietzky University | Oldenburg, Germany
O. Zielinski, D. Voß

GEOMAR Helmholtz Centre for Ocean Research Kiel | Kiel, Germany
T. Browning

Max-Planck-Institute for Meteorology | Hamburg, Germany
S. Kinne

The transit cruise SO267/2 of RV SONNE from Suva (Fiji) to Manzanillo (Mexico) involved underway and in-situ measurements that were conducted within the framework of the three projects (i) OceanLight (ICBM), (ii) MORE-1 (MPI-M) and (iii) EqPac co-Limit (GEOMAR). Within a transit cruise of 16 days', with short stops for station work, various underway measurements were performed in international waters across the Pacific Ocean.

OCEANLIGHT

In general, natural light in the ocean is an essential climate variable useful in understanding dynamics, processes and proxy status of biogeochemical and physical variables that possess an optical signature (Garaba and Zielinski, 2013; GCOS, 2011). Natural light in the ultra-violet to visible spectrum is an important source of energy to heat the land and the sea driving the global atmospheric and ocean currents, photosynthesis hence aquatic primary production and it influences health and behavior of the regional to global aquatic biome (Kirk, 2011). Arising from this, also natural water bodies and their constituents are strongly influenced by light abundance. Integral understanding of light interactions is a key element to understand and predict environmental processes in aquatic ecosystems (Dickey et al, 2011). Utilizing the interactions of light with water constituents via optical sensors enables an assessment of spatial, temporal as well as spectral variability of optical properties and proxies that are associated to them (Moore et al. 2009; Zielinski et al. 2009). The Pacific Ocean is among some of the most oligotrophic waters in the world (Bricaud et al., 2010; Claustre and Maritorena, 2003; Morel et al., 2007). Although optical properties in the open ocean have been extensively studied and robust algorithms to predict the inherent bio-optical status are available, little is known about remote zones of the Pacific Ocean biome (Claustre and Maritorena, 2003; Tedetti et al., 2010).

The focus of the OceanLight project was set on shipborne ocean color remote sensing. It aimed to determine the above- and underwater light field in the Pacific Ocean for bio-optical algorithm development, validation and calibration relevant to ocean colour remote sensing. These observations can help to support satellite remote sensing and act as point references. To address how is the light propagated in the UV to visible spectrum the underwater light field was examined at stations by using a hyperspectral HyperPro II light profiler to collect apparent and inherent optical properties, combined with a shipborne set of five hyperspectral radiometers for underway data. Data collected on the cruise SO267/2 will be combined with previous cruises with RV Sonne across the Pacific for detailed analyses related to optical properties of the Pacific Ocean. The underwater light field was already examined on SO245, SO248, and SO254. Processing of data include the implementation of quality control methods for hyperspectral underwater light field data and the calculation of optical ocean variables, e. g. diffuse attenuation coefficient (Kd), Forel-Ule index (FUI), Secchi depth (SD). A second focus of the project was to assess the performance of the underway flow-through measuring system integrated on board RV SONNE. Reference sensors and samples were taken in defined intervals to investigate the performance of the new integrated system.

EQPAC CO-LIMIT

Phytoplankton, photosynthetic microbes, are the base of marine food webs and sequester atmospheric carbon. Nutrient availability regulates growth rates of marine phytoplankton globally. Recent work has shown that multiple nutrients can 'co-limit' phytoplankton, but the distribution, causative mechanisms, and biogeochemical impacts of co-limitation are poorly constrained. The transit cruise SO267/2 across the Equatorial Pacific crossed strong gradients in availability of the growth-limiting nutrients, nitrogen and iron.

The EqPac co-Limit project integrated experimental, proteomics and fluorescence approaches to resolve nutrient co-limitation of phytoplankton productivity in the Equatorial Pacific. Therefore, continuous surface samples were taken underway via Towfish and analysed for dissolved macronutrient (nitrate / phosphate / silicate) concentrations, trace element concentrations, phytoplankton pigment composition, phytoplankton cell counts, particulate organic carbon (POC/N), biogenic silicate, chlorophyll-a concentrations, and active fluorescence physiological measurements. Five 48 hour duration on-deck incubation experiments were carried out in 1L trace-metal-clean Nalgene polycarbonate bottles, following protocols described in Browning et al. (2017).

MORE-1

Atmospheric data for aerosol, trace-gases and clouds were collected to address the need for atmospheric reference data over oceans. Scientists from different research institutes and universities operated a suite of remote sensing instruments. Using the sun and the sky as background, atmospheric properties can be determined at higher accuracy than by satellite remote sensing. Especially over the Pacific reference data are sparse, yet they are needed for evaluations of satellite retrievals and global models. During the transit,

data were collected via several sun-photometers (for aerosol and water vapor properties), via three differential absorption spectrometers (for trace-gas data) and via ceilometer and cloud camera system (to capture the properties of clouds). In addition, recorded ocean-floor data in international waters were processed and prepared for the data-base of the SEABED 2030 initiative.

Sun-photometers inform during the day, when the sun is not obscured by clouds on aerosol amount, on typical aerosol size and on water vapor content. Sampled data with the calibrated MICROTOPS instruments of the Maritime Aerosol Network, (MAN, Smirnov et al, 2009, 2011) were e-mailed each evening to the corresponding database and were immediately visualized. Daily AOD averages (for atmospheric aerosol amount) of the SO267/2 transit are presented in Figure 1.

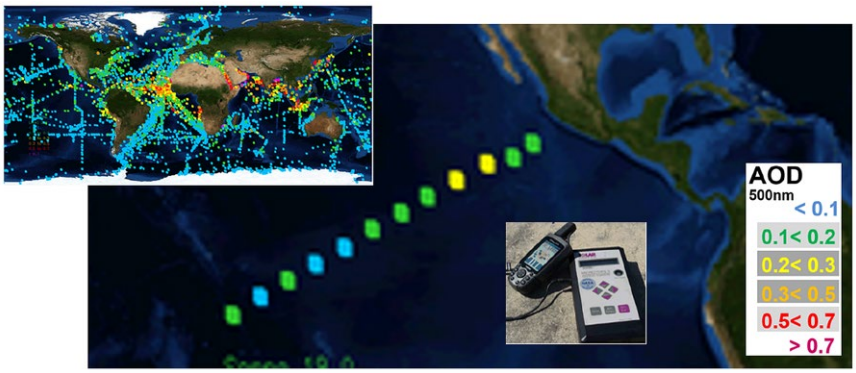

Fig. 1: daily AOD averages during the SO267/2 cruise in the context off all shipborne samples contributed to the MAN data-base over the last 18 years (left, upper corner).

In a general aerosol data application, all ship-borne (MAN) and land-based (AERONET) data were statistically (monthly and 1x1 degree lat/lon binned) processed to improve the MAC global aerosol climatology (Kinne 2019a). And in turn this updated MAC climatology was processed in an off-line radiative transfer scheme to revise aerosol radiative effects and to update likely aerosol climate impacts (Kinne 2019b).

Sky-spectrometers extract near surface trace-gas concentration profiles and atmospheric totals via the combined use of samples at different elevations above the horizon. Two MAX-DOAS (Multi-AXis Differential Optical Absorptions Spectrometer) instruments and a Pandora instrument offered data redundancy. As an example, NO_2 samples are compared to TROPOMI satellite retrievals and TM5 model data (Wang et al., 2020) in Figure 2.

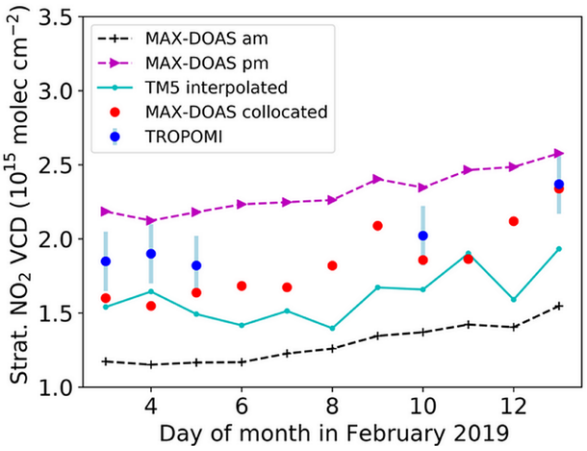

Fig. 2: Time-series of NO_2 vertical column densities during the SO267/2 transit cruise. Sampled MAX-DOAS data are presented for the morning (AM), for the evening (PM) and most importantly (in red) for the early afternoon TROPOMI satellite overpass. TROPOMI satellites retrievals (blue) with uncertainties were only available at cloud-free days. TM5 represents simulations with the TM5 global model.

A cloud camera system and a ceilometer provided continuously data on cloud cover. In summary Figure 3, cloud cover and cloud base statistics illustrate the most intense tropical convection well north (6-8N) of the equator.

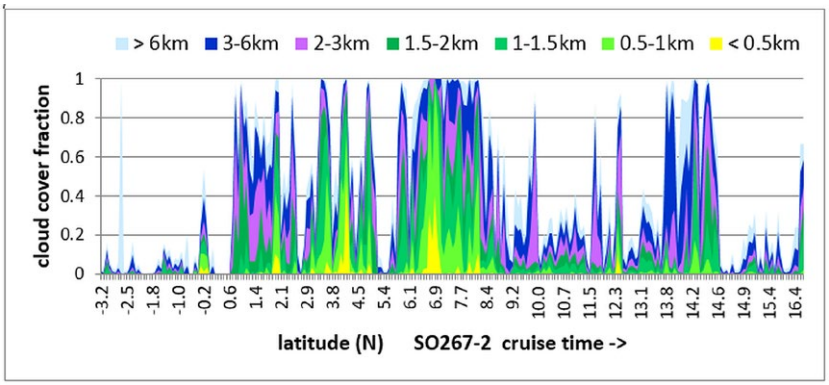

Fig. 3: Hourly averages of cloud cover fraction as function of the cruise track by the thermal camera images. Cloud fractions are presented as function of cloud-base altitude-regimes, according to the color scale. Cloud-free fractions are in white.

REFERENCES

Bricaud A, Babin M, Claustre H, Ras J, et al. Light absorption properties and absorption budget of Southeast Pacific waters: Journal of Geophysical Research: Oceans, 2010, v. 115, no. C8, p. C08009, doi:10.1029/2009jc005517.

Browning, T.J., Achterberg, E.P., Rapp, I., Bertrand, E.M., Engel, A., Tagliabue, A., & Moore, C.M. Nutrient co-limitation at the boundary of an oceanic gyre. Nature, 550, 242–246 (2017).

Claustre H, Maritorena S, The many shades of ocean blue: Science, 2003, v. 302, no. 5650, p. 1514–1515, doi:10.1126/science.1092704.

Dickey T D, Kattawar G W, Voss K J, Shedding new light on light in the ocean, Phys. Today, 2011, 64(4), 44–49.

Garaba S P, Zielinski O, Comparison of remote sensing reflectance from above-water and in-water measurements west of Greenland, Labrador Sea, Denmark Strait, and west of Iceland: Optics Express, 2013, v. 21, no. 13, p. 15938–15950, doi:10.1364/OE.21.015938.

GCOS, The Global Climate Observing System – Systematic Observation Requirements for Satellite-based Data Products for Climate: 2011 Update GCOS-154 (pp. 138), 2011, World Meteorological Organization – Geneva, Switzerland.

Kinne, S., The MACv2 Aerosol Climatology, Tellus B: Chemical and Physical Meteorology, 2019a, 71, 1, 1–21.

Kinne, S., Aerosol radiative effects with MACv2, ACP 19, 2019b, 10919–10959.

Kirk J T O, Light and photosynthesis in aquatic ecosystems, Cambridge, United Kingdom, Cambridge University Press, 2011, 662 p.

Moore C, Barnand A, Fietzek P, Lewis M, et al. Optical tools for ocean monitoring and research. Ocean Science, 2009, 5, pp 661–684, doi:10.5194/os-5-661-2009

Morel A, Gentili B, Claustre H, Babin M, et al. Optical properties of the "clearest" natural waters: Limnology and Oceanography, 2007, v. 52, no. 1, p. 217–229

Smirnov, A., et al., Maritime aerosol network as a component of AERONET – first results and comparison with global aerosol models and satellite retrievals, Atmos. Meas. Tech., 2011, 4, 583–597.

Smirnov, A., et al., Maritime Aerosol Network as a component of Aerosol Robotic Network, J. Geophys. Res., 2009, 114, D06204, doi:10.1029/2008JD011257.

Tedetti M, Charrière B, Bricaud A, Para J, et al. Distribution of normalized water-leaving radiances at UV and visible wave bands in relation with chlorophyll a and colored detrital matter content in the southeast Pacific: Journal of Geophysical Research: Oceans,

2010, v. 115, no. C2, doi:10.1029/2009JC005289.

Wang, P., et al., Shipborne MAX-DOAS measurements for validation of TROPOMI, Atmos. Meas. Tech., 2020, 1413–1426.

Zielinski O, Busch J A, Cembella A D, Daly K L, et al. Detecting marine hazardous substances and organisms: sensors for pollutants, toxins, and pathogens, Ocean Science, 2009, 5, pp 329–349, doi:10.5194/os-5-329-2009.

SO268

NoduleMonitoring – Assessing the impacts of nodule mining on the deep-sea environment

AUTHORS

GEOMAR Helmholtz Centre for Ocean Research Kiel | Kiel, Germany
M. Haeckel, P. Linke

OBJECTIVES

The JPI Oceans project MiningImpact consists of thirty partners from nine European countries and The International Seabed Authority (ISA). The project aims at assessing the environmental risks and impacts of polymetallic nodule mining in the deep sea. The main objective is to provide the scientific basis and recommendations for the "Regulations on Exploitation of Mineral Resources in the Area" drafted by the ISA.

In the second phase, the project's fieldwork focused on developing and conducting an independent scientific monitoring programme around the first industrial test of a pre-prototype collector system for polymetallic nodules by the Belgian company DEME-GSR. Originally, the tests had been planned for April 2019, but were aborted by DEME-GSR due to a technical failure of the umbilical cable of the collector system. Therefore, the work plan of SO268 had to be adjusted while the first leg was already ongoing. Instead of being able to conduct the monitoring of the collector test, extended baseline investigations of the designated trial sites and corresponding reference sites in the German and Belgian contract areas for polymetallic nodule exploration in the Clarion-Clipperton Zone (CCZ) in the Northeast Pacific were conducted. In addition, the sensor equipment for sediment plume monitoring was tested in a small-scale dredge experiment and a restoration experiment with artificial hard substrates for the recolonization of nodule-associated fauna was initiated.

Finally, in April to May 2021 DEME-GSR has carried out the intended tests of the nodule collector vehicle PATANIA II in the CCZ. MiningImpact partners conducted the monitoring of the tests and first post-impact studies from the commercial vessel Island Pride, which was chartered by the project partner BGR for this purpose.

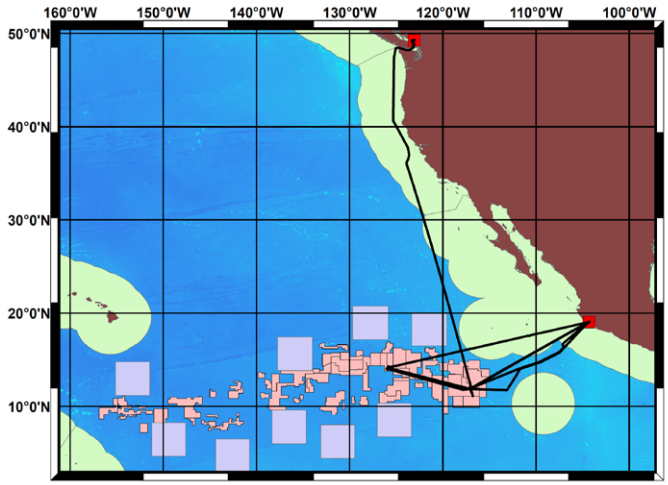

Fig. 1: Map of the Northeast Pacific Ocean showing the cruise track of SO268 (black lines), the harbours Manzanillo and Vancouver (red squares), the exploration license areas for polymetallic nodules in the CCZ (red areas) issued by the ISA and the Areas of Particular Environmental Interest (APEI, purple squares) as well as the Exclusive Economic Zones of neighbouring countries (EEZ, green areas).

STUDY SITES

The working areas of SO268 are located in the "Prospective Area #1" of the German contract area and in the B4S03 area of the Belgian contract area for polymetallic nodule exploration. In both working areas a collector trial and impact site were selected based on available pre-existing information, such as bathymetry, nodule size and abundance on the seabed as well as biological and biogeochemical data that indicated the possibility to have a suitable reference site nearby. While the German trial site exhibits a rather smooth terrain with slopes of 0–3° in water depths of 4080–4130 m and small nodules of typically less than 4 cm in size with an abundance of 20–26 kg/m^2 of wet weight (BGR, 2018), the Belgian trial site exhibits a rougher terrain with slopes of up to 3–7° in water depths of 4450–4530 m and nodule sizes of more than 4 cm with an abundance of 20–24 kg/m^2 of wet weight (GSR, 2018).

The reference sites were selected based on the following criteria: (i) data from previous years are available, (ii) these data indicate that they are representative for the ecosystem and environment of the trial sites, and (iii) they are located at sufficient distance and direction from the trial sites and will likely not be impacted by the collector trial, i. e. the suspended sediment plume.

The site of the small-scale dredge experiment (Dredge Site) in the German working area was chosen in an area that had been sampled on previous cruises and in sufficient distance from the trial and reference sites to avoid any impact on them. The Dredge Site exhibits a smooth topography with a few highs and lows (4115–4125 m water depth). It is located slightly north of the SO239-24-EBS track.

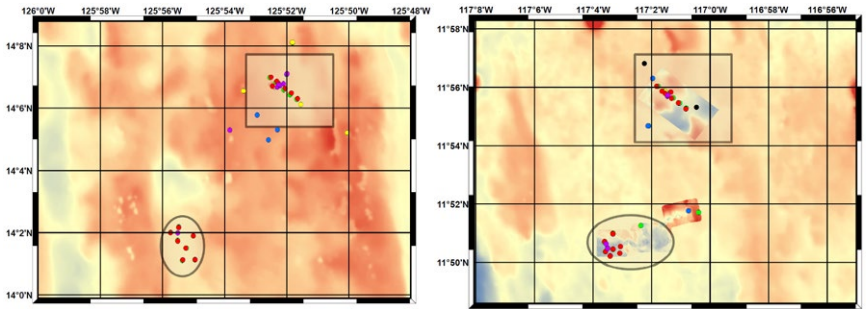

Fig. 2: Overview maps of the Belgian (left) and German (right) working areas showing the locations of the Reference Sites (ellipse) and Trial Sites (square), plotted on ship-based and AUV-based multibeam bathymetric data.

RESULTS

While leg 1 was dedicated to acquiring detailed environmental baseline data in the designated collector trial and reference sites, leg 2 focused on executing and sampling of the small-scale dredge experiment. The work comprised oceanographic, biological, microbiological, biogeochemical, and geological investigations, which required the deployment of a variety of seagoing equipment. ROV Kiel 6000 was used for sampling of sediments, nodules, and benthic fauna as well as carrying out in situ measurements and experiments. High-resolution multibeam data of the seafloor and video/photo surveys of the manganese nodule habitat was acquired with AUV Abyss and ROV Kiel 6000. Additional photo surveys were conducted with the OFOS system. Benthic landers and moorings equipped with acoustic and optical sensors were deployed for measurements of physical and chemical oceanographic variables. Several coring devices (i. e., box corer, gravity corer, TV-guided multiple corer, ROV-operated push cores) were used to collect sediment samples for biological, geochemical, and microbiological analyses. A CTD rosette water sampler, in situ pumps, and a bottom water sampler sampled the water column. The spatial and temporal spread of the sediment plume suspended during the dredge experiment was monitored by an array of intercalibrated acoustic and optical sensors on fourteen platforms, which were placed on the seafloor by ROV.

The research has documented that abyssal nodule ecosystems show unrivalled high biodiversity in combination with high spatial variability of sessile and mobile faunal populations and environmental variables. The BGR and GSR areas are considerably different from each other with respect to faunal densities and epifauna communities as well as biogeochemical and microbiological variables, whereas reference and trial sites in each area show sufficient similarities to be suitable for the purpose of impact assessments.

REFERENCE

Bundesamt für Geowissenschaften und Rohstoffe (BGR), Environmental Impact Assessment for the Testing of a Pre-protoype Manganese Nodule Collector Vehicle in the Eastern German License Area (Clarion-Clipperton Zone) in the Framework of the European JPI-O MiningImpact 2 Research Project, 2018, Hannover, Germany, 209p.

Global Sea Mineral Resources (GSR), Environmental Impact Statement: Small-scale Testing of Nodule Collector Components on the Seafloor of the Clarion-Clipperton Fracture Zone and its Environmental Impact, 2018, ISA_EIA_2018_GSRNOD2019, Zwijndrecht, Belgium, 337p.

SO268/3

MICRO-FATE – Characterizing the Fate and Effects of Microplastic Particles between Hotspots and Remote Regions in the Pacific Ocean

AUTHORS

Fraunhofer-Gesellschaft, Institute for Ceramic Technologies and Systems (IKTS) | Dresden, Germany
A. Potthoff

Helmholtz Centre for Environmental Research - UFZ | Leipzig, Germany
S. Wagner, T. Reemtsma, M. Schmitt-Jansen, K. Wendt-Potthoff, A. Jahnke

Leibniz-Institute for Baltic Sea Research Warnemünde (IOW) | Rostock, Germany
S. Oberbeckmann

INTRODUCTION

Plastic pollution of the environment is ubiquitous, and particularly the World's oceans are heavily impacted (MacLeod et al. 2021). Both modeling exercises (e. g., Maximenko et al. 2012) and first field measurements (e. g., Egger et al. 2020) indicated that the North Pacific Ocean includes one of the largest accumulation areas of marine plastic pollution world-wide, the so-called North Pacific Garbage Patch. Comprehensive field data from the sea surface as well as from deeper regions (water column, sediment) were lacking, so far. Hence, the MICRO-FATE project set out to investigate the transport, fate and potential effects of plastic in the North Pacific Ocean, covering the predicted centre of the North Pacific Garbage Patch and background regions with expected lower levels of plastic pollution. The transit SO268/3 of the R/V SONNE from Vancouver, Canada to Singapore (Figure 1) between May 30 and July 5, 2019, offered ideal conditions for collecting material and data needed for answering the research questions of the MICRO-FATE project.

Fig. 1: Weathered sample collected on expedition SO268/3.

BACKGROUND

Despite high research activities on the occurrence, fate and effects of plastic debris in marine environments, field data is still scarce, in particular covering subsurface layers that in many cases extend to several thousand meters of depth. This presentation gives an overview of the research outcomes of our interdisciplinary project MICRO-FATE that aimed at characterizing the fate and effects of field-aged plastic particles (macro, micro, nano) in hotspots and other regions of the North Pacific Ocean. Specifically, we addressed (i) visual inspection, collection, identification and characterization of plastic particles from the sea surface, water column and deep sea sediments, (ii) their weathering, fragmentation and aggregation that impacts its transport and fate, (iii) sorption and leaching of chemicals to/from the plastic material that makes it either a sink or source of chemicals to the surrounding medium, and (iv) biofilm growth on the particle surface. Taken together, these research topics provide contributions to the current understanding of the transport, fate and potential effects of plastic debris in the marine environment.

MICRO-FATE RESEARCH

We present an overview of MICRO-FATE, with a focus on the topics above: (i) Plastic particles have been collected at the surface using a neuston catamaran and with continuous sampling from a cascade filtration unit, from the water column using *in situ* pumps and from the seabed using a multiple corer to collect sediments. Our current data supports the expected elevated concentrations in the Great Pacific Garbage Patch. (ii) In addition to field-weathered material, we also performed on-board weathering experiments with pristine and pre-weathered polymer samples in mesocosms under flow-through conditions with local seawater, either exposed to solar radiation or covered as dark

controls. Our assessments indicate that weathering effects were detectable already during the 4-week exposure period. (iii) For the assessment of organic pollutants, we collected floating macro-litter and surface sediment and enriched pollutants from large volumes of water (60–100 L) from the surface and the water column on solid-phase extraction sorbent, which allowed for dozens of chemicals to be detected whereas the sediments seem to be rather unpolluted. Bioanalytical assessment of the mixtures of chemicals complements this data set. (iv) Biofilms from the surface of floating plastic debris were collected, submitted to structural and functional analyses, characterized using confocal laser scanning microscopy and cultivated to investigate the "plastisphere" which has allowed for the identification of several organisms and their lifestyles. Many of these have been found to be associated with marine plastic before by culture-independent methods. Furthermore, the early colonization stages from the mesocosm experiment have been investigated.

(I) DISTRIBUTION OF PLASTIC IN THE NORTH PACIFIC OCEAN

As part of the visual inspection of the sea surface while steaming, a so-called Litter Survey supported by a large team of scientists on board, we described the distribution of large floating plastic items (>5 cm) at the sea surface along the track of R/V SONNE on SO268/3. It represents the largest coverage area to date in the North Pacific and confirmed the model predictions. In addition, it indicates another accumulation area in the Western North Pacific Ocean (Figure 2). These data are complemented by the detailed plastic particle identification and quantification performed in samples collected with catamaran nets deployed at the stations, amongst others, with samples from the deeper water layers and the sediments under analysis.

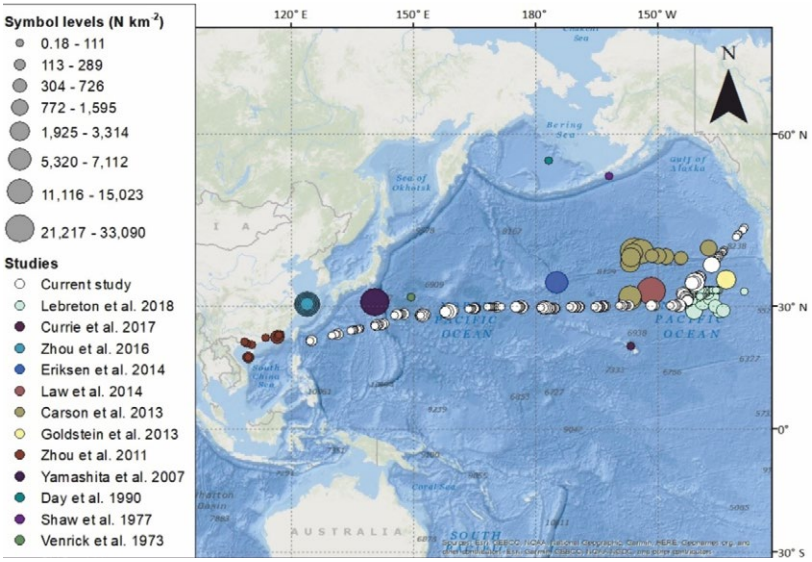

Fig. 2: Outcomes of the Litter Survey conducted on SO268/3.

(II) PARTICLE CHARACTERIZATION – KEY FOR UNDERSTANDING PLASTIC FATE

How fast do the properties of plastics change due to weathering processes, and how does this process impact its fate? How long has the collected plastic litter been travelling in the ocean? – Answering these questions requires bridging the gap between analysis in the lab and in the real environment, i. e., between short- and long-term weathering. Two approaches were followed: (i) We set up two mesocosms on deck of RV SONNE representing weathering processes close to the water surface (with UV exposure) and in the depth (w/o UV light) in which we exposed both well-defined polymer samples (partly pre-weathered) and a consumer product during the expedition. First changes of surface properties were detectable within a few days. (ii) Field-weathered plastics like canisters were collected, and in a few cases, we could purchase the corresponding new product. To find the link between complex long-term weathering in the field and short-term artificial weathering experiments in the lab, the new product is investigated. Advanced characterization including spectroscopic methods, X-Ray Tomography, contact angle measurement etc. was applied to observe chemical and physical changes. In particular Scanning Electron Microscopy (SEM) images offered a deeper look into the weathered coating and might become a valuable tool to roughly estimate timelines of the weathering process.

(III) PLASTICS – SOURCE OR SINK OF POLLUTANTS TO THE NORTH PACIFIC OCEAN

We seek to answer the following questions: What are the levels and patterns of pollutants in the surface seawater, at greater depths in the water column and in the sediment from the SONNE transit SO268/3? Does plastic litter aged in the marine environment show higher effects in cell-based bioassays (Rummel et al., 2019) and organism-based assays (Rummel et al., accepted) than the corresponding original material? Can we simulate environmental weathering artificially in the laboratory? Does the relevance of different endpoints vary over time and location, and how much of the observed effects can we explain by the detected chemicals? Our hypothesis was that sorbed chemicals and the degrading plastic from the North Pacific show higher effects than the original new product since we expect a highly diverse chemical mixture being sorbed from the water phase compared to a less substantial fraction of chemicals added during manufacturing. The results indicate that we can observe both phenomena, i. e., higher effects in the new vs. field-weathered items or the other way around, depending on the type of product and the investigated endpoint and/or pollutant. The identified chemicals are then linked to the observed effects by means of so-called iceberg modelling to determine the fraction of the total effect explained by the measured chemicals.

(IV) THE ‘ PLASTISPHERE’ – MICROBIAL CONSORTIA COLONIZING THE PLASTIC

We could show that biofilms, consortia composed of microalgae, bacteria, fungi and meiofauna embedded in a matrix of extracellular polymeric substances colonize on

environmental plastic within minutes to hours after a conditioning film was built (Rummel et al., 2021). Therefore, we asked the questions what plastic-related and environmental parameters shape the formation of biofilms on plastic surfaces. Community structural analysis based on amplicon sequencing (16/18S and ITS) revealed no differences of communities between plastic types (PP and PE) but clear differences to the pelagic microbial communities indicating plastic being a new habitat in the pristine areas of the North Pacific Ocean. Functional analysis (primary production) of the biofilms revealed comparable rates between different plastic fractions and P/R ratios close to zero.

ACKNOWLEDGEMENT

The MICRO-FATE team kindly acknowledges support and collaboration with additional scientists from the Alfred-Wegener-Institute Helmholtz Centre for Polar and Marine Research (AWI: M. Bergmann, M.B. Tekman) and Senckenberg Institute (SaM: G. Veit-Köhler, P. Martínez).

REFERENCES

Egger M, Sulu-Gambari F, Lebreton L. First evidence of plastic fallout from the North Pacific Garbage Patch. Scientific Reports 2020, 10, 7495 DOI: 10.1038/s41598-020-64465-8

MacLeod M, Arp HPH, Tekman MB, Jahnke A. The global threat from plastic pollution, Science 2021, 373, 61 DOI: 10.1126/science.abg5433

Maximenko N, Hafner J, Niiler P. Pathways of marine debris derived from trajectories of Lagrangian drifters. Marine Pollution Bulletin 2012, 65, 51 DOI: 10.1016/j.marpolbul.2011.04.016

Rummel, C.D. et al. (2019). 'Effects of Leachates from UV-Weathered Microplastic in Cell-Based Bioassays', Environ. Sci. Technol,. 53, pp. 9214-9223. doi: 10.1021/acs.est.9b02400.

Rummel C.D., Lechtenfeld O.J., Kallies R., Benke A., Herzsprung P., Rynek R., Wagner S., Potthoff A., Jahnke A., Schmitt-Jansen M. (2021) Conditioning film and early biofilm succession on plastic surfaces. Environ. Sci. Technol., 55, pp. 11006–11018. doi: 10.1021/acs.est.0c07875.

Rummel C.D., Schäfer H.,Arp HP., Jahnke A., Schmitt-Jansen M. (accepted). Effects of leachates from UV-weathered microplastic on the microalgae Scenedesmus vacuolatus. Analytical and Bioanalytical Chemistry.

SO269

South China Sea-natural laboratory under climatic and human induced stress

AUTHORS

Leibniz Institute for Baltic Sea Research | Warnemünde, Germany
J.J. Waniek, C. Deich, K. Fisch, D.E. Schulz-Bull

Institute for Geology, University Hamburg | Hamburg, Germany
B. Gaye, S. Tian, N. Lahajnar

School of Oceanography, Shanghai Jiao Tong University | Shanghai, PR. China
Y. Zhong, M. Zhou

Guangzhou Marine Geological Survey | Guangzhou, PR China
X. Zhen

The South China Sea (SCS), a marginal sea of the western Pacific, is oligotrophic in its distal parts and even on the shelf close to the coast, as it is a mostly stratified tropical region (Wu et al., 2003; Dai et al., 2013). Enhanced productivity occurs seasonally and is regionally limited to the upwelling areas off Vietnam, Luzon and Hainan, and off the river mouths, especially of the large rivers such as the Mekong in the southwest and the Pearl River in the northern SCS. The Pearl River is the largest river by volume discharged, delivering 326 billion m^3 of freshwater and 86 million tons of sediments into the SCS (Zu et al., 2014). Its catchment is population by 168 million inhabitants – a so-called megacity – and hosts among the biggest industries in China. The Pearl River is thus a conduit for wastewater from agriculture, industries and humans to the coastal SCS and potentially also to deeper parts of the SCS.

Our study area is therefore an excellent example of a subtropical adjacent sea and a natural laboratory to study the exchange processes between the land and the ocean (Pearl River), the variability of physical forcing (monsoon, circulation), the drastically increasing anthropogenic stress (nutrients/eutrophication, organic contaminants, microplastic, antibiotics) following the development of a Megacity within the area Guangzhou-Hong Kong. In particular SO269 aimed at improving our understanding of the impact of the Pearl River on it adjacent shelf and slope areas and to contribute to a better understanding of the widths of the halo of a megacity and the mechanisms driving it. We used established organic contaminants like polycyclic aromatic hydrocarbons, polychlorinated biphenyls and Dichlorodiphenyltrichloroethane as well as emerging contaminants (UV filters, hormones and microplastic) in combination with hydrographic

parameters (temperature, salinity, dissolved oxygen) as well as nutrient and suspended matter concentrations and composition along cross shelf transects in a sampling grid off the Pearl River mouth to understand the river impacts on productivity and sediment dispersal and assess the pollution status in the study area.

Here we are presenting a selection of results regarding the distribution of riverine material, resuspension processes on the shelf and slope as displayed by amino acids as tracers of organic matter sources. The pollution status is analysed using examples based on measurements of established organic pollutants and emerging pollutants.

The cruise took place in August/September when the Pearl River discharge was high and a river plume characterized by salinities below 30, enhanced nutrient and suspended matter concentrations was observed off the river mouth. Within this river plume the chlorophyll maximum occurred at the surface whereas in areas outside the river plume chlorophyll maxima were found at a subsurface nutricline with depths increasing from 30 m at the proximal to 80 m at the most distal stations. Suspended matter in the river plume was rich in organic carbon, nitrogen and amino acids and the organic matter was of fresh planktonic origin sustained by river derived nutrients. Organic matter was of similar quality in the deep chlorophyll maxima with slightly lower organic carbon and nitrogen concentrations. On the shelf and the shelf break, a distinct turbidity maximum was found above the sea floor forming a turbid layer of 5–20 m thickness. Amino acid spectra reveal that a large proportion of the organic matter in these turbidity maxima originates from sediments. Resuspension of sediments on the shelf and slope is thus an important process and can lead to the redistribution of contaminants supplied by the Pearl River into distal areas.

Our measurements of organic pollutants indicate that the concentrations of polycyclic aromatic hydrocarbons, dichlorodiphenyltrichloroethane, and polychlorinated biphenyls are below established sediment quality guidelines, suggesting no environmental risk. However, surprisingly their concentrations increase from the shelf to the deep northern SCS, and are higher in the east of the study area. The organic pollutant composition indicates that PAH were mainly derived from pyrogenic sources, and mostly degraded DDT and PCB were seen. However, in the deep northern SCS, considerable contribution of petrogenic PAH, low chlorinated PCB and p,p'-DDT suggest more recent input from different sources compared to the shelf. We have measured rather uniform PCB concentrations in the nearshore area. A comparison with measurements from the a cruise carried out in 2018 shows that the distribution and PCB concentrations in the aqueous phase in the South China Sea does not exhibit much interannual variation, with the Pearl River Delta acting as a sources of PCBs into the South China Sea, contrasting the results of Kaiser et al (2018), who identified the water SW of Taiwan as their source. The DDT compounds had a different distribution pattern than the PCBs, with higher concentrations in the water column on the shelf than in the open South China Sea compared to 2018. As for the PCBs, the Pearl River Delta is a major input source for the DDT compounds in the aqueous phase. Distribution patterns differ in the sediment compared to the water

phase. Both PCBs and DDTs were detected in higher concentrations on the slope than on the shelf. This indicates that the observed resuspension processes can lead to a considerable downslope redistribution of pollutants.

Our combined results from 2018 and 2019 (SO269) provide a first insight into the transport of pharmaceutical and personal care products (PPCPs) to the open sea and their different behaviour in the marine environment. Caffeine (CAF, alkaloid), phenylbenzimidazolesulfonic acid (PBSA, UV filter), octocrylene (OC, UV filter), and nonylphenoxyacetic acid (NP1EC, metabolite) were detected most abundantly in surface waters, but showed different distribution patterns. High concentrations of the metabolite NP1EC were measured on the western shelf of the sampling area with decreasing concentrations towards the open sea. CAF exhibits a similar pattern to NP1EC, but the decrease was less pronounced allowing its detection in the open South China Sea. Highly elevated CAF concentrations were detected in the nearshore area off Hong Kong, indicating a land-based source. PBSA and octocrylene showed slightly different distribution patterns, with the water-soluble UV filter PBSA detected at some stations and the poorly water-soluble octocrylene almost everywhere in the area.

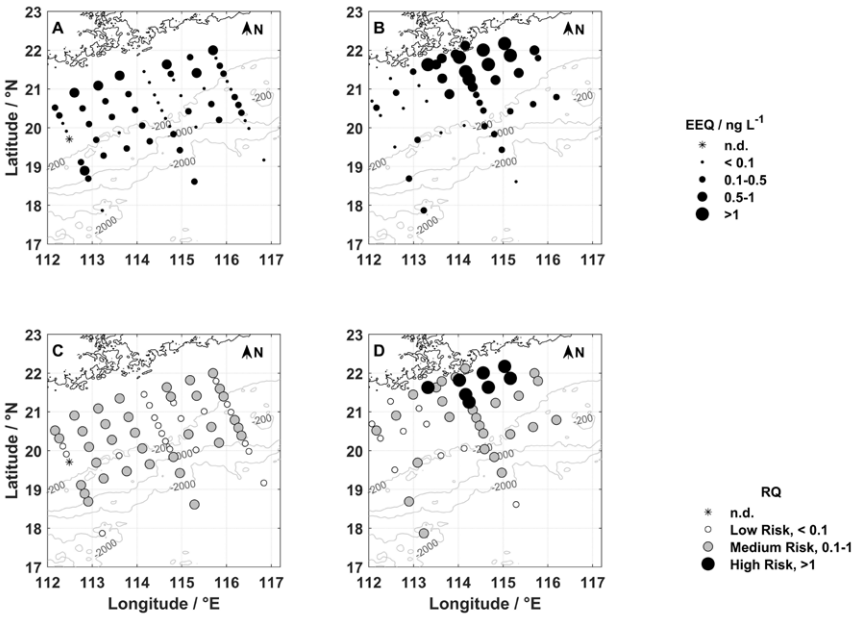

Fig. 1: Calculated estradiol equivalent concentration (EEQ) in the SO269 working area in the northern South China Sea a) in 2018 and b) in 2019. The size of ● is related to the detected concentration. Bathymetry lines are based on ETOPO1. The calculated risk quotient in the region in 2018 (c) and 2019 (d). The colour refers to the level of risk (Deich et al., 2021).

We have also used synthetic and natural hormones as indicators for human impact and analysed water samples for estrone (E1), 17-estradiol (E2), 17-ethinylestradiol (EE2),

genistein (GEN), daidzein (DAI), and zearalenone (ZEN). Within the target substances, mainly the naturally occurring hormones E1 and E2 as well as the synthetic EE2 were detected. Of the phytoestrogens and mycoestrogens, only GEN was detected at one station in August 2019 (1.2 ng L^{-1}, SCS-14; Deich et al., 2021). Elevated concentrations of the hormones E1 and EE2 were detected at nearshore stations in both years, 2018 and 2019. E1 was detected at up to 1.1 ng L^{-1} and EE2 at up to 0.6 ng L^{-1}. Furthermore, the natural hormone E2 was detected up to 0.7 ng L^{-1} in August 2019. Because hormones and hormone-like substances can interfere with the endocrine system of living organisms and cause lasting damage (Adeel et al., 2017), an initial risk assessment was carried out by calculating ratios between measured and predicted no effect concentrations (PNEC) following Hernando et al., (2006). In SCS the calculated risk quotients for the natural hormone E1 (PNEC = 6 ng L^{-1}, Caldwell et al., 2012) range from <0.1 to <1, indicating low to moderate risk. In comparison, concentrations of the natural hormone E2 (PNEC = 2 ng L^{-1}, Caldwell et al., 2012) may pose a moderate risk to aquatic organisms. The synthetic EE2 generally shows a very strong estrogenic effect, which is also reflected in the low PNEC (PNEC = 0.1 ng L^{-1}, Caldwell et al., 2012) leading to a comparatively high risk with quotients well above 1 (Deich et al., 2021). Since the estrogenically active substances are not present individually in environmental matrices and can thus act together on the endocrine system of organisms, the estrogenic activity was determined as well using the measured concentration and the substance-specific estrogenic potency (Fig. 1). Estrogenic activity is considered in relation to the natural E2 and consequently expressed as estradiol equivalent quotient (EEQ). In 2019 EEQ up to 1.4 ng L^{-1} were observed (Deich et al., 2021). Hereby EE2 accounted for a large part of the estrogenic activity due to its high estrogenic potency. It should be noted however, that conclusions about synergistic, antagonistic, or competitive effects between individual compounds cannot be currently assessed.

In summary the organic and emerging pollutants are of moderate concentrations. Their distribution in sediments evidently exceeds the region under direct land and river impact because of resuspension and near bottom downslope transport processes.

The SO269 cruise was the third joint cruise within the framework of the Sino-German project Megacity's fingerprint in Chinese marginal seas: Investigation of pollutant fingerprints and dispersal (MEGAPOL) with participants from 7 German and Chinese institutions. SO269 and the MEGAPOL consortium project contribute to the BMBF program marine research (Meeresforschung, PTJ) and are rooted in the WTZ-China initiative, dating back to 1986. Our activities continue the bilateral projects PECAI and BEIBU, both relevant to the programs Forschung für die Nachhaltigkeit (FONA) and System Erde. MEGAPOL and SO269-SOCLIS were founded by BMBF under contract 03F0786A and 03G0269, respectively.

REFERENCES

Adeel M., Song X., Wang Y., Francis D., Yang Y., Environmental impact of estrogens on human, animal and plant life: A critical review. Environment International, 99, 107–119. doi: 10.1016/j.envint.2016.12.010, 2017.

Caldwell D. J., Mastrocco F., Anderson P. D., Länge R., Sumpter J. P., Predicted-no-effect concentrations for the steroid estrogens estrone, 17β-estradiol, estriol, and 17α-ethinylestradiol. Environmental Toxicology and Chemistry, 31, 1396–1406. doi: 10.1002/etc.1825, 2012

Dai M. H., Cao Z. M., Guo X. H., Zhai W. D., Liu Z. Y., Yin Z. Q., Xu Y. P., Gan J. P., Hu J. Y., Du C. J., Why are some marginal seas sources of atmospheric CO_2?, Geophysical Research Letters, 40, 2154–2158, 10.1002/grl.50390, 2013.

Deich C., Frazão H.C., Appelt J.S., Li W., Pohlmann T., Waniek J.J., Estrogenic compounds in the Pearl River Estuary and northern shelf of the South China Sea. Science of the Total Environment, 770, doi.org/10.1016/j.scitotenv.2021.145239, 2021.

Hernanod M.D., Mezcua M., Fernandez-alba, A.R., Barcelo, D., Environmental risk assessment of pharmaceutical residues in wastewater effluents, surface waters and sediments, Talanta, 69, 334–342, 2006.

Kaiser D., Schulz-Bull D.E., Waniek J.J., Polycyclic and organochlorine hydrocarbons in sediments of the northern South China Sea. Marine Pollution Bulletin, 137, 668–676, doi.org/10.1016/j.marpolbul.2018.10.039, 2018.

Wu J., Chung S.-W., Wen L.-S., Liu K.-K., Chen Y. L., Chen H.-Y., Karl D. M., Dissolved inorganic phosphorus, dissolved iron and Trichodesmium in the oligotrophic South China Sea, Global Global Biogeochemical Cycles, 17, doi:10.1029/2002GB001924, 2003.

Zu T., Wang D., Gan J.,Guan W., On the role of wind and tide in generating variability of Pearl River plume during summer in a coupled wide estuary and shelf system, Journal of Marine Systems, doi.org/10.1016/j.jmarsys.2014.03.005, 2014.

SO270

The demise of a tropical reef system (Saya de Malha Bank, Indian Ocean)

AUTHORS

Institute of Geologie, University of Hamburg | Hamburg, Germany
C. Betzler, S. Lindhorst, T. Lüdmann, K. Emeis, J.O. Eisermann

Leibniz Centre for Tropical Marine Research | Bremen, Germany
T. Rixen

Departamento de Estratigrafía y Paleontología, Facultad de Ciencias | Granada, Spain
J. Braga, J. Reolid

Earth Science Department, Vrije Universiteit Amsterdam | Amsterdam, The Netherlands
J.J. Reijmer

Department of Geosciences, Faculty of Science, University of Malta, | Malta
O.M. Bialik

Department for Continental Shelf, Maritime Zones Administration & Exploration | Port-Louis, Mauritius
D. Bissessur

INTRODUCTION

Carbonate platforms are edifices several kilometers high and several hundreds of kilometers wide mostly produced by shallow-water organisms, and by detritus of these organisms. A common element is that coral reefs grow up to sea level, mainly along the platform rims. Light availability determines the depth down to which corals with their photosynthetic symbionts can thrive. Water temperature, turbidity, salinity, nutrient and hydrodynamic energy are further important parameters.

Sea-level change exerts a fundamental control on reef development at geological time scales. Reefs migrate seaward and landward following falling or rising sea level, whereas a sea-level rise outpacing reef growth interrupts reef development. In the Indo-Pacific realm some reefs were able to keep up with deglacial sea level rise but others, for reasons that are not fully understood, were not (Montaggioni, 2005; Webster et al.,

2018; Woodroffe and Webster, 2014). Those are today the sites of many mesophotic coral ecosystems (MCEs).

The Saya de Malha Bank (SMB; Fig. 1) in the Indian Ocean lies in the window of optimal conditions for shallow-water reef development, but the carbonate platform today is mostly populated by MCEs. Using geophysical, oceanographical and sedimentological data from the research cruise SO270 we show how ocean currents shape this platform and how – along with sea-level changes – they impede shallow-water reef growth.

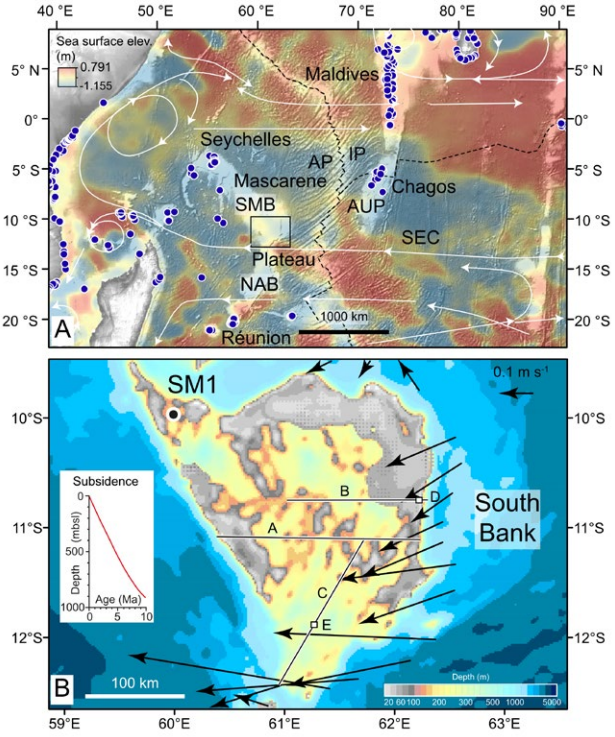

Fig. 1: A: Indian Ocean circulation with June 2004 sea-surface height tracing current speed, and shallow-water reefs (blue dots). SMB: Saya de Malha Bank; NAB: Nazareth Bank; SEC: South Equatorial Current. B: SMB with location of well SM1. Arrows: direction and speed of currents at a water depth of 27 m. Lines A–C: position of seismic lines in Fig. 2; white squares D and E: location of sea-floor views in Fig. 2. Subsidence curve for the southern SMB. From Betzler et al. (2021).

GEOLOGY AND SEISMIC STRATIGRAPHY

The SO270 seismic data allow a subdivision of the SMB succession into three units (Fig. 2). The base of the lowermost Unit 1 is not imaged in the profiles; at the top it is delimited by an unconformity at 0.9–1.2 s two-way travel time which corresponds to a depth of ca. 1.3–1.6 km below seafloor. The reflection pattern is mainly chaotic.

In Unit 2 a basin was laterally infilled by progradational clinoform strata (Fig. 2A, B). In view of the isolated nature of SMB without any siliciclastic input, the architecture is interpreted to reflect a flat-topped carbonate platform. Such platforms have an edge formed by reefs or shoals, inclined slopes, and flat-lying inner platform deposits. The carbonate edifice enclosed a basin several 10s to 100s m deep and at least 60 km wide (Fig. 2A, B). The progradation of the inner platform edge towards the inner basin was not controlled by margin orientation (Fig. 2A, B, C), which indicates that SMB at this time was an atoll.

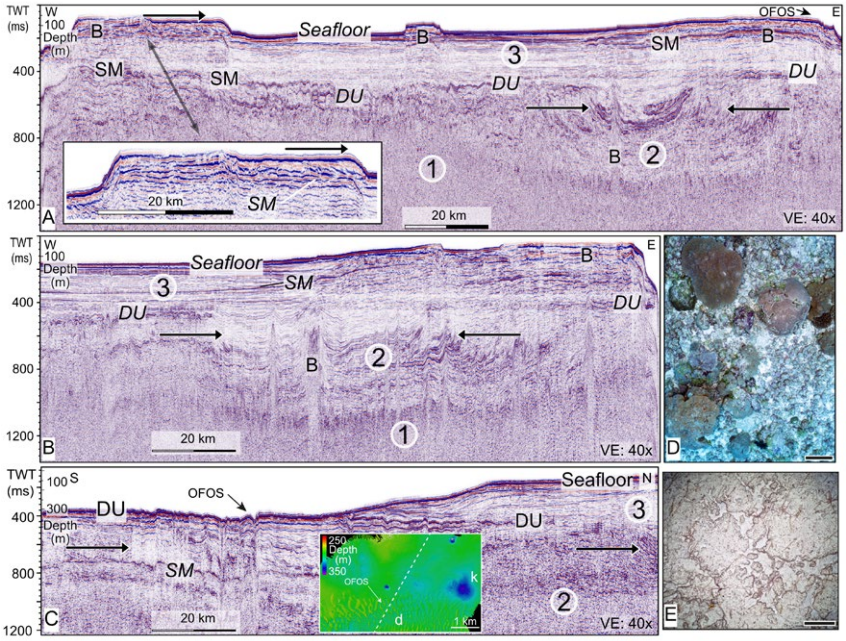

Fig. 2: Seismic profiles of SMB (Position in Fig. 1B) with clinoform progradations (arrows) and drowning unconformity DU. A: W–E line. B: Carbonate banks, SM: sea-floor multiple. Inlay: Detail showing progradation in carbonate body. OFOS: image shown in D. B: Eastern part of W-E Line. C: SSW–NNE line with DU hardground and sediment cover thickening towards the north. OFOS: image shown in E. Inlay with multibeam imagery and path of seismic profile (stippled line); d: submarine dunes; k: karst collapse. D: MEC (water depth: 30 m) with corals and coralline red algae. Scale bar: 40 cm. E: DU hardground (water depth: 302 m). Scale bar: 40 cm. From Betzler et al. (2021).

This growth mode of SMB terminated at a platform-wide seismic reflection (DU) (Fig. 2). Above DU, the succession is layered (Unit 3) and thinning out towards the south. In NE–SW oriented sections, Unit 3 has a backstepping carbonate ramp-like geometry (Fig. 2C). The layered sedimentation pattern of Unit 3 is interrupted by up to 12 km wide and flat-topped minor bodies, which reach up to a water depth of 20 m (Fig. 2A). Some show an internal stratification (Fig. 2A) with a succession of parallel to subparallel strata in the center, and some and prograding strata towards the margins. Today the bodies surfaces are populated by MECs with red algae, corals, and the green alga *Halimeda* (Fig. 2D).

The establishment of a horse-shoe shaped rim of SMB appears to correlate with changes in the stratal patterns above DU. In NE–SW oriented seismic lines (Fig. 2C) it is apparent that DU crops out at the seafloor as a hardground (Fig. 2E), locally covered by fields of submarine dunes (Fig. 2C).

OCEANOGRAPHY

Temperature, salinity, and oxygen concentrations indicate tropical surface waters of low salinity and more saline Arabian Sea water near the surface (Fig. 3A). Salt-rich Subtropical Surface Water and Indonesian Throughflow Water that is low in oxygen mix at around 200 m water depth (Fig. 3A, B). Below there is the relatively oxygen-rich Southern Indian Central Water (300–500 m), in turn underlain by oxygen-poor Red Sea/ Persian Gulf Intermediate Water. The temperature, the mean salinity of 34.8 psu, the low productivity, and the phosphate concentration of 0.11 µM (Fig. 3C-D) are well within the tolerance limits of coral reefs.

Zones of SMB impacted by highest current velocities (Fig. 1B) coincide with the areas where horizon DU is at the seafloor (Fig. 2C, E). In spite of the blocking position of SMB in the massive SEC water flow, there is no indication of topographic upwelling of nutrient-rich sub-thermocline waters into the euphotic zone (Fig. 3C, D).

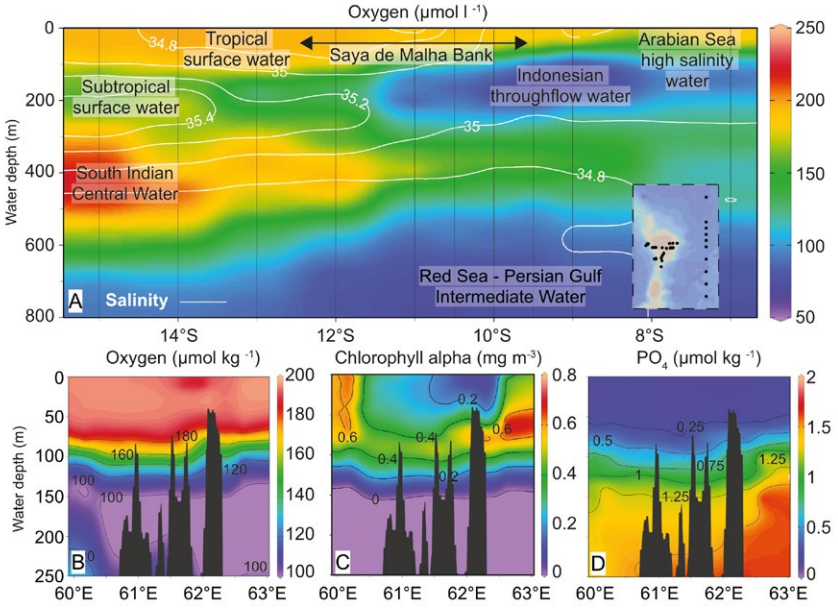

Fig. 3: A: Salinity and oxygen concentrations distributions in the upper water column along a CTD transect at 65°E. (B) fluorescence and oxygen content (C) from CTD casts and phosphate concentrations (D) in discrete samples. From Betzler et al. (2021).

DISCUSSION

The present-day platform state of partial drowning established during the younger Neogene, i. e. the Pliocene (Betzler et al., 2021). The most straightforward explanation for the SMB drowning thus appears to be the response to the Pliocene sea level rise. Other isolated carbonate platforms such as the Bahamas, the Maldives or the platforms off NE Australia also record this episode of high Pliocene eustatic sea level (Betzler et al., 2021). Subsequent recovery of these platforms, however, indicates that in addition to sea-level fluctuations other factors controlled drowning of SMB.

Today, the low phosphate and fluorescence concentrations in the water column on and around SMB (Fig. 3) exclude nutrient influx as reason for shallow-water reef demise. Conditions of low productivity in the Indian Ocean can be traced back for the last ca. 4 Myrs by carbonate mass accumulation rates (Dickens and Owen, 1999). Before 4 Ma, the same data indicate more elevated surface water productivity.

Ocean currents can trigger drowning (Betzler et al., 2021). This introduces the SEC as a major player of platform evolution. Today, SMB is sculpted by the SEC with sediment winnowing at the southern bank's tip (Fig. 2C, E). The SEC established at 3.3 Ma (Auer et al., 2019). Acceleration of the currents through trade-wind intensification started around 3 Ma as documented in upwelling records of the Benguela Current (Marlow et al., 2000), which is connected to the SEC through the Agulhas Leakage (Durgadoo et al., 2017).

If a shallow-water carbonate factory keeps up with sea-level rise depends on the amplitudes and frequencies of sea-level changes, but also on the antecedent topography. Coral colonization of a substrate during a rapid sea-level rise is only possible when there is substrate for corals to grow in the upper photic zone, as documented by many backstepping and submerged reef terraces around modern carbonate platforms (Woodroffe and Webster, 2014). Flat-topped platforms do not provide these conditions, and under elevated rates of sea-level rise thus drown quickly. The seismic stratigraphy of relict banks in SMB with margin progradation (Fig. 2A) here is proposed to reflect ephemeral past stages with bank-top carbonate production and export, i. e. short episodes when the bank tops were at sea level.

The onset of eccentricity-driven sea-level fluctuations around 3 Ma resulted in high amplitudes and rates of change, which later during the Pleistocene became even more pronounced. This onset impacted on many carbonate platforms which underwent a change from flat-topped banks to atolls (Droxler and Jorry, 2021). In the case of SMB, however, the SEC hindered the reefs to form a closed rim, thus drowning the bank, which from then on probably only was populated by shallow-water reefs during short periods of low sea level.

The drowning of SMB appears as a response to a combination of two effects, i. e. sea-level change and current intensification, which were the reason that the reef systems, although situated in a suitable setting did not produce sufficient sediment to infill the available accommodation. These findings are expected to be applicable to other Tertiary platforms in the Indopacific region, which were drowned at a certain point in their evolution, such as for example in the South China Sea.

REFERENCES

Betzler, C., Lindhorst, S., Lüdmann, T., et al., Current and sea level control the demise of shallow carbonate production on a tropical bank (Saya de Malha Bank, Indian Ocean). Geology 2021, doi.org/10.1130/G49090.1

Geology.Dickens, G. R., and Owen, R. M., The Latest Miocene-Early Pliocene biogenic bloom: a revised Indian Ocean perspective: Marine Geology 1999, 161, 75–91.

Droxler, A. W., and Jorry, S. J., The Origin of Modern Atolls: Challenging Darwin's Deeply Ingrained Theory: Annual Review of Marine Science 2021, 13, 537–573.

Durgadoo, J. V., Rühs, S., Biastoch, A., and Böning, C. W. B., Indian Ocean sources of Agulhas leakage: Journal of Geophysical Research: Oceans 2017, 122, 3481–3499.

Marlow, J. R., Lange, C. B., Wefer, G., and Rosell-Melé, A., Upwelling Intensification As Part of the Pliocene-Pleistocene Climate Transition: Science 2000, 290, 2288–2291.

Montaggioni, L., History of Indo-Pacific coral reef systems since the last glaciation: development patterns and controlling factors.: Earth Sci. Rev. 2005, 71, 1–75.

Montaggioni, L. F., and Martin-Garin, B., Quaternary development history of coral reefs from West Indian islands: a review: International Journal of Earth Sciences 2020, 109, 911–930.

Webster, J. M., Braga, J. C., Humblet, M., Potts, D. C., et al., Response of the Great Barrier Reef to sea-level and environmental changes over the past 30,000 years: Nature Geoscience 2018, 11, 426–432.

Woodroffe, C. D., and Webster, J. M., 2014, Coral reefs and sea-level change: Marine Geology, 352, 248–267.

POSTER

M147

Geochemical behaviour of neodymium and hafnium isotopes in the Amazon estuary: Tracing the river plume and quantifying continental inputs

AUTHORS

GEOMAR Helmholtz Centre for Ocean Research Kiel | Kiel, Germany
A. Xu, E. Hathorne, M. Frank

Radiogenic neodymium (Nd) and hafnium (Hf) isotopes have been demonstrated to be powerful tracers of water mass provenance and their present and past mixing, which is enabled by the quasi-conservative behavior of Nd and Hf in seawater and their average oceanic residence time of 300–1000 yr and 250–7500 yr, respectively (Frank, 2002; Rickli et al., 2009; Stichel et al., 2012a, b). In order to better understand the cycling of trace elements and their isotopes in the oceans and further their application in the reconstruction of past ocean circulation, their sources and sinks, as well as transport process in the modern ocean are key issues that need to be clarified. The Amazon River, the world's largest river, which discharges 6.15 % of the global suspended sediment and about 15 % of the global freshwater to the ocean is expected to have a key impact on the Atlantic Ocean's element and isotope budget (Guyot et al., 2011; Martinez et al., 2009; Merschel et al., 2017a; Mortatti and Probst, 2003).

Prior studies of the Amazon River have shown that it supplies a dissolved Nd flux of 42 Mg/year to the Atlantic Ocean (Rousseau et al., 2015). Nevertheless, our understanding of the sources that control the seawater Nd and Hf budgets in the oceans and their impact on the potential use of εNd and εHf as water mass tracers is not complete. In particular, the riverine Hf input into the global ocean is still not quantified. We therefore measured dissolved Nd and Hf concentrations and their isotopic compositions of estuarine waters in the Amazon estuary obtained during RV Meteor cruise M147, which was official process study GApr11 of the international GEOTRACES program (Fig. 1).

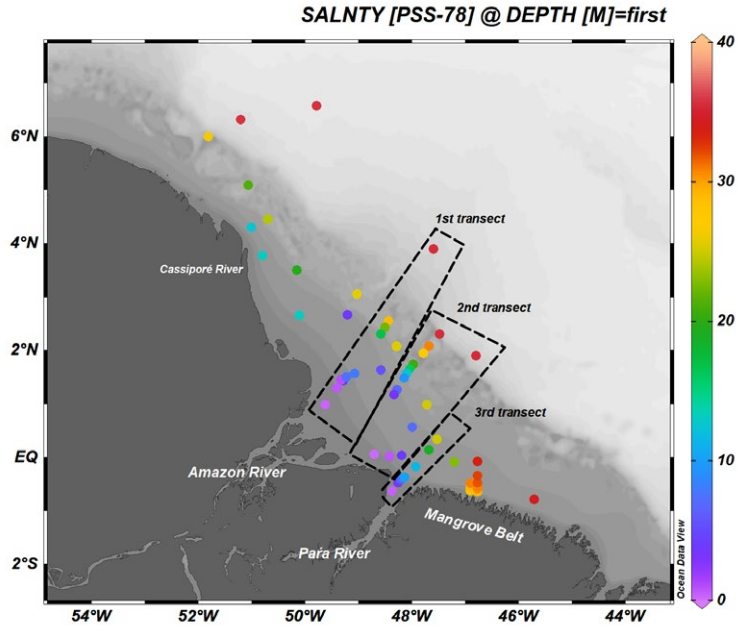

Fig. 1: Sampling stations in the Amazon estuary

ND AND HF CONCENTRATION CHANGES IN THE AMAZON RIVER AND PARÁ RIVER ESTUARIES

Our data show that dissolved Nd and Hf are removed rapidly in the low-salinity zone (0–10 psu) of the Amazon and Pará River estuaries due to the salt-induced coagulation of colloids (Fig. 2). The main factor controlling the removal of REEs is the immediate flocculation and precipitation of river-borne inorganic and organic nanoparticles and colloids when river waters and seawater mix (Hoyle et al., 1984; Pokrovsky and Schott, 2002; Merschel et al., 2017b). The maximum removal rates of dissolved riverine Nd and Hf are 93 % and 85 % in the Amazon River estuary and reach 94 % and 80 % in the Pará River estuary. Our Nd and Hf concentrations appear to increase in the low-salinity zone of the Amazon River estuary, which is most likely not caused by the dissolution of particles but either by entrained Pará River water or estuarine waters recirculated in the estuary. Moreover, slight increases of Nd and Hf concentrations occurred in the mid- to high-salinity range, which have been considered to be caused by dissolution of lithogenic suspended sediments in a previous study (Rousseau et al., 2015). However, Pará River water carries high Nd and Hf concentrations (1035.6 pmol/kg and 13.4 pmol/kg, respectively) and can therefore also supply significant amounts of additional Nd and Hf to Amazon River estuarine waters.

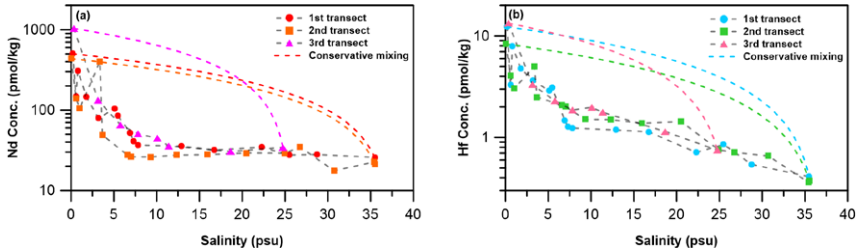

Fig. 2: Nd and Hf concentration vs. salinity

ND AND HF FLUXES FROM AMAZON RIVER AND PARÁ RIVER TO THE ATLANTIC OCEAN

The Amazon and Pará Rivers discharge an average of 2.05 x10^5 m^3/s and 2.09 x10^4 m^3/s of freshwater to the Atlantic, respectively. Therefore, the minimum dissolved Nd and Hf flux of the Amazon River to the Atlantic is calculated to be 3.2x105 mol/yr and 1.3x10^4 mol/yr based on an average of 7 % and 19 % of the total riverine Nd and Hf fluxes finally reaching the Atlantic Ocean. Moreover, the minimum dissolved Nd and Hf flux from the Pará River is 4.2 x10^4 mol/yr and 1.7x10^3 mol/yr, respectively, taking into account that about 6 % of the Nd and 20 % of the Hf are retained during estuarine mixing.

ND AND HF ISOTOPE BEHAVIOUR DURING ESTUARINE MIXING

The results show that the Amazon river has the most radiogenic Nd (-9.4) and Hf (1.8), signatures while mangrove groundwater displays the least radiogenic Nd (-17.5) and Hf (-9.7) signatures, with the Pará River and surface seawater having intermediate Nd (-14.1, -11.4, respectively) and Hf (-4.1, -1.0, respectively) signatures. Using these endmember values, conservative mixing of Nd and Hf isotopes was calculated (Fig. 3) revealing that most surface water signatures cannot be explained by conservative mixing between Amazon River water and seawater alone. Along the salinity gradient, both εNd and εHf are shifted towards less radiogenic signatures reaching values as low as -14 (εNd) and -4 (εHf), which in the case of Nd is less radiogenic than the seawater and sedimentary Nd isotope signatures (-11.4 and -10.6, respectively) (Rousseau et al., 2015). The calculation indicates that suspended sediment is not the source shifting the Nd and Hf isotopic compositions to unradiogenic signatures. Admixture of Pará River water with its high Nd and Hf concentrations and unradiogenic Nd and Hf signatures obviously also has a great impact on Nd and Hf signatures of Amazon estuarine waters. This is consistent with the Pará River discharge peaking in April at 3.8 x 10^5 m^3 s^{-1} (Prestes et al., 2020), which is higher than the discharge peak of the Amazon River in May (2.8× 10^5 m^3 s^{-1}) (Moquet et al., 2015). Therefore, the Pará River will most strongly influence the Amazon estuarine water during the period of high discharge and may have been missed by previous studies sampling at other times of the year.

The conservative mixing model of Nd and Hf isotopes shows that all surface water signatures in the Amazon estuary can be explained by mixing of the Amazon River, the

Pará River and seawater, except for the 2 surface water samples near the mangrove belt, which were strongly affected by mangrove groundwater.

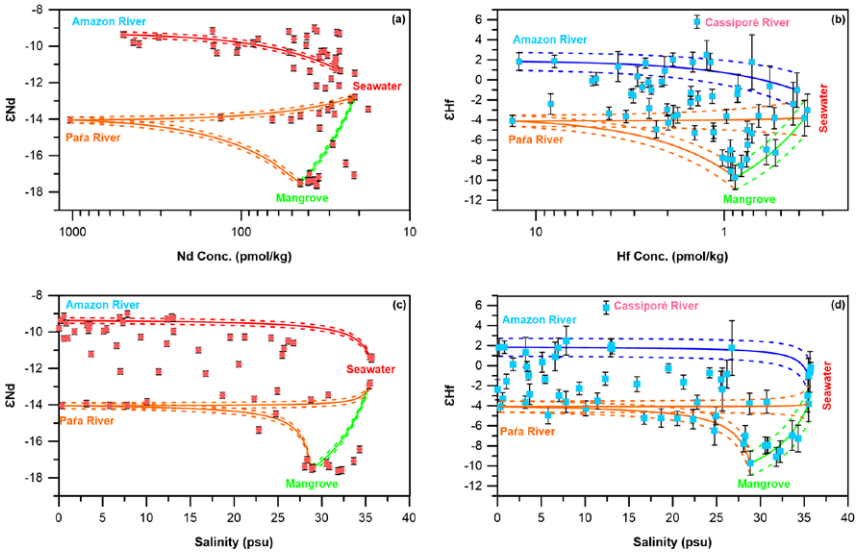

Fig. 3: Conservative mixing model of Nd and Hf isotopes

ND AND HF ISOTOPES TRACE THE AMAZON RIVER PLUME

Nd and Hf isotopes behave conservatively during estuarine mixing which allows tracing of the Amazon River and Pará River plume. Fig. 4 shows that the Pará River and Amazon River plumes were deviated northward by the vigorous North Brazil Current (NBC). The Amazon River and Pará River plumes merge in the low- to mid-salinity zone of the Amazon estuary. Estuarine water in the mid- to high-salinity zone was influenced strongly by the Pará River plume due to the deviation of the Amazon River freshwater plume to flow northward as a consequence of interaction with the NBC.

In summary, Nd and Hf isotopes are quasi-conservative tracers of water masses mixing in the estuary where river water and seawater mix. Therefore, Nd and Hf isotopes can be used to trace the Amazon River plume and Amazon River inputs. However, the admixture of waters and sediment from the Para River, which has a significant impact on the Amazon estuarine waters during periods of high discharge, also needs to be taken into account.

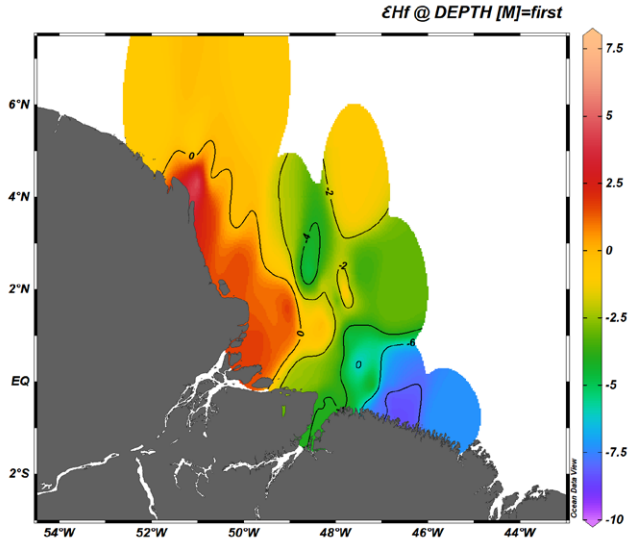

Fig. 4: εNd and εHf distribution in the Amazon estuary

REFERENCES

Frank M. Radiogenic isotopes: Tracers of past ocean circulation and erosional input. Reviews of geophysics, 2002, 40(1): 1-1-1-38.

Hoyle J, Elderfield H, Gledhill A, et al. The behaviour of the rare earth elements during mixing of river and sea waters. Geochimica et Cosmochimica Acta, 1984, 48(1): 143–149.

Martinez J M, Guyot J L, Filizola N, et al. Increase in suspended sediment discharge of the Amazon River assessed by monitoring network and satellite data. Catena, 2009, 79(3): 257–264.

Merschel G, Bau M, Dantas E L. Contrasting impact of organic and inorganic nanoparticles and colloids on the behavior of particle-reactive elements in tropical estuaries: an experimental study. Geochimica et Cosmochimica Acta, 2017b, 197: 1–13.

Merschel G, Bau M, Schmidt K, et al. Hafnium and neodymium isotopes and REY distribution in the truly dissolved, nanoparticulate/colloidal and suspended loads of rivers in the Amazon Basin, Brazil. Geochimica et Cosmochimica Acta, 2017a, 213: 383-399.

Moquet J S, Guyot J L, Crave A, et al. Amazon River dissolved load: temporal dynamics and annual budget from the Andes to the ocean. Environmental Science and Pollution Research, 2016, 23(12): 11405–11429.

Mortatti J, Probst J L. Silicate rock weathering and atmospheric/soil CO_2 uptake in the Amazon basin estimated from river water geochemistry: seasonal and spatial variations. Chemical geology, 2003, 197(1–4): 177–196.

Pokrovsky O S, Schott J. Iron colloids/organic matter associated transport of major and trace elements in small boreal rivers and their estuaries (NW Russia). Chemical Geology, 2002, 190(1–4): 141–179.

Prestes Y O, da Costa Borba T A, da Silva A C, et al. A discharge stationary model for the Pará-Amazon estuarine system. Journal of Hydrology: Regional Studies, 2020, 28: 100668.

Rickli J, Frank M, Halliday A N. The hafnium–neodymium isotopic composition of Atlantic seawater. Earth and Planetary Science Letters, 2009, 280(1–4): 118–127.

Rousseau T C C, Sonke J E, Chmeleff J, et al. Rapid neodymium release to marine waters from lithogenic sediments in the Amazon estuary. Nature communications, 2015, 6(1): 1–8.

Stichel T, Frank M, Rickli J, et al. The hafnium and neodymium isotope composition of seawater in the Atlantic sector of the Southern Ocean. Earth and Planetary Science Letters, 2012a, 317: 282–294.

Stichel T, Frank M, Rickli J, et al. Sources and input mechanisms of hafnium and neodymium in surface waters of the Atlantic sector of the Southern Ocean. Geochimica et Cosmochimica Acta, 2012b, 94: 22–37.

M147

Distribution and Flux of Trace Metals (Al, Mn, Fe, Co, Ni, Cu, Zn, Cd, Pb and U) in the Amazon and Pará River Estuary and Mixing Plume

AUTHORS

Jacobs University Bremen gGmbH, Department of Earth Sciences | Bremen, Germany
A. Hollister, A. Koschinsky

GEOMAR Helmholtz Centre for Ocean Research Kiel | Kiel, Germany
M. Gledhill

INTRODUCTION:

The Amazon River is the largest river on earth, accounting for 15–20 % of the global fluvial freshwater and discharging a volume of 100,200–240,000 m^3 s^{-1} water into the Atlantic (Espinoza-Villar et al. 2009). The Amazon Estuary is fed by the Amazon River as well as the smaller Pará River to the south (volume discharge: 9,000–38,000 m^3 s^{-1}), making it an important source of trace metals and organic matter on a global scale. Although the Amazon basin has been increasingly subject to anthropogenic impacts, however, sparse data existed for trace metals in the Amazon estuary and mixing plume prior to this project (Boyle et al. 1982). Importantly, no data exist to measure the dissolved flux of these dissolved trace metals from the Amazon estuary into the ocean. Trace metals are subject to a variety of removal and input processes in estuaries, including particle adsorption-desorption, colloidal fluctuation, biological uptake, sediment and porewater exchange, and ox(ihydrox)ide formation. Understanding and quantifying these processes is therefore crucial to understanding eventual fluxes of trace metals from the Amazon and Pará Rivers into the Atlantic Ocean. Toward this end, surface samples were collected for dissolved (<0.2 µm) trace metals (Al, Mn, Fe, Co, Ni, Cu, Zn, Cd, Pb and U) on a GEOTRACES process study (GApr11, cruise M147) throughout the Amazon estuary in Apr–May 2018 during a period of high river discharge. Here we present dissolved trace metal fluxes from the Amazon and Pará Rivers based on endmember concentrations and estuarine removal.

RESULTS

THE AMAZON AND PARÁ TRANSECTS SHOWED DISTINCT BEHAVIOR

Samples in the estuary were grouped based on salinity and source (Fig. 1). The Amazon estuary is influenced by the Amazon and Pará River transects, a mangrove belt to the southeast, an aging plume flowing northward and the North Brazil Current (NBC), which

serves as the seawater endmember. The Pará The Amazon and Pará transects showed distinct endmember signatures: the Pará was higher in dissolved Al, Ni, Co, Zn and Pb, while the Amazon was higher in dissolved Cu, Fe and Mn. The Pará is largely fed by the Tocantins River to the south, which has a drier catchment area with elevated anthropogenic influence compared to the Amazon. The higher levels of certain trace metals (e. g. Zn and Pb) in the Pará may reflect a more contaminated river compared to the Amazon.

In the Amazon transect, Fe, Pb and Mn declined rapidly at low salinity, indicating possible ox(yhydrox)ide formation, particle adsorption and/or colloidal flocculation (Fig. 2). These metals also declined initially in the Pará transect. However, several metals (Al, Mn, Fe, Co, Ni, Zn, Pb) showed an additional mid-salinity (S = 7–10) increase in the Pará transect only (Fig. 2). This may be caused by resuspension from sediments, possibly due to increased shipping traffic in the area, and reflects the different dynamics of the Pará transect compared to the Amazon. In addition to the Amazon and Pará Rivers, the Mangrove belt also represented a source of trace metals and organic matter to the estuary through groundwater exchange. For all metals, the river and mangrove belt transect signatures became indistinguishable at ca S > 15, indicating thorough estuary mixing.

Figure 1. Surface sample locations in the Amazon estuary. Symbols correspond to the Amazon and Pará River transects, a large mangrove forest to the southeast ("mangrove belt"), an aging mixing plume ("plume north"), and the North Brazil Current ("NBC") representing the seawater endmember.

Figure 2. Concentrations of dissolved (<0.2 μm) Al, Mn, Fe, Co, Ni, Cu, Zn, Cd, Pb and U plotted against salinity. Symbols correspond to the sample group locations described in Figure 1.

REMOVAL OF TRACE METALS

Removal of trace metals was calculated for the Amazon and Pará transects as follows:

$$(1)\ \text{removal fraction} = \left(M_{sample} - S_{sample} * \frac{(M_{river} - M_{sw})}{(S_{river} - S_{sw})} + M_{river}\right) / M_{sample}$$

where M is the dissolved metal concentration, S is salinity, and the subscripts "sample" represents a given sample, "river" represents the riverine endmember and "SW" represents the seawater endmember.

Removal and addition of trace metals during estuarine mixing may occur due to particle adsorption-desorption, ox(yhydrox)ide formation, porewater exchange and/or colloidal flocculation. In the Amazon transect, the particle-reactive elements Fe, Mn and Pb showed the greatest removal (86–94 %), consistent with known estuarine behavior. In general,

the Pará had lower removal than the Amazon, possibly related to a lower particle load or an additional source of input. In both transects, Cd had a net input owing to its mid-salinity maximum. This is in agreement with a well-documented phenomenon in estuaries: as Cd^{2+} reacts with Cl^- at increased salinity, Cd is mobilized from particles, resulting in increased dissolved concentrations (Comans and van Dijk 1988). In general, Cu, Ni and Co showed the lowest removal in the Amazon and Pará transects (6–39 %), possibly reflecting their organic complexation and relatively low particle reactivity (de Carvalho et al. 2021; Hollister et al. 2021).

GLOBAL FLUX COMPARISON

The removal of trace metals heavily influences their fluxes. Therefore, trace metal fluxes in the Amazon and Pará transects were calculated based on deviation from the two-endmember mixing line as a result of removal (or input) as described below:

$$\mathbf{(2)}\ Flux_M = V_{river} * (M_{river} - M_{river} * removal\ fraction_{avg})$$

where FluxM is the dissolved trace metal flux, Vriver is the river volume during the high-discharge sampling period and removal fractionavg is the average of the samples calculated in (1).

Using the fluxes at the high-discharge period, we estimate that the Amazon and Pará combined contribute up to 21 % of the global dissolved flux for Cu and 18 % for Ni, but only 5 % for Zn and Co and 3 % for Mn (based on global totals by Poulton and Raisewell 2000 and Carey et al. 2002). The dissolved Cu load in the Amazon alone (19 % of global totals) represents a flux greater than the combined total fo all major Asian Rivers. On the other hand, the Amazon flux is comparatively lower for the more particle-reactive elements Zn, Co, Mn and Fe relative to other rivers. We estimate that the Amazon delivers roughly the same flux of dissolved Fe as the Congo, the world's second largest river (Vieira et al. 2020), despite the Congo's considerably lower discharge (mean: 39,100 $m^3\ s^{-1}$). This can be attributed to the Congo's relatively low removal of Fe (ca 50 %), as well as its higher endmember concentration (Vieira et al. 2020).

Importantly, these flux estimates are based on the high discharge period. A future cruise to gather trace metal data in the low discharge period has approved and will compete the picture of total fluxes in the Amazon and Pará Rivers.

REFERENCES

Boyle, E., Huested, S. and Grant, B., 1982. The chemical mass balance of the Amazon Plume—II. Copper, nickel, and cadmium. Deep Sea Research Part A. Oceanographic Research Papers, 29(11): 1355–1364.

Carey, A.E., Nezat, C.A., Lyons, W.B., Kao, S.J., Hicks, D.M. and Owen, J.S., 2002. Trace metal fluxes to the ocean: The importance of high-standing oceanic islands. Geophysical research letters, 29(23): 14-1-14-4.

Comans, R.N. and van Dijk, C.P., 1988. Role of complexation processes in cadmium mobilization during estuarine mixing. Nature, 336(6195): 151–154.

de Carvalho, L.M., Hollister, A.P., Trindade, C., Gledhill, M., and Koschinsky, A. 2021. Distribution and size fractionation of nickel and cobalt species along the Amazon estuary and mixing plume. Marine Chemistry, 236: 104019.

Espinoza-Villar, J.C., Guyot, J.L., Ronchail, J., Cochonneau, G., Filizola, N., Fraizy, P., Labat, D., de Oliveira, E., Ordoñez, J.J. and Vauchel, P., 2009. Contrasting regional discharge evolutions in the Amazon basin (1974–2004). Journal of Hydrology, 375(3–4): 297–311.

Hollister, A.P., Whitby, H., Seidel, M., Lodeiro, P., Gledhill, M. and Koschinsky, A., 2021. Dissolved concentrations and organic speciation of copper in the Amazon River estuary and mixing plume. Marine Chemistry, 234: 104005.

Poulton, S.W. and Raiswell, R., 2000. Solid phase associations, oceanic fluxes and the anthropogenic perturbation of transition metals in world river particulates. Marine chemistry, 72(1): 17–31.

Vieira, L.H., Krisch, S., Hopwood, M.J., Beck, A.J., Scholten, J., Liebetrau, V. and Achterberg, E.P., 2020. Unprecedented Fe delivery from the Congo River margin to the South Atlantic Gyre. Nature communications, 11(1): 1–8.

M148 (M98/M120/M131/M158)

Seasonal mixed layer heat budget in coastal waters off Angola

AUTHORS

GEOMAR Helmholtz Centre for Ocean Research | Kiel, Germany
M. Körner, P. Brandt, M. Dengler

The coastal waters off Angola are home to a highly productive ecosystem (Ostrowski et al., 2009; Tchipalanga et al., 2018). To the south it is separated by the Angola-Benguela Frontal Zone (ABFZ) from colder waters in the Benguela upwelling region (Fig. 1a). Located at the coast of Africa it is connected to equatorial dynamics via poleward propagating coastally trapped waves (CTWs). The Angola Current (AC) is the main circulation feature in the Angolan ecosystem which transports warm water poleward (Kopte et al., 2017).

The Angolan upwelling system has a distinct seasonal cycle. During austral winter (June-September) productivity peaks and sea surface temperatures are at their seasonal minimum (Fig. 1b&c). At the same time, seasonally-prevailing upwelling-favorable winds are weakest (Fig. 1b). Thus, local wind-driven upwelling is not able to explain the upwelling signal in austral winter. Possible process that leads to changes of the mixed-layer heat content does not only include local mechanism but also the passage of remotely forced CTWs (Fig. 1c). The presence of a strong upwelling CTW in austral summer coincides with the high productive upwelling season. This suggests that CTWs communicating equatorial variability along the continental margin are important for the seasonal upwelling in coastal waters off Angola.

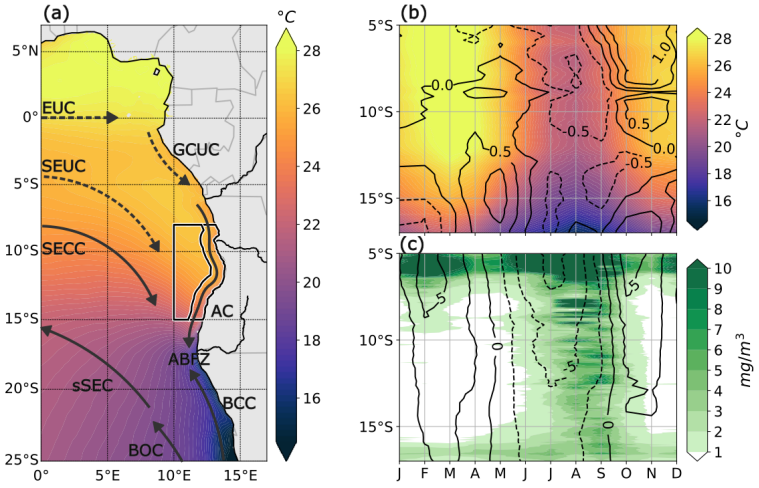

Fig.1: (a) Schematic circulation in the Southeast Atlantic Ocean. Colors show mean SST. Black lines indicate the offshore and coastal box. (b) Seasonal cycle of SST (color) and alongshore wind speed anomaly [m/s] (black lines) within 1.5° distance to the coast. (c) Seasonal cycle of chlorophyll-a (color) and sea level anomaly [cm] (black lines) within 1.5° distance to the coast.

Understanding the driving mechanism of changes in the mixed-layer heat content that may be locally or remotely forced are vital for understanding upwelling off Angola. Here, we investigate the seasonal mixed layer heat budget by analyzing atmospheric and oceanic causes for heat content variability.

Our mixed layer heat budget analysis follows the methodology of Hummels et al. (2014). Horizontal heat advection and surface heat flux are determined. The sum of these two terms is then compared to the local heat storage term. The difference between both is the residuum consisting of contributions we did not consider and uncertainties in the data sets. All terms of the budget are averaged over two boxes. The coastal box includes the area within 1° distance to the coast between 8°S and 15°S. The offshore box is located offshore of the coastal box up to 10°E (Fig. 1a). We use satellite data to calculate monthly estimates of surface heat fluxes, horizontal advection from near-surface velocities and heat storage changes.

Additionally, we use microstructure observations to estimate diapycnal heat loss at the base of the mixed layer due to turbulent mixing. Microstructure observation were conducted during five cruises in Angolan waters (M98, M120, M131, M148, M158). A section at about 11°S was heavily sampled during these cruises. From the microstructure measurements we obtain an estimate of turbulent dissipation rates (Fig. 2a). Average turbulent dissipation rates show distinct differences between the five cruises. In general, the dissipation rates are elevated below the mixed layer and decrease with depth. However, from the dissipation rates available from the five cruises, no clear seasonal dependence is found. Moreover, the average dissipation rates measured during the

same month, a cruise in October 2015 (M120) and a cruise in October 2016 (M131) differ greatly. During October 2016, the dissipation rates are considerably elevated, leading to a larger diapycnal heat loss of the mixed layer. Similarly, we find elevated differences of average dissipation rates between the two cruises conducted in austral winter. During cruise M98 (July 2013) much lower dissipation rates are found compared to cruise M148 (June 2018).

Stratification as well as the temperature gradient also differ between the five cruises (Fig. 2b&c). A very strong temperature gradient and stratification is measured in June 2018 (M148). Note that the stratification is higher in October 2015 (M120) than in October 2016 (M131) despite a similar temperature stratification. A layer off freshwater occupying the upper ocean in October 2015 is the reason for these stratification differences.

The resulting diapycnal heat loss is of different magnitude during the five cruises and also does not exhibit a seasonal dependence (Fig. 2d). Differences between cruises M131 and M120 both conducted in October are particularly pronounced. The mean diapycnal heat loss between 4 and 14 m below the mixed layer amounts to 4 W/m^2 in October 2015 and 57 W/m^2 in October 2016. For the cruises conducted during the upwelling season in austral winter (M98 and M148) diapycnal heat loss was 84 W/m^2 in June 2018 whereas in July 2013 the diapycnal heat loss is clearly reduced (21 W/m^2).

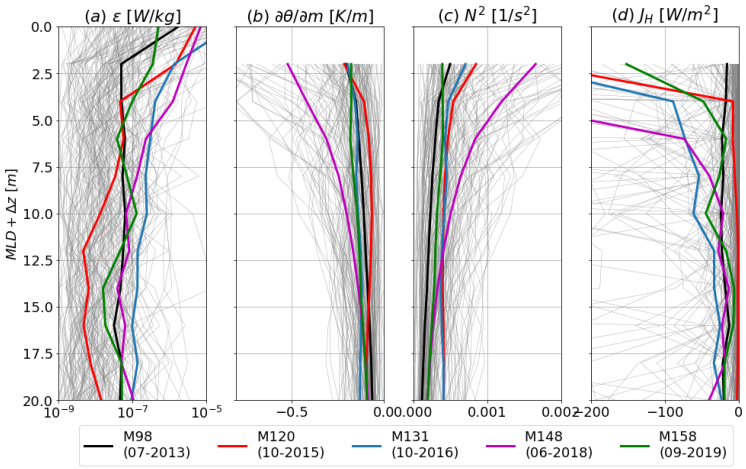

Fig. 2: (a)Turbulent dissipation (Ɛ), (b) temperature gradient, (c) buoyancy frequency and (c) turbulent heat flux as a function of depth below mixed layer. Colored lines give the mean for each cruise. Grey lines show the averages of each microstructure station.

The terms of the mixed layer heat budget show a similar seasonal cycle with different magnitudes in the coastal and the offshore box (Fig. 3a&b). The net surface heat flux is

positive throughout the year averaged over the coastal box. Averaged over the offshore box, the net surface heat flux is weaker and negative between May and June. The total horizontal heat advection has only a small contribution to the mixed layer heat budget. During the course of the year, it mostly contributes to the warming of the mixed layer. The maximum of the total horizontal heat advection is found in October and is larger at the coast.

Comparing the heat storage term with the sum of total horizontal heat advection and net surface heat fluxes reveals that the budget is not closed in the offshore box nor in the coastal box. In the coastal box, the residuum ranges between 45 W/m^2 and 90 W/m^2 and is considerably larger than in the offshore box (15–50 W/m^2). The residuum undergoes a seasonal cycle which differs between the boxes. In the offshore box the maximum residuum is found in January and its minimum in July. In the coastal box the maximum is found in May and the minimum in February.

Microstructure observation from five cruises indicate that heat loss due to diapycnal mixing is an important cooling term in the mixed layer heat budget (Fig. 3b&d). Averaged between 4 and 14m below the mixed layer the term ranges from 4 W/m^2 in October 2015 to 84 W/m^2 in June 2018. Especially, the high inter-annual variability between October 2015 (4 W/m^2) and October 2016 (57 W/m^2) is noteworthy. Adding diapycnal heat loss to the climatological sum of net surface heat fluxes and horizontal heat advection reduces the residuum (Fig. 3d).

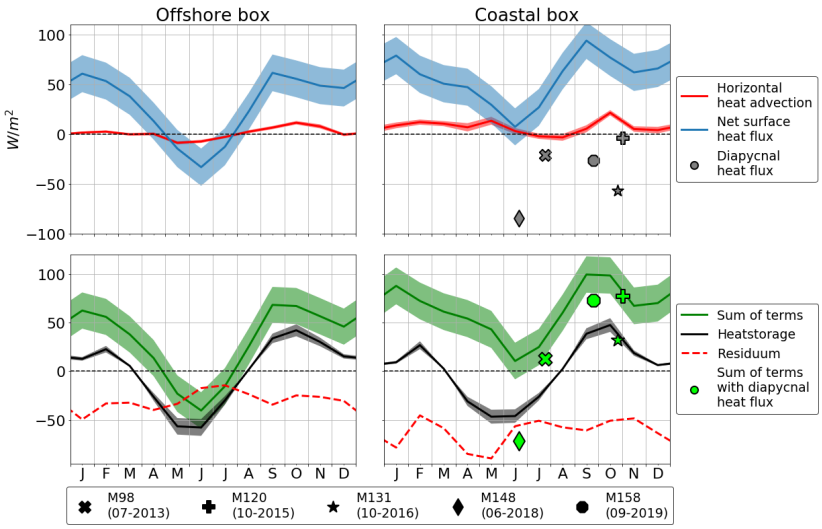

Fig. 3: (a) & (b) Climatology of terms of the mixed layer heat budget in W/m^2. Blue line shows the net surface heat fluxes. Red lines show the total horizontal heat advection. Grey markers display the mean heat loss due to diapycnal mixing averaged between 4 and 14m below the mixed layer measured during five cruises (see legend). (c) & (d) Green lines displays the sum of terms depicted in (a) & (b). Black lines show the heat storage term. The residuum between the sum of terms and the heat storage term is shown in red dashed lines. Green marker shows the climatological sum of terms including the measured diapycnal heat fluxes. (a) & (c) shows the spatial average over the offshore box, (b) & (d) shows the spatial average over the costal box.

Summarizing, the analysis of the mixed layer heat budget reveals that the budget is not closed by only considering the horizontal heat advection and the net surface heat fluxes. The horizontal heat advection term is small and does not contribute crucially to the cooling of the mixed layer. The diapycnal heat loss at the base of the mixed layer seems to be an important term of the mixed layer heat budget. However, the estimates calculated from observed microstructure data reveal a high variability. Further analysis has to be conducted to understand this variability.

REFERENCES

Hummels, R., Dengler, M., Brandt, P., & Schlundt, M. (2014). Diapycnal heat flux and mixed layer heat budget within the Atlantic Cold Tongue. Climate Dynamics, 43(11), 3179–3199. https://doi.org/10.1007/s00382-014-2339-6

Kopte, R., Brandt, P., Tchipalanga, P. C. M., Macueria, M., & Ostrowski, M. (2017). The Angola Current: Flow and hydrographic characteristics as observed at 11S. Journal of Geophysical Research: Oceans, 122, 1177–1189. https://doi.org/doi:10.1002/2016JC012374

Ostrowski, M., Da Silva, J. C. B., & Bazik-Sangolay, B. (2009). The response of sound scatterers to El Ninõ- and La Niña-like oceanographic regimes in the southeastern Atlantic. ICES Journal of Marine Science, 66(6), 1063–1072. https://doi.org/10.1093/icesjms/fsp102

Tchipalanga, P., Dengler, M., Brandt, P., Kopte, R., Macuéria, M., Coelho, P., Ostrowski, M., & Keenlyside, N. S. (2018). Eastern boundary circulation and hydrography off Angola building Angolan oceanographic capacities. Bulletin of the American Meteorological Society, 99(8), 1589–1605. https://doi.org/10.1175/BAMS-D-17-0197.1

M150

Morphospecies and genetic diversity of Bryozoa collected during M150 BIODIAZ in the remote Azores Archipelago

AUTHORS

CIBIO, Centro de Investigação em Biodiversidade e Recursos Genéticos, InBIO Laboratório Associado, Pólo dos Açores | Ponta Delgada, Portugal
L. Baptista, B. Berning, S.P. Ávila

BIOPOLIS Program in Genomics, Biodiversity and Land Planning, CIBIO, Campus de Vairão | Vairão, Portugal
L. Baptista, A.M. Santos, S.P. Ávila

MPB-Marine Palaeontology and Biogeography lab, Universidade dos Açores | Ponta Delgada, Portugal
L. Baptista, S.P. Ávila

Faculdade de Ciências da Universidade do Porto | Porto, Portugal
L. Baptista, A.M. Santos

Institute for Integrative Nature Conservation Research, University of Natural Resources and Life Sciences | Vienna, Austria
L. Baptista, H. Meimberg, M. Curto

Oberösterreichische Landes-Kultur GmbH, Geowissenschaftliche Sammlungen | Linz, Austria
B. Berning

Departamento de Biologia, Faculdade de Ciências e Tecnologia, Universidade dos Açores | Ponta Delgada, Portugal
S.P. Ávila

CIBIO, Centro de Investigação em Biodiversidade e Recursos Genéticos, InBIO Laboratório Associado, Campus de Vairão, Universidade do Porto | Vairão, Portugal
A.M. Santos

Department of Life Sciences, Natural History Museum | London, United Kingdom
A.W. Waeschenbach

MARE, Marine and Environmental Sciences Centre, Faculdade de Ciências, Universidade de Lisboa | Lisbon, Portugal
M. Curto

BRYOZOANS FROM THE CRUISE M150 BIODIAZ

The Cruise M150 BIODIAZ provided a unique opportunity to study the ecology, diversity, abundance, and geographical distribution of epibenthos in mid-shelf to bathyal waters around the Azores. Among the target taxa were bryozoans, a globally distributed group of aquatic, colonial, benthic, suspension-feeding invertebrates represented by over 6,500 described extant species Their role in the ecosystems is undeniable, acting as bioconstructors of habitat to other invertebrate taxa (Cocito 2004, Casoli et al 2020), providing food for micropredators (Lidgard 2008), and contributing to the production of carbonate sediments in shallow-water environments (Bone and James, 1993; Wisshak et al. 2015). About 70 cheilostome and 15 cyclostome bryozoan morphospecies were identified onboard the RV METEOR during the mission, several of which were regarded as new to science. The biological samples were collected from depths of 50 to 2,550 m, resorting to several sampling gears (Agassiz-Trawl, Epibenthic Sledge, Rock Dredge, Henning- and Shipek-Grabs, and Box Corer), and preliminary identification was conducted with a stereomicroscope (George et al. 2018).

BARCODING AZOREAN BRYOZOANS

To meet the BIODIAZ aim of conducting a comprehensive DNA barcoding survey of the Azorean marine fauna, we intend to amplify the mitochondrial marker Cytochrome Oxidase subunit I for the bryozoan morphospecies collected during the cruise M150 BIODIAZ. After extracting genomic DNA, amplification of the target barcode will be achieved with the primers cox1F_prifi/cox1R_prifi (Waeschenbach et al., 2012), specific for bryozoans, and Sanger sequencing will be conducted at Genewiz (Leipzig, Germany). The barcodes of Azorean bryozoans will then be assembled, creating a dataset for phylogeographic reconstructions to unveil their origin and real diversity in the archipelago. So far, barcodes have been produced for 96 specimens from M150, representing 32 cheilostome and 6 cyclostome morphospecies.

Unraveling the relationships among Azorean bryozoans and their closest relatives worldwide will contribute to a better understanding of the so-called "Azorean Biogeographical Paradox" (Ávila 2013, Freitas et al 2019). The oceanic volcanic archipelago of the Azores, sitting in the centre of the North Atlantic, is under a complex regime of sea-surface currents flowing predominantly eastward (for details see Baptista et al. 2021). However, Azorean marine taxa show strong biogeographical affinities with European and Mediterranean taxa, mismatching the circulation patterns in the region and giving rise to the paradox (Ávila 2013). By barcoding and determining the intricate relationships of Azorean bryozoans, we hope to shed light onto the first arrivals to the

archipelago and subsequent evolution and inter-island population genetic exchange in such a remote region.

RELATIONSHIPS WITHIN THE FAMILY PHIDOLOPORIDAE

The phidoloporid genus Reteporella was studied in detail, based on mitochondrial and nuclear markers for phylogenetic analyses, combined with microsatellite data for population genetic inferences. The dataset included individuals from several Azorean islands and seamounts (n=124), but also specimens from the Mediterranean Sea, aiming to put into perspective the evolution of Reteporella in the Azores. Molecular data was complemented with scanning electron microscopy images. Phylogenies were reconstructed following Bayesian Inference and Maximum Likelihood methods. Shot-gun genomic libraries were prepared with Illumina MiSeq at the Ludwig Maximillian Universität (München, Germany) to detect microsatellite regions and design specific primers for Reteporella. Microsatellite genotyping by amplicon sequencing (SSR-GBAS) was performed and analysed with the SSR_GBAS_pipeline.py script (Tibihika et al 2019, Curto et al 2019), generating a dataset suitable for population genetics and diversity inferences.

Historical records report ten *Reteporella* morphospecies in the Azores. The genetic analyses on recent material reveal the presence of at least 6 new species in this genus alone, with consistent genetic differentiation and supported by unique morphological characteristics. Major differences between two genetic groups might call for the need to split the genus *Reteporella* and to revise the taxonomic classification of these bryozoans. The retrieval of four major genetic groups may suggest the arrival of several distinct lineages of *Reteporella* in the archipelago. Locality-dependent genetic differentiation of (cryptic) taxa within some of the groups argues for the presence of an ongoing evolutionary radiation in these clades. This situation becomes clear within the *Reteporella atlantica* clade, as shallow-water samples (<25 m depth) form a well-supported and genetically differentiated lineage. We propose that these have evolved from deep-water ancestrals, taking advantage of adequate empty niches at lower depths. On the other hand, population genetic analyses suggest occasional genetic exchanges between lineages within an island, causing potential introgression in populations of deeper-waters. A wider interpretation of the diversity, biogeography, and evolution of the family Phidoloporidae will soon follow, also based on molecular tools, aiming to put into perspective the evolution of the entire family in the remote Azores Archipelago and to determine if the patterns observed in *Reteporella* are widespread in the family.

REFERENCES

Ávila SP, Unravelling the patterns and processes of evolution of marine life in oceanic islands: a global framework. In: Fernández-Palacios JM, Nascimento L, Hernández JC, Clemente S, González A, Díaz-González JP (eds) Climate Change Perspectives From the Atlantic: Past, Present and Future, Universidad de La Laguna, Tenerife, 2013, 95–125.

Baptista L, Santos AM, Melo CS, Rebelo AC, et al. Untangling the origin of the newcomer Phorcus sauciatus (Mollusca: Gastropoda) in a remote Atlantic archipelago, Marine Biology 2021, 168, doi: 10.1007/s00227-020-03808-5.

Bone Y, James NP, Bryozoans as carbonate sediment producers on the coolwater Lacepede Shelf, southern Australia, Sedimentary Geology 1993, 86, 247–271.

Casoli E, Piazzi L, Nicoletti L, Jona-Lasinio G, et al. Ecology, distribution and demography of erect bryozoans in Mediterranean coralligenous reefs, Estuarine, Coastal and Shelf Science 2020, 235, doi: 10.1016/j.ecss.2019.106573.

Cocito S, Bioconstruction and biodiversity: their mutual influence, Scientia Marina 2004, 68 (Suppl. 1), 137–144.

Curto M, Winter S, Seiter A, Schmid L, Scheicher K, Barthel LMF, et al. Application of a SSR-GBS marker system on investigation of European Hedgehog species and their hybrid zone dynamics. Ecology and Evolution 2019, 9, 2814–2832. doi:10.1002/ece3.4960.

Freitas R, Romeiras M, Silva L, Cordeiro R, et al. Restructuring of the 'Macaronesia' biogeographic unit: a marine multi-taxon biogeographical approach, Scientific Reports 2019, 9, doi: 10.1038/s4159 8-019-51786-6.

George KH, Arndt H, Wehrmann A, Baptista L, et al. Controls in benthic and pelagic BIODIversity of the AZores BIODIAZ, Cruise No. M150, 27.08.2018–02.10.2018, Cádiz (Spain) – Ponta Delgada, São Miguel (Azores). METEOR-Berichte, Gutachterpanel Forschungsschiffe 2018, 74 pp. doi:10.2312/cr_m150.

Lidgard S, Carter MC, Dick MH, Gordon DP, et al. Division of labor and recurrent evolution of polymorphisms in a group of colonial animals, Evolutionary Ecology 2011, 26, 233–257, doi:10.1007/s10682-011-9513-7.

Tibihika PD, Curto M, Dornstauder-Schrammel E, Winter S, et al. Application of microsatellite genotyping by sequencing (SSR-GBS) to measure genetic diversity of the East African Oreochromis niloticus, Conservation Genetics 2019, 20, 357–372. doi: 10.1007/s10592-018-1136-x.

Waeschenbach A, Taylor PD, Littlewood DTJ, A molecular phylogeny of bryozoans, Molecular Phylogenetics and Evolution 2012, 62, 718–735, doi: 10.1016/j.ympev.2011.11.011.

Wisshak M, Berning B, Jakobsen J, Freiwald A, Temperate carbonate production: biodiversity of sclerobionts from intertidal to bathyal depths (Azores), Marine Biodiversity 2015, 45(1), 87–112, doi: 10.1007/s1

M150

BIODIAZ – Vertical distribution of heterotrophic protists from Atlantic sublittoral to deep-sea sediments

AUTHORS

University of Cologne | Cologne, Germany
M. Hohlfeld, H. Arndt

Since the studies of the global Tara Ocean expedition, it is known that marine heterotrophic protists form the most diverse group of organisms on our planet (de Vargas et al., 2015). However, eukaryotic microbial life at abyssal depths and on seamounts is still widely uncharted, which contradicts its potential importance regarding the material flux and trophic interactions in these habitats. Only recently, protists inhabiting deep-sea sediments became subject of next-generation-sequencing studies revealing their high and specific diversity (Gooday et al., 2020, Schoenle et al., 2021, Scheckenbach et al., 2010). Next-generation-sequencing methods like metabarcoding of short marker regions are well suited to investigate the diversity of communities and their biogeographical distribution (Burki et al., 2021), while live-counting techniques offer the opportunity to gain information on the morphology and behavior of organsims beside quantitative estimates of taxa (Schoenle et al., 2016). Abundance estimations of heterotrophic flagellates in deep-sea sediments have revealed densities of a few hundred up to 105 cells cm-3 (e. g. Arndt et al., 2003, Bak and Nieuwland, 1997), but only little is known about vertical distribution patterns of benthic protists. Our studies on protists from the Great Meteor Seamount (expedition M79/1, 2009) south of the Azores are probably the only ones comparing benthic protists on shallow seamounts and the surrounding deep sea (Salani et al., 2012). Information on how the abundance and community composition of protists changes along vertical depth gradients is of special importance for analyzing the role of islands/seamounts for the dispersal of species.

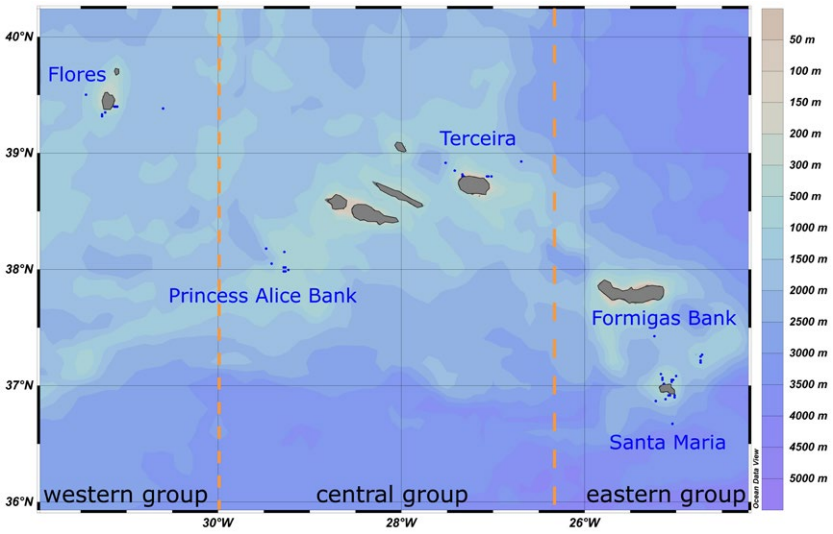

Fig. 1: Map showing stations (dark blue dots) of cruise M150 BIODIAZ, where sediment samples for metabarcoding analysis were taken. Map created with Ocean Data View (Schlitzer, 2012).

The Azores islands have an isolated position in the middle of the North Atlantic and are well suited to study whether they function as staging posts/stepping stones, enabling the constant gene flow over large distances, or if they act as trapping stones, where the gene flow is disconnected and species become "trapped" (George, 2013, Pinheiro et al., 2017). During cruise M150, we sampled sediment along vertical depth gradients from 50 to 3,000 m depth around three islands and two seamounts of the Azores archipelago (Fig. 1), which were analysed by metabarcoding of the hypervariable V9-region on the SSU rDNA, live-observations and cultivation techniques to resolve distribution patterns of protist communities. Besides benthic protist communities, we also investigated pelagic protists during cruise M150 to analyse benthic-pelagic interactions. A total of ten stations, including three open ocean stations (Caribbean Sea and southern North Atlantic) from cruise M139 as well as seven stations around the Azores islands, sampled during cruise M150 were examined.

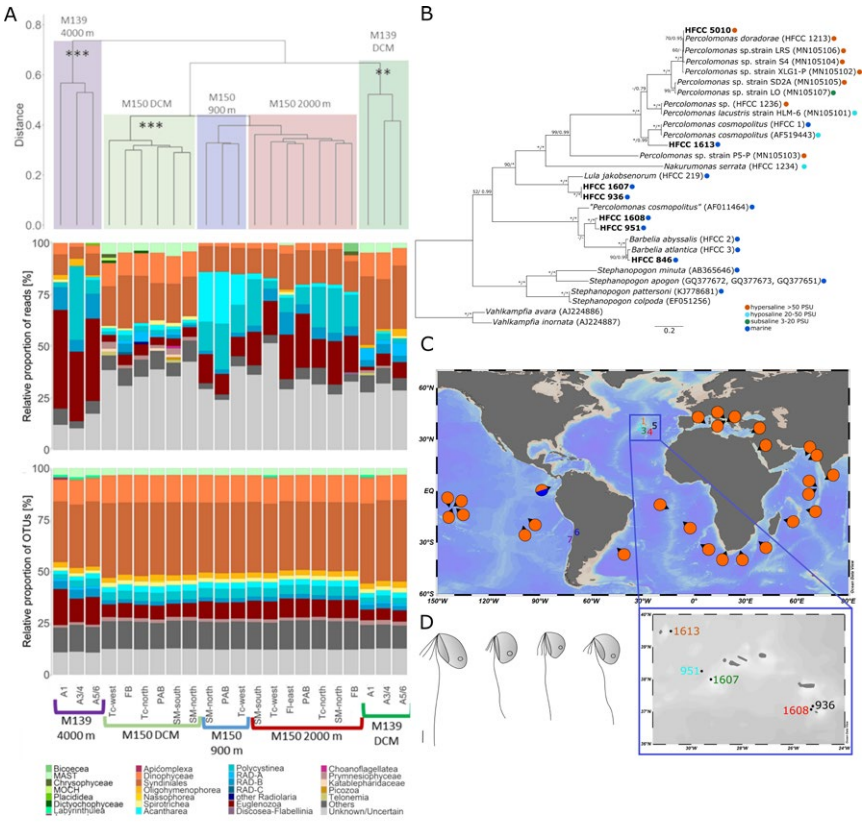

Fig. 2: (A) Community structure of pelagic protists at 22 stations of cruises M150 and M139. Upper panel showing a cluster dendrogram based on Jaccard distance, middle panel showing relative proportions of reads and lower panel showing relative proportions of OTUs with regard to taxonomic composition. (B) Maximum likelihood phylogeny of the Percolatea, one of the groups we investigated in more detail. (C) Map showing geographical positions of stations of the Tara Ocean project, where metabarcode sequences (V9-sequences of 18S rDNA) with 100 % similarity to the isolated percolomonads were found. (D) Drawings of the isolated and cultivated Percolomonadida.

Samples from surface to bathypelagic waters were analysed using a combined approach based on Illumina sequencing of the V9-region and a cultivation-based approach in order to study the vertical distribution of heterotrophic protists. Abundance and taxonomic composition of pelagic protist communities showed a depth and sampling area related pattern (Fig. 2, A). With the cultivation approach we were able to isolate and cultivate different protist species of various taxonomic groups. One example presented here are Percolomonadida, for which we could resolve the phylogeny by adding SSU sequences of five newly isolated strains (Fig. 2, B). The biogeographic distribution of strains was analysed by searching for the V9-regions (variable marker region located on SSU rDNA) of all isolated strains in two global NGS datasets (Fig. 2, C).

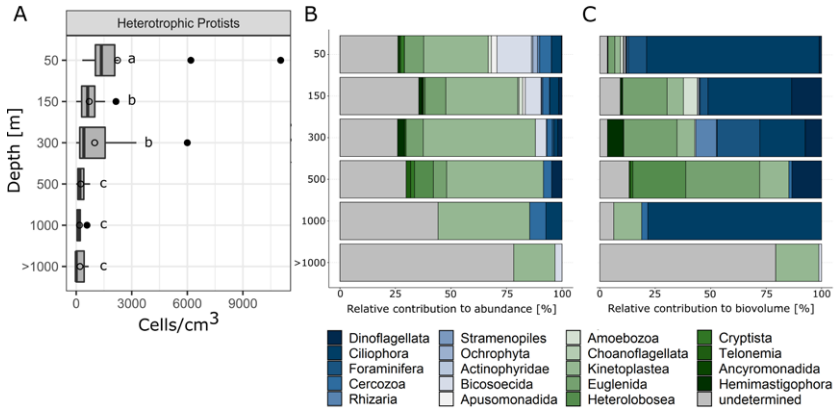

Fig. 3: (A) Boxplots showing the abundance of heterotrophic protists obtained by live-counting from 50 to 3,000 m depth. Results from Kruskal-Wallis test with Dunn's post hoc test are indicated by next to boxes. (B) Relative contribution to abundance and (C) to biovolume of taxonomic groups in different depths observed during live-counting on cruise M150 BIODIAZ.

The main focus of our investigations laid on the benthic protist community. In total 202 different morphotypes were identified during live-counting (Fig. 3). Abundances of heterotrophic protists were in the same range as abundances from literature (e. g. Arndt et al., 2003). The abundance of heterotrophic protists was significantly higher in samples from 50 m depth than in all other depths (Fig. 3, A). In 50 down to 1,000 m depth, the taxonomic group of Kinetoplastea made up the largest proportion of the abundance of heterotrophic protists (Fig. 3, B). In 500 m, Heterolobosea and in 1,000 m, Ciliophora and Cercozoa were frequently found. Organisms, which could not be identified at the deepest stations contributed with up to 78 % to the abundance, indicating the large number of so far undiscovered species inhabiting the deep sea. Ciliophora made up the largest relative contribution to the biovolume (Fig. 3, C). Sequencing of up to now 30 sediment samples resulted in a total of 49,889,149 filtered reads clustering into 1,138 operational taxonomical units (OTUs). Most reads with 100 % similarity to a reference sequence were assigned to Alveolata and Obazoa (Fig. 4, A).

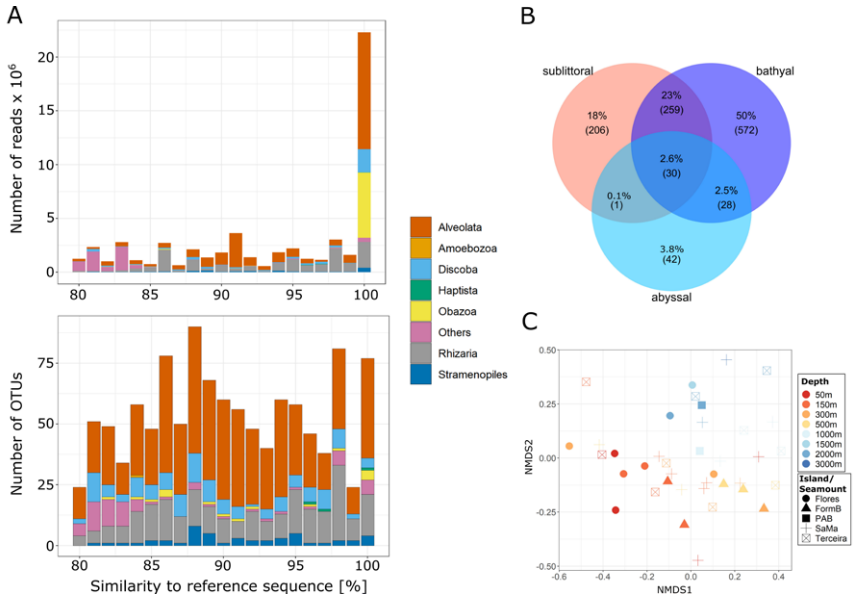

Fig. 4: (A) Similarity of reads and OTUs to sequences from the enlarged PR^2 database and their taxonomic affiliation. Only reads/OTUs with a similarity >80 % are shown. (B) Venn diagram showing shared and unique OTUs of sublittoral, bathyal and abyssal regions. (C) Non-metric multidimensional scaling (NMDS) plot based on the Jaccard distance comparing protist communities from different depths and different islands/seamounts.

The high number of OTUs with low sequence similarities indicate a high number of so far undiscovered genotypes, which are not yet covered by reference databases. The sublittoral and bathyal shared only low amounts of OTUs with the abyssal, which points towards a distinct deep-sea community (Fig. 4, B) which confirms the results of live-observations (see above). Samples from 50 to 500 m and samples from 1,000 to 3,000 m clustered closely together in the NMDS analysis, indicating a separation of protist communities by depth, while the island/seamount where samples were taken, seems to play a minor role for the community structure (Fig. 4, C). Relative contributions of reads and OTUs of taxonomic groups revealed diverse community structures in all depths (Fig. 5, A). In 50 m depth, Choanoflagellata and Ciliophora dominated the reads, while in 150 to 1000 m depth, Radiolaria, Dinoflagellata and Katablepharidophyta increased. Concerning the relative contribution of OTUs, Dinoflagellata and Radiolaria dominated. While OTUs belonging to some taxonomic groups were detected at all investigated islands and seamounts, others were found to be unique to single spots or occurred only at some islands/seamounts (Fig. 5, B), indicating that for some groups, the islands/ seamounts serve as stepping stones leading to a wide distribution of organisms, while others seem to be restricted in their dispersal. Samples from additional sampling sites are presently analyzed and will further resolve the distribution patterns of genotypes.

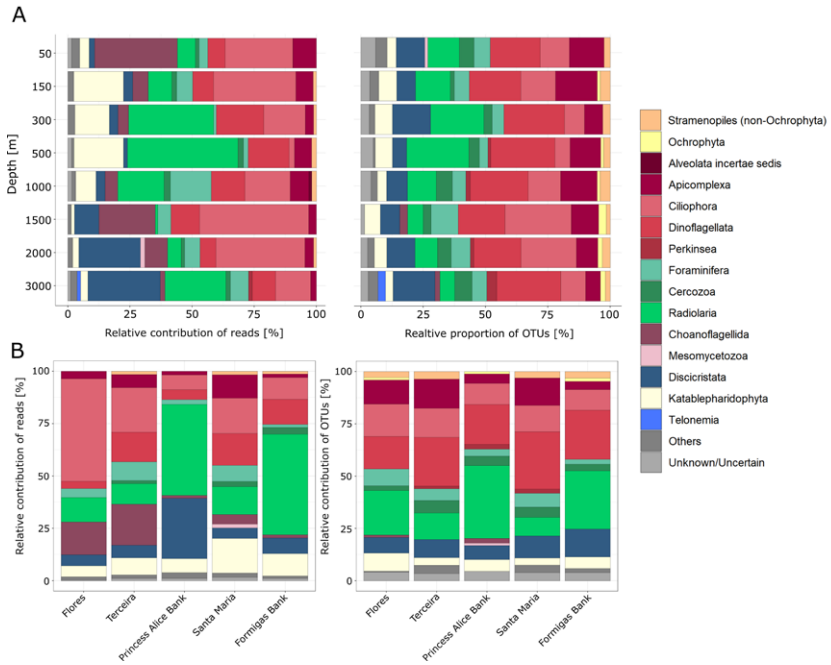

Fig. 5: Community structure of heterotrophic protists (A) in depths from 50 to 3,000 m and (B) at different islands/seamounts of the Azores sampled during cruise M150. Relative contribution of reads (left) and OTUs (right) assigned to taxonomic groups. Taxa with a relative abundance of <1 % are denoted as "Others". Reads/OTUS which could not be assigned to any taxonomic division are shown as "Unknown/Uncertain".

REFERENCES

Arndt H, Hausmann K, Wolf M, Deep-sea heterotrophic nanoflagellates of the Eastern Mediterranean Sea: qualitative and quantitative aspects of their pelagic and benthic occurrence, Mar. Ecol. Prog. Ser. 2003, 256, 45–56

Bak R, Nieuwland G, Seasonal variation in bacterial and flagellate communities of deep-sea sediments in a monsoonal upwelling system, Deep-Sea Research Part II 1997, 44(6–7), 1281–1292

Burki F, Sandin M, Jamy M, Diversity and ecology of protists revealed by metabarcoding, Current Biology 2021, 31, R1267–R1280, doi: 10.1016/j.cub.2021.07.066

de Vargas C, Audic S, Henry N, Decelle J, Mahé F, et al. Eukaryotic plankton diversity in the sunlit ocean, Science 2015, 348(6237), 1261605-1-11, doi: 10.1126/science.1261605

George KH, Faunistic research on metazoan meiofauna from seamounts – a review, Meiofauna Marina 2013, 20, 1–32

Gooday AJ, Schoenle A, Dolan, JR, Arndt H, Protist diversity and function in the dark ocean – challenging the paradigms of deep-sea ecology with special emphasis on foraminiferans and naked protists, Europ. J. Protistol. 2020, 75, 125721, doi: 10.1016/j.ejop.2020.125721

Pinheiro HT, Bernardi G, Simon T, Joyeux J-C, Macieira RM, Gasparini JL, Rocha C, Rocha LA, Island biogeography of marine organisms, Nature 2017, 549(7670), 82–85, doi: 10.1038/nature23680

Salani F, Arndt H, Hausmann K, Nitsche F, Scheckenbach F, Analysis of the community structure of abyssal kinetoplastids revealed similar communities at larger spatial scale, The ISME Journal 2012, 6(4), 713–723, doi: 10.1038/ismej.2011.138

Scheckenbach F, Hausmann F, Wylezich C, Weitere M, Arndt H, Large-scale patterns in biodiversity of microbial eukaryotes from the abyssal sea floor, PNAS 2010, 107(1), 115–120, doi: 10.1073/pnas.0908816106

Schlitzer R, Ocean Data View, 2012, http://odv.awi.de.

Schoenle A, Jeuck A, Nitsche F, Venter P, Prausse D, Arndt H, Methodological studies on estimates of abundance and diversity of heterotrophic flagellates from the deep-sea floor, J. Mar. Sci. Eng. 2016, 4(22), doi: 10.3390/jmse4010022

Schoenle A, Hohlfeld M, Hermanns K, Mahé F, de Vargas C, Nitsche F, Arndt H, High and specific diversity of protists in the deep-sea basins dominated by diplonemids, kinetoplastids, ciliates and foraminiferans, Communications Biology 2021, 4(501), doi: 10.1038/s42003-021-02012-5

M150

Preliminary insights into the gastrotrich community of sublittoral sediments of the Azores Archipelago (Portugal) obtained during METEOR cruise M150 Controls in benthic and pelagic BIODIversity of the Azores BIODIAZ

AUTHORS

Senckenberg am Meer, German Centre for Marine Biodiversity Research | Wilhelmshaven, Germany
A. Kieneke

In the course of the BIODIAZ project, a multitude of sediment samples from various depths were obtained during cruise M150 of R/V METEOR in the area of the Azores Archipelago. In order to gain preliminary insight into the community of marine Gastrotricha, a subset of samples from depths between 50 and 300 m was cultivated aboard (vented and stored at 10°C) and living meiofauna was subsequently extracted with a 7 % aqueous solution of MgCl2 for microscopic investigation and extraction of genomic DNA. This initial study yielded 18 species of the taxon *Macrodasyida* (Fig. 1). Added to the 13 species reported in the 'Global distribution of marine Gastrotricha' (one species probably concordant), we currently know at least 30 marine gastrotrich species from the Azores belonging to 20 different genera of both gastrotrich subclades Macrodasyida and Paucitubulatina. The new genus and species *Chimaeradasys oligotubulatus* was recently described from material of expedition M150 (Kieneke & Todaro 2021).

Fig. 1: A selection of gastrotrich species discovered during expedition M150. From left to right: *Diplodasys ankeli, Tetranchyroderma* sp. 3, *Crasiella azorensis, Acanthodasys* sp. 1, *Xenodasys eknomios, Oregodasys* sp. 1 (light microscopic images; not to scale).

Fourteen out of the 31 'Azorean morphospecies' known so far have also been reported from further coastal locations on both sides of the North Atlantic Ocean. Among the latter species are *Dactylopodola cornuta, D. typhle, Xenodasys riedli, Diplodasys ankeli, D. meloriae,* and *D. minor,* which have also been discovered in the sublittoral samples of expedition M150. The occurrence of such widespread morphospecies in remote oceanic biotopes like the Azores and associated seamounts may support their role as 'stepping stones' or 'staging posts' supporting a trans-oceanic long-distance dispersal of interstitial meiobenthic organisms. Initial analyses of DNA sequence data of the three species *Diplodasys ankeli, D. meloriae,* and *D. minor* demonstrate a rather high genetic diversity of *D. ankeli* across the whole archipelago. Furthermore, affinities between analyzed Azorean specimens of all three species and specimens from different European coastal populations emerged as well. This may be interpreted as an indication of past connectivity/gene flow between oceanic and continental populations. In order to identify putative source populations and pathways of past colonization of the Azorean sediments, however, comprehensive analyses with more satisfying sampling sizes and from various populations across the Atlantic Ocean are essential.

REFERENCE

Kieneke A & Todaro MA, Discovery of two 'chimeric' Gastrotricha and their systematic placement based on an integrative approach, Zoological Journal of the Linnean Society 2021, 192, 710–735. Https://doi:10.1093/zoolinnean/zlaa117

M150

BIODIAZ: Calcareous nanophytoplankton distribution around the Azores Archipelago (Central North Atlantic)

AUTHORS

University of Madeira, Faculty of Life Sciences | Funchal, Madeira Island, Portugal
Á. Narciso, M. Kaufmann

CIIMAR – Interdisciplinary Centre of Marine and Environmental Research | University of Porto, Matosinhos, Portugal
Á. Narciso, M. Kaufmann

Ocean Observatory of Madeira – OOM/ARDITI | Funchal, Madeira Island, Portugal
Á. Narciso, M. Kaufmann, T. Silva

Senckenberg am Meer, Marine Research Department | Wilhelmshaven, Germany
B. Springer

The enhanced productivity that occurs around oceanic islands in comparison to the surrounding waters is known as Island Mass Effect (IME). This process, recognised worldwide and shown in numerous studies (Hernández-León et al. 2001, Elliott et al. 2012), may rise the nearshore standing stock of phytoplankton biomass by more than 80 % over background oceanic productivity. Acting as natural barriers in the main current pathways, seamounts and islands lead to similar geophysical and biological effects when compared to the surrounding open ocean (Hasegawa et al. 2004).

Coccolithophores, which represent about 10 % of the global phytoplankton biomass (Tyrrell and Young 2009), are pelagic unicellular algae members of the haptophyte class Prymnesiophyceae Hibberd, distinguished by the ability to produce calcite platelets. Surrounding the living cell, which diameter vary from 2 to 75mm, these calcareous structures, referred as coccoliths, form an exoskeleton called coccosphere (e. g. Winter and Siesser, 1994). Being widely and abundantly distributed in the ocean, these nannoplankton organisms are one of the major contributors of pelagic carbonate on Earth (Beare et al., 2013) and dominate the phytoplankton biodiversity in the oligotrophic central gyres of the oceans (Winter et al., 1994).

The North Atlantic Subtropical Gyre (NAST; Longhurst et al., 1995), where the present work was developed, is characterized by relatively weak winter deep mixing, with high rates of productivity during the months of January to March, and minimum primary production rate in late summer (Waniek et al., 2005).

Being an isolated archipelago in the middle of the North Atlantic, the Azores may serve as a unique model system for biogeographic research of marine taxa. The present work was developed in the context of the BIODIAZ (BIODiversity of the AZores) project, which provided material from sublittoral down to deep-sea stations in order to incorporate innovative aspects into the study of island and seamount productivity. Thus, the main goals of the present study involve: i) to detect the influence of the islands on the abundance, composition and distribution of the phytoplankton community; ii) to check these differences among islands and between islands and seamounts; iii) to compare nearshore and offshore abundance and composition of the phytoplankton communities along several transects; iv) to compare the difference in abundance and species diversity along depth.

Sampling was performed during the oceanographic campaign M150 of RV Meteor, between 27th August and 2nd October of 2018, in the scope of the project BIODIAZ. This expedition provided material from different Azorean islands (Flores, Terceira and Santa Maria) and seamounts (Princesa Alice and Formigas).

For the present work a total of 50 stations along 9 transects were selected. Seawater samples were collected between 5 and 8 depths per station, from the first 150m, through a rosette with 24 Niskin bottles of 10L volume. CTD-profiles were recorded with the ship's CTD/Rosette system.

The present study was based on a total of 306 seawater samples. Onboard, between 3-4L from each depth were immediately filtered through Whatman nuclepore track-etched polycarbonate membranes, rinsed with about 1–2 ml of deionized water, to remove sea salt, and left to dry at ambient temperature in plastic Petri dishes, sealed with parafilm. At the laboratory, a randomly chosen 20 to 30° angular sector of each filter was cut and permanently mounted on a slide. Species diversity and abundances were determined under cross-polarized light microscopy (Leitz Ortholux II Pol-BK) at 1250x magnification. At least 400 coccospheres were counted through a randomly selected sequence of fields of view aligned parallel to the radius of the filter. The results are presented in absolute abundances (Coccosphere L^{-1}).

A total of 45 distinct taxa were recognized using polarizing light microscopy. Total cell densities ranged between $0.56x10^3$ and $79.79x10^3$ cell L^{-1}, being the highest coccolithophore densities observed at Formigas Bank, at a water depth of 60 m, whereas the lowest were observed south of the Flores Island, at a water depth of 25 m. In order to recognize the spatial distribution of coccolithophores in the studied regions of the Azores archipelago, the total cell integrated abundances over the water column (5 to 150 m) were plotted (Fig. 1). This figure shows a trend to higher concentrations in the southeast section, namely in the Formigas Bank and in its SW coast. The Princesa Alice Bank, positioned westwards, showed the lowest coccolithophore concentrations. The analysis of the several transects over the 5 regions does not show a consistent pattern,

however, and for Santa Maria Island in particular, there is a tendency for absolute abundance increases offshorewards.

Gephyrocapsa ericsonii together with *Emiliania huxleyi* are the most abundant species, making up to 59 % of the total abundance. Other pertinent taxa for the present study, in order of decreasing abundance were: *Umbellosphaera spp., Florisphaera profunda, Syracosphaera spp., Discosphaera tubifera, Gephyrocapsa oceanica, Algirosphaera robusta, Rhabdosphaera spp., Michaelsarsia spp., Ophiaster spp., Calciosolenia spp., Umbilicosphaera spp. (mostly U. sibogae), Reticulofenestra sessilis, Acanthoica spp., Gladiolithus flabellatus, Helicosphaera spp. (mostly H. carteri), Oolithotus spp. (mostly O. antillarum)*, and *Syracosphaera lamina*.

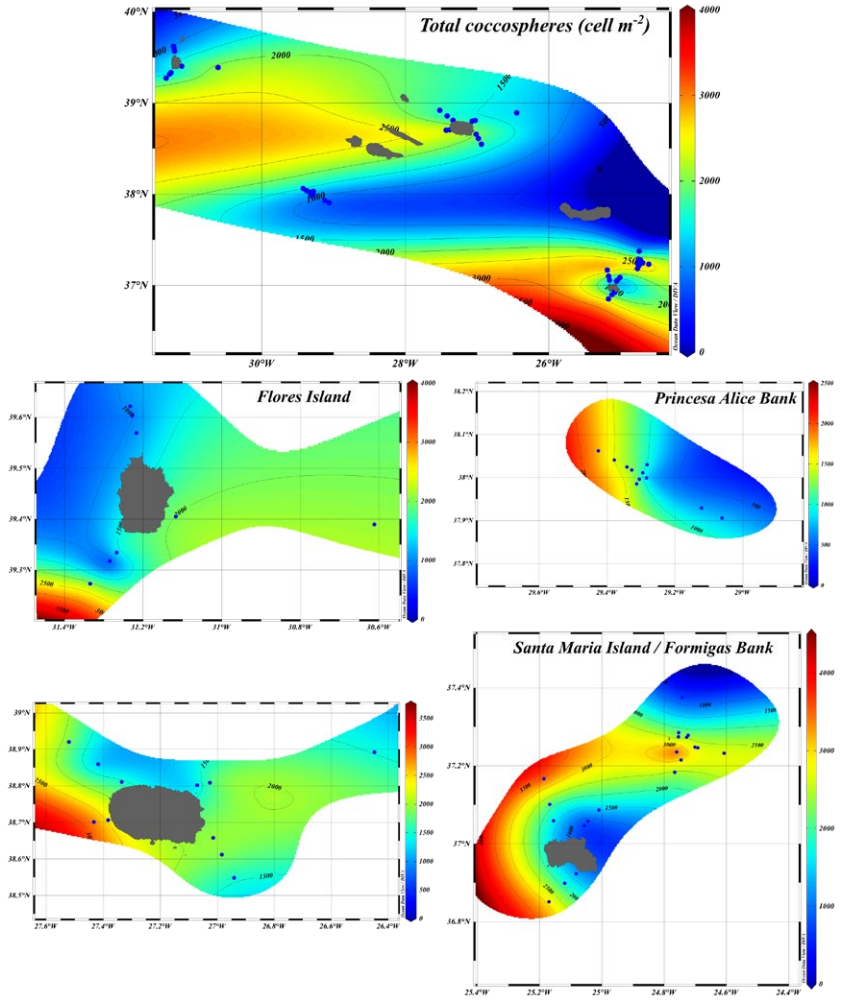

Fig. 1: Spatial distribution of the total coccolithophore densities based on its depth integrated data.

Concerning the taxa depth distribution, a vertical zonation was depicted: a shallower group, above 50–60m depth, represented by D. *tubifera, Rhabdosphaera spp., Umbellosphaera spp.* and the *holococcolithophores*; an intermediate group, between 60 and 80m depth, represented by the *coccolith-bearing E. huxleyi, G. ericsonii* and *G. oceanica*, as well as by *Syracosphaera spp.*; and a deeper group, below 75m depth, represented by *A. robusta* and *F. profunda*, with higher abundances until 100m depth, and represented by *G. flabellatus* and *S. lamina*, with higher abundances below 100m depth.

REFERENCES

Beare D, McQuatters-Gollop A, van der Hammen T, Machiels M, Teoh S J, Hall-Spencer J M, Long-Term Trends in Calcifying Plankton and pH in the North Sea. PLoS ONE 2013, 8(5), https://doi.org/10.1371/journal.pone.0061175

Elliott J, Patterson,M, Gleiber M, Detecting ' Island Mass Effect ' through remote sensing. Proceedings of the 12th International Coral Reef Symposium 2012, July, 9–13.

Hasegawa D, Yamazaki H, Lueck R G, Seuront L, How islands stir and fertilize the upper ocean, Geophysical Research Letters 2004, 31(16), 2–5, https://doi.org/10.1029/2004GL020143

Hernández-León S, Almeida C, Gómez M, Torres S, Montero I, Portillo-Hahnefeld A, Zooplankton biomass and indices of feeding and metabolism in island-generated eddies around Gran Canaria. Journal of Marine Systems 2001, 30(1–2), 51–66, https://doi.org/10.1016/S0924-7963(01)00037-9

Longhurst A, Sathyendranath S, Platt T, Caverhill C, An estimate of global primary production in the ocean from satellite radiometer data. Journal of Plankton Research 1995, 17(6), 1245–1271, https://doi.org/10.1093/plankt/17.6.1245

Tyrrell T, Young J R, Coccolithophores 2009, In Encyclopedia of Ocean Sciences (pp. 606–614), Elsevier. https://doi.org/10.1016/B978-012374473-9.00662-7

Waniek J J, Schulz-Bull D E, Blanz T, Prien R D, Oschlies A, Müller T J, Interannual variability of deep water particle flux in relation to production and lateral sources in the northeast Atlantic, Deep Sea Research Part I: Oceanographic Research Papers 2005, 52(1), 33–50, https://doi.org/10.1016/j.dsr.2004.08.008

Winter A, Siesser W G, Atlas of living Coccolithophores 1994, In A Winter & W G Siesser (Eds.), Coccolithophores (Vol 75, Issue 01), Cambridge University Press, https://doi.org/10.1017/S0025315400015496

Winter A, Jorda, R, Roth P, Biogeography of living coccolithophores in ocean waters, In: Winter A, Siesser W (Eds), Coccolithophores 1994, Cambridge University Press, Cambridge, pp. 161–177.

M150

BIODIAZ – Controls in sedimentary facies and related carbonate factories of volcanic islands, seamounts and shallow water platforms around the Azores

AUTHORS

Senckenberg am Meer, Marine Research Department | Wilhelmshaven, Germany
A. Wehrmann

Senckenberg am Meer, German Centre for Marine Biodiversity Research | Wilhelmshaven, Germany
K.H. George, A. Kieneke

University of Madeira, Faculty of Life Sciences | Funchal, Portugal
M. Kaufmann

University of Cologne | Cologne, Germany
H. Arndt

During M150 cruise the Shipek grab was applied in shallow waters down to 300m water depth. As a small-scale spatial variation in sediment composition has locally to be expected, up to 4 grabs were taken at stations where meiobenthos sampling and/or underwater video surveys revealed substrate heterogeneity. For sediment facies analysis we determined at least 400 particles of each grain size fraction (<0.125mm, 0.125–0.25mm, 0.25–0.5mm, 0.5–1mm, 1–2mm, >2mm) to calculate the relative proportion of each particle group (n=20) to the overall sediment composition (for details see Sarnthein 1971).

In total we analysed 53 samples of stations from 50 to 300 m water depth covering all transects of the 5 study areas, i. e., the three volcanic islands of different ages and tectonic settings (Flores, Terceira, Sta. Maria), one seamount (Princess Alice Bank, PAB) and one shallow water platform (Formigas Bank) (see George et al 2021).

GRAIN SIZE DISTRIBUTION

Most of the sediments can be classified as fine sands to coarse sands. These sands are most common around the volcanic islands and the Formigas. The sorting in general is good, however, heterogeneous or bimodal grain size distribution rarely occur, both ranging into the gravel fractions. Contrastingly, all sediments from the Princess Alice Bank are coarse sands to medium gravel showing a homogenous grain size distribution comparing to each other.

VOLCANIC ORIGIN VS. BIOGENIC SEDIMENT PRODUCTION

As postulated by our working hypothesis the terrestrial signal in sediment composition is clearly recognizable in the shallow water stations, especially around the volcanic Islands of Flores, Terceira and to a minor amount Santa Maria. The lithoclastic/volcanic sediment particles can reach more than 95 % of all particles (Flores, Terceira, PAB) whereas around St. Maria and the shallow-water platform Formigas the lithoclastic components are less than 9.5 % (mean) and 1.2 % (mean), respectively. On the other hand, this means that bioclastic components represent on average 72.5 % of the sediment composition over all stations irrespective water depth, transect orientation and geological setting.

FACIES ANALYSIS

The bioclastic sediments show a broad variety of components reflecting numerous different subhabitats/-environments. The biogenic composition of the sediments can be assigned to distinct groups of benthic and pelagic organisms, mainly erect rigid-branching bryozoan colonies, benthic foraminifera (e. g. *Miniacina miniace*a), echinoderms (sea urchins & brittle stars), corals, bivalves, benthic gastropods, tube-building polychaetes, and planktonic pteropods and globigerinids.

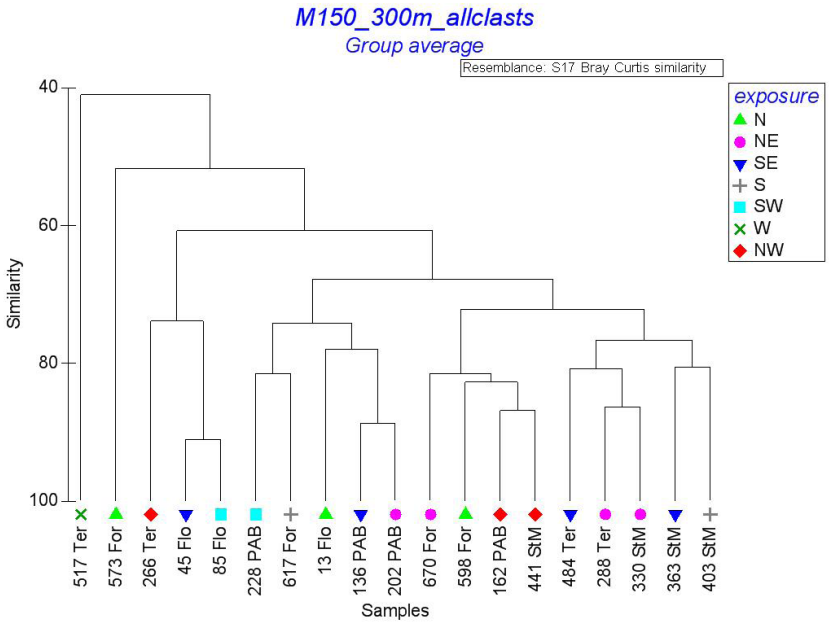

Fig. 1: Cluster analysis of sediments from all 300m Stations of M150 Cruise concerning the entire component spectrum (bioclasts, relictic material, lithoclasts). Ter = Terceira, Flo = Flores, StM = St. Maria, For = Formigas, PAB = Princess Alice Bank.

The bioclastic sediments can be classified as autochthonous to par-autochthonous showing a spatial relation to their so called "carbonate factories". Some of the 150m

and 300 m stations show relictic sediments, most probably originating from Pleistocene sea level lowstands. This is also true for findings of Verruca stroemia in sediments from the 150 m and 300m stations of PAB which clearly indicates previous larger stocks of macro algae (kelp) in the shallowest parts of PAB.

Some component groups show a clear preference to the main wind/wave direction (Fig. 1). Porifera as well as Echinoidea mostly occur in the eastern sector of the islands, i. e., on the leeward side. The opposite is true for the lithoclastic material which is most frequent in the western and southern sector. This scheme is also visible, e. g., in the cluster analysis of all 300m stations were the samples of the subfacies cluster to distinct directions of exposure. The statistic outliers of sample 517 Ter and 573 For (and 266 Ter) (Fig. 2) are due to the extreme amounts of distinct particle groups (bivalves, Miniacina miniacea, carbonate-tube polychaetes). In general, 4 facies groups can be recognized from statistical analyses of the sediments from the 300m stations which, however, show a higher grade of similarity.

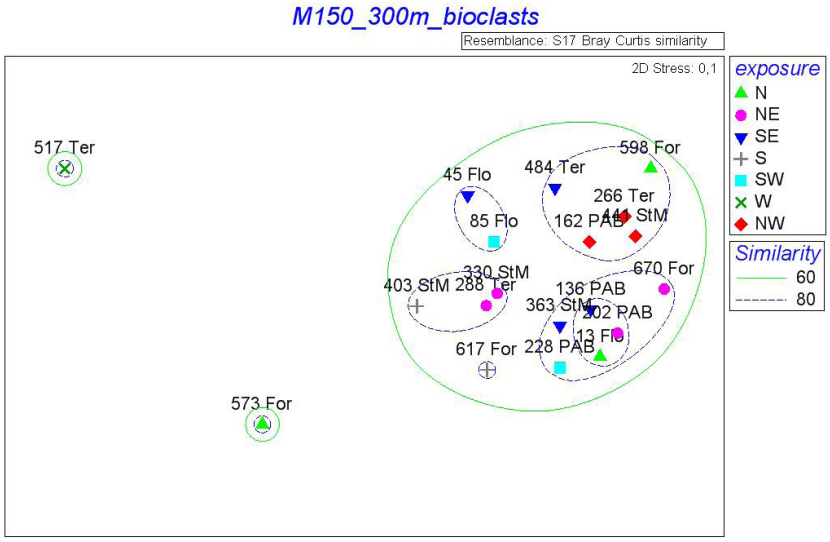

Fig. 2: nMDS plot of sediments from all 300m Stations of M150 Cruise concerning the entire bioclasts component spectrum. Ter = Terceira, Flo = Flores, StM = St. Maria, For = Formigas, PAB = Princess Alice Bank.

REFERENCE

Sarnthein M, Oberflächensedimente im Persischen Golf und Golf von Oman. II Quantitative Komponentenanalyse der Grobfraktion, „Meteor"-Forschungsergebnisse 1971, C, 5: 1–113

MPI-MET/NASA COLLABORATIONS

AUTHORS

Max-Planck-Institute for Meteorology | Hamburg, Germany
S. Kinne, T. Machnitzki, J. Menken

AEROSOL REFERENCES OVER OCEANS AND SATELLITE EVALUATIONS

Since 2008 the Max-Planck-Institute for Meteorology in Hamburg has distributed NASA owned sun-photometers to the science staff, that participated on transit and science cruises of German research vessels. The labor-intensive handheld operation yielded highly accurate data for the atmospheric aerosol and water vapour. These are needed to evaluate and improve space-retrievals and modeling of aerosol over oceans. The poster presents sampled daily average column aerosol amounts (quantified by the mid-visible aerosol optical depth, AOD) of more than 60 cruises with RV POLARSTERN, RV METEOR, RV MARIA S. MERIAN and RV SONNE. These data are a major contribution to NASA's Maritime Aerosol Network (MAN) open access data-base: https://aeronet.gsfc.nasa.gov/new_web/maritime_aerosol_network.html (Smirnov et al, 2009). All AOD quality data (at a visible 500nm wavelength) since 2006 as of June 2021 are summarized in Figure 1, showing higher aerosol associated with mineral dust (off the Sahara across the Atlantic, off Arabia), with wildfires (near Indonesia, off central Africa) and with urban pollution (off E. and S. Asia).

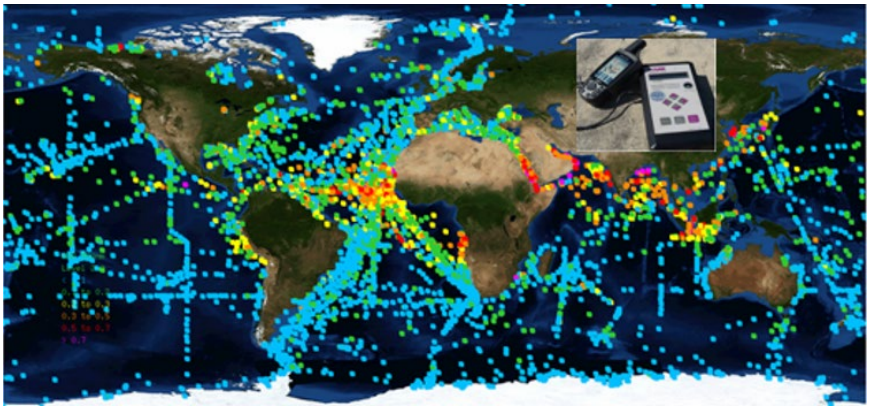

Fig. 1: Quality assured AOD (at 500nm) data by MICROTOPS sun-photometers (see inlet) since 2006 – collected on ocean cruises of opportunity. A significant fraction of contributions is provided from cruises with German research vessels, Atmospheric aerosol load strengths are indicated by color (blue:<0.01, green: 0.01–0.02, yellow: 0.02–0.03, orange: 0.3–0.5, red: 0.5–0.7, purple: >0.7 for AOD at 500nm).

In one application, the data were used to update the Max-Planck Aerosol Climatology (MAC, Kinne 2019a) and to determine (MAC) associated aerosol radiative and climate impacts (Kinne, 2019b). In addition, during the RV SONNE 268-3 cruise across the Pacific more recent 2015–2018 MAN data of AOD were matched to available satellite data to evaluate the retrieval performance over oceans. Major retrieval biases (green for overestimates, red for underestimates) for AOD data with popular MODIS sensor (Levy et al., 2013) are summarized – by ocean location – in Figure 2.

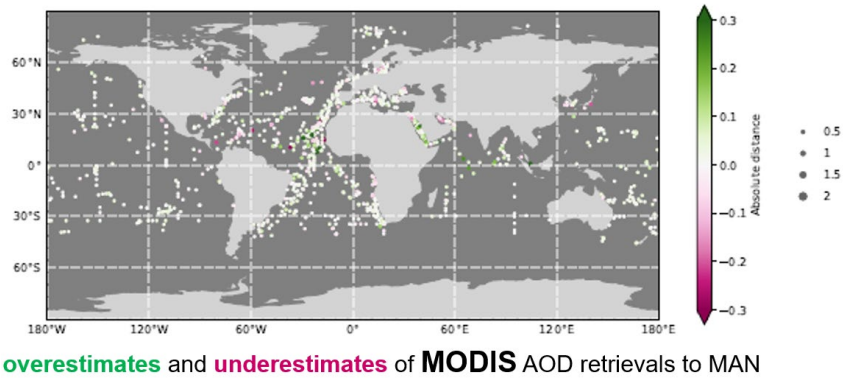

Fig. 2: Differences between MODIS AOD retrievals and space/time matching MAN vessel-based sunphotometer data, revealing likely aerosol optical depth (AOD) retrieval biases over oceans (overestimates in green, underestimates in red).

Generally, there is a good MODIS retrieval performance over oceans, with an overall tendency to overestimate AOD (green color) over many remote ocean regions. The poster presents – in addition to MODIS evaluations – also performance evaluations of AOD retrievals with satellite sensor data of MISR (Limbacher and Kahn, 2019) for the 2015–2018 period and of VIIRS (Sayer et al., 2018) for 2018.

REFERENCES

Kinne, S., The MACv2 Aerosol Climatology, Tellus B: Chemical and Physical Meteorology, 2019a, 71, 1, 1–21.

Kinne, S., Aerosol radiative effects with MACv2, ACP 19, 2019b, 10919–10959.

Levy, R., et al., The collection 6 MODIS aerosol products over land and ocean, Atmos. Meas. Techn., 2013, 6 (11).

Limbacher J. and R. Kahn, Updated MISR over-water research aerosol retrieval algorithm – Part 2: A multi-angle aerosol retrieval algorithm for shallow, turbid, oligotrophic, and eutrophic waters, 2019, Atmos. Meas. Tech., 2019, 12, 675–689.

Sayer, A., et al., Satellite Ocean Aerosol Retrieval (SOAR) algorithm extension to S-NPP VIIRS as part of the 'Deep Blue' aerosol project, J Geophys. Res. Atmos., 2018, 123, 380–400.

Smirnov, A., et al., Maritime Aerosol Network as a component of Aerosol Robotic Network, J. Geophys. Res., 2009, 114, D06204, doi:10.1029/2008JD011257.

MSM71

LOBSTER: Basin opening and inversion insights from seismic data in the Ligurian Sea

AUTHORS

GEOMAR Helmholtz Centre for Ocean Research Kiel | Kiel, Germany
A. Dannowski, I. Grevemeyer, H. Kopp, D. Lange

Christian-Albrechts-University (CAU) Kiel | Kiel, Germany
M. Thorwart

Laboratoire de Géosciences Marines, Institut de Physique du Globe de Paris, IPGP | Paris, France
W. C. Crawford

Université Grenoble Alpes, Université Savoie Mont Blanc, CNRS, IRD, UGE, ISTerre | Grenoble, France
A. Paul

IDPA-CNR, Istituto per la dinamica dei processi ambientali | Milano, Italy
G. Caielli, R. de Franco

INTRODUCTION

The Ligurian Basin was generated by the south-eastward trench retreat of the Apennines-Calabrian subduction zone. The basin underwent a long-lasting phase of extension from Late Oligocene to Miocene (Rehault et al., 1984; Gueguen et al., 1998), progressively opening from south to north with a high syn-rift sedimentation (Sage et al., 2011). The Corsica-Sardinia Block underwent a counter-clockwise (CCW) rotation of 23° to 53° that stopped ~16 Ma (Speranza et al., 2002; Gattacceca et al., 2007; Le Breton et al., 2017). Today, seismic activity is highest along the Côte d'Azur and the Ligurian coast with compressional earthquakes (Larroque et al., 2011) and decreases towards the central basin and Corsica (Figure 1). The geodynamic setting of the area is controlled by the convergence of the African and Eurasian plates (e. g. Dercourt et al., 1986). Despite the existing large collection of seismic and other geophysical data, the present-day crustal architecture of the Ligurian Basin is still under discussion and the kinematic boundaries are poorly resolved, in particular the continent–ocean transition along the margins as well as its termination to the north-north-east. It is proposed that at the late phase of the opening oceanic spreading occurred or the basin extended until atypical oceanic crust was created (Rollet et al., 2002) (white dashed lines in Figure 1). Imaging

clear fault structures within the crust has proven challenging due to the presence of thick Messinian salt. Deep-drilling data are lacking, and the magnetic data are complex and their anomalies discontinuous (Bayer et al., 1973).

In the frame of the AlpArray initiative and the SPP 4D-MB, new marine passive seismic data have been acquired covering the Ligurian Sea from the Gulf of Lion and from offshore southern Corsica towards the Gulf of Genoa. This data set will help to study the recent deformation of the plate interior that in general should predominantly be aseismic (McKenzie and Parker, 1967). Additionally, two modern refraction seismic profiles have been shot to study the crustal structure and the origin of the crust.

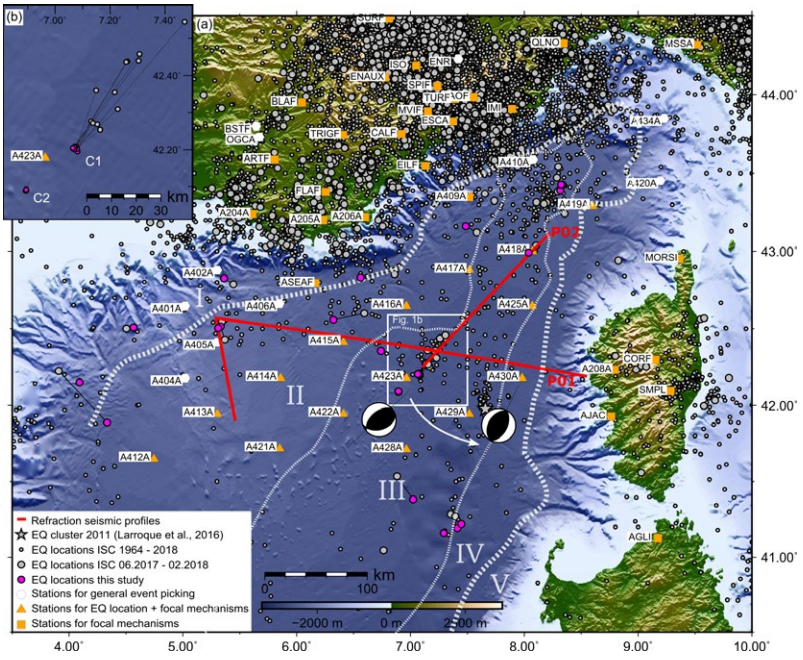

Fig. 1: Bathymetric map of the Ligurian Sea and surrounding. Superposed the wide-angle profiles from the MSM71 cruise (red lines P01 and P02), orange triangles and squares for the long-term broad-band ocean bottom seismometers and land-stations. The magenta circles show the locations of earthquakes during June 2017 and February 2018. White dashed lines mark the different proposed crustal domains after Rollet et al. (2002): continental domain (I and V), transitional domain (II and IV), and oceanic domain (III). Average focal mechanisms for the 2017 cluster events (western) and the EQ cluster 2011 (eastern).

DATA AND METHODS

RV Maria S. Merian set out to acquire a modern refraction seismic data set and to recover the long-term AlpArray ocean bottom seismometer (OBS) network that recorded continuously data from June 2017 to February 2018 on broad-band seismometers from DEPAS (Schmidt-Aursch and Haberland, 2017), IPGP and GEOMAR pools. Data on short-period OBS were recorded along two active seismic profiles (P01 and P02, red

lines in Figure 1). Simultaneously, a mini-streamer recorded multi-channel seismic (MCS) data to image the shallow sediment units down to the Messinian salt and Parasound was used to image the uppermost sediment layers.

The airgun shots were registered at most of the stations for offsets up to 60 km (Figure 2). Land stations registered shots from more than 200 km distance. The data show clear sedimentary arrivals and wide-angle Moho reflections (PmP) as well as mantle phases (Pn) at a critical distance between 25 km and 35 km to the stations. These arrivals were picked by hand and served as input for 2D travel time tomography (Korenaga et al., 2000). Additionally, satellite derived gravity data were used to confirm the seismic models.

During the long-term OBS deployment, 39 seismic events were detected within the Ligurian Basin excluding the Alps-Liguria junction zone (Figure 1, magenta circles). This work focuses on two earthquake clusters in the centre of the Ligurian Basin, near OBS A423A. The first cluster (C1) consists of 13 events that occurred from June to November 2017 and the second cluster (C2) consists of three events that occurred during one day in January 2018, about 25 km southwest of C1. Three onsets predominated the observed events: The P-wave is weak in amplitude and followed by a stronger Ps-phase, which was observed on all OBS stations but not on land stations; and an S-wave with a strong amplitude. The phases were picked on all stations shown on the map. Only stations within the basin were used for event location. To estimate fault plane solutions, the first motion direction of the P-wave was determined for on- and offshore stations where clearly visible. The amplitude ratio of P- and S-wave was determined on the vertical component at land stations only.

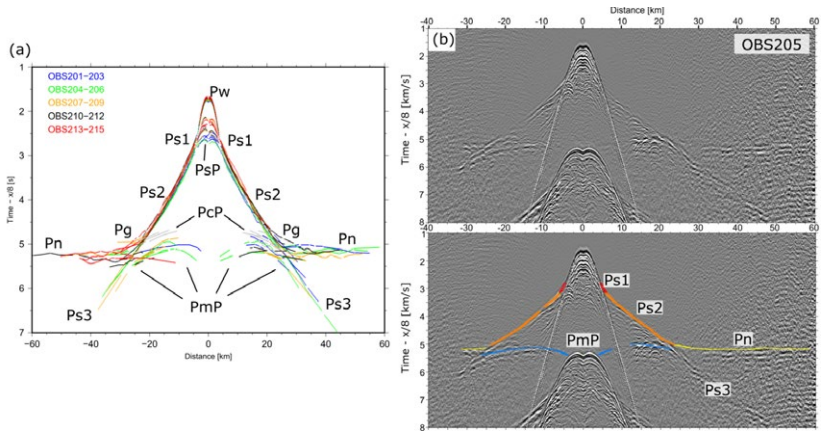

Fig. 2: (a) Stacked travel time picks of all 15 stations from profile P02, showing very similar arrivals suggesting an almost 1D structure along the profile. (b) Record section of station OBS205 (time reduced with a velocity of 8 km/s). The lower panel shows the calculated travel time picks from the final velocity model superimposed on the seismic data.

RESULTS AND CONCLUSIONS

The P-wave velocity models determined in this study image the uppermost lithospheric structure of the central Ligurian Basin. Syn- and post-rift sediments of ~6–8 km thickness filled the basin during and after the ~15 Ma long lasting opening phase. Based on the image of the seismic velocity distribution in the basin centre, it remains enigmatic if the mantle is overlain directly by syn-rift sediments or by extremely thin continental crust of up to 2.5 km. The northern half of profile P02 indicates a northward thickening of continental crust and a deepening crust-mantle boundary from 11 km to 13 km (Dannowski et al., 2020). Along profile P01, at the Corsican margin, the Moho is deepening abruptly from ~11 km to ~24 km depth within a short distance of 30 km in the so-called necking zone. There sediments thin out and the crust thickens from <3 km west of the Corsica margin to ~24 km underneath Corsica. In the basin centre, along P01, a gap in mantle phase observations could be explained by an area of serpentinised mantle or by a thick Messinian salt unit and related salt tectonics. Based on the retrieved velocity distribution, gravity modelling and results of surrounding studies, we conclude that the extension of the Ligurian Basin led to: (1) Extended and very thin continental crust or exhumed, partially serpentinised mantle. It remains enigmatic if the mantle is overlain directly by sediments or by extremely thinned continental crust of up to 2.5 km thickness. (2) Continental crustal thinning from north to south related to the increase of extension with increasing distance from the rotation pole of the anti-clockwise rotation of the Corsica-Sardinia block. Furthermore, our study documents that seafloor spreading and formation of mantle-derived oceanic crust was not initiated during the extension of the Ligurian Basin.

Our seismicity study (Thorwart et al., 2021) confirms that the entire Ligurian Basin is characterised by sparse but wide-spread micro-earthquakes of magnitude <3. The two earthquake clusters that show thrust faulting mechanisms support a model of inversion of the Ligurian Basin, in which the basin's centre is under compression and stresses are taken up by reactivated faults in the crust and uppermost mantle. The location of the cluster events and their focal mechanisms indicate that they occurred in reactivated pre-existing rift-related structures. Slightly different striking directions of faults in the basin centre compared to faults further east and hence away from the rift basin may reflect the counter-clockwise rotation of the Corsica-Sardinia block. In general, observations of earthquakes in continental mantle lithosphere are rare. A high mantle S-wave velocity of Vs=4.7 km/s and a low Vp/Vs ratio of 1.72 reveal a strengthening of the crust and uppermost mantle during the Oligocene-Miocene rifting. The observed event clusters indicate local weak zones possibly through local mantle serpentinisation in an otherwise strong lithosphere and support the interpretation that rifting failed in the northern Ligurian Basin.

REFERENCES

Bayer, R., Le Mouel, J. L. and Le Pichon, X., Magnetic anomaly pattern in the western mediterranean, Earth Planet. Sci. Lett. 1973, 19(2), 168–176, doi: 10.1016/0012-821X(73)90111-8.

Dannowski A, Kopp H, Grevemeyer I, Lange D, Thorwart M, Bialas J, Wollatz-Vogt M, Seismic evidence for failed rifting in the Ligurian Basin, Western Alpine domain, Solid Earth 2020, doi:10.5194/se-11-873-2020.

Dercourt, J., Zonenshain, L. P., Ricou, L.-E., Kazmin, V. G., Le Pichon, X., Knipper, A. L., Grandjacquet, C., Sbortshikov, I. M., Geyssant, J., Lepvrier, C., Pechersky, D. H., Boulin, J., Sibuet, J.-C., Savostin, L. A., Sorokhtin, O., Westphal, M., Bazhenov, M. L., Lauer, J. P. and Biju-Duval, B., Geological evolution of the tethys belt from the atlantic to the pamirs since the LIAS, Tectonophysics 1986, 123(1–4), 241–315, doi: 10.1016/0040-1951(86)90199-X.

Gattacceca, J., Deino, A., Rizzo, R, Jones, D.S., Henry, B., Beaudoin, B., Valeboin, F., Miocene rotation of Sardinia: new paleomagnetic and geochronological constraints and geodynamic implications. Earth Planet. Sci. Lett. 2007, 258, 359–377, doi: https://doi.org/10.1016/j.epsl.2007.02.003.

Gueguen, E., Doglioni, C. and Fernandez, M., On the post-25 Ma geodynamic evolution of the western Mediterranean, Tectonophysics 1998, 298(1–3), 259–269, https://doi.org/10.1016/S0040-1951(98)00189-9.

Korenaga, J., Holbrook, W. S., Kent, G. M., Kelemen, P. B., Detrick, R. S., Larsen, H.-C., Hopper, J. R. and Dahl-Jensen, T., Crustal structure of the southeast Greenland margin from joint refraction and reflection seismic tomography, J. Geophys. Res. Solid Earth 2000, 105(B9), 21591–21614, doi:10.1029/2000JB900188.

Larroque, C., Mercier de Lépinay, B., Migeon, S., Morphotectonic and fault–earthquake relationships along the northern Ligurian margin (western Mediterranean) based on high resolution multibeam bathymetry and multichannel seismic reflection profiles, Mar. Geophys. Res. 2011, 32 (1–2), 163–179, doi: http://dx.doi.org/10.1007/s11001-010-9108-7.

Le Breton, E., Handy, M. R., Molli, G. and Ustaszewski, K., Post-20 Ma Motion of the Adriatic Plate: New Constraints From Surrounding Orogens and Implications for Crust-Mantle Decoupling: Post-20 Ma Motion of the Adriatic Plate, Tectonics 2017, 36(12), 3135–3154, doi: https://doi.org/10.1002/2016TC004443.

McKenzie, D. P. and Parker, R. L., The North Pacific: an Example of Tectonics on a Sphere, Nature 1967, 216(5122), 1276–1280, doi: https://doi.org/10.1038/2161276a0.

Réhault, J.-P., Boillot, G. and Mauffret, A., The Western Mediterranean Basin geological evolution, Mar. Geol. 1984, 55(3), 447–477, doi: 10.1016/0025-3227(84)90081-1.

Rollet, N., Déverchère, J., Beslier, M.-O., Guennoc, P., Réhault, J.-P., Sosson, M. and Truffert, C., Back arc extension, tectonic inheritance, and volcanism in the Ligurian Sea, Western Mediterranean: LIGURIAN SEA BACK ARC STRUCTURE AND EVOLUTION, Tectonics 2002, 21(3), 6-1-6–23, doi: https://doi.org/10.1029/2001TC900027.

Sage, F., Beslier, M.O., Thinon, I., Larroque, C., Dessa, J.X., Migeon, S., Angelier, J., Guennoc, P., Schreiber, D., Michaud, F., Stéphan, J.F., Sonnette, L., Structure and evolution of a passive margin in a compressive environment: example of the southwestern Alps-Ligurian basin junction during the Cenozoic, Mar. Pet. Geol. 2011, 28, 1263–1282, doi:10.1016/j.marpetgeo.2011.03.012.

Schmidt-Aursch, M. C. and Haberland, C., DEPAS (Deutscher Geräte-Pool für amphibische Seismologie): German Instrument Pool for Amphibian Seismology, J. of large-scale res. Facilities 2017, 3, 122, https://doi.org/10.17815/jlsrf-3-165.

Speranza, F., Villa, I. M., Sagnotti, L., Florindo, F., Cosentino, D., Cipollari, P. and Mattei, M., Age of the Corsica–Sardinia rotation and Liguro–Provençal Basin spreading: new paleomagnetic and Ar/Ar evidence, Tectonophysics 2002, 347(4), 231–251, doi: https://doi.org/10.1016/S0040-1951(02)00031-8.

Thorwart M, Dannowski A, Grevemeyer I, Lange D, Kopp H, Petersen F, Crawford W, Paul A, and the AlpArray Working Group: Basin inversion: Reactivated rift structures in the Ligurian Sea revealed by OBS, Solid Earth Discussions 2021, doi:10.5194/se-2021-9.

MSM71

Lobster — First results of 3D travel time tomography of the Ligurian Sea and Coastal Western Alps using data from Cruise

AUTHORS

GEOMAR Helmholtz Center for Ocean Research Kiel | Kiel, Germany
L. Murray-Bergquist, D. Lange, A. Dannowski, H. Kopp

Christian-Albrechts-University (CAU) Kiel | Kiel, Germany
M. Thorwart

Freie Universität Berlin | Berlin, Germany
E. Le Breton

Institut de Physique du Globe de Paris | Paris, France
W. Crawford

INTRODUCTION

The Ligurian Sea is a highly complex tectonic setting lying between two major orogenies, the Western Alpine belt and the Apennine system. The Ligurian Sea formed as a back-arc basin related to the Apennines-Calabria subduction zone retreat (Rollet et al., 2002). Opening began in the late Oligocene and continued into the early Miocene by the counter-clockwise rotation of the Corsica-Sardinia block. The area is now under compression with shortening of 0.3–1.5 mm/year along the northern margin (Nocquet, 2012). The region's tectonic activity has produced large topographic gradients, with heights of >3 km in the Alps descending to water depths of 2.5 km in the center of the Ligurian Basin over a horizontal distance of only 100 km. The crust and upper mantle show strong heterogeneity, and a strong gradient in the Moho which is fairly shallow in the basin center ~12.5 km depth, and then deepens sharply at the coastlines to ~50 km under the Alps and ~25 km under Corsica. The area has hosted large, destructive earthquakes, such as the 1887 Mw 6.3–7.5 Imperia earthquake (Larroque et al., 2012) with devastating effects on the densely populated Ligurian sea coast. To better estimate these hazards, we must improve our understanding of the shallow and deep structures and processes in the Ligurian basin. In this way we can better estimate the seismic hazard posed to cities along the coast, as well as broadening our understanding of the evolution of the Alpine orogen. Within the framework of the DFG Priority Program "Mountain Building Processes in Four Dimensions (MB-4D)", we focus on the deep structure of the Ligurian Sea from Corsica to the South-Western Alps which we aim to model with 3D body wave tomography. To do this we use data from OBS stations deployed on the June 2017 RV Pourquoi Pas? cruise, and collected with RV Maria S. Merian in February 2018.

DATA AND METHODS

In June 2017 29 broadband ocean-bottom seismometers (OBS) were deployed from the RV Pourquoi Pas? The instruments were supplied and installed jointly by scientists from the Institut de physique du globe de Paris (IPGP, Paris, France), the Institute des Sciences de la Terre (ISTerre, Grenoble, France) and GEOMAR Helmholtz Centre for Ocean Research Kiel (Kiel, Germany). An additional station was operated by GeoAzur in Nice, forming an array of 30 OBS stations, shown in Figure 1. Land stations and OBSs used were installed in the frame of the European AlpArray initiative (Hetényi et al., 2018) or are permanent stations from the Mediterranean seismological networks.

The goal of the February 2018 RV Maria S. Merian cruise MSN71 (LOBSTER, Kopp et al., 2018) was to recover the 29 stations deployed by the RV Pourquoi Pas?, and to shoot two seismic refraction/reflection profiles in the center of the basin. Profile 1 (P01, Figure 1) ran roughly from the eastern side of the Ligurian Basin near Corsica west across the basin. 35 short period OBS were installed along this profile with a spacing of 4 nm, and the profile was continued onto the west side of Corsica with three temporary land stations. Two G-gun arrays with total volume 84l were used with one array towed from each side of the ship, and a 280m long geo-eel streamer was deployed along the profile; this was recovered on passing the last OBS station. The profile was traversed from east to west, the ship then turned and continued shooting for another 45 nm along a southeastward course to pass closer to some of the AlpArray broadband seismometer array. Profile 2 (P02) ran roughly NE to SW, slightly crossing P01 at the SW end of the line. 15 stations were deployed along P02, 12 OBS and 3 OBH, and the same air gun and streamer configuration was used. These profiles and the short term station deployments along the profiles are shown in Figure 1.

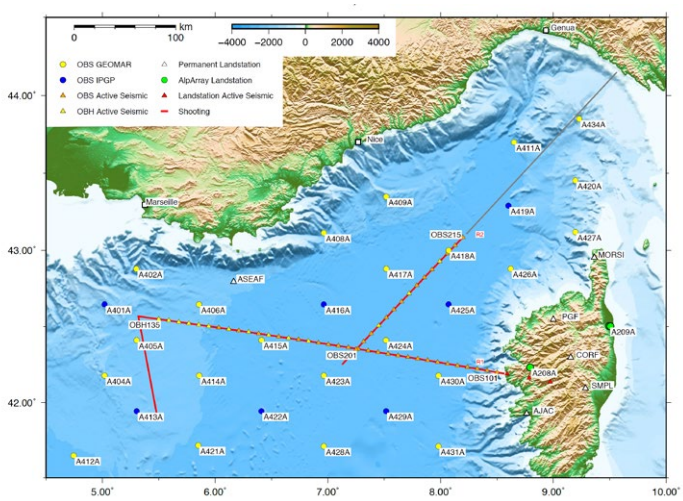

Fig. 1: Map of the Ligurian Sea and Coastal area with OBS stations and the two refraction/reflection profiles (red lines). The grey line shows the profile recorded by Makris et al. 1999. (Kopp et al., 2018)

The shots recorded at the OBS stations were analysed using PasteUp (Fujie et al., 2008) and the P and Pn arrival times were manually picked. These picktimes were then reformatted for input into the tomographic inversion code TOMO3D (Meléndez et al., 2019).

OUTLOOK

The data quality is generally very good, with clear arrivals at stations along the profiles and on Corsica, and shots recorded on OBS and mainland stations. The data collected on cruise MSM71 has been used to create 2D tomographic profiles and to examine the crustal structure of the basin (Dannowski et al., 2020, Thorwart et al., 2021). In the context of a doctoral project a 3D S-wave velocity model from ambient noise tomography is available for the crust and uppermost mantle (Wolf et al., accepted).

In this ongoing project we are working towards inverting a robust 3D P-wave velocity model of the crust and upper mantle of the Ligurian Sea and South-Western Alps using body wave tomography. The current model still has very high error, but as more stations are added the result is improving. We intend to further improve this model by adding picked arrivals of local earthquakes at the 30 OBS stations that were recording between June 2017 and February 2018. To improve the ray coverage we plan to add picked arrival times of local seismicity and shots observed at land stations, which also improves the time coverage as most land stations recorded over a longer period.

The tomographic code TOMO3D allows for anisotropy which could be interesting to observe in the Ligurian Basin, especially in the upper mantle. Once a robust tomographic model of the area has been achieved we plan to explore the anisotropy of the basin which could provide interesting insight into the local tectonics.

REFERENCE

Dannowski A, Kopp H, Grevemeyer I, Lange D, Thorwart M, Bialas J, Wollatz-Vogt M, Seismic evidence for failed rifting in the Ligurian Basin, Western Alpine domain, Solid Earth 2020, doi:10.5194/se-11-873-2020.

Fujie G, Kasahara J, Murase K, Mochizuki K, Kaneda Y, Interactive analysis tools for the wide-angle seismic data for crustal structure study (Technical Report), Exploration Geophysics 2008, 39, pp. 26–33; Butsuri-Tansa 2008, 61, pp. 26–33; Mulli-Tamsa 2008, 11, pp. 26–33, doi: 10.1071/EG08006

Hetényi, G. et al.: The AlpArray Seismic Network: A Large-Scale European Experiment to Image the Alpine Orogen, Surv. Geophys. 2018, doi:10.1007/s10712-018-9472-4.

Kopp H, Lange D, Thorwart M, Paul A, Dannowski A, et al., RV MARIA S. MERIAN Fahrtbericht/Cruise Report MSM71 LOBSTER: Ligurian Ocean Bottom Seismology and

Tectonics Research, Las Palmas (Spain) – Heraklion (Greece) 07.02.-27.02.2018, GEOMAR Report N. Ser. 041, 2018. GEOMAR Helmholtz-Zentrum für Ozeanforschung Kiel, Kiel, Germany, 47 pp. doi: 10.3289/GEOMAR_REP_NS_41_2018

Larroque C, Scotti O, Ioualalen M, Reappraisal of the 1887 Ligurian earthquake (western Mediterranean) from macroseismicity, active tectonics and tsunami modelling, Geophysical Journal International 2012, 190, doi: 10.1111/j.1365-246X.2012.05498.x

Makris J, Egloff F, Nicolich R, Rihm R., Crustal structure from the Ligurian Sea to the Northern Apennines — a wide angle seismic transect, Tectonophysics 1999, doi:10.1016/S0040-1951(98)00225-X.

Meléndez A, Jiménez C.E., Sallarès V, and Ranero C.R., Anisotropic P-wave travel-time tomography implementing Thomsen's weak approximation in TOMO3D, Solid Earth Discussions 2019, https://doi.org/10.5194/se-2019-44

Nocquet J.M., Present-day kinematics of the Mediterranean: A comprehensive overview of GPS results, Tectonophysics 2012, 579.

Rollet N, Déverchère J, Beslier M.O., Guennoc P, Back arc extension, tectonic inheritance, and volcanism in the Ligurian Sea, Western Mediterranean, Tectonics 2002, 21(3), doi:10.1029/2001TC900027

Thorwart M, Dannowski A, Grevemeyer I, Lange D, Kopp H, Petersen F, Crawford W, Paul A, and the AlpArray Working Group: Basin inversion: Reactivated rift structures in the Ligurian Sea revealed by OBS, Solid Earth Discussions 2021, doi:10.5194/se-2021-9.

Wolf F.N., Lange D, Dannowski A, Thorwart M, Crawford W, Wiesenberg L, Grevemeyer I, Kopp H, the AlpArray Working Group. 3D crustal structure of the Ligurian Sea revealed by ambient noise tomography using ocean bottom seismometer data. Solid Earth Discussions (accepted), doi:10.5194/se-2021-55.

MSM71

LOBSTER: 3D Crustal Structure of the Ligurian Sea Revealed by Surface Wave Tomography using Ocean Bottom Seismometer Data

AUTHORS

GEOMAR Helmholtz Centre for Ocean Research Kiel | Kiel, Germany
F. N. Wolf, D. Lange, A. Dannowski, I. Grevemeyer, H. Kopp

Christian-Albrechts-University (CAU) Kiel | Kiel, Germany
M. Thorwart, L. Wiesenberg, H. Kopp

Laboratoire de Géosciences Marines, Institut de Physique du Globe de Paris, IPGP | Paris, France
W. C. Crawford

AlpArray Working Group
AlpArray members listed at www.alparray.ethz.ch

INTRODUCTION

This document is summarizing the work of Wolf et al., published in Solid Earth, doi: 10.5194/se-2021-55.

The Liguro-Provençal basin was formed as a back-arc basin of the retreating Calabrian-Apennines subduction zone during the Oligocene and Miocene. It is still debated whether oceanic or atypical oceanic crust was formed or if the crust is continental and experienced extreme thinning during the opening of the basin. We perform ambient noise tomography, also taking into account teleseismic events, using an amphibious network of seismic stations, including 22 broadband Ocean Bottom Seismometers (OBS), to investigate the lithospheric structure of the Ligurian Sea (Figure 1).

DATA AND METHODS

The OBS instruments were installed in the Ligurian Sea for eight months between June 2017 and February 2018 as part of the AlpArray seismic network (Hetényi et al., 2018). The 22 broadband ocean-bottom seismometers (OBS, Figure 1) used were installed jointly by the *Institut de physique du globe de Paris* (IPGP, Paris, France), the *Institut des Sciences de la Terre* (ISTerre, Grenoble, France), *Deutscher Geräte-Pool für amphibische Seismologie* (DEPAS, Schmidt-Aursch and Haberland, 2017) and *GEOMAR Helmholtz Centre for Ocean Research Kiel* (Kiel, Germany). The instruments were deployed from the

RV Pourquoi Pas? in June 2017 and were recovered in February 2018 by *RV Maria S. Merian* during cruise MSM71.

Because of additional noise sources in the ocean, OBS data are rarely used for ambient noise studies. Pre-processing included corrections for instrument tilt and seafloor compliance and excluding higher modes of the ambient-noise Rayleigh waves. We calculate daily cross-correlation functions for the AlpArray OBS network and surrounding land stations. We also correlate short time windows that include teleseismic earthquakes (e. g. Meier et al., 2004), allowing us to derive surface wave group velocities for longer periods than using ambient noise only. We obtain group velocity maps by inverting Green's functions derived from the cross-correlation of ambient noise and teleseismic events. We use the Fast Marching Surface Tomography method (FMST, Rawlinson & Sambridge, 2004) to derive 2D Rayleigh group velocity maps (see Wolf et al., accepted, for group velocity maps) from the picked dispersion curves. We then used the resulting 3D group velocity information to invert for 1D S-wave velocities using the software provided by Herrmann (2013).

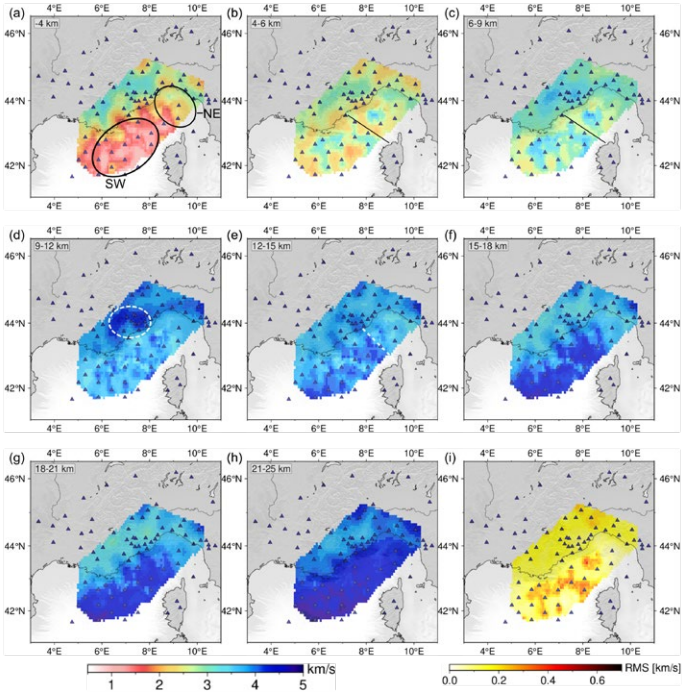

Fig. 1: 2D shear velocity maps derived from the 1D inversion (Wolf et al., accepted). Layer depth is stated in the upper left corner. Depths (in km) are relative to the sea surface. The annotations in (a) mark the southwestern and central (SW) and the northeastern (NE) Ligurian Basin. The solid black line in (b) and (c) show the location of profile LISA01 (Contrucci et al., 2001). The dashed circle in (d) marks a high-velocity area north of Nice, and the dashed white line in (e) represents the proposed prolongation of the Alpine front. Panel (i) shows the root mean square (RMS) value for the 1D shear-wave-inversion in map view. Blue triangles mark stations. The topography is plotted based on a GMRT grid (Ryan et al., 2009).

RESULTS AND DISCUSSION

The group velocity and shear-wave velocity results compare well to existing large-scale studies that partly include the study area. Onshore France, we observe a high-velocity area beneath the Argentera Massif, roughly 10 km below sea level (Figure 1d). We interpret this as the root of the Argentera massif (Wolf et al., accepted). In addition to existing seismic profiles (e. g. Makris et al., 1999, Contrucci et al., 2001, Dannowski et al., 2020), our results add spatial information to the knowledge on seismic velocities in the Ligurian Basin. In agreement with existing seismic studies, our shear-wave velocity maps indicate a deepening of the Moho from 12 km at the southwestern basin centre to 20–25 km at the Ligurian coast in the northeast and over 30 km at the Provençal coast. The maps also indicate that the southwestern and northeastern Ligurian Basin are structurally separated. We do not observe high vp/vs ratios which would indicate mantle serpentinisation in the southwestern Ligurian Basin.

CONCLUSIONS

Applying ambient noise techniques and the correlation of teleseismic events to amphibious data results in the first 3D high-resolution seismic group and shear velocity models for the Ligurian Sea. This document summarizes the findings published in Wolf et al. (accepted). The dataset differs from most previous ambient noise by combining amphibious data. Our OBS stations are comparably shallow, and the fundamental mode is not always the most prominent signal in the marine ray paths. Higher modes are primarily observed in the southeast. We reveal a high-velocity area at the Argentera Massif, approximately 10 km below sea level. Offshore, the lithospheric structure in the Ligurian Basin mostly mimics the geometry of the basin. Shear-wave velocity maps indicate a gradual deepening of the Moho from 12–15 km in the southwestern basin centre towards 20–25 km in the northeastern basin and a more rapid deepening from the basin axis to the Provençal coast (> 30 km). Based on the low vp/vs ratios of 1.74, we exclude mantle serpentinisation in the basin centre. Overall, the off-shore region north of Corsica is faster than the southwestern basin at shallow depths (<12 km) and slower at greater depth. This is linked to the varying sediment cover and the crustal thickness.

ADDITIONAL INFORMATION

For data availability and extended acknowledgements, we would like to refer to Wolf et al. (accepted).

REFERENCES

Contrucci, I., Nercessian, A., Béthoux, N., Mauffret, A., and Pascal, G.: A Ligurian (Western Mediterranean Sea) geophysical transect revisited, Geophys. J. Int., 2001, doi:10.1046/j.0956-540x.2001.01418.x.

Dannowski, A., Kopp, H., Grevemeyer, I., Lange, D., Thorwart, M., Bialas, J., and Wollatz-Vogt, M.: Seismic evidence for failed rifting in the Ligurian Basin, Western Alpine domain, Solid Earth 2020, doi:10.5194/se-11-873-2020.

Herrmann, R. B.: Computer Programs in Seismology: An Evolving Tool for Instruction and Research, Seismol. Res. Lett. 2013, doi:10.1785/0220110096.

Hetényi, G. et al.: The AlpArray Seismic Network: A Large-Scale European Experiment to Image the Alpine Orogen, Surv. Geophys. 2018, doi:10.1007/s10712-018-9472-4.

Makris, J., Egloff, F., Nicolich, R., and Rihm, R.: Crustal structure from the Ligurian Sea to the Northern Apennines — a wide angle seismic transect, Tectonophysics 1999, doi:10.1016/S0040-1951(98)00225-X.

Meier, T., Dietrich, K., Stöckhert, B., and Harjes, H. P.: One-dimensional models of shear wave velocity for the eastern Mediterranean obtained from the inversion of Rayleigh wave phase velocities and tectonic implications, Geophys. J. Int. 2004, doi:10.1111/j.1365-246X.2004.02121.x.

Rawlinson, N. and Sambridge, M.: Wave front evolution in strongly heterogeneous layered media using the fast marching method, Geophys. J. Int., 156, 2004, doi:10.1111/j.1365-246X.2004.02153.x.

Ryan, W. B. F., Carbotte, S. M., Coplan, J. O., O'Hara, S., Melkonian, A., Arko, R., Weissel, R. A., Ferrini, V., Goodwillie, A., Nitsche, F., Bonczkowski, J., and Zemsky, R.: Global Multi-Resolution Topography synthesis, Geochem. Geophys. Geosystems, 2009, doi:10.1029/2008GC002332.

Schmidt-Aursch, M. C. and Haberland, C., DEPAS (Deutscher Geräte-Pool für amphibische Seismologie): German Instrument Pool for Amphibian Seismology, J. of large-scale res. Facilities 2017, 3, 122, https://doi.org/10.17815/jlsrf-3-165.

Wolf, F.N., Lange, D., Dannowski, A., Thorwart, M., Crawford, W., Wiesenberg, L., Grevemeyer, I., Kopp, H., the AlpArray Working Group. 3D crustal structure of the Ligurian Sea revealed by ambient noise tomography using ocean bottom seismometer data. Solid Earth (accepted), doi:10.5194/se-2021-55.

MSM79

18 years of dinoflagellate cyst export flux and benthic foraminifera deposition recovered from a sediment trap in the upwelling region off Cape Blanc (NW Africa)

AUTHORS

Center for Marine Environmental Sciences – MARUM, University of Bremen | Bremen, Germany
E. Roza, G. Versteegh, K. Zonneveld

The upwelling system off Cape Blanc (NW Africa) is one of the most productive areas in the world. Year-round upweliing and frequent input of Sahara dust results high nutrient concentrations throughout the year. Although upwelling is a permanent feature in the region, upwelling intensity and dynamics are highly diverse, depending on seasonal variability as well as dynamics of local weather, notably wind strength and direction (e. g. Romero et al., 2020).

Here we present results from an 18-years study (2002–2020) on the dynamics of the particulate organic export flux formed by dinoflagellate cysts and benthic foraminifera. Material has been collected by sediment trap CBeu at ca 1260 m depth, which is deployed as part of the long-term MARUM/GeoB sediment trap monitoring program at 20°50' N/18°44' W (off Cape Blanc). The trap is located just west of the active upwelling cell locations below the track of offshore drifting surface water upwelling filaments.

We document a long-term trend in the phyto- and zooplankton export flux composition with major association shifts recorded during the years 2005 and 2009. The record also shows multi-annual cyclic plankton association changes. The dynamics of the system are very high with each upwelling event having a different plankton export flux association.

Furthermore, we show that the export flux in the region not only consists of particulate organic matter formed in the upper waters near the trap location but also includes a considerable amount of reworked shelf material that most probably has been transported offshore by subsurface nepheloid layers.

REFERENCE

Romero, R.E., Baumann, K-H., Zonneveld, K.A.F., Donner, B., Hefter, J., Bambaye, O.H., Pospelova, V. and Fischer , G. Flux variability of phyto- and zooplankton communities in the Mauritanian coastal upwelling between 2003 and 2008. Biogeosciences 17, 2020, 187–214

MSM79

Export flux succession of dinoflagellate cysts and planktonic foraminifera in an active upwelling cell off Cape Blanc (NW Africa) in November 2018

AUTHORS

Center for Marine Environmental Sciences – MARUM, University of Bremen | Bremen, Germany
K.A.F. Zonneveld, J. Meiland, B. Donner, G.J.M. Versteegh

To better understand production, succession, excystment and transport of dinoflagellate cysts (dinocysts) and planktonic foraminifera in the upper water column, we investigated their fluxes during a 7-day survey in the active upwelling off Cape Blanc (NW Africa) in November 2018 with drifting traps at 100 m, 200 m and 400 m water depth. The survey covered a change from active upwelling to stratified conditions (Zoneveld et al., 2021). Highest production of organic dinocysts and planktonic foraminifera was observed during active upwelling conditions and decreased drastically towards the end of the survey. Calcareous dinocysts appeared later during upwelling relaxation. Cytoplasm-bearing (full) dinocysts and foraminifera were produced in the water column above the traps (<100 m depth). Some of the empty dinocysts were resuspended, implying that sediments below the survey site contain both local and allochthonous cyst assemblages. This is the first demonstration that excystment in the upper water column is species-specific. *Brigantedinium* excysted in the upper water column before reaching deeper depths, whereas no upper water column excystment was observed for the other dinoflagellate species.

Dinoflagellate and planktonic foraminifera associations showed a clear succession. During active upwelling, *Echinidinium zonneveldiae, Brigantedinium* spp., other peridinioids, *Echinidinium* spp., cysts of *Pentapharsodinium dalei*, 'other photosynthetic organic-walled dinocysts', *Neogloboquadrina incompta* and *Globigerinella calida* were collected. During upwelling relaxation, Lingulodinium machaerophorum was produced; and under stratified conditions *Gymnodiniaceae* cysts (*G. microreticulatum, G. catenatum*) and the *foraminifera Globigerina* bulloides and *Orbulina universa* were sampled. Apart from enhancing knowledge of these species, our observations allow more detailed reconstructions of upwelling history in the Cape Blanc region based on sedimentary archives using fossilized dinoflagellate and planktonic foraminifera assemblages.

REFERENCE

Zonneveld K.A.F., Donner B., Meiland J., Versteegh G.J.M. Export flux succession of dinoflagellate cysts and planktonic foraminifera in an active upwelling cell off Cape Blanc (NW Africa). European Journal of Phycology, 2021, doi: 10.1080/09670262.2021.1885066

MSM79

Better molecular preservation of organic matter in an oxic than in a sulphidic depositional environment: evidence from from modern and fossil dinoflagellate cysts

AUTHORS

Center for Marine Environmental Sciences – MARUM, University of Bremen | Bremen, Germany
K. Zonneveld, G.J.M. Versteegh

Geological Survey of the Netherlands, TNO | Utrecht, The Netherlands
A.J.P. Houben

Anoxic sediments as compared to oxic settings encompass a much higher proportion of relatively labile and thus more reactive organic matter, naturally giving rise to structural changes of the organic molecules themselves, as well as cross-linking between them (e. g. through reactive sulphur species). Both processes transform the original biomolecules into geomolecules. For the oxic environment, these inter- and intramolecular transformations also operate, but cross-linking may be less important since the labile, reactive, component is rapidly removed. As such, one may expect a structurally better preservation of the more refractory initial biomolecules in the oxic environment. To test this hypothesis, initially identical biomolecules need to be compared between different preservational environments.

Here, we use the species-specific morphology of organic microfossils to assure a single initial biosynthetic product (the cysts of the fossil dinoflagellate species *Thallasiphora pelagica* for comparison (Versteegh et al., 2020). We assess the macromolecular structures of cysts from the Eocene (~40 Ma) sulphidic Rhine Graben and the oxic Kerguelen Plateau and compare them with each other and the structures of recent cysts collected during several cruise, such as MSM79. While between the sites the T. pelagica cysts are morphologically identical and show no signs of morphological modification, pyrolysis gas chromatography, mass spectroscopy and micro-Fourier transform infra red analyses show that their macromolecular characteristics are strongly different. Comparison with recent cysts shows that the cysts deposited in the sulphidic Rhine Graben show a strong additional contribution of long-chain aliphatic moieties and thus less diagenetic intermolecular cross-linking. The presence of organic sulphur, identifies natural volcanisation as one of the diagenetic processes. Our result shows that excellent morphological preservation doesn't imply excellent chemical preservation. It also leads to the conclusion that the best preservation of molecular structure is not necessarily where most organic matter gets preserved, which, in turn, is important for

understanding the nature and fate of sedimentary organic matter and its isotopic signature.

REFERENCE

Versteegh G.J.M, Houben A.J.P., Zonneveld K.A.F. Better molecular preservation of organic matter in an oxic than in a sulfidic depositional environment: evidence from Thalassiphora pelagica (Dinoflagellata, Eocene) cysts. Biogeosciences 2020, 17, 3545–3561, 2020.

MSM82

The complex volcanic evolution of the Rio Grande Rise, SW Atlantic

AUTHORS

GeoZentrum Nordbayern, Friedrich-Alexander-University Erlangen-Nuremberg | Erlangen, Germany
P. A. Hoyer, K. M. Haase, M. Regelous, J. M. O'Connor

GEOMAR Helmholtz Centre for Ocean Research Kiel | Kiel, Germany
S. Homrighausen

Alfred Wegener Institute Helmholtz Centre for Polar and Marine Research | Bremerhaven, Germany
W. H. Geissler, W. Jokat

The Rio Grande Rise and the Walvis Ridge are the most prominent bathymetric features of the South Atlantic Ocean and have been interpreted as rifted parts of a Late-Cretaceous Large Igneous Province related to the Tristan-Gough mantle plume (e. g., Wilson 1965) or as a detached microcontinent embedded in plume-influenced oceanic crust (Mohriak et al., 2010; Santos et al., 2019). In general, the Rio Grande Rise can be subdivided in an eastern and a western part, whereby both provinces are cut by the Cruzeiro do Sul Rift. On the prolongation of the rift structure lie the Jean Charcot Seamount Chain pointing towards the Brazilian coast. Much about the structure and geochemical composition of the western Rio Grande Rise is known from volcanic rocks recovered from Deep Sea Drilling Project Site 516 (e. g., Weaver et al., 1983) and one previous dredge position (Fodor et al., 1977). In contrast, the eastern Rio Grande Rise and the Jean Charcot Seamount Chain remained unsampled yet, which is why their geochemical compositions and relation to the Western Rio Grande Rise is unknown.

It is believed that between ~120 and ~80 Ma, the Tristan-Gough mantle plume was situated beneath or in close proximity to the new emerging Mid-Atlantic Ridge resulting in the formation of the Walvis Ridge and western Rio Grande Rise in a setting that is similar to present-day Iceland (e. g., O'Connor and Duncan, 1990). Between ~80 and ~60 Ma, continuous volcanic activity separated the Walvis Ridge and western Rio Grande Rise along a southward propagating plume-fed spreading axis, which subsequently led to the formation of the N-S trending eastern Rio Grande Rise and its corresponding counterpart on the African Plate (e. g., O'Connor and Duncan, 1990). At ~60 Ma, the Walvis Ridge and Rio Grande Rise were finally separated by several ridge jumps, which isolated the Rio Grande Rise on the South American Plate and temporarily

terminated its magmatic formation (Graça et al., 2019). In contrast, plume-related volcanism continued on the African Plate forming the Guyot Province consisting of two age-progressive and isotopically distinct volcanic tracks extending from the Walvis Ridge to the volcanically-active ocean islands of Tristan da Cunha and Gough (Rohde et al., 2013). Recent Ar-Ar ages from the samples recovered from the crest of western Rio Grande Rise indicates a magmatic rejuvenation or late-stage volcanism at ~46 Ma with a distinct geochemical signature compared to the main plateau forming stage (e. g., Rohde et al., 2013). It is assumed that almost simultaneously, the Rio Grande Rise was cut by the Cruzeiro do Sul Rift that is up to 20 km wide and 1 km deep (e. g., Mohriak et al., 2010). Since the Cruzeiro do Sul Rift also affected the South American continent forming alkaline complexes at the Brazilian shore, it is believed to reflect a major plate reorganization in the Paleogene and Neogene (e. g., Mohriak et al., 2010.

In contrast to exclusively magmatic models, recent geophysical and petrological studies claim that the western Rio Grande Rise is a continental crustal fragment detached from the Brazilian margin that has been preserved as a 'microcontinent' embedded in plume-influenced oceanic crust (Mohriak et al., 2010; Santos et al., 2019). The submarine plateau exhibits a negative Bouguer anomaly indicating a mass deficiency relative to the surrounding seafloor crust (Mohriak et al., 2010). Further, submersible sampling recovered boulders of gneiss, granite and pegmatite of Proterozoic age suggesting that the western Rio Grande Rise may be underlain by slivers of continental crust (Santos et al., 2019). These recent findings draw the previous models for the volcanic origin of the Rio Grande Rise into question.

Here we present new major and trace element data for volcanic rocks from Deep Sea Drilling Project Site 516 and dredged samples from different locations of the Rio Grande Rise which yield detailed information about the temporal and spatial evolution of this isolated oceanic plateau. We show the first geochemical data for the eastern Rio Grande Rise and the Jean Charcot Seamount Chain providing new insights into the magmatic history of the western South Atlantic Ocean. All the samples used in this study are variably altered volcanic rocks, predominantly basaltic with a geochemical signature reflecting formation on oceanic lithosphere with varying thickness. We find that the Rio Grande Rise was formed by at least two magmatic stages erupting first tholeiitic and second alkaline lavas that reflect a change from high degrees of shallow mantle melting at a plume-influenced spreading centre to intraplate volcanism. Whereas the first volcanic stage is probably related to the Tristan da Cunha mantle plume, the second stage may be due to lithospheric rifting and formation of the Jean Charcot Seamount Chain northeast of the Rio Grande Rise. We find no clear geochemical indications for crustal assimilation which could possibly indicate fragments of a microcontinent beneath the Rio Grande Rise.

REFERENCES

Fodor R V, Husler J W and Kumar N, Petrology of volcanic rocks from an aseismic rise: implications for the origin of the Rio Grande Rise, South Atlantic Ocean. Earth and Planetary Science Letters 1977, 35, doi: 10.1016/0012-821X(77)90125-X

Graça M C, Kusznir N and Stanton N S G, Crustal thickness mapping of the central South Atlantic and the geodynamic development of the Rio Grande Rise and Walvis Ridge, Marine and Petroleum Geology 2019, 101, doi: 10.1016/j.marpetgeo.2018.12.011

Mohriak W U, Nóbrega M, Odegard M E, Gomes B S et al. Geological and geophysical interpretation of the Rio Grande Rise, south-eastern Brazilian margin: extensional tectonics and rifting of continental and oceanic crusts, Petroleum Geoscience 2010, 16, doi:10.1144/1354-079309-910

O'Connor J M and Duncan R A, Evolution of the Walvis Ridge-Rio Grande Rise hot spot system: Implications for African and South American plate motions over plumes, Journal of Geophysical Research: Solid Earth 1990, 95, doi: 10.1029/JB095iB11p17475

Rohde J K, van den Bogaard P, Hoernle K, Hauff F et al. Evidence for an age progression along the Tristan-Gough volcanic track from new 40Ar/39Ar ages on phenocryst phases, Tectonophysics 2013, 604, doi:10.1016/j.tecto.2012.08.026

Santos R V, Ganade C E, Lacasse C M, Costa I S L et al. Dating Gondwanan continental crust at the Rio Grande Rise, South Atlantic. Terra Nova 2019, 31, doi:10.1111/ter.12405

Weaver B L, Marsh N G and Tarney J, TRACE-ELEMENT GEOCHEMISTRY OF BASALTIC ROCKS RECOVERED AT SITE-516, RIO-GRANDE RISE, DEEP-SEA DRILLING PROJECT LEG-72. Initial Reports of the Deep Sea Drilling Project 1983, 72

Wilson J T, Submarine fracture zones, aseismic ridges and the International Council of Scientific Unions line: proposed western margin of the east Pacific ridge, Nature 1965, 207, doi:10.1038/207907a0

MSM82/2

Protistan diversity along a transect across the South and North Atlantic Ocean exemplified by choanoflagellates

AUTHORS

University of Cologne | Cologne, Germany
F. Nitsche, S. Schiwitza

Within marine habitats, unicellular eukaryotes (protists) are important components in ecosystem functioning as they form the major part of primary production and food-web dynamics (Worden et al., 2015). Heterotrophic protists play an essential role as they remineralize nutrients from bacterial and phytoplankton production and provide them to higher trophic levels (Massana et al., 2009; Pernthaler, 2005). Exemplified by studies from the Atlantic Ocean, only few approaches have been attempted to study the abundance (Mangot et al., 2018), taxonomic composition (Countway et al., 2007), distribution (de Vargas et al., 1999) and diversity (Patterson et al., 1993) of heterotrophic flagellates in the off-shelf waters. Most studies focused on neritic pelagic zones (Bergesch et al., 2008; Gran-Stadniczeñko et al., 2019), which differ in their community composition compared to pelagic oceanic habitats. The first global metabarcoding approach (Tara Oceans) revealed different protist community patterns in the sunlit ocean (de Vargas et al., 2015). As this study is mainly hindered by the lack of reference sequences for the assignment of reads and the limitation of the used primer set, the species composition of these communities remains uncertain. Still, cultivation-based studies are of great necessity to create reliable data for reference databases and hence increase our knowledge on the ecological function of protists in marine ecosystems and refine biogeographical patterns by molecular and morphological characterization.

Within our study, we focused on the investigation of heterotrophic choanoflagellates. As efficient filter feeders, choanoflagellates have great ecological impact on the pelagic zone of marine ecosystems. Several studies revealed positive correlations of choanoflagellates to autotrophic nanoplankton and bacterioplankton abundance respectively making them a key component in marine habitats (Becquevort et al., 1992; Kivi and Kuosa, 1994). Despite their important role, choanoflagellates were dominantly studied from polar regions and neritic environments (e. g. Disco Bay, Greenland; Weddell Sea, Antarctica; Kattegat, Denmark; Southampton Bay, UK or Shark Bay, Australia) (Nitsche et al., 2017; Thomsen et al., 1997, 2016; Thomsen and Østergaard, 2017; Tong, 1997a, 1997b). Only recent morphological studies broadly extended the knowledge on warm water acanthoecid choanoflagellates (e. g. Thomsen and Østergaard, 2019). Although molecular data is missing, as these samples were fixed for microscopy, these studies show that the warm water regions harbor along with ubiquitous

distributed species a morphological distinct acanthoecid community. Mainly due to their unique morphological characteristic, the species-specific siliceous lorica, most quantitative and qualitative data are available for acanthoecid choanoflagellates. Craspedid species (only organic covering), although frequently found, are barely assigned to species level, hindered by the lack of distinct morphological traits.

Within a recent revision of the order of Craspedida, the polyphyly of the genus Codosiga with its freshwater type species *Codosiga botrytis* (Ehrenberg) Bütschli, 1878 was revealed by molecular data, which separated the species into two distinct phylogenetical and ecological clades (Carr et al., 2017). The marine clade, composed of *C. gracilis* (Saville-Kent) de Saedeleer, 1927, *C. balthica* Wylezich and Karpov, 2012 and *C. minima* Wylezich and Karpov, 2012, was amended by introducing the new genus *Hartaetosiga*. The type species of the genus *Hartaetosiga, H. gracilis* (Saville-Kent) Carr, Richter, Nitsche, 2017 was isolated from a tide pool of a salt marsh bordering the Wash at Freiston Shore, England, indicating its marine character. The further findings of *H. balthica* (Wylezich and Karpov) Carr, Richter and Nitsche, 2017 and *H. minima* (Wylezich and Karpov) Carr, Richter and Nitsche, 2017 from the Baltic Sea extended the clade with relevant data on its ecological function as relevant players for hypoxic water bodies, underlined by isolates found in over 200 m depth (Wylezich et al., 2012).

For further insights into the systematics and biogeography of the genus Hartaetosiga, we sampled surface water of a transect across the Atlantic Ocean (35 °S to 23 °N) as the pelagic provinces do affect biological and ecological patterns (Spalding et al., 2012). The Atlantic Ocean is the second largest aquatic ecosystem on Earth and physically structured by varying abiotic conditions, like changes in salinity (influenced by the influx of river systems and high equatorial evaporation) and temperature shifts due to the spatial expansion (e. g. artic waters and tropics) (Fuglister, 1960; Parrilla et al., 1994). The South and North Atlantic are separated by equatorial counter currents at about 8 °N, dividing the surface waters of both regions (Richardson and Walsh, 1986). With a high isolation and cultivation effort, we were able to enlarge the clade of the genus *Hartaetosiga* with several strains (see Figure 1, left), including a new species, *H. australis*. This new species was recorded only from sampling stations in the Southern Hemisphere, which may indicate a potential biogeographic distribution likely caused by the Equatorial Counter Current (ECC), dividing the northern and southern surface waters.

Aside of the cultivation success regarding craspedid choanoflagellates during the cruise, we were able to record a high morphological diversity of acanthoecid choanoflagellates based on a standardized protocol for SEM (scanning electron microscopy) (see examples in Figure 1, right). We were able to record acanthoecid species which were previously not reported from the off-shelf region of the Atlantic Ocean as well as morphotypes that cannot be assigned to any known loricate species, indicating a hidden diversity within the well-studied group of acanthoecids. Our data extends the dataset on biogeographic distribution patterns and provides further information on the dispersal potential for marine choanoflagellates.

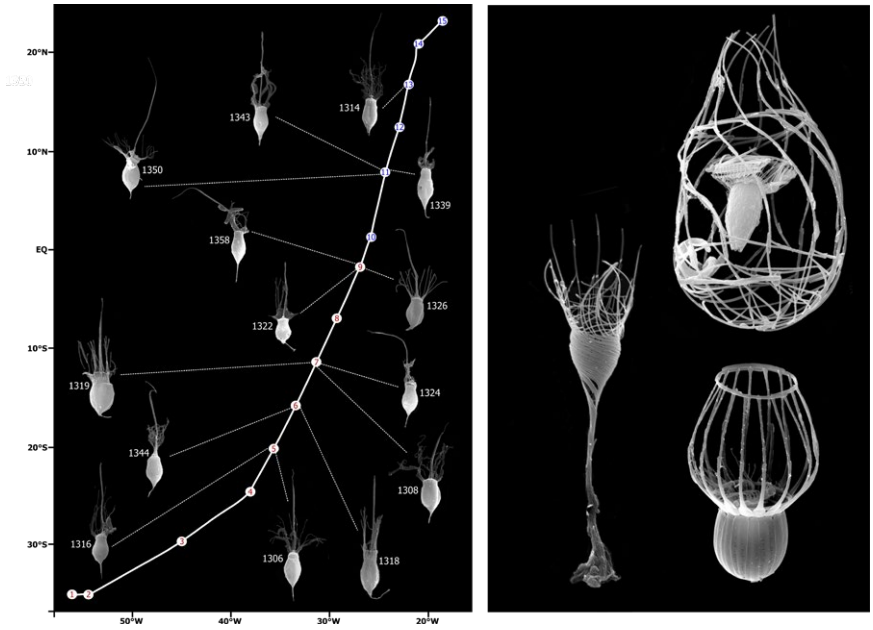

Fig. 1: Choanoflagellate diversity along a transect across the South and North Atlantic Ocean. Left: cultivated strains (see strain number) of the craspedid genus *Hartaetosiga* from different stations (in total 15) along the cruise, right: acanthoecid choanoflagellates exemplified by *Acanthoeca spectabilis*, *Diaphanoeca grandis* and *Didymoeca costata*.

REFERENCES

Becquevort S, Mathot S, Lancelot C, Interactions in the microbial community of the marginal ice zone of the northwestern Weddell Sea through size distribution analysis, Polar Biology 1992, 12, 211–218, doi:10.1007/BF00238262

Bergesch M, Odebrecht C, Moestrup Ø, Loricate choanoflagellates from the South Atlantic coastal zone (~32 °S) including the description of Diplotheca tricyclica sp. nov., Biota Neotropica 2008, 8, 111–122, doi: 10.1590/S1676-06032008000400010

Carr M, Richter DJ, Fozouni P, Smith TJ, Jeuck A, Leadbeater BSC, Nitsche F, A six-gene phylogeny provides new insights into choanoflagellate evolution, Molecular Phylogenetics and Evolution 2017, 107, 166–178, doi: 10.1016/j.ympev.2016.10.011

Countway PD, Gast RJ, Dennett MR, Savai P, Rose JM, Caron DA, Distinct protistan assemblages characterize the euphotic zone and deep sea (2500 m) of the western North Atlantic (Sargasso Sea and Gulf Stream), Environmental Microbiology 2007, 9, 1219–1232, doi: 10.1111/j.1462-2920.2007.01243.x

de Vargas C, Audic S, Henry N, Decelle J, Mahe F, Logares R, Lara E, Berney C, Le Bescot N, Probert I, Carmichael M, Poulain J, Romac S, Colin S, Aury J-M, Bittner L,

Chaffron S, Dunthorn M, Engelen S, Flegontova O, Guidi L, Horak A, Jaillon O, Lima-Mendez G, Luke J, Malviya S, Morard R, Mulot M, Scalco E, Siano R, Vincent F, Zingone A, Dimier C, Picheral M, Searson S, Kandels-Lewis S, Tara Oceans Coordinators, Acinas SG, Bork P, Bowler C, Gorsky G, Grimsley N, Hingamp P, Iudicone D, Not F, Ogata H, Pesant S, Raes J, Sieracki ME, Speich S, Stemmann L, Sunagawa S, Weissenbach J, Wincker P, Karsenti E, Boss E, Follows M, Karp-Boss L, Krzic U, Reynaud EG, Sardet C, Sullivan MB, Velayoudon D, Eukaryotic plankton diversity in the sunlit ocean, Science 2015, 348, 1261605–1261605, doi: 10.1126/science.1261605

de Vargas C, Norris R, Zaninetti L, Gibb SW, Pawlowski J, Molecular evidence of cryptic speciation in planktonic foraminifers and their relation to oceanic provinces, Proceedings of the National Academy of Sciences of the United States of America 1999, 96, 2864–2868, doi: 10.1073/pnas.96.6.2864

Fuglister FC, Atlantic Ocean atlas of temperature and salinity profiles and data from the international geophysical year of 1957-1958, Woods Hole Oceanographic Institution 1960, 1–209

Gran-Stadniczeñko S, Egge E, Hostyeva V, Logares R, Eikrem W, Edvardsen B, Protist diversity and seasonal dynamics in Skagerrak plankton communities as revealed by metabarcoding and microscopy, Journal of Eukaryotic Microbiology 2019, 66, 494–513, doi: 10.1111/jeu.12700

Kivi K, Kuosa H, Late winter microbial communities in the western Weddell Sea (Antarctica), Polar Biology 1994, 14, 389–399, doi: 10.1007/BF00240259

Mangot J-F, Forn I, Obiol A, Massana R, Constant abundances of ubiquitous uncultured protists in the open sea assessed by automated microscopy, Environmental Microbiology 2018, 20, 3876–3889, doi: 10.1111/1462-2920.14408

Massana R, Unrein F, Rodríguez-Martínez R, Forn I, Lefort T, Pinhassi J, Not F, Grazing rates and functional diversity of uncultured heterotrophic flagellates, The ISME Journal 2009, 3, 588–596, doi: 10.1038/ismej.2008.130

Nitsche F, Thomsen HA, Richter DJ, Bridging the gap between morphological species and molecular barcodes – exemplified by loricate choanoflagellates, European Journal of Protistology 2017, 57, 26–37, doi: 10.1016/j.ejop.2016.10.006

Parrilla G, Lavín A, Bryden H, García M, Millard R, Rising temperatures in the subtropical North Atlantic Ocean over the past 35 years, Nature 1994, 369, 48–51, doi: 10.1038/369048a0

Patterson DJ, Nygaard K, Steinberg G, Turley CM, Heterotrophic flagellates and other protists associated with oceanic detritus throughout the water column in the mid North Atlantic, Journal of the Marine Biological Association of the United Kingdom 1993, 73, 67–95, doi: 10.1017/S0025315400032653

Pernthaler J, Predation on prokaryotes in the water column and its ecological implications, Nature Reviews Microbiology 2005, 3, 537–546, doi: 10.1038/nrmicro1180

Richardson PL, Walsh D, Mapping climatological seasonal variations of surface currents in the tropical Atlantic using ship drifts, Journal of Geophysical Research 1986, 91, 10537–10550, doi: 10.1029/JC091iC09p10537

Spalding MD, Agostini VN, Rice J, Grant SM, Pelagic provinces of the world: a biogeographic classification of the world's surface pelagic waters, Ocean & Coastal Management 2012, 60, 19–30, doi: 10.1016/j.ocecoaman.2011.12.016

Thomsen HA, Garrison DL, Kosman C, Choanoflagellates (Acanthoecidae, Choanoflagellida) from the Weddell Sea, Antarctica, taxonomy and community structure with particular emphasis on the ice biota; with preliminary remarks on choanoflagellates from Arctic sea ice (Northeast Water Polynya, Greenland), Archiv fuer Protistenkunde 1997, 148, 77–114

Thomsen HA, Nitsche F, Richter DJ, Seasonal occurrence of loricate choanoflagellates in Danish inner waters, Protist 2016, 167, 622–638, doi: 10.1016/j.protis.2016.09.002

Thomsen HA, Østergaard JB, Acanthoecid choanoflagellates from the Atlantic Arctic Region – a baseline study, Heliyon 2017, 3, e00345, doi: 10.1016/j.heliyon.2017.e00345

Thomsen HA, Østergaard JB, Loricate choanoflagellates (Acanthoecida) from warm water seas. I. Conioeca gen. nov. and Nannoeca Thomsen, European Journal of Protistology 2019, 67, 77–88, doi: 10.1016/j.ejop.2018.11.001

Tong SM, Choanoflagellates in Southampton water, including the description of three new species, Journal of the Marine Biological Association of the United Kingdom 1997a, 77, 929–958, doi: 10.1017/S0025315400038546

Tong SM, Heterotrophic flagellates from the water column in Shark Bay, Western Australia, Marine Biology 1997b, 128, 517–536, doi: 10.1007/s002270050118

Worden AZ, Follows MJ, Giovannoni SJ, Wilken S, Zimmerman AE, Keeling PJ, Rethinking the marine carbon cycle: Factoring in the multifarious lifestyles of microbes, Science 2015, 347, 1257594–1257594, doi: 10.1126/science.1257594

Wylezich C, Karpov SA, Mylnikov AP, Anderson R, Jürgens K, Ecologically relevant choanoflagellates collected from hypoxic water masses of the Baltic Sea have untypical mitochondrial cristae, BMC Microbiology 2012, 12, 271, doi: 10.1186/1471-2180-12-271

MSM89

Atmospheric Turbulence and Clouds in the Tropics: Shipborne Lidar Measurements of Dynamics and Thermodynamics During EUREC4A

AUTHORS

University of Hohenheim, Institute of Physics and Meteorology | Stuttgart, Germany
D. Lange, A. Behrendt, F. Spath, S. Abbas, V. Wulfmeyer

University of Colorado and NOAA (National Oceanic and Atmospheric Administration) Chemical Sciences Laboratory | Boulder CO, USA
C. Senff

During the EUREC4A campaign (Bony et al., 2017, Stevens et al, 2021), a unique combination of lidar systems for temperature, humidity and wind measurements was operated on the German research vessel R/V Maria S Merian (MSM89 cruise) between 18 January and 18 February 2020 in the trade wind alley east of Barbados and in the "Boulevard des Tourbillons" east of Venezuela. These systems observed the maritime boundary layer (MBL) with turbulence-resolving resolution which shows the dependence of cloud evolution on sea surface temperature and MBL properties as well as the interaction with the trade wind layer.

ARTHUS

For the first time, the Atmospheric Raman Temperature and Humidity Sounder (ARTHUS) (Lange et al., 2019) was operated on a shipborne platform.

Due to an advanced design of the transmitter and the receiver, simultaneous profiling of temperature and water-vapor mixing ratio is possible with unprecedent accuracies and resolutions. Typical resolutions are a few seconds and meters in the lower troposphere. With the measurements themselves, also the statistical uncertainties are derived (Wulfmeyer et.al., 2016). The design of the system permits measurements in all weather conditions and even in clouds and rain up to an optical thickness of approx. 2. Stable 24/7 operations over long periods were achieved during several field campaigns and at the Land Atmosphere Feedback Observatory (LAFO) at the University of Hohenheim accumulating more than a year of data until now and covering a huge variety of weather conditions.

EUREC4A

During EUREC4A, the measurements were made in vertically staring mode. ARTHUS provides water-vapor mixing ratio (Figure 2), temperature, and aerosol profiles with a

high resolution of 7.5 m and 10 s in the lower troposphere and was combined with one Doppler lidar in vertically staring mode and a second one in a 6-beam scanning mode, both with resolutions of 1 s and 15 m. The Doppler lidars provide vertical (Figure 3) and horizontal wind profiles as well as the statistics of higher-order moments of turbulent fluctuations of these parameters and thus, e. g., turbulent kinetic energy and momentum flux. Synergetic parameters from the combination of all three lidars are, e. g., sensible and latent heat flux profiles (Figure 4, Behrendt et al. 2020).

ARTHUS data is available between 24 January 2017 and 19 February 2017, while the Doppler lidars measured between 17 January 2017 and 19 February 2017. At the conference, highlights of the measurements will be presented.

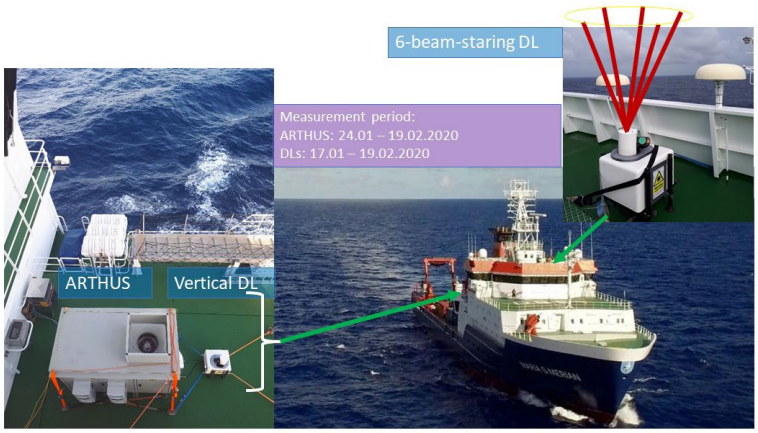

Fig. 1: ARTHUS and Doppler lidars setup on board R/V Maria S Merian during EUREC4A campaign (MSM89 cruise). Credits: D. Lange and http://eurec4a.eu/index.php?id=5154.

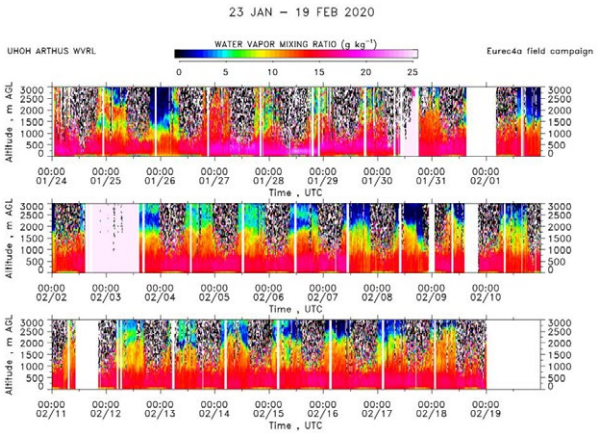

Fig. 2: Time-height cross section of water-vapor mixing ratio measured between 24 January 2017 and 19 February 2017. The resolution of the data is 50 m and 600 s.

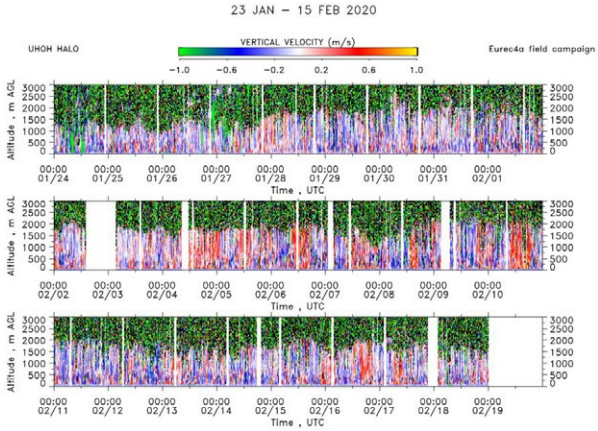

Fig. 3: Time-height cross section of vertical velocity measured between 24 January 2017 and 19 February 2017. The resolution of the data is 50 m and 600 s.

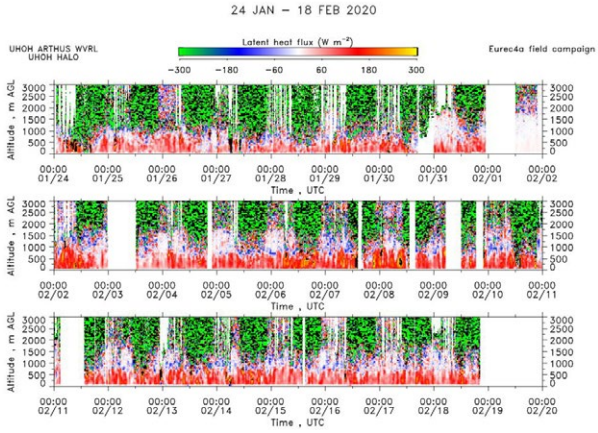

Fig. 4: Time-height cross section of latent heat flux between 24 January 2017 and 19 February 2017. The resolution of the data is 50 m and 600 s.

REFERENCES

Behrendt, A., Wulfmeyer, V., Senff, C., Muppa, S. K., Späth, F., Lange, D., Kalthoff, N., and Wieser, A.: Observation of sensible and latent heat flux profiles with lidar, Atmos. Meas. Tech. 2020, 13, 3221–3233, https://doi.org/10.5194/amt-13-3221-2020.

Bony, S. et al. EUREC4A: A Field Campaign to Elucidate the Couplings Between Clouds, Convection and Circulation 2017. Surv Geophys 38, 1529–1568. https://doi.org/10.1007/s10712-017-9428-0.

Lange, D., Behrendt, A., Wulfmeyer, V. Compact operational tropospheric water vapor and temperature Raman lidar with turbulence resolution. Geophysical Research Letters 2019, 46, 14,844–14, 853. https://doi.org/10.1029/2019GL085774

Stevens, B. et.al. EUREC4A, Earth Syst. Sci. Data 2021, 13, 4067–4119, https://doi.org/10.5194/essd-13-4067-2021.

Wulfmeyer, V., et.al. Determination of Convective Boundary Layer Entrainment Fluxes, Dissipation Rates, and the Molecular Destruction of Variances: Theoretical Description and a Strategy for Its Confirmation with a Novel Lidar System Synergy. Journal of the Atmospheric Sciences 2016, 73(2), 667–692. https://doi.org/10.1175/JAS-D-14-0392.1

POS539

Nitrous oxide cycling under low oxygen concentrations in the water column of the Western Black Sea

AUTHORS

Max Planck Institute for Marine Microbiology | Bremen, Germany

J. N. von Arx, K. Kitzinger, J. Graf, H. K. Marchant, G. Lavik, M.M.M. Kuypers, J. Milucka

Nitrous oxide (N_2O) is the third most abundant greenhouse gas in the atmosphere, making it a significant driver of climate change. Marine habitats are estimated to contribute 33 %, of total natural N_2O emissions; predominantly from oxygen minimum zones (OMZs). The low oxygen concentrations found in OMZs allow both aerobic and anaerobic microbial processes to co-occur. As such N_2O can be formed in OMZs by both aerobic ammonia oxidation, the conversion of ammonia to nitrite, and denitrification, the stepwise reduction of nitrate to dinitrogen gas (N_2). During aerobic ammonia oxidation, ammonia oxidising archaea form N_2O as a by-product, through a little understood side reaction, while ammonia-oxidising bacteria can produce N_2O in a process sometimes called "nitrifier-denitrification". During canonical denitrification, microorganisms produce N_2O when they reduce nitric oxide and consume N_2O via reduction to N_2. The latter process is the only biological process that contributes substantially to N_2O removal. However, while N_2O production and consumption are part of the denitrification process, they are not necessarily carried out by the same microorganisms, and instead a complex community of co-occurring N_2O producers and consumers exists in marine systems. Both aerobic ammonia oxidation and denitrification are well documented N_2O sources in the major oxygen minimum zones that exist at eastern boundary upwelling systems, however, their contribution to N_2O emissions has received little attention in the largest meromictic sea in the world, the Black Sea. This unique ecosystem is not only the largest surface water reservoir for methane (CH_4) but, unlike many other oxygen minimum zones, it is considered a negligible source of N_2O to the atmosphere. In this study, we aim to constrain and quantify the processes and organisms responsible for N_2O cycling, to understand the underlying mechanisms for the Black Sea's low N_2O emissions.

As part of the cruise POS539 on board FS Poseidon N_2O cycling was investigated at six stations in the Western Black Sea (Figure 1.). At each station, high-resolution nutrient profiles were collected with a pump cast conductivity temperature depth system for ammonium, nitrite, nitrate, phosphate, silicate and sulphide concentration measurements. From selected depths, water was sampled for gas concentration analyses, as well as for visualising biogeochemically relevant microbes with fluorescent *in-situ* hybridisation.

Furthermore, at each station, three to four discrete depths were selected to conduct stable isotope incubation measurements, using ^{15}N labelled isotopes, to determine the production rates of N_2O from both ammonium and nitrite as precursors, as well as ^{15}N-N_2O consumption rates. The incubation depths targeted the upper suboxic zone, the nitrate maximum, the nitrite maximum and the depth where both the CH_4 and ammonium increase. In addition to the incubations, water was also filtered for metagenomic and metatranscriptomic analysis and, upon the completion of the incubation experiments, incubated samples were also filtered for nanoscale secondary ion mass spectrometry analysis to track stable isotope incorporation at a single cell level.

Oxygen concentrations rapidly decreased with depth, with the oxycline situated between 100–120m (Figure 2.). This depth also marked the transition zone for sulphide, ammonium and CH_4 concentrations, which were depleted in the oxic water column but increased in the lower part of the oxycline and at deeper depths. Although not always forming distinct maxima, nitrate concentrations reached up to 6 µM, while nitrite remained mostly below detection limit. Therefore, the chosen incubation depths (Figure 2.) could potentially be areas of intense nutrient cycling. The rate incubation experiments showed significant N_2O production from both nitrite and ammonium as precursors. N_2Oproduction rates were in the picomolar per day range; a magnitude comparable to a previous study conducted in the centre of the Western Gyre (Westley et al., 2006). There was one exception, the deepest incubation depth of station POS539_08, where the N_2O production was in the nanomolar per day range; an order of magnitude higher than all other incubations. Overall, nitrite seemed to be the main precursor for N_2O formation, but not at all depths or stations, especially in the suboxic zone ammonium derived N_2O was dominant. N_2O reduction was also quantifiable, with consumption rates partly exceeding N_2O formation rates. This potentially tight coupling of the two processes explains the insignificant N_2O accumulation in the water column. Future research will focus on the molecular aspects of the observed N_2O cycling in this environment by identifying the key organisms involved. It will be especially interesting to determine whether the community differed at the enigmatic depth at station POS539_08 where N_2O production was unusually high. To answer these questions, a combination of metagenomics and fluorescent *in-situ* hybridisation are going to be applied to help further the understanding of this fascinating ecosystem.

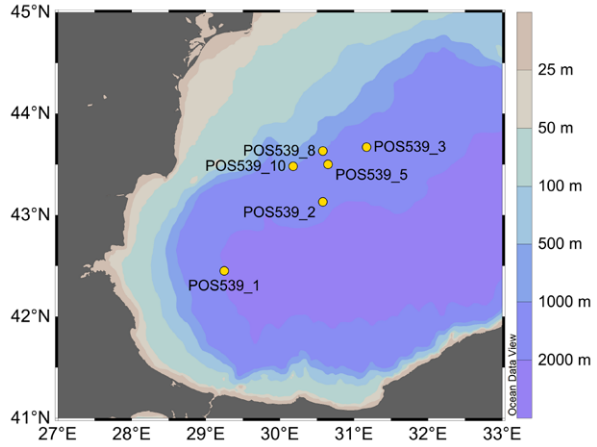

Fig. 1: Station map of the cruise POS539, investigating the Western Black Sea.

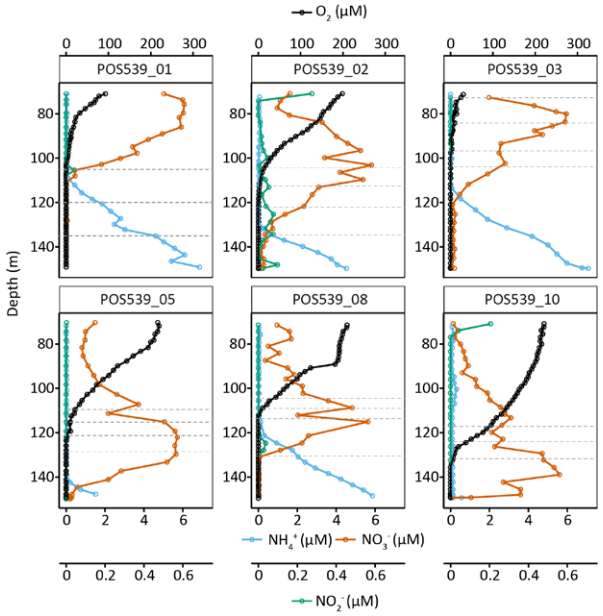

Fig. 2: Oxygen and nitrogen concentration profiles from the lower water column taken from the six incubation stations from cruise POS539. Samples were taken with a pump cast system, continuously sampling the water column around every 3m. The grey dotted lines indicate the sampling depths for the incubation experiments.

REFERENCE

Westley M B, Yamagishi H, Popp B N, N Yoshida, Nitrous oxide cycling in the Black Sea inferred from stable isotope and isotopomer distributions, Deep-Sea Research Part II 2006, 53 (17–19), doi: 10.1016/j.dsr2.2006.03.012

SO259/3

CAROL – Collecting Atmpspheric Reference Data Over Oceans

AUTHORS

Max-Planck-Institute for Meteorology | Hamburg, Germany
S. Kinne, J. Frontzek

Koninklijk Nederlands Meteorologisch Instituut | DeBilt, The Netherlands
P. Wang

Max-Planck-Institute for Chemistry | Mainz, Germany
S. Dörner

Hamburg City University | Hamburg, Germany
H. Sternberg, T. Dufek

University of Montevideo | Montevideo, Uruguay
L. Kühne

COLLECTING ATMOSPHERIC REFERENCE DATA OVER OCEANS

The poster presents images and results of the RV SONNE transit SO-259/3 from Emden via Brest to Buenos Aires. Consistent with the scientific purpose (to collect reference data over oceans) meridional Atlantic cross-sections by late December are displayed for (water and air) temperatures, relative humidity, wind-speed, water vapor, cloud cover, cloud base altitude, aerosol load and even typical aerosol size. The poster also shows extra instrumentation and highlights results and images of specific events, as the passing of an atmospheric squall line (with heavy rain), a major dust event (sharply reduced visibility) and several ARGO float deployments.

Fig. 1: daily averages of the atmospheric aerosol column load during (quantified by the aerosol optical depth, AOD) and the arrival of the dust event on Christmas Day 2017 off Africa, comparing good visibility during an ARGO float deployment in the morning with poor visibility in the evening, when the sun's image was diffused by dust.

SO263

Chemical and isotopic variations in hydrothermal sulfides from Niuatahi caldera, Tonga rear-arc

AUTHORS

GeoZentrum Nordbayern, Friedrich-Alexander University (FAU) | Erlangen, Germany

J.J. Falkenberg, M. Keith, K.M. Haase

Submarine hydrothermal vent systems are actively forming massive sulfide deposits on the seafloor and can be enriched in precious (Ag, Au) and volatile (Te, Se, Bi) elements in subduction zone-related environments. These elements are of economic interest, since they are key commodities for the green energy transition. The magmas in these subduction zone-related settings can reach volatile saturation during ascent and fractional crystallization, resulting in the release of a metal(loid) and gas-rich magmatic volatile phase influencing the metal budget of the overlying hydrothermal system. Due to the shallower water depth (<2000 mbsl) in subduction zone-related hydrothermal systems, trace element fractionation between a Cl-rich liquid and a Cl-poor vapour phase during fluid boiling is another effective process changing the metal(loid) contents of the hydrothermal fluids. Hence, such processes commonly overprint the signature of the metal sources (host rock vs. magmatic volatiles) in the fluids and as a consequence cause distinct variations in the mineralogical and chemical composition of seafloor hydrothermal sulfides, which remain poorly constrained.

The giant andesitic-dacitic submarine caldera of Niuatahi volcano in the Tonga rear-arc hosts four active vent sites associated with younger magmatic cones along the caldera wall (Niuatahi North and Southwest) and in the central parts of the caldera (Niuatahi Motutahi and Niuatahi South-Central; Fig. 1). The discharge of high temperature fluids (up to 334°C) with variable salinities (369 to 583 mM Cl) is indicative for the influence of fluid boiling, whereas acid-sulfate alteration together with massive native S precipitation is evidence for a magmatic volatile influx (Kim et al. 2011). These variable processes might be recorded by the chemical and isotopic composition of the hydrothermal precipitates. Thus, comparing the in-situ trace element and radiogenic Pb and stable S isotope composition of hydrothermal sulfides (pyrite, chalcopyrite, sphalerite) from the different vent sites allows us to define key ore-forming processes. We decipher deep source-related (magmatic volatile vs. host rock leaching) vs. shallow hydrothermal (fluid boiling) signatures and constrain spatially selective trace element enrichments within the seafloor mineralization in the submarine hydrothermal systems of Niuatahi caldera.

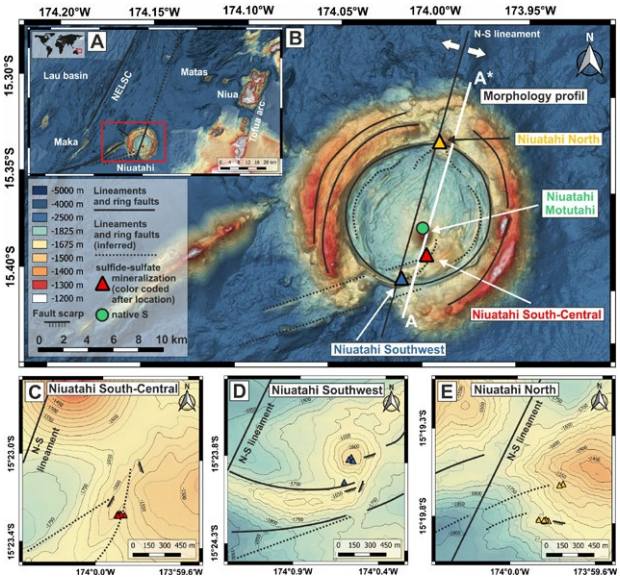

Fig.1: (A) Overview of the NE Lau basin and the northern end of the Tonga arc. (B) Detailed bathymetric map of the Niuatahi caldera based on data from the SO263 cruise. (C-E) Detailed bathymetric maps of ROV dives and sampling locations during SO263.

The seafloor mineralization at Niuatahi caldera includes Cu-Fe-rich massive sulfides talus as well as zoned Cu-Fe and Zn-Ba-rich chimneys that actively discharge fluids. The main sulfide minerals (pyrite, chalcopyrite, sphalerite) show distinct trace element compositions between the different vent sites. Niuatahi South-Central shows high Te, Se, Bi ± Co contents, whereas those from Niuatahi North are enriched in Zn, Cd, Pb, and Tl. Sulfides from Niuatahi Southwest show intermediate trace element contents between the signatures of the other two vent sites. The S isotope composition of hydrothermal sulfides suggests that S is derived from distinct sources with variable contribution in the Niuatahi caldera vent sites. For instance, the low $\delta^{34}S$ signatures of sulfides and native S from Niuatahi Motutahi (-8.2 to 0.8‰, Kim et al. 2011) and Niuatahi South-Central (-10.6 to 2.7‰) suggest a strong influence of magmatic derived SO_2 by magmatic volatile influx, which strongly enhances the volatile element budget (e. g., Te, Se, Bi) of the respective fluids and precipitates. Accordingly, the occurrence of native S mineralization at Niuatahi Motutahi reveals, that the magmatic volatile phase reached the seafloor and its chemical signature might be recorded in the native S condensates (Kim et al. 2011). Therefore, the high contents of volatile Se, Te, and Bi as well as similar Te/As, Te/Au, and Bi/As ratios of pyrite at Niuatahi Southwest and in native S from Niuatahi Motutahi (Fig. 2) propose at least a minor or infrequent contribution of magmatic volatiles to Niuatahi Southwest. However, the higher and variable $\delta^{34}S$ values (1.7 to 6.3‰) of sulfides at Niuatahi Southwest rather imply a mixing of host rock and seawater-derived sulfur (up to 26 %), which might have been overprinted by minor or infrequent magmatic signatures (Ono et al. 2007). By contrast, the $\delta^{34}S$ signature of seafloor sulfides from Niuatahi North (-0.6

to 0.8‰) display only slight variation and is consistent with leaching of host rocks with a $\delta^{34}S$ composition that is presumably represented by the $\delta^{34}S$ composition of basaltic glass from the nearby Mata volcano (0.2 to 2.0‰, Keller et al. 2009).

Distinctly higher Te/As and Te/Au ratios in the sulfides from Niuatahi South-Central compared to sulfides from Niuatahi Southwest and North as well as native S from Niuatahi Motutahi (Fig. 2) however cannot be the result of magmatic degassing as similar ratios in the magmatic host rocks and native S imply no major fractionation of Te in favor of As and Au. Instead, we propose, that the high Te/As and Te/Au ratios are the result of distinct trace element fractionation between the Cl-poor vapour and Cl-rich liquid phase during subseafloor boiling at Niuatahi South-Central. This is consistent with the venting of fluids with a vapour component (369–460 mM Cl) and with experimentally derived fluid-melt and vapor-liquid partitioning coefficients during magmatic degassing and phase separation, respectively (Pokrovski et al. 2002; Grundler et al. 2013; Pokrovski et al. 2013; Guo and Audétat 2017; Zelenski et al. 2021).

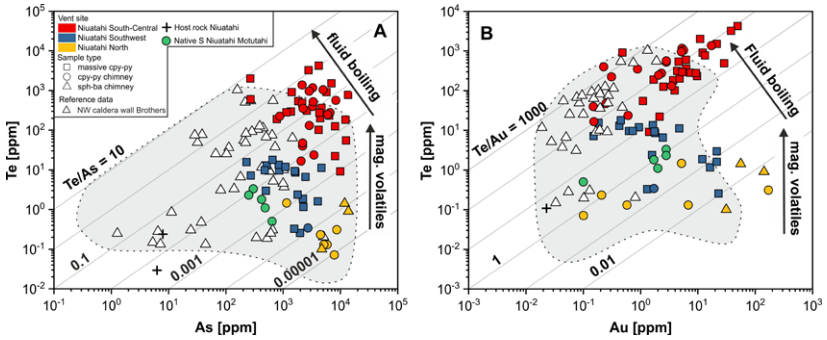

Fig. 2: In-situ LA-ICP-MS composition of hydrothermal pyrite compared to the composition of the magmatic host rock (this study), native S from Niuatahi Motutahi (Kim et al. 2011) and pyrite from other subduction zone-related systems (Keith et al. 2016).

The Pb isotope ratios in seafloor sulfides are distinct between the northern caldera wall compared to the vent sites in the central and southern (Niuatahi South-Central and Southwest) portion of Niuatahi caldera. However, Pb isotope ratios at Niuatahi South-Central and Southwest are comparable. In combination with the sulfide chemistry and the S isotope constraints this suggests, that venting at the Niuatahi North vent site at the distal northern caldera wall is decoupled from the magmatic SO_2 source in the caldera center, whereas venting at Niuatahi Motutahi, Niuatahi South-Central ± Southwest proximal to the caldera centre are coupled systems. Therefore, we conclude, that the observed hydrothermal fractionation processes (e. g., fluid boiling) and the distinct metal(loid) sources (magmatic volatiles vs. host rocks) at Niuatahi represent stages along a continuum of magmatic volatile-dominated to seawater-derived fluid venting. This leads to seafloor mineralizations with a distinct composition represented by spatially selective

trace element enrichments, such as Te, Se, Bi, and Co (± Au, Ag) in the central caldera compared to Au, Ag, Zn, Cd, Tl, and Pb at the northern caldera wall.

REFERENCES

Grundler, P.V.; Brugger, J.; Etschmann, B.E.; Helm, L.; Liu, W.; Spry, P.G. et al. (2013): Speciation of aqueous tellurium (IV) in hydrothermal solutions and vapors, and the role of oxidized tellurium species in Te transport and gold deposition. Geochimica et Cosmochimica Acta 120, 298–325.

Guo, H.; Audétat, A. (2017): Transfer of volatiles and metals from mafic to felsic magmas in composite magma chambers: an experimental study. Geochimica et Cosmochimica Acta 198, 360–378.

Keith, M.; Häckel, F.; Haase, K.M.; Schwarz-Schampera, U.; Klemd, R. (2016): Trace element systematics of pyrite from submarine hydrothermal vents. Ore Geology Reviews 72, 728–745.

Keller, N.S.; Rubin, K.H.; Clague, D.A.; Michael, P.J.; Resing, J.A.; Cooper, L.B. et al. (2009): Sulfur in submarine eruptions: Observations and preliminary data from West Mata, NE Lau Basin. American Geophysical Union, Fall Meeting, V43I-08.

Kim, J.; Lee, K.-Y.; Kim, J.-H. (2011): Metal-bearing molten sulfur collected from a submarine volcano: Implications for vapor transport of metals in seafloor hydrothermal systems. Geology 39, 351–354.

Ono, S.; Shanks, W.C.; Rouxel, O.J.; Rumble, D. (2007): S-33 constraints on the seawater sulfate contribution in modern seafloor hydrothermal vent sulfides. Geochimica et Cosmochimica Acta 71, 1170–1182.

Pokrovski, G.S.; Zakirov, I.V.; Roux, J.; Testemale, D.; Hazemann, J.-L.; Bychkov, A.Y.; Golikova, G.V. (2002): Experimental study of arsenic speciation in vapor phase to 500°C: implications for As transport and fractionation in low-density crustal fluids and volcanic gases. Geochimica et Cosmochimica Acta 66, 3453–3480.

Pokrovski, G.S.; Borisova, A.Y.; Bychkov, A.Y. (2013): Speciation and transport of metals and metalloids in geological vapors. Reviews in mineralogy and geochemistry 76, 165–218.

Zelenski, M.; Simakin, A.; Taran, Y.; Kamenetsky, V.S.; Malik, N. (2021): Partitioning of elements between high-temperature, low-density aqueous fluid and silicate melt as derived from volcanic gas geochemistry. Geochimica et Cosmochimica Acta 295, 112–134.

SO263

Hydrothermal vent fluids and sulphides from Maka volcano, North Eastern Lau Spreading Centre

AUTHORS

Jacobs University Bremen | Bremen, Germany
L. Klose, C. Kleint, A. Koschinsky

GeoZentrum Nordbayern, University of Erlangen-Nuremberg | Erlangen, Germany
M. Keith, D. Hafermaas, R. Klemd, R. von Geldern, K. Haase

Center for Marine Environmental Sciences (MARUM) and Faculty of Geosciences, University of Bremen | Bremen, Germany
W. Bach, A. Diehl, F. Wilckens

Department for Geology and Palaeontology, University of Münster | Münster, Germany
H. Strauss, C. Peters

INTRODUCTION

Back-arc spreading centres and related volcanic structures are known for their intense hydrothermal activity. Heat loss during the cooling of the oceanic crust is the driver for hydrothermal fluid circulation (e. g. Von Damm, 1995; German and Seyfried, 2013; Humphris and Klein, 2018). Seawater that percolates through the oceanic crust is chemically modified due to water-rock interaction during low temperature alteration (<250°C) in the recharge zone and temperatures up to 400°C in the reaction and upflow zone, where most of the metals are leached from the adjacent host rocks (German and Von Damm, 2003; Bach et al., 2013; Humphris and Klein, 2018). In addition to the leaching process, metals may be contributed by magmatic volatiles, as known from island arc and some back-arc hydrothermal systems (de Ronde et al., 2011; Keith et al., 2018; Seewald et al., 2019; Fox et al., 2020; Martin et al., 2020). Previous studies highlighted that fluid boiling is an efficient process for metal fractionation and precipitation in arc and back-arc hydrothermal systems (i. e., 3060 m water depth; Stoffers et al., 2006; Monecke et al., 2014). Although, liquid-vapour partitioning and precipitation affect the fluid chemistry in predictable ways (e. g., Von Damm et al., 1997; Stoffers et al., 2006; Schmidt et al., 2017) it is still unclear how these processes are recorded in the geological archive by sulphide chemistry (Tardani et al., 2017; Román et al., 2019; Keith et al., 2020; Falkenberg et al., 2021; Nestmeyer et al., 2021; Schaarschmidt et al., 2021).

GEOLOGICAL OVERVIEW AND SAMPLING SITE

The North Eastern Lau Basin in the SW Pacific Ocean (Fig. 1A) is known for its intense hydrothermal activity and complex tectonic setting (Zellmer and Taylor, 2001; Lupton et al., 2015; Embley and Rubin, 2018; Baker et al., 2019; Baxter et al., 2020; Anderson et al., 2021). The North Eastern Lau Spreading Centre (NELSC, Fig. 1B) is situated in the western part of the Lau back-arc basin and follows a NE-orientation with an estimated spreading rate of ~42 mm yr^{-1} (Baxter et al., 2020). Maka is the southernmost axial volcanic edifice at the NELSC, where first evidence for hydrothermal activity was indicated by a plume survey in 2004 (German et al., 2006). At the summit of Maka volcano two active hydrothermal vent sites occur at 1525 to 1543 m water depth, which are characterised by distinct vent structures and fluid discharge. At the Maka hydrothermal field (Maka HF) vigorously venting black smoker-type fluids were observed together with smaller chimneys emitting clear fluids (Haase et al., 2018). Less than a hundred meters south of Maka HF, a second vent site named Maka South was discovered, where clear to white fluids are discharged at several sites from flanges and diffuse areas (Haase et al., 2018).

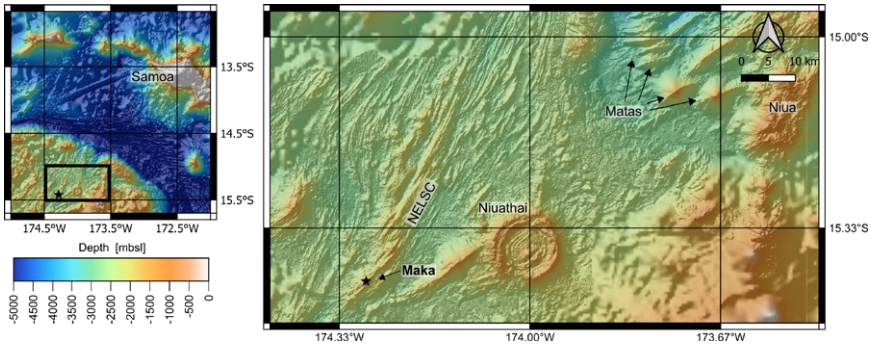

Fig. 1: (A) Large scale bathymetry of the northern Lau Basin, SW Pacific Ocean. The black star marks the study site situated within the North East Lau Basin. Bathymetric data taken from (GEPCO Compilation Group, 2021). (B) Detailed bathymetric map of the North East Lau Basin. The sample location at Maka volcano is marked with a black star. Bathymetric data presented in (B) taken from (Merle et al., 2018).

RESULTS AND DISCUSSION

At Maka HF black smoker-type fluids actively discharge at temperatures of 329 °C and are characterized by low pH values (2.8–3.0) and a depletion in Mg (5.5 mmol/kg) and SO_4 (0.5 mmol/l) relative to seawater. High metal (e. g., Fe up to ~6 mmol/kg) and rare earth element (REE) contents in the fluids, are indicative for a rock-buffered hydrothermal system at low water/rock ratios (2–3). At Maka South, venting of white smoke with temperatures up to 301°C occurs at chimneys and flanges. Measured pH values range from 4.5 to 5.4 and Mg (31.0 mmol/kg), SO_4 (8.2 mmol/l), Cl (309 mmol/kg), Br (0.50 mmol/kg) and Na (230 mmol/kg) are depleted compared to seawater, whereas metals like Li and Mn are typically enriched together with H_2S.

Pyrite, chalcopyrite, sphalerite and marcasite occur throughout the chimney walls in variable proportions and exhibit distinct textures between the outer chimney wall and the central fluid conduit. The sulphide-sulphate samples from Maka HF and Maka South overlap in their bulk chemical composition. However, differences were observed with respect to the overall compositional range, as reflected by elevated Mn, Co and Bi contents at Maka HF and a tendency towards higher Cu, Zn, Se, Mo, Ag, Cd, Sb and Ba contents (max. values) at Maka South. Significant variations were also observed in the trace element composition of pyrite between Maka HF and Maka South. On average, pyrite from Maka HF is enriched in Mn, Co, Ni, Se, Mo, Te, Tl and Bi, but depleted in Cu, Zn, As, Cd, Sb, Au and Pb compared to pyrite from Maka South. Trace element ratios in pyrite between Maka HF and Maka South show systematic variations. A negative correlation is described between Co/Ni – As/Co and Se/Ge – As/Co, in which respect pyrite from Maka South is characterized by a tendency to higher As/Co (>10), as well as lower Co/Ni (<10) and Se/Ge (<10) ratios.

We propose a three-component mixing model with respect to the fluid composition at Maka South including seawater, a boiling-induced low-Cl vapour and a black smoker-type fluid similar to that of Maka HF, which is also preserved by the trace element signature of hydrothermal pyrite. At Maka South, high As/Co (>10 to 100) and Sb/Pb (>0.1) in pyrite are suggested to be related to a boiling-induced element fractionation between vapour (As, Sb) and liquid (Co, Pb). By contrast, lower As/Co (<100) and a tendency to higher Co/Ni values in pyrite from Maka HF likely reflect the black smoker-type fluid. The Se/Ge ratio in pyrite provides evidence for fluid-seawater mixing, where lower values (<10) are the result of a seawater contribution at the seafloor or during fluid upflow. Sulphur and Pb isotopes in hydrothermal sulphides indicate a common metal(loid) source at the two vent sites by host rock leaching in the reaction zone, as also reflected by the REE patterns in the vent fluids.

CONCLUSION

The reported vent fluid chemistry in combination with *in situ* trace element and isotope data of associated sulphide precipitates from two adjacent vent sites at Maka Volcano, North Eastern Lau Spreading Centre, SW Pacific Ocean provides important new insights into the evolution of submarine hydrothermal systems and the preservation of traces of mixing and boiling in the geological record, as preserved by sulphide chemistry. Furthermore, the combined use of vent fluid and sulphide chemistry allows to define new geochemical tracers in hydrothermal sulphides that can provide important insights into understanding water-rock interaction, fluid boiling and seawater mixing during the formation of fossil/extinct seafloor mineralizations that formed under temporally variable fluid conditions.

This work is currently under review for publication in the journal Frontiers in Earth Science under the title: *"Trace element and isotope systematics in vent fluids and sulphides from Maka volcano, North Eastern Lau Spreading Centre: Insights into three-component fluid mixing"*.

REFERENCES

Anderson M. O., Norris-Julseth C., Rubin K. H., Haase K., Hannington M. D., Baxter A. T. and Stewart M. S. (2021) Geologic and Structural Evolution of the NE Lau Basin, Tonga: Morphotectonic Analysis and Classification of Structures Using Shallow Seismicity. Front. Earth Sci. 9, 1–24.

Bach W., Jöns N. and Klein F. (2013) Metasomatism within the ocean crust. In Metasomatism and the Chemical Transformation of Rock, Lecture Notes in Earth System Sciences (eds. D. E. Harlov and H. Austrheimm). Springer-Verlag, Berlin Heidelberg. pp. 253–288.

Baker E. T., Walker S. L., Massoth G. J. and Resing J. A. (2019) The NE Lau Basin: Widespread and Abundant Hydrothermal Venting in the Back-Arc Region Behind a Superfast Subduction Zone. Front. Mar. Sci. 6, 1–15.

Baxter A. T., Hannington M. D., Stewart M. S., Emberley J. M., Breker K., Krätschell A., Petersen S., Brandl P. A., Klischies M., Mensing R. and Anderson M. O. (2020) Shallow Seismicity and the Classification of Structures in the Lau Back-Arc Basin. Geochemistry, Geophys. Geosystems 21.

Von Damm K. L. (1995) Controls on the Chemistry and Temporal Variability of Seafloor Hydrothermal Fluids. In Seafloor Hydrothermal Systems: Physical, Chemical, Biological, and Geological Interactions (eds. S. E. Humphris, R. A. Zierenberg, L. S. Mullineaux, and R. E. Thomson). AGU Monograph. American Geophysical Union. pp. 222–247.

Von Damm K. L., Buttermore L. G., Oosting S. E., Bray A. M., Fornari D. J., Lilley M. D. and Shanks W. C. (1997) Direct observation of the evolution of a seafloor "black smoker" from vapor to brine. Earth Planet. Sci. Lett. 149, 101–111.

Embley R. W. and Rubin K. H. (2018) Extensive young silicic volcanism produces large deep submarine lava flows in the NE Lau Basin. Bull. Volcanol. 80.

Falkenberg J. J., Keith M., Haase K. M., Bach W., Klemd R., Strauss H., Yeo I. A., Rubin K. H., Storch B. and Anderson M. O. (2021) Effects of fluid boiling on Au and volatile element enrichment in submarine arc-related hydrothermal systems. Geochim. Cosmochim. Acta 307, 105–132. Available at: https://doi.org/10.1016/j.gca.2021.05.047.

Fox S., Katzir Y., Bach W., Schlicht L. and Glessner J. (2020) Magmatic volatiles episodically flush oceanic hydrothermal systems as recorded by zoned epidote. Commun. Earth Environ. 1, 1–9. Available at: http://dx.doi.org/10.1038/s43247-020-00051-0.

GEPCO Compilation Group (2021) GEBCO 2021 Grid. Available at: https://www.gebco.net/data_and_products/gridded_bathymetry_data/.

German C. R., Baker E. T., Connelly D. P., Lupton J. E., Resing J., Prien R. D., Walker S. L., Edmonds H. N. and Langmuir C. H. (2006) Hydrothermal exploration of the Fonualei Rift and Spreading Center and the Northeast Lau Spreading Center. Geochemistry, Geophys. Geosystems *7*, 1–15.

German C. R. and Von Damm K. L. (2003) Hydrothermal Processes. In Treatise on Geochemistry Elsevier Inc. pp. 181–222.

German C. R. and Seyfried W. E. (2013) Hydrothermal Processes. 2nd ed., Elsevier Ltd. Available at: http://dx.doi.org/10.1016/B978-0-08-095975-7.00607-0.

Haase K. M., Beier C., Bach W., Kleint C., Anderson M., Büttner H., Dede B., Diehl A., Ernst D., Funganitao C., Giguere T., Gonzales Porras M. A., Günther T., Hüttich D., Krumm S. H., Leymann T., Meierhoff I., Moje A., Monien P., Murdock S., Nowald N., Peters C., Planer-Friedrich B., Ratmeyer V., Reuter C., Reuter M., Rubin K., Schade T., Schleifer B. K., Schönhofen M., Sopke S., Storch B., Ücker M., Türke A. and Wilckens F. (2018) RV Sonne Cruise Report Tonga Rift Cruise No. SO263.

Humphris S. E. and Klein F. (2018) Progress in deciphering the controls on the geochemistry of fluids in seafloor hydrothermal systems. Ann. Rev. Mar. Sci. 10, 315–343.

Keith M., Haase K. M., Klemd R., Smith D. J., Schwarz-Schampera U. and Bach W. (2018) Constraints on the source of Cu in a submarine magmatic-hydrothermal system, Brothers volcano, Kermadec island arc. Contrib. to Mineral. Petrol. 173, 1–16. Available at: http://dx.doi.org/10.1007/s00410-018-1470-5.

Keith M., Smith D. J., Doyle K., Holwell D. A., Jenkin G. R. T., Barry T. L., Becker J. and Rampe J. (2020) Pyrite chemistry: A new window into Au-Te ore-forming processes in alkaline epithermal districts, Cripple Creek, Colorado. Geochim. Cosmochim. Acta 274, 172–191.

Lupton J., Rubin K. H., Arculus R., Lilley M., Butterfield D., Resing J., Baker E. and Embley R. (2015) Helium isotope, C/3He, and Ba-Nb-Ti signatures in the northern Lau Basin: Distinguishing arc, back-arc and hotspot affinities. Geochemistry Geophys. Geosystems 16, 1133–1155.

Martin A. J., Keith M., Parvaz D. B., McDonald I., Boyce A. J., McFall K. A., Jenkin G. R. T., Strauss H. and MacLeod C. J. (2020) Effects of magmatic volatile influx in mafic VMS hydrothermal systems: Evidence from the Troodos ophiolite, Cyprus. Chem. Geol. 531.

Merle S., Chadwick W. and Rubin K. (2018) Processed gridded bathymetry data from the Tonga Volcanic Arc acquired during R/V Falkor expedition FK171110 (2017)., Interdisciplinary Earth Data Alliance (IEDA0).

Nestmeyer M., Keith M., Haase K. M., Klemd R., Voudouris P., Schwarz-Schampera U., Strauss H., Kati M. and Magganas A. (2021) Trace Element Signatures in Pyrite and Marcasite From Shallow Marine Island Arc-Related Hydrothermal Vents, Calypso Vents, New Zealand, and Paleochori Bay, Greece. Front. Earth Sci. 9, 1–18.

Román N., Reich M., Leisen M., Morata D., Barra F. and Deditius A. P. (2019) Geochemical and micro-textural fingerprints of boiling in pyrite. Geochim. Cosmochim. Acta 246, 60–85.

de Ronde C. E. J., Massoth G. J., Butterfield D. A., Christenson B. W., Ishibashi J., Ditchburn R. G., Hannington M. D., Brathwaite R. L., Lupton J. E., Kamenetsky V. S., Graham I. J., Zellmer G. F., Dziak R. P., Embley R. W., Dekov V. M., Munnik F., Lahr J., Evans L. J. and Takai K. (2011) Submarine hydrothermal activity and gold-rich mineralization at Brothers Volcano, Kermadec Arc, New Zealand. Miner. Depos. 46, 541–584.

Schaarschmidt A., Haase K. M., Klemd R., Keith M., Voudouris P. C., Alfieris D., Strauss H. and Wiedenbeck M. (2021) Boiling effects on trace element and sulfur isotope compositions of sulfides in shallow-marine hydrothermal systems: Evidence from Milos Island, Greece. Chem. Geol. accepted.

Schmidt K., Garbe-Schonberg D., Hannington M. D., Anderson M. O., Bohring B., Haase K., Haruel C., Lupton J. and Koschinsky A. (2017) Boiling vapour-type fluids from the Nifonea vent field (New Hebrides Back- Arc, Vanuatu, SW Pacific): Geochemistry of an early-stage, post-eruptive hydrothermal system. Geochim. Cosmochim. Acta 207, 185–209.

Seewald J. S., Reeves E. P., Bach W., Saccocia P. J., Craddock P. R., Walsh E., Shanks W. C., Sylva S. P., Pichler T. and Rosner M. (2019) Geochemistry of hot-springs at the SuSu Knolls hydrothermal field , Eastern Manus Basin : Advanced argillic alteration and vent fluid acidity. Geochim. Cosmochim. Acta 255, 25–48. Available at: https://doi.org/10.1016/j.gca.2019.03.034.

Stoffers P., Worthington T. J., Schwarz-Schampera U., Hannington M. D., Massoth G. J., Hekinian R., Schmidt M., Lundsten L. J., Evans L. J., Vaiomo'unga R. and Kerby T. (2006) Submarine volcanoes and high-temperature hydrothermal venting on the Tonga arc, southwest Pacific. Geology 34, 453–456.

Tardani D., Reich M., Deditius A. P., Chryssoulis S., Sánchez-Alfaro P., Wrage J. and Roberts M. P. (2017) Copper–arsenic decoupling in an active geothermal system: A link between pyrite and fluid composition. Geochim. Cosmochim. Acta 204, 179–204.

Zellmer K. E. and Taylor B. (2001) A three-plate kinematic model for Lau Basin opening. Geochemistry Geophys. Geosystems 2, 1–26.

SO263

Geochemical investigation of hydrothermal fluids from Niuatahi rear-arc volcano, North East Lau Basin, SW Pacific

AUTHORS

Jacobs University Bremen | Bremen, Germany
L. Klose, C. Kleint, A. Koschinsky

Center for Marine Environmental Sciences (MARUM) and Faculty of Geosciences, University of Bremen | Bremen, Germany
W. Bach, A. Diehl, F. Wilckens

Department for Geology and Palaeontology, University of Münster | Münster, Germany
H. Strauss, C. Peters

GeoZentrum Nordbayern, University of Erlangen-Nuremberg | Erlangen, Germany
K. Haase

INTRODUCTION

During research cruise SO263 in June 2018 hydrothermal vent fluids were sampled from Niuatahi rear-arc volcano, North East Lau Basin, SW Pacific. Hydrothermal activity in the North Eastern Lau Basin has previously been shown to be a widespread phenomenon in the area between the North Eastern Lau Spreading Center (NESLC) and the Tofua oceanic island arc with much of the hydrothermal activity occurring at the rear-arc Mata volcanoes and Niuatahi (Baker et al., 2019).

GEOLOGICAL SETTING AND SAMPLING SITE

The Niuatahi volcano, also known as volcano "O" or "MTJ-1", is an off-axis dacitic volcanic caldera complex, located ~17 km east of the NELSC and ~35 km west of the Tofua oceanic island arc (Kim et al., 2009; Kim et al., 2011; Berkenbosch et al., 2015; Park et al., 2016). The near circular caldera is ~8 km in diameter and a prominent post-caldera cone (Motutahi) is located in the center. Two apparently older faulted cones occur to the southwest and to the north (Kim et al., 2009; Berkenbosch et al., 2015). High temperature hydrothermal activity with chalcopyrite-sulfate chimneys occur at the caldera ring faults (Berkenbosch et al., 2015), as well as metal-rich molten sulfur on top of the Motutahi cone (Kim et al., 2011). The latter displays direct evidence for degassing of metal-bearing magmatic vapors. Besides dredge samples of altered rocks, which show fillings of native sulfur and alunite (Kim et al., 2009), several studies focused on the

hydrothermal plume above Motutahi. Respective results also indicate venting of magmatically influenced acid sulfate fluids (Merle and Walker, 2008; Kim et al., 2009; Kim et al., 2011; Resing and Embley, 2012; Baker et al., 2019). Ongoing east-west extension of the Niuatahi caldera is indicated by short gaps in the caldera wall (Baker et al., 2019; Anderson et al., 2021), close to the locations of hydrothermal activity at the Northern Cone and Southwestern Cone.

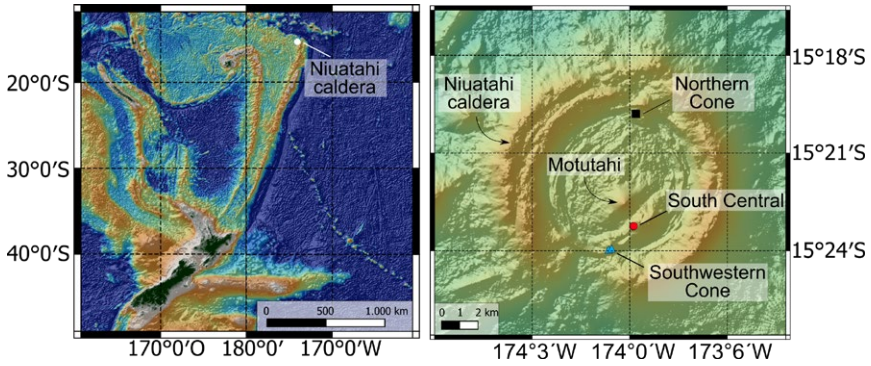

Fig. 1: (A) Overview of the southwest Pacific and the Kermadec and Tofua island arc. The white circle marks the location of Niuatahi caldera volcano. Bathymetry data taken GEPCO Compilation Group (2021) GEBCO 2021 Grid (doi:10.5285/a29c5465-b138-234d-e053-6c86abc040b9) (B) Detailed map of the study site at the off-axis caldera volcano Niuatahi and the hydrothermal sites sampled during research cruise SO263. Bathymetry data taken from R/V Falkor expedition FK171110 (2017) Merle et al. (2018). Data DOI: 10.1594/IEDA/324445.

Hydrothermal fluids were recovered from three vent sites within the Niuatahi caldera at South Central, Southwestern Cone and Northern Cone in water depths between 1607 and 1699 m. The samples were taken from grey to black smokers, expelling diffuse as well as focused hot fluids, using the ROV MARUM QUEST 4000 (University of Bremen). At South Central, a ~10 m tall multi-spired chimney complex was venting black smoke from multiple beehive orifices with maximum measured temperatures of up to 334 °C. At the Southwestern Cone, the chimneys appeared to grow along a ~10 m extending lineament. The spires were column-like, with flanges and a rough outer surface. At the Northern Cone, grey-black smoke was venting from several orifices from a ~3–5 m tall chimney, along with a large beehive orifice venting shimmering water, and thick flanges that appear bulbous and were inactive.

RESULTS AND DISCUSSION

All sampled fluids are characterized by depletions in Mg, SO_4 and U as well as an enrichment of (trace) metals (e. g., Fe, Mn, K, Li) and dissolved gases (e. g., H_2S, CO_2, H_2) compared to seawater. Water-rock (W/R) ratios were calculated to estimate the intensity of W/R interaction using the concentrations of fluid mobile elements, such as K, Li, Rb, Cs as well as $\delta^{11}B$, $\delta^{7}Li$ and $^{87}Sr/^{86}Sr$ isotopic values. W/R ratios calculated for the Niuatahi caldera wall sites (Northern and Southwestern Cone) display slightly lower values

compared to the South Central site, ranging from 1 to 6 and 1 to 9, respectively. The overall low W/R ratios suggest that fluid-rock interactions under rock-dominated conditions are predominant at all sampling sites. The chondrite-normalized rare earth element (REE) distribution patterns in calculated hydrothermal end-member fluids overlap with other high-temperature black smoker fluids from oceanic island arc and back-arc volcanoes as well as from sediment-starved MOR hydrothermal systems (Mitra et al., 1994; Douville et al., 2002; Craddock et al., 2010; Cole et al., 2014; Schmidt et al., 2017; Kleint et al., 2019; Diehl and Bach, 2020). The patterns are consistent with REE solubility controlled by chloro-complexation, which is expected at high temperatures and under rock-controlled redox conditions (e. g. Craddock et al., 2010). However, despite multiple similarities there are also differences in the geochemical composition of the individual fluids, e. g. in the chloride, volatile or metal concentrations, which can be related to additional processes besides W/R interaction (e. g. phase separation, ongoing W/R interaction, subsurface mineral precipitation, conductive cooling, cooling by mixing with seawater).

At South Central, Cl concentrations as low as (~300 mmol kg^{-1}) are indicative for phase separation. Furthermore, these fluids show the lowest pH (2.8–3.1), highest H_2S and lowest H_2, CH_4 and CO_2 concentrations of the three sampled sites. Geochemical proxies, such as Fe/Mn geothermometer (Pester et al., 2011) or Si-Cl geothermobarometer (Fournier, 1983; Von Damm et al., 1991; Fontaine et al., 2009) can be used to infer subsurface p-T conditions of the reaction zone. The above-mentioned proxies indicate a deep hydrothermal root zone and phase-separation close to/above the critical point of seawater. Based on the fluid composition, we believe that the Cl-depleted fluids originate from subcritical phase separation and subsequent partial remixing of vapor and brine phases. Furthermore, we attribute the high concentrations of (trace)-metals to W/R interaction after phase separation and during fluid ascent. Additionally, there is no clear evidence of significant input from magmatic SO_2, as the overall geochemical composition (e. g. Mg concentrations, chondrite-normalized REE patterns, low W/R ratios) differs significantly from previously described acid sulfate fluids from the Manus Basin or Brothers volcano in the Kermadec island arc that show clear evidence for SO_2 degassing and disproportionation (e. g. Kleint et al., 2019; Seewald et al., 2015).

Despite being situated at opposite sides of the caldera, hydrothermal fluids from the Northern and Southwestern Cone show a similar geochemical composition. Fluids from these sites show lower Fe/Mn ratios (<1) and H_2S concentrations than those from South Central suggesting that they are affected by subsurface cooling and sulfide precipitation. We attribute the similar geochemical compositions of hydrothermal fluids from the Northern and Southwestern Cone to similar conditions in the hydrothermal root zones. Furthermore, high temperature hydrothermal activity at the Northern Cone indicates a reactivation of this system after 2006 (Kim et al., 2009).

Hydrothermal fluid data from the three vent sites at Niuatahi do not show a contribution of magmatic SO_2 in contrast to $\delta^{34}S$ isotopes ratios as low as -10.6 ‰ of hydrothermal

sulfides sampled from Niuatahi South Central (Falkenberg et al., 2021). Overall, the hydrothermal fluid compositions suggest a dynamic system controlled by variable input of magmatic volatiles (SO_2 and CO_2) as well as permeability changes. These changes are probably related to the complex tectonic and magmatic activity within the Niuatahi caldera, which is supported by a recent study of the regional structural geology (Anderson et al., 2021). Based on the reported fluid composition and recent investigations conducted at Brothers volcano, Kermadec island arc (e. g. Berkenbosch et al., 2019; Kleint et al., 2019; Diehl et al., 2020), we believe that there might also be a stronger temporal variability than previously known. In these dynamic systems it is much harder to estimate the influence of (trace) metal input into the oceans. Therefore, more time-series data sets, especially covering shorter periods of days to months, in oceanic island arc and back-arc environments are needed to elucidate the effects of short-term variability proposed here, as well as to characterize their impact on (trace) metal fluxes into the oceans.

This work is currently under review for publication in the journal Geochimica et Cosmochimica Acta under the title: *"Hydrothermal activity and associated subsurface processes at Niuatahi rear-arc volcano, North East Lau Basin, SW Pacific: Implications from trace elements and stable isotope systematics in vent fluids."*.

REFERENCES

Anderson M. O., Norris-Julseth C., Rubin K. H., Haase K., Hannington M. D., Baxter A. T. and Stewart M. S. (2021) Geologic and Structural Evolution of the NE Lau Basin, Tonga: Morphotectonic Analysis and Classification of Structures Using Shallow Seismicity. Front. Earth Sci. 9, 1–24.

Baker E. T., Walker S. L., Massoth G. J. and Resing J. A. (2019) The NE Lau Basin: Widespread and Abundant Hydrothermal Venting in the Back-Arc Region Behind a Superfast Subduction Zone. Front. Mar. Sci. 6, 1–15.

Berkenbosch H. A., de Ronde C. E. J., Paul B. T. and Gemmell J. B. (2015) Characteristics of Cu isotopes from chalcopyrite-rich black smoker chimneys at Brothers volcano, Kermadec arc, and Niuatahi volcano, Lau basin. Miner. Depos. 50, 811–824.

Berkenbosch H. A., De Ronde C. E. J., Ryan C. G., McNeill A. W., Howard D. L., Gemmell J. B. and Danyushevsky L. V. (2019) Trace element mapping of copper- and zinc-rich black smoker chimneys from brothers volcano, kermadec arc, using synchrotron radiation XFM and LA-ICP-MS. Econ. Geol. 114, 67–92.

Cole C. S., James R. H., Connelly D. P. and Hathorne E. C. (2014) Rare earth elements as indicators of hydrothermal processes within the East Scotia subduction zone system. Geochim. Cosmochim. Acta 140, 20–38. Available at: http://dx.doi.org/10.1016/j.gca.2014.05.018.

Craddock P. R., Bach W., Seewald J. S., Rouxel O. J., Reeves E. and Tivey M. K. (2010) Rare earth element abundances in hydrothermal fluids from the Manus Basin, Papua New Guinea: Indicators of sub-seafloor hydrothermal processes in back-arc basins. Geochim. Cosmochim. Acta 74, 5494–5513. Available at: http://dx.doi.org/10.1016/j.gca.2010.07.003.

Von Damm K. L., Bischoff J. L. and Rosenbauer R. J. (1991) Quarz solubility in hydrothermal seawater: an experimental study and equation describing quart solubility for up to 0.5 M NaCl solutions. Am. J. Sci. 291, 977–1007.

Diehl A. and Bach W. (2020) MARHYS (MARine HYdrothermal Solutions) Database: A Global Compilation of Marine Hydrothermal Vent Fluid, End Member, and Seawater Compositions. Geochemistry, Geophys. Geosystems 21, 1–17.

Diehl A., De Ronde C. E. J. and Bach W. (2020) Subcritical Phase Separation and Occurrence of Deep-Seated Brines at the NW Caldera Vent Field, Brothers Volcano: Evidence from Fluid Inclusions in Hydrothermal Precipitates. Geofluids 2020.

Douville E., Charlou J. L., Oelkers E. H., Bienvenu P., Jove Colon C. F., Donval J. P., Fouquet Y., Prieur D. and Appriou P. (2002) The rainbow vent fluids (36°14′N, MAR): The influence of ultramafic rocks and phase separation on trace metal content in Mid-Atlantic Ridge hydrothermal fluids. Chem. Geol. 184, 37–48.

Falkenberg J. J., Keith M., Haase K. M., Klemd R., Strauss H., Peters C. and Kim J. (2021) Spatial variations in submarine caldera-hosted hydrothermal systems: Insights from sulfide chemistry, Niuatahi caldera, Tonga rear-arc. In GeoKarlsruhe 2021

Fontaine F., Wilcock W., Foustoukos D. and Butterfield D. (2009) A Si-Cl geothermobarometer for the reaction zone of high-temperature, basaltic-hosted mid-ocean ridge hydrothermal systems. Geochemistry Geophys. Geosystems 10.

Fournier R. (1983) A method of calculating quartz solubilities in aqueous sodium chloride solutions. Geochim. Cosmochim. Acta 47, 579–586.

GEPCO Compilation Group (2021) GEBCO 2021 Grid. Available at: https://www.gebco.net/data_and_products/gridded_bathymetry_data/.

Kim J., Son S. K., Son J. W., Kim K. H., Shim W. J., Kim C. H. and Lee K. Y. (2009) Venting sites along the Fonualei and Northeast Lau Spreading Centers and evidence of hydrothermal activity at an off-axis caldera in the northeastern Lau Basin. Geochem. J. 43, 1–13.

Kim Jonguk, Lee K. and Kim Jung-hoon (2011) Metal-bearing molten sulfur collected from a submarine volcano : Implications for vapor transport of metals in seafl oor hydrothermal systems. , 351–354.

Kleint C., Bach W., Diehl A., Fröhberg N., Garbe-Schönberg D., Hartmann J. F., de Ronde C. E. J., Sander S. G., Strauss H., Stucker V. K., Thal J., Zitoun R. and Koschinsky A. (2019) Geochemical characterization of highly diverse hydrothermal fluids from volcanic vent systems of the Kermadec intraoceanic arc. Chem. Geol.

Merle S., Chadwick W. and Rubin K. (2018) Processed gridded bathymetry data from the Tonga Volcanic Arc acquired during R/V Falkor expedition FK171110 (2017)., Interdisciplinary Earth Data Alliance (IEDA0).

Merle S. and Walker S. (2008) North East Lau Basin R/V Thompson Expedition TN227 cruise report. Available at: https://www.pmel.noaa.gov/eoi/laubasin/documents/tn227-nelau-report-final.pdf.

Mitra A., Elderfield H. and Greaves M. J. (1994) Rare earth elements in submarine hydrothermal fluids and plumes from the Mid-Atlantic Ridge. Mar. Chem. 46, 217–235.

Park J. W., Campbell I. H. and Kim J. (2016) Abundances of platinum group elements in native sulfur condensates from the Niuatahi-Motutahi submarine volcano, Tonga rear arc: Implications for PGE mineralization in porphyry deposits. Geochim. Cosmochim. Acta 174, 236–246. Available at: http://dx.doi.org/10.1016/j.gca.2015.11.026.

Pester N. J., Rough M., Ding K. and Seyfried Jr. W. E. (2011) A new Fe/Mn geothermometer for hydrothermal systems: Implications for high-salinity fluids at 13°N on the East Pacific Rise. Geochim. Cosmochim. Acta 75, 7881–7892. Available at: http://dx.doi.org/10.1016/j.gca.2011.08.043.

Resing J. and Embley R. W. (2012) Submarine Ring of Fire-2012 (SRoF-12) Northeast Lau Basin_ Cruise Report. Cruise Rep.

Schmidt K., Garbe-Schönberg D., Hannington M. D., Anderson M. O., Bühring B., Haase K., Haruel C., Lupton J. and Koschinsky A. (2017) Boiling vapour-type fluids from the Nifonea vent field (New Hebrides Back-Arc, Vanuatu, SW Pacific): Geochemistry of an early-stage, post-eruptive hydrothermal system. Geochim. Cosmochim. Acta 207, 185–209.

Seewald J. S., Reeves E. P., Bach W., Saccocia P. J., Craddock P. R., Shanks W. C., Sylva S. P., Pichler T., Rosner M. and Walsh E. (2015) Submarine venting of magmatic volatiles in the Eastern Manus Basin, Papua New Guinea. Geochim. Cosmochim. Acta 163, 178–199. Available at: http://dx.doi.org/10.1016/j.gca.2015.04.023.

SO263

Volcanic geomorphology, tectonics and geochemical character of the submarine rear-arc caldera Niuatahi in the SW Pacific, examined through ROV-dives and TVG sampling during cruise

AUTHORS

GeoZentrum Nordbayern, Friedrich-Alexander University | Erlangen, Germany
B. Storch, K.M. Haase, M. Regelous, R.H.W. Romer

Department of Earth Sciences, University of Hawaii at Manoa | Honolulu, USA
K.H. Rubin

Korea Institute of Ocean Science & Technology | Ansan, South Korea
J.Kim

With 15 km in diameter, Niuatahi forms an unusually large volcanic structure in the rear-arc (around 175 km west of the trench) of the northernmost Tonga-Lau region in the southwest Pacific. The Niuatahi Caldera and the Diagonal Ridge in the southwest were sampled during the cruise SO263 with the R/V Sonne in 2018. New major element data reveal that the lavas from small edifices outside of the caldera are basaltic to basaltic andesite. In contrast the youngest lavas inside the caldera show dacitic to rhyolitic composition. However, evolved lava flows were also sampled outside of the caldera to the north and south of Niuatahi (Embley & Rubin, 2018). This implies a change in magma evolution from little fractionation during early stages to extensive crystal fractionation and longer magma stagnation during the caldera stage. Thus, the magma plumbing system may have evolved from small sills at different depths in the crust to a larger shallow magma reservoir that collapsed forming the caldera. Trace element and isotope data suggest that the Niuatahi lavas are fed by different magma chambers but formed from a relatively homogenous mantle wedge. The cross-cutting of two different stress regimes (NNE–SSW and ENE–WSW) in the northern Lau Basin possibly facilitated the eruption of the magma (Anderson et al., 2021). We distinguish five different formation stages from geomorphological and tectonic observations. (1) The ENE trending volcanic ridge SW of the caldera (the 'Diagonal Ridge') and the small ridge, trending NNE, outside of the caldera to the north are considered as pre-caldera structures. (2) The Niuatahi volcano formed as a large volcanic edifice around 800 m in height with a flat top and 17 km in diameter. (3) Large volumes of lavas erupted outside the caldera causing the down-sag of the magma chamber roof. Numerous ring faults formed in the caldera and on its rim which functioned as pathways for ascending magmas and later for hydrothermal circulation of heated fluids. (4) The later E-W extension caused breaches in the caldera walls (Baker et al., 2019). Dikes intruded parallel this NNE-SSW trending

extensional zone and probably fed several eruptions within in the caldera. (5) An ENE-trending normal fault in the southwest, outside of the caldera dissects the caldera rim with a similar orientation to the Diagonal Ridge.

Several of the young cones within the caldera are dissected by the ring faults implying young tectonic activity and caldera subsidence. For example, a cone at the northern caldera wall was dissected by the reactivation of the inner caldera ring fault. It is possible that this subsidence caused hydrothermal activity in 2018, but no hydrothermal plume was found in 2015 (Wang et al., 2019), suggesting very young tectonic and hydrothermal activity. The youngest volcanism along the NNE-SSW fault zone caused the formation of Motutahi cone in the center of the caldera and possibly a smaller cone further to the south. Motutahi is a 465 m tall submarine cone and consists of dacitic lavas (Park et al., 2015) and shows active SO_2 venting (Kim et al. 2009).

The new trace element concentrations of the sampled lavas show a stronger subduction influence for the Diagonal Ridge in the southwest compared to lavas from the caldera, implying different evolutionary stages. The Diagonal Ridge may have formed closer to the trench, probably reflecting the fast clockwise rotation of the Tonga island arc and associated rear-arc extension. The Niuatahi lavas show a geochemical composition that is less depleted than those from the volcanic front in northern Tonga. However, the samples show a slightly higher subduction input (e. g. Ba/Nb, Th/Nb) than the magmas from the North East Lau Spreading Centre. The pre-caldera Diagonal Ridge and the Niuatahi lavas evolved from a similar source, since the new isotope ratios (e. g. Pb) show a similar range. The Niuatahi and pre-caldera samples show very radiogenic Pb isotopes and lavas from the Diagonal Ridge have the highest $^{206}Pb/^{204}Pb$ ratios in the entire northern Tonga-Lau region. However, the $^{207}Pb/^{204}Pb$ and $^{208}Pb/^{204}Pb$ ratios from the volcano and the ridges are lower compared to the very close North-East Lau Spreading Centre (<10 km distance to Diagonal Ridge). The Pb isotope signature implies transport of subducted Louisville seamount chain material (Regelous et al., 2010) into the mantle wedge beneath the rear-arc. This material influenced not only the island arc lavas, but also the rear-arc structures. The significant differences between Niuatahi + pre-caldera structures and North-East Lau Spreading Centre lavas further imply the different evolutionary stages.

REFERENCES

Anderson, M.O., Norris-Julseth, C., Rubin, K.H., Haase, K.M., et al. Geological and Structural Evolution of the NE Lau Basin, Tonga: Morphotectonic Analysis and Classification of Structures Using Shallow Seismicity. Front, Earth Sci 2021, 9, 665185, doi: 10.3389/feart.2021.665185.

Baker E.T., Walker, S.L., Massoth, G.J., Resing, J.A., The NE Lau Basin: widespread and abundant hydrothermal venting in the back-arc region behind a superfast subduction zone, Frontiers in Marine Science 2019, 6, 382, doi: 10.3389/fmars.2019.00382.

Embley, R.W., Rubin K.H., Extensive young silicic volcanism produces large deep submarine lava flows in the NE Lau Basin, Bulletin of Volcanology 2018, 80(4), 1–23, doi: 10.1007/s00445-018-1211-7.

Kim, J., Son, S. K., Son, J. W., Kim, K. H., et al. Venting sites along the Fonualei and Northeast Lau Spreading Centers and evidence of hydrothermal activity at an off-axis caldera in the northeastern Lau Basin, Geochemical Journal 2009, 43(1), 1–13, doi: 10.2343/geochemj.0.0164.

Park, J.W., Campbell, I.H., Kim, J., Moon, J.W., The role of late sulfide saturation in the formation of a Cu- and Au-rich magma: insights from the platinum group element geochemistry of Niuatahi-Motutahi lavas, Tonga rear arc, Journal of Petrology 2015, 56(1), 59–81, doi: 10.1093/petrology/egu071.

Regelous, M., Gamble, J.A., Turner, S.P., Mechanism and timing of Pb transport from subducted oceanic crust and sediment to the mantle source of arc lavas, Chemical Geology 2010, 273 (1–2), 46–54, doi: 10.1016/j.chemgeo.2010.02.011.

Wang, Z., Park, J. W., Wang, X., Zou, Z., et al. Evolution of copper isotopes in arc systems: insights from lavas and molten sulfur in Niuatahi volcano, Tonga rear arc, Geochimica et Cosmochimica Acta 2019, 250, 18-33, doi: 10.1016/j.gca.2019.01.040.

SO267

Investigating the crustal structure and tectonic evolution of the northern Lau Basin with reflection and refraction seismic and magnetic data acquired during SO267 – ARCHIMEDES I

AUTHORS

GEOMAR Helmholtz Centre for Ocean Research | Kiel, Germany
A. Beniest, A. Dannowski, F. Schmid, A. Jegen, H. Kopp

Vrije Universiteit Amsterdam | Amsterdam, The Netherlands
A. Beniest

Federal Institute for Geosciences and Natural Resources | Hanover, Germany
M. Schnabel, U. Barckhausen

The northeastern Lau Basin is one of the fastest opening and magmatically most active back-arc regions on Earth (Sleeper and Martinez, 2016). Although the current pattern of plate boundaries and motions in this complex mosaic of microplates is fairly well understood, the structure and evolution of the back-arc crust are not. The complex tectonic setting of this part of the Lau Basin, caused by the roll-back of the Pacific slab subducting at the Tonga trench, hampers our understanding of how extension is accommodated in this region and its tectonic history.

During the ARCHIMEDES-I expedition in December 2018 – January 2019 (Hannington et al., 2019), we acquired multi-channel seismic (MCS) reflection data along six profiles and refraction seismic data using Ocean Bottom Seismometers (OBS) along three profiles (Figure 1). We combined this data with magnetic anomaly profiles to investigate the crustal structure and tectonic evolution.

The OBS data were processed with a predictive deconvolution and Butterworth filtering, manually picking of phase arrivals and picking errors. A P-wave velocity model was established and used as a starting model for a tomographic inversion that allows us to investigate the crustal thickness and velocity structure.

The MCS reflection data were processed at the BGR using standard seismic processing steps, including deconvolving the raw data, binning to common depth point, band-pass filtering, true amplitude recovery, moveout-correction of CDP gathers, stacking and post-stacking Kirchhoff time migration. The seismic sections were depth-converted prior to interpretation. The MCS reflection data were manually interpreted structurally and seismic stratigraphically to investigate the tectonic activity.

The magnetic data were acquired with a ship-towed marine magnetics SeaSpy-II gradiometer system. The data were processed with subtraction of a reference field IGRF2015 (Thebault et al., 2015).

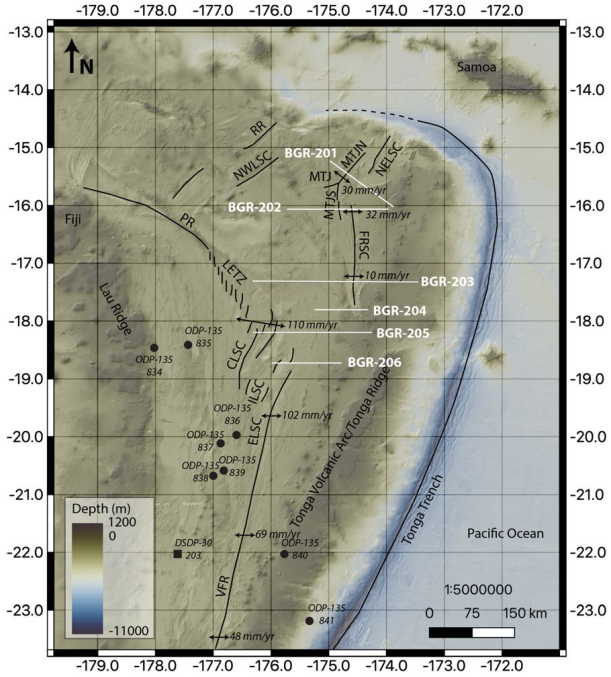

Fig. 1: Bathymetric map with the location of the multi-channel seismic reflection data profiles (BGR-201 – BGR-206) and refraction seismic data profiles (BGR-202, BGR-203 and BGR-205).

Our longest refraction seismic profile (Figure 2, Schmid et al., 2020) was acquired along a 300 km long east-west oriented transect crossing the back-arc, the Fonualei Rift and Spreading Centre (FRSC) and the volcanic arc at 17°20'S. Our P-wave tomography model shows strong lateral variations in the thickness and velocity-depth distribution of the crust.

Our P wave tomography model (Figure 2) and density modelling suggest that past crustal accretion inside the southern FRSC was accommodated by a combination of arc crust extension and magmatic activity. The absence of magnetic reversals inside the FRSC supports this and suggests that focused seafloor spreading has until now not contributed to crustal accretion.

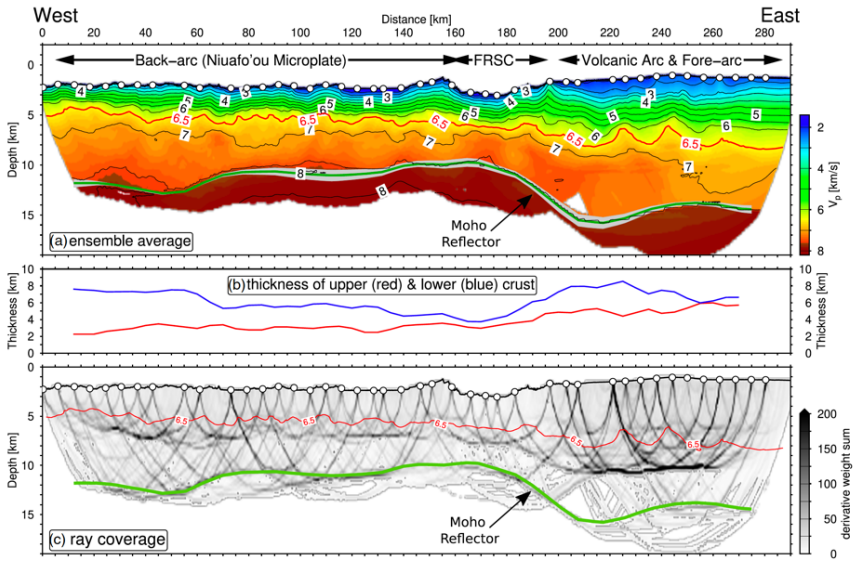

Fig. 2: a) Final P wave tomographic model for BGR-203 with the major tectonic regions indicated. b) Thickness of the upper crust and lower crust. c) Derivative weight sum for individual nodes of the model grid, representing the ray coverage. Red line represents the 6.5 km/s contour, which marks the boundary between upper and lower crust. Solid green line represents the Moho reflector. Image from Schmid et al. (2020).

Our most southern refraction seismic profile (Figure 3) was shot along a 200 km long east-west oriented transect between the Central Lau Spreading Center and the southern tip of the Fonualei Rift and Spreading Centre (FRSC). Our P-wave tomography model shows moderate lateral variations in the thickness of the crust, typical back-arc crust (9 km thick) in the west and arc-crust (12–14 km thick) in the east.

The interpreted MCS profiles revealed two types of normal faults that have been observed on all profiles, from the MTJ in the north, to south of the FRSC in the south of the northern Lau Basin. These are 1) inactive normal faults that cross-cut the acoustic basement and are covered by sediments, and 2) the currently active, steeply-dipping normal faults that do reach the surface. With the use of the magnetic data, buried volcanoes and lava flows have been observed closer to the arc on the MCS profiles. The recognized fault pattern points to a two-phase tectonic evolution: 1) are the result of an initial wide-rift phase, 2) and became active more recently and are the result of a second, focused extension phase that is still ongoing. Two-phase extension has been proposed before for this region (Parson and Hawkins, 1994).

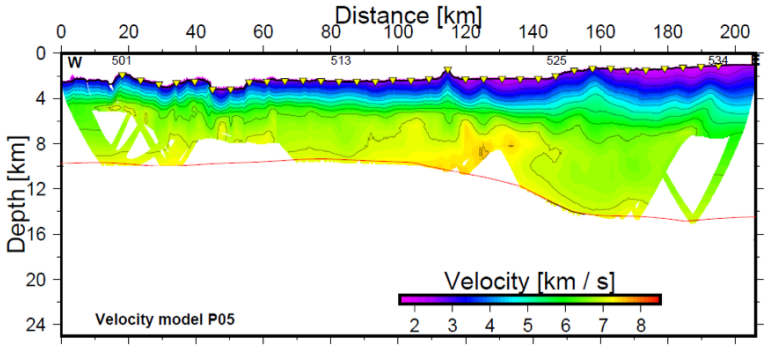

Fig. 3. a) Preliminary P-wave tomographic model for BGR-205, showing typical back-arc crust thickness (9 km) in the west and arc crust thickness (12–14 km) in the east.

In the investigated back-arc region we identify two distinct locations in the tomographic models, representing different opening phases of the northeastern Lau Basin. On the MCS seismic data we recognised two different sets of faults that belong to an initial wide-rift phase, dominated by rifting and more advanced opening phase, dominated by narrow rifting and, in places, seafloor spreading. Thickening of the crust below the arc is the result of magmatic underplating, which is supported by elevated upper mantle temperatures in this region.

REFERENCES

Hannington, M.D., Kopp, H., Schnabel, M., 2019. RV Sonne Cruise Report SO267 – ARCHIMEDES 1: Arc Rifting, Metallogeny and Microplate Evolution – an Integrated Geodynamic, Magmatic and Hydrothermal Study of the Fonualei Rift System, NE Lau Basin. Geomar Rep. 49.

Parson, L.M., Hawkins, J.W., 1994. Two-Stage Ridge Propagation and the Geological History of the Lau Backarc Basin. Proc. Ocean Drill. Program, 135 Sci. Results. https://doi.org/10.2973/odp.proc.sr.135.153.1994

Schmid, F., Kopp, H., Schnabel, M., Dannowski, A., Heyde, I., Riedel, M., Hannington, M., Engels, M., Beniest, A., Klaucke, I., Augustin, N., Brandl, P., Devey, C., 2020. Crustal structure of the Niuafo'ou Microplate and Fonualei Rift and Spreading Center in the northeastern Lau Basin, Southwestern Pacific. J. Geophys. Res. – Solid Earth In review.

Sleeper, J.D., Martinez, F., 2016. Geology and kinematics of the Niuafo'ou microplate in the northern Lau Basin. J. Geophys. Res. Solid Earth 121, 4852–4875. https://doi.org/10.1002/2016JB013051

Thebault, E., 2015. International Geomagnetic Reference Field: the 12th generation. Earth, Planets Sp. 67–79. SO267

SO267

ARCHIMEDES: A multi-methodical approach to decipher the extensional dynamics of the northern Lau Basin at 16°S

AUTHORS

Geomar Helmholtz Centre for Ocean Research | Kiel, Germany
A. Jegen, A. Dannowski, H. Kopp, F. Schmid, M. Riedel

Federal Institute for Geosciences and Natural Resources | Hanover, Germany
M. Schnabel, U. Barckhausen, I. Heyde

Vrije Universiteit Amsterdam | Amsterdam, The Netherlands
A. Beniest

University of Ottawa | Ottawa, Canada
M. Hannington

The Lau Basin is a young back-arc basin that is steadily forming at the Indo-Australian-Pacific plate boundary and was in fact the first back-arc basin ever to be identified as such (Karig, 1970). Because of this, it has coined our conceptual model of back-arc basins significantly and its study can help hone our understanding of their formation and mechanics. The generally accepted concept of the Lau Basins formation began with the roll-back of the pacific plate, which produced the extensional forces necessary for the creation of a back-arc basin (Heuret and Lallemand, 2005). This roll-back of the Pacific plate created extensional forces, which caused the overriding plate to extend until the point of crustal break was reached. After this point of crustal breakage, spreading initiated and young oceanic crust is formed at about 5 Ma (Wiedicke and Collier, 1993; Taylor et al., 1996).

While this model might be reasonably accurate for the southern Lau Basin, two tectonic mechanisms affect and therefore complicate the northern Lau Basins stress regime (Bonnardot et al., 2007). The first mechanism is a tear in the northern end of the subducting pacific plate, which spans from 18 to 88km in depth and thus through the entire Lithosphere (Millen and Hamburger 1998). The second mechanism is the proximity to the Subduction Edge Propagator, which marks the end of a progressive, northward transition from trench to transform fault (Eguchi et al., 1984, Bevis et al., 1995). These additional mechanisms create a more complex stress regime, which in return has led to the formation of a multitude of spreading centres and zones of active rifting.

Two of these zones are the southern arm of the Mangatolu Triple Junction (MTJ-S2) and the Northern tip of the Fonualei Rift Spreading Centre (FRSC1). As is typical for slow spreading ridges, both the FRSC1 and the MTJ-S2 are dominated by an axial valley with a neovolcanic zone. The neovolcanic zone of the MTJ-S2 is smaller than that of the FRSC1, implying a lower magmatic budget (Sleeper and Martinez, 2016; Anderson et al., 2021). The larger magmatic budget of the FRSC1 is likely caused by a higher influence of hydrous melting, since it is offset only ~ 75 km from the volcanic arc at the latitude of the profile (Escrig et al., 2012).

However, neither the seafloor magnetisation nor the seafloor morphology indicate seafloor spreading at either of the zones of active rifting or spreading (Sleeper and Martinez 2016). We therefore conclude that, if still active, both the MTJ-S2 and the FRSC1 are in the rifting phase. Yet, to fully confirm this first hypothesis, more detailed studies of the crustal structure were needed.

Research vessel RV Sonne (cruise SO267) set out to conduct seismic refraction and wide-angle reflection data along a 185 km long transect crossing the Lau Basin at ~16 °S from the Tonga arc in the east, over the overlapping spreading centres, FRSC1 and MTJ-S2, and extending as far as a volcanic ridge in the west. The refraction seismic profile consisted of 30 ocean bottom seismometers. Simultaneously, 2D MCS reflection seismic data, Parasound data, as well as magnetic and gravimetric data were acquired.

The results of our P-wave traveltime tomography show a crust that varies between 6–8 km in thickness with a largely even Moho, which thickens towards the volcanic arc in the east and towards a volcano chain in the west. The upper crust shows velocities between 2.5 km/s and 6 km/s and a mostly stable thickness of about 3 km, which only visibly thickens under the FRSC1 and the crossed volcano chain. In contrast, the lower crust is thinnest (~2 km) under the FRSC1 from where its thickness gradually decreases toward the crossed volcanic chain in the west and the arc in the east. The p-wave velocities in the lower crust range between 6 km/s and 7.2 km/s and show an overall even Vp gradient of 0.5, with only one extensive positive anomaly from 110–160 km profile offset.

Those locations where the upper crust thickened, coincide with areas of decreased Vp gradients and with areas of decreased density in the shallowest parts of the upper crust. Since the boundary between the upper and lower crust was deducted using the 6 km/s Vp isoline, a decrease of the lower crustal Vp (e. g by faulting) will seemingly shrink the lower crust, resulting in an artificially raised Vp gradient in the lower crust and a thickening of the upper crust.

Similar, though less pronounced, the MTJ-S2 also shows decreased Vp gradients and densities in the shallow upper crust. Consulting the catalogued seismicity of the area (Conder and Wiens, 2011), we suggest that the FRSC1 shows more pronounced

anomalies, compared to the MTJ-S2, because it is still tectonically active. Hence even though the FRSC1 and MTJ-S2 have a similar underlying rifting mechanism that produced the observed anomalies, the FRSC1 has had a longer time span over which to accumulate deformation and therefore appears more pronounced.

The MCS data profile shows a ragged seabed with numerous grabens, which grow more extensive and deeper towards the arc, which is the main sediment source of the area. These sediment-filled grabens were studied closer using Parasound data in order to identify the zones of active rifting. Even though multiple basins were consulted (just east of the FRSC1 and just west of the MTJ-S2), only the sediment basin between MTJ-S2 and FRSC1 showed signs of active faulting. This one-sided occurrence of active faulting around the FRSC1 suggests an asymmetric rifting with higher opening rates towards the west, away from the rolling-back subducting slab.

REFERENCES

Anderson, Melissa O., Chantal Norris-Julseth, Kenneth Howard Rubin, Karsten M. Haase, Mark Hannington, Alan T. Baxter, und Margaret Stewart. „Geologic and Structural Evolution of the NE Lau Basin, Tonga: Morphotectonic Analysis and Classification of Structures Using Shallow Seismicity". Preprint. Earth and Space Science Open Archive. Earth and Space Science Open Archive, 8.02.2021. World. https://doi.org/10.1002/essoar.10502463.2.

Bevis, Michael, F. W. Taylor, B. E. Schutz, Jacques Recy, B. L. Isacks, Saimone Helu, Rajendra Singh, u. a. „Geodetic Observations of Very Rapid Convergence and Back-Arc Extension at the Tonga Arc". Nature 374, Nr. 6519 (03.1995): 249–51. https://doi.org/10.1038/374249a0.

Bonnardot, M.-A., M. Régnier, E. Ruellan, C. Christova, und E. Tric. „Seismicity and State of Stress within the Overriding Plate of the Tonga-Kermadec Subduction Zone". Tectonics 26, Nr. 5 (2007). https://doi.org/10.1029/2006TC002044.

Eguchi, Takao. „Seismotectonics of the Fiji Plateau and Lau Basin". Tectonophysics, Geodynamics of Back-Arc Regions, 102, Nr. 1 (20.02.1984): 17–32. https://doi.org/10.1016/0040-1951(84)90006-4.

Escrig, S., A. Bézos, C. H. Langmuir, P. J. Michael, und R. Arculus. „Characterizing the Effect of Mantle Source, Subduction Input and Melting in the Fonualei Spreading Center, Lau Basin: Constraints on the Origin of the Boninitic Signature of the Back-Arc Lavas". Geochemistry, Geophysics, Geosystems 13, Nr. 10 (2012). https://doi.org/10.1029/2012GC004130.

Heuret, Arnauld, und Serge Lallemand. „Plate Motions, Slab Dynamics and Back-Arc Deformation". Physics of the Earth and Planetary Interiors, Thermal Structure and

Dynamics of Subduction Zones: Insights from Observations and Modeling, 149, Nr. 1 (15.03.2005): 31–51. https://doi.org/10.1016/j.pepi.2004.08.022.

Karig, D. E. (1970). Ridges and Basins of the Tonga-Kermadec Island Arc System. J. Geophys. Res. 75, 239–254. doi:10.1029/JB075i002p00239

Millen, David W., und Michael W. Hamburger. „Seismological Evidence for Tearing of the Pacific Plate at the Northern Termination of the Tonga Subduction Zone". Geology 26, Nr. 7 (1.07.1998): 659–62. https://doi.org/10.1130/0091-7613(1998)026<0659:SEFTOT>2.3.CO;2.

Sleeper, Jonathan D., Fernando Martinez, und Richard Arculus. „The Fonualei Rift and Spreading Center: Effects of Ultraslow Spreading and Arc Proximity on Back-Arc Crustal Accretion". Journal of Geophysical Research: Solid Earth 121, Nr. 7 (2016): 4814–35. https://doi.org/10.1002/2016JB013050.

Taylor, Brian, Kirsten Zellmer, Fernando Martinez, und Andrew Goodliffe. „Sea-Floor Spreading in the Lau Back-Arc Basin". Earth and Planetary Science Letters 144, Nr. 1 (1.10.1996): 35–40. https://doi.org/10.1016/0012-821X(96)00148-3.

Wiedicke, Michael, und Jenny Collier. „Morphology of the Valu Fa Spreading Ridge in the Southern Lau Basin". Journal of Geophysical Research: Solid Earth 98, Nr. B7 (1993): 11769–82. https://doi.org/10.1029/93JB00708.

SO267

Relationship between saucer-shaped igneous sills and sedimentary layers: an example from the Tofua volcanic arc

AUTHORS

Federal Institute for Geosciences and Natural Resources | Hanover, Germany
M. Schnabel, M. Engels, B. Schramm

GEOMAR Helmholtz Centre for Ocean Research | Kiel, Germany
H. Kopp, F. Schmid

Vrije Universiteit Amsterdam | Amsterdam, The Netherlands
A. Beniest

University of Ottawa | Ottawa, Canada
M. Hannington

INTRODUCTION

Rising magma within sedimentary basins generally form sheet intrusions like dykes and sills. These shallow-level magmatic systems may trigger the generation of earth natural resources, and they may also have a strong impact on climate change (Rocchi and Breitkreuz, 2018). The geometry of sills largely depends on the depth and on the stress field within the sedimentary column, leading in most cases to characteristic saucer-shaped structures (Malthe-Sørenssen et al., 2004). Above such intrusions, the sediments typically form domal structures – but the process of formation of such domes is not fully understood. Based on seismic data from the NE Atlantic Margin, Hansen and Cartwright (2006) proposed that these structures are forced folds, where its relief could be directly related to the thickness of the intrusion. On the other hand, Thomson (2007) proposed a different interpretation of the same data set. He demonstrated that the strata above the sill is not only folded but also thickened, and he describes these domes as complex volcanic centres.

Existing seismic examples covering such structures are rare within the literature and mainly rely on the interpretation of post-stack seismic sections in the time domain (e. g., Medialdea et al., 2017). Here, we present depth-migrated seismic data covering several shallow-level magmatic systems, as well as a domal structure related to a magmatic intrusion. This allows us to further discuss the nature and the history of these structures.

DATA AND PROCESSING

During SO267, we acquired reflection seismic data crossing the Tofua Volcanic Arc in the northern Lau Basin (SW Pacific). The profile discussed here crosses the arc at 17° 20′ S just south of Volcano J South. The data was recorded with a 3900 m active cable and a fixed source point interval of 50 m. The recording of the far-field source signature allowed for a shot-by-shot deconvolution, which sharpened thesource wavelet and therefore increased the vertical resolution. The data was iteratively depth-migrated in the pre stack domain, and a migration velocity analysis (MVA) using a layer-stripping approach was applied within the common reflection point gathers. This method allows for the determination of reliable seismic velocities even within geological complex areas. For a subsequent amplitude analysis, these velocities were used to improve the processing in the time domain.

RESULTS

The processing scheme resulted in a subsurface image in true depth as well as in a high-resolution velocity field and we used it as an additional input for interpretation. Figure 1 shows a part of the profile east of the volcanic arc. Tilted blocks can be seen in a depth between 600 and 800 m below seafloor. The half-grabens show a fault throw of about 200 m. These blocks are likely the result of extension during the creation of the Tofua Trough during late Miocene or early Pliocene times. Further on, the sedimentary layers show a general thickening to the east. This implies that the main source for sedimentation was the Tonga Ridge.

The seismic image allowed us to describe and quantify several igneous structures in the vicinity of volcano J South. Around CDP 56800, a saucer-shaped intrusion with a diameter of about 2.300 m is imaged in a depth of 400 m below the seafloor. The sedimentary horizons in this area show an upward bending in the range of 150 m. The intrusion itself is imaged as a high-amplitude reflection with a broad black-white-black waveform. This seismic response is typical for intrusions and indicates that the intrusion is much thinner than the mean seismic wavelength. This leads to interference between the reflections from the upper and lower boundary of the sill. Due to this, it was also not possible to resolve the intrusive body directly within velocity analysis. On the other hand, the interval containing the sill showed a mean velocity of 2.250 m/s, while the surrounding sediments show velocities of 2.000 m/s. With an assumed velocity for the sill ranging between 4.800 and 6.000 m/s we can conclude than the thickness of this body would be in the range of 16 to 23 m. Therefore, the magnitude of the domal structure could not be explained be the thickness of the intrusive body alone, and additional processes – e. g. upwelling due to rising magma before the emplacement of the sill – have to be taken into account.

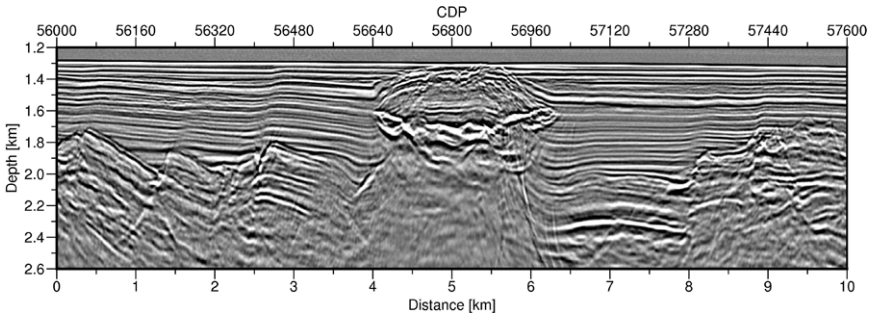

Fig. 1: Depth-migrated seismic line BGR18-203. The central part shows a pronounced saucer-shaped intrusion in a depth below seafloor of about 400 m.

REFERENCES

Hansen DM, Cartwright J, The three-dimensional geometry and growth of forced folds above saucer-shaped igneous sills, Journal of Structural Geology 2006, 28, 1520–1535, doi:10.1016/j.jsg.2006.04.004.

Malthe-Sørenssen A, Planke S, Svensen H, Jamtveit B, Formation of saucer-shaped sills, Geological Society, London, Special Publications 2004, 234, 215–227, doi:10.1144/gsl.sp.2004.234.01.13.

Medialdea T, Somoza L, González FJ, Vázquez JT, at al. Evidence of a modern deep water magmatic hydrothermal system in the Canary Basin (eastern central Atlantic Ocean), Geochemistry, Geophysics, Geosystems 2017, 18, 3138–3164, doi:10.1002/2017GC006889.

Rocchi S, Breitkreuz C, Physical Geology of Shallow-Level Magmatic Systems—An Introduction, In Breitkreuz, C. and Rocchi, S. (Eds.), Physical Geology of Shallow Magmatic Systems: Dykes, Sills and Laccoliths 2018 (Springer International Publishing), doi:10.1007/11157_2017_32.

Thomson K, Comment on "The three-dimensional geometry and growth of forced folds above saucer-shaped igneous sills" by Hansen and Cartwright, Journal of Structural Geology 2007, 29, 736–740, doi:10.1016/j.jsg.2006.10.009.

SO268/3

Plastic-associated chemicals – are plastics a sink or source of organic chemicals to the North Pacific Ocean?

AUTHORS

Helmholtz Centre for Environmental Research – UFZ, Departments of Ecological Chemistry and Bioanalytical Ecotoxicology | Leipzig, Germany
C.D. Rummel, E. Rojo-Nieto, A. Jahnke, collaborators

To date, risk assessments of plastics in the environment usually focus on the particles themselves. However, recent research acknowledges the importance of sorbed chemicals in addition to the physical presence of the particles for comprehensive assessments of the fate and potential effects of plastics (Bucci and Rochman, 2021). Some scientists have raised concerns about the potential of environmental plastics to represent a vehicle of these sorbed and industrially added chemical mixtures for long-range environmental transport of the chemicals, the so-called vector effect (Gouin 2021), whereas others assume that equilibration with the surroundings is faster than the particle transport so that floating plastics do not substantially alter the transport and fate of associated chemicals.

Some polymers have high sorption capacity for hydrophobic organic compounds (HOCs), and particularly polyethylene has been used for decades as passive sampling material in environmental chemistry. For marine plastic litter, thermodynamic gradients between the polymer and the surrounding medium drive the partitioning of chemicals between these two phases in direct contact. That means that chemicals are sorbed to each phase according to its relative sorption capacity, and partitioning proceeds along the thermodynamic gradient to achieve an equilibrium distrubution between these two phases. The anticipated processes regarding floating plastic litter are two-fold: (i) additives from the production process are present in the newly emitted plastic, and leaching of these chemicals to the environment occurs during residence at sea; (ii) plastics are initially low in levels of environmental pollutants such as HOCs, and partitioning from the seawater to the plastic occurs, with the plastic representing a sink for such chemicals relative to its surroundings.

Following sufficiently long exposure times, the plastics and surrounding seawater are expected to approach equilibrium partitioning. Assuming that 80 % of all marine plastic is exposed to the marine environment for more than 4 years (Koelmans et al., 2016), pollutants in the polymer are expected to be close to equilibrium partitioning relative to the surrounding seawater. In MICRO-FATE, we comprehensively characterize the chemicals present in the environmental media (surface seawater, water from greater depths and sediments) and in the floating plastic items collected during expedition

SO268/3 crossing the North Pacific Ocean (Figure 1). Furthermore, we investigate the mixture effects that additives, sorbed pollutants and weathering-induced degradation products jointly elicit in cell-based bioassays covering different endpoints used as bioanalytical tools (Rummel et al., 2019) to further elucidate the plastics' role as a source or sink of pollutants to the North Pacific Ocean.

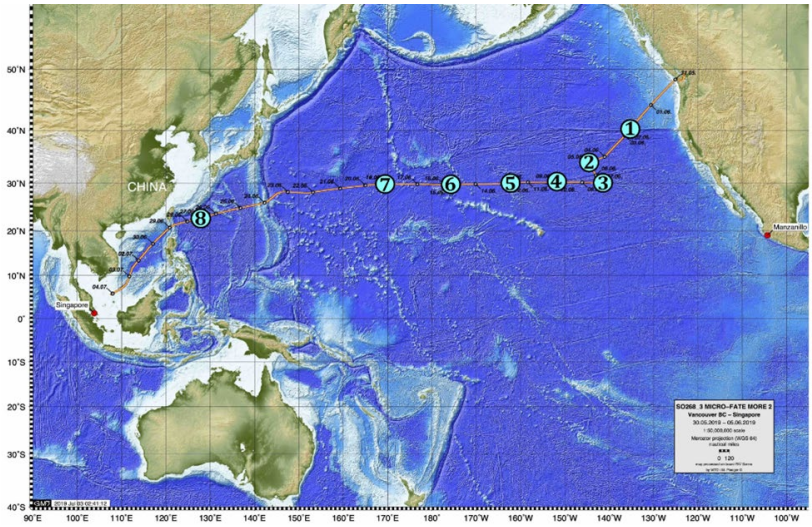

Fig. 1: Track of expedition SO268/3 on research vessel SONNE with major sampling stations.

We seek to answer the following questions: What are the levels and patterns of pollutants in the surface seawater, at greater depths in the water column and in the sediment from the SONNE transit SO268/3? Does plastic litter aged in the marine environment show higher effects than the corresponding original material? Can we simulate environmental weathering artificially in the laboratory? Does the relevance of different endpoints vary over time and location? Our hypothesis was that sorbed chemicals and the degrading plastic from the North Pacific show higher effects than the original new product since we expect a highly diverse chemical mixture being sorbed from the water phase compared to a less substantial fraction of chemicals added during manufacturing. Restrictions include that the composition of the original material may have varied over time or that the new product is not identical to the field-weathered one, and that the exact duration and location of the weathering in the field are largely unknown. To address these questions, material was sampled, photographed and labelled on board (Figure 2) for comprehensive analyses under controlled laboratory conditions at UFZ.

Based on the obtained data, we compare the chemical partitioning status between floating plastics and the surrounding seawater determined by chromatographic separation techniques coupled to advanced high-resolution mass spectrometry to the

known equilibrium partitioning status and can hence derive for which chemicals and under which circumstances plastics in the environment represent a source or sink of chemicals. Furthermore, cell-based bioassays help to characterize mixture effects of the known and unknown chemicals present in the samples. In particular, for the paired samples of field-weathered items, the corresponding new products and the artificially weathered products, we compare (a) analytical chemical and bioanalytical results of the solvent extracts (new to field-weathered) and (b) bioanalytical results of enriched leachate waters of the new products that we artificially weathered under strong UV light irradiation (new to artificially weathered). The results indicate that we can observe both phenomena, i. e. higher effects in the new vs. field-weathered items or the other way around, depending on the type of product and the investigated endpoint and/or pollutant. The identified chemicals are then linked to the observed effects by means of so-called iceberg modelling to determine the fraction of the total effect explained by the measured chemicals. This study helps to elucidate the vector role of added and sorbed chemical mixtures in plastic debris from the North Pacific Ocean which is of utmost importance to understand the ecotoxicological relevance and the long-range environmental transport pathways of marine plastic pollution.

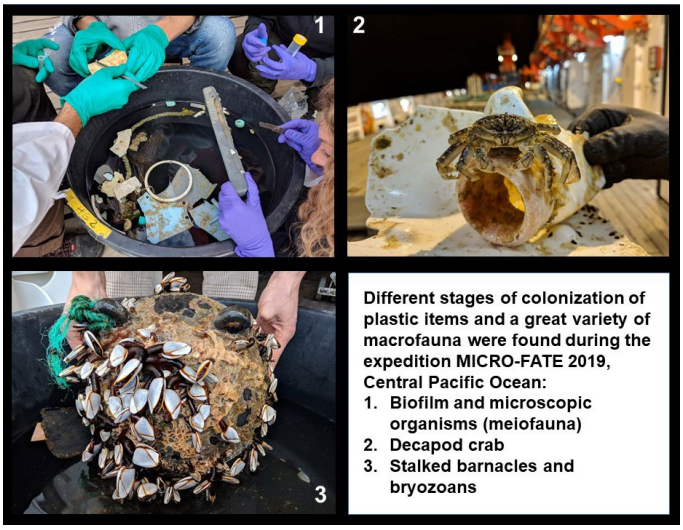

Fig. 2: Impressions of the samples collected on expedition SO268/3 of research vessel SONNE.

REFERENCES

Bucci, K. and Rochman, C. (2021) 'A Proposed Framework for Microplastics Risk Assessment', presentation at the SETAC North American 42nd Annual Meeting, Portland/ Scicon, November 14–18.

Gouin, T. (2021) 'Addressing the importance of microplastic particles as vectors for long-range transport of chemical contaminants: perspective in relation to prioritizing research and regulatory actions', Micropl.&Nanopl. 1, p. 14. doi: 10.1186/s43591-021-00016-w

Koelmans, A.A. et al. (2016). 'Microplastic as a Vector for Chemicals in the Aquatic Environment: Critical Review and Model-Supported Reinterpretation of Empirical Studies', Environ. Sci. Technol,. 50, pp. 3315–3326. doi: 10.1021/acs.est.5b06069.

Rummel, C.D. et al. (2019). 'Effects of Leachates from UV-Weathered Microplastic in Cell-Based Bioassays ', Environ. Sci. Technol,. 53, pp. 9214–9223. doi: 10.1021/acs.est.9b02400.

SO268/3

On-board systematic polymer weathering in mesocosms

AUTHORS

Fraunhofer-Gesellschaft, Institute for Ceramic Technologies and Systems (IKTS) | Dresden, Germany
A. Benke, M. Schneider, A. Potthoff

Topas GmbH | Dresden, Germany
K. Oelschlägel

To improve the understanding of the mechanisms of natural weathering of polymers, on-board weathering experiments were conducted in mesocosms during the voyage of the research vessel SONNE from Vancouver to Singapore across the Pacific Ocean (Figure 1). The polymer samples were exposed to natural sunlight and seawater, and the environmental conditions were permanently monitored. A scenario of natural weathering under controlled conditions was realized. The experiments fill a gap between the analysis of field-weathered material (e. g. Krause et al. 2020), where the duration of weathering is unknown, and artificial weathering in the laboratory (e. g. Horne et al. 2020), where the environmental conditions are often very different from those in nature.

Two mesocosms, each holding approx. 1 m^3 of water, were installed on board the research vessel. LDPE (low density polyethylene), PET (polyethylene terephthalate) and PS (polystyrene) were chosen as plastic materials due to their strong commercial use. They were fixed as sheets and granules in the mesocosms, either exposed to the solar radiation or covered as dark controls. Samples were taken for analysis after 1, 3, 6, 12, 20 and 28 days, so that the weathering process could be analyzed for 28 days. The natural UVB irradiation was varied by positioning the samples at different depths below the water surface.

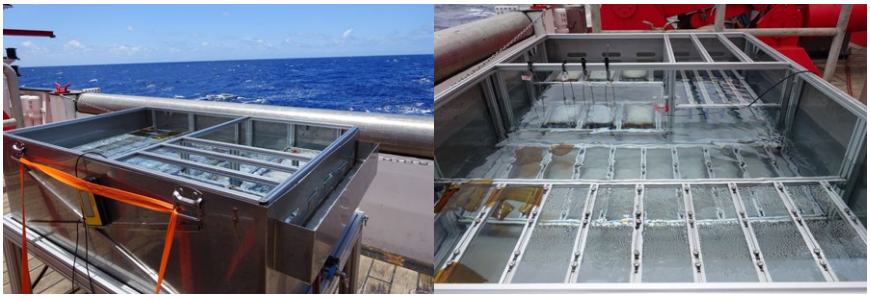

Fig. 1: View of one of the mesocosms installed on board the ship (left) and position of the samples: Sheets and PET bottles in the foreground, granules in nets in the background (right).

Throughout the weathering period, water samples were taken from the Pacific Ocean and temperature, conductivity, pH, density, solute concentrations, and ions (Ca^{2+}, Mg^{2+}, total salts) were analyzed. Figure 2 shows the pH value of the seawater, measured on the route between Vancouver and Singapore, and as a function of water depth. In addition, the global solar radiation and the UVB radiation component essential for polymer weathering were measured. By logging the environmental data accurately, it is possible to relate the weathering conditions to the weathering states of the samples in the mesocosms.

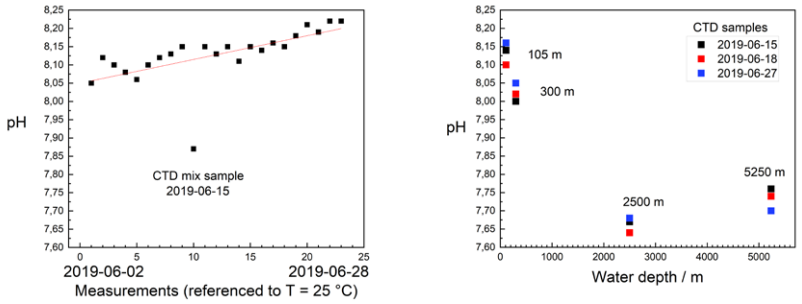

Fig. 2: pH values of the Pacific Ocean: increase in the pH value of the surface seawater between Vancouver and Singapore (left) and decrease in the pH value with water depth (right).

To assess the weathering status, the surfaces and bulk of the polymer samples were characterized using the following methods: light and scanning electron microscopy to visualize biofilms and salt deposits, contact angle measurements to assess the wettability with water, UV/VIS spectroscopy for color measurement to quantify the yellowing, computer tomography for visualization of weathering phenomena in the bulk, FTIR spectroscopy to analyze chemical changes on the surface, like breaking and formation of chemical bonds due to weathering progress.

The wettability of polymer surfaces plays an important role in transport and fate and influences the sedimentation and dispersion of plastic particles in the water body. It is therefore important to know how the wettability changes due to weathering. A suitable technique to quantify the wettability of a solid surface by a liquid is the measurement of the contact angle.

It was found that the contact angle for the three polymers investigated decreases with weathering time, wetting increases for all samples (Figure 3). The contact angle depends on polymer material. LDPE wets worst, sheets from the closed mesocosm are unchanged after 4 weeks. Wettability of PS changes most until complete wettability is achieved for samples with UV irradiation. Furthermore, the contact angle depends on the biofilm growth. If measured on the biofilms, the contact angle decreases more than on the

cleaned samples without biofilm. The contact angle is also influenced by the presence of UV radiation. After removal of the biofilm, small differences depending on the irradiation were always measured, showing the influence of light on surface changes during weathering. Both the weathering of the polymer itself and the associated increase in polar functional groups and the influence of eco-corona and biofilm formation are discussed as causes for the increase in wettability with weathering time (Benke et al. 2022).

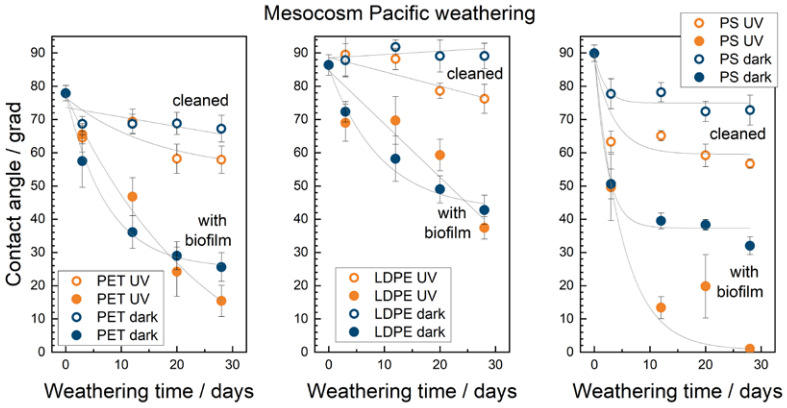

Fig. 3: Evolution of the contact angle of PET, LDPE, and PS sheet samples during weathering under controlled, natural conditions in the mesocosms. Significant decrease in contact angle for sheets with biofilm compared to cleaned sheets. UV: Sheets with UV light irradiation in open mesocosm, Dark: Dark control samples in closed mesocosm.

REFERENCES

Krause, S.; Molari, M.; Gorb, E. V.; Gorb, S. N.; Kossel, E.; Haeckel, M. (2020): Persistence of plastic debris and its colonization by bacterial communities after two decades on the abyssal seafloor. Scientific reports 10 (1), S. 9484. DOI: 10.1038/s41598-020-66361-7.

Horne, F. J.; Liggat, J. J.; MacDonald, W. A.; Sankey, S. W. (2020): Photo-oxidation of poly(ethylene terephthalate) films intended for photovoltaic backsheet. J Appl Polym Sci 137 (17), S. 48623. DOI: 10.1002/app.48623.

Benke, A.; Sonnenberg, J.; Oelschlägel, K.; Schneider, M.; Lux, M.; Potthoff A. (2022): Can contact angle measurements contribute to assessing the weathering of plastics? Paper in preparation.

SO268/3

Quantification of microplastic particles in surface water collected during SO268/3 between Vancouver and Singapore

AUTHORS

Helmholtz Centre for Environmental Research – UFZ | Leipzig, Germany
R. Rynek, S. Wagner, A. Jahnke, T. Reemtsma

The global plastic production reached 368 million tons in 2019. (PlascticEurope, 2020) Incorrect waste disposal and insufficient waste management lead to the fact that up to 10 % of the annual produced plastic mass reaches the oceans. (Thompson, 2007) Assuming a constantly increasing plastic production mass and no change in handling plastic waste, more than 250 million tons of plastic could have reached the oceans by 2025. (Jambeck et al., 2015) In the oceans plastic particles are influenced by ocean currents and winds which lead to the formation of accumulation zones. (Maximenko, Hafner and Niiler, 2012) One of the biggest known accumulation zone is the Great Pacific Garbage Patch between California and Hawaii. (Lebreton et al., 2018)

The aim of this study is to determine the lateral distribution of plastic particles in the Pacific Ocean. Therefore particle samples from surface waters were obtained during cruise SO268/3 between Vancouver and Singapore from May to July 2019 (Fig. 1).

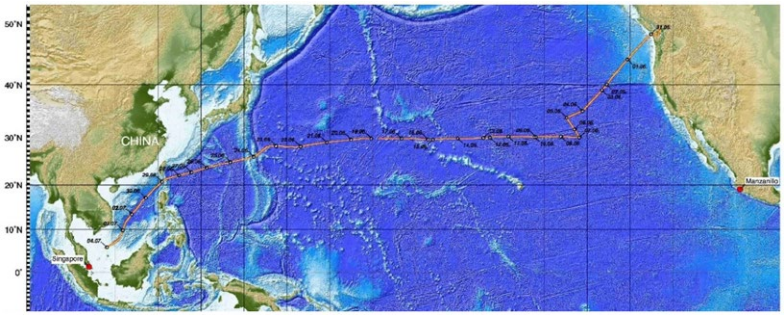

Fig. 1: track of cruise SO268/3 on research vessel SONNE

Here we present the general workflow from sampling to quantification of plastic particles and preliminary results for the lateral distribution of micro plastic in surface water.

Samples were obtained with a Neuston catamaran (> 330 µm). Sample suspensions were wet sieved (2 mm) and possible plastic particles were extracted from the sieve with

tweezers and stored individually. Organic matrix in the smaller size fraction was removed by an enzymatic digestion protocol. (Löder et al., 2017) The residue was wet sieved again (500 µm) and possible plastic particles were extracted and stored individually. The smaller size fraction was filtered onto Anodisc filters (0,2 µm). Extracted particles were analyzed by ATR-FT-IR and filter samples by FT-IR imaging in transmission mode.

We found plastic debris at every sampling station ranging from 11000 to 172000 items per km². Elevated concentrations were found in the area of the Great Pacific Garbage Patch (Fig. 2, A) and the Papahānaumokuākea Marine National Monument. (Fig. 2, B)

Fig. 2: Comparison of concentrations of surface floating plastic particles. A – Great Pacific Garbage Patch, B – Papahānaumokuākea Marine National Monument

REFERENCES

Jambeck, J. R. et al. (2015) 'Plastic waste inputs from land into the Ocean', Science, 347(6223), pp. 768–771. doi: 10.1126/science.1260352.

Lebreton, L. et al. (2018) 'Evidence that the Great Pacific Garbage Patch is rapidly accumulating plastic', Scientific Reports. Springer US, 8(1), pp. 1–15. doi: 10.1038/s41598-018-22939-w.

Löder, M. G. J. et al. (2017) 'Enzymatic Purification of Microplastics in Environmental Samples', Environmental Science and Technology, 51(24), pp. 14283–14292. doi: 10.1021/acs.est.7b03055.

Maximenko, N., Hafner, J. and Niiler, P. (2012) 'Pathways of marine debris derived from trajectories of Lagrangian drifters', Marine Pollution Bulletin. Elsevier Ltd, 65(1–3), pp. 51–62. doi: 10.1016/j.marpolbul.2011.04.016.

PlascticEurope (2020) 'Plastics – the Facts 2020', PlasticEurope, pp. 1–64.

Thompson, R. C. (2007) 'Plastic debris in the marine environment: consequences and solutions', Marine Nature Conservation in Europe 2006, (May 2006), pp. 107–116.

SO268/3

The role of the 'plastisphere' in the North Pacific Ocean Gyre

AUTHORS

Helmholtz Centre for Environmental Research – UFZ, Department Bioanalytical Ecotoxicology | Leipzig, Germany
M. Schmitt-Jansen, S. Lips, C.D. Rummel

Helmholtz Centre for Environmental Research – UFZ | Department Lake Research Leipzig, Germany
K. Wendt-Potthoff

Leibniz Institute for Baltic Sea Research Warnemuende (IOW), Biological Oceanography | Rostock, Germany
B. Scales, S. Oberbeckmann

and collaborators

Environmental biofilms readily colonize all surfaces available in aquatic systems, including plastic material (Rummel et al., 2017). Consisting of microbial consortia of bacteria, archaea, autotrophic microalgae, fungi and the meiofauna, biofilms comprise all food chain components and contribute substantially to the matter and energy cycling of aquatic systems. The importance of marine microbial communities for the global biogeochemical cycles is indisputable (Azam et al., 1983), however, the role of the plastisphere, the plastic-specific microbial community, from the North Pacific Ocean Gyre is less investigated. Plastic material, free-floating in high abundance in the Pacific Gyre may create a new ecological environment for colonizing microbial communities. Although the diversity and composition of epiplastic communities is increasingly investigated, little is known about the initial processes and succession of plastic colonization and the ecological functions of epiplastic communities. Using a holistic approach, our research on the RV SONNE cruise (SO268/3) addressed following objectives:

(i) understanding early biofilm formation on plastic material

(ii) structural and functional characterization of biofilms on environmental plastic

(iii) identification of different life strategies in plastic biofilms.

(i) The early formation of biofilms on plastic as subject to the eco-corona was studied on virgin and lab-aged polymers in mesocosm experiments. After exposure, the corona of adsorbed organic matter (using FT-ICR MS) and subsequent bacterial colonisation (using 16S amplicon sequencing) was analysed, over time. Our results revealed a fast colonisation of pristine material after one day with unique communities, however, community structure converged over time on all materials (Rummel et al., 2021).

(ii) The structure of microbial communities from plastic items, derived from the Pacific Ocean was analysed using Confocal laser-scanning microscopy and molecular methods (16S, 18S and ITS amplicon sequencing) and compared to the pelagic environment. We have not been able to compare the structure of the plastisphere to autochthonous particulate material, as no natural substrates like wood were found during the cruise. Whereas no differences in the community structure was detectable in dependence of the plastic type (PP and PE), distinct differences to the pelagic community of the Pacific Ocean were revealed. The functional capacity of the biofilms was assessed in terms of primary production, by quantifying the photosynthesis capacity (on-board PAM-Fluorometry) and pigment profiling using HPLC coupled to DAD. Tracer techniques using ^{13}C incorporation as well as oxygen measurements were applied to directly measure primary production. Medium-size microplastic was put on-board into closed glass vessels equipped with oxygen detection spots which allowed contactless, non-destructive oxygen measurements with a Fibox oxygen meter. Incubation in light and dark conditions was performed over 24 hours to calculate primary production rates and revealed P/R ratios close to zero indicating closed and small cycles of matter and energy within the biofilms.

(iii) Different life strategies in plastic biofilms were traced via cultivation of microorganisms from the same material as used for structural and functional analysis. To obtain strains that might be able to degrade plastic or associated chemicals, sampled particles and aliquots of the peeled-off and resuspended biofilms were put into different liquid media prepared before the campaign. Media were incubated during the campaign (room temperature, dark conditions, accompanied by temperature loggers) and sequenced afterwards. Back in the lab, 69 colonies were selected for sequencing their entire 16S rRNA gene revealing, among others, members of the *Pseudoalteromonas, Halomonas, Brachybacterium, Labrenzia, Qipengyuania, Kocuria* and *Vibrio* genera. The majority of 16S sequences from isolated colonies matched with ≥99 % sequence identity with OTUs from the structural community analysis (ii) indicating the viability and metabolic activity of the microorganisms of the plastisphere.

In conclusion, plastic material of the North Pacific Ocean Gyre forms a new habitat, which is colonized quickly with a functionally vital and active community of microorganisms. Thus the plastisphere has to be considered in all processes related to the fate and effects of environmental plastic pollution.

REFERENCES

Azam, F., T. Fenchel, J. G. Field, J. S. Gray, L. A. Meyer-Reil and F. Thingstad (1983). The Ecological Role of Water-Column Microbes in the Sea. Marine Ecology Progress Series 10(3): 257–263.

Rummel, C.D., Jahnke, A., Gorokhova, E., Kühnel, D., Schmitt-Jansen, M. (2017) Impacts of biofilm formation on the fate and potential effects of microplastic in the aquatic environment. Environ. Sci. Technol. Lett. 4 (7), 258–267. (DOI: 10.1021/acs.estlett.7b00164)

Rummel C.D., Lechtenfeld O.J., Kallies R., Benke A., Herzsprung P., Rynek R., Wagner S., Potthoff A., Jahnke A., Schmitt-Jansen M. (2021) Conditioning film and early biofilm succession on plastic surfaces. Environ. Sci. Technol. 55 (16), 11006–11018.

SO271/1

Exploring the Indian Ocean: results from cruise SO271/1

AUTHORS

Federal Institute for Geosciences and Natural Resources | Hanover, Germany
T. Kuhn, U. Schwarz-Schampera, R. Freitag, S. Fuchs, C. Kriete, A. Lückge

University of Hamburg | Hamburg, Germany
N. Harms, N. Lahajnar

Senckenberg am Meer, German Centre for Marine Biodiversity Research | Wilhelmshaven, Germany
T. Kihara

Laurentian University | Sudbury, Canada
H. Gibson

The expedition SO271/1 (INDEX 2019) of BGR with TFS SONNE targeted the German license area for polymetallic sulfides in the Indian Ocean. Cruise participants included the Universities of Hamburg, HCU Hamburg, Kiel, Erlangen, Padua, the DZMB Senckenberg am Meer Wilhelmshaven and INES GmbH, and GEOMAR in Kiel. The cruise focused on the detailed bathymetric and geological exploration for active vents and inactive sulfide fields in the license clusters #01, #04, #05, #06, #07, #10 and #12. The license area was also sampled for environmental, i. e., (paleo) oceanographic, sedimentary and faunal base line studies by sediment coring stations, water sampling, biodiversity in the water column and in vent fields, and sediment trap and current meter moorings. Very few environmental and geological studies exist in this part of the Indian Ocean so far. Our work therefore contributes to the understanding of regional and ocean-wide oceanographic and sedimentation processes and to the faunal census.

Cruise SO271/1 (INDEX 2019) was very successful. Sea conditions were generally good with only a half day of limited operational capability. There were no problems with the ship operation despite the high number of different tools we deployed during the cruise and the limited space on SONNE's working deck. A total of 131 stations with survey, observation and sampling operations were completed in the license clusters #01, #04, #05, #06, #07, #10, and #12. A total of 12 different operational tools were used for diverse and extensive exploration and environmental studies during this cruise within the license area, including

- 6 vertical CTD rosette casts for environmental, water masses and sedimentary studies;
- 7 gravity corer and 3 multicorer stations for paleooceanographic and biogeochemical studies;
- 8 heat flow probe measurements for crustal temperature regime estimations;
- 24 wax corer and 15 dredge stations for petrological reconnaissance and spreading ridge and triple junction evolution studies;
- 10 sediment trap and two ADCP mooring operations for biogeochemistry, particle flux and ocean current measurements;
- 7 vertical multinet casts for planktonic base line studies in the license area. The biodiversity in total was studied and sampled with 4,125 samples and 5,477 individuals. 89 samples were collected for microbiological analyses;
- 20 deep-towed HOMESIDE surveys for high-resolution bathymetric mapping, magnetics and water anomaly surveys (total of 330 km, 202 km^2 in 153 hours);
- 11 tow-yo stations with the SOPHI sensor sled for plume hunting (183 km, 116 hours);
- 18 ROPOS operations for detailed site surveys and sampling;
- bathymetric surveys with 938 hours of survey time (total of 4,541 km) with EM122 and 994 hours (4,828 km) of survey with the echo-sounder EK60 for water column imaging and analyses.

Two new sites (SURYA, SOORAJ; both Sanskrit/Hindi for Sonne) were identified in the license clusters #06 and #07, respectively. SURYA is the very first identified vent site on the western flank of the entire SEIR. The new findings again attest to the high potential for sulfide mineralization in all clusters of the German license area. Additionally, 24 hydrothermal vent fluids were sampled from five different sulfide areas during the ROPOS dives and shipboard characterized. Swath bathymetric mapping and scientific echosounder measurements for water column imaging were carried out during the entire cruise outside the EEZ of Mauritius. The biodiversity was studied and sampled at 79 stations with 1972 sediment, rock, water and sulfide samples and more than 10,000 individuals.

The results with respect to the sulfide exploration during SO271/1 (INDEX 2019) are represented by

- The discovery of the SURYA sulfide area in cluster #06. The site extends over 40x40m and is composed of five sulfide sites with diameters of several meters. Two sites are

inactive, three others show diffuse venting with fluid temperatures up to 32°C. The site is associated with the outer edge of a normal graben fault, similar to the setting that was identified at the NEW SONNE field in cluster #11. The location is situated about 6.8 km west of the central SEIR graben axis. The site is associated with a number of young pillow mounds. The graben fault plane is covered with talus material from the pillow mounds and the sulfide site, possibly covering parts of the site. Fragments of chimney debris and frequent indications for former high-temperature venting were observed. The field is in the waning stage of venting with low fluid discharge temperatures. The normal graben fault shows outcrops of stockwork-type mineralization with highly altered pillow basalts and mineralized stringers in pillow volcanic talus and pillow basalt flows. The biodiversity is similar to other sites along the SEIR and at KAIREI. The scaly-foot gastropod chrysomallon squamiferum is also present.

- The discovery of the SOORAJ sulfide area in Cluster #7 extending over about 100x140m. The area is associated with a very prominent inner corner high and the association with exhumed deeper oceanic crust (megamullion or oceanic core complex), is suggested. The area is associated with redox, particle and self-potential anomalies, as well as a recorded plume. At least three vent sites and chimney-like edifices were located by high-resolution swath bathymetry mapping. The sulfide mound is flat and irregular and occurs on a gentle slope. A steeper slope occurs to the East. The inner corner high displays a generally rough terrain with slopes >40°. Similarities can be drawn to the KAIMANA field and its strongly fault-controlled occurrence of sulfide mineralization and chimneys, respectively.

- The discovery of vast extensions of the HUNA area in cluster #12. The size extends to about 2,400 m in length and a width of about 400 m. In total, the Huna area hosts six high-temperature sites, 16 diffuse, low-temperature sites and 18 inactive sulfide patches.

- The significant extension of PENUMBRA (four more active vent sites, 2.6 x 0.5 km) and KAIMANA (three new sulfide sites) areas.

Cruise SO271/1 (INDEX 2019) attests to the high prospectivity of the spreading ridges in the Indian Ocean and of the German license area. The new discovery of larger and extending sulfide areas in two more clusters at greater distances from the actual spreading axes defines off-axis areas lacking high magmatic heat production and fluid pathways by traditional definition as new and prime exploration targets. Sulfide areas associated with exhumed deeper oceanic crust become a more significant exploration target as more sulfide sites are found.

Fig. 1: Overview of the SO271/1 (INDEX 2019/1) working area, the cruise plot for Leg 1 and courses along the southern Central and the northern Southeast Indian Ridge, Central Indian Ocean. The cruise started and ended in Port Louis, Mauritius. Numbers refer to dates in November and December.

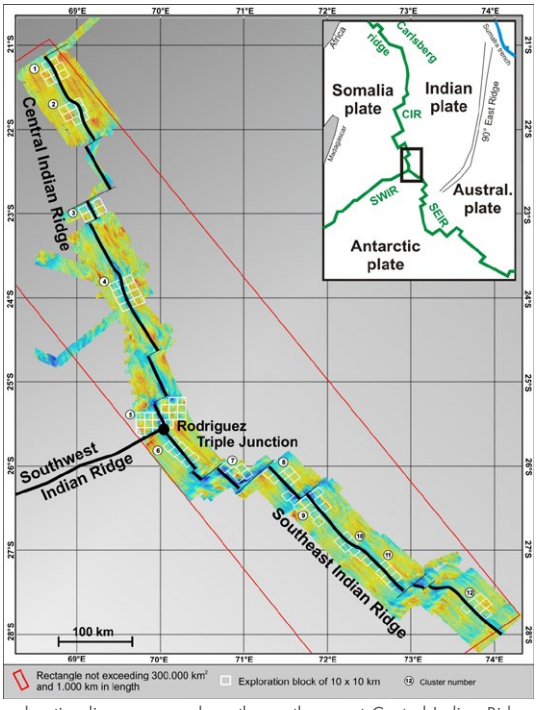

Fig. 2: The German exploration license area along the southernmost Central Indian Ridge and the northernmost Southeast Indian Ridge. Cruise SO271/1 (INDEX 2019) with TFS SONNE addressed the clusters #01, #04, #05, #06, #07, #10, and #12 along the southern Central and the northern Southeast Indian Ridges.

SO271/2

Exploring the Indian Ocean: results from cruise SO271/2

AUTHORS

Federal Institute for Geosciences and Natural Resources | Hanover, Germany
U. Barckhausen, A. Ehrhardt, I. Heyde, H. Müller, K. Schwalenberg

Senckenberg am Meer, German Centre for Marine Biodiversity Research | Wilhelmshaven, Germany
K. Gerdes, K. Kniesz

Cruise SO271/2 was the second Leg of expedition INDEX2019 of BGR with TFS SONNE and was dedicated to geophysical investigations in the German license area for polymetallic sulfides in the Indian Ocean. Cruise participants included the DZMB Senckenberg am Meer Wilhelmshaven and INES, the University of Bremen, and the Landesamt für Bergbau, Energie und Geologie Niedersachen.

The cruise focused on the detailed electromagnetic exploration of four known sulfide areas in the clusters #04 and #05 of the German license area with the electromagnetic profiler GOLDEN EYE. The work was accompanied by high resolution deep-tow bathymetric and magnetic measurements. An array of 16 Ocean Bottom Seismometers was deployed for a long term monitoring of the local seismic activity along the southernmost part of the Central Indian Ridge. Systematic mapping of the seafloor around the four sulfide areas, investigated with a high resolution camera, contributed to the faunal census.

Cruise SO-271/2 (INDEX2019 Leg 2) was carried out without any major problems and all planned scientific work could be completed. The weather and the sea conditions were generally good with fresh winds most of the time. During two relatively short periods with rougher conditions, magnetic mapping was carried out which is not depending on low to moderate sea states as much as instruments like GOLDEN EYE, which need to be navigated very precisely at the seafloor. The balance of this rather short cruise with 14 working days amounts to 15 stations completed in clusters #04 and #05. Swath bathymetric mapping and scientific echosounder measurements for water column imaging were carried out during the entire cruise outside the EEZ of Mauritius.

The seven deployments of GOLDEN EYE amounted to a total of 238 hours, during which the magnetic and electrical properties of the sub-seafloor at and around the sulfide areas Kairei and Kaimana (both cluster #05) and Alpha and Score (both cluster #04) could be mapped in great detail. The data show the distribution of material with a high electrical

conductivity, which is a strong indication for the presence of massive sulfides. Different modes of measuring were tested in order to find the most effective working mode in terms of data quality and minimized measuring time for future deployments of GOLDEN EYE.

Magnetic measurements were carried out on the transits to and from the German License area on profile tracks designed to fill gaps in the already existing data coverage. In addition, the entire cluster #05 was mapped magnetically with a dense grid of profiles at 2.5 km distance. In total, 1772 km of magnetic profiling were completed. During one deployment of the deep-towed instrument platform HOMESIDE in the Kairei area, another 22 profile km of magnetics were acquired at a height of ~100 m above the seafloor simultaneously with high resolution bathymetry.

An array of 16 Ocean Bottom Seismometers (OBS) was deployed around the Kairei site and along the southernmost part of the Central Indian Ridge. These recorded the local seismicity with a high sensitivity for a period of nine months. The OBS were recovered in August 2020 in a rescue mission because the originally planned recovery in September 2020 during cruise SO-277 had to be cancelled due to the Covid-19 pandemic.

Gravity data, multibeam bathymetry with EM122, and water column imaging with EK 710 were collected throughout the cruise from leaving until reentering the EEZ of Mauritius.

The main purpose of SO-271/2 was the acquisition of as many electromagnetic data as possible in order to gain much needed information on the 3D-structure of the sulfide areas Kairei and Kaimana (both cluster #05) and Alpha and Score (both cluster #04). From earlier work at the Edmond-Gauss-Score sulfide area it was known that significant parts of the massive sulfides can be hidden under a sedimentary cover (Müller et al., 2018). In addition, at the moment electromagnetics is the only method available to us for gaining detailed insight into the upper 30 meters of the massive sulfide bodies.

The electromagnetic profiler GOLDEN EYE carries powerful lights and three cameras, one of them a high resolution camera pointing directly downwards. The design of the seafloor surveys with a regular pattern of parallel lines at a distance of 50 m allows a systematic and representative census of the deep sea fauna over the sulfide areas and their immediate surroundings.

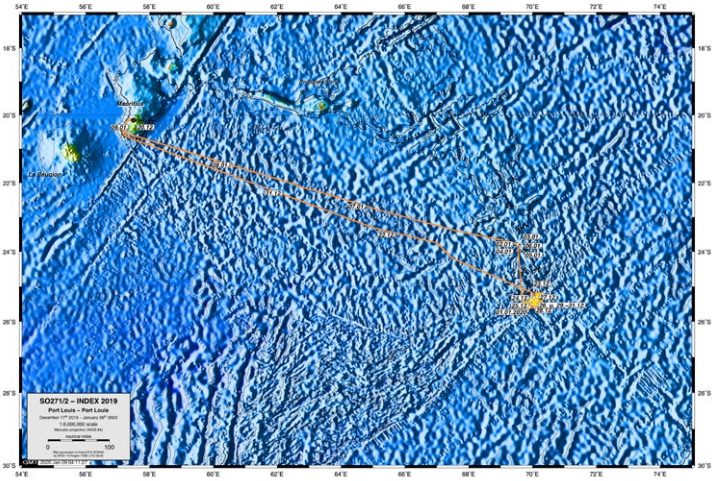

Fig. 1: Cruise plot for SO271/2 (INDEX2019 Leg 2), and courses along the southern Central Indian Ridge, Central Indian Ocean. The cruise started and ended in Port Louis, Mauritius. Numbers refer to dates in December 2019 and January 2020.

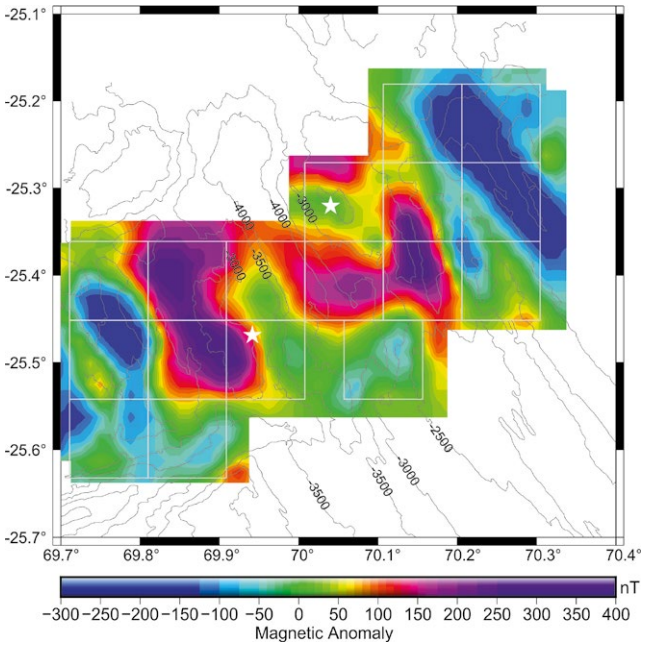

Fig. 2: Magnetic anomaly map of cluster #05 just north of the Rodriguez Triple Junction. Data acquired during Cruise SO271/2 (INDEX 2019 Leg 2) with TFS SONNE.

SCHRIFTENREIHE PROJEKTTRÄGER JÜLICH

1. Technologie- und Erkenntnistransfer aus der Wissenschaft in die Industrie
   Eine explorative Untersuchung in der deutschen Material- und Werkstoffforschung
   hrsg. von A. Pechmann, F. Piller und G. Schumacher (2010), 230 Seiten
   ISBN: 978-3-89336-624-8

2. STATUSTAGUNG SCHIFFFAHRT UND MEERESTECHNIK
   Tagungsband der Statustagung 2010 (2010), 173 Seiten
   ISBN: 978-3-89336-677-4

3. STATUSTAGUNG SCHIFFFAHRT UND MEERESTECHNIK
   Tagungsband der Statustagung 2011 (2011), 227 Seiten
   ISBN: 978-3-89336-745-0

4. STATUSTAGUNG SCHIFFFAHRT UND MEERESTECHNIK
   Tagungsband der Statustagung 2012 (2012), 206 Seiten
   ISBN: 978-3-89336-832-7

5. STATUSTAGUNG MARITIME TECHNOLOGIEN
   Tagungsband der Statustagung 2013 (2013), 188 Seiten
   ISBN: 978-3-89336-922-5

6. STATUSTAGUNG MARITIME TECHNOLOGIEN
   Tagungsband der Statustagung 2014 (2014), 179 Seiten
   ISBN: 978-3-95806-006-7

7. STATUSTAGUNG MARITIME TECHNOLOGIEN
   Tagungsband der Statustagung 2015 (2015), 196 Seiten
   ISBN: 978-3-95806-104-0

8. STATUSTAGUNG MARITIME TECHNOLOGIEN
   Tagungsband der Statustagung 2016 (2016), 220 Seiten
   ISBN: 978-3-95806-187-3

9. STATUSSEMINAR MEERESFORSCHUNG mit FS SONNE
   14.–15. Februar 2017 in Oldenburg–Tagungsband (2017), 221 Seiten
   ISBN: 978-3-95806-207-8

10. STATUSTAGUNG MARITIME TECHNOLOGIEN
    Tagungsband der Statustagung 2017 (2017), 224 Seiten
    ISBN: 978-3-95806-277-1

11. STATUSTAGUNG MARITIME TECHNOLOGIEN
    Tagungsband der Statustagung 2018 (2018), 224 Seiten
    ISBN: 978-3-95806-366-2

12. STATUSTAGUNG MARITIME TECHNOLOGIEN
Tagungsband der Statustagung 2019 (2018), 187 Seiten
ISBN: 978-3-95806-439-3

13. STATUS CONFERENCE RESEARCH VESSELS 2020
Conference transcript
Online-Publikation (2020), 411 Seiten
ISBN: 978-3-95806-479-9

14. STATUSTAGUNG MARITIME TECHNOLOGIEN
Tagungsband der Statustagung 2021 (2021), 300 Seiten
ISBN: 978-3-95806-594-9

15. STATUS CONFERENCE RESEARCH VESSELS 2022
Conference transcript
Online-Publikation (2022), 476 Seiten
ISBN: 978-3-95806-608-3

Projektträger Jülich
Forschungszentrum Jülich

HELMHOLTZ
RESEARCH FOR GRAND CHALLENGES